DOE/ER/40150--75

DE89 014430

Proceedings

CEBAF/SURA

1987 Summer Workshop

Continuous Electron Beam Accelerator Facility

Newport News, Virginia

June 22-26, 1987

Edited by: Franz Gross and Claude Williamson

Sponsored by: CEBAF/SURA

and

The Department of Energy

Endorsed by: The National Science Foundation

Continuous Electron Beam Accelerator Facility

12070 Jefferson Avenue

Newport News, VA 23606

(804) 875-7800

October 1987

Workshop Editors: Franz Gross (CEBAF/W&M)
Claude Williamson (MIT)

Local Organizing Committee

Volker Burkert (CEBAF)
Mike Finn (W&M)
Franz Gross (CEBAF/W&M)
Bernhard Mecking (CEBAF)
Jean Mougey (CEBAF)
Christine-Anne Bach (CEBAF)
R.Roy Whitney (CEBAF)

CEBAF User's Group - Board of Directors

Chairman (1986-1987) - Claude Williamson (MIT)

Chairman Elect (1987-88) - Jack Lightbody (NBS)

Past Chairman (1985-1986) - Ralph Minehart (UVa)

Members at Large: Mike Finn (W&M)
Wade Sapp (MIT)
Bernhard Mecking (CEBAF)

CEBAF User Liaison - R. Roy Whitney

Printed in the United States of America

To order a copy of the Proceedings, send $25 ($35 for overseas mail) to:

CEBAF 1987 Summer Workshop
12070 Jefferson Avenue
Newport News, VA 23606

Preface

The 4th annual CEBAF Summer Workshop was the first workshop to be held after the actual start of construction of CEBAF. Further evidence of the existence of an ongoing project was the written report of the first Program Advisory Committee (PAC) sent to the Users by the Scientific Director, J. Dirk Walecka. The Users had also received a letter from Dirk describing the response of the CEBAF management to the PAC recommendations. They had been informed that CEBAF was proceeding at full speed with plans to instrument Hall A with two high resolution spectrometers and Hall B with a Large Acceptance Spectrometer. Finally, Users had been told that a $5 million trust fund had been set aside for the instrumentation of Hall C with the final decision on the configuration of its equipment to be made in October 1988.

This Workshop therefore presented the Users with a unique opportunity to influence the plans for the experimental equipment. Since this equipment must reflect the experimental program for the facility, the emphasis for this Workshop was the organization of collaborations for carrying out the first round of CEBAF experiments. Users responded to this challenge by a record attendance at the Workshop. We were particularly pleased to welcome one very special group, namely the graduate students attending the second annual summer program of Hampton University Graduate Studies (HUGS) at CEBAF.

All of the Workshop sessions were held at neighboring Christopher Newport College, a recent associate member of SURA. A large, new auditorium and several classrooms were placed at our disposal for the various plenary sessions and collaboration meetings. We are indeed grateful to Christopher Newport College for hosting our Summer Workshop for a second year, and we extend to them our sincere thanks for allowing us to use their excellent facilities.

The organization of these Proceedings parallels the program of the 1987 Summer Workshop. It consists of summary talks on the CEBAF project, invited talks on theoretical and experimental subjects related to the CEBAF program, and summary reports of the collaboration meetings held during the Workshop. The collaboration meetings held at this Workshop reflect the fact that CEBAF is now a under construction and replaced the working group meetings of previous Workshops. In preparation for the collaboration meetings, a survey was sent to the Users in April to determine the areas of greatest interest in the community. Two types of collaboration meetings were organized, referred to as program collaborations and physics collaborations.

The physics collaborations focused on the design of individual experiments. Six hours were set aside during the first three days of the Workshop for these meetings, and summary reports from the nine groups which were formed are given in the third section of these Proceedings. In addition, a theory group also met for one session and made suggestions for the organization of activities for the summer of 1988.

Program collaborations were organized around major experimental programs, in principal drawing ideas from several physics collaborations and focusing them

into a well-defined experimental facility. Four program collaborations were identified before the Workshop began, and a fifth "new" program collaboration was organized by the participants at the Workshop. Spokespersons for these collaborations made initial presentations on Monday afternoon, and the collaborations met for one and one-half hours during the week. Final reports were made by spokespersons on Friday morning. The program collaborations were:

High Resolution Spectrometers (Hall A)
C. Papanicolas (Illinois) and J. Mougey (CEBAF)

Large Acceptance Spectrometer (Hall B)
R.D. McKeown (Caltech) and B. Mecking (CEBAF)

The (γ,K) Program
R.E. Chrien (BNL) and E. Hungerford (Houston)

Parity Measurements
R. Carlini (LAMPF) and R. Siegel (William & Mary)

Moderate Resolution Spectrometers
D. Day (Virginia)

We are very grateful to the leaders of the physics and program collaborations for their contributions to the Workshop.

The CEBAF Users Group held its fourth annual meeting on June 24. The outgoing Chairperson, Claude Williamson, presided over a short business meeting. This was followed by presentations by Jean Mougey and Bernhard Mecking, the CEBAF project managers for the two identified major equipment efforts, on the state of the planning for these instruments. The meeting was then opened for a very productive discussion between the Users and the CEBAF management. The incoming Chairperson, Jack Lightbody of the National Bureau of Standards, assumed office at the end of the meeting.

We are deeply indebted to the CEBAF Research Division support staff for their cheerful and efficient management of the Workshop. In particular, a special thanks are due to Chris Bach, Administrative Assistant, who assumed full responsibility for the organization of the Workshop only a few months before it was held, and to Ai Choo Ashe who only recently joined the CEBAF staff. All involved did an outstanding job and are heartily thanked by CEBAF and the CEBAF Users Group.

The discussions at the Workshop were a very valuable contribution to the planning for the CEBAF scientific program. We sincerely thank all the participants for coming and sharing their ideas and expertise.

Franz Gross
CEBAF & College of W&M

Claude Williamson
Massachusetts Institute of Technology

Workshop Co-chairpersons and Editors

TABLE OF CONTENTS

PHYSICS COLLABORATION REPORTS

PROGRAM COLLABORATION REPORTS

CONTRIBUTED PAPERS

APPENDICES

THE CONTINUOUS ELECTRON BEAM ACCELERATOR FACILITY

H. A. Grunder, J. J. Bisognano, W. I. Diamond, B. K. Hartline
C. W. Leemann, J. Mougey, R. M. Sundelin, R. C. York
CEBAF, 12070 Jefferson Avenue, Newport News, Virginia 23606

Presented at the International Particle Accelerator Conference, Washington, D.C., March 16–19, 1987.

ABSTRACT

On February 13, 1987, construction started on the Continuous Electron Beam Accelerator Facility—a 4-GeV, 200-μA, continuous beam, electron accelerator facility designed for nuclear physics research. The machine has a racetrack configuration with two antiparallel, 500-MeV, superconducting linac segments connected by recirculator beam lines to allow four passes. The accelerating structure consists of 1500-MHz, five-cell niobium cavities developed at Cornell University. A liquid helium cryogenic system cools the cavities to an operating temperature of 2 K. Beam extraction after any three of the four passes allows simultaneous delivery of up to three beams of independently variable currents and different, but correlated, energies to the three experimental areas. Beam breakup thresholds exceed the design current by nearly two orders of magnitude. Project completion and the start of physics operations are scheduled for 1993. The total estimated cost is $255 million.

INTRODUCTION

The Continuous Electron Beam Accelerator Facility (CEBAF) will be a 4-GeV, 200-μA, continuous beam, electron accelerator facility for nuclear physics research. The Vogt Subcommittee of the Nuclear Science Advisory Committee has stated succinctly the physics objective of this new accelerator:

The search for new nuclear degrees of freedom and the relationship of nucleon-meson degrees of freedom to quark-gluon degrees of freedom in nuclei is one of the most challenging and fundamental questions of physics.[1]

Consistent with this objective, CEBAF's purpose is to study the structure of the nuclear many-body system, its quark substructure, and the strong and electroweak interactions governing the behavior of nuclear matter.

To accomplish this objective, CEBAF must provide electron beams of sufficient

- energy to provide the kinematic flexibility required to study the transition region;[1]
- intensity (current) to allow precise measurement of relatively small electromagnetic cross sections;
- duty factor to allow the detection of hadronic components emitted from the nucleus in coincidence with the scattered electron;
- beam quality and resolution to allow detailed probing of the multifaceted elements of nuclear structure.

It is this combination of characteristics—high energy $\otimes$ high current $\otimes$ high duty factor $\otimes$ beam quality—which will make CEBAF the world's most powerful microscope for studying the nucleus.

Such an accelerator was called for in 1976 by the National Academy of Science panel (G. Friedlander, Chairman) convened to delineate the future opportunities and objectives of nuclear science.[2] Subsequent panels[3,4,5,6] reaffirmed the need for a high-energy cw electron accelerator, refined its requirements, and established its priority. In 1980, Professor James McCarthy of the University of Virginia submitted a proposal to the Department of Energy (DOE) under the auspices of the newly incorporated Southeastern Universities Research Association (SURA). The submission of the SURA proposal triggered activity within the electromagnetic nuclear physics community to prepare a formal scientific justification and to develop alternative designs. By 1982, five proposals were in

hand, including a revised proposal from SURA. During the winter of 1982/83, the NSAC Panel on Electron Accelerator Facilities (D. A. Bromley, Chairman) reviewed and evaluated the proposals at the request of NSF and DOE.[7] NSAC endorsed the panel's recommendation to accept the SURA proposal, and DOE accepted the recommendation.

Originally proposed as a 2-GeV, SLAC-type linac with two-pass, head-to-tail recirculation and pulse stretcher ring, CEBAF was converted to a cw, superconducting, four-pass recirculating linac after a technology review in the summer and fall of 1985.[8,9,10,11] DOE directed CEBAF to proceed with the superconducting linac design, and proposed the project to Congress for construction start in FY 1987. The superconducting accelerating structure that was adopted had been developed and tested by Cornell University's Newman Laboratory of Nuclear Studies, and had proven its capability to meet CEBAF's requirements.[12]

BASIC CHOICES: CONCEPT AND TECHNOLOGY

The beam performance design objectives are:

Energy, E	0.5 GeV $\leq$ E $\leq$ 4.0 GeV
Duty factor	100%
Average current	$\leq$200 μA
Emittance ($4\sigma^2 = \epsilon\beta$)	$\leq 2 \cdot 10^{-9}$ m-radian
Momentum spread $4\sigma_E/E$	10^{-4}
User multiplicity	3 beams, 3 energies

An intrinsically cw device is the approach of choice to meet these objectives. RF superconductivity is the preferred technology, because it allows higher gradients in cw operation and lower power consumption than room-temperature technology. Even so, beam recirculation is necessary for a cost-effective solution.

THE RECIRCULATING LINAC CONCEPT

Figure 1 illustrates schematically the solution adopted by CEBAF. Four-pass recirculation, close to the cost minimum, was chosen. The accelerating structure is arranged in two separate linac segments located in the straight sections of the racetrack-shaped configuration, thus minimizing the total accelerator circumference. Each segment is made of 25 cryomodules containing eight cavities apiece, with each cryomodule separated from its neighbors by a warm section containing vacuum equipment, beam diagnostics, and quadrupole and steering dipole magnets. The beam transport system connecting the two linac segments is designed to be strongly focusing, with beam lines of moderately large radii of curvature to minimize quantum excitation effects. Beam transport from linac to linac is achromatic, isochronous, and provides the required match in transverse phase space.

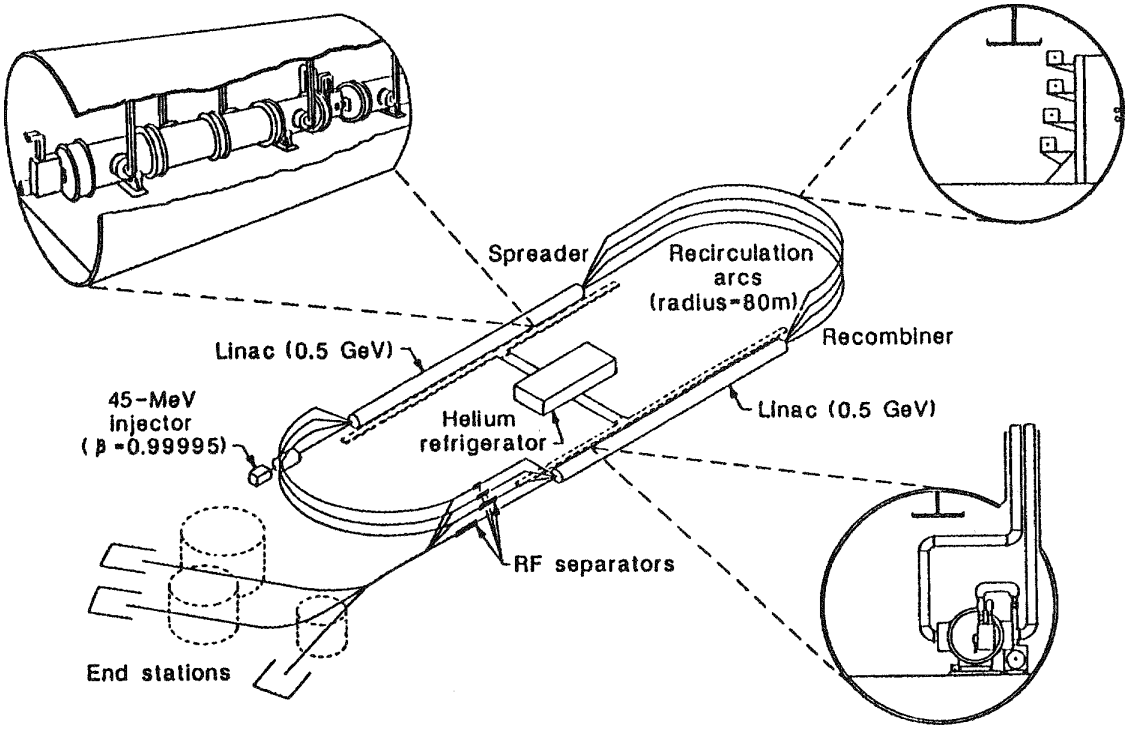

Figure 1. Schematic representation of four-pass recirculating linac concept.

Nominal injection energy is 45 MeV, sufficiently relativistic for the electrons to experience less than 2° of phase slip throughout the entire four-pass acceleration cycle, most of it in the first half of the first linac segment. The injector creates three interspersed 499-MHz bunch trains ($\{1,4,7..\}, \{2,5,8,..\}$, $\{3,6,9,..\}$) with individually adjustable current levels. Extraction at fractional energies, i.e., on the 1st, 2nd, or 3rd pass, is accomplished by deflecting bunches to a septum magnet by rf separators operating at 2495-MHz (i.e., 5/3 of the fundamental frequency). This choice of frequency allows the selective extraction of one (or two) of the 499-MHz bunch trains, leaving the remaining ones for further acceleration. Similarly, if all trains are accelerated to the maximum energy, an rf separator allows distribution among three channels. Thus, the recirculation, the differential bunch loading at the injector, and the extraction (or distribution) by rf separators achieve the goal of serving three users with beams of individually adjusted current and up to three different, although correlated, energies.

STATUS OF RF SUPERCONDUCTIVITY

Since 1979, rf superconductivity has made significant strides in structures designed for accelerating speed-of-light particles. In 1979, it was fortuitously found at the University of Genoa[13] that cavities with continuously curving outer walls do not multipactor. Multipacting had long blocked progress to higher gradients in superconducting rf accelerating cavities. Lyneis *et al.*[14] showed that cylindrical cavities exhibit one-point multipacting at their outer walls. Building upon this work, Klein and Proch[15] verified by simulation that spherical outer walls do not exhibit this multipacting.

Other important developments have followed. Development of the rastered[16] or defocused electron beam weld has eliminated vacuum voids that cause break-

down by interfering with heat transport. Input couplers and heavily coupled higher-order-mode (HOM) couplers are both mounted on the beam pipes to suppress beam instabilities, avoid local field enhancement, and minimize multipacting.[17] High thermal conductivity niobium, as supplied by manufacturers or as improved by yttrium[18] or titanium[19] gettering, stabilizes the temperature of the niobium surrounding rf-heated hot spots and suppresses breakdown.

A niobium cavity having all of the above improvements was beam-tested in the Cornell CESR storage ring at a gradient of 6.5 MV/m and Q_{res} of 5×10^9. Cavities of somewhat different designs, but incorporating all of the above improvements and operating in accelerators at gradients $\geq$ 5 MV/m and Q_{res} values $\geq 3 \times 10^9$, are planned in the near future at CERN, DESY, and KEK. KEK plans to use superconducting cavities in Tristan to boost the energy. DESY plans to use them to increase the energy gain per turn in the HERA electron ring. CERN plans to use them to upgrade LEP to LEP II. Darmstadt is building a recirculating superconducting linear accelerator. Saclay, Frascati, Stanford, TRW, and LANL are at various stages of planning accelerators using superconducting cavities.

BEAM BREAKUP

Recirculating a beam through a linac can lead to a transverse instability in which transverse displacement on successive recirculations can excite modes which further deflect the beam. The recirculated beam and cavities form a feedback loop that can be driven unstable at sufficiently high currents. This multipass beam breakup can severely limit current in a superconducting linear accelerator, due to the inherently high Q of transverse deflecting modes of the rf cavities.

Beam breakup at CEBAF has been investigated both with bunch-by-bunch simulations and analytic modeling. This work indicates that the HOM damping designed into CEBAF cavities successfully suppresses HOMs. Threshold currents are nearly two orders of magnitude above the CEBAF design current of 200 μA.[20]

The dominant mechanism for multipass beam breakup can be modeled in an impulse approximation. This is also the regime appropriate to single-pass cumulative beam breakup as observed in SLAC, where extensive computer modeling has been successful. A CRAY computer code has been developed that models beam behavior with multiple, transverse modes distributed along the linac.[21]

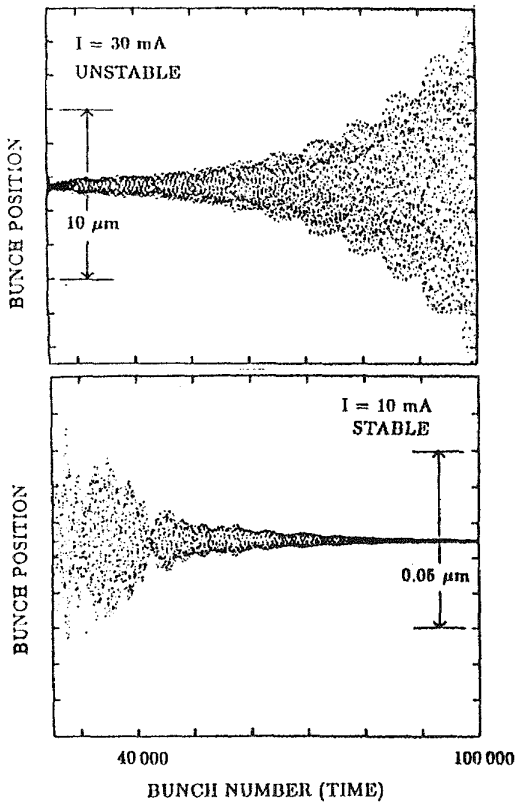

Figure 2. Simulation results clearly show instability for an average current of 30 mA and stability for 10 mA. Bunches are injected off-axis, thereby exciting deflecting modes. Shown is their centroid transverse position leaving the linac after four passes, plotted vs. bunch number, i.e., time.

Diagnostics to determine threshold currents for instablity and to estimate any steady-state emittance degradation due to the differential bunch loading have been included. In parallel with this effort, an analytic model has been developed. For N passes and M cavities, the solution reduces to finding M zeros of a $2(N\text{-}1)$ dimensional determinant, or equivalently the M eigenvalues of an M-dimensional matrix.[22] Excellent agreement is found between the two techniques.[21]

Stability of the CEBAF linac has been evaluated for the full 400-cavity array distributed along the linac with a FODO lattice. The four strongest HOMs of the cavity were included. The threshold current was found to be 19 mA at 4 GeV and 11 mA at 2 GeV after four passes through the linac (Figure 2). Furthermore, simulation of subthreshold excitation of HOMs, e.g. by differential bunch loading and injection offset, shows no significant emittance increase.

The CEBAF Design

Table I summarizes the CEBAF accelerator parameters.

Table I

Design Parameter List

CEBAF Superconducting Radio-Frequency CW Linac

Beam characteristics	
Electron energy E [GeV]	$0.5 \leq E \leq 4.0$
Average current [μA]	200
Transverse emittance (95%, 1 GeV) [m]	2×10^{-9}
Energy spread (95%)	1×10^{-4}
Duty factor	100%
Simultaneous beams	3
Simultaneous energies	≤ 3

Continued on next page

Table I, *continued*

Linac parameters	
Concept	Superconducting cw recirculating linac
Number of passes	4
Number of linac segments	2
Segment length [m]	235
Maximum energy gain per pass [GeV]	1.0
Recirculation time per pass [μs]	4.2
Focusing	FODO
Phase advance per cell (pass 1)	120°
Half-cell length [m]	9.4
Number of cavities per half-cell	8
Number of half-cells per segment	25
Vacuum (before cooldown) [torr]	10^{-9}
Cavity parameters	
Type	Superconducting
Frequency [MHz]	1497
Electric length [m]	0.5
Shunt impedance (r/Q) [ohm/m]	960.0
Design gradient [MV/m]	5.0
Design Q_0 at 2 K, 5 MV/m	2.4×10^9
Typical HOM Q_{external}	10^3 to 10^5
Clear aperture [mm]	70
Transverse HOM Z''/Q [ohms/m^3]	$\leq 16.4 \times 10^4$
Loaded Q (fundamental mode)	6.6×10^6
RF system	
Number of klystrons	418
Klystron power rating [kW]	5.0
Phase control	$< 1°$
Gradient regulation	$< 10^{-4}$

(Continued on next page)

Table I, *continued*

Injector parameters	
Gun energy [MeV]	0.10
Injection energy [MeV]	45
Average current [μA]	200
Transverse emittance (at 0.1 MeV) [mm-mr]	1
Longitudinal emittance [keV-degrees]	$< 15\pi$
Bunch length [degrees]	< 1.0
Pulse capability [μs]	0.05 to 10
Recirculation arc beam lines	
Number	7
Magnetic radii [m]	11.5 to 28.6
Phase advance per period	$2\pi(5/4)$
Periods per arc	4
Cryogenic system	
Total rf load (2.0 K) [W]	2510
Total heat load (2.0 K) [W]	3310
Total heat load (45 K) [W]	8000
System capacity (2.0 K) [W]	4800

INJECTOR

The injector provides a high-quality electron beam that is sufficiently relativistic (nominal 45 MeV) to stay in phase with the rf and the recirculating electron beams in the first half of the linac. The bunching, capture, and initial acceleration (up to about 1 MeV) regions are modeled after proven injector designs.[23,24] This beam is then further bunched and accelerated to just over 5 MeV in two five-cell superconducting cavities in a short cryostat, and then accelerated in two full-sized cryomodules to the required 45 MeV before injection into the linac. The entire injector has been modeled with PARMELA, a two-dimensional particle simulation code that calculates phase and radial properties, including space charge effects, for an electron beam. Calculations indicate

that a bunch of less than 1° phase angle and 20-keV full width should be obtained at the exit of the injector.[25] The injector enclosure has been designed to accommodate two electron guns to provide both polarized and unpolarized beams.

ACCELERATION SYSTEMS: CAVITIES, CRYOGENIC SYSTEM, AND RF SYSTEM

The accelerating cavities are five-cell, 1497-MHz, elliptical cavities developed at Cornell University (Figure 3). The cavities operate in the π mode, and have a fundamental coupler on the beam line at one end and an HOM coupler on the beam line at the other. The elliptical cavity shape yields low peak surface electric fields, a good chemical rinsing geometry, and good mechanical rigidity. The HOM coupler has two waveguides for extraction of HOMs. HOM Q's are typically in the range of $500 \lesssim Q_{\mathrm{HOM}} \lesssim 170{,}000$, which represents five orders of magnitude of damping.

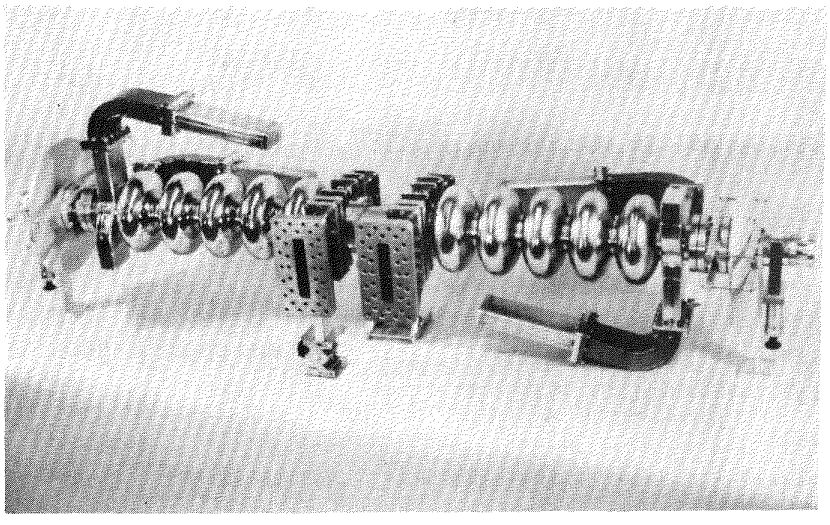

Figure 3. An assembled pair of CEBAF-Cornell superconducting five-cell cavities.

The Cornell cavity was adopted for CEBAF for four important reasons: suitable frequency, gradients in excess of 5 MV/m in laboratory and beam tests, damping of HOMs, and technical maturity, i.e., readiness for industrial prototyping.

Frequency optimization is based on minimizing transverse impedance, which scales as f^3, and delivering a pulse train with a high enough frequency that it appears effectively continuous to the detectors. Since 500 MHz appears continuous to the physics instrumentation, 1500 MHz allows simultaneous service to three users.

CEBAF is engaged in a cavity prototyping program in collaboration with Cornell and five industrial vendors—two European and three American firms. The design specifications are a cw accelerating gradient of at least 5 MV/m and a Q_0 of at least 2.4×10^9 at 2.0 K and 5 MV/m. Ten tests on four prototypes at Cornell have yielded an average gradient of 8.2 MV/m and an average Q_0 of 3.1×10^9. In acceptance tests, the first six prototypes produced by industry for CEBAF have achieved an average gradient of 7.1 MV/m. Each test exceeded the gradient and Q_0 specifications. In subsequent tests, the industrial prototypes have achieved gradients as high as 12.0 MV/m. Q_0 values of CEBAF prototypes average 6.5×10^9.

The operating temperature was selected on the basis of a cost optimization study. Liquid helium refrigeration systems become more expensive (capital and operating costs) as their design temperature decreases. Yet rf heat losses in the cavities increase exponentially with temperature. For CEBAF the optimum is around 2.0 K.

The cryogenic system for CEBAF consists of a 5-kW central helium refrigerator and a transfer line system to supply 2.2-K, 2.8-atm helium to the cavity

cryostats, 45-K helium at 4.0 atm to the radiation shields, and 4.5-K helium at 2.8 atm to the superconducting magnetic spectrometers in the experimental halls. Both the 2.2-K and the 4.5-K helium are expanded by Joule-Thompson (JT) valves in the cryostats, yielding 2.0 K at 0.031 atm and 4.4 K at 1.2 atm, respectively. The central helium refrigerator is located in the center of the CEBAF racetrack with the transfer lines located in the linac tunnels. The system capacity as a function of operating temperature is illustrated in Figure 4.

The CEBAF rf system consists of 418 individual rf amplifier chains. Each superconducting cavity is phase-locked to the master drive reference line to within 1°, and the cavity field gradient is regulated to within 1 part in 10^4 by an rf control module. Continuously adjustable, modulo-360° phase shifters are used to generate the individual phase references, and a compensated rf detector is used for level feedback. The close-coupled digital system enhances system accuracy, provides self-calibration, and continuously checks the system for malfunction. Calibration curves, the operating program, and system history are

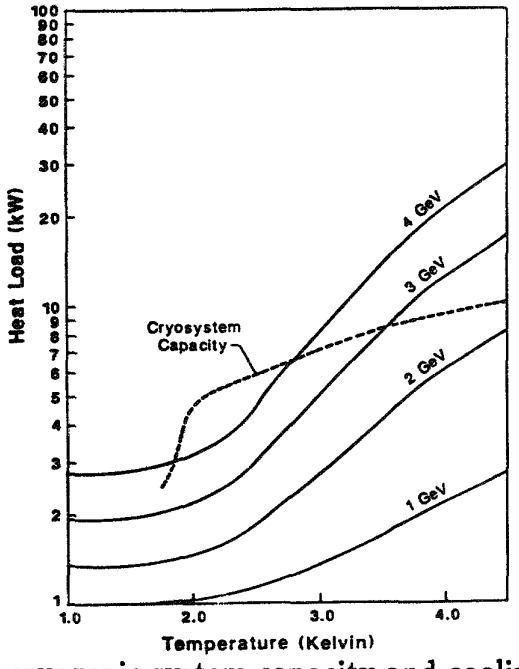

Figure 4. CEBAF cryogenic system capacity and cooling requirements for 1, 2, 3, and 4 GeV at minimum acceptable cavity quality factors Q.

stored in an on-board electrically erasable programmable read only memory (E^2PROM). The rf power is generated by a 5-kW, water-cooled, permanent-magnet-focused klystron. The klystrons are clustered in groups of eight and powered from a common supply.

Losses in the superconducting cavity are completely negligible from an rf point of view. Therefore all the power not used to accelerate the beam is reflected. Since CEBAF must cover operating conditions ranging from virtually no current to 800 μA in the cavities, a wide range of load conditions must be accommodated. The choice of the proper strength of cavity coupling, i.e., the loaded quality factor ($Q_L = 6.6 \times 10^6$), is based on the goal of achieving accelerating gradients up to 10 MV/m at full design current and with incident power $P_{\text{in}} \lesssim 5$ kW. Figure 5 shows the accessible gradient and current range.

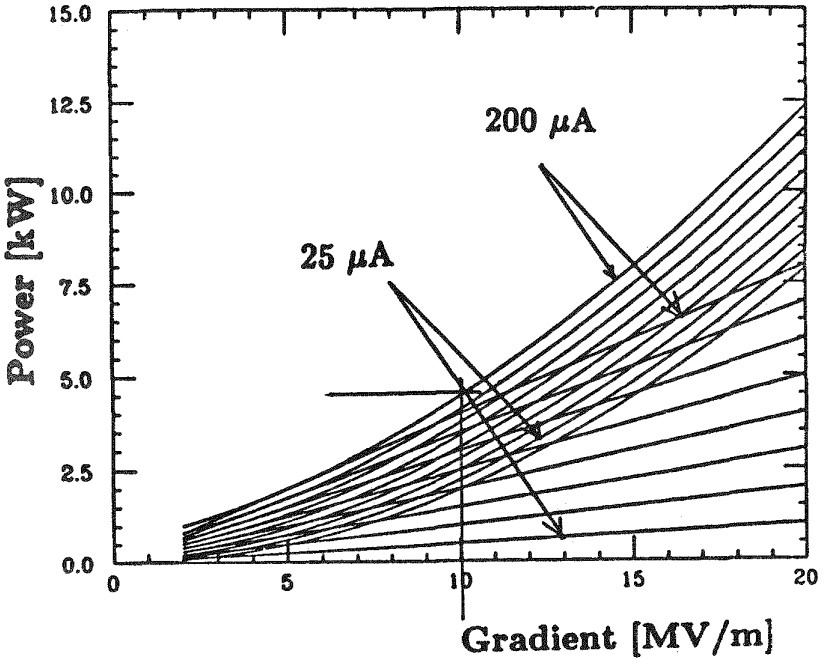

Figure 5. Power requirements versus cavity gradient for linac output from 0 to 200 μA. Design Q_L is $6.6 \cdot 10^6$ and power available from planned klystron is 5 kW. Straight lines represent powr into the beam, curved lines the required incident power.

OPTICS AND BEAM TRANSPORT SYSTEM

The beam transport system, consisting of main dipoles, quadrupoles, sextupoles and small steering dipoles, serves to guide and confine the beam through up to four passes through the accelerator, and to distribute it to the three experimental end stations. Within the accelerator, the three major areas are the two linac segments, the recirculation arcs (seven beam lines bending by 180°), and the sections connecting the linacs to the arcs. Key requirements for the optics are achromaticity, isochronicity, control of beam envelope (β,η functions) and of overall phase advance, and proper matching from linac to linac in transverse phase space. Another important concern is the minimization of synchrotron radiation effects. The design of the optics and beam transport system follows a modular phil-osophy, attempting as much as possible a one-to-one correspondence between a particular optical function and a subset of magnets.[26]

The linac optics for the first pass are simple FODO arrays with a phase advance per cell of 120° on the beam's first pass. The quadrupole spacing is 9.4 m, set by the pitch of the 8.4-m cryomodule accelerating units separated by 1-m regions for focusing and beam diagnostics. On subsequent passes the beams are acceptably matched to the optics by creating an increasingly larger β function for each pass as the beam enters the first linac.

The linac segments are connected to the arcs by spreaders and long matching sections, while the connection from arcs back to the linac segments is accomplished by recombiners and short matching sections. The long matching sections in the spreader regions provide space for extraction elements.

Spreaders and recombiners are vertical, achromatic bends consisting of a dipole common to all beams bending by an angle (α) inversely proportional to the beam energy, followed by magnets bending by $-\alpha$, now acting separately

on each beam. To achieve achromaticity in this arrangement, strong focusing to create 2π phase advance from dipole to dipole is required. The matching sections following the spreaders (or preceding the recombiners) match the beam from linac to arcs, or vice versa, with regard to vertical and horizontal beam ellipse parameters.[26]

The recirculation arc regions are achromatic and isochronous, based upon the second-order achromat principle. In addition, the lattice minimizes the six-dimensional beam-quality degradation due to synchrotron radiation by incorporating sufficiently large bending radii (~30 m magnetic radius for the high-energy beam lines) and strong focusing.

The extraction system, which provides the ability to deliver multiple simultaneous beams of correlated energy, is based upon the use of an "optical amplifier," an rf separator operating at 2495 MHz, and a magnetic septum to complete the separation between recirculated and extracted current. The "optical amplifier" is used to reduce the transverse kick required from the rf separator. The choice of rf separator frequency meets the criterion of $f_s = mf/3$ where f is the accelerator fundamental frequency (1497 MHz) and where m is an integer, but not a multiple of 3. With this choice, every third bunch receives the same kick, while the separator rf phase determines the relative strength of the kick that each bunch of the three-bunch train receives. The rf phase can be set to accomplish a two-beam split (extracted and recirculated) in the three low-energy beam lines, or a three-beam split in the highest-energy beam line. Thus, the system provides three extracted beams, which may consist of any one of the three lower energies together with two beams of the highest energy, or any two of the three lower energies together with one beam of the highest energy, or three beams of the highest energy.[26]

INSTRUMENTATION AND CONTROL

The central elements of beam instrumentation are several hundred beam current and position monitors that are based on cavities with loaded Q-values around 1000 and operating at 2994 MHz. Profile monitors at the low-energy end in the injector area will be wire scanners, while several beam parameters, such as profile and bunch length, will be measured in the arcs with synchrotron radiation monitors.

The control system's key feature is a two-level computer structure using extensively distributed intelligence and high-power, local capabilities. It provides sufficient capability in the control room to implement such tools as automated tune-up procedures, on-line machine modeling, and simulation.[27]

EXPERIMENTAL EQUIPMENT

As electrons and photons are known to be precise and quantitative probes, the physics program at CEBAF will rely heavily upon high-precision detection systems. To perform coincidence experiments, sets of two or three large angular and momentum acceptance spectrometers around the same pivot, or 4π detectors with magnetic analysis, will be used.

The CEBAF facility includes three experimental halls—A, B, and C—fed simultaneously by continuous beams of different (correlated) energies and independently controlled intensities.

Hall A, designed for high-resolution experiments (1.0 to 0.1 MeV) will house two high-resolution (10^{-4} or better) spectrometers with large solid angle (10 msr) and momentum acceptance (10–15%). The 4-GeV/c (expandable to 6-GeV/c) electron and 3-GeV/c hadron spectrometers are made of several homogeneous-field, iron-dominated superconducting dipoles and high-gradient,

large-aperture, superconducting $\cos 2\theta$ quadrupoles, with higher-order correcting coils. The spectrometer arrangement will allow operation with long gas targets, use of polarized beam and/or target, and measurements involving non-coplanar kinematics.

The large acceptance spectrometer in hall B has been designed for photonuclear and low-luminosity ($\leq 10^{33}$ cm^{-2} sec^{-1}) electronuclear studies. It consists of eight superconducting coils generating a toroidal field in eight nearly independent sectors. Fully instrumented, it will allow multiparticle detection and identification within ~80% of 4π and 0.1 to 3 GeV/c in momentum.

Hall C will be devoted to double- or triple-arm experiments with moderate (~10 MeV) resolution. Initial plans include a large momentum acceptance (30%) electron spectrometer and two non-focusing hadron spectrometers with very large acceptances, associated with neutron time-of-flight detectors.

COST AND SCHEDULE

Congress authorized CEBAF's construction in FY 1987 with a first-year budget of $16.2 million. On February 13, 1987—the same day the Program Advisory Committee held its first meeting to discuss and recommend priorities for the scientific program—CEBAF signed its first construction contract, and site clearing began.

The president's budget for FY 1988 requests $33.5 million for construction. The proposed funding profile projects $65 million in FY 1989 and FY 1990, $55 million in FY 1991, and $20.3 million in FY 1992, for a total estimated cost of $255 million. Project completion and the start of physics operations are scheduled for FY 1993.

REFERENCES

[1] "Report of the NSAC Ad Hoc Subcommittee on a 4 GeV CW Electron Accelerator for Nuclear Physics," September 1984.

[2] Future of Nuclear Science, NAS 1977. Friedlander Panel, National Research Council, National Academy of Science, 1977.

[3] Long Range Plan for Nuclear Science, DOE/NSF Nuclear Science Advisory Committee, 1979.

[4] The Role of Electron Accelerators in U.S. Medium Energy Nuclear Science ORNL/PPA-77/4, 1977.

[5] The Role of Electromagnetic Interaction in Nuclear Science, DOE/NSF Nuclear Science Advisory Committee, 1982.

[6] Long Range Plan for Nuclear Science, DOE/NSF Nuclear Science Advisory Committee, 1983.

[7] A Report of the Panel on Electron Accelerator Facilities, DOE/NSF Nuclear Science Advisory Committee, 1983.

[8] CEBAF Pre-Construction Technology Review, 1985.

[9] Scientific and Technological Assessment Report (STAR), CEBAF, Nov. 1985.

[10] Preliminary Conceptual Design Report (PCDR), CEBAF, Nov. 1985.

[11] Conceptual Design Report (CDR), CEBAF, Feb. 1986.

[12] Ronald M. Sundelin, "High Gradient Superconducting Cavities for Storage Rings," IEEE Trans. Nucl. Sci. **NS-32**, No. 5, October 1985, pp. 3570–3573.

[13] V. Lagomarsino *et al.*, "Measurements on Niobium Superconducting C Band Cavities for Linear Accelerator Applications," IEEE Trans. Magn., Vol. Mag-15, No. 1, January 1979, pp. 25–26.

[14] C. M. Lyneis, H. A. Schwettman, and J. P. Turneaure, "Elimination of Electron Multipacting in Superconducting Structures for Electron Accelerators," Appl. Phys. Lett., Vol. 31, No. 8, October 1977, pp. 541–543.

[15] U. Klein and D. Proch, "Multipacting in Superconducting RF Structures," in Proceedings: Conference on Future Possibilities for Electron Accelerators, Charlottesville, Virginia, 1979, pp. N–N-17.

[16] R. Sundelin, "Superconducting RF Activities at Cornell University," in Proceedings of the Second Workshop on RF-Superconductivity, ed. H. Lengeler, Geneva, Switzerland, July 1984, Part 1, pp. 49–61.

[17] B. Dwersteg *et al.*, "Status Report of the Petra 18-Cell Superconducting Cavity Experiment," in Proceedings of the Second Workshop on RF-Superconconductivity, ed. H. Lengeler, Geneva, Switzerland, July 1984, Part 1, pp. 235–253; R. Sundelin, "What Did We Learn From Storage Ring Tests?" *ibid.*, pp. 203–223.

[18] H. Padamsee, U.S. Patent No. 4,487,637 (1984).

[19] P. Kneisel, Cornell Laboratory of Nuclear Studies, Internal Report SRF-840702, 1984.
[20] J. J. Bisognano and G. A. Krafft, "Multipass Beam Breakup in the CEBAF Superconducting Linac," in 1986 Linear Accelerator Conference Proceedings, pp. 452–454.
[21] G. A. Krafft and J. J. Bisognano, "Two-Dimensional Simulations of Multipass Beam Breakup," to be published in the proceedings of the 1987 Particle Accelerator Conference.
[22] J. J. Bisognano and R. L. Gluckstern, "Multipass Beam Breakup in Recirculating Linacs," *ibid.*
[23] M. Wilson *et al.*, "NBS-LANL RTM Injector Installation," IEEE Trans. Nucl. Sci. **NS-30**, No. 4, 1983, p. 3021.
[24] Nuclear Physics with a 450 MeV Cascade Microtron, University of Illinois Nuclear Physics Laboratory report, March 1986.
[25] W. Diamond, "The Injector for the CEBAF CW Superconducting Linac," to be published in the proceedings of the 1987 Particle Accelerator Conference.
[26] R. C. York and D. R. Douglas, "Optics of the CEBAF CW Superconducting Accelerator," *ibid.*
[27] Rolf Bork, "The CEBAF Control System Architecture," *ibid.*

1987 SUMMER WORKSHOP
CEBAF - A LABORATORY FOR NUCLEAR PHYSICS

JOHN DIRK WALECKA
SCIENTIFIC DIRECTOR

I would like to welcome all the participants to this 1987 CEBAF Summer Workshop.

Let me begin at the beginning. Why do we do nuclear physics? First, the nucleus is a unique form of matter. It consists of many baryons in close proximity. All the forces of nature are present in the nucleus: strong, electromagnetic, weak, and even gravitation if one includes neutron stars which are nothing more than enormous nuclei held together by the gravitational attraction. The nucleus presents a unique microscopic laboratory to test the structure of the fundamental interactions. Furthermore, the nuclear many-body problem is of intrinsic intellectual interest. In addition, most of the mass and energy in the visible universe comes from nuclei and nuclear reactions. If the goal of physics is to understand nature, then surely we must understand the nucleus. Finally, in sum, nuclear physics is really the study of the structure of matter.

Why do we do electron scattering [1,2]? First, the interaction is known. It is given by quantum electrodynamics (QED) which is the most accurate physical theory we have. The electron provides a clean probe. We know what we measure. The interaction is with the local electromagnetic current density in the target. In addition, this interaction is relatively weak, of order α, the fine structure constant. Thus one can make measurements on the target without greatly distrurbing its structure. What one basically measures in electron scattering, with large spectrometers in the laboratory, is a macroscopic diffraction pattern. This pattern is determined by the Fourier transform of the charge and current densities in the target. By inverting this Fourier transform, one can measure the detailed microscopic spatial distribution of these charge and current densities in the target. The Fourier transform variable is the momentum transfer of the electron, and thus there is an inverse relationship between the momentum transfer and the distance scale probed in the target - to study short distances one needs

high momentum transfer. Figure 1 shows the macroscopic diffraction pattern observed when scattering electrons elastically from ^{40}Ca. This data is from Saclay [3]. Figure 2 shows the charge density of ^{40}Ca deduced from these experiments plotted as a function of the distance from the center of the nucleus measured in Fermis ($1F = 10^{-13}cm$). The hatched area indicates the uncertainty in our knowledge of this charge distribution. Our best knowledge of what the nucleus actually looks like comes from electron scattering. The electron is also a versatile nuclear probe. Not only is there an interaction with the charge density, but also with the convection current density arising from the motion of the charges (e.g. protons) in the nucleus. Furthermore, neutrons and protons are little magnets, and the distribution of nucleons over the nucleus gives rise to an intrinsic magnetization density (or spin density). The curl of this magnetization density gives rise to an additional current in the nucleus with which the electron interacts.

How do we do nuclear physics? The traditional approach to nuclear physics [4] starts from static two-body potentials fit to two-body scattering and bound-state data. These potentials are then inserted in the non-relativistic many-particle Schrödinger equation, and that equation is then solved in some approximation. The three-body problem can essentially be solved exactly within this framework using modern techniques. Electroweak nuclear currents are then constructed from the properties of free nucleons and used to probe the structure of the nucleus.

Although this traditional approach to nuclear structure has had many successes, it is clearly inadequate for a more detailed understanding of the nucleus. A more appropriate set of degrees of freedom consists of the hadrons, the strongly interacting mesons and baryons. There are many arguments one can give for this. For example, the long-range part of the Paris potential, probably the most accurate two-nucleon potential currently available, consists of the exchange of mesons: $\pi(0^-,1)$, $\sigma(0^+,0)$, $\omega(1^-,0)$, and $\rho(1^-,1)$. Also, one of the significant recent successes of this field has been the unambiguous identification of exchange currents in nuclei. These are additional convection currents present in the nucleus because of the flow of charged mesons between baryons in the many-baryon system. We shall return to this.

Furthermore, a current goal of nuclear physics is to obtain a description of nuclear matter under extreme conditions. For example, one wants the behavior at high density and temperature in applications to astrophysics or relativistic heavy-ion collisions. In addition, one wants the response of the nuclear system to high q^2 probes, where q, the momentum transfer may be large compared to the nucleon mass. In developing any theoretical

description of the nucleus which allows one to extrapolate away from the known properties of terrestrial nuclei, it is essential to incorporate general principles of physics, such as quantum mechanics, special relativity, and microscopic causality.

The only consistent theory we have of such a relativistic interacting many- body system is relativistic quantum field theory based on a local lagrangian density. I like to refer to relativistic quantum field theories of the nuclear system based on hadronic degrees of freedom, baryons and mesons, as quantum hadrodynamics (QHD) [5].

One of the great intellectual achievements of our era is the unification of the electromagnetic and weak interactions due to Weinberg, Salam, Glashow, and others [6,7,8]. This is akin to Maxwell's unification of electricity and magnetism. It is essential to continue to put this theory to rigorous tests.

Furthermore, we currently have a theory of the strong interactions binding quarks into the observed hadrons. This is a Yang-Mills non-abelian gauge theory [9] based on an internal color symmetry. It is called quantum chromodynamics (QCD) [10].

We thus now have a standard model of the strong and electroweak interactions. This standard model is a local gauge theory based on the underlying symmetry structure $SU(3)_C \otimes SU(2)_W \otimes U(1)_W$. In this talk, I will discuss how one can use the electroweak interactions to probe the structure of this standard model of the strong, electromagnetic, and weak interactions. In addition, we will discuss how nuclei can be used to study the structure of the strong interactions.

Before beginning the discussion, it is important to recall two remarkable properties of QCD [10]. The first is asymptotic freedom, which roughly states the following: when all the momenta entering into a process are large, or equivalently at very short distances, the renormalized coupling constant for that process goes to zero. In this regime, one can do perturbation theory. The second property is confinement. One never sees the underlying degrees of freedom in the theory, the quarks and gluons (the massless spin-one bosons mediating the force), as free asymptotic scattering states in the laboratory. The quarks and gluons are confined to the interior of the observed hadrons, and at large distances, it is only the composite hadrons which are observed. There is strong evidence from lattice gauge theory calculations, where QCD is solved as a strong-coupling theory on a finite space-time lattice, that confinement is indeed a dynamical property of QCD arising from the non-linear gluon couplings in the theory.

We start the discussion with an example which exhibits relativistic

aspects of nuclear structure. Consider elastic magnetic electron scattering (e,e) from ^3He. The experimental results for the square of the magnetic form factor are shown in Figure 3 [11]. The dashed curve is the result obtained in the traditional nuclear physics picture. Here the three-body Faddeev equations are solved with a static two-body potential and the nucleus is assumed to consist only of nucleons, protons and neutrons. The solid curve is obtained by adding in the contribution of exchange currents arising from the exchange of mesons between the nucleons. At large distances, or low momentum transfer, this exchange current arises from pions, and can be calculated exactly using low-energy theorems. Evidently, while the exchange current contributions are very small at low q^2, they soon become a large effect, and they dominate the form factor by orders of magnitude at high momentum transfer. The exchange currents are clearly needed to fit the data. The two different solid curves at high q^2 are two different theoretical calculations that include higher mass hadronic degrees of freedom [12,13].

There are several morals that can be drawn from this comparison:

1) The intermediate q^2 results illustrate the marginal role of exchange currents in the traditional nuclear physics domain.

2) The high q^2 results illustrate the need for an explicit treatment of the subnucleonic hadronic degrees of freedom, or for QHD.

3) The appropriate set of degrees of freedom depends on the distance scale at which we probe the system.

Where are we today in nuclear physics? Properties of the nuclear system are studied experimentally with electron accelerators at laboratories such as Bates, Saclay, and NIKHEF. One can then accurately interpret this data in terms of nucleons and subnucleonic hadronic degrees of freedom, baryons and mesons. On the other hand, we have dynamic evidence for a point-like substructure of the hadrons from deep inelastic electron scattering (e,e') experiments pioneered at SLAC [14,15,16]. In these deep-inelastic experiments $q^2 \rightarrow \infty$ and $\nu = \epsilon - \epsilon' \rightarrow \infty$ while their ratio is fixed. The observed point-like substructure is interpreted in terms of a new underlying set of degrees of freedom for the hadrons themseves, quarks and gluons. One concludes that:

> *There must be interesting, important physics in the intermediate range of energy loss and momentum transfer.*

Indeed, the report of the Vogt Subcommittee of NSAC, the last national committee to reexamine the top priority given by the field of nuclear physics to the construction of a 4 GeV CW electron accelerator states that:

The search for new nuclear degrees of freedom and the relationship of nucleon-meson degrees of freedom to quark-gluon degrees of freedom in nuclei is one of the most challenging and fundamental questions of physics.

The picture of the nucleus in the standard model of the strong and electroweak interactions is shown in Figure 4. This is only a cartoon, but it is important to realize that underneath this cartoon there is a local lagrangian density and local currents. We can make several observations here:

1) The structure of confinement in the many-baryon system, as well as in the single-baryon system is an unsolved problem. A way to study this problem is to vary the environment in which the hadrons find themselves, and this means looking at nuclei under a wide variety of conditions.

2) The electroweak interactions with a lepton arise from the exchange of a virtual γ, Z^0, or $W^{\pm}$. In the standard model, these electroweak interactions couple directly to the quarks.

3) The gluons, whose non-linear interactions presumably give rise to confinement, are absolutely neutral to the electroweak interactions in the standard model.

4) The electroweak interactions are colorblind; they are the same for all quarks regardless of color.

5) While it is the quark that is struck by the electroweak interaction, it is only hadrons that emerge from the nucleus to form free asymptotic scattering states in the laboratory. The process of "hadronization" by which this takes place is largely unexplored. CEBAF, with its 100% duty factor and corresponding coincidence capability, is in a unique position to make important contributions in this area.

Let us discuss one consequence of this standard model of the nucleus. Consider the difference in cross section for the scattering of right- and left-handed longitudinally polarized electrons. This difference reflects parity-violation arising from the interference of the exchange of a virtual photon and a Z^0 which governs the weak neutral current interaction (Figure 5). Recall that parity is conserved to all orders in the electromagnetic interaction. Now assume only that the weak neutral current has a V-A structure and consider elastic scattering from a 0^+ target. The parity violating asymmetry is then given by [1]

$$A_{ee'} = \frac{d\sigma_\uparrow - d\sigma_\downarrow}{d\sigma_\uparrow + d\sigma_\downarrow} \qquad (1)$$

$$= -\frac{q^2 G}{2\pi\alpha\sqrt{2}} \cdot \left[\frac{F^{(0)}(q^2)}{F^{(\gamma)}(q^2)}\right] \tag{2}$$

Here $F^{(\gamma)}(q^2)$ is the familiar electromagnetic form factor which measures the distribution of electromagnetic charge over the nucleus. Similarly $F^{(0)}(q^2)$ measures the distribution of weak neutral charge over the nucleus. *A priori* these quantities have absolutely nothing to do with each other. Suppose that one now invokes the standard model in the nuclear domain. Here the Hilbert space is truncated to that sector containing only the light u and d quarks and their antiparticles. This sector provides a description of all the non-strange and non-charmed hadrons of interest. Suppose further that the nucleus has isospin $T = 0$. In this case the weak neutral current density and electromagnetic current density are exactly proportional, and consequently the form factors are exactly proportional. The asymmetry then reduces to [17,1,2]

$$\mathcal{A} = \frac{q^2 G}{\pi\alpha\sqrt{2}} \sin^2\theta_W \tag{3}$$

Now this is a spectacular result! It is independent of the details of the strong interaction structure of the target. The charge densities and form factors are the same at all q^2 and hence at all distance scales. This holds at low q^2 and large distances where one only samples the gross properties of the nucleus, out to higher q^2 and shorter distances where one sees the proton and neutron substructure, out to still larger q^2 and shorter distances where one sees the charges residing in the subnucleonic hadronic degrees of freedom, and on out to the highest q^2 where the point- like quark substructure itself is manifest. This, to me, provides a true test of the unification of the electroweak interactions. This is why I personally give the $^{12}C(\vec{e},e)$ experiment at Bates such a high priority.

Why CEBAF? There is no single feature that makes CEBAF unique. Rather it is the combination of qualities

$$energy \oplus duty\ factor \oplus intensity \oplus beam\ quality \tag{4}$$

which makes CEBAF the world's most powerful microscope for studying the nucleus.

I have tried to capture my own vision of CEBAF in a few words:

CEBAF will provide the most precise, accessible probe of matter. The interaction if known, and one knows what is being measured. It is a

unique time for nuclear physics. What we are really discussing is a tool and capability for the next generation of nuclear physicists.

My version of CEBAF's scientific goal is the following:

CEBAF's scientific goal is to study the structure of the nuclear many-body system, its quark substructure, and the strong and electroweak intreractions governing the behavior of this fundamental form of matter.

In February of this year we had the first meeting of the CEBAF Program Advisory Committee (PAC1). The charge and membership are shown in Figure 6. It is a first-rate PAC. We got the very best people we could think of, and experienced people. We are fortunate to have John Schiffer serve as Chairman of the PAC, and John will give a talk on the PAC report at this workshop. To organize the first meeting, steering committees were appointed in conjunction with the Board of Directors (BOD) of the CEBAF Users Group. We built on the work of the previous CEBAF workshops and summer studies and established steering committees in the areas shown in Figure 7. The PAC subsequently confirmed that these are indeed the anticipated major areas of research at CEBAF. The steering committees were asked to work with the users community and to:

1) Choose a spokesman

2) Prepare the strongest possible physics case for that particular area of research

3) Design a prototype experiment. What would be required to carry through such an experiment from beginning to end?

4) Identify groups in the users community which would like to take responsibility for the development of that particular program

As John will tell you, the PAC established an initial set of relative priorities, and made recommendations concerning the development of the experimental facilities required to implement the scientific program. The PAC Report, with a covering letter outlining the laboratory response to the report, went out to all members of the CEBAF Users Group on 3/23/87. You should all have received it. In any event, the material is appended to this talk; I will not repeat it here. These highlights are shown in Figures 8-12.

During the PAC Hermann told me that he really wanted to get in on some of the fun. He organized a task force (Figure 13) to work on the design of the end stations. This task force met religiously at 8:00 a.m. all winter, and I am really pleased with the results. The end station layouts are shown in Figures

14 and 15. Hall A is designed to house, with maximum kinematic flexibility, the pair of high-resolution electron and hadron spectrometers (HRS^2) shown in Figures 16 and 17. Hall B will house the large-acceptance spectrometer (LAS) shown in Figure 18. The size of hall C is maximized within the civil construction budget; it is left open for now (see above). Each hall is designed to independently take full beam intensity. Equipment access to the floor will be by hoistable truck platform. There is a common counting house, with personnel access through elevator and labyrinth to the experimental areas. Crane coverage will be provided, and a test beam is available off hall C. There are 60° bends, and dispersed beam will be available, in halls A and C. The incident electron beam will be transported through a discrete set of channels, with individual beam dumps, to provide an out-of-plane capability in hall A. You will hear much more about the spectrometers and end stations at this workshop.

My own top priority during the past year has been to arrange academic appointments for future CEBAF scientific research scientists. I believe that contact with students and young people, as well as with colleagues in other areas of physics, and related fields, is absolutely essential to the long-term intellectual health and vitality of this organization. I want these to be regular academic appointments, where the individual spends a finite fraction of his or her time at the academic institution doing classroom teaching, working with graduate students, carrying out independent research, and interacting with colleagues. Indeed, I see this academic connection as an essential part of the job function of these research scientists. This is a two-way street. These appointments will allow the universities to have close intellectual contact with the physics at CEBAF, and to directly participate in that physics. Figure 19 indicates the SURA universities I have visited so far. The visits consisted of talks with physics faculty, department chairmen, deans, and provosts. I would also give a colloquium. The response from all of these institutions was extremely rewarding. All are eager to participate in this exciting new venture in basic research. Each university is an individual institution with individual needs and requirements, but I could not be more pleased with the progress we have made toward constructing these academic positions. I think I can safely say that there will be academic appointments of this type for approximatly 15-20 research scientists at CEBAF.

Graduate education at CEBAF is another of my major concerns. I gave a series of lectures on "Electron Scattering" this winter and spring at CEBAF [2]. These were an update of the lectures given at Argonne a few years ago [1]. Approximately 20-30 people attended, and roughly half of these were students and postdocs from the surrounding area. Lecture notes were

prepared; they are available outside my office. I was very pleased with this initial venture. The current plan is to offer the sequence of graduate level courses indicated in Figure 20 at CEBAF over the next three years. These are aimed at the CEBAF scientific/engineering staff and at people in the vicinity. The goal is to establish an intellectual environment during the construction phase of the project, and to prepare researchers for the physics that will be done when CEBAF is in operation. Lecture notes will be prepared, and the lectures will be put onto video tape. Anyone at a SURA university, or at any other university for that matter, is welcome to participate and encouraged to do so.

The growth in staffing in the Research Division in FY87 and FY88 is presented in Figure 21. Our highest priority is to recruit the individual recommended by the national search committee we established to identify an Associate Director for Research. I am guardedly optimistic here. We are also trying to recruit the individual recommended by the second national search committee established to identify a Head of the Theory Group. We have added the indicated staff, after extensive and rigorous searches and evaluations. We intend to continue these searches, casting an even wider net, to fill the indicated positions in FY88.

The most immediate issue is to appoint an *ad hoc* Technical Advisory Panel (TAP) to provide technical advice to the CEBAF directorate on the design, construction, cost, schedule, and implementation of the LAS. The membership of this TAP was selected in consultation with the BOD immediately following the workshop. It is shown in Figure 22. We are extremely fortunate to have John Peoples, Jr. as Chairman of this TAP. The letter establishing the TAP was also written immediately following the workshop (7/14/87). It is based on the presentation in this talk, and it is appended to this material. The issues for the TAP are spelled out in detail in that letter.

Some key dates are the following:

- TAP(LAS) — August, 1987
- Freeze out-of-plane capability — October, 1987
- Freeze extended target capability — October, 1987
- Freeze conceptual design of end stations — October, 1987
- PAC2 — October 8-10, 1987
- Freeze conceptual design of spectrometers — January, 1988
  - LAS
  - HRS[2]

In closing, I would just like to reiterate our institutional goal at CEBAF:

> *GOAL: Build a world-class, user friendly laboratory for nuclear physics research and graduate education centered around a high-intensity 4-GeV, CW electron accelerator.*

REFERENCES

[1] J. D. Walecka, "Electron Scattering", ANL-83-50, Argonne Nat. Lab., Argonne, Illinois (1984)

[2] J. D. Walecka, "Electron Scattering", CEBAF Lecture Notes (1987) - *unpublished*

[3] B. Frois **et al.**, Lect. Notes in Phys. **108**, Springer, Berlin (1979), p. 52

[4] A. L. Fetter and J. D. Walecka, **Quantum Theory of Many-Partical Systems**, McGraw-Hill, New York (1971)

[5] B. D. Serot and J. D. Walecka, "The Relativistic Nuclear Many-Body Problem", Adv. in Nucl. Phys. Vol. **16**, eds. J. W. Negele and E. Vogt, Plenum Press, New York (1986)

[6] S. Weinberg, Phys. Rev. Lett **19**, 1264 (1967); Phys. Rev. **D5**, 1412 (1972)

[7] A. Salam and J. C. Ward, Phys. Lett. **13**, 168 (1964)

[8] S. L. Glashow **et al.**, Phys. Rev. **D2**, 1285 (1970)

[9] C. N. Yang and R. Mills, Phys. Rev. **96**, 191 (1954)

[10] F. Wilczek, Ann. Rev. of Nucl. Sci. **32**, 177 (1982)

[11] J. M. Cavedon **et al.**, Phys. Rev. Lett. **49**, 986 (1982)

[12] D. Riska, Nucl. Phys. **A350**, 227 (1980)

[13] E. Hadjimichael, B. Goulard, and R. Bornais, Phys. Rev. **C27**, 831 (1983)

[14] J. D. Bjorken, Phys. Rev. **179**, 1547 (1969)

[15] R. E. Taylor, "Proc. 4^{th} Int. Sym. on Electron and Photon Inter. at High Energy", ed. D. W. Braben, Daresburg Nuclear Phys. Lab. (1969) p. 251

[16] J. I. Friedman and H. W. Kendall, Ann. Rev. Nucl. Sci. **22**, 203 (1972)

[17] G. Feinberg, Phys. Rev. **D12**, 3575 (1975)

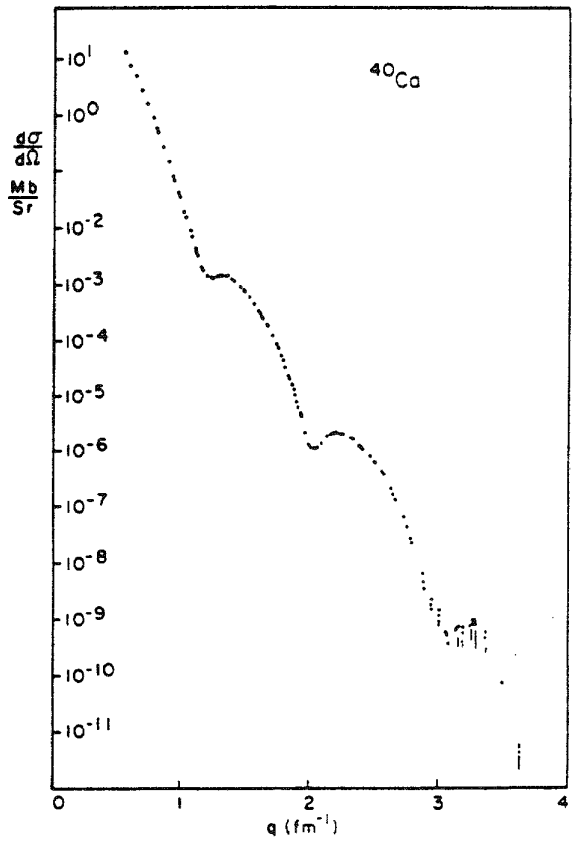

Fig. 1 Elastic (e,e) cross section for ^{40}Ca vs. momentum transfer [3]. The scattering here is from the charge distribution.

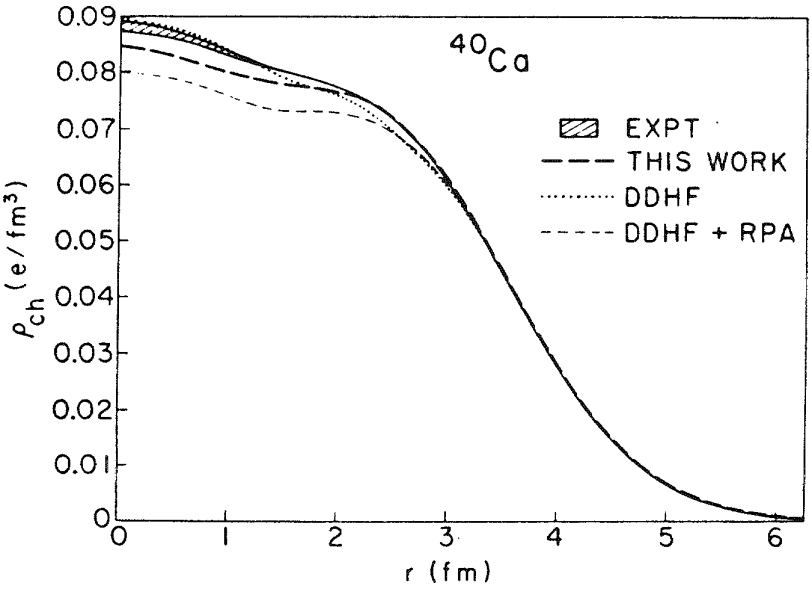

Fig. 2 Experimental charge density of ^{40}Ca with estimated uncertainty from elastic electron scattering (solid lines and shaded area) and relativistic Hartree calculations of this quantity within the framework of QHD (heavy dashed line). Taken from refs. [3,5].

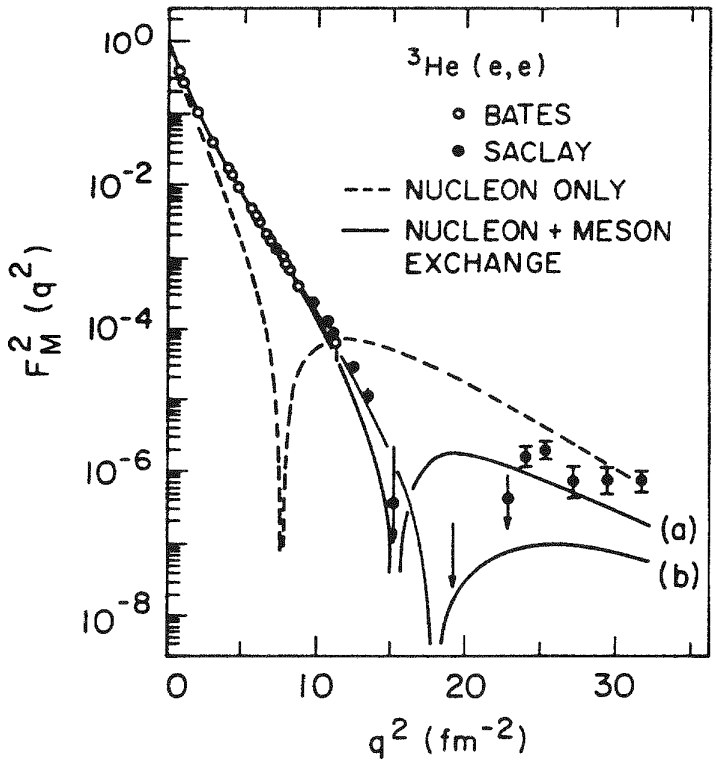

Fig. 3 Elastic magnetic form factor for ^3He (e,e) out to high q^2 [11]. Two exchange current theories are shown [12(b), 13(a)].

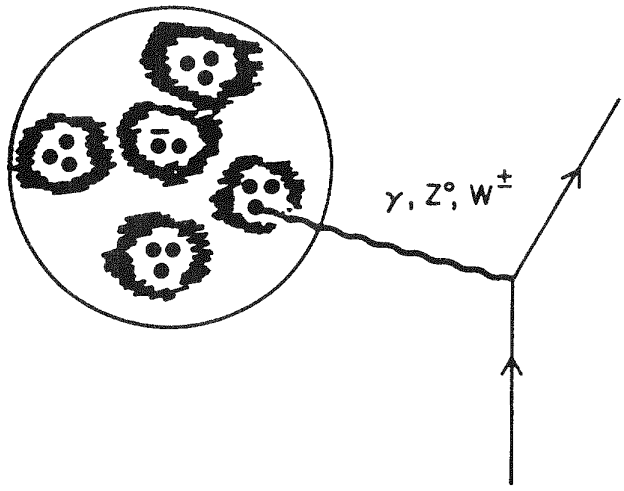

Fig. 4 Picture of the nucleus in the standard model.

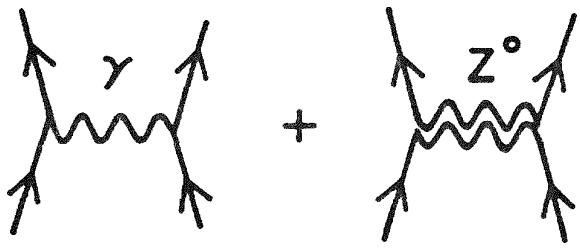

Fig. 5

PROGRAM ADVISORY COMMITTEE (PAC) CEBAF

- **Function**

  Advise CEBAF Directorate on scientific directions and relative scientific priorities for the experimental program

- **Membership**

  J. Schiffer (Argonne), Chairman
  P. Barnes (Carnegie-Mellon)
  W. Bertozzi (MIT)
  T. W. Donnelly (MIT)
  R. Eisenstein (Illinois)
  J. Friar (LANL)
  S. Kowalski (MIT)
  R. McKeown (Caltech)
  E. Moniz (MIT)
  I. Sick (Basel)
  H. Thiessen (LANL)
  C. Williamson (MIT)
  S. Wojcicki (Stanford)

- **First Meeting**

  February 13-15, 1987

- **Report completed**

Fig. 6

SUBJECT AREAS FOR STEERING COMMITTEES — CEBAF

- o (e,e′ nucleon)
- o (e,e′K) and (e,eπ)
- o (e,e′ two nucleon)
- o (e,e′ multihadron)
- o p($\vec{e}$,e)p parity
- o few nucleon systems
- o (e,e′N*)
- o (e,e′X) deep inelastic transition to x scaling

Fig. 7

RESPONSE TO PAC REPORT — CEBAF

End Stations

Three independent structures, each adequately shielded

- o Halls A, B, and C
- o Provide maximum versatility within budget constraints
- o Leave Hall C open and establish "trust fund" for equipment
- o Entertain proposals at the October 1988 PAC to determine development of experimental equipment for Hall C

Fig. 8

RESPONSE TO PAC REPORT — CEBAF

Large Acceptance Spectrometer (LAS)

- Appoint Co-Program Managers
  - B. Mecking - CEBAF
  - Person to be named from physics community
  - Assign senior engineer
- Establish Technical Advisory Panel (TAP)
- LAS will go into Hall B, designed to take full beam intensity

Fig. 9

RESPONSE TO PAC REPORT — CEBAF

High Resolution Spectrometers

- Design Studies
  - Study design modification to accommodate extended targets with moderate resolution
  - Examine modifications required to accommodate polarized hydrogen and deuterium targets
  - Re-examine design with an eye to maximize the resolution in the missing mass at an electron energy of approximately 2 GeV
  - Take resulting resolution at 4 (6 GeV) consistent with quality of accelerator
  - If design modifications appear acceptable, appoint at TAP

Fig. 10

RESPONSE TO PAC REPORT — CEBAF

High Resolution Spectrometers (Cont'd)

- Appoint Co-Program Managers
  - Jean Mougey - CEBAF
  - Person to be named from physics community
  - Assign senior engineer

Fig. 11

RESPONSE TO PAC REPORT — CEBAF

Additional Steps

- Polarized Beam
- Parity Violation
  - Continue to develop design
  - Work to ensure accelerator development is consistent with a quality parity experiment
  - Actively encourage research and development on sources
- (e,e'K^+)
  - Hire scientific staff member to design an optimal spectrometer system
- Low Intensity Test Beam
  - Initiate change request to include a low-intensity test beam
- Data Acquisition
  - Examine projected laboratory manpower and hardware needs

Fig. 12

END STATION TASK FORCE — CEBAF

Membership

- H. Grunder (Chair)
  - P. Brindza
  - G. Doddy
  - O. Matherny
  - B. Mecking
  - J. O'Meara
  - J. Mougey
  - G. Stapelton
  - R. Whitney
  - R. York

Fig. 13

END STATION LAYOUT

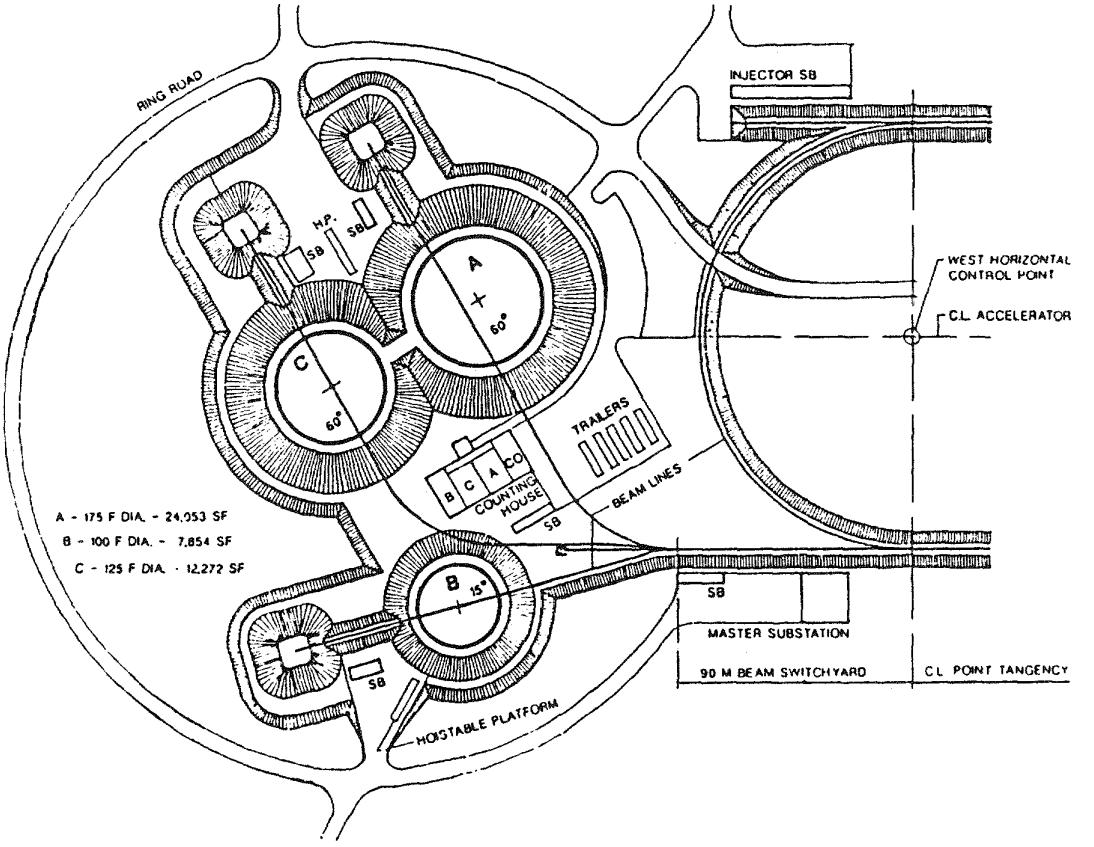

Fig. 14

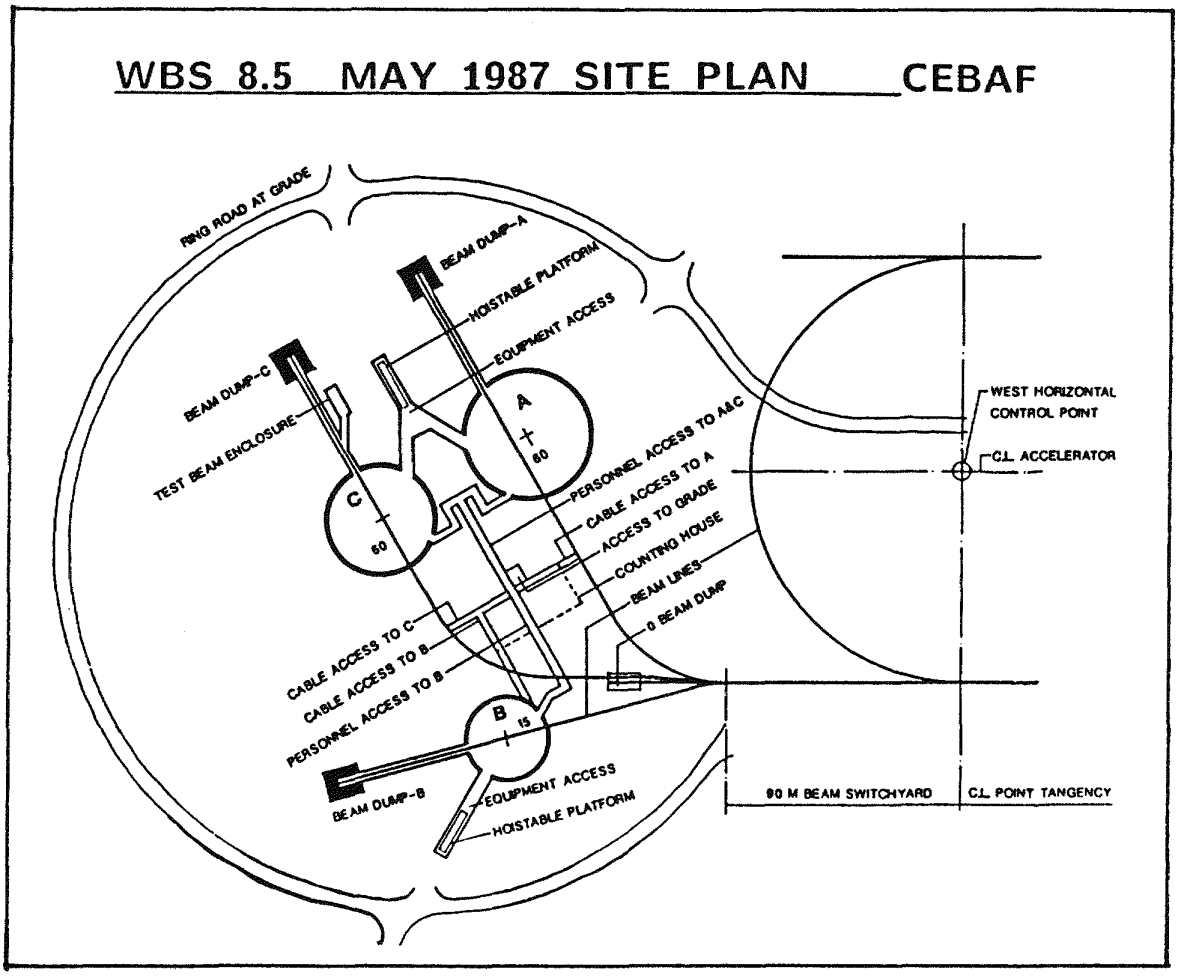

Fig. 15

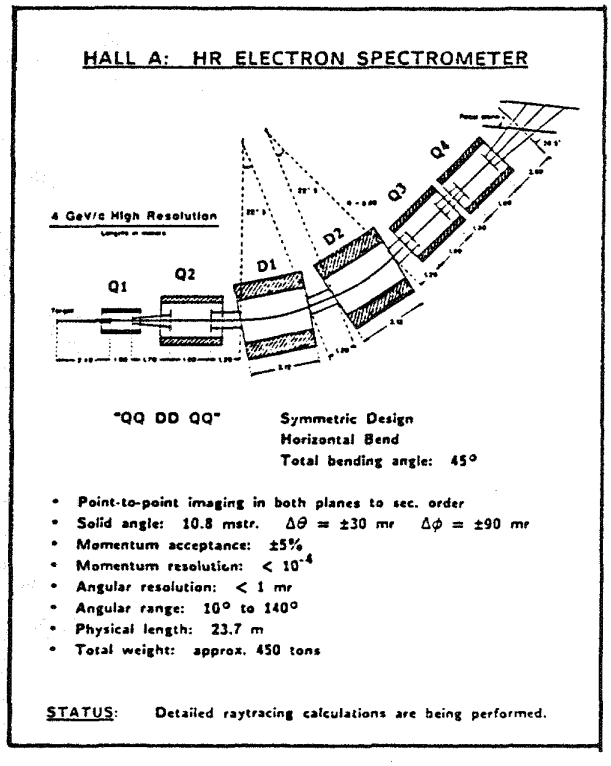

Fig. 16

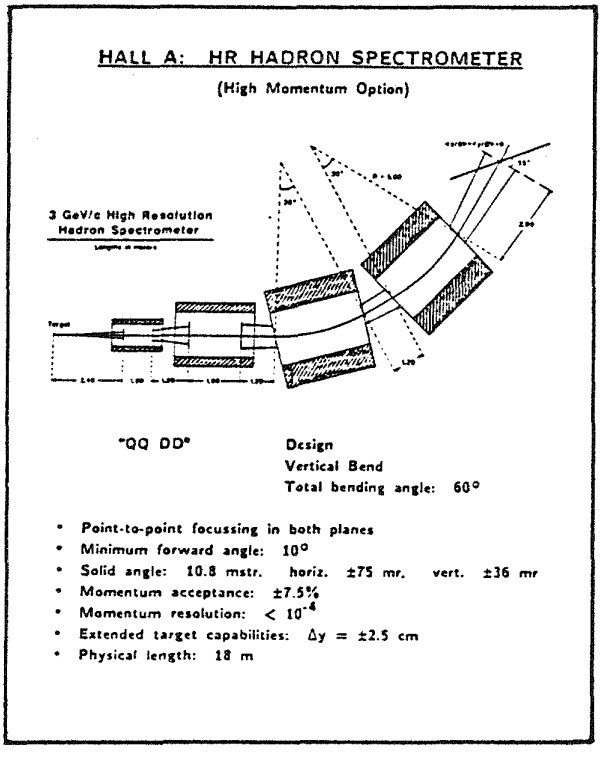

Fig. 17

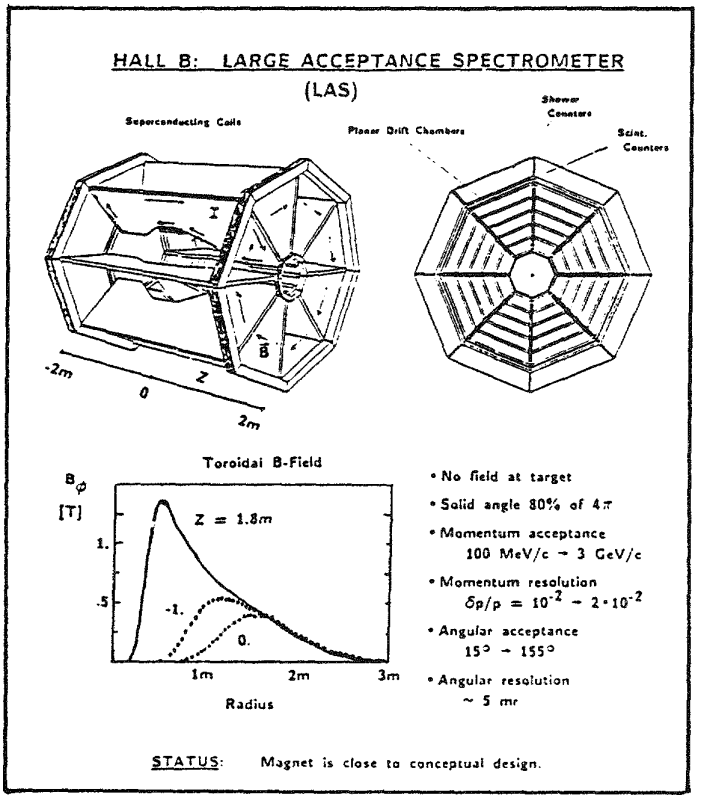

Fig. 18

SURA ACTIVITIES — CEBAF

Academic Appointments for CEBAF Scientists

Visits to SURA Universities 9/1/86 - 5/5/87

Duke University	University of Tennessee
George Washington University	Virginia Commonwealth
Georgia Tech	Virginia Tech
Hampton University	University of Virginia
University of Maryland	West Virginia University
University of North Carolina	College of William & Mary
North Carolina State	

Fig. 19

SURA ACTIVITIES — CEBAF

Graduate Education at CEBAF

- Continuing Electron Scattering Lectures
- Plan to offer graduate level courses
  - Graduate Quantum Mechanics 1987
  - Advanced Quantum Mechanics ⊕ Field Theory 1988
  - Nuclear and Particle Physics 1989

Fig. 20

Research Division — CEBAF

Staffing

- Associate Director for Research
  - National Search Committee
  - Offer out
  - Governor's Distinguished CEBAF Professor
- Head of Theory Group
  - National Search Committee
  - Offer out
  - Governor's Distinguished CEBAF Professor
- CEBAF Search Committees - Hires (FY 87)
  - A. Saha
  - S. Nanda
  - P. Dunn - Head of Detector Group
  - LAS - Offer
- CEBAF Search Committees - Positions (FY 88)
  - Staff Scientists (3)
  - Technical Support Personnel (2)
  - Postdocs (2)

Fig. 21

TAP MEMBERSHIP — CEBAF

John Peoples, Jr. (Chair)
Doug A. Bryman (TRIUMF)
John M. Cameron (U. of Alberta)
David G. Cassel (Cornell)
Martin D. Cooper (LANL)
Paul T. Debevec (U. of ILL)
Jay N. Marx (LBL)
Clyde Taylor (LBL)
Albert Ulbricht (ORNL)
Karl A. VanBibber (LLNL)
Jon Zbasnik (LBL)

Fig. 22

Continuous Electron Beam Accelerator Facility

12070 Jefferson Avenue
Newport News, Virginia 23606
804-875-7883

Attachment 1

Prof. John Dirk Walecka
Scientific Director

March 23, 1987

Dear Member of the CEBAF Users Group:

On February 13, 14, 15, 1987 the first meeting of the Program Advisory Committee (PAC) was held at CEBAF. It was held in conjunction with a Users meeting, and overall we had approximately 90 physicists participating. On the first day, the Steering Committees described in my previous two letters to you made their presentations on the potential physics programs at CEBAF. On Saturday morning, the CEBAF staff presented the best current efforts at equipment and end station designs. The general level of the presentations and discussion was high. It was a good meeting, and I was pleased with it. It is also a first-rate PAC, and I want to take this opportunity to thank the members for their contributions. Hermann Grunder and I were fortunate to be allowed to sit in as observers at the executive sessions, so we have a good feeling for the opinions expressed and the tone of the discussions.

On March 16, we received the final written report of the PAC. I am enclosing a copy with this letter. The most significant result is that the PAC has delineated a set of physics priorities which will guide our development of the laboratory. The PAC observed:

> "The overall physics program presented by the Steering Committees certainly does represent a broad program, spanning the nuclear physics interests in CEBAF."

and further

> "Indeed, the essential point is that in the opinion of the PAC, their presentations encompassed the CEBAF core program."

Hermann Grunder and I have discussed the PAC meeting and report. We have formulated a course of action which we feel is responsive and which we believe will lead to an outstanding physics program at CEBAF which is our common goal. I want to communicate the broad outline of that course of action to you in this letter so that you will be fully informed. The essential points are the following:

1) <u>End Stations</u>

Hermann decided he wanted to share in some of the fun, and he is actively participating in the design of the end stations. He chairs a working group which is meeting regularly with a goal of setting the physical dimensions and design criteria for the end stations. The plan is to have three independent structures, each adequately shielded. The end stations are referred to as halls A, B, and C. They will each be designed to provide maximum versatility within the overall budget constraints. We are confident that our goal of setting the physical requirements for the end stations by April, 1987 will be achieved.

2) Large Acceptance Spectrometer (LAS)

CEBAF will proceed with the construction of the LAS through the following series of steps:

i) Co-program managers will be appointed, one from CEBAF and one from the national nuclear physics community. Bernhard Mecking will be the program manager from CEBAF. A senior engineer will then be appointed for the LAS, and a charter written for just how the program will be managed. The program managers will be instructed to aggressively recruit from throughout the country active user participation in the construction and implementation of the LAS.

ii) An ad hoc Technical Advisory Panel (TAP) will be appointed by CEBAF, after consultation with the Board of Directors (BOD) of the CEBAF Users Group, to give the LAS the extensive review recommended in the PAC report. We anticipate completing this review before the Summer Workshop at the end of June.

iii) The LAS will go into hall B, which is being designed to take full beam intensity.

3) Magnetic Spectrometers

CEBAF will start from the current designs for the 4(6) GeV electron spectrometer and the 3 GeV hadron spectrometer and do the following:

i) Design modification to accommodate extended targets with moderate resolution will be studied to see if one can accomplish a significant fraction of the top-priority few nucleon studies with this system. Modifications required to accommodate polarized hydrogen and deuterium targets will also be examined.

ii) The design will be re-examined with an eye to maximizing the resolution in the missing mass at an electron energy of approximately 2 GeV. One will then take what resolution one can get with this system at 4 GeV, consistent with the overall quality of the resolution of the accelerator itself. The electron spectrometer will be designed so that it can be upgraded to 6 GeV, should the need arise.

iii) Co-program managers will be appointed for the magnetic spectrometer program at CEBAF, one from CEBAF and one from the national nuclear physics community. Jean Mougey will be the CEBAF program manager. A senior engineer will then be appointed for the program, and a charter written to define how the program will be managed. The program managers will be instructed to aggressively recruit from throughout the country active user participation in the construction and implementation of this project.

iv) If the design modifications discussed in i) and ii) appear acceptable, CEBAF will proceed to appoint a TAP for this magnetic spectrometer project just as discussed in LAS ii). If things go well, we anticipate convening the TAP for this project before the next PAC meeting on October 8-10, 1987.

v) These magnetic spectrometers will go in hall A.

4) End Station C

CEBAF will keep end station C open for the time being with the following intent:

i) A "trust fund" of approximately $5M in equipment money will be set aside for this end station

ii) Proposals will be solicited from the national users community. Procedures will be developed through discussions with your BOD.

iii) Proposals will be heard by the PAC at its meeting a year from this October, that is in October, 1988. The PAC, relying on its delineation of the physics priorities for CEBAF, will at that time provide advice on how to proceed with developing experimental equipment for hall C.

5) Additional Steps

CEBAF will take the following additional steps to implement the advice of the PAC:

i) The design of the parity experiment will continue to be developed by the CEBAF staff, with the participation of the users community. The CEBAF staff will work to see that the accelerator development is consistent with a quality parity experiment. Research and development on sources with improved polarization will be actively encouraged.

ii) A scientific staff member will be hired at CEBAF and instructed to design an optimal spectrometer system for studying the $(e,e'K^+)$ reaction. One component of this clearly involves the design of an innovative, short, high-resolution kaon spectrometer.

iii) A change request will be submitted to include a low-intensity test beam at CEBAF.

iv) CEBAF will examine in depth its data acquisition goals. This includes an examination of the projected laboratory manpower and hardware needed to effectively serve the data acquisition function.

Finally, I would just like to conclude with the observation that CEBAF is now on the move. We have a projected physics program and we are going to take steps to implement that program. CEBAF is a reality, and it is your laboratory. It is time for you to get aboard if you want to participate in the physics program when it is ready to run.

I will be in touch.

Sincerely yours,

John Dirk Walecka
Scientific Director of CEBAF

cc: H. Grunder

ARGONNE NATIONAL LABORATORY
9700 South Cass Avenue, Argonne, Illinois 60439

(312) 972-4066
BITNET address: SCHIFFER at ANLPHY

SCIENTIFIC
DIRECTOR'S OFFICE

March 16, 1987

MAR 18 1987

CEBAF

Professor John Dirk Walecka
Scientific Director, CEBAF
12070 Jefferson Avenue
Newport News, Virginia 23606

Dear Dirk,

Enclosed is the final-final version of our report that I sent you by BITNET on Saturday.

Best regards,

John P. Schiffer

JPS/bw

Encl:

cc: H. Grunder

REPORT OF THE PROGRAM ADVISORY COMMITTEE FOR CEBAF

March, 1987

The first meeting of the Program Advisory Committee for CEBAF took place February 13 through 15, 1987. On the first day the Committee heard presentations on elements of the proposed research program from the eight 'Steering Committee'-s, then, on the second day, plans for the experimental system were presented.

The charge to the PAC was as follows:

The CEBAF PAC is established to provide advice and guidance to the CEBAF Directorate on scientific directions and relative scientific priorities for the experimental program.

Specific Issues for the initial PAC are as follows:

1. The PAC should examine the overall physics program as presented to it by the Steering Committees and advise on what, if anything, is missing or underemphasized by the proposed program.

2. The PAC should evaluate the spectrometer designs, including the end station civil construction layout, presented by the CEBAF staff; specifically it should evaluate the designs for the:

   a. Electron and hadron spectrometers for End Station A
   b. Electron and hadron spectrometers for End Station C
   c. Large acceptance spectrometer for End Station B

3. In the context of the physics program presented by the Committees, and the spectrometer designs, the PAC should recommend relative priorities among the major components of the research program at CEBAF.

4. The PAC should provide advice on the optimum level of involvement by user groups in the design and construction of the experimental equipment for CEBAF. The PAC should also suggest mechanisms for achieving that optimum level of involvement.

1. THE OVERALL PHYSICS PROGRAM

CEBAF is intended to address central issues of nuclear physics, ones where the level of current knowledge is either lacking or in a very qualitative and unsatisfactory stage. In particular CEBAF is directed at questions involving non-nucleonic degrees of freedom in nuclei and the duality between hadronic and quark-gluon descriptions of nuclear structure and

interactions. Its high energy resolution, high beam current, and continuous beams make it an ideal instrument for the program of measurements, many of them requiring time coincidence between detected particles, that have been envisioned by the nuclear physics community over the past decade. The overall physics program presented by the Steering Committees certainly does represent a broad program, spanning the nuclear physics interests in CEBAF.

The central question asked of this first PAC meeting requested advice on establishing a set of scientific priorities among the various classes of experimental programs anticipated at CEBAF and thereby helping develop a plan for the commitment of resources to specific spectrometer designs. The PAC is very enthusiastic about the possible set of measurements on the form factors of elementary systems and feels that this class of measurements must be accommodated from the beginning of the program. The areas of hypernuclear spectroscopy, of coincidence studies [i.e., (e,e'N) (e,e'NN), etc.] and of baryon resonance and meson production were also found to be very attractive and of central importance to the CEBAF program. The capabilities must be provided for all of these programs as early as possible within budgetary and manpower constraints. The electroweak program is potentially of great significance and should be explored further, but the PAC does not feel that a commitment to proceed with this program is called for at this time. We stress the obvious point that the present statements regarding priorities are not intended to fix the experimental program indefinitely, or to narrow options for future proposals. Priorities will have to be the subject of periodic review over the coming years.

A set of reasonable spectrometer baseline designs was presented. It is not anticipated that the entire complement of instruments discussed can (or should) be built with the initial equipment budget. Consequently, the priorities should be viewed as guides to the iterative process of advancing and modifying the baseline designs in a manner consistent with our best estimate of the equipment needs projected at the commencement of the research program in 1993.

2. SPECTROMETERS AND OTHER FACILITIES

It is, of course, difficult for a group such as the PAC to offer a detailed evaluation of spectrometer plans presented in one hour talks. As far

as could be judged from the presentations and the discussions, careful work has gone into these designs and they represent a baseline starting point for more detailed final planning. The size of the target halls appears to be adequate.

a. The Electron and Hadron Spectrometers for End Stations A and C.

The PAC sees the designs of the spectrometers for a high resolution program as a reasonable basis for more detailed planning. A priority judgment on the spectrometers must consider not only the technical designs, but how the parameters of the devices match the needs of the experimental program, a question that is particularly acute since it seems unlikely that all the spectrometers discussed can be built in the first go-around. It would be useful to have more thought given to the question of how to adjust the designs in such a way as to develop a subset of spectrometers, perhaps with somewhat modified design goals, that could address a majority of the physics program. Clearly a spectrometer that can utilize the high resolution of CEBAF needs to be built early. Also, the highest priority experiments require an electron spectrometer that could accept 4 (6) GeV/c with a matching hadron spectrometer, both with large solid angles, capable of viewing extended targets (> 20 cm), though for these measurements requiring modest (10^{-3}) resolution. It would be desirable to determine whether the proposed high-resolution spectrometers could be adapted through reconfiguration or some design modification to serve these ends. Also, though some spectrometers must be built to utilize the unique high-resolution features of the CEBAF beam, the physics implications of the possibility that the initial high-resolution spectrometers might accept less than the full beam momentum should be assessed.

It is the recommendation of the PAC that the designs be examined in order to develop options for the initial set of spectrometers for CEBAF, to accommodate as many of the high-priority programs as possible.

b. The Large Acceptance Spectrometer.

The LAS design, if it can meet its stated goals, could provide the basis of a large part of the CEBAF experimental program. In addition to high-multiplicity reactions, the detector could provide an effective alternative to

other spectrometer designs for much of the proposed (e,e'N) and (e,e'2N) work. However, optimization of the design must be examined critically by a group of technically experienced physicists, from every perspective, the magnets, detectors, backgrounds, counting rates, requirements on tracking of particles, the software needs, with particular attention to the feasibility of extracting complex information from the recorded data expeditiously, and the manpower requirements needed for bringing such a system together to be ready in time for the first CEBAF beams. It is the recommendation of the PAC that a rigorous technical and cost review take place in order to examine the feasibility of achieving high luminosity and versatility for supporting a broad spectrum of potential experiments with a variety of users and to insure that the design is optimized for maximum physics output.

c. Polarized Electrons.

The PAC feels that the need for a polarized electron source exists independent of the demands of the parity experiment. We recommend that CEBAF undertake a plan to begin such development as soon as is practical, and that a polarized electron beam be one of the initial objectives of CEBAF. The development of a source with higher polarization might be undertaken collaboratively with another laboratory.

d. Other Matters.

During the course of our meetings we also heard presentations concerning the development of other aspects of the facility. Since several of these items will have direct relevance to the experimental program, we discuss the PAC's reaction to current plans.

The development of first-rate data acquisition and computing capabilities is crucial for a successful CEBAF experimental system. A serious effort in this direction should be started reasonably soon and can be usefully reviewed by the PAC from time to time.

A number of experiments would require or would benefit from out-of-plane measurements. In the original design for Hall C a placement of detectors (VAS spectrometers, neutron detectors, or polarimeters) out of the scattering plane defined by the electron spectrometer, can be envisioned. In Hall A, with the original design, movement of the beam to two discrete angles out of the

spectrometer plane looks more realistic, but requires further study. In particular, the radiation problems caused by electrons that have lost energy in the target and cannot be bent back into the beamstop also needs investigation.

The PAC felt that the question of neutron detection in Area C has not been addressed adequately; this is urgent only in that the implications of this capability on the layout of the experimental halls needs to be assessed very soon.

The possibility of providing a test beam should be investigated.

3. PRIORITIES.

Any assessment of scientific priorities six years in advance is difficult and detailed judgments are subject to large uncertainties that can be resolved only after the fact, in the face of specific proposals for experiments. In assessing priorities the PAC judged that the capability for measurements on elementary form factors should be accommodated in the first capabilities available at CEBAF. A number of other components of the program were also thought to be very attractive and the design for the initial complement of experimental spectrometers must be reviewed with a view towards accommodating as many of these as possible. While in the following the programs are listed in the order in which the PAC regarded their priorities, the differences between adjacent programs are often represented by a single vote, and the ordering should not be regarded as firm or immutable. Indeed, the essential point is that in the opinion of the PAC, the presentations encompassed the CEBAF core program.

a.) Form Factors in Simple Systems

The measurement of the form factors of elementary systems -- neutron and proton charge form factors, C_0/C_2 form factors of the deuteron, nucleon spin structure functions, and deuteron electro-disintegration -- will provide fundamental information on observables that have been the subject of interest for a long time and that are essential for the quantitative pursuit of the scientific goals of nuclear physics, in particular the central goal of understanding nuclei in terms of the underlying quark-gluon degrees of freedom. The requirements of these experiments are well matched to the capabilities of CEBAF.

Many of these measurements require an electron spectrometer with large solid angle, medium resolution (10 MeV) and the capability to work with long targets (> 20 cm). Some would profit from the highest energy (6 GeV). Most of the experiments need (or would profit from) polarized electrons. We therefore recommend that a polarized electron beam be one of the initial objectives of CEBAF. Most of the experiments need polarized targets or recoil detectors, development projects that may be well suited to the capabilities of the user community.

b.) Hypernuclear Physics

The committee sees high-resolution studies of hypernuclear spectroscopy as a unique contribution that CEBAF can make. The very gross outlines of hypernuclear structure have been delineated over the past two decades through the study of the (K^-,π^-) reaction, requiring long runs and yielding very limited statistics and resolution. CEBAF holds the potential of providing a new window to observe this added dimension in nuclear symmetries and structure. Determination of the effective N-Λ interaction and its relation to the NN force will test our models of the baryon-baryon interaction. The committee was concerned about the low event rates discussed, perhaps because less than optimal instruments were assumed and a very far from favorable case was picked for the prototype calculation of rates. The program is worth carrying out only if it can be done well. The PAC recommends that further study be made of the advantages of a 0° electron tag spectrometer with a kaon spectrometer of as short a length and as large a solid angle as possible, consistent with the requisite resolution. Other configurations with smaller angles between the electron and the kaon should also be explored; it seems entirely possible that more carefully tailored spectrometers for the relatively low momentum electrons and kaons (where a short spectrometer would be very desirable) should be explored. A scenario including modest, dedicated spectrometers optimized for these studies should be investigated. Use of auxiliary tags (using for example nonmesonic lambda decay) which will remove the quasifree production contribution to the hypernucleus excitation spectrum should be explored.

c.) The (e,e'2N) and Other Multihadron Reactions

The (e,e'2N) reaction may provide crucial information about the nature of 2-nucleon correlations in nuclear matter. Both the (e,e'2p) reaction and the (e,e'pn) reaction should be studied; the latter, while much more difficult, will provide essential information about reactions proceeding through the quasi-deuteron mechanism. Study of a larger kinematic region will be essential in order to separate clearly two nucleons emerging because of correlations from two nucleons that are produced through the formation of an intermediate delta resonance. The possibility of studying such outgoing channels as π-N, π-π-N, K-Λ, etc., using both real and virtual photons of CEBAF energies, is an important component of the CEBAF program. It is clear that these studies can be adequately done with energy resolutions on the order of 10 MeV (to separate the major shells). Therefore, only moderate resolution spectrometers will be required; perhaps it will be possible to do the (e,e'2p) reaction using the LAS detector if the luminosity it can accept can be increased. It is also important that CEBAF develop good neutron detection capability; the (e,e'pn) reaction provides a motivation for this development.

d.) The (e,e'p) Reaction

The single nucleon reaction has proven to be a powerful tool, providing a benchmark for studies of nuclear structure. It has elaborated the quantitative aspects of the validity of our understanding of the structure of nuclei in terms of single-particle motion in a nuclear mean field. Much remains to be done with 100% duty-factor facilities. Nucleon degrees of freedom prevail below 800 MeV/c insofar as the q-dependence of the quasielastic (e,e'p) knockout predictions is preserved. On the other hand, it is suggestive from the transverse/longitudinal separations that other currents are present for the deeply bound nucleons. CEBAF is poised to extend this work to much higher momentum transfers and an enormous dynamical range will become available for study with cross-section sensitivity that is more than three orders of magnitude larger than our present knowledge. With the high duty-factor and high quality beams from CEBAF, another level of spatial resolution and sensitivity will be reached that could dramatically alter our understanding of the hadronic degrees of freedom, and the hadronic structure essential to nuclear physics.

e.) Parity

The goal of this experiment is a test of the Standard Model resulting from measuring $\sin^2(\theta_W)$ to 1% accuracy at low q^2. Combined with the anticipated high precision results at high q^2 from SLC and LEP, this would constitute an important test of the Standard Model at the level of radiative corrections and thus possibly be sensitive to new physics (e.g. additional Z_0's). A complete set of measurements with H and D targets permit separation of the neutral current structure functions F_1, F_2, F_A at low q^2. The PAC is concerned both about the physics impact of the experiment given the possibility of other low-q^2 measurements (e.g., the proposed LCD experiment) and about the enormous facility impact the experiment could have on the CEBAF program. We think it likely that this will not be a "first generation" CEBAF experiment; in any case, a commitment to this experiment can wait for 2-3 years without substantially delaying it. However, steps should be taken now in order to insure that the capability for making such measurements exists at CEBAF; important areas include accelerator and beamline diagnostic instrumentation and polarization monitoring to very high precision. Further, the possibilities for a polarized electron source with very high polarization should be explored; such a development would greatly reduce the facility impact of this, and of many other experiments requiring polarized beams.

f.) Nucleon Resonances and Meson Production

The PAC sees a strong potential at CEBAF for an important program of electroproduction from the nucleon that must form the basis of any understanding of the behavior of resonances and mesons in the nucleus. Interest in studying the q^2 dependence of resonance multipole amplitudes is driven by developments of quark model dynamics. These experiments appear well suited to CEBAF, given the development of polarized beams and polarized targets in addition to spectrometers similar to the ones discussed above. The PAC sees strong interest in a study of the higher resonance region, where CEBAF will provide a capability far more powerful than those previously available but a more quantitative evaluation of the precision achievable for the multipole amplitudes should be developed. The LAS will play an important role in these studies. The elementary amplitudes for K^+,η,η' production can be measured well at CEBAF. The mechanism of strangeness production, including

the role of the spin variables, is a problem of considerable interest, and electromagnetic hyperon production has been studied only very poorly.

g.) Deep-Inelastic Scattering

The scaling phenomena observed in high-energy inelastic electron scattering have played a central role in revealing the parton structure of matter, in determining modified quark distributions in nuclei, and more recently in providing a new approach to the nucleon momentum distribution in nuclei. The goal of coincidence studies in these same kinematic regimes is in understanding of how different hadronic channels conspire to produce the scaling phenomenon. The PAC feels that more theoretical work is needed in this area, and that the design of the experimental system will be able to accommodate the measurements that are presently foreseen.

4. USERS

The active involvement of the experimental community in the planning and implementation of the CEBAF experimental system is essential. It is entirely appropriate that this issue is treated very seriously even at this early stage in the facility's development. The PAC recommends that CEBAF should solicit help from users. CEBAF is a unique major facility for all of nuclear physics, and it is particularly important that the active participation of strong experimental groups be sought, with special attention devoted to attracting those who have not previously concentrated on research at electron accelerators.

It appears that the designs for spectrometers have evolved to the point where more manpower would be beneficial. A reasonable course of action would be to actively solicit user collaborators (and user co-spokespersons where practical) for various aspects of these projects in the near future. A possible model is the MEGA collaboration at LAMPF, a large collaboration which is managed from LAMPF by the spokesman, with assistance from the Director of LAMPF. Commitments and progress by all collaborators are carefully monitored and frequent collaboration meetings are held. Within some similar scheme, appropriate spokespersons who were CEBAF physicists could be appointed and begin soliciting collaborators from the user community. Specific groups with appropriate skills could be approached not with generalities but with a well

thought-out scheme of options whereby these groups could contribute their effort. While the need for this is urgent it is also important that the user groups feel that they have real tasks to do and not just be participating in pro-forma symbolic activities. If these collaborations could begin working soon, substantial progress could take place before further reviews come up. It would be a good sign if such activities were well underway when the PAC meets again.

Continuous Electron Beam Accelerator Facility

12070 Jefferson Avenue
Newport News, Virginia 23606
804-875-7883

Attachment 3

Prof. John Dirk Walecka
Scientific Director

July 14, 1987

TO: Technical Advisory Panel

FROM: Dirk Walecka
Scientific Director
CEBAF

SUBJECT: Technical Advisory Panel (TAP) for the Large Acceptance Spectrometer (LAS)

Dear Panel Member:

Thank you for agreeing to serve on CEBAF's Technical Advisory Panel for the Large Acceptance Spectrometer. John Peoples (Fermilab) has agreed to chair the panel, and a list of the membership is attached. We feel this is a first-rate panel and we look forward to having you here at CEBAF and benefiting from your experience and advice.

Co-Program Managers have been named for the LAS. One is from CEBAF, the other from the CEBAF Users Community.

CEBAF Program Manager	B. Mecking
USERS Program Manager	R. McKeown (Cal Tech)

Dena Polyhronakis has administrative responsibility for the TAP at CEBAF, please feel free to contact her (804 875-8910 or bitnet address POLYHRONAKIS@CEBAFVAX) regarding this panel.

I have prepared an outline of the proposed method of operation of the TAP as well as a list of the issues we would like the TAP to address:

MEETINGS

It is proposed that the TAP meet in (at least) two stages:

Stage I	August, 1987
Stage II	Summer, 1988

CHARGE

To provide technical advice to the CEBAF directorate on the design, construction, cost, schedule, and implementation of the LAS.

GOAL OF STAGE I

First-stage approval of the conceptual design of the LAS by the second PAC meeting (PAC2) on October 8-10, 1987.

PROPOSED TAP ISSUES

STAGE	ITEM
I	1) Critique Design
I	2) Technical Feasibility?
I	3) Has Anything Been Missed? o Design o Instrumentation o Data Acquisition o High Energy Experience
I	4) Alternate Designs?
I	5) Maximum Luminosity?
I and II	6) Cost?
I and II	7) Schedule?
I and II	8) Manpower Requirements?

USER PARTICIPATION

Some of the questions which must be answered regarding the user participation in the LAS are the following:

1) Design

- Are the users satisfied that the device will allow them to do the physics that they want to do?
- Review of design at Summer Workshop and by users' collaboration

2) Technical, Hardware Aspects (Component Participation)

- Drift chambers
- Scintillation counters
- Shower counters
- Bremsstrahlung tagging
- Neutron counters
- Polarized targets

3) Software Aspects (Component Participation)

- Data acquisition system (both software and hardware)
- Track reconstruction
- Acceptance determination
- Efficiency determination

4) Practical Aspects of User's Collaboration

- Rules of the Game?
- User input in fabrication?
- Experimental use of LAS?
  - Preferred treatment?
  - Commissioning phase?
  - Demonstration of technical competence?
- Funding?
- Charter?
- Principle: Collaboration recommends to CEBAF management

CHARTER

In order to write a charge for the collaboration, and to establish clear lines of responsibility, we are using as a model the Cover Agreement for the Collider Detector (CD0) at Fermilab. This was provided to us by Phil McGee, who helped write it. Although our collaboration will be on a smaller scale, the problems will be quite similar.

Again, let me thank you for your willingness to serve on this Panel. A packet of briefing material will be sent to you during the next week to give you some background information. I look forward to seeing you August 10-11, 1987.

Best regards,

John Dirk Walecka

J. Dirk Walecka

cc: H. Grunder
R. McKeown (Cal Tech)
B. Mecking
D. Polyhronakis

Coincidence Measurements from Nuclei

William Bertozzi and Robert W. Lourie
Department of Physics and Laboratory for Nuclear Science
Massachusetts Institute of Technology
Cambridge, MA 02139 USA

and

John M. Finn
Department of Physics
The College of William and Mary
Williamsburg, VA 23185 USA

I. Introduction

Our motivation for pursuing inclusive electron scattering and coincidence measurements with electrons has several origins. One goal is to elaborate on our accepted view of the nucleus as a mean field system of neutrons and protons and to explore more complex details about standard nuclear structure. Another goal is to learn more about degrees of freedom that we cannot include via the nucleonic coordinates of the mean field. Finally, part of our motivation is provided by anomalies in experimental data not explained by our mean field picture and we shall review some of these as part of this discussion.

The electromagnetic interaction is our premier probe of nuclear currents and thus nuclear structure. This follows because it is relatively weak and can be treated in first order perturbation theory. These characteristics have enabled (e,e′) and (e,e′p) reactions to make very valuable contributions to our knowledge about nuclei and it is worthwhile to review some of these.

1) Ground state charge and magnetization densities have been determined for many nuclei. These densities are very precise and provide unique bench marks for fundamental theories of the few-body systems and more complex nuclei.

2) In nuclei with N=Z and for $\Delta T=0$ transitions, the transition charge densities from (e,e′) are also interpretable as neutron densities since the nuclear force is charge symmetric and charge independent.

3) Quasielastic (e,e′) provides our best and most accurate information that nuclei are mostly composed of neutrons and protons. It also provides us with some of our most interesting puzzles.

4) Nonnucleonic currents have been definitely observed in the threshold electrodisintegration of the deuteron [1] and in elastic magnetic scattering from ^{3}He [2] and ^{3}H. [3] We understand much of this phenomenology in terms of meson exchange currents.

5) The (e,e′p) coincidence reaction has established the basic validity of the shell-model or mean field view of the nucleus. This follows from observation of explicit single particle orbits even those that are deeply bound — such as the s-shell protons in ^{16}O. [4] This is in striking contrast to the results from stripping, pick-up and other hadronically induced reactions where only the surface character of the nucleus is studied and only the valence nucleon orbitals are accessible. The (e,e′p) reaction has a hadron in the final state. Our interpretations are based primarily on the physical premise that the reaction is representable to a good approximation by expressions of the form σ(e,e′p)= $K\sigma_{ep}S(\vec{p_i},\epsilon_m)$, where K is a kinematic factor, σ_{ep} is the elementary or free electron-proton cross section and $S(\vec{p_i},\epsilon_m)$, the spectral function, gives the distribution of the struck proton in terms of its initial momentum and energy respectively. For the independent particle shell model we have :

$$S(\vec{p_i},\epsilon_m) = \sum_\alpha |\Phi_\alpha(\vec{p_i})|^2 \delta(\epsilon_m - \epsilon_\alpha) \quad ,$$

where $\Phi_\alpha(\vec{p_i})$ is the momentum space wavefunction and the sum is over all occupied orbitals whose quantum numbers are denoted by $\alpha = (n,\ell,j,\ldots)$

From these contributions as well as other reactions, we have come to see that our central view of the nucleus as a shell model or mean field problem has served us well but is roughly only one-half of the story. Our main evidence comes from rather universal observations of quenched single-particle occupations and transition strengths.

1) From the ground state charge distribution of ^{208}Pb we have known for some time that only 60% of the $3s_{1/2}$ orbit appeared to be occupied. Recent detailed studies [5] show that the difference of the ground state charge densities in ^{206}Pb and ^{205}Th exhibits the $3s_{1/2}$ shape but with only 60% occupation.

2) Stretched Mλ transitions are universally at the 50% level. An example of these transitions is given by the excitation of the 4^- states in ^{16}O [6] formed by coupling a $d_{5/2}$ particle and a $p_{3/2}$ hole. The high angular momentum of these states is otherwise difficult to form except by excitations at considerably higher energy so they are considered to be good single particle excitations. Such transitions indicate that only 50% of the ground state is represented by our fully occupied $(1s_{1/2})^4(1p_{3/2})^8(1p_{1/2})^4$ mean field configuration.

3) From other reactions such as β-decay and mainly (p,n) charge exchange we also learn that 65% of the Gamow-Teller sum is observed. [7] This could also be a problem of ground state occupations although interesting conjectures about Δ-hole configurations have been invoked. [8]

We generally accept that the solution to our occupation problem lies in the need for more complex configurations. That is, our nuclei are not only Hartree-Fock or shell model ground states, but they also include a large contribution from multiparticle-multihole configurations. This, of course, ties us to the old term two-body correlations and also to the old concepts of multiparticle clustering etc. The important thing to recognize is that about one-half of the nuclear ground state involves these configurations in addition to those of the zero-temperature independent particle shell model. Important concepts include surface excitations, pairing, tensor force correlations and others. In addition to these structure problems associated with our zeroth order view of the nucleus we have encountered problems with the (e,e′) reaction mechanism and with effective hadronic interactions. We have encountered them in (e,e′p) studies, in studies of the quasifree reaction regions in (e,e′) and in our synthesis of (p,p′) and (e,e′) reactions. For now we simply list some of these situations and return to them in more detail in our later discussions.

1) Anomalous behavior of the transverse/longitudinal ratio of the response functions from quasielastic (e,e′).

2) Anomalies in quasifree Δ excitation.

3) Excess yield in the dip rigion between the quasielastic peak and the quasifree Δ excitation.

4) The local-density-approximation (LDA) representation of nucleon-nucleus interactions versus the Dirac phenomenology.

Finally, before turning to our discussion of recent coincidence experiments, let us review the generic figure (fig. 1) we all use to describe the (e,e′) process. We see the peaks referred to above describing the quasielastic (e,N) scattering and the quasifree Δ excitation, the dip region and scattering to discrete states of the nucleus. Along the vertical solid line we show the momentum transfers of most of the experiments we discuss. These vertical lines establish the kinematics of the (e,e′) process associated with any (e,e′p) study.

Specifically, we write for the energy transfer, ω, at the quasielastic peak:

$$\omega = \frac{\vec{q}^{\,2}}{2m} + \epsilon$$

where $\vec{q}^{\,2}$ is the square of the momentum transfer and non-relativistically ϵ is an energy derived from the momentum dependence of the effective nucleon-nucleus interaction while relativistically it is related to the nucleon effective mass m^*. For Δ excitation, ϵ includes the excitation energy of the nucleon $\sim$ 340 MeV. In the case of the (e,e′p) reaction, the kinematics of the problem are established in a similar manner but include the quantities $\vec{p_i}$ and ϵ_m, which are respectively the initial momentum of the struck proton and the eigenenergy of the proton referred to zero at large separation distance:

$$\omega = \frac{(\vec{p_i} + \vec{q})^2}{2m} + \frac{\vec{p_i}^{\,2}}{2M_{A-1}} + \epsilon_m.$$

We have used the non-relativistic expression for kinetic energy but the qeneralization to the relativistic expression is straightforward. In this quasifree model, the final proton momentum $\vec{p_f} = \vec{p_i} + \vec{q}$ and, along with $\vec{q}$, determines the initial momentum. The eigenenergy of the proton, ϵ_m, is then determined by ω. We

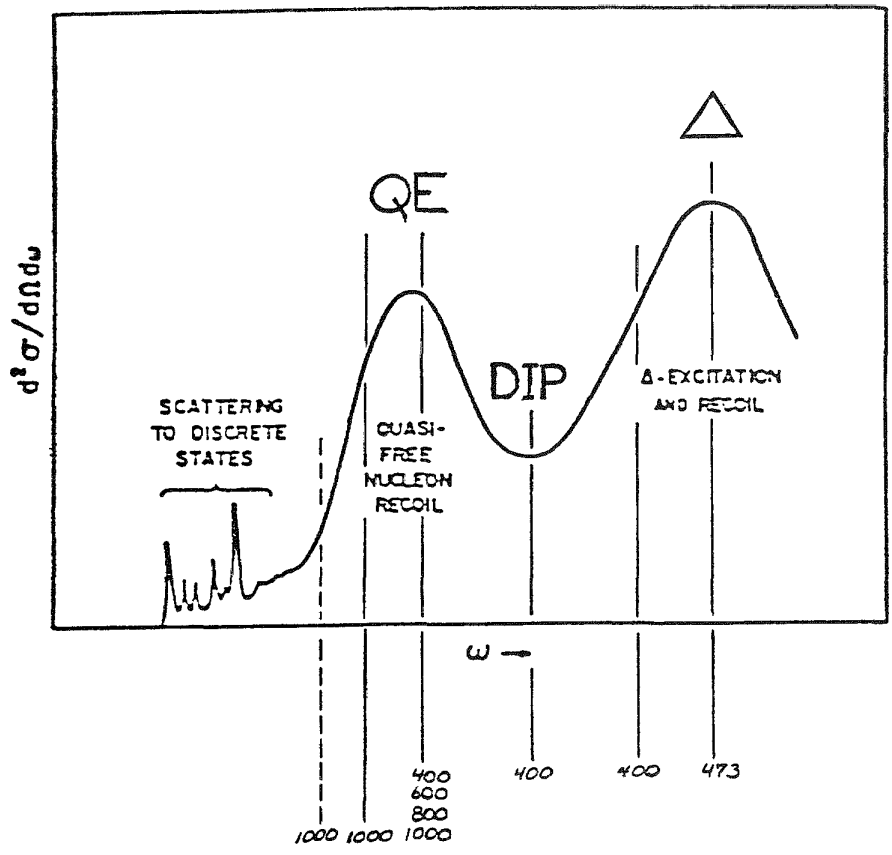

Figure 1. Generic (e,e′) cross section illustrating the relevant kinematic regions. The solid lines indicate the momentum transfers of specific experiments to be discussed.

also speak of ϵ_m as the missing energy since it is given by (neglecting the small recoil term):

$$\epsilon_m = \omega - T_p = \omega - \frac{(\vec{p_i} + \vec{q})^2}{2m}$$

Notice also that in this simple model the quasielastic peak appears at $\vec{p_i} = 0$, and, although a relation between ϵ from (e,e′) and the various ϵ_m from (e,e′p) can be established empirically within any set of assumptions, the connection between these parameters is rather vague. A more detailed model is required to interpret (e,e′p) data than is required to interpret (e,e′) data, and this feature shows up right at the start when we introduce the kinematic definitions for the reactions. This is only natural since we are not integrating over kinematic quantities in (e,e′p), rather, they are explicitly part of our measurements.

II. High Resolution (e,e'p) Results

The work at NIKHEF has the highest resolution and is illustrative of the concepts developed by the pioneering work of Jacob and Maris [9] and by the experimentalists at Frascati [10] and at Saclay. [11] In Figures 2 and 3 we show missing energy spectra and momentum distributions respectively, measured at NIKHEF in the ^{12}C(e,e'p)^{11}B reaction. In these figures, $\vec{p}_m$ is the same as our $\vec{p}_i$ and E_x is the excitation energy of ^{11}B and is related to ϵ_m by adding the separation energy of a proton. The first feature of note is the resolution. At this laboratory they routinely achieve resolutions of 100 KeV in E_x and this allows them to isolate states at high excitation energies such as the $\frac{1}{2}^+$ state at 9.87 MeV. [12] Before this work, resolutions were about 1 MeV. The distributions of intensity versus $|\vec{p}_m|$ for the states of E_x = 0, 2.12 and 5.02 MeV all have an $\ell = 1$ parentage with almost identical distributions up to $|\vec{p}_m| > 200$ MeV/c. Therefore, they share a common $\ell = 1$ orbital, the 1p-hole state, and we see its distribution in E_x. This nucleus is a classic case for intermediate coupling and in the impulse approximation we are learning about the $1p_{3/2}$ and $1p_{1/2}$ parentage of the ground state of ^{12}C and we are learning about this parentage at distances less than 1 fm.

The positive parity states at 6.79, 7.29, 7.98 and 9.87 MeV ($J^\pi = \frac{1}{2}^+, \frac{5}{2}^+, \frac{3}{2}^+$ and $\frac{1}{2}^+$ respectively) have a special significance as they require the existence of configurations of positive parity in the ground state. The $(2s)^2$ and $(1d)^2$ terms are obvious contributors. The distributions of intensity for the $\frac{1}{2}^+$ states with respect to $\vec{p}_m$ are maximal at $|\vec{p}_m| = 0$ indicating $\ell = 0$ but the absence of a minimum means that the 1s must also be important. The momentum distributions of the $\frac{3}{2}^+$ and $\frac{5}{2}^+$ states exhibit a minimum, indicating the presence of 1d components. In the impulse approximation, these excitations lead us to the two-particle-two-hole parentage in the ^{12}C ground state. These configurations arise from the longer range part of two-body correlations and perhaps more complex correlations as well.

One may argue that short range correlations, because of the curvature of the wavefunction, will result in, for the most part, continuum excitations of ^{11}B and thus two nucleon (or more) emission. Nevertheless, low-lying 2p-2h states must be part of the story and indeed are an important part.

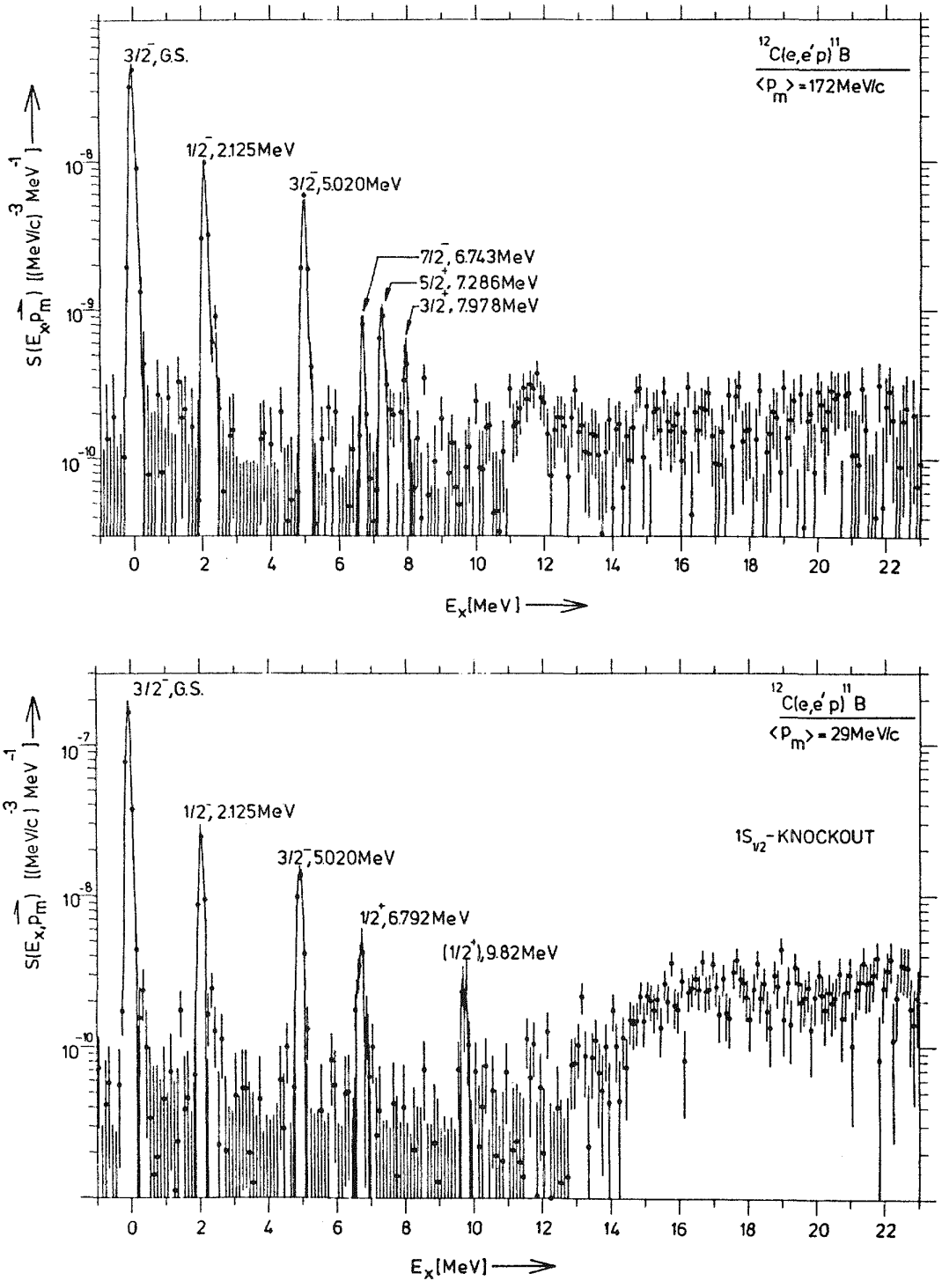

Figure 2. High resolution $^{12}C(e,e'p)$ missing energy spectra measured at NIKHEF for high (top) and low (bottom) initial momenta.

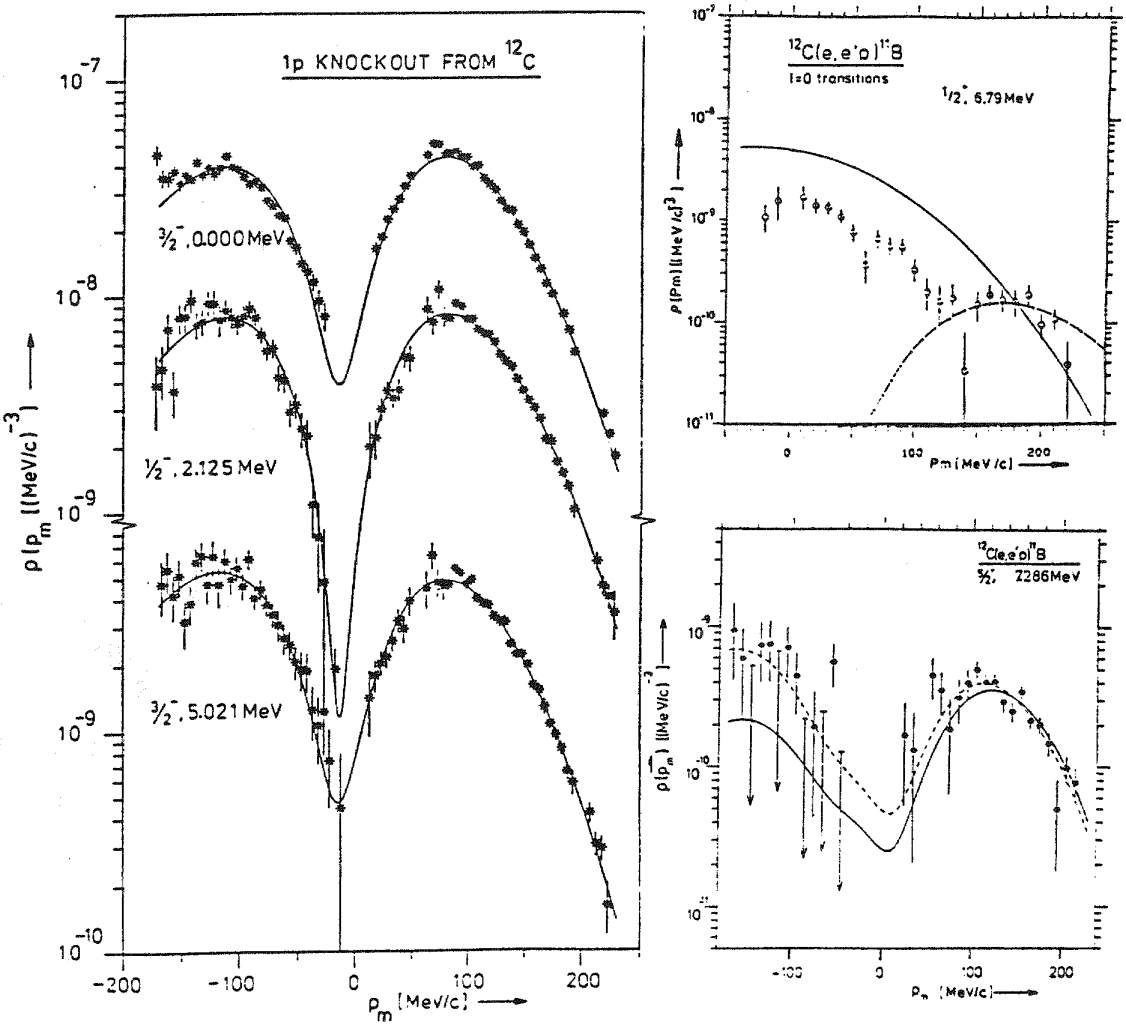

Figure 3. Momentum distribution for the negative parity p-shell states (left) and the positive parity states (right) at 6.79 MeV ($\frac{1}{2}^+$) and 7.29 MeV ($\frac{5}{2}^+$) in ^{11}B.

An important aspect of these discussions of (e,e'p) reactions is the accuracy of our treatment of the strongly interacting hadron in the final state. Is the impulsive idea that is central to first order thinking largely correct with manageable corrections? There is a growing body of evidence from (p,p') that hadronic probing of nuclei can be quantitative. There is also evidence that (e,e'p) reactions can be treated quantitatively. However, many quantitative questions, e.q. coupled channel effects, charge exchange etc., are just beginning to be dealt with and this is an open theoretical field. There is, however, a tantalizing bit of evidence in the data from NIKHEF that we bring to your attention, the $\frac{5}{2}^-$ state at 4.45 MeV in ^{11}B. It is not excited in the (e,e'p) process.[13] This tells us two things — it does not have a parent configuration in the ^{12}C ground state, which

is not unreasonable, and secondly, it is not excited by a two-step process by final state interactions of the outgoing proton. Just this bit of experimental evidence gives us hope that the (e,e'p) probe can evolve into a much better understood probe of multiparticle configurations.

These issues will not be settled by computation alone. As experimentalists we must have the fortitude to search for a large body of systematic data that demonstrates the independence of interpretation to final state energies, momentum transfer, etc. These data will provide the hints to guide theorists to formulate useful concepts to interpret our data with a sophistication beyond our simplest ideas and to formulate theories that yield well-defined experimental questions. Breaking this barrier will allow us to enter a realm of understanding in many areas of strong interaction physics. We believe this to be one of the most important challenges to those of us studying electromagnetically induced reactions, in particular high resolution (e,e'p).

Let us turn to some high resolution results from (e,e'p) studies on ^{90}Zr.[14] These workers use two different final proton energies (70 MeV, 100 MeV) to probe different regions of $|\vec{p}_m|$. Notice, in Figure 4, their mapping of the 1f-hole strength up to 20 MeV of excitation in ^{89}Y. Our standard nuclear physics with pick-up and stripping can only supply us with such data for the first few MeV of excitation. The unique spectroscopic contributions possible from (e,e'p) are very clear from this example and should form an important part of new and more comprehensive understandings of nuclear excitations.

Another interesting result from the ^{90}Zr(e,e'p)^{89}Y study [15] is exhibited in Figure 5. Here, a DWIA calculation is used to fit the momentum distribution data for the $2p_{3/2}$ and $2p_{1/2}$ hole states in ^{89}Y. A poor fit is provided by potentials that come from (p,p') studies. it is possible to find an energy-dependent potential can fit both the (p,p') and the (e,e'p) data though it has significantly different parameters, in particular a stronger imaginary part in the interior where the (p,p') probe is a more ambiguous source of information.

The (e,e'p) reaction will be a clear contributor to detailed knowledge of effective proton-nucleus interactions and we have much to understand in this area. We remind you that we have two distinct treatments of these interactions. One, successfully attempted up to about 200 MeV, uses a medium corrected effective two-body interaction and typical versions are from Brieva, Rook and von

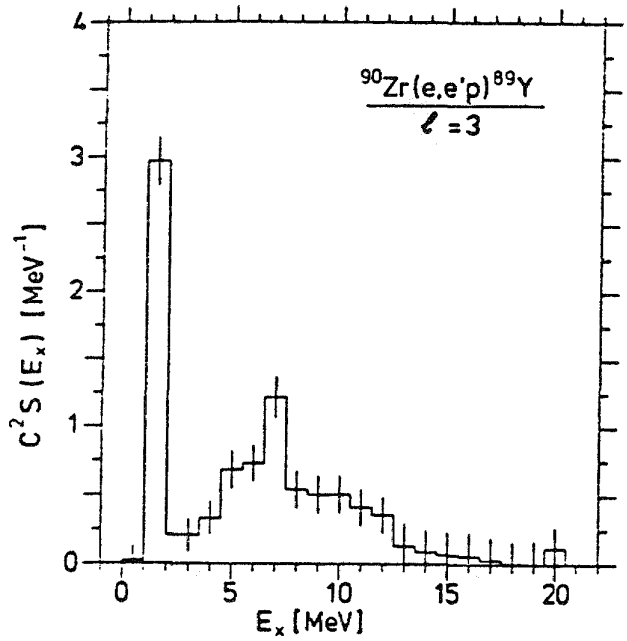

Figure 4. Fragmentation of 1f hole strength in the ^{90}Zr(e,e'p)^{89}Y reaction studied at NIKHEF.

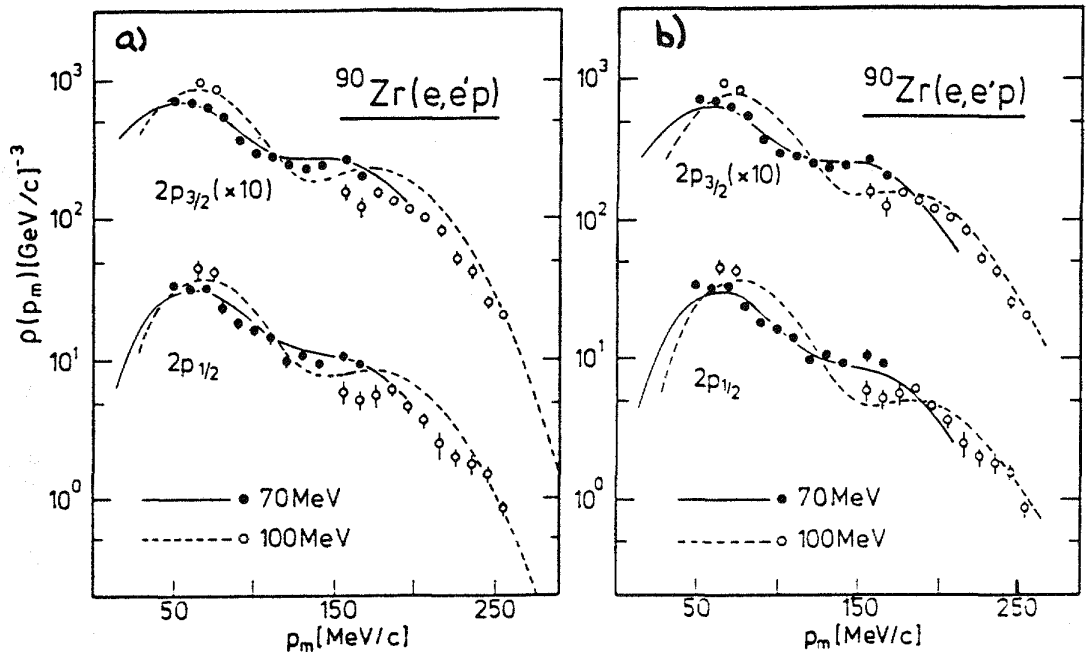

Figure 5. Fits to the $2p_{3/2}$ and $2p_{1/2}$ momentum distributions in ^{90}Zr with a) standard and b) modified proton optical potentials.

Geramb. [16] In Figure 6 we show the density dependence (via the Fermi momentum) for such an interaction compared to the free nucleon-nucleon interaction of Love. [17] Much of the quality of this approach involves the synthesis with (e,e')

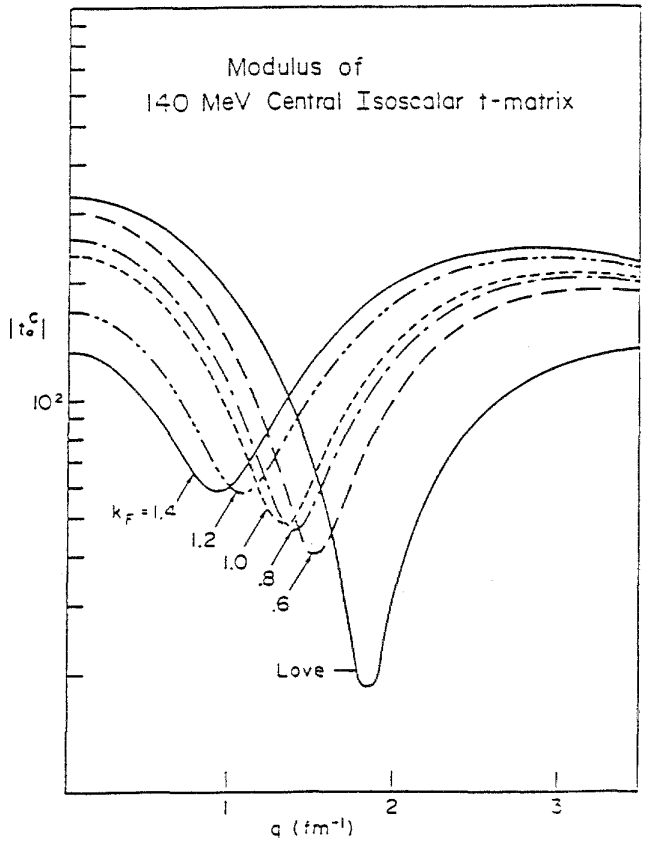

Figure 6. Density dependence of the central isoscalar effective interaction.

studies to specify the neutron and proton densities of isoscalar transitions. [18]

The second approach to nucleon-nucleus interactions uses the Dirac phenomenology. The spin-orbit $(\vec{L} \cdot \vec{S})$ interaction has a classic origin and the ability to describe data is greatly improved. This is exhibited in Figure 7 dealing with the elastic scattering of 497 MeV protons from ^{40}Ca. [19] Notice the considerably improved fits to the cross section and polarization data by the Dirac phenomenology compared to the nonrelativistic optical models. Clearly the small components of the spinor are important. However, where are the effects of the nuclear medium observed earlier? These media effects are clearly important in Hartree-Fock representations of nuclear ground states as are relativistic effects. How do we bring these ideas together?

To conclude this part on high resolution, we list a few thoughts about high resolution (e,e'p) reactions:

a) Our resolution goal should at least approach 100 keV.

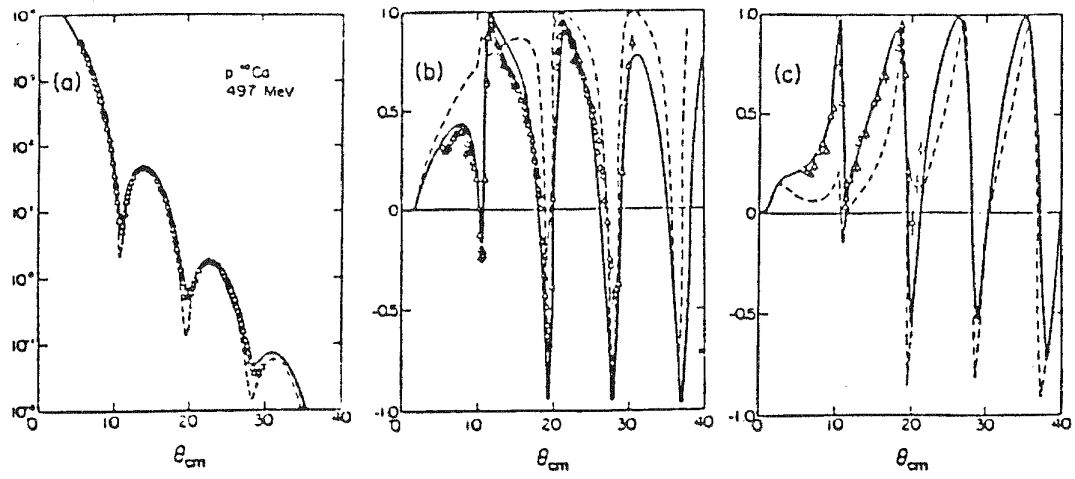

Figure 7. Relativistic (solid) and non-relativistic (dashed) calculations of a) cross section (mb/sr), b) polarization P and c) spin rotation parameter Q for ^{40}Ca(p,p') at 497 MeV.

b) With the duty ratio and intensity available at CEBAF we expect more that a 10^3 improvement in cross section sensitivity. In terms of physical amplitudes we will be more than thirty times more sensitive than present work. This challenges our ability to extend our present knowledge in order to conceive of exactly what we will see. Most of our present knowledge is represented by the mean field ideas and we should be *very* careful not to limit our experimental capabilities by these ideas — in particular our ability to do (e,e'p) at the highest energies and out-of-plane to secure all of the invariant amplitudes (more on this later). Remember that CEBAF will be unique in the World!

c) We will map intensities in momentum space to values of $|\vec{p}_m| > 600$ MeV/c. We will observe these distributions to excitations of more that 20 MeV. (In fact, we have no idea whether structures will not exist at considerably higher excitations energies in this new regime of $\vec{p}_m$.) We will map out the intensity in momentum space for natural parity (hole) and unnatural parity (multiparticle-multihole) states of many differing spins and isospins. This will help provide us with a more complete specification of the ground state configurations of nuclei — knowledge that is presently limited to that 50% which is well-represented by the shell-model mean field.

d) For many of the states observable, the separation of transverse, longitudinal and interference structure functions will provide unique information about effective two-nucleon interactions in the nuclear medium. For example, the $p_{1/2}$ and $p_{3/2}$ hole states differ in energy because of the difference in the $\vec{L} \cdot \vec{S}$ interaction. In terms of the two-nucleon interaction, this is of very short range (exchanged mass $\sim$ 1 GeV). We may well acquire important knowledge about the origin of the spin-orbit force by examining the longitudinal and transverse contributions to (e,e'p) at low and high values of $\vec{p}_m$. The same comments are true about the importance of tensor force correlations and also those states resulting from 2p-2h configurations in the ground state.

High resolution (e,e'p) studies at CEBAF have the potential for novel information which is enormous compared to our present knowledge.

III. The (e,e') and (e,e'p) Reaction Processes

Contrary to our one-body predjudices formed by the existence of well-defined (e,e') peaks that correspond quasielastic scattering and quasifree Δ-production, there are some severe problems with our understanding of the (e,e') reaction process. These problems provide part of the motivation for a series of explorations at MIT-Bates, NIKHEF and Saclay with the (e,e'p) reaction. The following is a brief review of these topics and a summary of some of the experimental results.

The (e,e') process, in Born approximation, can be written as a composite of two response functions which are separable experimentally:

$$\frac{d\sigma}{d\Omega d\omega} = \left(\frac{d\sigma}{d\Omega}\right)_{Mott} [v_L R_L(\vec{q},\omega) + v_T R_T(\vec{q},\omega)]$$

where $v_L = (q_\mu/\vec{q})^4$ and $v_T = \frac{1}{2}(q_\mu/\vec{q})^2 + \tan^2\theta/2$. If we also make the assumption that the (e,e') process involves interactions with quasifree nucleons with appropriate off-shell cross sections, then the longitudinal and transverse responses (R_L, R_T) can be reduced to longitudinal and transverse scaling functions, $f_L(y)$ and $f_T(y)$ respectively, where the free nucleon longitudinal and transverse form factors have been removed. In Figure 8 these reduced response functions [20] for ^{12}C(e,e') are plotted as a function of the scaling variable y

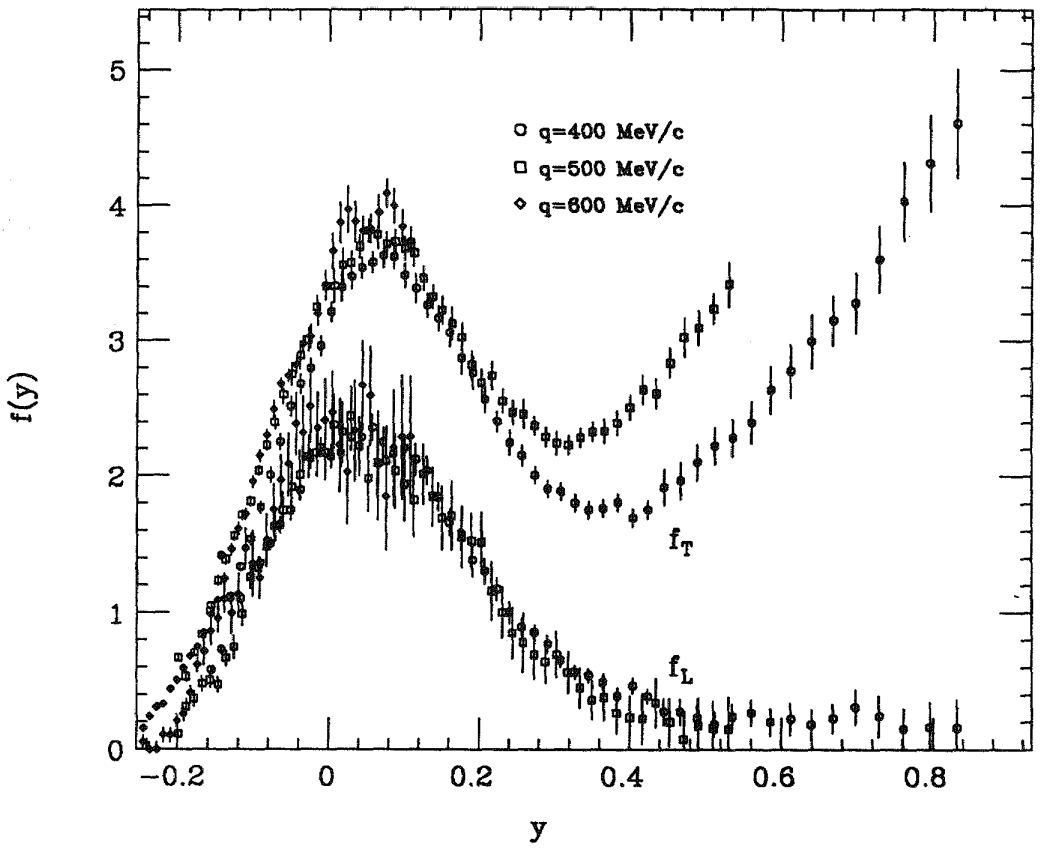

Figure 8. Reduced structure functions for ^{12}C(e,e') at quasielastic kinematics.

which is effectively the component of initial momentum along $\vec{q}$ in units of m, the nucleon mass:

$$y = -\frac{|\vec{q}|}{2m} + \frac{\omega}{|\vec{q}|}\sqrt{\frac{\vec{q}^{\,2}}{q_\mu^2}\left(1 + \frac{q_\mu^2}{4m^2}\right)}$$

Several things are important to notice in this figure. First, over the quasielastic peak and up to y = 0.2, both the transverse and longitudinal responses scale independently of $|\vec{q}|$ for the range of $|\vec{q}|$ indicated. This lends validity to the idea that the quasielastic process is dominant. The longitudinal $f(y)$ scales to even higher values of y. For $y > 0.3$, the transverse $f(y)$ no longer scales as the quasielastic assumption requires and we expect this deviation since the Δ resonance is now important.

The real problem is that the quasielastic assumption requires that $f_L = f_T$ over the quasielastic peak while experiment yields $f_T \approx 1.7 f_L$. There are discussions which try to relate this result to f_L being too small with a resulting lack of

strength in the longitudinal sum rule.[21] Some discussions argue that f_T is larger than expected on the basis of a nuclear shell model.[22] Others try to use the result to argue for an effect that is equivalent to a swollen nucleon.[23] [24] We remark only that the result is contrary to the elementary expection that $f_L = f_T$ and that there is an alteration of the (e,e′) reaction mechanism in the quasielastic regime. The result cannot be explained by final state hadronic interactions and a new current or modification of nucleonic structure is required.

In Figure 9 we show the results of O'Connell *et al.*[25] for (e,e′) from several light nuclei. Notice the standard phenomenology with increasing ω — quasielastic peak, dip region and quasifree Δ production peak. The experimental cross section is divided by A, the number of nucleons. In the dip region we see the yield basically saturate for $A \geq 9$. If ^{3}He were included in the data set it would be only 65% of ^{4}He in the dip region. We are unable to explain the experimental yield in the dip region of nuclei with $A > 4$ with reasonable models for quasielastic scattering, quasifree delta production and meson exchange currents. The theory is always about one-half of the experimental yield unless one invokes specialized phenomenologies like the quasideuteron model to enhance and localize in ω the effects of meson currents.

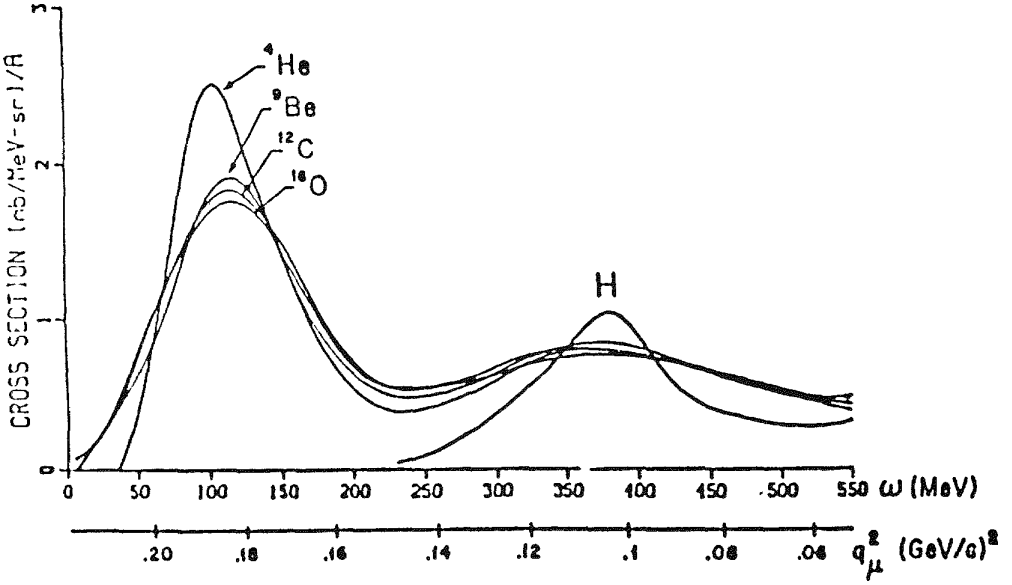

Figure 9. Inclusive quasielastic electron scattering from light nuclei.

Finally, we note that in these data the Δ production peak in complex nuclei is wider than one would expect from nucleon momentum distributions and that the

integrated yield is about 30% larger than expected from a quasifree production model.[25]

Clearly the (e,e′) reaction mechanism is more complex than one would glean from the simple observation of kinematic peaks corresponding to quasifree processes smeared by nucleon motion. In fact, much earlier (e,e′) quasielastic work[26] done at about 60° and with $|\vec{q}| \sim 400$ MeV/c was very coincidentally the appropriate combination of transverse and longitudinal to demonstrate excellent fits by a Fermi Gas model or a shell model with accurate demonstrations that $\sigma = Z\sigma_p + N\sigma_n$. This happenstance contributed much to our early predjudice of simplicity and is an excellent example for the need for complete experimentation in experimental physics.

The abovementioned problems have led us to the program we describe here in studying the ^{12}C(e,e′p) reaction at the MIT-Bates Laboratory.

1) The reaction has been studied with ω at the quasielastic peak for $|\vec{q}| = 400$ MeV/c to derive the transverse and longitudinal spectral functions. The data integrate one a wide range of $\vec{p}_i$ and focus on the the missing energy dependence.

2) The ^{12}C(e,e′p) reaction was studied with ω at the quasielastic peak for $|\vec{q}|$ = 400, 600, 800 and 1000 MeV/c always integrating over the same range of $\vec{p}_i$. The question to be addressed is the dependence on q_μ, the momentum transfer. Is it different from that of the free nucleon?

3) For $|\vec{q}| = 1000$ MeV/c, the ω-dependence is also under study through the quasielastic peak.

4) The ^{12}C(e,e′p) reaction was studied in the dip region to examine the missing energy spectra for indications of new processes.

5) The ^{12}C(e,e′p) reaction was studied in the region of the Δ resonance. The missing energy spectra clearly exhibit separate reactions: those with pions in the final state and those that have only nucleons in the final state.

This program is diagrammed in Figure 1 by the vertical lines. Where available, we will include results from NIKHEF and Saclay.

IIIA. R_L/R_T Separations and $|\vec{q}|$-dependence in (e,e'p)

We discuss first the results of Ulmer *et al.* [27] with $|\vec{q}| = 400$ MeV/c and $\omega = 200$ MeV.This is about 30 MeV above the quasielastic peak so that $\vec{p_i} > 0$ for the p-shell in ^{12}C. In fact, the results integrate the p-shell momentum distribution from $30 \leq |\vec{p_i}| \leq 110$ MeV/c. These results were obtained at electron scattering angles of 60° and 120° to allow a longitudinal/transverse separation. The longitudinal and transverse response function R_L and R_T are shown in Figure 10. Also shown is the difference between the transverse and longitudinal spectral function $S^d(\vec{p_i}, \vec{p_f}, \epsilon_m)$ derived from the assumption that σ(e,e'p)= $K\sigma_{ep}S^d(\vec{p_i}, \vec{p_f}, \epsilon_m)$, where the superscript d denotes distortion corrections for final state absorbtion and $\vec{p_f}$ is the final state proton momentum. The results are integrated by the experiment over the same range of iniitial momenta for the forward and backward angles. In the nonrelativistic quasielastic impulse approximation $S_L = S_T$.

For the p-shell, the ^{11}B ground state is the strongest contributor by far and the results are integrated over a bin in ϵ_m that includes the first excited state of ^{11}B. For plotting purposes the p-shell data have been reduced by 1/3. For the p-shell, there is no difference between the transverse and longitudinal spectral functions. Table 1 gives the integration region in ϵ_m and corresponding L/T ratio. The p-shell shows no effect within the errors, statistical and systematic respectively.

In the case of the s-shell, the result is different. R_L is localized in ϵ_m with essentially zero strength above 48 MeV. R_T has a bump localized somewhat like R_L, but it has an additional flat contribution that is appreciable and extends up to 64 MeV where the data end. In the graph of $S_T - S_L$, this shows up as a distribution starting at about $\epsilon_m \approx 28$ MeV, approximately the threshold for two nucleon emission. In Table 1 the results are shown compared to the expectation of a DWIA calculation for different regions of integration for the s-shell. The s-shell is appreciably more transverse than longitudinal, and the degree of this increased transversality depends on the upper limit of the variable ϵ_m.

These results are not like the simple expectations of a one-body model wherein the properties of the nucleon, i.e. its magnetic and coulombic form factors, might be altered, but the spectral distributions remain the same. Perhaps the energy dependence of the transverse process can be included in such a view.

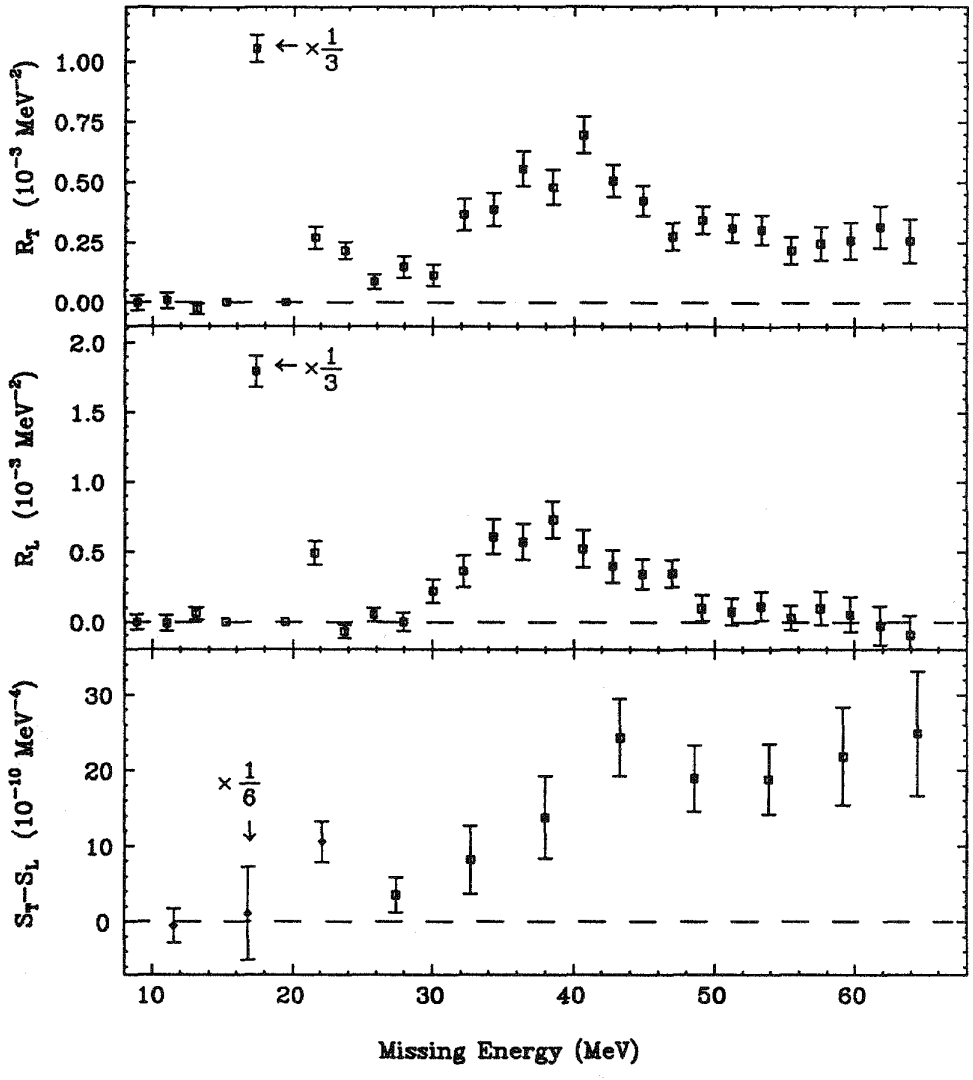

Figure 10. Separated ^{12}C(e,e'p) response functions and their difference. Transverse (4a) and longitudinal (4b) response functions and the difference in the spectral functions (4c) vs. missing energy.

On the other hand, it may be more appropriate to describe the large additional transverse contribution as due to a new current, perhaps a two-body current. This seems to be a common thread through much of our data although in this experiment the association with the two-nucleon threshold may be largely circumstantial.

It should be noted that the ratio of transverse to longitudinal inclusive scaling functions, $f_T(y)/f_L(y)$, can be made consistent with our data by simply ex-

Integration Region	$(S_L/S_T)_{EXP}/(S_L/S_T)_{DWIA}$
p-shell ($13 < \epsilon_m < 26$ MeV)	0.89±0.09±0.12
s-shell ($27 < \epsilon_m < 50$ MeV)	0.69±0.09±0.08
s-shell ($27 < \epsilon_m < 60$ MeV)	0.61±0.09±0.07

Table 1. Ratio of longitudinal to transverse spectral functions compared to DWIA predictions at $|\vec{q}|$=400 MeV/c.

tending the flat transverse yield to about 80 MeV in ϵ_m, about 15 MeV beyond our measurements, but allowed by our kinematics with $\omega = 120$ MeV. If the angular distribution (relative to $\vec{q}$) of the supposed two-body transverse piece is broader than the one-body (e,e'p) distribution, then a lesser extension of the data in ϵ_m is required. At any rate, it appears that this new component in the transverse response is the culprit behind the large transverse/longitudinal anomaly in (e,e').

Our next set of experiments focussed on the $\vec{q}$-dependence of the (e,e'p) reaction. This work tests the quasifree assumption that the momentum transfer dependence of the (e,e'p) cross section is determined by that of the (e,p) cross section when $\omega \sim q_\mu^2/2m$, that is, when we select kinematics in the quasielastic region. The MIT experiments, as well as the others we report on, are in parallel kinematics i.e the proton final momentum is along the direction of $\vec{q}$. In these experiments the terms parallel or antiparallel are sometimes used to denote that the initial momentum is opposite to, or along, $\vec{q}$.

Let us first show the results from NIKHEF [28] where longitudinal/transverse separations were made for various values of q_μ^2 in the 1p-shell of ^{12}C and in the 1s and 1p-shells of ^{6}Li. The results in Figure 11 are exhibited in terms of the ratio

$$R_G = \sqrt{\frac{2m^2\vec{q}^2}{q_\mu^4}\frac{R_T}{R_L}}$$

which is equal to G_M/G_E for a free proton (G_M and G_E are respectively the magnetic and electric form factors of the proton). They interpret R_G as representing this same quantity for the bound proton though off-shell effects (small in quasielastic kinematics) can also modify the ratio. Proton distortion corrections

and radiative corrections have been applied which are small in such ratio results. The solid horizontal line is the ratio of G_M/G_E for the free proton. The error bars on the NIKHEF data are purely statistical. The data from MIT–Bates for ^{12}C at $|\vec{q}| = 400$ MeV/c are also shown on Figure 11 as the large rectangular points. From Figure 11 we can conclude that the quasifree knockout picture does not require a strong momentum dependence of G_M/G_E for the p-shell in ^{12}C and ^{6}Li and the s-shell in ^{6}Li.

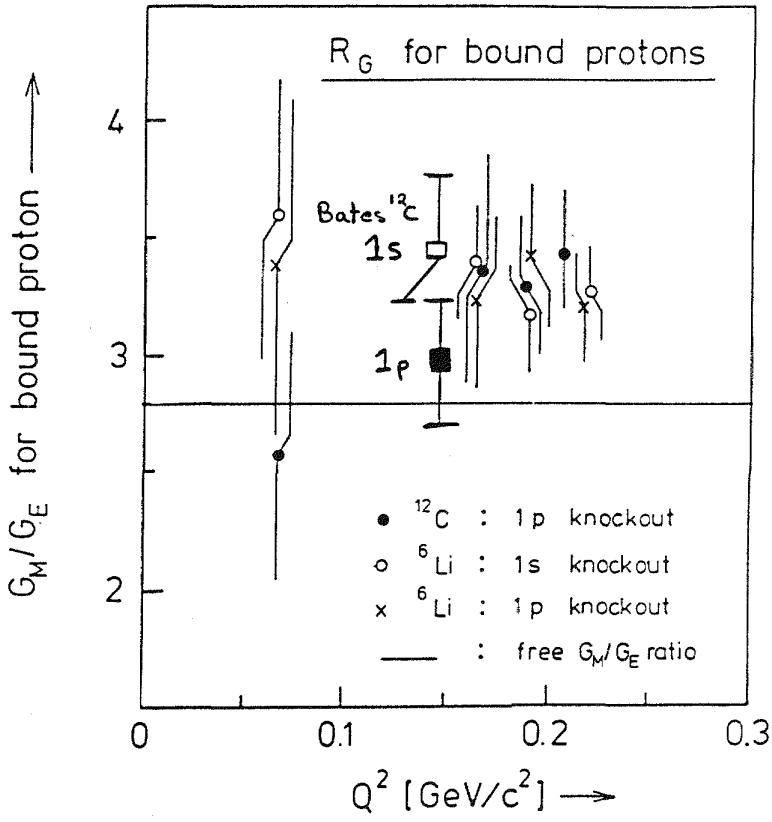

Figure 11. The ratio R_G of the magnetic to electric form factor for a bound proton.

Unpublished results by Cohen *et al.* [29] using a relativistic formalism show that the small deviations from the free proton values of the type shown in Figure 11 for the p-shell in ^{12}C and ^{6}Li can be a natural result of including the small components of the Dirac wavefunctions. Their results also fall below the free proton value in the region $0.10 < q_\mu^2 < 0.14$ GeV/c. However, we need a considerable improvement in experimental precision to play this game seriously as well as a large range of kinematic variation to demonstrate a systematic effect related to dynamical properties of the nucleon in the nuclear medium.

As we mentioned earlier, we need these more complete sets of data to guide our theoretical colleagues in their efforts to construct a more accurate representation of the (e,e'p) reaction process. For example, corrections due to electron-neutron scattering with charge exchange present us with a non-negeligible transverse amplitude leading to proton emission. Similarly, the importance of electron-neutron interactions with (np) pairs leading to the final states we investigate should be calculated. We have a long way to go beyond final state optical potentials before we can interpret modest deviations from our quasifree picture as modifications of nucleon electromagnetic structure.

Returning to the experiments, we show in Figure 12 some results from Saclay [30] for the (e,e'p) reaction in ^{40}Ca ranging from just below 400 MeV/c to just above 800 MeV/c in three-momentum transfer. The final proton momentum is in the direction of $\vec{q}$ and parallel and antiparallel mean that the initial momentum is antiparallel or parallel to $\vec{q}$ respectively. In these experiments the magnitude of the initial momentum was centered at 115 MeV/c for each point. The momentum transfer was varied causing the final momentum to vary. The results integrate over missing energy with $\epsilon_m < 60$ MeV. Radiative corrections and corrections for final state proton distortions were applied. The data are presented as a double ratio after a longitudinal/transverse separation is made. The point at the highest momentum transfer has no forward angle partner for a separation and is assumed to be mostly transverse. The quantity $\sigma_T^P(q)$ is the proton's apparent transverse cross section required to yield the experimental result based on a quasifree knockout model. The data are normalized to the point at $|\vec{q}| = 560$ MeV/c and compared to the same ratio for various models for the q_μ-dependence of the transverse cross section of the proton.

Except for the antiparallel situation, there does not appear to be a q_μ-dependence of significance. Certainly the specific version of the soliton model of Celenza *et al.*[24]shown on the figure is ruled out. The antiparallel results are contrary to intuition since they correspond to an energy transfer in (e,e') that is larger than that of the quasielastic maximum, where an increased relative transversality in the inclusive cross section is usually exhibited in the data, as we showed in Figure 8. Nevertheless, these results are preliminary and we await final results from these researchers. The Saclay results also show no q_μ-dependence in the longitudinal cross sections where the data extends up to $|\vec{q}| \approx 670$ MeV/c.

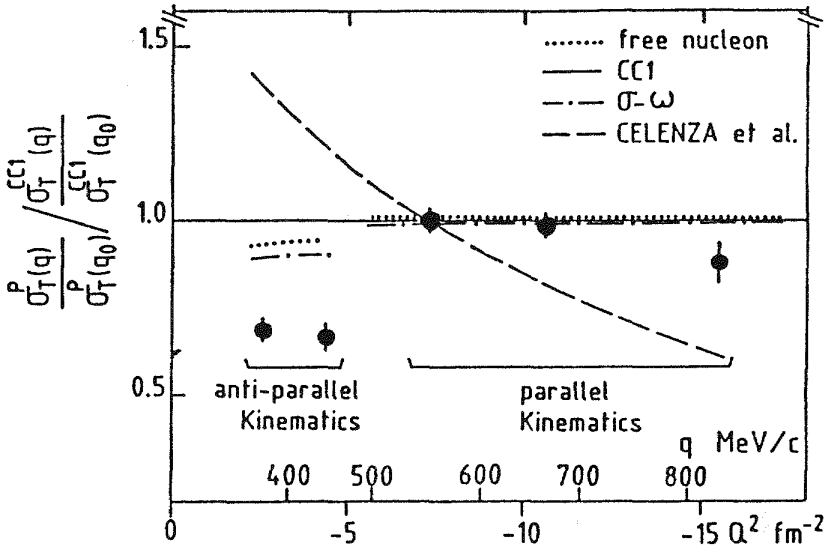

Figure 12. Momentum transfer dependence of the transverse ^{40}Ca(e,e'p) cross section (relative to the DeForest "CC1" (e,p) cross section) measured at Saclay.

In Figure 13 we present preliminary results from an MIT-Bates study of the $|\vec{q}|$-dependence of the (e,e'p) reaction in ^{12}C. These data are mostly transverse since backward angles are involved (except for one of the 400 MeV/c points taken at an (e,e') angle of 60°). The data involve the same range of the initial momentum we reported at $|\vec{q}| = 400$ MeV/c, $30 \leq |\vec{p}_i| \leq 110$ MeV/c.

The p-shell and s-shell regions are defined by the same regions of missing energy given in Table 1. The data are radiatively corrected and corrected for final state absorption. It should be noted that the final proton energy increases with increasing $|\vec{q}|$ and this feature is accounted for in optical model parameters.[31] Using the off-shell proton cross section of DeForest,[32] the data are represented by an occupation number. For the p-shell this number is about 4. Earlier results of Mougey *et al.*[11] obtained a number of 2.6 but no errors are given. At this preliminary stage of analysis this is not a serious problem. The integration over missing energy for the p-shell includes some positive parity states because of experimental resolution and should be reduced by 10-15%. The error bars have a large contribution due to theoretical uncertainty in applying final state optical model corrections. For the s-shell the data are the same as earlier results of Mougey *et al.*[11]

The important feature of these preliminary results is the lack of a momentum transfer dependence of the occupation numbers. Over the range of $|\vec{q}|$, 400

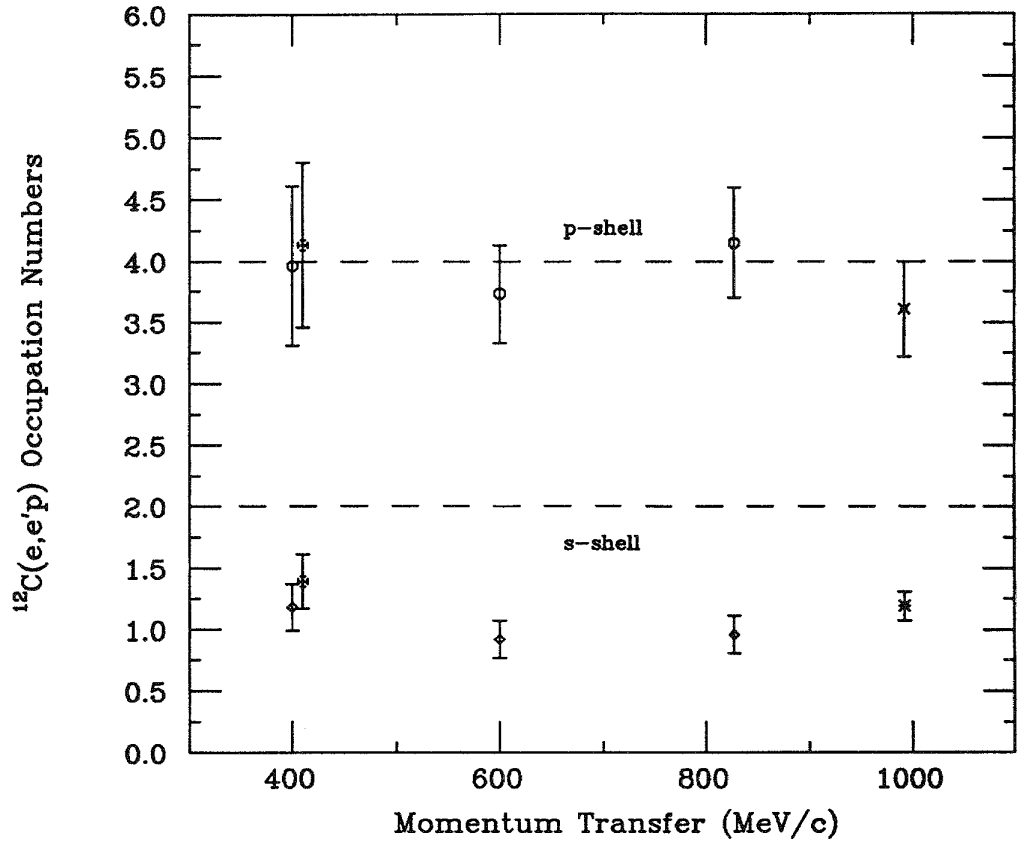

Figure 13. Ratio of the measured p- and s-shell cross sections to DWIA predictions expressed as occupation numbers.

MeV/c to 1000 MeV/c, G_E^2 of the proton varies from 0.42 to 0.04. This change of an order of magnitude is all that is required to explain the data. No additional alteration of the total proton form factor as a function of momentum transfer is allowed by these data above the 10-20% level.

As the momentum transfer increases beyond 400 MeV/c, the identification of the quasielastic peak in (e,e′) becomes increasingly more difficult. The so-called "dip region" between the quasielastic peak and quasifree Δ production peak is filled in so that these distinct nucleon peaks are obscured. This result is demonstrated by the data in Figure 14 from ^{12}C(e,e′) at CEA.[33] As $|\vec{q}|$ increases, the widths of the quasifree peaks increase in proportion to $|\vec{q}|\,|\vec{k}_f|$ where $|\vec{k}_f|$ is the Fermi momentum. The filling in of the dip region requires more than just this kinematic broadening, as we pointed out earlier when $|\vec{q}|$=400 MeV/c. Natural questions that arise at higher momentum transfers in quasielastic kinematics are:

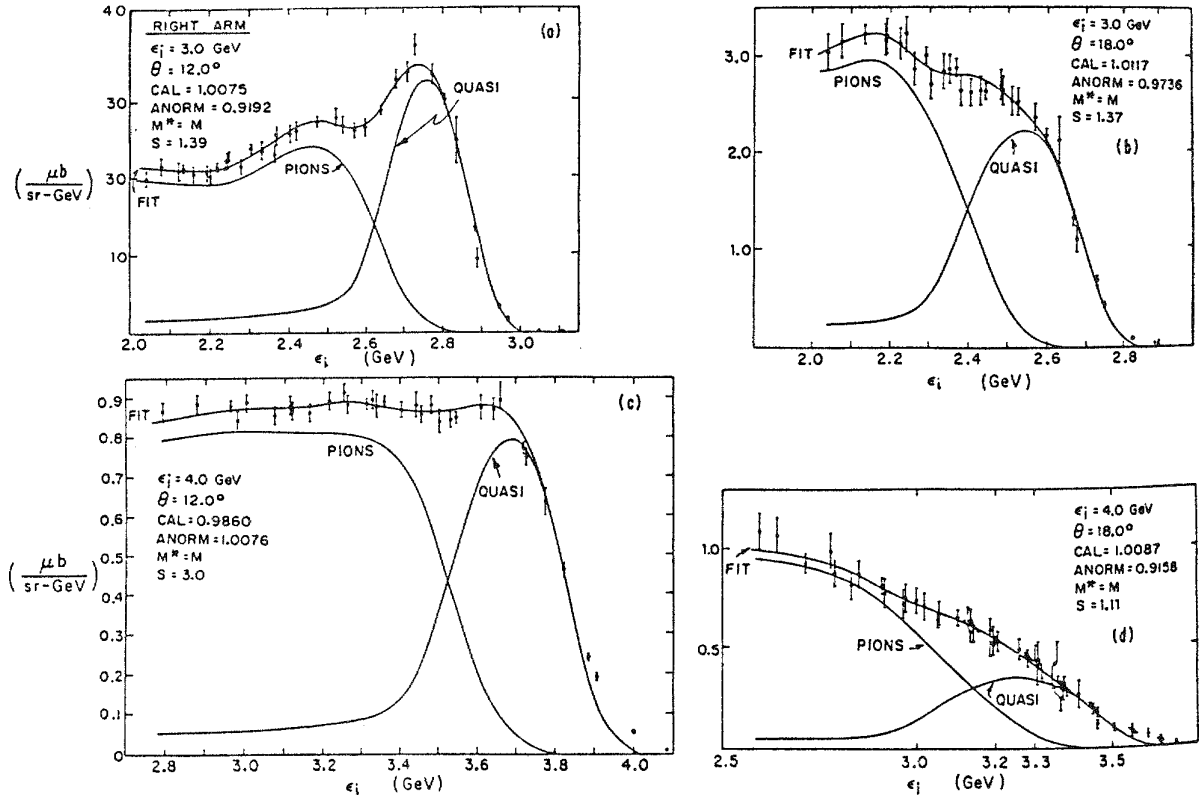

Figure 14. High energy quasielastic ^{12}C(e,e') from CEA.

a) Is there a contribution from the low-energy-loss tail of the Δ?

b) Is there still a distinct quasielastic signature in the missing energy spectrum?

c) Does the missing energy spectrum exhibit any other reaction component, for example, the additional one demonstrated in the transverse response function at $|\vec{q}|$=400 MeV/c?

Towards these ends, we have examined the missing energy spectra at $|\vec{q}| = 600$ MeV/c, 800 MeV/c and 1000 MeV/c in predominantly transverse kinematics. At the highest momentum transfer two values of ω were used: $\omega = q_\mu^2/2m + 35$ MeV $= 470$ MeV; and $\omega = 330$MeV, about halfway down the low-ω side of quasielastic peak. The preliminary results are shown in Figures 15 and 16.

The first conclusion is that no pion production of consequence is observed since no increase in yield is observed for $\epsilon_m > 160$ MeV, the pion production threshold. Even when $\omega = 470$ MeV, pion production is not an important process when the

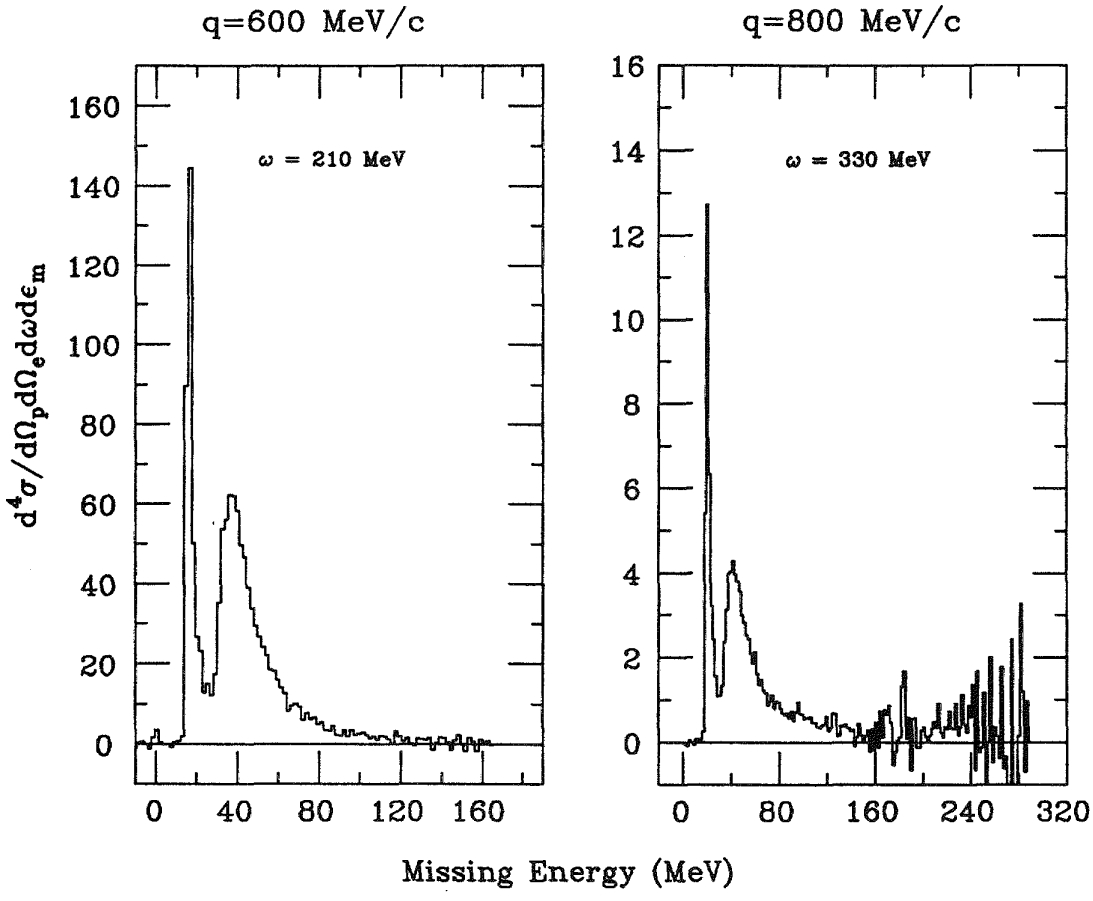

Figure 15. Missing energy spectra from ^{12}C(e,e'p) at $|\vec{q}|$ =600 MeV/c (left) and 800 MeV/c (right).

kinematics selects the quasielastic process. The p-shell and the s-shell strengths are clearly observed and were used to derive the occupation numbers in Fig. 13.

The continuum strength above the s-shell is significant. Perhaps this continuum strength is due to the same process observed in the transverse response at $|\vec{q}|$ = 400 MeV/c. Two-nucleon and multinucleon reaction processes fill the dip region and they seem to increase in importance as either $|\vec{q}|$ or ω increases.

IIIB. The (e,e'p) Reaction in the Dip and Δ-Resonance Regions

In Figure 17, we show the missing energy spectrum for ^{12}C(e,e'p) in parallel kinematics when we probe the dip region using the condition $|\vec{q}|$ = 400 MeV/c and ω = 200 MeV.[34] The electron scattering angle was 60° and $\vec{q}$ was pointing at −34.3° with respect to the incident electron beam. The p-shell (^{11}B ground state) is very clear and the cross section is in agreement with that expected on

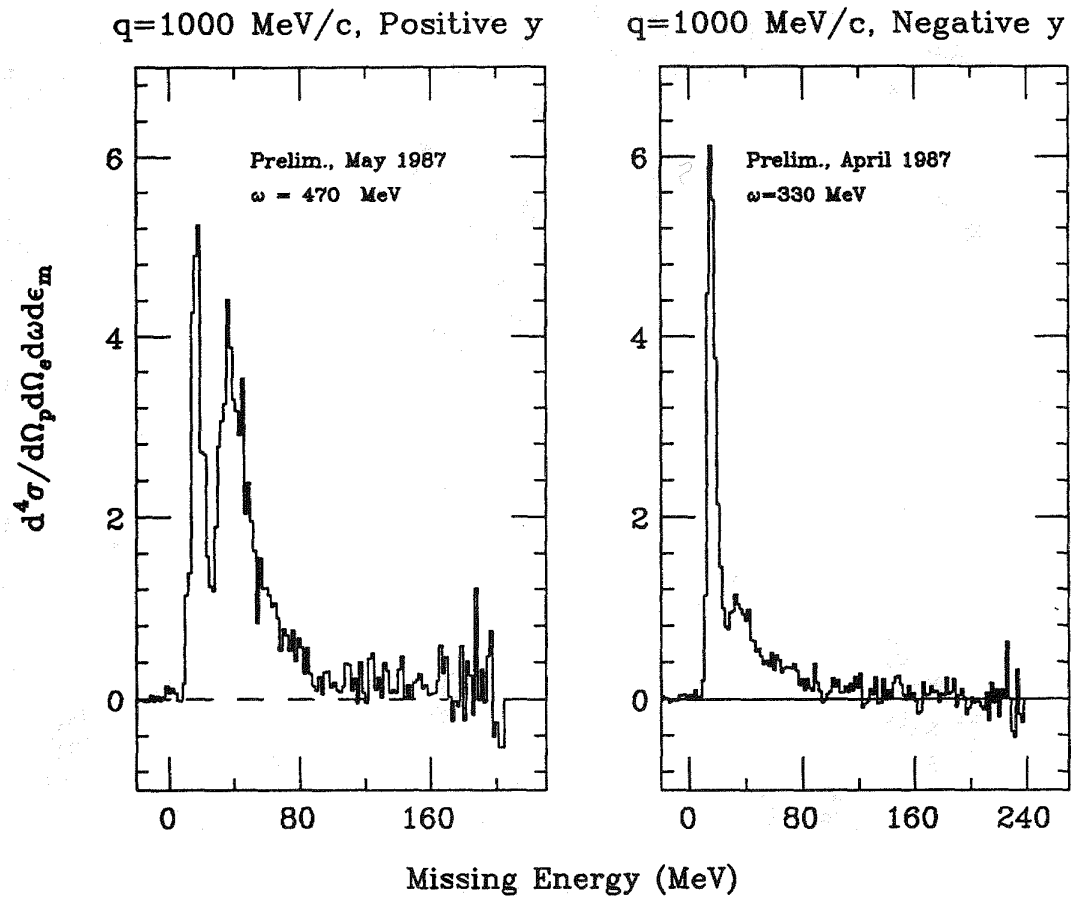

Figure 16. Missing energy spectra from ^{12}C(e,e'p) at $|\vec{q}|$ =1000 MeV/c. The spectrum on the left was obtained on the high-ω side of the quasielastic peak (positive y) while the one on the right is on the low-ω (negative y) side.

the basis of momentum distributions measured in perpendicular kinematics by Mougey*et al.*[11] On the basis of the same measurements, the area above the dashed line represents the s-shell. The rest of the yield, which is flat out to $\epsilon_m \sim 155$ MeV, is in excess over our simple idea of quasifree proton knockout. This excess yield is much more than one can produce by radiative processes or by final state interactions scattering protons into our kinematics from protons and neutrons originating from (e,e') but headed in other directions. Indeed, only about 15% of the strength above 80 MeV can be accounted for by these processes. Laget[22]is able to account for the excess yield in the region of the s-shell by a quasideuteron model but this model does not provide strength above 75 MeV. We have not performed a longitudinal/transverse separation in this region. However, since the (e,e') process is predominantly transverse, it is reasonable to assume that this (e,e'p) yield is also predominantly transverse. With

a reasonable assumption about the angular distribution of the excess yield relative to $\vec{q}$, over half of the (e,e′) process is associated with this yield. Clearly, a new transverse current over and above quasifree nucleon knockout is required leading to large missing energies and multinucleon knockout.

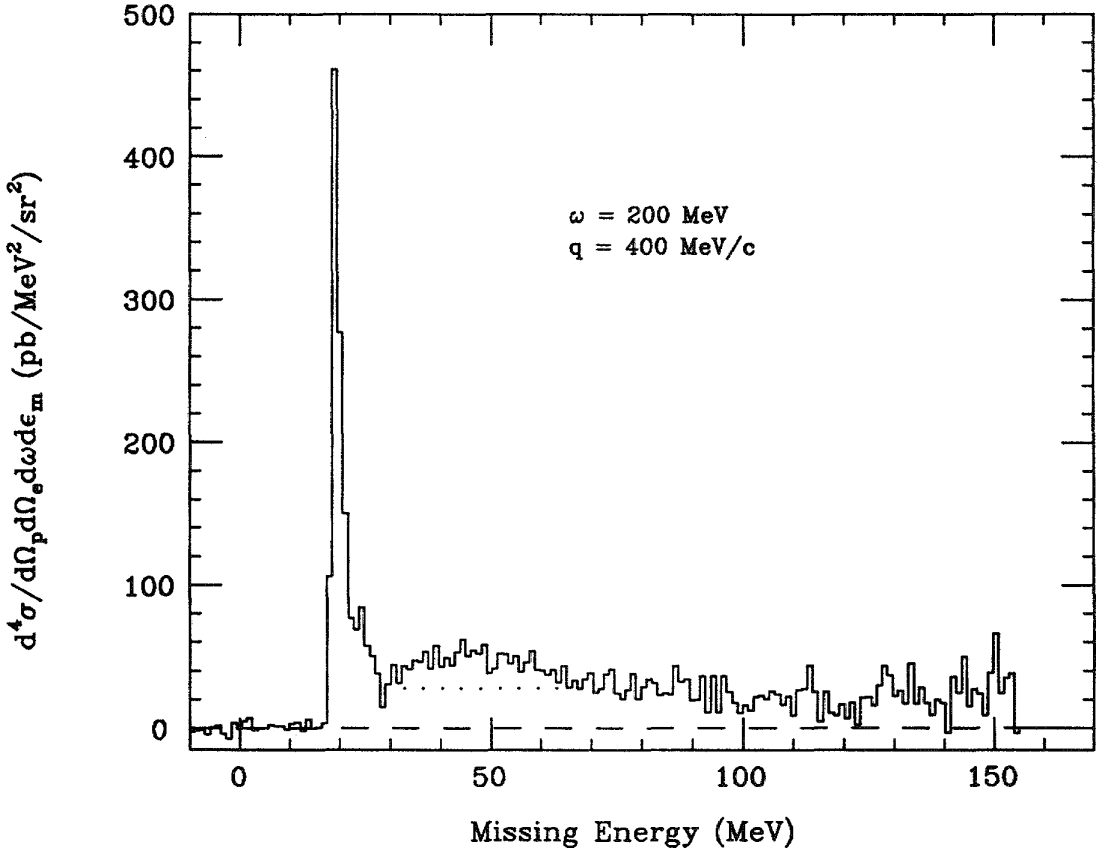

Figure 17. Missing energy spectrum from ^{12}C(e,e′p) in the dip region. The area above the dotted line is attributed to 1s proton knockout.

In Figure 18, results on ^{3}He(e,e′p) from Saclay [35] are shown. The values of $|\vec{q}|$ and ω place the experiment in the dip region and two different initial (= −recoil) momenta were probed. The figure caption is almost self explanitory. The narrow peak corresponds to 1s-shell knockout. The broad continuum peak is associated with the electromagnetic interaction with a correlated np pair. The kinematic shift with initial momentum seems to follow this model. The results also show the importance of meson exchange currents. Specific diagrams contributing to direct two-nucleon emission are also shown in the figure.

We have also examined ^{12}C(e,e′p) in the region of Δ kinematics. [36] Two kinematic situations are involved: with kinematics I, $|\vec{q}| = 400$ MeV/c and $\omega = 275$

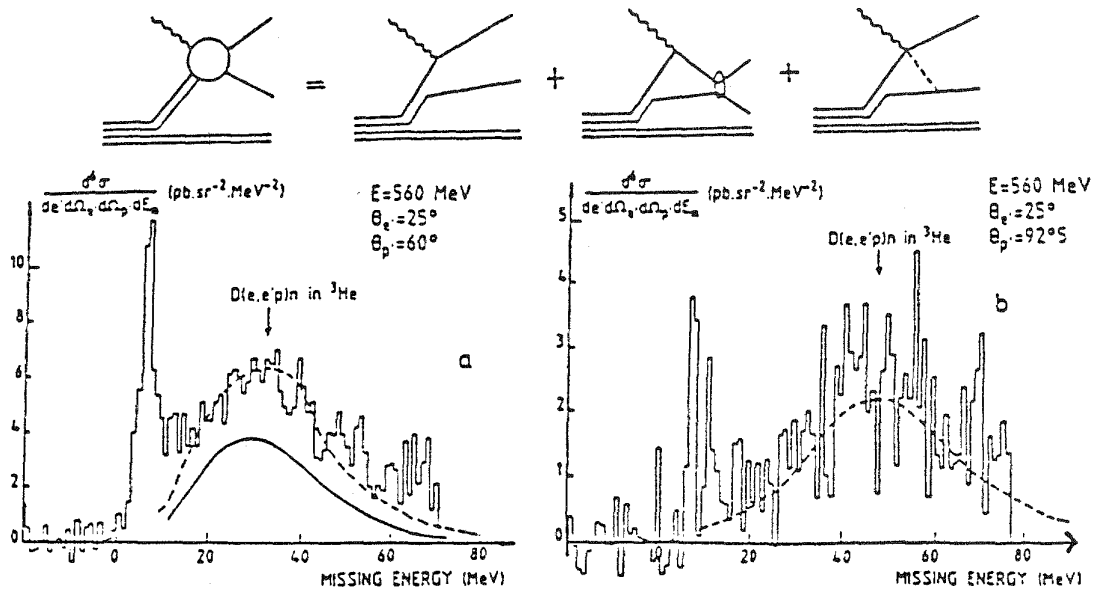

Figure 18. Missing energy spectra from ^{3}He(e,e'p) in the dip region measured at Saclay. The arrow indicated the expected position from the D(e,e'p) reaction. The dashed (solid) curve is with (without) meson exchange currents. In a) the recoil momentum is 310 MeV/c and 403 MeV/c in b).

MeV; with kinematics II, $|\vec{q}| = 473$ MeV/c and $\omega = 382$ MeV. Kinematics I are located about one-third of the way up the low-ω side of the (e,e') Δ resonance in ^{12}C while kinematics II are near the peak of the Δ resonance.

The results of Baghaei *et al.*[36] are shown in Figure 19. The very large increase in yield for $\epsilon_m > 160$ MeV, the pion threshold, is clear. This is in distinct contrast to the situation with $|\vec{q}| = 1000$ MeV/c and $\omega = 470$ MeV where no pions were observed. It is clear that quasifree Δ production with pion emission is selected by the kinematic situation and determined only by the electromagnetic vertex via $(\vec{q}, \omega)$. There is also a significant yield for $\epsilon_m < 160$ MeV with no pions in the final state. With kinematics I, there is also yield in the region of the p- and s-shell as this corresponds to lower values of $|\vec{p}_i|$.

The lower half of Figure 19 show Gaussian fits to the data using two peaks: one for the yield for $\epsilon_m < 160$ MeV and one for $\epsilon_m > 160$ MeV. The Gaussian centroid at low ϵ_m follows the kinematics of direct emission of a correlated pair or a quasideuteron:

$$\gamma_v + \text{“}D\text{”} \rightarrow n + p$$

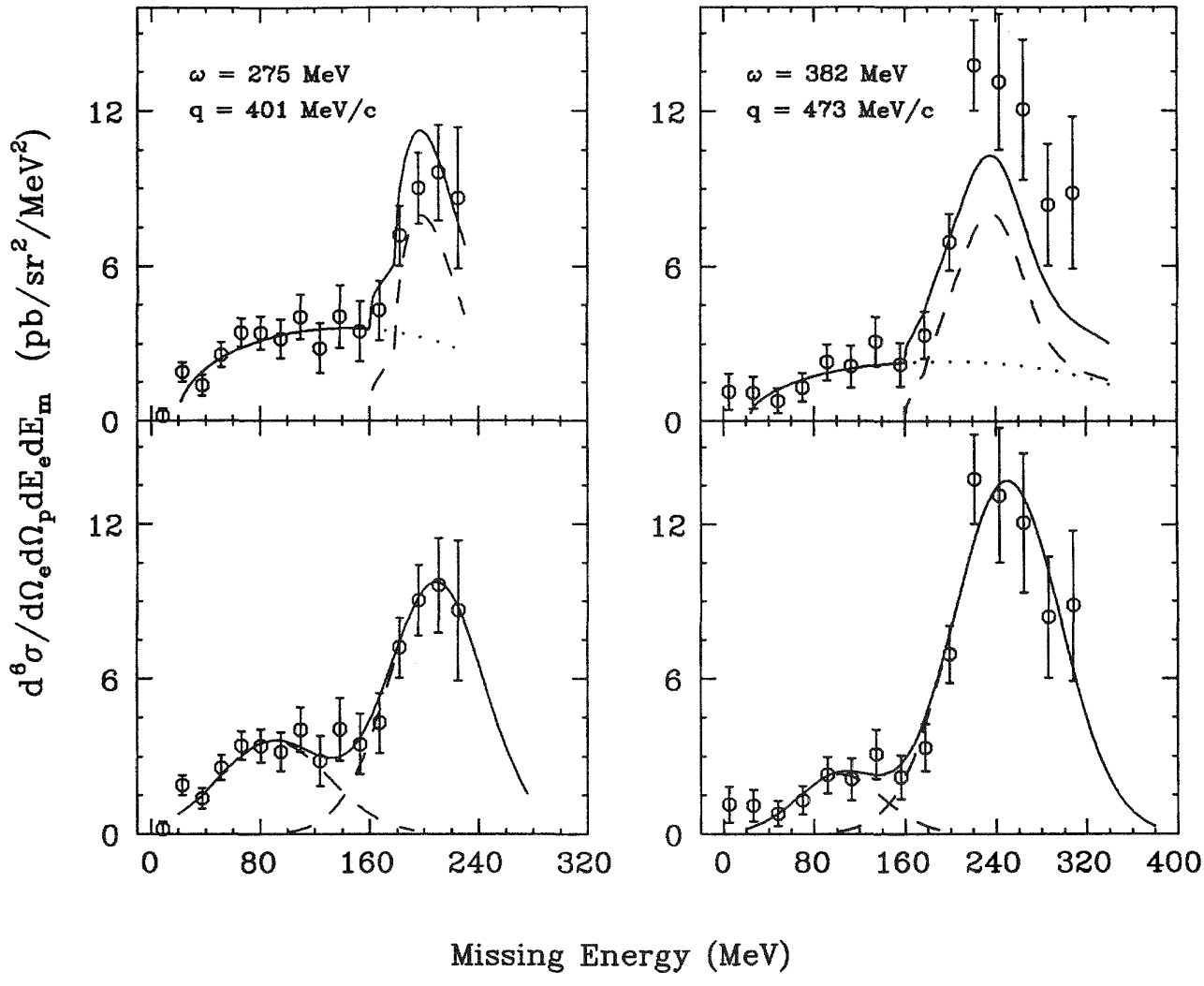

Figure 19. Missing energy spectra obtained in the region of the Δ resonance. Kinematics I (left) corresponds to a point approximately halfway between the dip region and the Δ peak while kinematics II (right) are at the maximum of the peak. In the lower half of the figure the curves are Gaussian fits while the upper half shows the results of a quasifree pion production calculation (dashed) along with the phase space for two nucleon knockout (dotted) and their sum (solid).

The kinematics of the peak at high ϵ_m follows that of quasifree pion production via the Δ resonance:

$$\gamma_v + p \rightarrow \Delta^+ \rightarrow p + \pi^\circ$$

$$\gamma_v + n \rightarrow \Delta^0 \rightarrow p + \pi^-$$

In going from kinematics I to kinematics II, the yield under the Gaussian peak at low ϵ_m follows more closely the decreasing yield of the free deuteron (γ, p) cross section rather than the increasing yield of ^{12}C(e,e′) in the Δ resonance region. Nevertheless, the Δ is known to be an important part of the deuteron

photoproton yield.

These results are very similar to the results of Homma *et al.*[37] and Kanazawa *et al.*[38] using tagged photons in $^{12}C(\gamma, p)$. This is demonstrated in Figure 20 where the results of kinematics II are plotted (with a reversed missing energy scale) along with the results of Homma *et al.*[37] for $E_\gamma = 320$ MeV and $\theta_p = 30°$. In (e,e'p) the higher the missing energy, the lower the final proton energy since ω is fixed and $\epsilon_m = \omega - T_p$. These authors have shown that the peak at high proton momentum has the kinematic behavior of direct knockout of a correlated nucleon pair. As a function of E_γ the yield follows (γ,p) from the deuteron. The yield of the peak at lower proton momentum follows the behavior of Δ-dominated quasifree pion production.

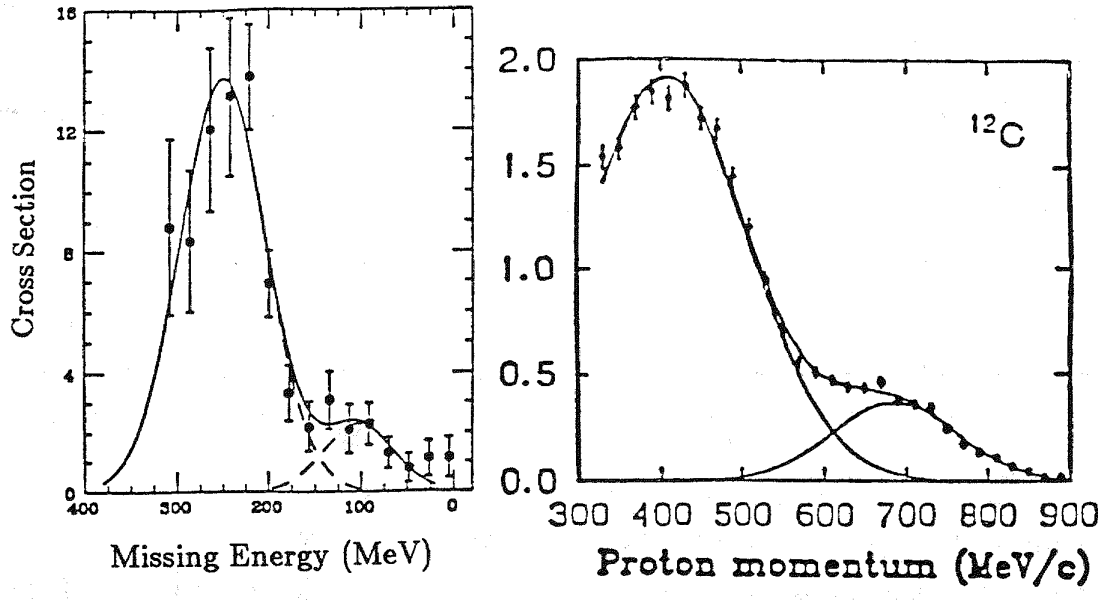

Figure 20. Comaparision of ^{12}C(e,e'p) (left) and $^{12}C(\gamma, p)$ (right) spectra in the Δ-resonance region.

In Figure 21 we reproduce a figure from Kanazawa *et al.*[38] that gives the detailed breakdown of the partial reactions that lead to $^{9}Be(\gamma,p)X$ with $E_\gamma =$ 320 MeV. They were determined by coincidence studies of $(\gamma, p\gamma)$, $(\gamma, p\pi)$, (γ, pn) and (γ, pp). One can see that (γ, pn) dominates the character of the small peak

we have come to call the quasideuteron or two nucleon peak. The large peak we associate with Δ production and pion emission indeed results predominantly in p-π pairs. In Figure 21 the same reactions are also shown with the deuteron as a target.

In the upper half of Figure 19, the MIT–Bates data for the two kinematics are compared with a calculation[36] assuming quasifree delta production. That is, we assume

$$\sigma(e,e'p) = K\sigma'_{eN}S(\vec{p}_i,\epsilon_m)$$

where K is a kinematic factor and σ'_{eN} is derived from the free nucleon processes:

$$\gamma_v + p \rightarrow p + \pi^\circ$$

$$\gamma_v + n \rightarrow p + \pi^-$$

assuming only the M1 Δ amplitude. $S(\vec{p}_i,\epsilon_m)$, the p-shell and s-shell spectral functions, use harmonic oscillator momentum distributions and δ-functions in missing energy located at the centroids of the two shell energies. All of the relevant transformations of electromagnetic amplitudes to moving nucleon frames and back to the laboratory were made. The results are shown by the dashed curves. They are considerably below the experimental yields. Although the Born terms and the E2 and other contributions to the Δ are neglected, these contributions roughly cancel the effect of neglecting final state proton absorbtion which is about 30-40%. A reasonable conclusion is that there is an additional process in the pion production region.

Perhaps a hint comes from the ^{9}Be(γ,pn) yield in Figure 21. Rather than limit the (γ,np) process to the region defined by the smaller Gaussian peak in Figure 19 one might consider a three-body phase space distribution scaled to the two-nucleon (plus residual nucleus) data. This assumption gives a yield extending under the Δ peak and the solid line in Figure 19 shows a better fit to the data although the experimental yield in kinematics II remains larger than our M1-only assumption. Clearly there is room for much more detailed experimental and theoretical work.

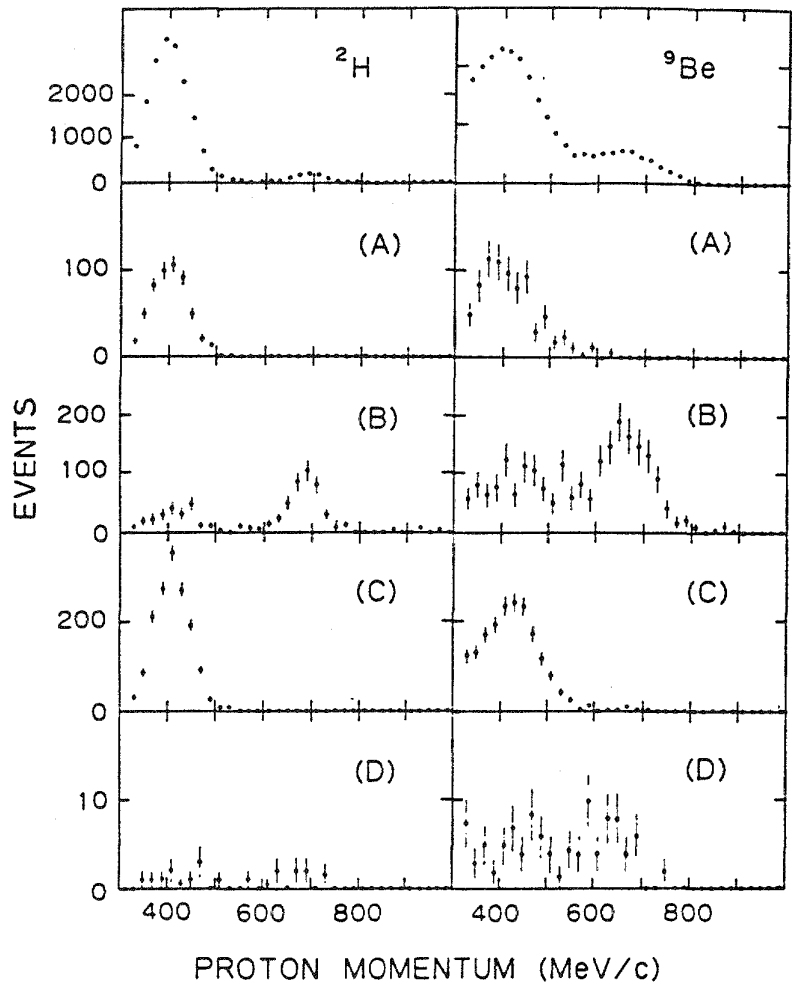

Figure 21. Tagged photon coincidence studies on ^{9}Be (right) and the deuteron (left). From top to bottom, the reactions are $(\gamma,p),(\gamma,p\gamma),(\gamma,pn),(\gamma,p\pi)$ and (γ,pp).

IV. Some Experimental Requirements

In this part of the presentation we take the opportunity to comment briefly on some of the aspects of accelerator and spectrometer precision and resolution that are important to an (e,e'p) program. We take this opportunity in part because we are somewhat alarmed by the extreme need for care that has surfaced in some of our plans at MIT for ^{2}D(e,e'p), in part because of our recognition of the error sources in longitudinal/transverse separations we have performed and in part because we have become concerned with the view projected in casual but important discussions that resolution is only needed at the lower energies of CEBAF. We hope to stimulate more discussion and, if necessary, a revised performance critera for the instruments.

We mentioned earlier the examples of experiments dealing with the longitudinal-transverse momentum structure of $p_{1/2}$- and $p_{3/2}$-hole states and the unnatural parity states in the spectrum dealing with two nucleon correlations. An important condition for a broad kinematic program is scanning the low-ω side of the quasielastic peak. This choice should alter as much as possible some of the two nucleon processes we have discussed earlier and that are apparent on the high-ω side of the quasielastic peak. We consider the spectral function at an initial momentum -600 MeV/c to study. This is a high momentum compared to our present limits (300 MeV/c) but it might be attainable depending on the real dynamical situation in nuclei. It is not out of bounds even for some mean field models. One map would involve varying the momentum transfer to change the final proton energy from 100 MeV to 800 MeV – the dynamical range we know well from experiments at Indiana and Los Alamos. The final proton is in parallel kinematics to limit the cross section to transverse and longitudinal components. From the point of view of ^{12}C, ^{16}O and a few other nuclei where the reaction leads to nuclei whose density of states is not too large, an energy resolution in missing energy of about 100 KeV is necessary. In Table 2 we show the incident electron energy required for two scattering angles (20° and 45°) for each proton energy and the longitudinal polarization of the virtual photon. One should remember, in particular, that transverse structure functions beome dominant at high momentum transfers and that the longitudinal world is highly compressed into small angles. It is clear that the high resolution is needed at the highest energies possible with CEBAF.

Turing to the question of our ability to define the initial proton momentum, we examine first the sensitivity to the definition of electron scattering angle. In any longitudinal/transverse separation we must control the values of $|\vec{p}_i|$ since $|\Phi(\vec{p}_i)|^2$ changes dramatically in the regions of interest which will generally be far away from the regions where $|\Phi(\vec{p}_i)|^2$ is a maximum. For the conditions mentioned above, $\vec{p}_i = -600$ MeV/c, $T_p = 100$ MeV and $\theta_e = 20°$ we find that:

$$\frac{1}{|\vec{p}_i|}\frac{d|\vec{p}_i|}{d\theta_e} = 51\,\mathrm{MeV/c/degree}$$

Combining this with the variation:

$$\frac{1}{|\Phi(\vec{p}_i)|^2}\frac{d|\Phi(\vec{p}_i)|^2}{d|\vec{p}_i|} \approx -8\%/\mathrm{MeV/c}$$

T_p (MeV)	$\|\vec{q}\|$ (GeV/c)	E_0 ($\theta_e = 20°$) (GeV)	ϵ ($\theta_e = 20°$)	E_0 ($\theta_e = 45°$) (GeV)	ϵ ($\theta_e = 45°$)
100	1.044	3.051	0.941	1.423	0.741
200	1.244	3.638	0.939	1.719	0.738
300	1.408	4.109	0.938	1.962	0.733
400	1.554	4.519	0.937	2.179	0.730
500	1.690	4.891	0.935	2.379	0.724
600	1.819	5.235	0.934	2.567	0.719
800	2.063	5.866	0.931	2.918	0.709

Table 2. Incident energy, momentum transfer and longitudinal polarization (at electron scattering angles $\theta_e = 20°$ and $45°$) required for ^{12}C(e,e'p) with $\vec{p}_m = -600$ MeV/c at various outgoing proton energies.

we find that the cross section is expected to vary by about 50%/mrad. This makes it vital to be in control of θ_e to the level of 0.1 mrad if we expect to produce a cross section at $\theta_e = 20°$ that is accurate to 5%. We neglect the additional variation of σ_{ep} with θ_e which further exacerbates the problem.

Consider combining a measurement at $\theta_e = 20°$ with a measurement at $\theta_e = 90°$ and assume that

$$\frac{R_L}{R_T} = \frac{G_E^2}{G_M^2}\frac{2m^2|\vec{q}|^2}{q_\mu^4} = 0.21$$

At 90° the longitudinal polarization $\epsilon = 0.33$. For a 5% measurement of σ at each angle we find $\Delta R_L/R_L = 35\%$ and $\Delta R_T/R_T = 9.5\%$. In other words, an L/T separation which is crucial to our understanding of (e,e'p) currents, at these modest accuracies requires a resolution in θ_e of 0.1 mrad.

One might argue that one can use much worse angular resolution and average over an acceptance. Then only the centroid must be known with this accuracy. However, this is only possible when cross section variations are linear or the same at both angles. This is hardly something we can plan on. Measuring θ_e to 0.1 mrad is possible within the limits of multiple scattering and feasible with point-to-parallel optics and we should do all we can to approach this capability.

When (e,e'p) measurements are performed at other than parallel kinematics, two more response functions are measurable: f_{TT}, the transverse-transverse

interference term and f_{LT}, the longitudinal-transverse interference term. These depend on $|\vec{q}|$, ω, T_P and θ_p; θ_p is the angle of the proton momentum relative to $\vec{q}$. In the cross section f_{TL} is modulated by $\cos\phi$, where ϕ is the angle of the plane $(\vec{q},\vec{p}_f)$ relative to the (e,e') scattering plane; f_{TT} is modulated by $\cos 2\phi$. A measure of f_{TT} thus requires hadron detection out of the (e,e') plane, with at least three values of ϕ. We have begun to plan a measurement of f_{TT} in ^{2}D(e,e'p) with $\theta_e = 22.5°$, $E_0 = 800$ MeV and $\omega = 167$ MeV.[39] At these kinematics, Fabian and Arenhövel[40] predict that f_{TT} is very sensitive to meson exchange currents and isobar configurations as we can see from Figure 22 reproduced from their work. Note that f_{1-1} in this figure is f_{TT} in our notation. We discuss the experiment for $\theta_p = 42.5°$, corresponding to $\theta_{np}^{cm} = 60°$, $|\vec{p}_i| = 320$ MeV/c and $|\vec{p}_f| = 472.3$ MeV/c. σ_{TT} is about 30% of σ_T or σ_L. As a result, there is a large magnification of the error in f_{-11} compared to the error in the cross sections at each of three values of $\phi(90°, 135°, 180°)$. This is shown in Figure 23 by the solid curve. Notice that a set of 1% measurements result in a 20% determination of f_{-11}. The dashed curve is for $\theta_p = 66.3°(\theta_{np}^{cm} = 90°)$ and in this case a set of 1% measurements results in a 10% error. We point out that this is a favorable case since in other nuclear situations f_{TT} is much smaller than f_L or f_T.

If we try to do this experiment with one hadron spectrometer we must keep many things constant as we vary ϕ. The sensitivity of the cross section to E_0 and to ω is about 8%/MeV and 5%/MeV respectively. Thus a 1% measurement of the cross section at each ϕ requires

$$\Delta E_0 \approx \Delta\omega \approx 100\,\mathrm{KeV}$$

As the incident energy grows, these requirements generally are about the same or become worse as we sample regions farther away from the quasielastic peak.

The important message is that high resolution is important not only to isolate discrete states, it is important in the continuum in order to define the dynamics of the problem under study. The physics we will be studying will generally be far from the quasielastic peak region and cross sections will vary very rapidly. The unique contributions of CEBAF to this field will most certainly come not only from the 100% duty ratio but also from the high resolution of the energy of the beam and the high energy resolution of its spectrometers at the highest energies.

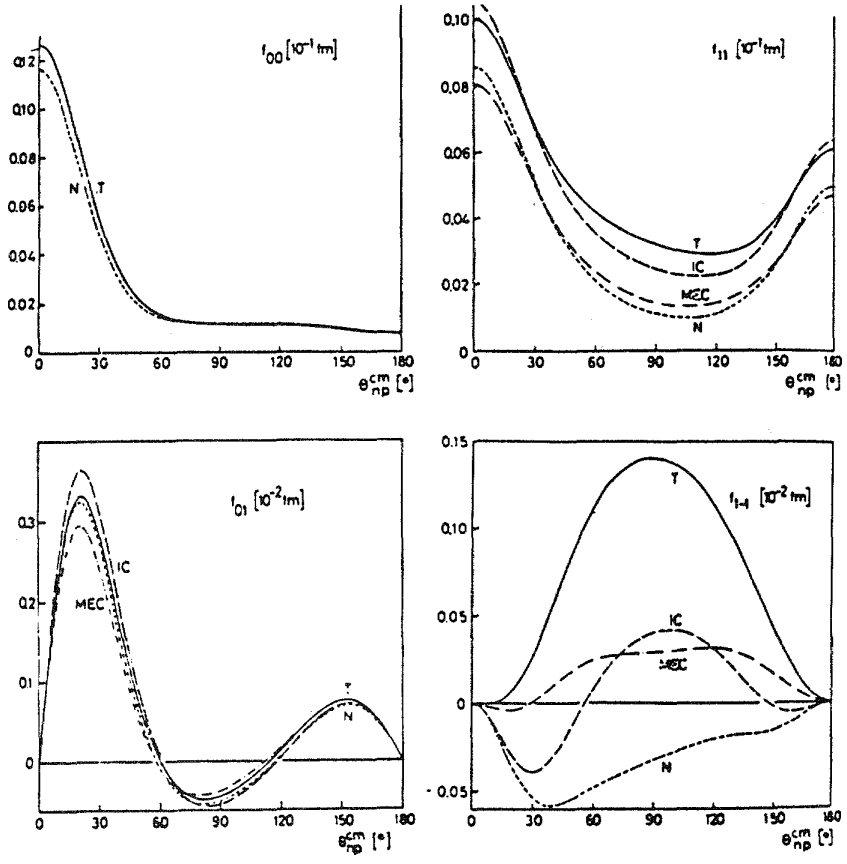

Figure 22. The (e,e'p) structure functions of the deuteron calculated by Fabian and Arenhövel. The curves show the nucleon-only (short dashes), nucleon+meson exchange currents (long dashes), nucleon+isobar configurations (dot-dashed) and nucleon+MEC+IC (solid).

Using three proton spectrometers at different ϕ's to simultaneously sample the (e,e') kinematics, some relaxation of these conditions is possible but generally we always require excellent electron energy resolution. For the proton spectrometers, the energy resolution for these continuum studies depends on the dynamical situation. However, the general condition is set by the variation of $|\Phi(\vec{p}_i)|^2$ which we expect to be about 8%/MeV/c.

Before leaving this subject, it is important to mention (e,e'2N) reactions. Often these are discussed as not requiring much in the way of electron or proton energy resolution. This can only be true for the most crude of surveys. Any experiment requiring a L/T separation or any experiment sensitive to the relative momenta will naturally require the same order of precision that we have discussed above. For this reason, one must look to Hall A as the location where at least two hadron spectrometers will eventually be located. This will occur sooner, rather than later, since this is the hall where the best resolution devices will reside and

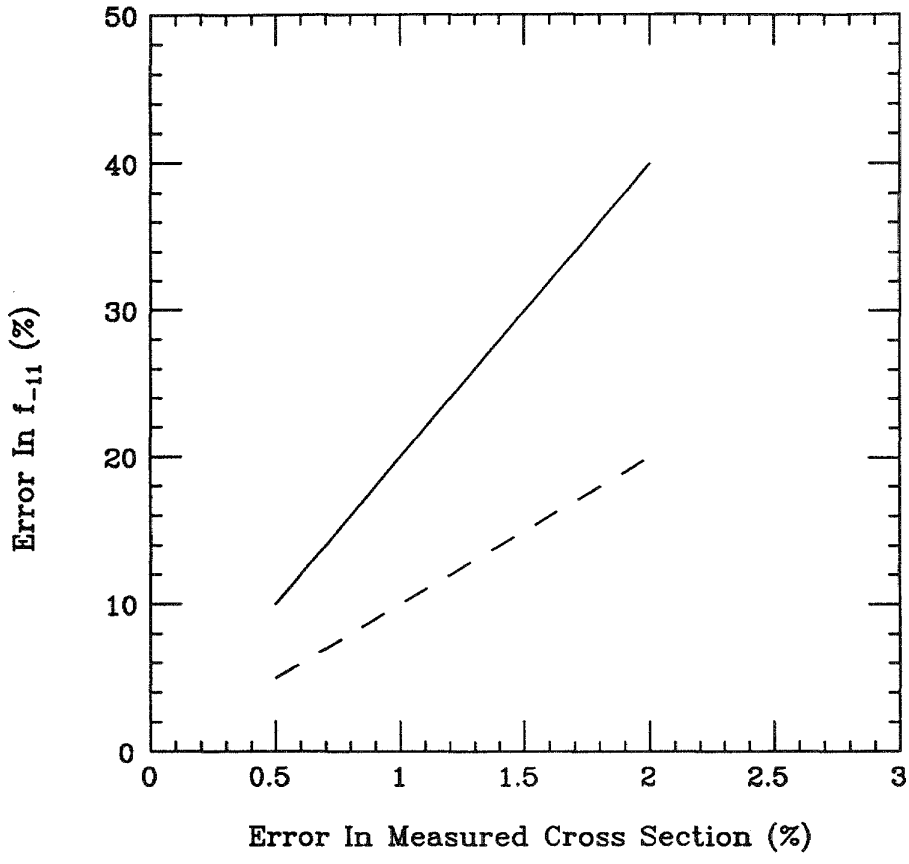

Figure 23. Error in f_{-11} vs. the error in the cross section measurements. The solid (dashed) curve is for $\theta_{np}^{cm} = 60°$ ($\theta_{np}^{cm} = 90°$).

which will be essential to quality (e,e'2N) studies. We suggest that this idea be carefully factored into our planning of all the features in this hall.

V. Concluding Comments

We have observed that the study of nuclei via the (e,e'p) reaction is a rich one. The concept of a system of quasifree nucleons in a mean field is a good starting point for some of our phenomenology, but we observe the strong influence of additional currents resulting specifically from two-body interactions and perhaps more complex many-body phenomena. We observe these influences in high resolution work involving individual states and we observe them in the deep continuum with excitation of hundreds of MeV. The (e,e'p) reaction connects the electromagnetic study directly with the work of our colleagues using hadronic probes and enlarges the scope of investigation to encompass the nature of continuum nucleon-nucleon interactions deep in the nuclear interior. Compared

to (e,e′) involving discrete states, the interpretation of data is more complex because more features of the hadronic system are involved. Nevertheless, the well-understood nature of the electromagnetic probe and its selectivity remains demonstratably available to us. Thus it gives great advantage to our efforts to study new phenomena and to provide the data that will guide the development of more quantitative general frameworks for understanding nuclei beyond our inadequate mean field ideas. No single experiment can do the job. Rather, broad systematic studies are required to demonstrate the adequacy of formalisms and generality of concepts under a variety of dynamical conditions.

References

[1] S. Auffret *et al.*, Phys. Rev. Lett. **55**, 1362, (1985).

[2] J. M. Cavedon *et al.*, Phys. Rev. Lett. **49**, 986 (1982).

[3] F. P. Juster *et al.*, Phys. Rev. Lett. **55**, 2261 (1985).

[4] S. Frullani and J. Mougey, *Advances in Nuclear Physics*, Vol. 14, Ed. J. W. Negele and E. Vogt, Plenum, (1984).

[5] J. M. Cavedon *et al.*, Phys. Rev. Lett. **49**, 978 (1982).

[6] C. E. Hyde-Wright *et al.*, Phys. Rev. **C35**, 880 (1987).

[7] C. D. Goodman *et al.*, Phys. Rev. Lett. **44**, 1755 (1980).

[8] A. Bohr and B. Mottelson, Phys. Lett. **100B**, 10, (1981).

[9] G. Jacob and Th. A. J. Maris, Nucl. Phys. **31**, 139 (1962).

[10] U. Amaldi *et al.*, Phys. Rev. Lett. **13**, 341 (1964).

[11] J. Mougey *et al.*, Nucl. Phys. **A262**, 461 (1976).

[12] G. van der Steenhoven *et al.*, Phys. Lett. **156B**, 151 (1985).

[13] G. van der Steenhoven *et al.*, Phys. Rev. **C32**, 1787 (1985.)

[14] J. W. A. Den Herder *et al.*, Phys. Lett. **184B**, 11 (1987).

[15] J. W. A. Den Herder *et al.*, Phys. Lett. **161B**, 65 (1985).

[16] H. V. von Geramb, F. A. Brieva and J. R. Rook, *Microscopic Optical Potentials*, ed. H. V. von Geramb, Springer-Verlag, Berlin (1979).

[17] W. G. Love *et al.*, Phys. Lett. **73B**, 277 (1979).

[18] W. Bertozzi and J. J. Kelly, Proc. Conf. on *New Horizons in Electomagnetic Physics*, ed. J. V. Noble and R. R. Whitney (1982).

[19] B. C. Clark *et al.*, Phys. Rev. Lett. **50**, 1644 (1983).

[20] J. M. Finn, R. W. Lourie and B. H. Cottman, Phys. Rev. **C29**, 2230 (1984).

[21] J. W. Van Orden and T. W. Donnelly, Ann. of Phys. **132**, 4 (1981.)

[22] J. M. Laget, *From Collective States to Quarks in Nuclei*, Lecture Notes in Physics, vol. 137, ed. by H. Arenhövel and A. M. Sarais, Springer, Berlin (1981).

[23] J. V. Noble, Phys. Rev. Lett. **46**, 412 (1981).

[24] L. S. Celenza *et al.*, Phys. Rev. **C31**, 946 (1985).

[25] J. S. O'Connell *et al.*, Phys. Rev. Lett. **53**, 1627 (1984).

[26] R. R. Whitney *et al.*, Phys. Rev. **C9**, 2230 (1974).

[27] P. E. Ulmer *et al.*, MIT Ph.D Thesis (1987) and Submitted to Phys. Rev. Lett.

[28] G. van der Steenhoven *et al.*, Phys. Rev. Lett. **58**, 1727 (1987); G. van der Steenhoven *et al.*, Phys. Rev. Lett. **57**, 182 (1986).

[29] T. D. Cohen, J. W. Van Orden and A. Picklesimer, U. Md. Preprint 87–255.

[30] D. Reffay-Pikeroen *et al.*, Report DPh-N/Sacaly **2424**, (1987).

[31] D. J. S. Findlay *et al.*, Phys. Lett. **74B**, 305 (1978).

[32] T. DeForest Jr., Nucl. Phys. **A392**, 232 (1983).

[33] K. C. Stanfield *et al.*, Phys. Rev. **C3**, 1448 (1971).

[34] R.W. Lourie *et al.*, Phys. Rev. Lett. **56**, 2364 (1986).

[35] J. Morgenstern, Proc. of the Fourth Miniconference, NIKHEF-K (1985).

[36] H. Baghaei *et al.*, MIT Ph.D. Thesis (1987) and To be submitted to Phys. Rev. Lett.

[37] S. Homma *et al.*, Phys. Rev. **C27**, 31 (1983).

[38] M. Kanazawa *et al.*, Phys. Rev. **C35**, 1828 (1987).

[39] We acknowledge the efforts of Dr. W. Boeglin in this regard.

[40] W. Fabian and H. Arenhövel, Nucl. Phys. **A314**, 253 (1979).

MEDIUM EFFECTS IN INELASTIC ELECTRON SCATTERING ON THE A=3 SYSTEM

J. A. Tjon and E. van Meijgaard
Institute for Theoretical Physics, P.O. Box 80.006
3508 TA Utrecht, The Netherlands

ABSTRACT

Work in progress on electrodisintegration of the trinucleon system is reviewed. Final state interaction effects are calculated exactly by solving the Faddeev equations for the continuum state. Comparisons are made for various exclusive two body breakup experiments. The role of FSI contribution is discussed as a possible explanation of the experiments, which have led to the suggested modification of the nucleon properties in a nuclear medium.

INTRODUCTION

The subject of what kind of underlying degrees of freedom are needed for describing the dynamical behaviour of the nucleus at intermediate energy is of considerable interest. For this purpose electron scattering can be an useful tool and such studies may lead to important new insights in the relevant physical processes. Both inclusive and exclusive scattering processes have been studied in recent years for various nuclei. Interesting results have thereby been obtained on y-scaling phenomena and the suggestion of a possible medium modification of the nucleon properties in the nuclear system.

In the above investigations particular attention has been focussed on the few nucleon system in view of the feasibility to obtain in principle exact solutions to the quantum dynamical equations of these systems and consequently have precise predictions available. Here we would like to report on some work[1] in progress on the study of (e,e',N) reactions on the trinucleon system, including the effects of final state interactions (FSI). Theoretically this problem is non trivial, because of the need to compute the continuum wavefunction of the three particle system. In particular, the calculation of the half off shell $3 \rightarrow 3$ scattering is called for in the case of electrodisintegration into the final state of three free nucleons.

In general the (e,e',N) reaction with unpolarized electrons can be characterized kinematically by two planes, one defined by the ingoing and outgoing electrons and the other one defined by the momentum transfer and the knocked out nucleon[2]. In fig. 1 is shown the kinematics of this process, where $\vec{p}_r$ is the recoil momentum of the residual nuclear system. In the case we are interested in the residual system can be either the deuteron or two free nucleons.

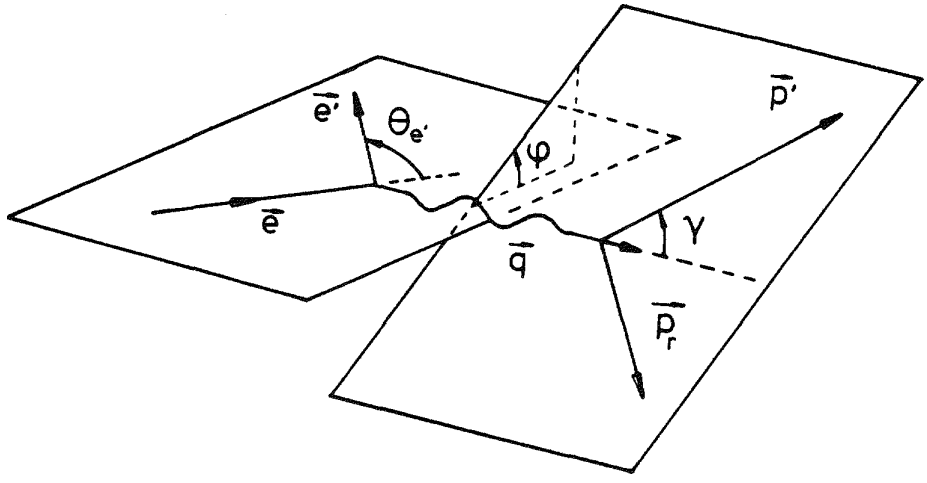

Fig. 1. Kinematics of the (e,e',N) reaction. The knocked out nucleon carries a momentum $\vec{p}'$, while the residual nuclear system has a total momentum $\vec{p}_r$

Relativistic covariance and gauge invariance considerations show that the differential cross section for the coincidence reaction process can be described in terms of four structure functions W_C, W_T, W_I and W_S^3. We have

$$\frac{d^6\sigma}{de'd\Omega_{e'}dE_{p'}d\Omega_p} = k\,\sigma_{Mott}\left[\left(\frac{q^2}{\vec{q}^2}\right)^2 W_C + \left(\frac{q^2}{2\vec{q}^2} + \tan^2\left(\frac{\theta_{e'}}{2}\right)\right) W_T\right. \tag{1}$$

$$\left. + \frac{q^2}{\vec{q}^2}\left(\frac{q^2}{\vec{q}^2} + \tan^2\left(\frac{\theta_{e'}}{2}\right)\right)^{1/2} \cos\phi\, W_I + \left(\frac{q^2}{\vec{q}^2}\cos^2\phi + tg^2\left(\frac{\theta_{e'}}{2}\right)\right) W_S\right]$$

where k is a kinematical factor, $\vec{q} = \vec{e}' - \vec{e}$, $\omega = e' - e$ and $q^2 = \vec{q}^2 - \omega^2$. For the special case of (anti)parallel kinematics, in which the photon and the outgoing nucleon have equal or opposite direction, the reaction process is characterized by only the longitudinal and transversal structure functions W_C and W_T^3.

BORN ANALYSIS

Considering the case of two body breakup and neglecting FSI effects, there are two contributions to the scattering amplitude.

One contribution, shown schematically in fig. 2a, is the coupling of the photon to the nucleon, which is directly knocked out. The other one corresponds to the photon interacting with the pn pair, forming the deuteron in the final state (fig. 2b). In the quasi free region it is usually assumed that the scattering amplitude can be determined in the PWIA approximation, corresponding to diagram 2a. In this approximation we get

$$\frac{d^6\sigma}{de' d\Omega_{e'} dE_{p'} d\Omega_{p}} = p' \; E_{p'} \; \sigma_{eN} \; S_n \; (p_m, E_m) \qquad (2)$$

The differential cross section factorizes into a part σ_{eN} corresponding to the free electron-nucleon scattering and a part S_n which contains the information about the nuclear structure, n being 2 if the residual nuclear system is the deuteron and otherwise 3 for the case of three body breakup. σ_{eN} is in general off the energy shell, since the knocked out nucleon is originally in a bound state. In the calculations we have carried out we have used the prescription as has been suggested by de Forest[4]. It has the advantage of satisfying gauge invariance. In particular the nucleon current operator is taken to be

$$J_{\mu}^{em} = i \; \bar{u}(\vec{p}') \left[\gamma_{\mu} \; F_1(q^2) - \frac{\kappa}{2m} \sigma_{\mu\nu} \; q_{\nu} \; F_2(q^2) \right] u(\vec{p}) \qquad (3)$$

where the off shell dependence of the e.m. nucleon form factors F_n is neglected and the on shell ones are used. In the kinematic

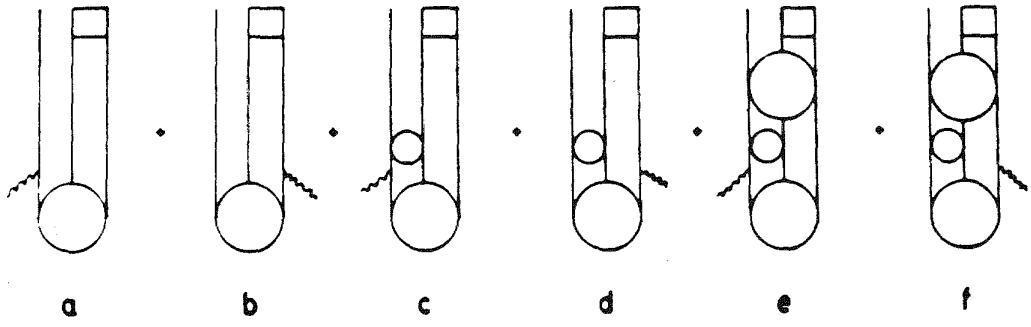

Fig. 2. Diagrammatic representation of the various contributions to the inelastic electron scattering on the A=3 system for the case of two body breakup. Graphs a and b are the Born amplitudes, representing the PWIA and γpn contributions respectively. The lowest order FSI are given by the graphs c and d, being the rescattering contributions, while graphs e and f are the contributions from the (higher order) connected graphs in the FSI.

regions we have studied we did not find substantial differences in the observables when changing from the e.m. dipole form factors[5] to the parameterization of Höhler et. al.[6]. The spectral distribution function S_n represents the probability to remove a nucleon with momentum p_m from the nucleus, leaving the residual nucleus in a state with mass $M_{A-1} = M_A - M + E_m$. In fig. 3 is shown the two body

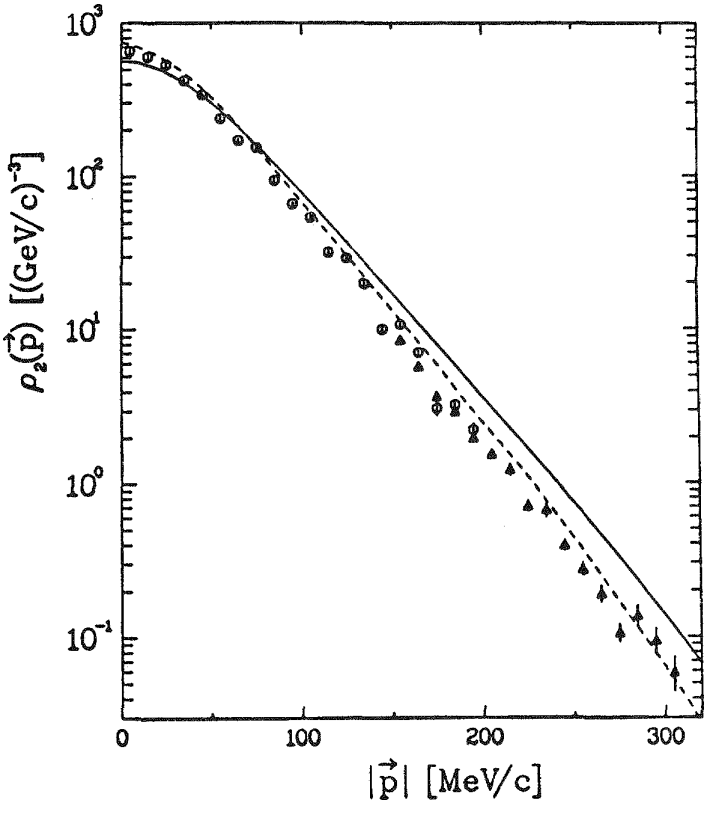

Fig. 3. Two body spectral distribution function for the RSC interaction (dashed curve) as calculated by Laget[14] and the MT I-III s-wave interaction (solid curve).

spectral function S_2, with the residual system being a deuteron, as calculated using the Reid soft core (RSC) interaction and the MT I-III s-wave Yukawa type potentials[7]. Up to a momentum of 320 MeV the spectral functions of these two interactions show a close resemblance, whereas for larger momenta the RSC starts to be considerably higher because of the contribution from the D-state.

In certain kinematic regions, where the missing momentum p_m of the nucleon is large the other Born diagram contribution (fig. 2b) becomes important. This is realized in the NIKHEF experiment. In contrast to the PWIA contribution no factorization of the electron-nucleon cross section and a nuclear structure part takes place. It is rather natural in this case to try a phenomenological approximation[8], where one assumes that a factorization takes place in terms of the e-D cross section. This corresponds to the Ansatz

that the pn pair in the trinucleon system is predominantly forming a deuteron. As is seen from fig. 4, this approximation describes remarkably well the experiment. On the other hand the exact γpn contribution yields a significantly higher prediction, indicating that the continuum contributions of the pn pair cannot simply be neglected. This shows that the success of the phenomenological form may be fortitious. Also is shown the PWIA contribution, which is one order of magnitude smaller.

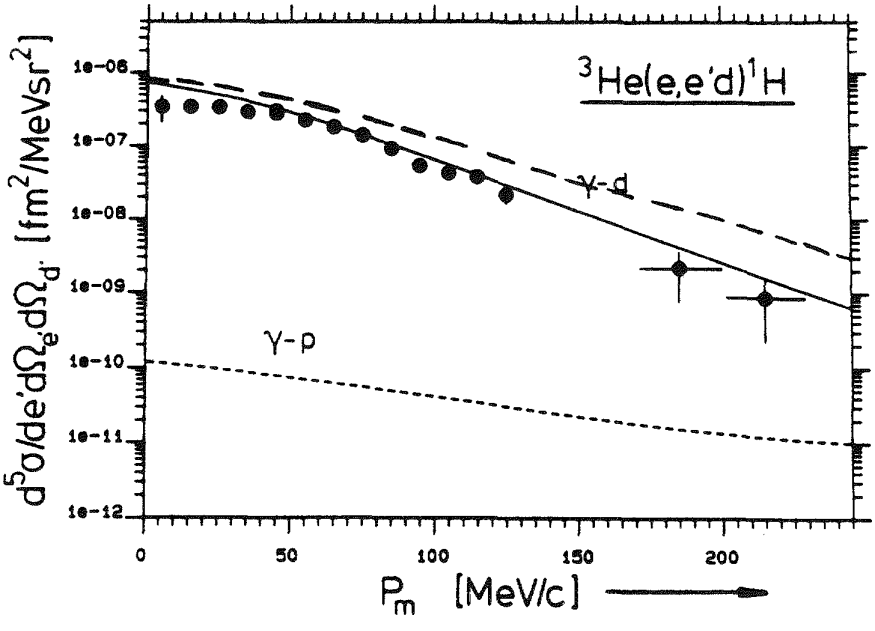

Fig. 4. Deuteron knock out at a fixed momentum transfer q = 380 MeV/c from ref. 18. Solid curve corresponds to the factorized approximation in terms of σ_{eD}, while the long dashed curve corresponds to the γpn graph 2b. The PWIA is given by the short dashed curve.

CONTINUUM FADDEEV CALCULATIONS

We now turn to describing the FSI calculation. To account for the complete FSI contributions we have to consider in addition to the two Born graphs, discussed up to now, the remaining graphs in fig. 2. These graphs consist of all connected graphs, describing the half off shell scattering of three free nucleons in the initial state and a final state with either three free nucleons or a nucleon and deuteron. Since the existing experiments have a moderate proton deuteron cm energy, it is a good approximation to assume non relativistic dynamics. In the calculations we have carried out the NN interaction is taken to be given by central s-wave Yukawa type

potentials in the $^1S_0$ and $^3S_1$ channel[7]. With this interaction the bound state properties of the trinucleon system together with the unpolarized elastic and inelastic scattering data of neutron-deuteron scattering is well described at the corresponding energies.[7,9]

The scattering amplitude needed for the complete FSI calculation can be constructed by solving the Faddeev equations for the continuum states. This is done by first determining the multiple scattering solution and resumming this exactly by Padé approximant techniques. The main problem one encounters in determining multiple scattering graphs is to account properly for the various singularities occuring in the integrals. This specifically applies for the case of the $3 \rightarrow 3$ S-matrix, where the singularity structure is more complex. By calculating the off shell rescattering graph in this case with high precision the Faddeev equations can also be solved in this case. To facilitate the calculations we are making use of separable expansions of the two nucleon T-matrices and partial wave expansions are employed. Typically 10 to 15 partial waves are sufficient in the energy range considered to reconstruct the full three body amplitude.

FSI EFFECTS FOR TWO BODY BREAKUP

In order to check the rather complex calculations, we have studied one specific case, for which a complete continuum calculation already exists. Using a separable Yamaguchi potential and a multipole expansion of the e.m. operator an exact analysis of the FSI has been carried out by Lehman et al.[10] for the kinematics of the Johansson experiment[11]. Our calculation with this potential agrees well with their results. With the MT I-III interaction the calculated cross sections increases significantly, yielding predictions in accordance with the reanalyzed data[12].

Two kinematic regions have been explored recently in some detail experimentally by the SACLAY and NIKHEF groups. In the SACLAY experimental setup[13], the PWIA contribution is dominant and in one case the effects of the D-state in ^3H_e are important. In fig. 5 are shown the results of our calculations, together with those of Laget[14], who carried out an approximate analysis of the FSI based on the rescattering graph of the multiple scattering series. As input of the latter calculation the Faddeev bound state wavefunction for the RSC[15] has been used. From this we see that the PWIA dominates, while the FSI tends to decrease the cross section. This happens in both calculations. The RSC result of Laget agrees well with the experiment, mainly because of its lower PWIA prediction. Since the multiple scattering series is explicitly determined by us by subsequent iterations of the Faddeev equations, it is a natural question to ask how well the series converges. In

particular, is it just possible to account for the FSI by including only the rescattering contribution? From fig. 5 we see that such an approximation is rather poor in describing the FSI, at least in the kinematic region considered. From this we may conclude that in general the continuum wavefunction has to be determined exactly to have a reliable prediction. It should however be noted that the Laget rescattering contribution seems not to be same as the corresponding graph in the multiple scattering solution of the Faddeev equations.

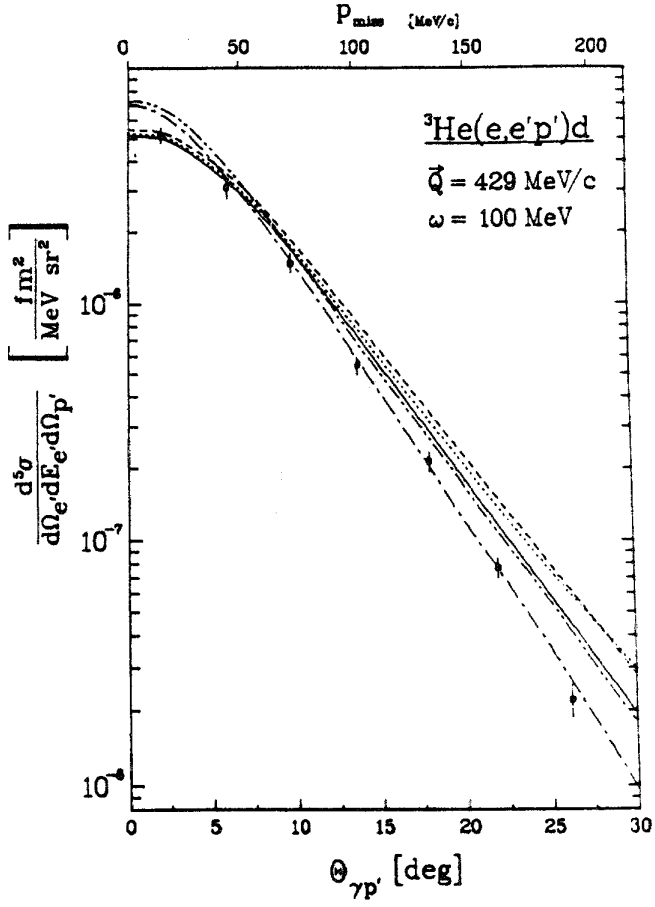

Fig. 5. Coincidence cross section for the MT I-III interaction. The dashed curve corresponds to the PWIA, while the solid curve is including the full FSI. Adding only the rescattering graph contribution to the PWIA graph gives a poor description of The FSI effect (dotted curve). Also are shown the Laget[14] calculations (PWIA -••- and including FSI -•-).

In fig. 6 is shown the SACLAY data obtained for the kinematics where the D-state contribution of the ^3H_e wavefunction plays a crucial role. A pure s-wave calculation as we are carrying out yields considerably lower cross sections. This is a consequence of the kinematics which is arranged in such a way that PWIA is the dominating process. However, since the corresponding missing momenta in this experiment are much greater than 300 MeV, the cross section is almost completely determined by the D-state components of the spectral function. To see this we have carried out a PWIA calculation using the RSC trinucleon boundstate wavefunction as parameterized by Hadjuk et al.[16]. From fig. 6 we indeed see that

good agreement is obtained with the experimental data. This is due to the presence of the D state. Also are shown in the figure the results of Laget[17] using the Paris potential. It should be noted that his estimates of the FSI contributions tend to increase the cross section, opposite to our findings for the s-wave interactions. It should be interesting to see whether this is because of the effects of the D-states.

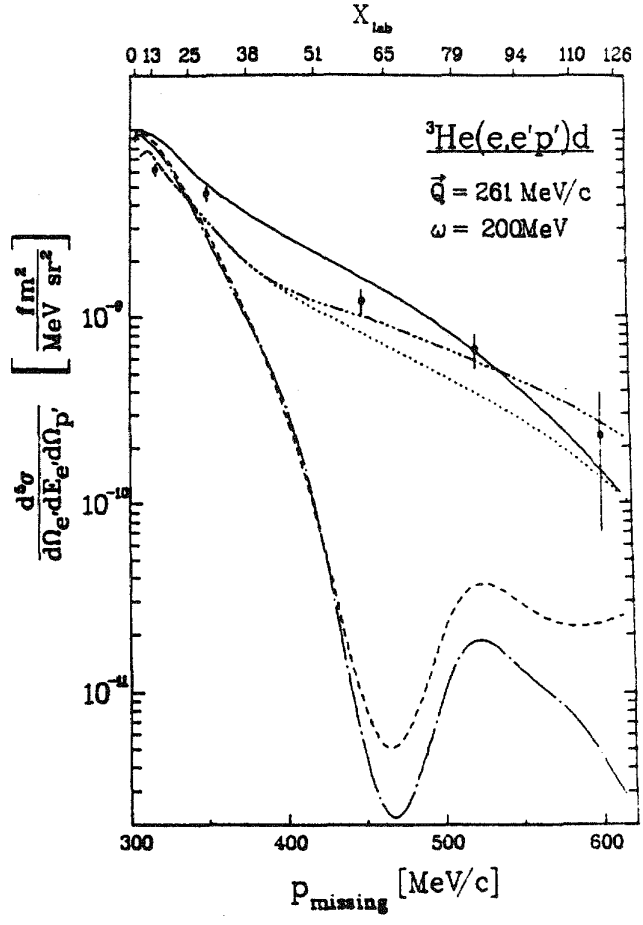

Fig. 6. Coincidence cross section for large missing momentum where D state contributions are important. The s-wave calculations are considerably below the data. Dashed and dashed-dotted curves are the PWIA and including FSI respectively. Also are shown a PWIA calculation with the RSC wavefunction (solid line) and results by Laget[17] for the Paris potential (PWIA ••••, including FSI -••••-). Experimental points are from ref. 13.

The NIKHEF experiments[8,10] are carried out at constant momentum transfer q = 250 MeV/c and energy transfer ν = 113 MeV. A missing momentum interval p_m from 200 MeV/c to 500 MeV/c is scanned varying the angle $\Theta_{\gamma p}$ between the photon and the outgoing nucleon from 0° to 180°. For experimental reasons the low missing momentum data (p_m<350 MeV/c) are taken at the angle ϕ=180°, whereas at high missing momenta the angle ϕ is switched to 0°, thereby remaining in plane. According to eq. (2) this different setting only affects the relative sign in front of the structure function W_I. The results

are summarized in fig. 7. The data set with $p_m < 350$ MeV (open circles) corresponds to the case where the PWIA is large. As can be seen from the figure the PWIA overestimates the cross section considerably. Including the FSI reduces it significantly, resulting in a good agreement with the experimental data except at higher missing momenta. In this region the D-state contribution should start to play a role. As a consequence we expect that the agreement will improve when these contributions are included. For the data set with $p_m > 350$ MeV , corresponding to the (e,e',D) reactions, the γpn graph cannot be neglected, in particular for larger values of the missing momentum p_m. From fig. 7 we see that the Born analysis predicts considerably higher values as compared to the experimental data. Including the FSI leads to a strong cancellation with the

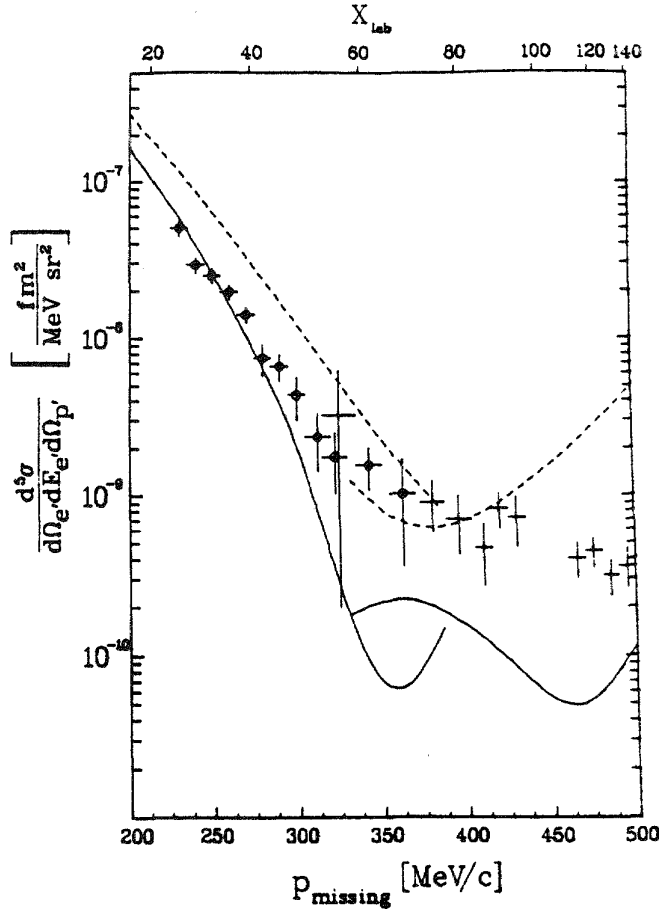

Fig. 7. Coincidence cross section as obtained by the NIKHEF group. Dashed curve is the Born calulation, while the solid curve is with FSI.

Born graphs. As a result the total result for the cross section is very small. In view of this strong cancellation it is expected that the result will be sensitive to other contributions. In particular inclusion of the D-state components will tend to increase the scattering cross section and as a result improve the agreement with the experiments. Also the results may depend strongly on the specific model used for the NN interaction.

PROTON MODIFICATION IN NUCLEAR MEDIUM

Some recent quasi-free (e,e',N) experiments have been carried out at NIKHEF on ^{12}C and ^{6}Li, where a longitudinal/transverse separation has been done[19,20]. Assuming the validity of the impulse approximation, these experiments suggest a significant effect of the nuclear medium on the effective e.m. coupling to the nucleon. The analysis is based on the factorized form as given in eq. (2). The experiments are carried out for so called parallel kinematics i.e. the momentum of the knocked out proton is opposite to the momentum transfer $\vec{q}$. As a consequence only the longitudinal and transverse structure functions contribute. Because of the form as given in eq. (2) all these structure dependence occur in the off shell electron proton cross section which in this case is given by

$$\sigma_{ep} = \sigma_{Mott} \left\{ \epsilon \, |F_L(q^2)|^2 + |F_T(q^2)|^2 \right\} \qquad (4)$$

with $\epsilon = \left[1 + \frac{2\vec{q}^2}{q^2} \tan(\theta_{e'}/2) \right]^{-1}$. By measuring at a forward and backward electron angle information can be obtained about the longitudinal and transverse structure functions F_L and F_T. To remove the dependence on the nuclear spectral function the ratio of reduced cross sections is measured. In fig. 8 are shown the experimental data for the ratio R, defined as

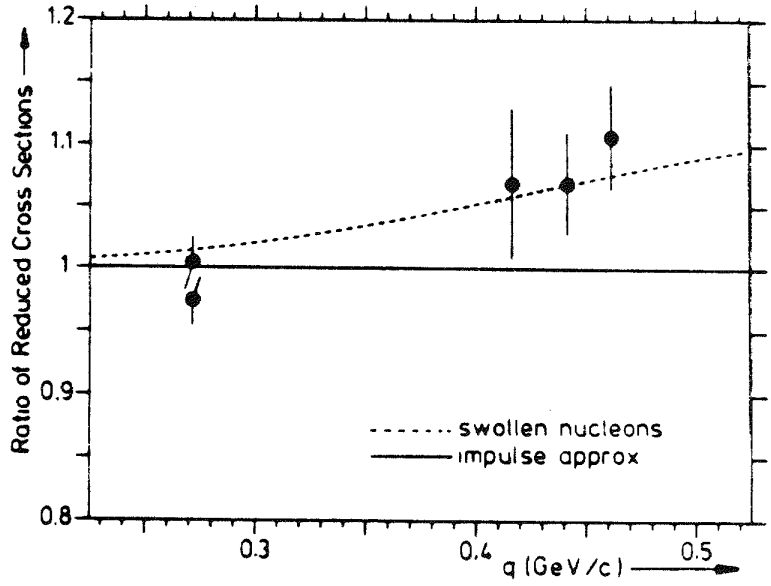

Fig. 8. The measured momentum transfer dependence of the ratio R for the reaction $^{12}C(e,e',p)^{11}B$ from ref. 19.

$$R = \left[\frac{d\sigma(exp)}{d\sigma_{ep}(de\ Forest)}\right]_{backward} / \left[\frac{d\sigma(exp)}{d\sigma_{ep}(de\ Forest)}\right]_{forward} \qquad (4)$$

for the case of ^{12}C. Effects of FSI interaction have been estimated in a DWBA type of model, indicating that the FSI effects would only modify eq. (2) by an additional factor depending only on the relative cm kinetic energy $T_{p,A-1}$ between the knocked out nucleon and the residual nucleus. Since the two electron angles are chosen such that the $T_{p,A-1}$ is the same, this implies that the FSI effects drop out in the ratio R (see however ref. 21).

From the above considerations it is clear, that in order to interpret the NIKHEF experiments in terms of single nucleon properties it is crucial that the electron proton cross section should be factorizable in the coincidence process. Since various assumptions have been made such as for the FSI effects in these measurements, it is worthwhile to study some model system, which is exactly soluble and where these assumptions can be tested. The few nucleon system is an excellent place for this. We have carried out a theoretical analysis in the trinucleon system to study this problem. The results for R are summarized in fig. 9, where a similar kinematic situation has been chosen as studied for the other nuclei. In analogy with the analysis of ref. 19 we may assume that the contributions from the e.m. interaction with the residual nucleus can be neglected. In our case this corresponds to dropping

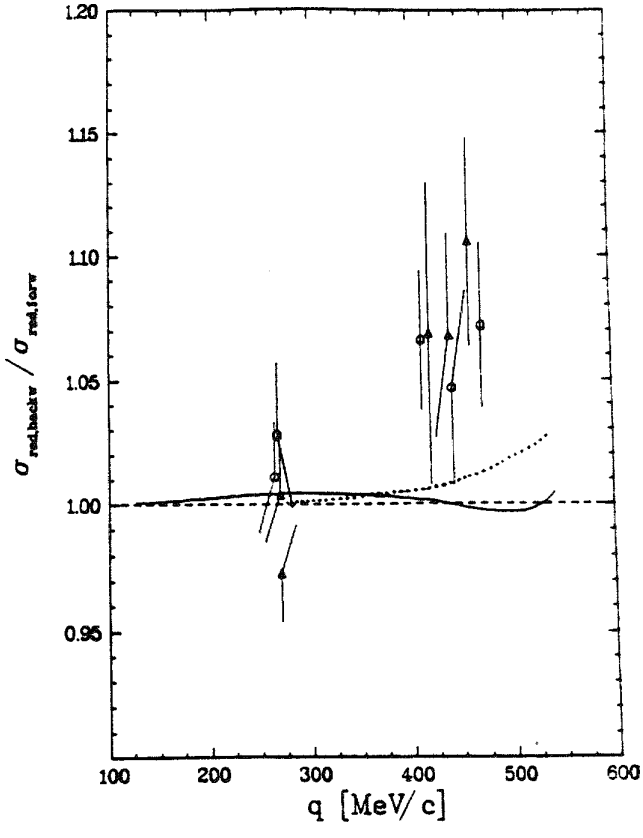

Fig. 9. The calculated ratio R for the case of the A = 3 system. Solid curve corresponds to the inclusion of all FSI contributions, while the dotted curve is obtained by neglecting the γpn type of graphs. Also are plotted the experimental results of refs. 19 and 20 for ^{12}C (o) and ^{6}Li (Δ).

the γpn contribution as given by figs. 2b, 2d and 2f. In doing so we find that the inclusion of the FSI graphs leads to the increase of R when we increase the momentum transfer. Hence, if for some particular reason we may neglect the interaction of the photon with the residual nucleus, the experimental finding of the increase of R could be attributed, at least partially, to FSI effects. It should however be emphasized that this increase cannot simply be interpreted in terms of a single nucleon property. The complete FSI contributions also contain a part coming from the γpn type of graphs. Although the contribution from the γpn Born graph can safely be neglected, the γpn FSI graphs are comparable in size to the results found for the graphs 2c and 2e. Including all the

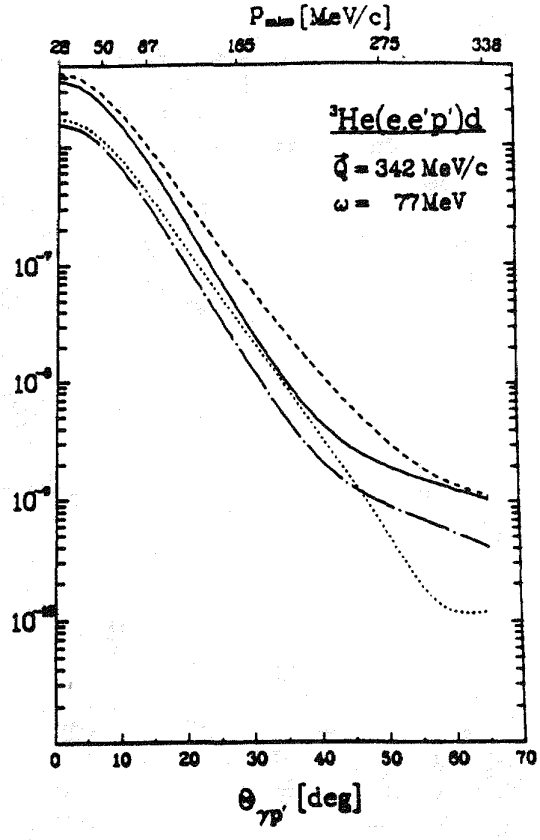

Fig. 10. Longitudinal structure function W_C (PWIA ••• with FSI -•- and transverse structure function W_T (PWIA ---- with FSI ——)

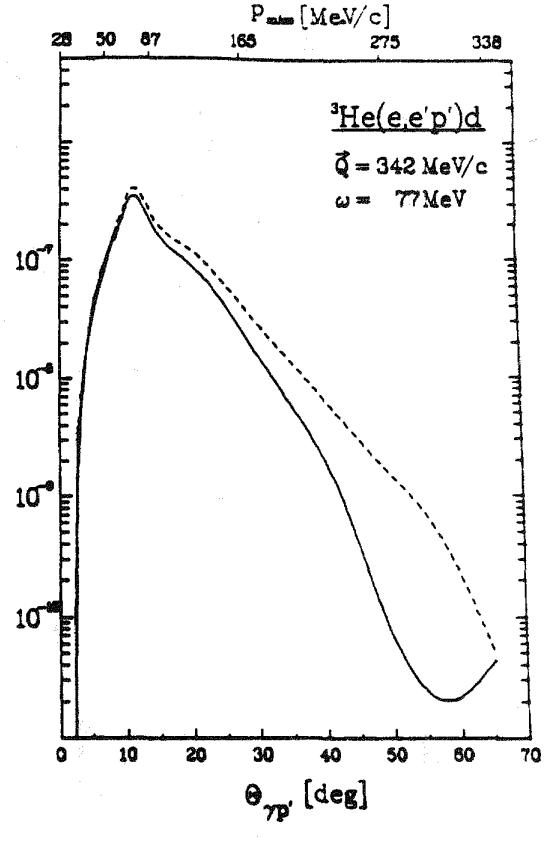

Fig 11. Structure function W_I (PWIA ---- with FSI ——)

FSI graphs lead to a result for R close to one. Hence the two types of FSI contributions tend to cancel each other in the observable R.

As noted before the parallel kinematics can be described by only two structure functions. Since the experiments allow for a certain geometric resolution we may like to see how the various structure functions behave if we allow for a non parallel kinematics. For this purpose we have calculated the dependence of the W's if we change the angle $\Theta_{\gamma p}$ between the knocked out proton and the momentum transfer, but still staying in plane (ϕ =180°). The results are shown in figs. 10 and 11. The fourth structure function W_S is small as compared to W_I and has therefore not been plotted. From the figures we see that W_I increases rapidly from zero when we gradually go away from the parallel kinematics. The three structure functions W_c, W_T and W_I become comparable in size. Moreover, FSI effects become more important in the non parallel direction. It should be interesting to see what actual effects there are on R due to the finite resolution.

CONCLUDING REMARKS

We have studied FSI effects in (e,e',N) reactions in certain kinematic regions for the trinucleon system and have shown that their contributions can be significant. In general however it is not obvious when they may be neglected or not. One possible situation where FSI are expected to be small is when the relative cm kinetic energy T_{pd} of the final state is large. On the other hand there exist some kinematic situations where the FSI is negligible even though T_{pd} is small. A systematic analysis should be interesting to understand this in detail.

Our work has demonstrated that exact dynamical calculations of the electrodisintegration process of the trinucleon system is feasible. Although the actual calculations carried out up to now concern the two body breakup, the three-body breakup process can also be handled if one is careful enough with treating the various singularities. Moreover more realistic NN interactions should be studied. In particular the non s-wave components like the D-states of the nuclear interaction should be included.

Exact dynamical calculations as described here may also serve another useful purpose. They can be used as a tool to study the validity of various approximations normally used in more complex nuclei. In this connection we have discussed the basic assumption of factorization of the electron nucleon scattering cross section used in the interpretation of the modification of the nucleon in the presence of a nuclear medium. At least for the case of the trinucleon system such an approximation can be criticized due to the presence of the FSI. It should be interesting to carry out a similar experiment for the trinucleon system as for ^{12}C and ^{6}Li.

In most (e,e',N) experiments carried out up to date the role of special relativity has been rather limited in estimating FSI effects

since the relative cm kinetic energies of the final states were of the order of 100 MeV. With possible future experiments at CEBAF it is clear that a relativistic dynamical treatment will become necessary.

REFERENCES

1. E. van Meijgaard and J.A. Tjon, Phys. Rev. Lett. 57, 3011 (1986).
2. S. Frullani and J. Mougey, Adv. Nucl. Phys. 14, 1 (1984).
3. T. de Forest, Jr., Ann. of Phys. 45, 365 (1967).
4. T. de Forest, Jr., Nucl. Phys. A392, 232 (1983).
5. T. Janssens et. al., Phys. Rev. 142, 922 (1966).
6. G. Höhler et. al., Nucl. Phys. B114, 505 (1976).
7. R. Malfliet and J.A. Tjon, Nucl. Phys. A127, 161 (1969).
8. P.H.M. Keizer et. al., Phys. Lett. 157B, 255 (1985), and to be published.
9. W.M. Kloet and J.A. Tjon, Ann. of Phys. 79, 407 (1973).
10. D.R. Lehman, Phys. Rev. C3, 1827 (1971); C. R. Heimbach et al., Phys. Lett. 66B, 1 (1977).
11. A. Johansson, Phys. Rev. 136, B1030 (1964).
12. B.F. Gibson an G.B. West, Nucl. Phys. B1, 349 (1967).
13. E. Jans et. al., Phys. Rev. Lett. 49, 974 (1982); J. Morgenstern, private communication.
14. J.M. Laget, Phys. Lett. 151B, 325 (1985).
15. H. Meier-Hadjuk et. al., Nucl. Phys. A395, 332 (1983).
16. Ch. Hadjuk et. al., Nucl. Phys. A337, 13 (1980).
17. J.M. Laget, SACLAY preprint (1987).
18. P. Keizer, Ph-D thesis, University of Amsterdam (1986).
19. G. van der Steenhoven et. al., Phys. Rev. Lett. 57, 182 (1986); ibid 58, 1727 (1987).
20. G. van der Steenhoven, Proc. CEBAF workshop (1986).
21. T.D. Cohen et. al., Maryland preprint (1987).

BARYON-BARYON INTERACTIONS IN THE QUARK CLUSTER MODEL

Makoto Oka

Department of Physics, University of Pennsylvania
Philadelphia, PA 19104

ABSTRACT

Quark cluster model approach to baryon-baryon interactions is reviewed. Emphasis is put upon a string model of quark confinement and its application to two-baryon systems. Results of the quark cluster model calculation for various baryon-baryon interactions are summarized. Roles of quark substructure of the nucleon in nuclei are also discussed.

INTRODUCTION

Strong interactions among hadrons are to be described by quantum chromodynamics (QCD) according to the standard model. Mesons and baryons are composite particles of quarks and gluons. An important feature of QCD is that the quark-gluon interaction varies with the momentum transfer q involved in the process. In high q the coupling is weak enough to allow perturbative calculations and there the (perturbative) QCD has been well confirmed by experiment. The low q behavior of QCD, however, is not yet very well understood, because the interaction is so strong that the perturbation is not applicable any more. Nonperturbative interaction is supposed to confine quarks and gluons in a small domain (≤ 1 fm), but mechanism of the confinement is not clear yet. Numerical simulations of discretized (lattice) QCD are available but still far from describing dynamical features of the confinement in multihadron systems. We are forced to model the confinement at this moment.

The nucleus is a unique existence in exploring the low energy QCD. The characteristic scale of the nuclear dynamics is the Fermi momentum, $k_F \simeq 0.25$ GeV, which is much lower than the scale of the perturbative QCD, but is comparable to the confinement scale ($\approx 0.2 - 0.4$ GeV). We may then expect interference between the nuclear dynamics and the quark confinement. In nuclear matter, the interaction with the nuclear medium may modify nucleon properties. In the lepton inclusive reactions from nuclei the EMC effect surprised us showing deviation of the structure functions from that of the free nucleon. The quark-gluon substructure may reveal the mechanism of the nucleon modification.

In few-nucleon systems, the nucleon substructure may play a major role at short distances. The size of the nucleon is larger than the range of the short-distance NN repulsion and of the same order as the range of the two-pion exchange, which is most responsible for the nuclear binding. It is therefore

not surprising that the conventional "nucleon-meson" picture of the nucleus is modified by the quark-gluon substructure of the nucleon. Nucleon-nucleon interaction has been studied in this context in many different ways.[1-8] In this report, we review recent attempts to understanding the baryon-baryon interactions based on the quark model. A potential quark model with the nonrelativistic kinematics is employed because it is quite successful in the study of hadron spectroscopy. Key ingredients of the model are (1) a quark confinement force and (2) a short-range color-magnetic interaction. The former sets the scale of the problem; especially the size of the baryon is determined by the balance of the quark kinetic energy and the confinement. In the next section, we discuss the quark confinement in detail, emphasizing its application to multi-hadron systems. The color-magnetic interaction is known to play an important role in the meson and baryon spectroscopy. This interaction, for instance, breaks the $SU(6)$ spin-flavor symmetry, and therefore explains the $N - \Delta$ mass difference. It also induces a mixed symmetry state in the nucleon, which explains the (negative) charge square radius of the neutron.

QUARK CONFINEMENT

A. From QCD to string

Quantum chromodynamics (QCD) is a gauge field theory for three colored quarks and eight colored gluons. Although QCD is analogous to quantum electrodynamics (QED), extra coupling among gluons gives the theory two important features, asymptotic freedom and color confinement. The asymptotic freedom makes perturbative calculations possible for high q (hard) processes, while our understanding is still limited on the confinement, which may be important in low energy processes. One of our goals is to seek a realistic model of the confinement which can be applied in multi-hadron systems. It should be stressed that the hadron spectroscopy is not sensitive enough to distinguish different confinement models, because most single-hadron observables are sensitive only on the overall size of the hadron but not on dynamical properties of the confinement.

When the $q-\bar{q}$ distance R is small in a meson system, the color confinement volume, or the bag, will be approximately spherical and the color-electric field around the quarks be analogous to the electric field around an $e^+ - e^-$ system. Energy of the system is then given by $E \approx -1/R$. Difference from QED will be seen at a large R, when due to the color confinement the color electric field is squeezed to a flux tube and forms a stretched bag. If R is so large that the cross section of the flux tube is about a constant, then the energy is given by $E \approx \sigma R$. This qualitative argument motivates string or flux-tube confinement models, where quarks are confined permanently in a linear rising potential, $V(R) = \sigma R$. The string tention σ can be determined so as to reproduce the high spin meson spectrum or the slope of the Regge trajectory, *i.e.* $\sigma \approx 1$ GeV/fm.

The string confinement is also "derived" by studying the strong coupling limit of lattice QCD (LQCD). The LQCD hamiltonian for the gluon gauge field is given by

$$\begin{aligned} H &= (g^2/2a)\sum (E_i^a)^2 \qquad \text{(electric)} \\ &\quad -(1/4ag^2)\sum \mathrm{Tr}[U_\mu U_\nu U_\mu^\dagger U_\nu^\dagger] \qquad \text{(magnetic)} \end{aligned} \tag{1}$$

where the first term counts the length of color-electric flux lines, while the second either creates or annihilates a plaquette flux configuration. In the strong coupling limit ($g \to \infty$) of a $q\bar{q}$ system, a color-electric flux runs from q to $\bar{q}$ along the straight line, giving $E = \sigma R$. The magnetic term modifies the shape of the flux from the straight line in the higher order and the string between q and $\bar{q}$ starts oscillating. Monte Carlo simulations of LQCD, in fact, give a long-range linear potential as well as a Coulomb-like short range force between q and $\bar{q}$.

B. String flip-flop model

We now consider a multi-hadron system, where quarks are not permanently confined, but certain combinations (color-singlet hadrons) are allowed to escape from the rest of the system. Then the interquark potential should (1) confine a single quark and any non-singlet groups of quarks, but (2) allow color-singlet hadrons to escape. Lenz et al.[9] proposed a potential model of confinement, so called string flip-flop model, which has the above properties. Following refs. 9 and 10, we choose a two-meson system as the simplest multi-hadron system. We also assume that the quarks are placed as is shown in fig. 1, and use two convenient variables, $x = \mathrm{r}_1 - \mathrm{r}_{\bar{1}} = -(\mathrm{r}_2 - \mathrm{r}_{\bar{2}})$, and $y = \mathrm{r}_1 - \mathrm{r}_{\bar{2}} = -(\mathrm{r}_2 - \mathrm{r}_{\bar{1}})$. If $x < y$ (fig. 1(a)), the two mesons are totally separated noninteracting. When the two approach to each other and reach $x = y$ (fig. 1(b)), then we have two energetically equivalent string configurations, $1\bar{1} - 2\bar{2}$ and $1\bar{2} - 2\bar{1}$. We assume that the string configuration can "flip-flop" between the two at $x = y$. For $x < y$ (fig. 1(c)), the new configuration $(1\bar{2} - 2\bar{1})$ becomes dominant. The potential energy is written in terms of x and y by

$$V(x, y) = \min\{2\sigma x, 2\sigma y\}, \tag{2}$$

which is plotted *v.s.* x for a fixed y in fig. 2.

Similar confining potential is suggested by the strong coupling expansion of LQCD.[11] In the $q\bar{q} - q\bar{q}$ system, creation of a plaquette can convert a color-flux configuration, say $1\bar{1} - 2\bar{2}$, to the other, $1\bar{2} - 2\bar{1}$. Recent Monte Carlo simulation of LQCD by Ohta *et al.*[12] shows that the transition occurs very quickly once x becomes smaller than y and that the potential curve is similar to fig. 2.

Meson-meson scatterings happen through a string rearrangement. In the $x - y$ plane, the initial state is incident from $+x$ to the origin, for instance, while

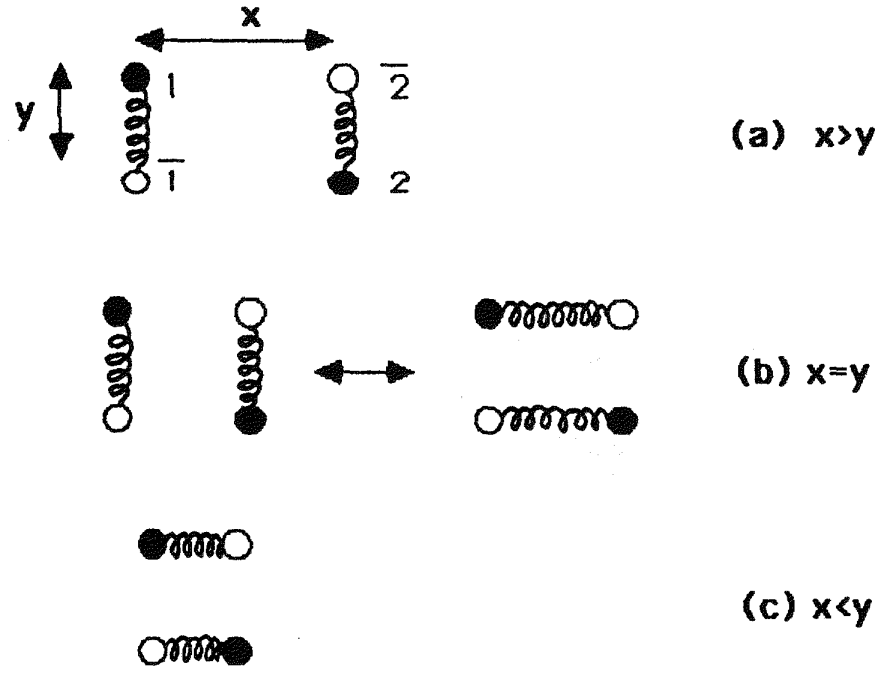

Figure 1 String configurations for a two-meson system.

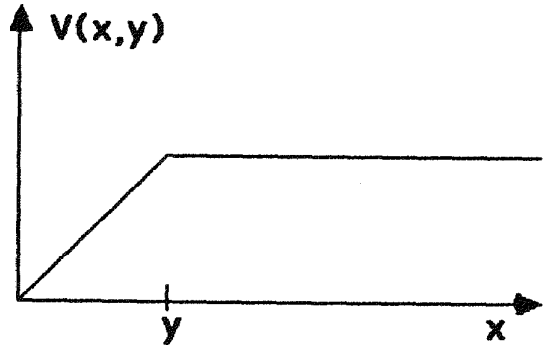

Figure 2 String flip-flop potential eq.(2).

the wave function is confined in the y direction. The final state after a string rearrangement will be a plane wave in the $+y$ direction. It is clear that $x-y$ symmetry property of the wave function plays an important role here. The $x-y$ symmetry is equivalent to the exchange symmetry between the quarks, *i.e.* the exchange of the quark labels 1 and 2 effectively interchanges x and y. Fig. 3 shows meson-meson scattering phase shifts calculated in the string flip-flop model with the antisymmetrized (3a) or the symmetrized (3b) wave function. For the antisymmetrized scattering, the meson-meson interaction is strongly repulsive and the phase shift behaves like that from a repulsive core, *i.e.* $\delta = -kc$, c being the core radius. On the contrary, when the wave function

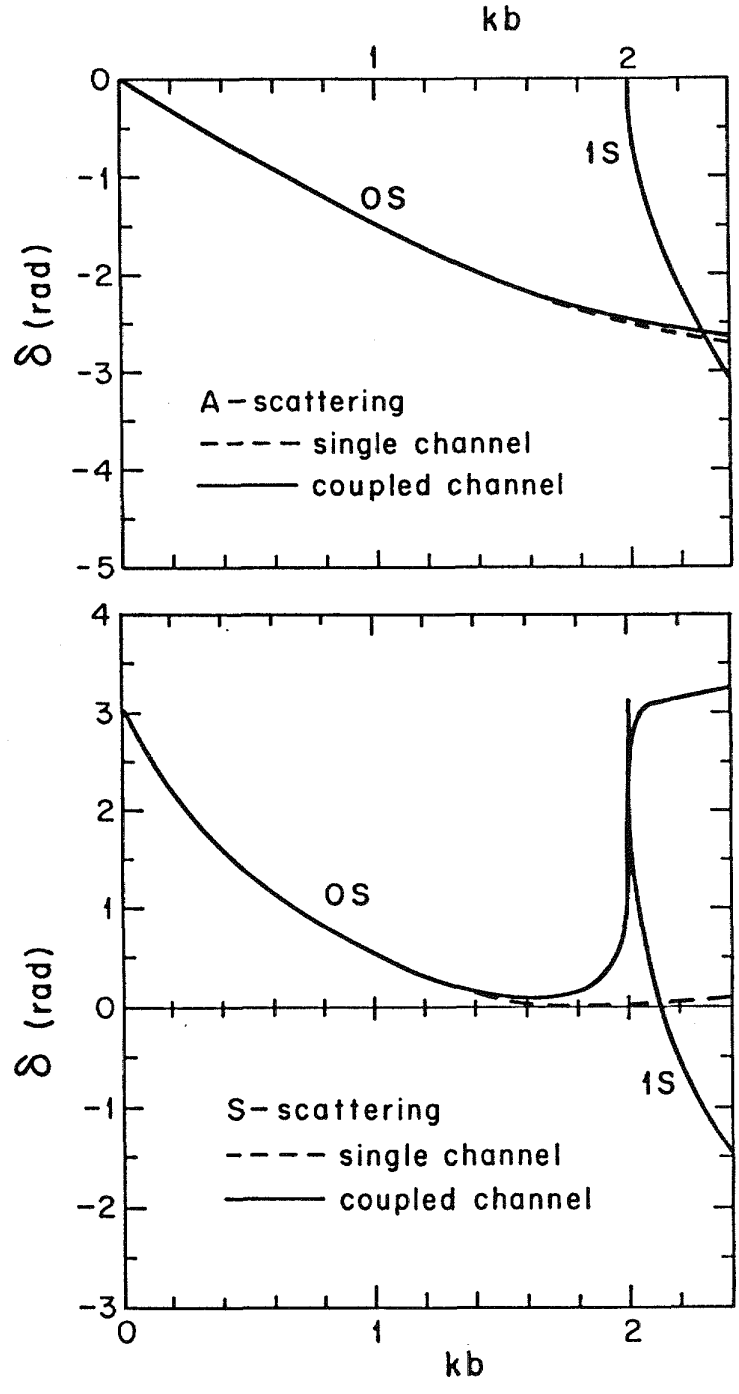

Figure 3 Meson-meson scattering phase shifts in the string flip-flop model: (a) antisymmetrized and (b) symmetrized. (ref. 10)

is symmetrized, we obtain a bound state, attractive interaction and resonances just below the threshold of internal excitations of the meson. It is remarkable that such a simple potential, eq. (2), shows these rich structures, which are, in

fact, characteristic of the realistic hadron dynamics.

Three valence quarks are confined in a baryon. The color-flux would have a Y-shaped configuration (fig. 4a). A potential which represents such confinement was given by Carson et al,[13]

$$V = \sigma \min_{\{r_0\}} \sum_i |\mathbf{r}_i - \mathbf{r}_0|^k, \tag{3}$$

where the minimization is for all possible juction points $\mathbf{r}_0$. V can be split into two parts: a two-body potential (fig. 4b)

$$V_2 = \sigma' \sum_{i<j} |\mathbf{r}_i - \mathbf{r}_j|^k, \tag{4}$$

and the rest V_3, which contains a three-body potential. It is easy to show that $V_3 = 0$ for a quadratic confinement $k = 2$ with $\sigma' = \sigma/3$. Even for a linear potential $k = 1$, contribution of V_3 is known to be less than 10% in the baryon spectrum. Therefore the two-body, triangle shaped, confinement is almost equivalent to the Y-shape one.

Figure 4 (a) Y-shape and (b) triangle string configurations for a baryon.

In the two-baryon system, we employ the triangle confinement for simplicity. A string flip-flop potential for a two-baryon system is given by[14]

$$V = \sigma \min \left\{ \sum_{i<j \in A} |\mathbf{r}_i - \mathbf{r}_j|^k + \sum_{\ell<m \in B} |\mathbf{r}_\ell - \mathbf{r}_m|^k \right\} \tag{5}$$

There the minimum is taken among ten possible clusterings of the six quarks into two clusters, A and B.

C. Colored string

One of the motivations of introducing the string flip-flop model is to avoid unphysical long-range forces between color-singlet hadrons. A traditional two-body confining potential,

$$V = (-a)\sum_{i<j}(\lambda_i \cdot \lambda_j)|\mathbf{r}_i - \mathbf{r}_j|^k, \tag{6}$$

is known to induce a long-range attraction, called color van der Waals force, $V \approx -1/R^3$.[15] The force results from mixing of an induced color-octet P-wave state of the hadrons. Matsuyama *et al.*[15] estimated the strength of the color van der Waals force between two nucleons and found that at $R \approx 2$ fm, it is comparable to the one-pion exchange potential and that it is a million times as big as the gravitation at $R \approx 1$ m. Such an unphysical force should be avoided. The string flip-flop potential, in fact, does not cause any long range force, because there is no interaction between two clusters separated far apart and therefore no polarization can be induced.

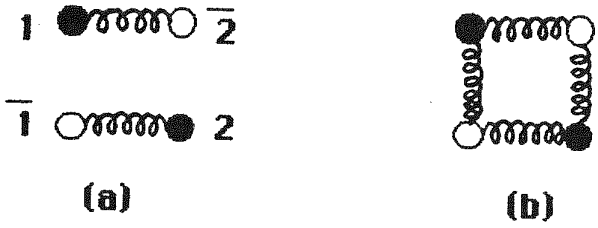

Figure 5 String configurations for (a) the singlet cluster (SC) state and (b) the hidden-color (HC) state (eq.(7)).

When the color is introduced in the string flip-flop model,[10] one notices that the rearrangement of quark-antiquark paring in the two-meson state leads to a "hidden color" (HC) state, $|(q\bar{q})_8(q\bar{q})_8\rangle$, as well as a singlet cluster (SC) state, $|(q\bar{q})_1(q\bar{q})_1\rangle$. The HC state should be confined in order not to allow free colored hadrons, while the SC state is not confined. We employ a simple potential which provides these properties: for $x < y$,

$$V = (v(1\bar{2}) + v(2\bar{1}))P + \frac{1}{\rho}(v(1\bar{1}) + v(2\bar{2}) + v(1\bar{2}) + v(2\bar{1}))Q \tag{7}$$

where P ($Q \equiv 1 - P$) is a projection operator onto the SC (HC) state (fig. 5). One encounters here an ambiguity in choosing the confinement of the HC state. The strength of the confinement in the color-singlet $q\bar{q}$ system is determined by the single meson spectrum. One cannot, however, relate the HC confinement to the meson spectrum, because the HC configuration arises only in the two-hadron system. In order to allow some freedom, we have introduced a parameter ρ in eq.(7), which controls the strength of the HC confinement.

The parameter ρ happens to be a very interesting one. When ρ is small, the HC confinement is so strong that all the HC states lie high above the SC states and couplings between them are negligible. On the contrary, for a large ρ, some HC states are low lying enough to couple to the SC states. This coupling will end up with bound states and resonances, which are dominated by the HC states. Fig. 6 shows meson-meson scattering phase shifts in the colored string flip-flop model obtained in a coupled channel calculation.[10] We observe a bound state for $\rho = 4$ and 6, and resonances for $\rho \geq 2$.

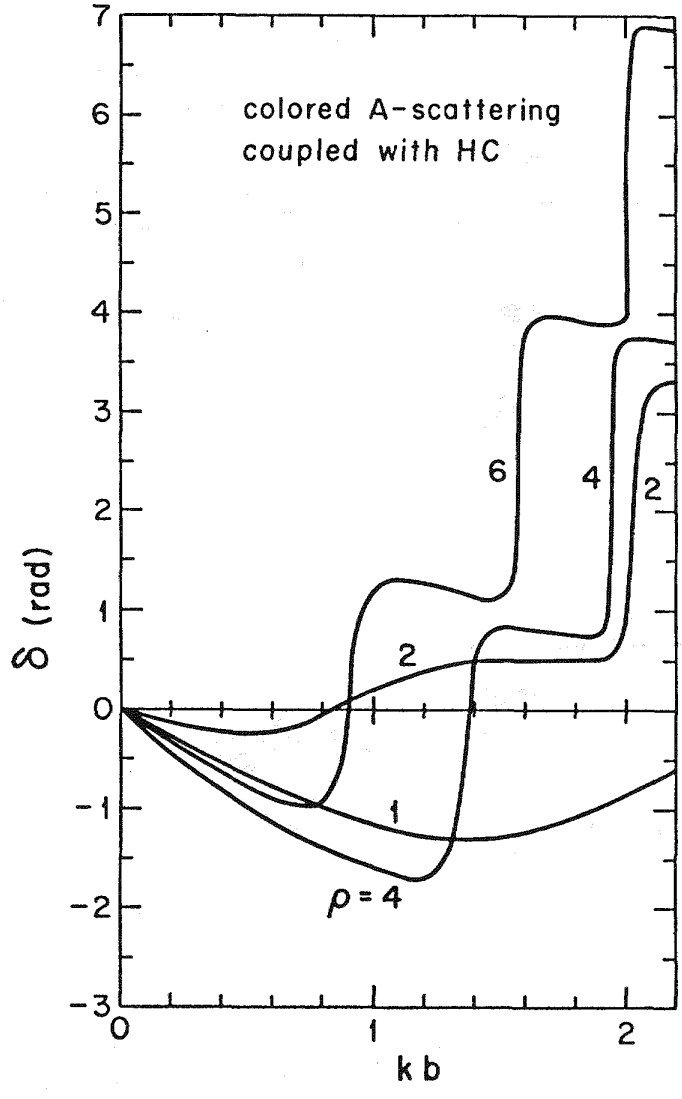

Figure 6 Meson-meson scattering phase shifts in the colored string flip-flop model.[10]

QUARK CLUSTER MODEL

A. Gluon exchange potential

In describing the quark dynamics in the hadron, the confinement is not the whole interaction. It is known that short range interactions due to the perturbative gluon exchange is important. According to DeRujula et al.,[16] the Briet-Fermi form of the semi-relativistic gluon exchange potential is employed traditionally, which contains the Coulomb, the color-magnetic, the tensor and the spin-orbit terms. The color-magnetic interaction, proportional to $(\lambda_i \cdot \lambda_j)(\sigma_i \cdot \sigma_j)\,\delta(r_{ij})$, plays an essential role in the baryon spectroscopy. It reproduces the $N - \Delta$ mass difference, the $\Lambda - \Sigma$ mass difference and the charge radius of the neutron, for instance.[17]

Because of the color dependence of the potential, which is due to the non-singlet color of the gluon, the gluon exchange potential does not carry a direct interaction between color-singlet hadrons. The lowest-order non-vanishing diagram is an exchange one, where a pair of quarks are exchanged between the hadrons (fig. 7). This gives a non-local exchange interaction, which is analogous to the Heitler-London force between two hydrogen atoms. The range of the exchange interaction is determined by the hadron size, because it requires that quark wave functions of the hadrons overlap with each other.

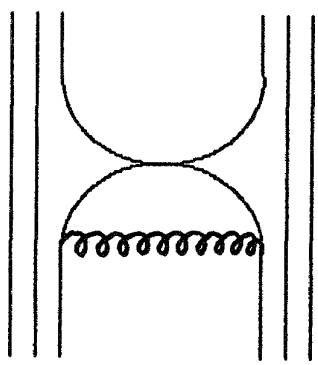

Figure 7 Quark exchange force.

B. Quark cluster model

Both the confinement and the short-range potential require a proper treatment of the exchange symmetry of the quark wave function. In order to include all the exchange interactions, we introduce the quark cluster model for the two-baryon system. The six-quark wave function is written as an antisymmetrized product of internal wave functions, ϕ_B, of the two baryons (clusters) and the relative wave function, χ,

$$\Phi(1,2,3,4,5,6) = \mathcal{A}[\phi_B(1,2,3)\,\phi_{B'}(4,5,6)\,\chi(\mathbf{R}_{123-456})] \qquad (8)$$

The Schrödinger equation is solved by using the resonating group method, which leads us to a nonlocal equation for χ,

$$\int d\mathbf{R}'[H(\mathbf{R},\mathbf{R}') - E\,N(\mathbf{R},\mathbf{R}')]\,\chi(\mathbf{R}') = 0 \tag{9}$$

The effective baryon-baryon interaction is nonlocal due to the antisymmetrization. The resonating group method is a popular approach in the cluster pictures of light nuclei and it is known that in some cases, *e.g.* $\alpha - \alpha$, a strong repulsion is observed due to the Pauli exclusion principle.[18] We have already seen an example in fig. 3a.

C. Baryon-Baryon interactions

Results of the quark cluster model calculation of the baryon-baryon interaction were already presented in several occasions.[3] We here briefly summarize them. Fig. 8 shows the S-wave NN scattering phase shifts for the string flip-flop model with various parameters. The parameter ϵ plays a similar role as ρ in eq.(7): for $\epsilon = 1$, the HC is confined strongly, while for $\epsilon \to 0$, the HC confinement is weak. (See ref. 14 for details.) We observe again wide variety in the NN interaction. This variety seems to be converged when the short-range interquark potential is turned on. From fig. 9, one concludes that the phase shift indicates a repulsive NN interaction, and that various models of quark confinement show qualitatively the same result. It is seen from the behavior of the phase shift around $100-200$ MeV in the c.m. NN system that the repulsion is as short range as the observed NN repulsive core. This short-range repulsion is a result of the cooperation of the quark antisymmetrization and the color-magnetic interaction (CMI). The mechanism is understood by considering the orbital symmetry structure of the quark wave function. We have two relevant orbital symmetries, [6] and [42]. The CMI is repulsive for the totally symmetric [6] state, which is favored by the kinetic energy. The mixed [42] symetric state feels an attraction by CMI, but is suppressed by the kinetic energy. Therefore at short distances both the [6] and [42] orbital states are pushed up to higher energies. By evaluating the CMI matrix elements in the quark shell model wave function, we obtain an adiabatic NN potential at $R = 0$,

$$V(R=0) \simeq 1.5(M_\Delta - M_N) \approx 450 \text{ MeV}. \tag{10}$$

$V(R)$ is related to the $N-\Delta$ mass difference, which is also caused by the CMI.

We have applied the quark cluster model to various two-baryon systems, *i.e.* $N-\Delta$, $\Delta-\Delta$, $\Lambda-N$, $\Sigma-N$ *etc.* A summary is given in table 1. Some conclusions are in the following: (1) The quark exchange interaction is repulsive in most two-baryon systems. Its strength varies from a state to state. Especially, the hyperon-nucleon ($Y-N$) short range repulsion seems not $SU(3)$ symmetric.[19] The $SU(3)$ symmetry is usually assumed in phenomenological potential models. (2) One finds two channels which show attractive interactions.

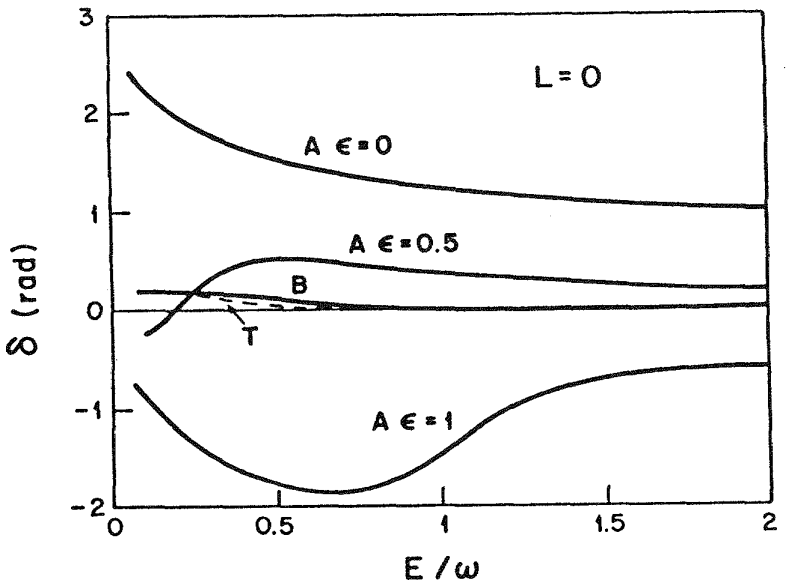

Figure 8 S-wave NN scattering phase shifts in the string flip-flop model.[14]

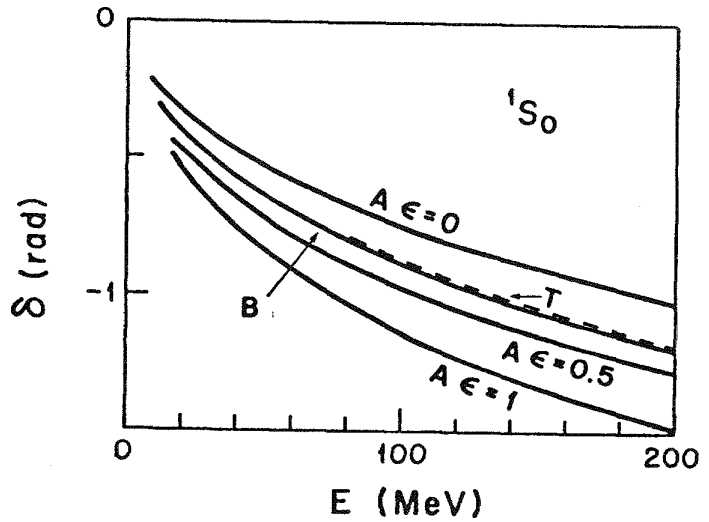

Figure 9 $^1S_0$ NN scattering phase shifts with the short-range gluon exchange potential.[14]

$\Delta - \Delta$ ($L = 0$, $I = 0$, $S = 3$) has a modest attraction. A coupled $\Lambda - \Lambda$, $N - \Xi$, $\Sigma - \Sigma$ ($L = I = S = 0$) system also shows an attraction, which causes a resonance state. Considering that the realistic nuclear force is a result of cancellation of the strong short-range repulsion and the strong meson-exchange attraction, nonexistence of the short-range repulsion may suggest deeply bound dibaryon states in these channels.[19]

BB'	$(S,\ I)$	*core radius*
$\Delta\Delta$	(3, 2)	0.81 fm
$\Delta\Delta$	(2, 3)	0.83 fm
$N\Delta$	(1, 1)	0.80 fm
$N\Delta$	(2, 2)	0.82 fm
$\Delta\Delta$	(3, 0)	*attractive*
$\Delta\Delta$	(0, 3)	*weakly repulsive*
$NN - \Delta\Delta$	(1, 0)	0.44 fm
$NN - \Delta\Delta$	(0, 1)	0.50 fm
$N\Delta - \Delta\Delta$	(2, 1)	*repulsive*
$N\Delta - \Delta\Delta$	(1, 2)	*repulsive*
$N\Lambda$	(0, 1/2)	0.44 fm
$N\Sigma$	(0, 1/2)	0.72 fm
$N\Lambda$	(1, 1/2)	0.37 fm
$N\Sigma$	(1, 1/2)	0.30 fm
$N\Sigma$	(0, 3/2)	0.40 fm
$N\Sigma$	(1, 3/2)	0.77 fm
$\Lambda\Lambda - N\Xi - \Sigma\Sigma$	(0, 0)	*resonance*

Table 1 S-wave baryon–baryon interaction

D. Deuteron form factors

We have seen that the quark exchange mechanism gives a short-range NN repulsion. On the other hand, traditional meson exchanges provide long range interactions, which are mostly attractive for NN. There have been many attempts to construct a realistic nuclear force combining these two interactions.[20] It has been shown that the quark exchange repulsion is capable to reproduce experimental data with the help of a long range attraction. Is the quark exchange force equivalent with phenomenological potentials? Both of them describe the NN scattering phase shifts fairly well. A major difference is the nonlocality of the quark exchange interaction, which will manifest itself in the off-shell behavior of the interaction.

To study the off-shell behavior, we calculate the deuteron form factors in a realistic model, which reproduces the on-shell scattering phase shifts and also the deuteron static properties.[21] Fig. 10 shows the monopole form factor of the deuteron, Fourier transformed, compared with that obtained by the Reid soft core potential model. One sees that the quark exchange interaction shows a significant enhancement around the origin due to the nonlocality. It is, however, hard to say that the nonlocality is a clear signature of quark participation, because the nucleon-meson picture may also provide a nonlocality due to retardation effect. If both the pictures give a similar nonlocality, it might be difficult to claim the quark exchange effect in a study of form factors and response functions of few-nucleon systems.

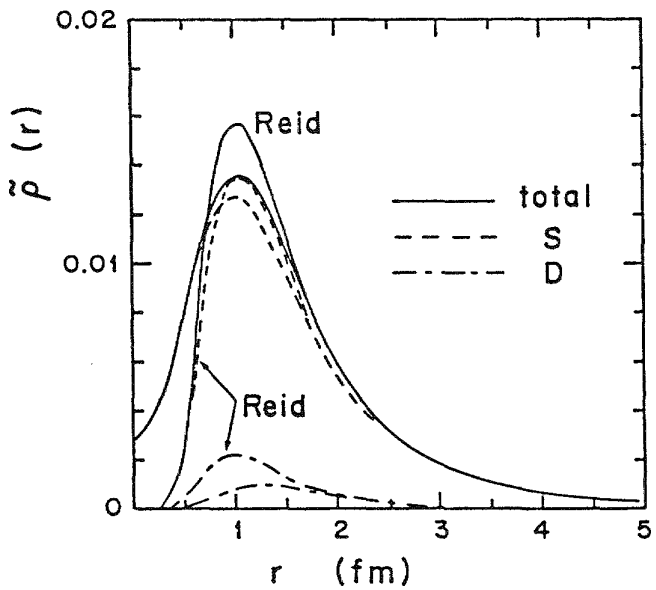

Figure 10 Nucleon density distribution of the deuteron by the quark cluster model compared with that by the Reid soft core potential.

QUARKS IN NUCLEI

One of the most interesting questions in nuclear physics is what is a significant role of quarks in nuclear medium. Is there a signature of quarks in nuclei which distinguishes the quark-gluon dynamics from the nucleon-meson dynamics. We here want to discuss two possibilities: (1) effect of quark antisymmetrization and the Pauli exclusion principle in few-nucleon systems, and (2) nucleon swelling mechanism in the quark model.

A. Pauli exclusion effect

A possible signature of the quark participation to the nuclear dynamics is effects of the Pauli exclusion principle in multi-nucleon systems. In the two-nucleon system, the Pauli effect is not strong, because the number of valence quarks is too small. In the quark shell model, where all quarks are in a single potential well, each single-particle orbit may be occupied by twelve quarks (two from the spin, two from the isospin and three from the color). The two-nucleon system is far from the saturation. This fact is quantitatively expressed by a suppression factor on the quark exchange diagram, *i.e.* (1/9) due to the spin, isospin and color exchange.

In some other two-baryon systems, the Pauli principle plays a dominant role. For instance, $\Delta\Delta$ ($I = I_z = 3$, $S = S_z = 2$) is made of five spin-up u quarks and one spin-down u quark. When two Δ's are on the top of each other, not all the quarks can sit in the lowest lying orbit, but the Pauli principle requires that at least two spin-up u quarks should occupy a higher orbit. This

effect produces a short-range $\Delta\Delta$ repulsion in this channel. Twice of the single particle excitation energy ($\hbar\omega \approx 200 - 300$ MeV) gives a rough estimate of the adiabatic $\Delta\Delta$ potential at $R = 0$. In table 1, the Pauli principle is responsible for the large repulsive core radii (0.7 – 0.85 fm) observed in $\Delta\Delta$ (3,2), $\Delta\Delta$ (2,3), $N\Sigma$ (0,1/2), $N\Sigma$ (1,3/2) *etc.* The state dependence of the short range repulsion will be a signature of the Pauli exclusion effect among quarks.

The lowest single particle orbit of the quark shell model is saturated in ^{4}He ($= 2p + 2n = 6u + 6d$). A hypernucleus $^5_\Lambda$He ($=^4$ He $+ \Lambda$) is unique in the study of the Pauli effect. If the extra Λ has no quark structure, it does not show any exclusion effect. In the quark shell model, however, Λ ($= u + d + s$) is partly excluded by the Pauli principle, because the lowest u, d orbits have already been fully occupied in ^{4}He. Although the quark shell model picture of $^5_\Lambda$He is, of course, an extreme one, the Pauli principle might be effective partially on Λ.[22] This effect has been noticed in the context of the overbinding problem of $^5_\Lambda$He. The Pauli effect might reduce the binding energy of Λ.

B. Nucleon swelling

Nucleons may be polarized in nuclear medium. A simple polarization is a monopole one, which is usually studied in the context of the nucleon swelling. We showed[23] that on very general grounds the size of a bound nucleon increases due to the attractive nature of the binding potential. A simple proof is given that a quantum system is expected to expand (contract) in an external attractive (repulsive) field. We use first order perturbation theory with a hamiltonian,

$$H(\mathbf{r}, \mathbf{R}) = H_0(\mathbf{r}) + V(|\mathbf{R} - \mathbf{r}|). \tag{11}$$

Here, H_0 is the internal hamiltonian of the system and $\mathbf{r}$ its dynamical coordinate. The system is exposed to a local central external field V centered at $\mathbf{R}$. If r in the quantum system is less than R, we may expand V in powers of r. For large R, keeping terms to order r^2 and taking only the monopole term, we get

$$V(|\vec{R} - \vec{r}|) \simeq V(R) + r^2 \nabla^2 V(R) + \text{higher multipoles.} \tag{12}$$

The "size" of the system evaluated in first order perturbation is then

$$\frac{\langle r^2 \rangle}{r_0^2} = 1 - \alpha(\mu r_0)^2 \frac{V(R)}{\Delta E_M}, \tag{13}$$

where r_0 is the rms radius of the ground state, μ the range of V ($\nabla^2 V = \mu^2 V$), α a positive numerical constant and ΔE_M a typical excitation energy of the monopole states. We clearly see in eq. (13) that an attractive (repulsive) potential makes the size of the system bigger (smaller). We have made a rough estimate of the effect for the nucleon and found a few % increase in nucleon size for the NN system at $R \simeq 1.5$ fm.

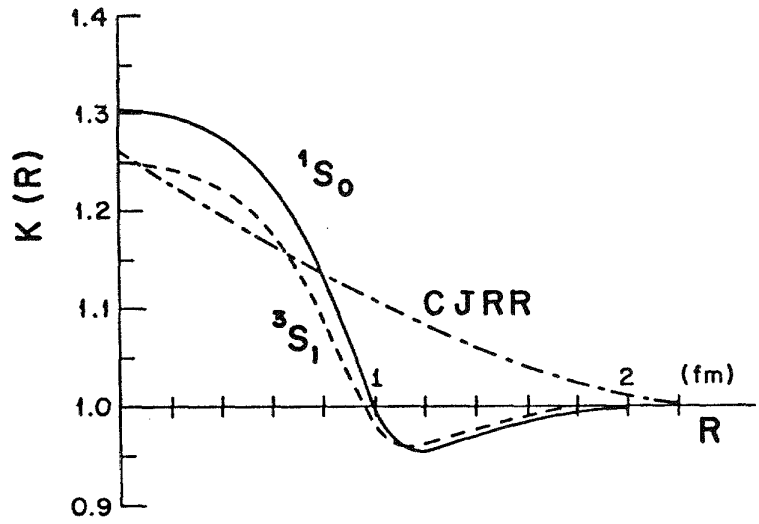

Figure 11 $K(R)$ in the two-nucleon system.[24] The curve CJRR shows the ratio used in the rescaling model analysis of the EMC effect.[25]

The quark cluster model predicts a nucleon size change in the interacting multi-nucleon system. We calculate the average quark momentum in the the quark cluster state by using an adiabatic approximation.[24] The ratio

$$K(R) \equiv \left(\langle p^2\rangle_R / \langle p^2\rangle_\infty\right)^{-1/2} \tag{14}$$

is plotted *v.s.* the NN distance R in fig. 11. This change of the average quark momentum is mostly due to the size change of the individual cluster in the cluster wave function. One sees a significant size enhancement in the internal region, while at large R it is slightly suppressed. The latter is, in fact, consistent with the above general argument, when we consider that the quark exchange mechanism provides only a repulsive NN interaction. Although this adiabatic approach to the nucleon polarization may only be qulitative, one sees a sizable interference effect between the nuclear interaction and the nucleon substructure.

In conclusion, the quark cluster model provides us with a realistic picture of the short distance baryon-baryon dynamics. It seems interesting to study few-nucleon systems including hypernuclei, and possible polarizations of the nucleon in nuclear medium.

This work was supported in part by a grant from the National Science Foundation.

REFERENCES

1. D.A. Liberman, Phys. Rev. D 16, 1542 (1977); C. DeTar, Phys. Rev. D 17, 302 (1978); *ibid.*, 323 (1978).

2. M. Oka and K. Yazaki, Phys. Lett. B 90, 41 (1980); Prog. Theor. Phys. 66, 556 (1981); *ibid.*, 572 (1981).
3. M. Oka and K. Yazaki, in *Quarks and Nuclei*, ed. by W. Weise (World Scientific, 1985); M. Oka, in *Proceedings of the 2nd Conference on the Intersection between Particle and Nuclear Physics*, (Lake Louise, 1986), ed. by D.F. Geesman, AIP Conference Proceedings 150, (AIP, New York 1986), and references therein.
4. J.E.T. Ribeiro, Z. Phys. C5, 27 (1980); C.S. Warke and R. Shanker, Phys. Rev. C 21, 2643 (1980); M. Cvetic, B. Golli, N. Mankoc-Borstnik and M. Rosina, Phys. Lett. B 93, 489 (1980); *ibid.* 99, 486 (1981); Nucl. Phys. A395, 349 (1983); H. Toki, Z. Phys. A294, 173 (1980).
5. M. Harvey, Nucl. Phys. A352, 301 (1981); *ibid.*, 326 (1981); M. Harvey, J. LeTourneux and B. Lorazo, Nucl. Phys. A424, 428 (1984).
6. A.F. Faessler, F. Fernandez, C. Lübeck and K. Shimizu, Phys. Lett. B 112, 201 (1982); Nucl. Phys. A402, 555 (1983).
7. Y. Suzuki and K.T. Hecht, Phys. Rev. C 27, 299 (1983); *ibid.* 28, 1458 (1983).
8. K. Maltman and N. Isgur, Phys. Rev. Lett. 50, 1827 (1983); 1827 (1983); Phys. Rev. D 29, 952 (1984).
9. F. Lenz, J.T. Londergan, E.J. Moniz, R. Rosenfelder, M. Stingl and K. Yazaki, Ann. Phys. 170, 65 (1986); J.T. Londergan, in *Hadron Substructure in Nuclear Physics*, ed. by W.Y.P. Hwang and M.H. Macfarlane (AIP, 1984); K. Yazaki, Nucl. Phys. A416, 87c (1984).
10. M. Oka, Phys. Rev. D 31, 2274 (1985); MIT preprint CTP#1194.
11. O.W. Greenberg and J. Hietarinta, Phys. Rev. D 22, 993 (1980); D. Robson, in *Hadron Substructure in Nuclear Physics*, ed. by W-Y.P. Hwang and M.H. Macfarlane (AIP, 1984); Phys. Rev. D 35, 1018 (1987); *ibid.*, 1029 (1987). N. Isgur and J. Paton, Phys. Lett. B 124, 247 (1983); Phys. Rev. D 31, 2910 (1985).
12. S. Ohta, M. Fukugita and A. Ukawa, Phys. Lett. B 173, 15 (1986).
13. I. Barbour and D.K. Ponting, Z. Phys. C4, 119 (1980); J. Carson, J.B. Kogut and V.R. Pandharipande, Phys. Rev. D 27, 233 (1983); *ibid.* 28, 2807 (1983).
14. M. Oka and C. Horowitz, Phys. Rev. D 31, 2773 (1985); Y. Koike, Nucl. Phys. A454, 509 (1986); Y. Koike and K. Yazaki, Phys. Lett. B 179, 332 (1986).
15. P.M. Fishbane and M.T. Grisaru, Phys. Lett. B 74, 98 (1978); T. Appelquist and W. Fischler, Phys. Lett. B 77, 405 (1978); S. Matsuyama and H. Miyazawa, Prog. Theor. Phys. 61, 942 (1979).
16. A. DeRujula, H. Georgi and S.L. Glashow, Phys. Rev. D 12, 147 (1975).

17. D. Gromes and I. Stamatescu, Nucl. Phys. B112, 213 (1976); 213 (1976); W. Celmaster, Phys. Rev. D 15, 1391 (1977); N. Isgur and G. Karl, Phys. Lett. B 72, 109 (1977); *ibid.* 74B, 353 (1978); A.J.G Hey and R. Kelly, Phys. Rep. 96C, 71 (1983).

18. J.A. Wheeler, Phys. Rev. 32, 1083 (1937); *ibid.*, 1107 (1937); K. Wildermuth and Th. Kanellopoulos, Nucl. Phys. 7, 150 (1958); 150 (1958); I. Shimodaya, R. Tamagaki and H. Tanaka, Prog. Theor. Phys. 27, 793 (1962).

19. M. Oka, K. Shimizu and K. Yazaki, Phys. Lett. B 130, 365 (1983); Nucl. Phys. A464, 700 (1987); in *Proceedings of 1986 INS International Symposium on Hypernuclear Physics*, (Tokyo, 1986), ed. by H. Bando et al.

20. M. Wakamatsu, R. Yamamoto and Y. Yamauchi, Phys. Lett. B 146, 148 (1984); Y. Yamauchi, R. Yamamoto and M. Wakamatsu, Phys. Lett. B 146, 153 (1984); K. Shimizu, Phys. Lett. B 148, 418 (1984); K. Bräuer, A. Faessler, F. Fernandez and K. Shimizu, Z. Phys. A320, 609 (1985); A. Faessler and F. Fernandez, Phys. Lett. B 124, 145 (1983); Y. Fujiwara and K.T. Hecht, Nucl. Phys. A444, 541 (1985); *ibid.* A451, 625 (1986); Phys. Lett. B 171, 17 (1986); Nucl. Phys. A456, 669 (1986).

21. M. Oka and K. Yazaki, Nucl. Phys. A402, 477 (1983); S. Takeuchi and K. Yazaki, Nucl. Phys. A438, 605 (1985); S. Takeuchi, K. Shimizu and K. Yazaki, Nucl. Phys. A449, 617 (1986).

22. S. Takeuchi and K. Shimizu, to be published; T. Yamazaki, Nucl. Phys. A446, 467c (1985); *ibid.* A463, 39c (1987).

23. M. Oka and R.D. Amado, Phys. Rev. C 35, 1586 (1987).

24. M. Oka, Phys. Lett. B 165, 1 (1985).

25. F.E. Close, R.G. Roberts and G.G. Ross, Phys. Lett. B 129, 346 (1983); R.L. Jaffe, F.E. Close, R.G. Roberts and G.G. Ross, Phys. Lett. B 134, 449 (1984); F.E. Close, R.L. Jaffe, R.G. Roberts and G.G. Ross, Phys. Rev. D 31, 1004 (1985).

NUCLEAR PHYSICS WITH STRANGE PARTICLES

Thomas Walcher
Universität Mainz, D-6500 Mainz, W.-Germany

ABSTRACT

The introduction of strangeness in strong interaction physics at low momentum transfers may provide a link between the conventional meson field theories and quark-gluon pictures of the nucleon and nucleus. Three experimental fields are discussed having this idea in mind: 1.) Strangeness content of the nucleon, 2.) Strange dibaryons and 3.) hypernuclei. In a 4th chapter some perspectives of electroproduction of strange nuclear systems are given.

INTRODUCTION

One of the interesting problems of present nuclear physics is the question of the constituents of the nucleus. We know from high energy physics that nucleons and consequently the nucleus is made up of the pointlike quarks and gluons. However, the very successful standard model of nuclear physics, the shell model, assumes pointlike nucleons as basic constituents which interact via meson exchange. At low energies these two pictures are essentially indistinguishable since the meson exchange can be represented as diquark- and soft gluon exchanges. Until recently this was only a theoretical problem. It was only the EMC effect, an effect which manifests itself at high energies, which showed us experimentally that quarks and gluons are present in the nucleus.

One of the few hopes to find also effects due to quark-gluon degrees of freedom at low energies is by marking a quark by strange flavour. It is this idea which makes the introduction of strangeness in nuclear physics so attractive. Strangeness may provide an additional constraint which will help to reduce the ambiguities of the two pictures.

This paper deals with three topics of nuclear physics with strangeness which could be addressed at a continuous electron beam accelerator of a few GeV: 1.) Strangeness content of the nucleon, 2.) Strange dibaryon resonances and 3.) Hypernuclei. It will show by means of examples of recent experiments where we stand. In a 4th paragraph some perspectives of electroproduction of strange nuclear systems are given. However, no systematic attempt will be made to device experiments for CEBAF. This is largely covered by special contributions to this workshop.

STRANGENESS CONTENT OF THE NUCLEON

From deep inelastic scattering at high energies we know that

$$\frac{2\,s}{\bar{u} + \bar{d}} = 0.57 \pm 0.1 \qquad \text{for } (\nu) \approx 30 \text{ GeV} \qquad (1)$$

where s, $\bar{u}$, $\bar{d}$ are the quark momentum distribution functions of the sea quarks. This means that the s and $\bar{s}$ sea quarks carry about 2 % of the momentum at $Q^2 \to \infty$. On the other hand arguments based on the pion-nucleon sigma term ($\Sigma_{\pi N}$) derived from the chiral symmetry breaking indicate a very large strange quark content at small momentum transfers[1]. Quantitatively

$$\langle p|\bar{s}s|p\rangle = 0.5\ \langle p|1/2(\bar{u}u+\bar{d}d)|p\rangle \qquad (2)$$

where $\bar{q}q$ projects out the respective quark content in the proton with momentum p. Since $\bar{u}u$ and $\bar{d}d$ contain the valence quarks this would be indeed a very large strangeness content. Unfortunately, we have no direct experimental information of the strangeness content at small momentum transfers. A possibility to study this interesting question is electroproduction of Kaons from the nucleon.

In the traditional picture of the nucleon at low momentum transfers, the pion is considered to be a kind of parton in the nucleon at low momentum transfers. If the resolution of the photon is moderate (photon mass $Q^2 < 1\ \text{GeV}^2$) the pion electroproduction in the direction of the momentum transfer can be considered as the quasi-elastic scattering $e(\pi N) \to e\pi N$. F.Güttner et al.[2] have analysed data of π electroproduction using this idea and derived a pion distribution function $G_{\pi/p}(x)$ where x is the momentum fraction of the proton carried by the π. The somewhat surprising result was that the proton is only to 3% a $n\pi^+$ state and that the $n\pi^+$ state carries 0.6% of

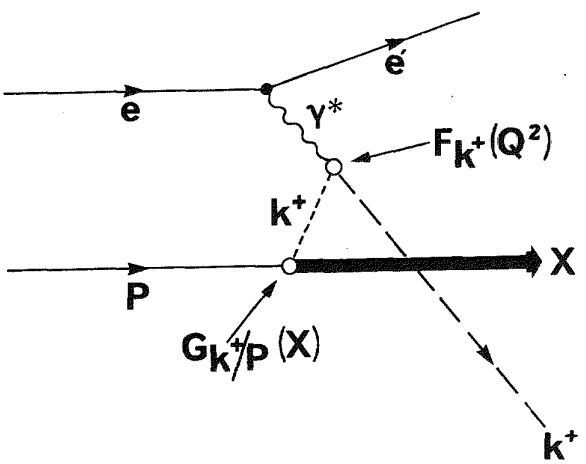

Fig. 1. Diagram for Kaon photoproduction.

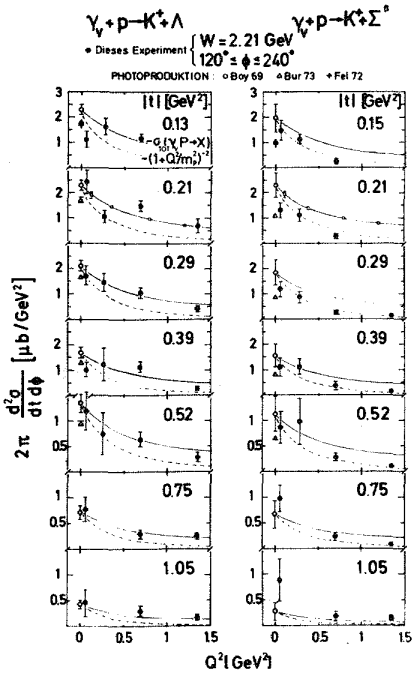

Fig. 2. The Q^2 dependence of the $K^+\Lambda$ and $K^+\Sigma^0$ cross sections $2\pi\, d^2\sigma/dtd\Phi$. The full line is proportional to $\sigma_{tot}(\gamma p \to X)$ and the dashed line to the vector dominance behaviour $(1+Q^2/m_\rho^2)^{-2}$ (from ref. 4)

the proton momentum. It is obvious that one might also try to determine the strangeness content of the nucleon at low energies. However, the pole term of fig. 1 is determined by the longitudinal cross section. Therefore, a separation of longitudinal and transverse cross sections are needed. The precision of the data which could be achieved with the old accelerators was not sufficient to do this separation. As an example the data of a DESY experiment[3,4] are shown in fig. 2. Plotted is the double differential cross section where t is the four-momentum transfer of the virtual photon to the Kaon and $\phi \approx 180°$ is the off-scattering plane angle. As reference the Q^2 dependence given by the vector-dominance model is plotted as well as the result of the $\sigma_{tot}(\gamma_v p \to X)$ with a ratio of $\sigma_L/\sigma_t = 0.18$.

STRANGE DIBARYON RESONANCES

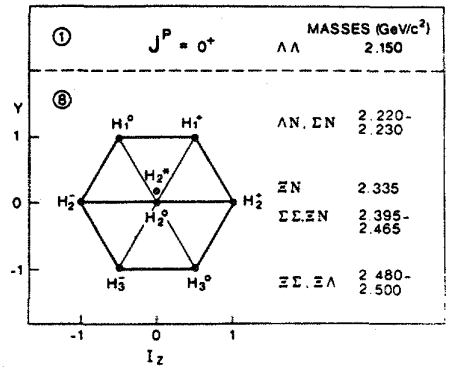

Fig. 3. Singlet and Octet representation of strange dibaryons[6]. The masses are predictions in the MIT bag model[6].

Dibaryon resonances would be probably the best cases to test the interplay between meson exchange interaction and the quark gluon picture. However, for light quarks the only dibaryon which is established beyond any doubts is the deuteron[5]. The most promising candidates for further dibaryons should be therefore, the SU(3) flavour partners with strangeness S = -1 and -2 of the deuteron. In the MIT bag model Jaffe[6] predited an octet of strange dibaryons (see fig. 3). Beside

this octet a singlet, usually called H with the most symmetric quark content {2u, 2d, 2s} all in a S state which would be bound by 80 MeV, is predicted. The masses predicted by Jaffe have been recalculated several times in more refined calculations (for a summary see e.g. Locher et al.[5]). As indicated in fig. 3 all proposed resonances are close to hyperon-nucleon or hyperon-hyperon thresholds and are difficult to distinguish from cusp effects.

The experimental search for these resonances has been, therefore, rather obscure. The search for the H particle has been negative so far[5]. A most promising AGS proposal[7] to search for the H using a two step reaction with intermediate (Ξ^- d) atom formation has not yet produced results.

A positive result for a S = -1 state was, however, presented by a Rome-Saclay-Vanderbilt collaboration[8] at CERN. They searched by means of the reaction $K^- d \to \pi^- X^+$ and the line inverted reaction $\pi^+ d \to K^+ X^+$ for the X = H_1^+ dibaryon. Fig. 4 shows a missing mass spectrum with the

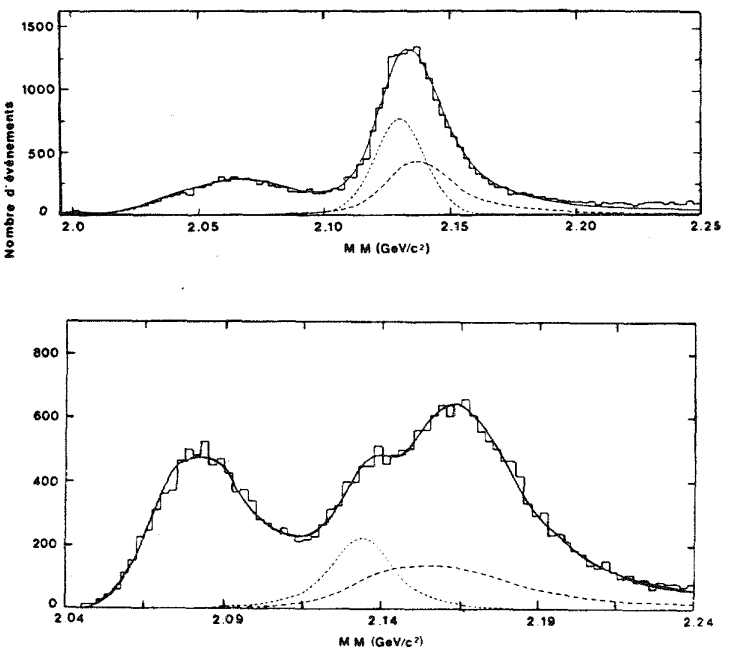

Fig. 4. Missing mass spectra for the $K^- d \to \pi^- X$ (upper) and $\pi^- d \to K^- X$ (lower) reactions[6]. The widely dashed curve is the calculated shape of the quasielastic reactions $K^-(\pi^+)d \to \pi^-(K^+)p\Sigma^0$ and $\to \pi^-(K^+)n\Sigma^+$ and the narrowly dashed curve indicates the H_1^+.

indication for a bump not explainable with the quasielastic reaction. The mean of its parameters derived from three momenta and for different decay multiplicities is M_X = 2129.8±0.2 MeV/c^2 and Γ = 16.7±1.9 MeV/c^2. It is most naturally identified with the H_1^+ resonance. However, this identification depends on the reliability of the calculation of the quasi-elastic background.

A more recent result from the AGS experiment 773 [9] is indicating hints to another kind of dibaryons. The H particles are partner of the deuteron and belong to the colour representation $(Q^6)_1$ and the mentioned flavour octet and have $L^P=0^+$. On the other hand, by grouping the six quarks of a dibaryon to different quark clusters, one can get states of $(Q^4)_3 - (Q^2)_{3^*}$ colour representation with $\underline{3}$-$\underline{3}^*$ or $\underline{6}^*$-$\underline{3}^*$ flavour SU(3) representation. They are denoted $D_J^C = D_{I,O}^{\pm}$ and have $L^P = 1^-$. Table 1 shows a compilation of these states with S = -1 by Piekarz[9] based on calculations by Mulders et al.[10].

TABLE 1 Strange dibaryons, S = -1

	Mass (GeV)	J,I	L^P	Quarks clusters and colours	Flavor	E
D_0	2.11	0,1/2	1^-	$(Q^4)_3-(Q^2)_{3^*}$	$\underline{3}$-$\underline{3}^*$	60
D_1	2.16	1,1/2	1^-	$(Q^4)_3-(Q^2)_{3^*}$	$\underline{3}$-$\underline{3}^*$	110
	2.17	1,1/2	0^+	$(Q^6)_1$	$\underline{8}$	130
	2.24	2,1/2	0^+	$(Q^6)_1$	$\underline{8}$	200
	2.27	1,1/2	1^-	$(Q^4)_3-(Q^2)_{3^*}$	$\underline{6}$-$\underline{3}^*$	230
	2.29	1,1/2	1^-	$(Q^4)_3-(Q^2)_{3^*}$	$\underline{6}$-$\underline{3}^*$	250

Missing mass spectra at different reaction angles $\Theta_{K\pi}$ of the $K^-d\rightarrow\pi^-X$ reaction obtained by Piekarz et al.[9] are depicted in fig. 5. At M_X = 2128 MeV/c^2 a peak on top of a background is seen which may be the cusp/resonance of Pigot et al.. At larger reaction angles a further indication of a peak at M_X = 2139 MeV/c^2 is appearing. The angular distributions of the assumed two peaks is shown in fig. 6. The bumb at 2129 MeV/c^2 behaves as a $\Delta L = 0$ transition consistent with the hypothesis that it is composed of a cusp and the H_1^+. The cross section for the possible peak at 2139 MeV/c^2, however, disappears in forward direction as it should if it is a D^1 for which $\Delta L = 1$.

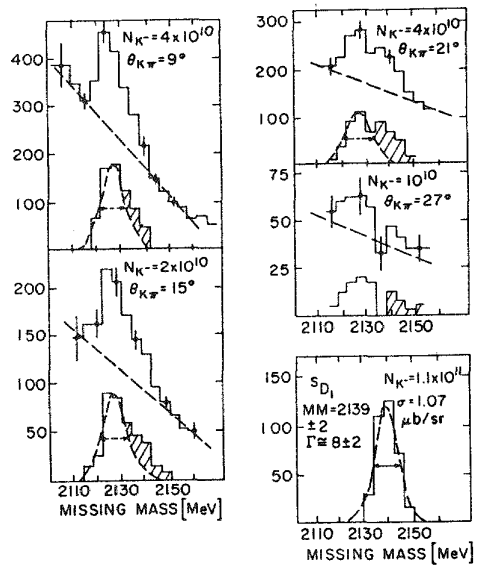

Fig. 5. Missing mass spectrum from the $K^-d\to\pi^-X$ reaction at different reaction angles[9]. The spectrum at the right hand lower side is the sum of all shaded areas after subtraction of a cusp/resonance at 2129MeV/c².

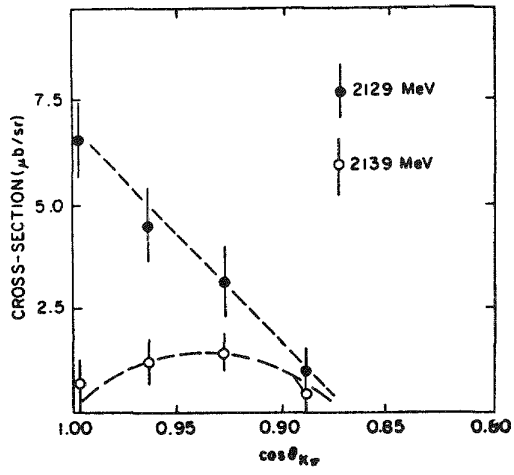

Fig. 6. The differential cross section for the maximum at 2129 MeV/c² and 2139 MeV/c².

All indications on strange dibaryon resonances are not yet very firm. Clearly better statistics and may be also some selectivity by measuring the decay channels are needed. Such improvements are likely to come about at an high intensity, Hadron Facility as e.g. LAMPF II, TRIUMF or EHF. A short comment on the perspectives at a high intensity electron accelerator will be made later.

HYPERNUCLEI

Hypernuclei are a direct extension of the idea of dibaryons, however, providing a much richer spectroscopy. Most of the existing data could be interpreted by assuming that a hyperon replaces a nucleon in a shell orbit. It is, however, tempting to relate the short range part of the effective interaction as e.g. the spin-orbit force to the quark degree of freedom. The experimental situation of hypernuclear production in the (K^-,π^-) strangeness exchange reaction has been summarized several times in recent years[11,12,13]. Only few experiments could be performed recently and, therefore, only few new results can be mentioned.

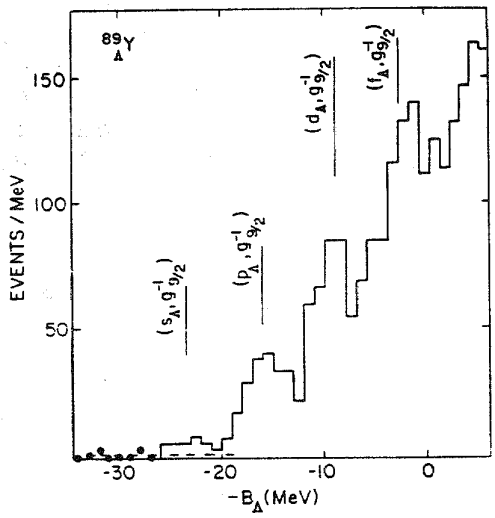

Fig. 7. Hypernuclear Spectrum of $^{89}_{\Lambda}$Y as obtained by the BNL(π^+,K^+) collaboration[15]. B_Λ denotes the binding energy of the Λ.

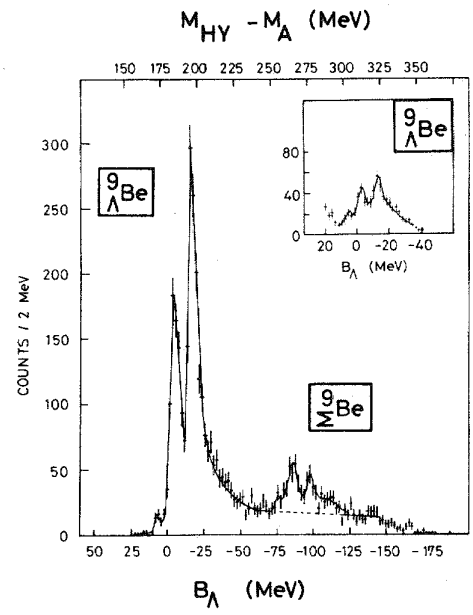

Fig. 8. Hypernuclear spectrum of ^{9}Be which covers the region of Λ and Σ hypernuclear states[21].

A most exciting result is the possible first observation of ground states of heavy hypernuclei by means of the (π^+,K^+) reaction[14] at the AGS of BNL[15]. Fig. 7 shows as an example $^{8,9}_{\Lambda}$Y. The configurations of the supposed hypernuclear states is indicated with (s_Λ, $g^{-1}{}_{9/2}$) being the ground state. The momentum transfer to the Λ at a pion momentum of 1.05 GeV/c is about 320 MeV/c, a value which would be also typical for hypernuclear production in (e,e'K) at CEBAF. In this kinematical situation it is possible to populate states with large angular momentum transfer. These may be as indicated in the example of $^{89}_{\Lambda}$Y deeply-lying Λ shell model states. A more detailed investigation of these states may provide for the first time a test of the shell model for deeply-bound shells.

A disappointing news is that the Σ hypernuclear states claimed by a Tokyo University group[16] in hypernuclear production with stopped Kaons could not be confirmed by a Tokyo-Heidelberg collaboration[17] at KEK.

This failure to reproduce the earlier spectra has been taken as a corroboration of theoretical claims that Σ hypernuclei can be interpreted as quasifree production of Σ from nuclei[18,19]. However, this model cannot explain the whole of all observations[20].

Fig. 8 shows a hypernuclear spectrum from ^{9}Be measured by Bertini et al. at CERN[21]. Fairly high above the binding energy threshold in the continuum two bumps due to a mixture of several Λ hypernuclear states are seen. At a mass just 77 MeV higher, the mass difference between the Σ^{0} and the Λ^{0} a very similar structure is seen. The width of these states is about 8 MeV suggesting that narrow Σ hypernuclear states in the continuum exist. The same is indicated if one compares the Λ and Σ spectra from ^{12}C (fig. 9). Though the statistical precision is only moderate due to the limitations of todays Kaon beams it is difficult to deny the similarity in the $(K^{-},\pi^{\pm})$ spectra. Beside the broad shoulder due to quasi free transitions a narrow peak about 5 MeV side is visible. The feature of narrow peaks cannot be reproduced by the quasi free models.

The quasi free calculations predict no cross sections. However, there are inconsistencies[20] within the measured cross sections if one assumes they are due to the quasi free mechanism which also sheds some doubt on this interpretation of the Σ production from nuclei.

Of course the existence of narrow Σ hypernuclear states which should not exist due to the strong transition $\Sigma N \rightarrow \Lambda N$ is highly provocative in the realm of the standard shell model. Numerous explanations have been discussed[22] and some of them have been questioned[23].

If the existence of narrow Σ states proves to be a general phenomenon, some new physics may be involved. Furthermore, the spectroscopy of Λ hypernuclei will be extended to a new dimension due to the different quark spin coupling and the isospin of the Σ hyperons.

PERSPECTIVES OF ELECTRO-PRODUCTION OF STRANGE NUCLEAR SYSTEMS

The three topics covered in this paper are all relevant to future program containing strangeness at CEBAF. The elementary cross sections are not only needed as an input for the multibaryon systems. Their study will allow a determination of the $KN\Lambda$ and $KN\Sigma$ coupling constants. Furthermore by separating the longitudinal and transverse part of the cross section the Born terms may be determined and in this way a measure of the strangeness (K) content of the nucleon be derived.

In the electroproduction (τ_{v},K) from the deuteron the final state interaction of the produced hyperon with the spectator nucleon may allow the study of YN scattering and YN dibaryon resonances. However, final state interaction effects are small and together with the small (τ_{v},K) elementary cross only rather low event rates can be expected for the YN resonance production. A separate calculation of the size of the final state interaction

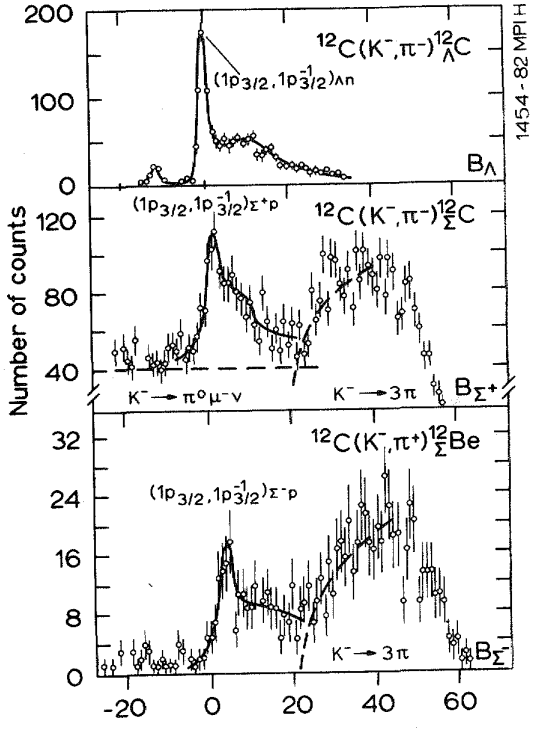

Fig. 9. Comparison of $^{12}_{\Sigma}C$ (measured at p_K=400 MeV/c), $^{12}_{\Sigma}Be$ (450 MeV/c) with $^{12}_{\Lambda}C$ (720 MeV/c). The continuous backgrounds of the $K^-\to 3\pi$ and $K^-\to\pi^0\gamma\mu^-$ decays are indicated. The binding energy scale is in MeV.

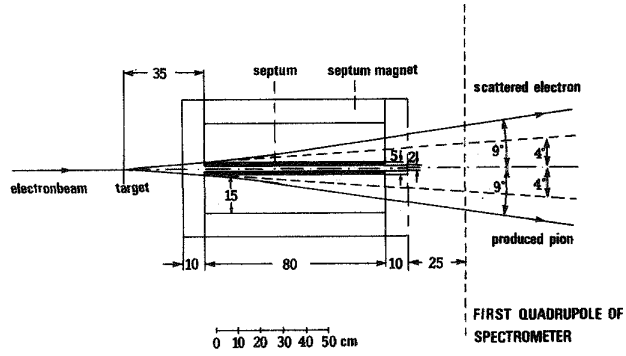

Fig. 10. A system of two septum magnets allowing to approach very forward angles in electroproduction experiments.

effects in the quasi free kinematics has been performed for the $(\bar{p},p)$ reaction[24] (see also[8]). The search for dibaryon resonances and the study of YN interactions will be probably done more effectively at a hadron facility.

The electroproduction of hypernuclei at CEBAF has been discussed several times in earlier papers[25,26]. One of the very important questions which where addressed was the count rate. Since different authors used rather different kinematical situations, very different count rates resulted.

For easily accessible scattering angles $\Theta_e \approx 15°$ and $\Theta_K \approx -15°$ about 5 coincidence events per hour were derived[26]. If one could reach e.g. $\Theta_e \approx 10°$ and $\Theta_K = -10°$ a factor 10 could be gained. This is a counting rate comparable to the (K^-,π) reaction. However, the resolution of the (e,e'K) hypernuclear could be ~300keV against the 2 MeV which are typical for the (K^-,π) reaction. A possi-

bility to reach very small reaction angles is indicated in fig. 10. The proposed set up[27] uses two independent septum magnets of conventional design. In this way the intense electron beam would go straight in the normal beam dump.

It is important to emphasize that the (e,e'K) reaction will deliver much more information on hypernuclear states than the (K^-,π) reaction. The Matrix element measured in (e,e'K) is given by[25]

$$M_{fi} \sim \langle \psi^f_\Lambda (njl) | \Phi^+_{K^+} \; e^{-i\vec{Q}x} \; O_{tr} \; | \psi^i_N \rangle$$

where Φ^+ is the outgoing Kaon wave function, $\vec{Q}$ the momentum of the virtual photon and O_{tr} the electromagnetic transition operator. By varying $\vec{K}$ and $\vec{Q}$ one can, therefore, test the Λ wavefunction ψ_Λ and study the distortions of the Kaon wave. More important may be the possibility to separate longitudinal and transverse contributions to the cross sections for some few selected cases. The longitudinal may be more sensitive to unexpected behaviour, i.e. non shell model, than the transverse part.

In summary it is clear that a hypernuclear program at CEBAF would make this field accessible with a more informative probe and an improved precision. Since the strangeness in nuclei is conceptionally a way to unravel possible quark degrees of freedom in nuclei a great potential for new physics exists here.

REFERENCES

1. R. L. Jaffe, inv. talk presented at the XI. Int. Conf. on Particles and Nuclei (PANIC), Kyoto 1987, to appear in the proceedings.
2. F. Güttner, G. Chanfray, H. I. Pirner, and B. Povh, Nucl. Phys. A429, 389 (1984).
3. P. Brauel et al., Z. f. Physik C3, 101 (1979).
4. P. Brauel, Dr. Dissertation, Univ. Hamburg, DESY-Report F22-78/04.
5. M. P. Locher, M. E. Sainio, and A. Svarc, Advances in Nuclear Physics, Vol. 17, 47 (1987).
6. R. L. Jaffe, Phys. Rev. Let. 38, 195 (1977).
7. G. Franklin, P. Barnes et al., AGS Proposal 813 (1985).
8. C. Pigot et al., Nucl. Phys. B249, 172 (1985).
9. H. Piekarz et al., AGS Experiment 773 (1985), Nucl. Phys. A450, 85c (1986).
10. P. Y. Mulders et al., Phys. Rev. D21, 2653 (1980).
11. B. Povh: "Nuclear Physics with Strange Particles" in Progress in Particle and Nuclear Physics, Vol. 18, 183 (1987).

12. E. H. Auerbach et al., Ann. Phys. (NY) 148, 381 (1983). D. I. Millner et al., Phys. Rev. C31, 499 (1985).
13. Th. Walcher, Nucl. Phys. A434, 343c (1985).
14. J. C. Peng, Nucl. Phys. A450, 129c (1986).
15. R. E. Chrien et al., contribution to the XI. Int. Conf. on Particles and Nuclei (PANIC), Kyoto 1987, and contribution to this conference.
16. T. Yamazaki et al., Nucl. Phys. A450, 1c (1986).
17. R. S. Hayano, invited talk at the XI. Int. Conf. on Particles and Nuclei (PANIC), Kyoto 1987, to appear in the proceedings.
18. R. E. Chrien, E. V. Hungerford, and T. Kishimoto, Phys. Rev. C35, 1589 (1987).
19. M. Kohno, R. Hausmann, P. Siegel, and W. Weise, Regensburg Preprint TPR-87-2
20. Th. Walcher, "Production of Hypernuclei in the K-π Reaction", invited paper at the International Symposium on Strangeness in Hadronic Matter (1987), proceedings to appear in Nucl. Phys. A.
21. R. Bertini et al., Phys. Lett. 90B, 375 (1980).
22. see e.g. C. B. Dover and A. Gal, Comments Nucl. Part. Phys. 12, 155 (1984).
23. H. Feshbach, Nucl. Phys. A450, 339 (1986).
24. R. Bertini et al., Nucl. Phys. B209, 269 (1982).
25. T. W. Donnelly and S. R. Cotanch in Research Program at CEBAF, Report of the 1985 Summer Study Group 1985, Newport News, VA, pp. 7.1 and references therein.
26. B. Mecking, in cit. ref.[25], pp. 7.25
27. W. Brückner et al., DESY-Proposal for p(e,e'π^+)n, MPI Heidelberg, 1982

EXPERIMENTAL STUDIES OF ELECTROMAGNETIC PROPERTIES OF FEW BODY SYSTEMS*

P. E. Bosted

The American University, Washington D.C. 20016
and
Stanford Linear Accelerator Center, Stanford, CA 94305

ABSTRACT

An overview is given of some recent and planned experiments which have or will substantially increase our knowledge of the electromagnetic properties of the few body systems. Specific examples include the proton and neutron elastic form factors, the deuteron elastic form factors, deuteron threshold electrodisintigration and quasi-elastic scattering, deuteron photodisintigration, and finally measurements of R in deep inelastic scattering from hydrogen, deuterium, and iron.

INTRODUCTION

The availability of a large current, medium energy electron beams at institutions such as SLAC, Bates, and Saclay has been combined with improvements in detectors and experimental techniques to push our knowledge of the electromagnetic properties of the few body systems to ever higher momentum transfer Q^2 and ever greater accuracy. The topic is too vast to cover completely in a paper such as this, so that I will concentrate on a few areas where recent or planned experiments are making significant contributions. See Ref. 1 for reviews that cover additional topics such as elastic and inelastic scattering from the tri-nucleon systems.

PROTON ELASTIC FORM FACTORS

Probably the simplest few body system of interest to nuclear physicists is the nucleon. In most cases the properties of nuclei can be explained in terms of systems of bound nucleons, ignoring the internal structure of the nucleons. Recent experimental evidence, especially the 'EMC Effect', has shown that at high energies this assumption breaks down. A central question has become to what extent are nucleon properties changed when in a nucleus, and what is the probability that two nucleons form a dibaryon state when placed close together. Answers to these and other questions require the best possible knowledge of the free nucleon properties and the development of good theoretical frameworks for explaining them.

* Work supported in part by the Department of Energy, contract DE-AC03-76SF00515 (SLAC) and by the National Science Foundation, Grant PHY85-10549 (American University).

Measurements of the nucleon form factors are usually given in terms of the Sachs form factors

$$G_E = F_1 - \frac{Q^2}{4M^2} F_2 \tag{1}$$

$$G_M = F_1 + F_2 \tag{2}$$

where F_1 and F_2 are the Dirac and Pauli form factors, which give information on the charge and spin distributions respectively. At low energies, a successful phenomenological description of the form factors can be given in terms of vector dominance models[2] (VDM) in which the interaction is pictured to be composed of two parts: a bare photon and vector meson components to the photon. At sufficiently high energy the role of vector mesons is expected to diminish, and calculations of the hard photon scattering should be possible using perturbative QCD. A major question has been how high does the energy transfer have to be for PQCD to work?

Recent experimental data[3] has shed some light on this question. Electrons with energies up to 20 GeV were scattered from a 60 cm long hydrogen target in End Station A at SLAC. The use of longer target, more forward angle, better detectors in the spectrometer, and the masking of the target endcaps were the principal factors that permitted measurements from $Q^2 = 2.9$ to 31.3 $(\mathrm{GeV/c})^2$ with considerably smaller errors than previous measurements. The results for the quantity $Q^4 G_M^p/\mu_p$ are shown in Figure 1, extracted from the measured cross sections assuming that $G_E^p = G_M^p/\mu_p$. The results show $Q^4 G_M^p$ attaining an approximately constant value around 5 to 10 $(\mathrm{GeV/c})^2$. This is consistent with the PQCD prediction[4] that F_1 should fall as Q^{-4} (times a slowly falling function of Q^2 due to the running of the strong coupling constant α_s and terms proportional to $\ln(Q^2)$), while F_2 should fall as Q^{-6} due to the extra helicity flip. Explicit calculations have so far been done for F_1 only. The results have been found to be quite sensitive to the choice of quark wave function. A symmetric wave function gives a curve[4] with the right shape (solid curve normalized to the

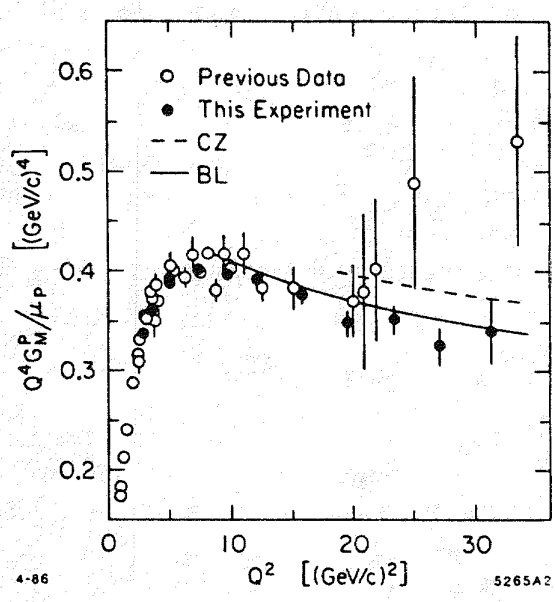

Fig. 1. New results for the proton form factor G_M^p from Ref. 3. The perturbative QCD curves are from Ref. 4 (BL) and Ref. 5 (CZ).

data at $Q^2 = 10$ (GeV/c)^2) but a magnitude that is about a hundred times too small. Chernyak and Zhitnitsky[5] have derived a set of asymmetric wave functions which satisfy the constraints from QCD sum rules and also give good agreement with the size and shape for G_M^p (dashed curve in Fig. 1).

Several developments should take place before one could conclude that PQCD becomes applicable around $Q^2 = 5$ (GeV/c)^2 and that the valence quarks in the nucleon do not share momentum equally. The first is that numerical calculations of F_2 are required. It is quite possible that the slow decrease in $Q^4 G_M^p$ with Q^2 is not due to the running of α_s and the $\ln(Q^2)$ terms, but to there being a substantial contribution to G_M^p from F_2 in this Q^2 range. This can be seen in an extended VDM fit (which required that $F_1 \sim C_1/Q^4$ and $F_2 \sim C_2/Q^6$ at high Q^2) made by Gari and Krumpelmann[6] (see Figure 2). On the experimental side, measurements of G_E^p are sorely needed. For example, if $G_E^p = G_M^p$ above $Q^2 = 6$ (GeV/c)^2, rather than $G_E^p = G_M^p/\mu_p$, as suggested by one diquark model,[7] than the values for $Q^4 G_M^p$ extracted from the measured cross sections would be almost completely independent of Q^2 above $Q^2 = 6$ (GeV/c)^2, instead of showing the slow decrease seen in Figure 1.

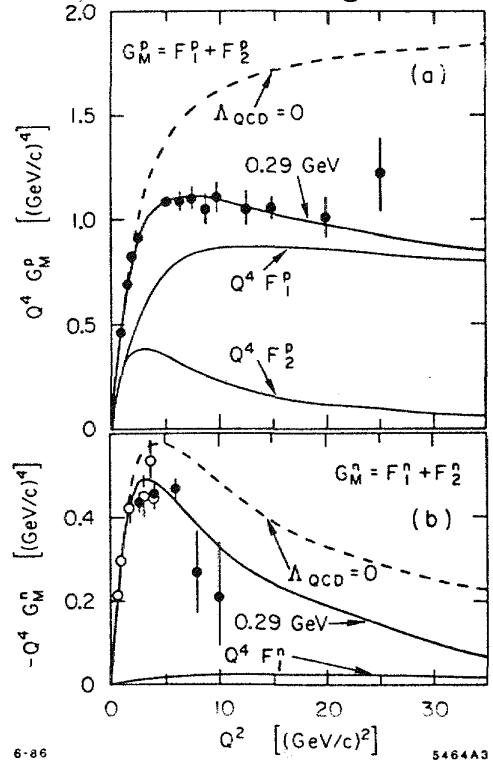

Fig. 2. Data for a) G_M^p and b) G_M^n compared to VDM + QCD fit of Ref. 6.

Aside from their value in interpreting the high Q^2 SLAC data, measurements of G_E^p are interesting in their own right in providing additional constraints on the VDM fits and probing the transition region to PQCD. The existing data (divided by the dipole law $G_D = 1/(1 + Q^2/.71)^2$) are shown in Figure 3, along with some of the VDM models. The error bars do not permit discrimination among models above $Q^2 = 3$ (GeV/c)^2. Not shown are preliminary results from a recent Rosenbluth experiment[8] at SLAC which made measurements up to $Q^2 = 3$ (GeV/c)^2. The new data do not show any significant deviation from the dipole law. Further measurements[9] at SLAC using the Rosenbluth separation method are planned up to approximately $Q^2 = 6$ (GeV/c)^2 with an error on G_E^p/G_D of ± 0.15 at the highest Q^2 (open rectangles in Figure 3). To achieve these small errors requires measurements over a large range of the polarization parameter ϵ. Forward angle measurements are needed with beam energies of 10 GeV or more, while backward angle measurements require a spectrometer

with a large solid angle to maintain reasonable count rates. Very good control over systematic errors is also required. Due to its limited beam energy, CEBAF will probably not be able to go much higher in Q^2 using the Rosenbluth method, but could likely obtain significantly smaller errors at moderate Q^2 by using combinations of polarized beams, polarized targets, and polarimeters to measure assymetries which are directly proportional to G_E^p.

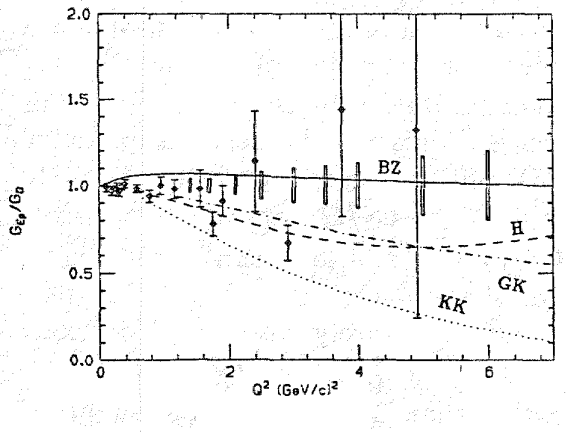

Fig. 3. Existing data for G_E^p compared to some VDM fits.[2] The open rectangles show the expected errors from a future SLAC experiment.[9]

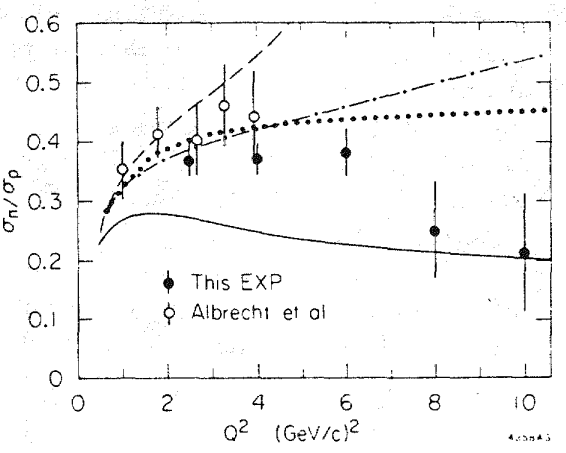

Fig. 4. Data[10] for σ_n/σ_p compared to VDM models of Höhler et al.[2] (dashed) and Blatnik and Zovdko[2] (solid) and to form factor scaling (dotted) and the dipole law (dashed-dot).

NEUTRON ELASTIC FORM FACTORS

Experimental knowledge of the neutron form factors has been necessarily much more limited than that of the proton due to the lack of a free neutron target. Most experiments have been performed using the deuteron as a target and subtracting the contribution from the proton. Existing measurements[10] of the ratio of neutron to proton cross sections at forward angles are shown in Figure 4. The results were all obtained from quasi-elastic scattering from the deuteron, and the error bars are dominated by the uncertainty in subtracting inelastic contributions rather than by statistics. The data show a fairly constant ratio between $Q^2 = 1$ and 6 $(\mathrm{GeV/c})^2$, then a slow decrease at high Q^2. The agreement with older VDM fits (done before the neutron data was available) is not particularly good, nor do the high Q^2 data seen to be in good agreement with empirical relations such as form factor scaling ($G_M^p/\mu_p = G_E^p = G_M^n/\mu_n$ and $G_E^n = 0$) or the dipole law ($G_M^n/\mu_n = G_D$ and $G_E^n = 0$). The best description of the data comes from models[6,11] in which F_1^n is small compared to F_2^n (see Figure 2). Calculations in PQCD have yet to be performed, but would likely shed light on the origin of the differences between proton and neutron cross sections.

The separation of the electron and magnetic form factors of the neutron has proven to be extremely difficult experimentally. The existing data for $(G_E^n/G_D)^2$ (see Figure 5) show that G_E^n is much smaller than G_M^n at low Q^2, and are equally compatible with either $F_1^n = 0$ or $G_E^n = 0$. The experiment[9] approved to run at SLAC to extend the measurements of G_E^p to high Q^2 will also try to extend the separation of G_M^n and G_E^n to $Q^2 = 4$ (GeV/c)^2 by performing Rosenbluth separations on quasi-elastic scattering from deuterium. The anticipated error bars from this experiment are shown as the tall rectangles in Figure 5 and should be small enough to distinguish between $F_1^n = 0$ and $G_E^n = 0$. While much of the relatively large errors come from counting statistics and the need to subtract the effect of the proton, a detailed knowledge of how the cross section deviates from the impulse approximation will be needed to have full confidence in the results. The error bars shown include estimates for all these possible sources of uncertainty. Plans also exist to make precision measurements of G_E^n at Bates at relatively low Q^2 using both polarization transfer (polarized beam and neutron polarimeter) and the scattering of polarized electrons from a polarized ^3He target. These measurements could be extended to higher Q^2 at CEBAF.

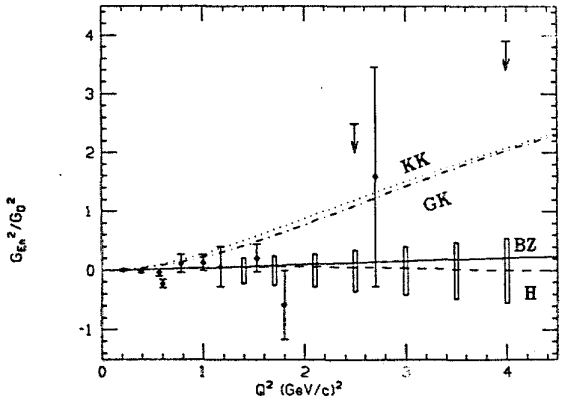

Fig. 5. Existing (solid circles) and potential (open rect.) data for $(G_E^n/G_D)^2$. Curves GK[6] and KK[11] have $F_1^n = 0$.

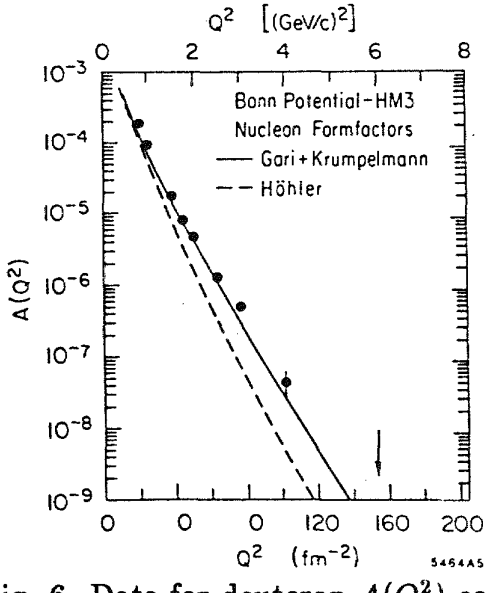

Fig. 6. Data for deuteron $A(Q^2)$ compared to IA calculations[12] with nucleon form factors from Refs. 2 and 6.

A better knowledge of the nucleon form factors will be important in interpreting existing and potential data from nuclear targets. A first example is the forward angle form factor of the deuteron $A(Q^2)$. As shown in Figure 6, the choice of form factors can change the calculations by a factor of 4 at $Q^2 = 4$ (GeV/c)^2. Another example is in quasi-elastic scattering from nuclei, where the longitudinal strength has been found to be smaller than expected.[13]

The choice of form factors can change[14] the predicted longitudinal strength at $Q^2 = 1$ (GeV/c)^2 by 25% for most nuclei and as much as 40% for ^3H. The effect is even larger at higher Q^2. It is vital to know the nucleon form factors before one can blame the disagreement between calculations and data for the longitudinal response function on more exotic effects.

DEUTERON ELASTIC FORM FACTORS

The electromagnetic form factors of the deuteron at high momentum transfer have long been of interest for the information they contain on the short range nucleon-nucleon interaction and the role of meson exchange currents and relativistic effects. There are three form factors (charge G_C, magnetic G_M, and quadrupole G_Q) which can be determined from three experimentally measurable quantities:

$$A(Q^2) = G_C^2 + \frac{8}{9}\tau^2 G_Q^2 + \frac{2}{3}\tau G_M^2 \tag{3}$$

$$B(Q^2) = \frac{4}{3}\tau(1+\tau)G_M^2 \tag{4}$$

$$P(Q^2) = \frac{4\sqrt{2}}{3}\frac{\tau G_Q(G_C + \frac{\tau}{3}G_Q)}{(G_C^2 + \frac{8}{9}\tau^2 G_Q^2} \tag{5}$$

where $\tau = Q^2/4M_d^2$. The quantities $A(Q^2)$ and $B(Q^2)$ are measured using unpolarized electrons and deuterons at forward and backward angles respectively, while measurements of $P(Q^2)$ require the use of polarization.

The existing data[16] for $A(Q^2)$ are shown in Figure 6. Non-relativistic impulse approximation calculations tend to fall below the data, but can be brought into agreement using non-zero values for G_E^n, wave functions with strong high momentum components, or large relativistic corrections. Fits have also been made using parton models (see Ref. 15 for a review of calculations).

The structure function $B(Q^2)$ is a more sensitive test of models than $A(Q^2)$ since it is proportional to only one form factor (rather than three) as is predicted to have a diffraction minimum around $Q^2 = 2$ (GeV/c)^2. New data[17] have recently become available from an experiment at SLAC which detected electrons backscattered at 180° is coincidence with deuterons recoiling at 0°. The new data are shown as the solid circles in Figure 7 and do indeed show a minimum around $Q^2 = 2$ (GeV/c)^2. The non-relativistic impulse approximation using the Pairs wave function[18] has the minimum at too low a Q^2 (solid curve), but this is improved when isobar admixtures and isoscalar meson exchange currents are taken into account[19] (dashed curve) or when the wave function is treated relativistically[18] (dotted curve). Interestingly, the Skyrme model (expected to

work best at low Q^2) gives a result[20] indistinguishable from the dotted curve. Perhaps the most significant result is the strong disagreement with the smooth falloff of parton model predictions, an example[21] of which is shown as the dot-dashed curve.

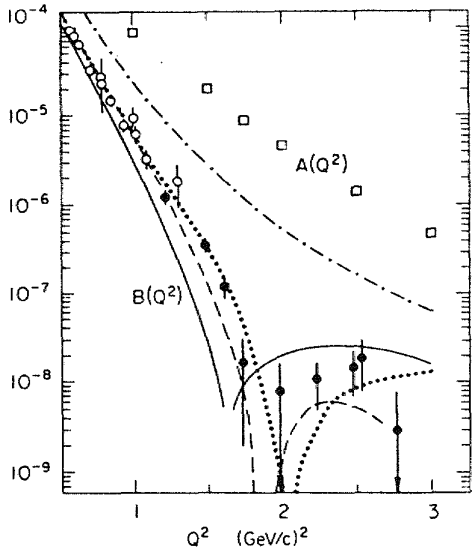

Fig. 7. Data for $B(Q^2)$ compared to various models (see text).

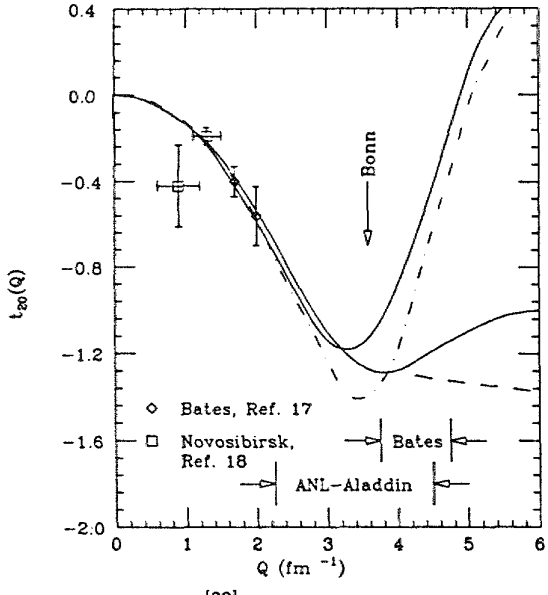

Fig. 8. Data[22] for t_{20} along with Q^2 ranges for future data. The dashed curve[23] is a QCD result, while the other curves are discussed in Ref. 24.

The data[22] for t_{20}, which is directly related to $P(Q^2))$ are shown in Figure 8. Data will soon be taken at Bates (see Figure for Q^2 range) which will go to high enough Q^2 to distinguish among various models. It will be especially interesting to see if QCD predictions[23] that t_{20} remain negative at large Q^2 are borne out. If the results support the traditional impulse approximation calculations (solid and dot-dashed curves in Figure 8), then increasingly tight constraints will be placed on models to simultaneously explain all the data for $A(Q^2)$, $B(Q^2)$, t_{20}, and the nucleon-nucleon scattering data.

DEUTERON THRESHOLD ELECTRODISINTIGRATION

The electrodisintigration of the deuteron near threshold has been shown to be one of the most sensitive reactions to non-nucleonic degrees of freedom (specifically isovector meson exchange currents).[26] The data[25] at backwards angles (where the M1 transition to the almost bound isospin triplet $^1S_0$ state dominates) averaged over excitation energies $E_{np} = 0$ to 3 Mev are shown in Figure 9. Impulse approximation calculations (not shown) fall far below the data at the higher Q^2, but the inclusion of MEC and isobar admixtures can bring calculations into reasonable agreement with the data.[26,27] Two areas of

uncertainty in the calculations are whether to use F_1^V or G_E^V in calculating the MEC, and in either case what is the size of G_E^n (see the four curves[26] shown in Figure 9). The somewhat more speculative hybrid quark cluster models[28] can find agreement with the data but predict a minimum in the cross section just where the data ends. This is contradiction to preliminary cross section data from experiment NE4 at SLAC[29] which continue to fall smoothly up to $Q^2 = 70$ fm^{-2}. The NE4 results have poor energy resolution ($\delta E_{np} = \pm 8$ MeV typically) but can still place significant limits on the cross section near threshold. A new experiment at Bates[30] has been approved to take data up to $Q^2 = 50$ fm^{-2} with good energy resolution. This new data will provide severe constraints on current models, complementary to those provided by measurements of $B(Q^2)$.

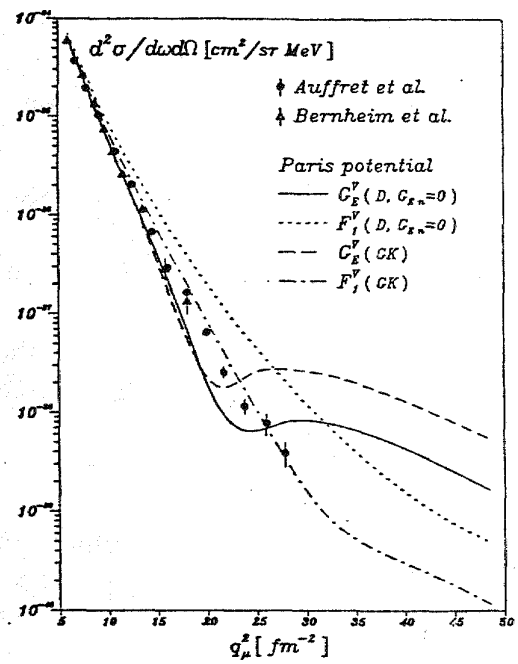

Fig. 9. Data[25] for $d(e,e')np$ averaged over $E_{np} = 0$ to 3 MeV compared to predictions[26] with different form factors.

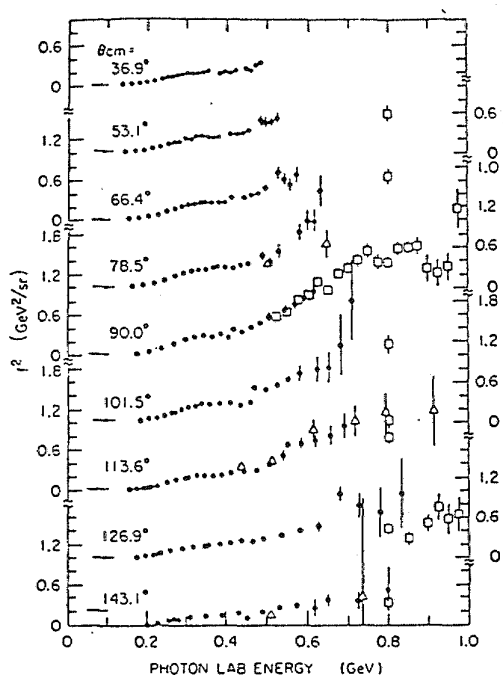

Fig. 10. Existing data[31] for photodisintigration of the deuteron with the s-dependence of QCD scaling[32] removed.

PHOTODISINTIGRATION OF THE DEUTERON

Another area where the importance of non-nucleonic degrees of freedom can be tested is in the photodisintigration of the deuteron. This is perhaps one of the simplest nuclear reactions, and has been studied in detail both experimentally[31] and theoretically at beam energies below 500 MeV, where the data is reasonably well described in terms of conventional meson-exchange theory.[33] Between 500 Mev and 1 Gev the small sample of data fall below the predictions. This has led

Brodsky and Hiller[32] to suggest that (at least around 90° in the c.m. system) the onset of dimensional scaling may have been reached. Dimensional scaling is based on lowest order perturbative QCD arguments and does very well is describing the energy dependence of meson photoproduction from the nucleon at energies above a few GeV. Dimensional scaling predicts that the reduced cross section

$$f^2(\theta_{CM}) = \frac{d\sigma}{d\Omega} \frac{\sqrt{s(s - M_d^2)}}{F_p(t_p)F_n(t_n)} \tag{6}$$

should be independent of s, the total energy in the c.m. system. The values for $f^2(\theta_{CM})$ for existing data[31] are plotted in Figure 10, where it can be seen that there is a hint of energy independence above 700 MeV. An experiment[34] is planned at SLAC in the near future to extend the data with reasonably small error bars up to 1.8 GeV. By the very nature of the kinematics involved, the new data will be very sensitive to the short range description of the nucleon-nucleon interaction, whether it be described in terms of extensions of the conventional model with additional N^* resonances, hybrid models including 6-quark clusters, bag models, or perturbative QCD.

QUASI-ELASTIC SCATTERING FROM DEUTERIUM

Quasi-elastic scattering from the lightest nucleus, the deuteron, is of particular interest since (below pion threshold) the final state is completely determined and relatively exact calculations can be made. As was discussed in a previous section, the area near the quasi-elastic peak can be used to determine the neutron form factor since the impulse approximation is believed to work well in this region. The region between threshold and the quasi-elastic peak is of particular interest because it is sensitive to the high-momentum components of the deuteron wave function. There exists a considerable amount of data at forward angles[35] which was compared[36] to the non-relativistic impulse approximation to estimate the deuteron wave function. Good agreement with the Paris wave function was found at low momenta ($P < 200$ MeV), but substantially higher values were found for $200 < P < 600$ MeV. Recent work[37] has shown that most of this discrepancy can be removed if the cross sections are compared to a calculation that takes into account final state interactions.

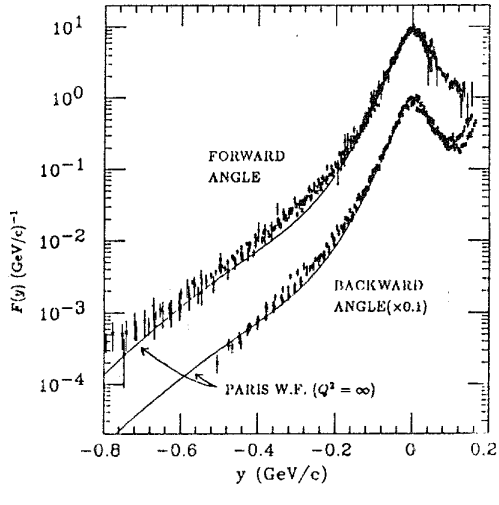

Fig. 11. $F(y)$ for forward angle data[35] (above) and preliminary backward angle data[29] (below).

There has recently become available cross section measurements at backward angles from Bates[38] at low Q^2, at Kharkov[39] for $0.5 < Q^2 < 1.0$ $(\mathrm{GeV/c})^2$, and at SLAC[29] for $1.0 < Q^2 < 2.75$ $(\mathrm{GeV/c})^2$. The new data allow comparisons of forward angle structure functions $W_2(Q^2,\nu)$ with backward angle structure functions $W_1(Q^2,\nu)$. The Kharkov data show that the ratio

$$R = \frac{\sigma_L}{\sigma_T} = \frac{W_2}{W_1}(1 + \frac{\nu^2}{Q^2}) - 1 \qquad (7)$$

is small (< 0.3) near the quasi-elastic peak, as expected if scattering from spin-$\frac{1}{2}$ nucleons dominates, but becomes larger than 1.0 close to threshold. Calculations of R using the new SLAC data are presently underway. It will be interesting to see if this trend continues. Large values of R could indicate important contributions from scattering of spin-0 or spin-1 clusters.

Another common way of analyzing quasi-elastic data is in terms of y-scaling. First proposed by West[40] as a way of searching for universal single-particle momentum distributions in nuclei, it has been found to be remarkably successful in describing data over a large range of Q^2 and A. In the case of the deuteron a direct connection can be made between scaling functions and models, which can be shown to scale more or less well depending on the choice of variable and scaling function. For the definitions of y and $F(y)$ used in Ref. 36, both the forward angle[35] and preliminary backward angle SLAC data scale remarkably well, as shown in Figure 11. While the two data sets agree very well at the quasi-elastic peak, the backward angle $F(y)$ tends to be somewhat lower than the forward angle $F(y)$ for $y < 0.2$ GeV/c. Further analysis will be needed to interpret this difference.

THE EMC EFFECT AND R IN DEEP INELASTIC SCATTERING

The discovery of the difference in the structure functions $F_2(x)$ for iron and deuterium targets (the 'EMC effect') has sparked considerable activity in the theoretical study of deep inelastic scattering from nuclear targets. Models for the EMC effect (see Ref. 41 for a review) are built of ideas such as Q^2 rescaling, x-rescaling, binding effects, and contributions from clusters of pions, isobars, and so on. Some models[42] predict large differences for $R = \sigma_L/\sigma_T$ between iron and deuterium, while QCD models and others predict a negligible difference. An experiment to measure the difference in R was recently performed at SLAC. The preliminary results[43] are shown in Figure 12. It can be seen that the difference $R_{FE} - R_D$ is negligible over the x and Q^2 range studied, showing that there are no significant spin-0 constituents or higher twist effects in nuclei as compared to free nucleons. The new data also show that a nuclear dependence to R cannot be used to explain the difference between the lower Q^2, larger angle SLAC data and the higher Q^2, smaller angle CERN data for

σ^{FE}/σ^{D} at low x, as proposed by some authors.[44] It should be noted that the discrepancy at low x has been much reduced with the new CERN data (see Ref. 41 for a review).

The Q^2 dependence of R for hydrogen or deuterium is a sensitive probe of the transition region to perturbative QCD. At very large Q^2, R should be zero for scattering from spin-$\frac{1}{2}$ quarks, but at lower Q^2 target mass effects lead to a form of R which falls like powers of $1/Q^2$, while gluon processes lead to a form which falls like $1/\ln(Q^2/\Lambda^2)$ (see for example Ref. 45). The preliminary data from SLAC E140 for R_D at $x = .2$ (and a high Q^2 data point from CDHS for iron) are shown as a function of Q^2 in Figure 13. Good agreement is found with the upper curve, which includes both gluon contributions and target mass corrections. Similar agreement is found at higher values of x. The errors on the SLAC R_D values will shrink when the analysis of radiative corrections is completed.

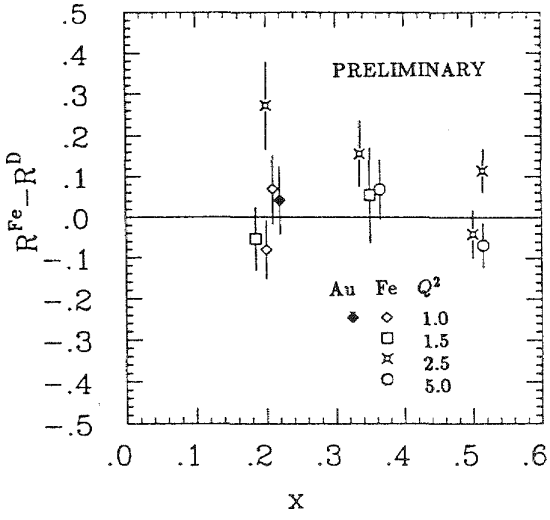

Fig. 12. Preliminary values of $R_{FE} - R_D$ as a function of x for various Q^2 values from SLAC E140 experiment.[43]

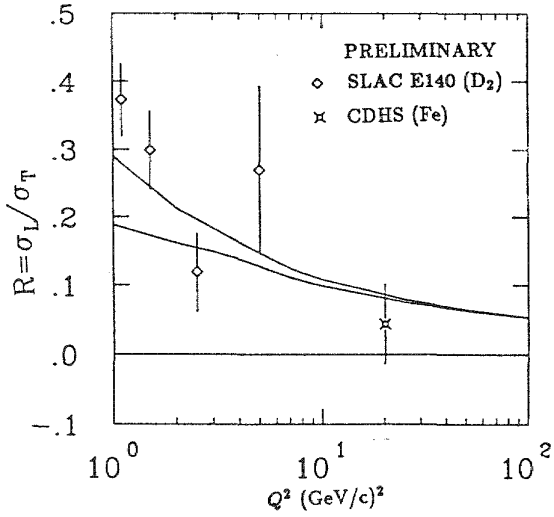

Fig. 13. R vrs Q^2 at $x = 0.2$. The lower curve is a perturbative QCD calculation including gluon contributions, while the upper curve also includes target mass contributions.

CONCLUSIONS

The examples cited in this paper show that experiments measuring the electromagnetic properties of few body systems are pushing towards ever higher energies and precision. These data provide stringent tests of our understanding of short range properties and non-nucleonic degrees of freedom. Theoretical approaches using PQCD, bag models, relativistic nucleon and meson models, the Skyrme model, and so-called hybrid models are making progress in their

ability to quantitatively understand the results obtained so far and make predictions that will be tested by future experiments. The availability of 4 to 6 GeV high current, high duty factor polarized electron beams at CEBAF, in combination with polarized targets or polarimeters, will open a new frontier in making precision measurements of quantities such as the neutron form factor, the transition form factors of the nucleon resonances, the deuteron t_{20} at high Q^2; and the ΛN interaction. Experiments which require higher energy, such as hadronization in deep inelastic scattering or measurements of the deep inelastic spin structure functions of the nucleon are being studied for feasibility using internal targets at the PEP storage ring. At very high energies, measurements in the deep inelastic region using muons continue to be made at Fermilab[46] and CERN.[47] Pushing the frontiers of the few-body electromagnetic problem will continue to keep us busy for many years to come.

REFERENCES

1. R. G. Arnold, AIP Conference Proc. 150, p.83 (1986); R. R. Whitney, 'Electromagnetic Interactions with Few-Body Systems', XI Int. Conf. Part. Nuclei, Kyoto, Japan, April 1987; B. Frois and C. Papanicolas, 'Electron Scattering and Nuclear Structure', U. Illinois preprint P/87/7/118.
2. G. Höhler et al., Nucl. Phys. B114, 505 (1976); S. Blatnk, N. Zovko, Acta Phys. Austriaca 39, 62 (1974); F. Iachello, A. Jackson, A. Lande, Phys. Lett. 43B, 191 (1973).
3. R. Arnold et al., Phys. Rev. Lett. 57, 174 (1986).
4. S. Brodsky, G. Lepage, Phys. Rev. D22, 2157 (1980).
5. V. L. Chernyak, I. R. Zhitnitsky, Nucl. Phys. B246, 52 (1984): V. L. Chernyak, I. R. Zhitnitsky, Phys. Rep. 112, 1973 (1984).
6. M. Gari, W. Krumpelmann, Z. Phys. A322, 689 (1986).
7. M. Anselmino, P. Kroll, B. Pire, WU B 87-2, February 1987.
8. R. Walker et al., SLAC experiment E140, to be published.
9. SLAC experiment NE11, P. Bosted spokesman.
10. S. Rock et al., Phys. Rev. Lett. 49, 1139 (1982); R. J. Budnitz et al., Phys. Rev. 173, 1357 (1968); W. Albrecht et al., Phys. Rev. 26B, 642 (1968).
11. J. G. Körner, M. Kuroda, Phys. Rev. D16, 2165 (1977).
12. R. Arnold et al., Phys. Rev. C21, 1426 (1980).
13. Z. Meziani et al., Phys. Rev. Lett. 54, 1233 (1985) and references therein.
14. O. Benhar et al., INFN-ISS-87/1 (1987).

15. V. M. Muzafarov et al., Fiz. Elem. Chastits At Yadra 14, 1112 (1983) [Sov. J. Part. Nucl. 14, 467 (1983)].

16. R. G. Arnold et al., Phys. Rev. Lett. 35, 776 (1975).

17. R. G. Arnold et al., Phys. Rev. Lett. 58, 1723 (1987).

18. R. S. Bhalero and S. A. Gurvitz, Phys. Rev. C24, 2273 (1981).

19. E. Lomon et al., Proc. IUPAP Int. Nucl. Phys. Conf., Vol. I, p. 478.

20. M. Nyman and D. O. Riska, Phys. Rev. Lett. 57, 3007 (1986).

21. M. Chemtob and S. Furui, Nucl. Phys. A454, 548 (1986).

22. M. E. Schultz et al., Phys. Rev. Lett. 52, 597 (1984); Y. F. Dmitriev et al., Phys. Lett. 157B, 143 (1985).

23. C. E. Carlson and F. Gross, Phys. Rev. Lett. 53, 127 (1984).

24. W. Turchinetz, Proc. Eur. Work. Few-Body Phys., Rome, 1986, p. 326.

25. S. Auffret et al., Phys. Rev. Lett. 55, 1362 (1985); M. Berheim et al., Phys. Rev. Lett. 46, 402 (1981).

26. H. Arenhovel, Mainz Preprint MKPH-T-87-4.

27. J. Mathiot, Nucl. Phys. A412, 210 (1984).

28. T.-S. Cheng, L. S. Kisslinger, Nucl. Phys. A457, 602 (1986): Y. Yamauchi et al., Nucl. Phys. A443, 628 (1985).

29. SLAC Experiment NE4, G. Petratos and P. Bosted, private communication.

30. R. Miskamen and G. Peterson, spokesmen.

31. J. Arends et al., Nucl. Phys. A412, 509 (1984) and references therein.

32. S. J. Brodsky and J. R. Miller, Phys. Rev. C28, 475 (1983).

33. J. M. Laget, Nucl. Phys. A312, 265 (1978).

34. SLAC Experiment NE8, R. Holt spokesman.

35. W. P. Schultz et al., Phys. Rev. Lett., 38, 259 (1977); S. E. Rock et al., Phys. Rev. Lett., 49, 1139 (1982).

36. P. E. Bosted et al., Phys. Rev. Lett., 49, 1380 (1982).

37. C. degli Atti et al., Nucl. Phys. A463, 127 (1987).

38. B. Parker et al., Phys. Rev. C 34, 2354 (1986): A. Bernstein et al., to be published.

39. Yu. I. Titov, Kharkov Preprint KPTI 87-38.

40. G. B. West, Phys. Rep. 18C, 263 (1975).

41. E. L. Berger and F. Coster, ANL-HEP-PR-87-13 (1987).

42. B.-Q. Ma and Ji Sun, Print-86-1217, Beijing U. (1986).

43. S. Dasu et al., UR-991 and UR-998 (Rochester 1987).

44. I. A. Savin and G. I. Smirnov, Phys. Lett. 145B, 438 (1984).

45. G. Altarelli and G. Martinelli, Phys. Lett. 28B, 89 (1978).

46. Fermilab experiment E665, PHY-4622-ME-85.

47. D. Allasia et al., the New Muon Collaboration, CERN Proposal SPSC/P210.

STUDY OF NUCLEAR CORRELATIONS AND THREE-BODY FORCES WITH ELECTRONS

J.M. Laget
Service de Physique Nucléaire - Haute Energie
CEN Saclay, 91191 Gif-sur-Yvette Cedex, France

The one-body properties of nuclei are nowadays well under control. For instance, the extensive study of elastic or inelastic electron scattering have made possible precise measurements of the nuclear shapes, and the single particle orbitals have been singled out and studied by means of the (e,e'p) reaction. While those results have provided us with strong constraints on the self consistent mean field picture of nuclei, in which nucleons are bound by effective long ranged two-body forces, we are still left with the two following open questions :

- What is the nature, and how can we study the effects, of the short range correlations in nuclei?
- What is the size and what are the effects of the three-nucleon force?

Those are very old problems [1,2] which are still unsolved.

The reason is that the meson and Δ degrees of freedom dominated all the attempts which have been made so far to study the short range behavior of nuclei : the use of probes of increasing energy requires to take into account the deformation of the nucleon and to consider also the coupling with each mechanism which drives the nucleon-nucleon force.

While the study of these meson and Δ degrees of freedom in nuclei has been an important achievement of the last two decades, the major task of Nuclear Physics is now to go beyond and to study nuclei in kinematical regions where their effects are strongly suppressed or with probes to which they couple weakly.

I have already dealt with these problems in [3] where a complete summary and a general background can be found. To day I will try to review the relevant experiments to be performed at a few Gev electron machines, and the problems raised by their analysis.

1. The high momentum conponents of the nuclear wave function

Provided that final state interaction and meson exchange current effects are fully taken into account the analysis [4,5] of the (e,e'p) reactions, recently studied at Saclay [6,7] and Amsterdam [8] for small values of the four momentum of the virtual photon, has led to strong contraints on the D and ^{3}He wave functions, up to momenta as large as 500 MeV/c.

Fig. 1 beautifully illustrates this point. It summarizes the cross sections of the D(e,e'p)n and ^{3}He(e,e'p)d reactions which have been measured at Saclay [6,7] during the past few years. The three kinematical settings have been chosen in such a way that the increase of the Mott cross section, when the electron scattering angle moves forward, compensates the rapid fall-off of the nuclear wave function. These kinematics, which maximize the longitudinal component of the cross section, minimize the effects of meson exchange currents (MEC). Although the corrections to the impulse approximation are significant and are necessary to reproduce the experiment, they do not dominate the cross-section. Moreover, they are strongly constrained by gauge invariance, which links in a consistent way the wave functions of the initial and final states and the various interaction effects.

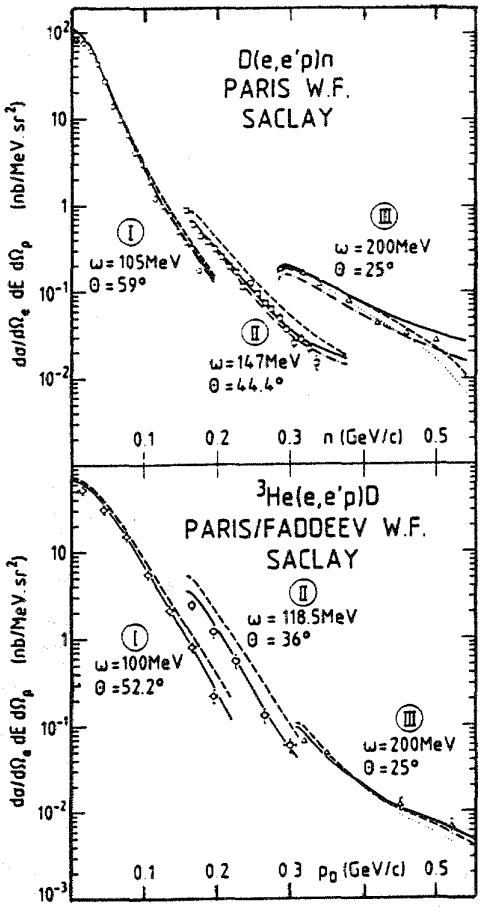

To day the cleanest signature of two-nucleon correlations is the spectrum of the protons emitted in the continuum of the reactions ^{3}He(e,e'p) x [7] and ^{3}He(γ,p) x [9], which have been recently measured at Saclay. The top of the peak, which appears in fig. 2, corresponds to the electrodisintegration of a nucleon pair at rest, and its width is due to its Fermi motion in ^{3}He.

While the (γ,p) spectra are dominated by the exchange current contribution and the Δ-formation mechanism, the (e,e'p) spectra are more directly sensitive to the relative wave function of the two active nucleons.

Fig. 1 - The cross sections of the D(e,e'p)n and ^{3}He(e,e'p)d reactions recently measured at Saclay [6,7] are plotted against the momentum of the undetected nuclear fragment. The electron scattering angle θ and the energy ω of the virtual photon are given for each kinematics. The dotted line curves are the impulse approximation. The dashed line curves correspond to the plane wave treatment and include the neutron exchange or the two nucleon exchange graph. The dash-dotted line curves correspond to the distorted wave treatment. The full line curves include also the meson exchange contribution.

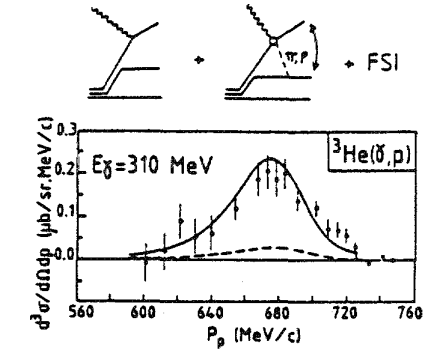

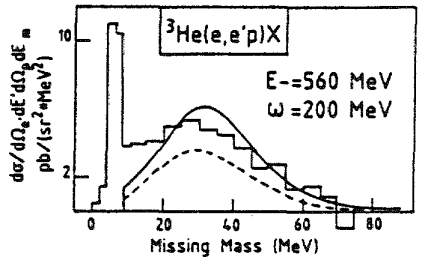

Fig. 2 - In the upper part, the spectrum of the protons emitted at θ_p = 23° in the reaction $^3He(\gamma,p)$ is plotted against the proton momentum. In the lower part, the spectrum emitted in the $^3He(e,e'p)$ at θ_p = 60° is plotted against the missing mass of the undetected system. The full curves are the result of the complete calculation [4,10]. Meson exchange currents and Δ-formation mechanisms are not included in the dashed curves.

Fig. 3 shows, the ratio of the experimental to the theoretical cross sections computed with the latest Hannover-Paris [11] wave function. It is compared to the ratio of the theoretical cross-sections computed with recent three-body wave functions [12, 13] and the Hannover-Paris one. It is very close to the ratio of the corresponding momentum distributions. However, the discontinuity, when two kinematics overlap, clearly shows that the cross section does not factorize into the momentum distribution and the electron nucleon elastic scattering cross section. It is therefore not possible to correct for the interaction effects the spectral function usually extracted from the

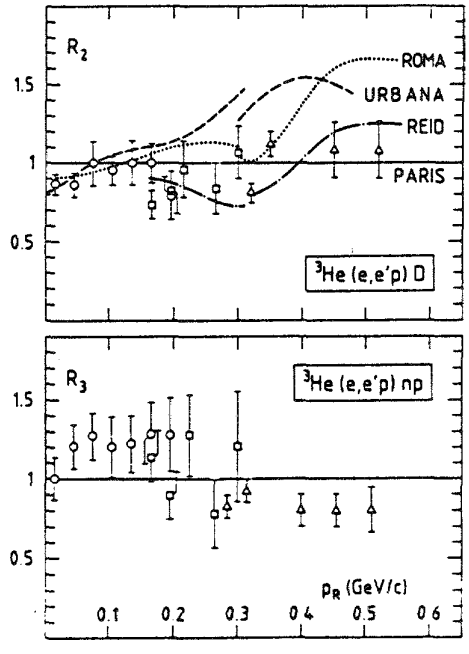

Fig. 3 - The ratio R_2 between the experimental cross-section [7] of the $^3He(e,e'p)d$ and the theoretical cross-section computed with the Hannover-Paris [11] wave function, is plotted against the momentum of the deuteron. The dashed, dotted, and dash-dotted line curves are the ratio between the theoretical cross sections, computed respectively with the Urbana [12], Roma [13] or Faddeev-Reid [14] wave functions, and the Hannover-Paris one [11]. The ratio R_3 has the same meaning for the $^3He(e,e'p)np$ channel, and is plotted against the momentum of the undetected np pair.

experiment [6,7] with the popular Plane Wave Impulse Approximation (PWIA). Only direct comparison of the cross sections makes sense. While the experiment hardly distinguishes between the Faddeev wave functions obtained with similar potentials as the Paris [11] or the Reid [14] one, it rules out the variational wave functions [12,13] whose high momentum components are too large.

This comparison of the theory and the experiment summarizes the present status of our knowledge of the high momentum components of the few body system, and clearly indicates the measurements to be performed in the future. While the high momentum components of D and ^{3}He are determined at the level 20 % up to 500 MeV/c, a more accurate determination requires a significant increase of the duty factor and the extension of such an analysis to higher momenta, and shorter distances, calls for electron beams of higher energies than those of the present generation of accelerators. Moreover the separation of the transverse and longitudinal components of the cross section is the necessary step to get rid of the exchange current contribution, and to study more directly the wave functions in the longitudinal cross section.

2. The pd capture reactions

Therefore no freedom is left to play with the high momentum components of the three-body wave function. It can be used to analyse other channels as for instance, the pd → $T\pi^+$ [15] and the pd → $^3He\gamma$ [16] reactions. Fig. 4 represents the analysis [15] of the angular distribution of the pd → $T\pi^+$ reaction at T_p = 500 MeV [17] and T_p = 800 MeV [18]. The relevant graphs are given in fig. 5. The analysis [16] of the 90° excitation function of the γ^3He → pd reaction [19-25] is shown on fig. 6.

Due to large momentum transfers, the one-body mechanisms are strongly suppressed. Two-body mechanisms dominate the cross section and lead to a fair agreement with a large bulk of experimental data [3, 26]. While the unpolarized differential cross sections and spin observables are well reproduced at forward angles, strong deviations appear around 90° and larger angles. For instance, at θ= 90° the cross section of the pd → $T\pi^+$ and γ^3He → pd reactions are respectively underestimated by one order of magnitude and more than a factor two. This discrepancy is really significant, since the two-body matrix elements have been calibrated against the D(π,p)p and D(γ,p)n reaction [3], and since we have seen that the three-body wave function has been checked in the same range of momenta.

The meson double scattering mechanism, depicted in fig. 5 for the pd → $T\pi^+$ channel and in fig. 7 for the γ^3He → pd channel, accounts for a large part of the disagreement between the theory and the experiment. When the momentum transfer increases, its contribution becomes more important than the contribution of the two-body mechanisms. First, it is more likely to be shared between three rather

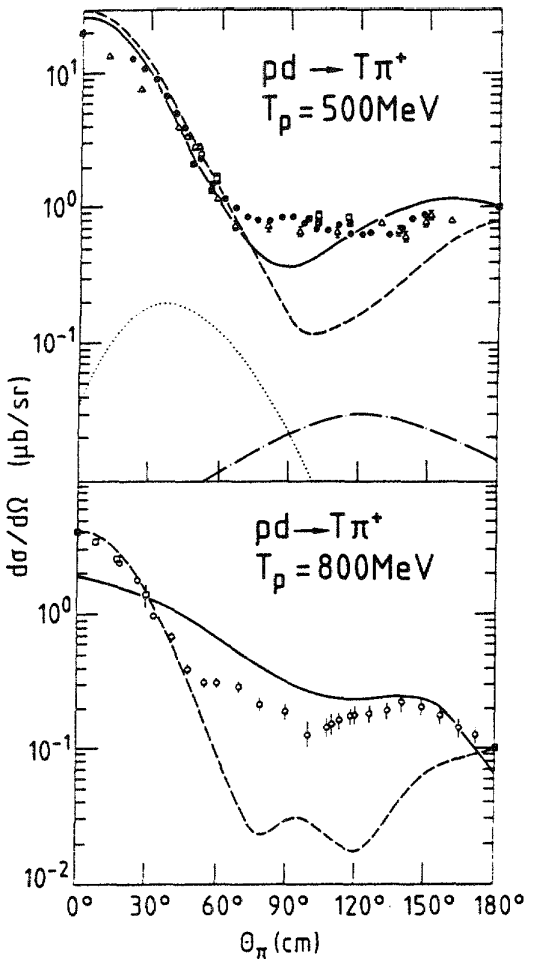

Fig. 4 - The unpolarized angular distribution of the pd → Tπ+ reaction at T_p = 500 MeV [17] and T_p = 800 MeV [18] is plotted against the pion angle. The full line curves include the three- body mechanisms, whereas the dashed line curves do not. The contributions of the nucleon exchange graph and the two nucleon exchange graph (resp. Ia and Ib in fig. 5) alone are represented respectively by the dotted and the dash-dotted line curves.

than two nucleons. Second, one of the exchanged pion is very close to its mass shell (on its mass shell above the pion threshold), and the corresponding triangular singularity enhances this three-body amplitude.

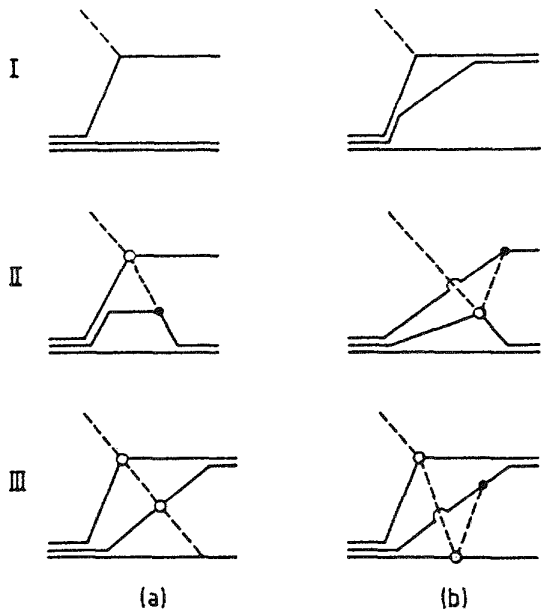

Fig. 5 - The relevant graphs in the pd → Tπ+ reaction. I : the one-nucleon (a) and the two-nucleon (b) exchange graphs. II : the two-body meson exchange graphs. III : the three-body meson exchange graph. Graphs IIb and IIIb come from the antisymmetrization of the two-body meson capture amplitude.

Contrary to the pd → Tπ+ reaction the γ3He → pd reaction has the advantadge to be opened below the pion production threshold. Here both mesons are off shell and this meson double scattering is a prototype of a three-body exchange current, which is related via gauge invariance to the corresponding part of the three nucleon force. The amplitude has the same expression as above thre-

shold, where only on shell elementary amplitudes enter the calculation. Therefore the excitation function, shown in fig. 6, offers us the opportunity to start from a kinematical domain where the calculation is founded on solid ground, and to extrapolate below the pion threshold where the usual problems, due to the virtual nature of the exchanged mesons (from factors, heavy mesons), come in to the game.

It should also be noted that due to the strong suppression of pion absorption by T = 1 nucleon pairs, only pion absorption by T = 0 pairs has to be considered. Since the total isospin of the pd channel is 1/2 the formation of the Δ is forbiden at the first pion scattering or production vertex. For instance, in the $\gamma\,^3He \to pd$ channel only Born terms are relevant, and the dominant graphs are the pion photoelectric and contact terms shown in fig. 7. They are really three nucleon exchange currents which are linked to a given part of the three-body forces.

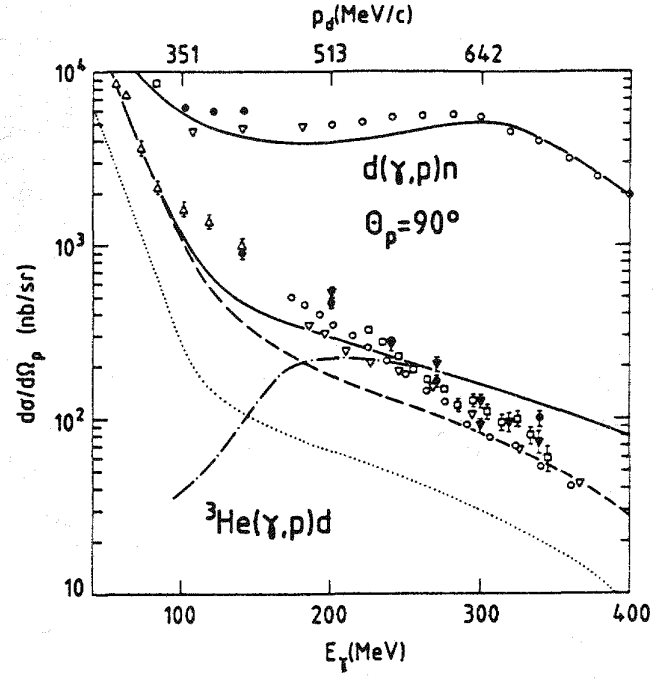

Fig. 6 - The excitation functions, at $[\theta_p]_{c.m.} = 90°$, *of the* $d(\gamma,p)n$ *reaction* [3,21] *and the* $^3He(\gamma,p)d$ *reaction* [19-25] *are plotted against the incoming photon energy. The momentum of the outgoing deuteron is also plotted as abscissa. The dotted-line curve is the contribution of the one-body mechanisms alone. The dashed-line curve includes also the two-body mechanisms. The full line curve takes also into account the meson double scattering mechanisms. Its contribution is the dash-dotted line curve.*

The agreement with the pd radiative capture data is not as good as in the analysis of the $pd \to T\pi^+$ reaction. Presumably this is a hint that other mechanisms, which do not occur in pion induced reactions, must be considered in photon induced reactions. Two examples are depicted in fig. 7 (diagram II). It is well known that ρ exchange contributes significantly to the πN S-wave scattering amplitudes. While the coupling of the photon to the pion is accounted for by diagram Ib, the direct coupling to the exchanged ρ, diagram IIb, must also be considered, especially near the pion threshold and below. It is also well known [27] that two-pion photoproduction proceeds primarily through the emission of a $\pi\Delta$ system in a relative S-wave. When these two pions are virtual (diagram IIa) the

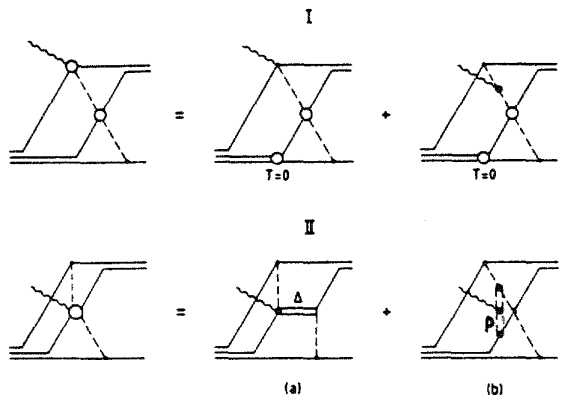

Fig. 7 - The three-body exchange currents in the $\gamma\,^3He \to pd$ reaction. I: The meson double scattering mechanisms is decomposed into its two dominant parts. II: The two relevant graphs which do not reduce to a sequential meson scattering.

amplitude extrapolates smoothly below the $\pi\Delta$ threshold, and the corresponding three-body exchange current might interfer with the meson double scattering amplitude.

To summarize, meson double scattering appears to be a capital ingredient of the cross section of the $^3He(\gamma,p)d$ reaction at high momentum transfer. However, it cannot alone reproduce all the data, and other three-body exchange currents must be considered before any definite conclusion can be reached. All these different mechanisms must be singled out and extensively studied. The flexibility of the three-body kinematics of the $^3He(\gamma,2p)n$ or the $^3He(e,e'2p)n$ reactions will provide us with the way to achieve this goal and to avoid the calculation of a nine fold integral.

3. The three-body forces

Contrary to the $^3He(\gamma,pn)$ reaction, two body mechanisms are strongly suppressed in the $^3He(\gamma,2p)$ reaction, or the transverse part of the $^3He(e,e'2p)$ reaction, because (i) a pp pair has no dipole moments to couple with, (ii) the charged exchange currents are vanishing, and (iii) the formation of the Δ as an intermediate state is forbidden (since the dominant $J^\pi=1^+$ $p\Delta^+$ state cannot decay in the pp channel). When the spectator neutron is at rest, the cross section of the $^3He(\gamma,2p)n$ reaction does not exceed 1 % of the cross section of the $^3He(\gamma,pn)p$ reaction (fig. 8). The calculation is fully described in [3,10]. One of the detected proton is assumed to be emitted at $\theta p = 90°$, with respect to the incoming photon, in the center of mass frame of the active pair. In the pp channel, the background is due to all the graphs due to final state interactions or corresponding to pion reabsorption is a pn active pair. It does not include the pion reabsorption graph in a pp pair, which dominates the (γ,pp) cross section.

Fig. 9 shows the relative importance of the two and three-body mechanisms (fig. 10) in the $^3He(\gamma,pn)$ and $^3He(\gamma,pp)$ reactions [28]. The reduced cross section $d\sigma/d\Omega\, d\underline{n}$ is directly related to the measured cross section (being J the Jacobian) :

$$\frac{d^3\sigma}{dp_1\ d\Omega_1\ d\Omega_2} = J\ \frac{d^2\sigma}{d\Omega_1\ d\underline{n}} \qquad (1)$$

If the neutron is assumed to be a spectator, and if it moves in a relative S-state with respect to the active proton pair, this reduced cross section is basically the product of its momentum distribution and the cross section of the disintegration of a pp pair (see [27] for instance). The mass of the detected nucleon pair and the angle of the proton, measured in the c.m. frame of this pair with respect to the direction of the incoming photon in the Lab system, are kept constant respectively at the values W = 2160 MeV and $[\theta_1]_{c.m.} = 90°$. The reduced cross section is plotted against the momentum of the undetected nucleon which is emitted at $\theta = 45°$ in the Lab frame. The plane wave cross section exhibits the variation of its momentum distribution, and the rise around 500 MeV comes from the antisymmetry of the outgoing three nucleons. At high momentum transfer, final state interactions become important, but the cross section is dominated by the three body mechanisms. In the $^3He(\gamma,pn)$ channel, the flattening

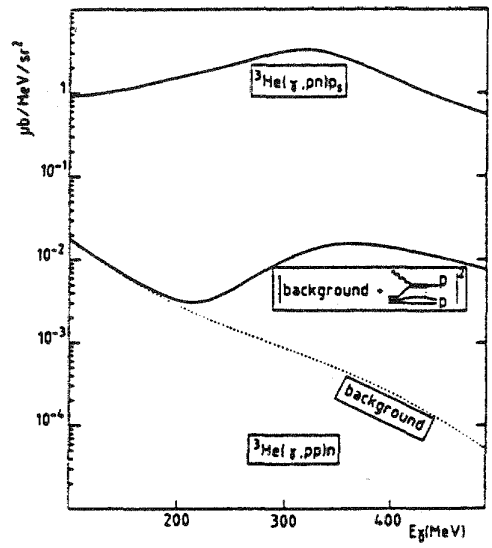

Fig. 8 - The photodisintegration cross section of the pn (upper part) and pp pair (lower part) at rest in ^3He (see text).

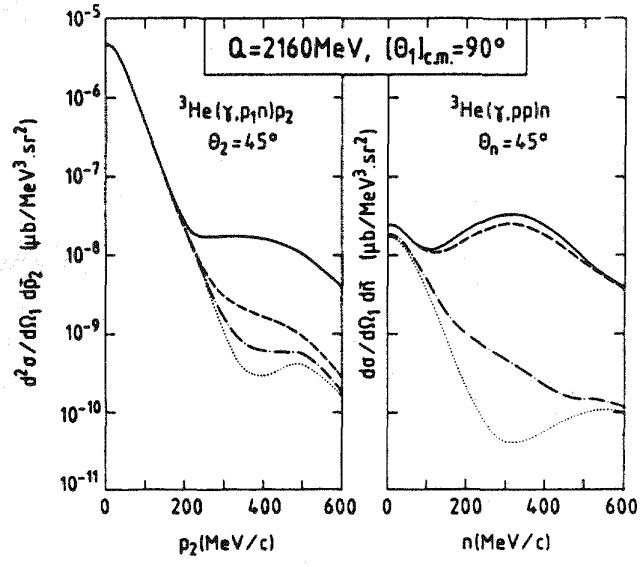

Fig. 9 - The reduced cross sections of the $^3He(\gamma,pn)p$ and the $^3He(\gamma,2p)n$ reactions are plotted against the momentum of the undetected nucleon when it is emitted at 45°, and when the mass of the detected pair is Q = 2160 MeV. The dotted and dash dotted lines represent the contributions of the two body mechanisms, without and with final state interactions respectively. The dashed lines include the three body graph when a π^+ is absorbed by a np pair. The full lines include also the absorption of a π^0 by a np pair.

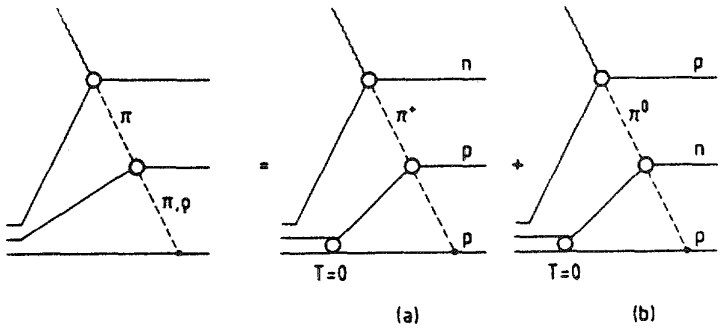

Fig. 10 - The meson double scattering graph in the $^3He(\gamma, 2p)n$ reaction is expressed in terms of the two most important parts : the absorption of a positive (a) or a neutral (b) pion by a T = 0 neutron proton pair.

of the cross section above 200 MeV/c, at the level of 1 % of the peak corresponding to the disintegration of a pn pair at rest, is consistent with a recent study [29] of pion capture by ^3He. In the $^3He(\gamma, 2p)$ channel, two body mechanisms are suppressed by two orders of magnitude and the cross section is entirely driven by the three-body mechanisms. As expected π^+ capture followed by the emission of two protons dominates the $(\gamma,2p)$ channel, whereas π^0 capture leading to the emission of a pn pair dominates the (γ,pn) channel.

This kinematics has been deliberately chosen in such a way to maximize the kinematical domain where the first pion propagates on shell and to enhance the effect of the triangular singularity. Indeed, the three body mechanism dominates the cross section in a small part of the phase space. It is maximized when the neutron is emitted at 45° with a momentum around 300 MeV/c. This corresponds to the most likely kinematics of the recoil nucleon in pion photoproduction on a nucleon at rest. This characteristic behavior of the cross section should be used to single out and study the three body mechanisms, in a domain where the calculation is basically free of parameters. Since it depends only on the low momentum part of the three body wave function and on shell elementary amplitudes which are calibrated independantly. Such a measurement is in progress at Saclay.

The next step consists of going far from the singularity in such a way that both mesons travel off shell. This graph can still be viewed as a virtual meson rescattering, but also as a genuine three body meson exchange current, which in turn is linked to the corresponding three body forces. An example is given in [28] : here the three-body effects are sizeable when the available energy is roughly shared by the three nucleons. Now,the calculation heavily depends on the way the elementary amplitudes are extrapoled off-shell. While pion baryon form factors, must be considered in the pion photoproduction and scattering amplitudes, the size of the corresponding cut-off mass is

still an open problem in three body forces [2]. While the description of S-wave pion nucleon scattering in terms of experimental phase shifts, or scattering lengths, is excellent on shell it might not be accurate enough to extrapolable below threshold, and a more microscopic treatment, based a low energy theorems, should be used instead. Finally, pion absorption on T = 1 pairs, as well as other three body mechanisms fig. 7 which do not reduce to a meson sequential scattering, should also be considered.

All those problems are open, and the extension to the ^{3}He(e,e'2p)n reaction is expected to provide us with a way to disentangle all these mechanism. Besides the flexibility of the three-body kinematics, this channel offers us the possibility of measuring transition form factors and to take advantage of a new degree of freedom : the variation of the four momentum of the virtual photon. However we have also to deal with the longitudinal cross section which is directly linked to the short range nucleon correlations.

4. The two nucleon correlations

The transverse cross section of the ^{3}He(e,e'2p) reaction is strongly suppressed for the same reason as the cross section of the ^{3}He(γ, 2p) reaction. Charged meson exchange currents and Δ-formation mechanisms do not contribute at all to the longitudinal cross section. This is the best place to study in details the two-body correlations provided that final state interactions are carefully taken into account [30].

Fig. 11 shows the excitation function of the electrodisintegration of a pp pair at rest, when the two protons are emitted at $\theta_{cm} = 90°$, in a kinematical range typically accessible with future electron machines. The plane wave treatment leads to a very simple and elegant picture. The transverse cross section vanishes. The two protons are emitted symmetrically around the direction of the virtual photon, with equal momenta of which the value

$$P = \left[\frac{1}{4}(\omega + M_3 - m_n)^2 - m^2_p\right]^{1/2}$$

depends only on the energy of the incoming virtual photon, regardless of the variations of the other kinematical quantities. Apart from a trivial phase-space factor, and the variations of the proton form factor, the longitudinal cross section exhibits a universal shape and directly maps out the square of the relative wave function of the two protons in ^{3}He. The effects of the final state interaction are very important, even for high values of the relative energy of the two outgoing protons, where the Δ formation mechanism also makes the transverse cross section larger than the longitudinal one.

However the interference cross section between the two transverse amplitudes is of the same order of magnitude, but of opposite sign,

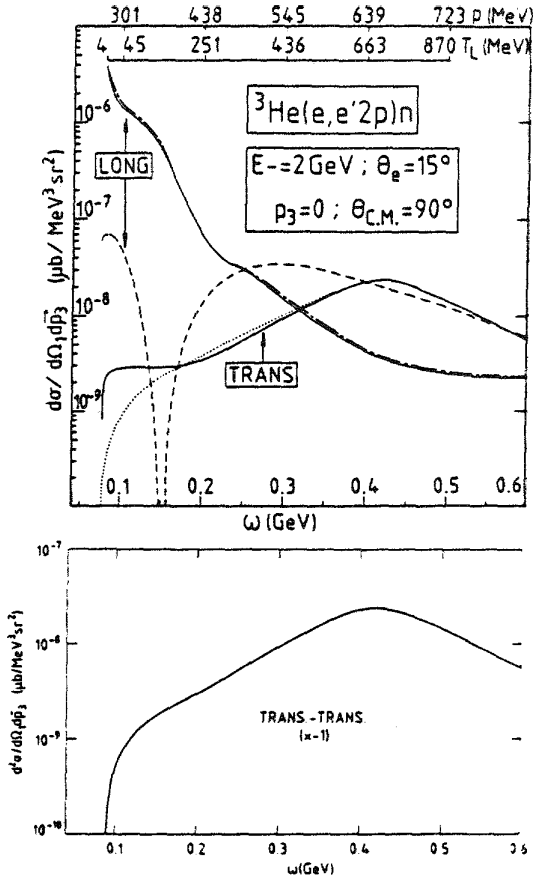

Fig. 11 - The excitation functions of the transverse and longitudinal reduced cross sections [30] of the electro-disintegration of a pp pair at rest in ^{3}He, when each proton is emitted at $\theta_{c.m.} = 90°$ with respect to the incoming virtual photon. The common value of the proton momentum P, as well as the proton relative kinetic energy T_L, is plotted on abcissa. Dashed lines : plane wave without meson exchange contribution. Dotted lines : plane wave with meson exchange amplitude. Dot-dashed lines : pp rescattering included Solid lines : all final state interactions included.

as the transverse cross section. This is a direct consequence of the behavior of the elementary amplitude of the p(e,e'π°)p channel which drives the two-body meson exchange amplitude. This provides us with a way of further reducing the transverse contribution. Let me go back to the expression of the cross section of the ^{3}He(e,e'2p) reaction [3,30].

$$\frac{d^2\sigma}{d\Omega_1\, d\eta} = \frac{d^2}{d\Omega_1\, d\eta}\left[\sigma_T + \varepsilon\,\sigma_L + \varepsilon(\cos 2\phi\;\sigma_{TT} + \sin 2\phi\;\sigma'_{TT}) - \sqrt{\frac{-q^2\varepsilon(\varepsilon+1)}{2\omega^2}}\,(\cos\phi\;\sigma_{TL} + \sin\phi\;\sigma'_{TL})\right] \qquad (2)$$

Where ε, q^2 and ω are respectively the polarisation the squared mass and the energy of the virtual photon. For symmetry reasons the two interference cross sections σ'_{TT} and σ'_{TL} vanishe when the pp pair is at rest. It turns out that the transverse longitudinal interference cross section σ_{TL} is negligible. Therefore the transverse cross section σ_T is canceled by the transverse-transverse interference cross section σ_{TT} in a coplanar kinematics (ϕ = 0), when the electron is scattered in the forward direction ($\varepsilon \simeq 1$). Fig. 12 illustrates this point and shows the total cross section of the ^{3}He(e,e'p) reaction in a coplanar kinematics for the same conditions as in fig. 11. It is entirely dominated by the longitudinal component. It is free of exchange current contamination and is a pure scalar transition between a $^1S_0$ pp bound pair and a $^1S_0$(or $^1D_2$, or $^1G_4$, etc...) pp scattering pairs.

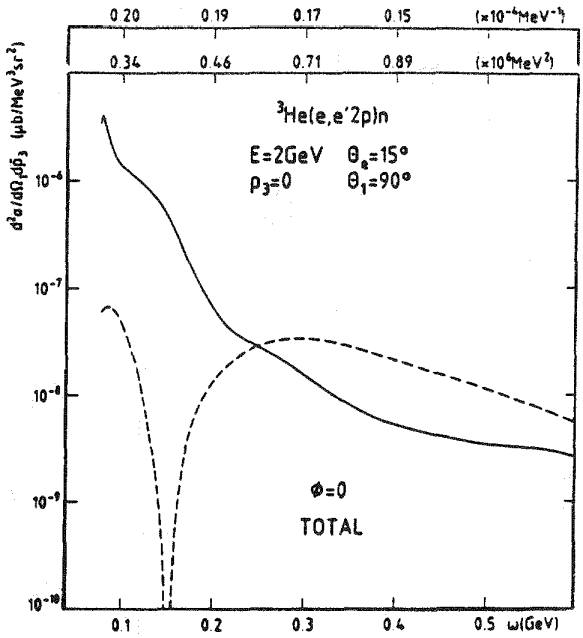

Fig. 12 - the total cross section, of the $^3He(e,e'2p)n$ reaction in the same kinematics as in Fig.11, when all the particles are scattered in the same plane (ϕ = 0). The meaning of the curve is the same as in Fig. 11. The values of the kinematical factor and of the photon flux, which multiply the induced cross section are also plotted on abscissa (see [30] for more details).

Of course, the size of the final state interactions prevents us to directly extract the correlation fonction between two-nucleons, but the measurement of the corresponding transition form factor is the cleanest and the strongest constraints. An example is given in fig 13 which represents the variation of the total cross section (eq. 2), in a coplanar kinematics (ϕ = 0), against the four momentum of the virtual photon, just at the pion production threshold. When the energy of the incoming electron is $E_- = 2$ GeV, the kinematics corresponds to ω = 250 MeV in fig. 11-12. Clearly 4 GeV is needed to measure the transition from factor up to $|q|^2 = 1(GeV/c)^2$.

When the pp pair is not at rest the physics is completely different. This is illustrated in fig. 14 and 15 which depict the variation of the various components of the cross section with the neutron momemtum. When the neutron is at rest fig. 14 corresponds to ω = 400 MeV (the top of the Δ) and fig. 15 to ω = 250 MeV (the pion production threshold). When the neutron momentum increases, the contribution of the two-body mechanisms decreases and follow the shape of the momentum distribution of the center of mass of the pp active pair. As in the $^3He(\gamma,2p)$ channel the transverse cross section are dominated by the three-body mechanisms. Their contribution is the most important when the available energy is almost equally shared between the three nucleons.

To summarize the (e,e'2p) reaction is dominated in a large part of the phase space by two and three-body exchange currents, although their contribution is strongly suppressed as compared to the (e,e'pn) reaction. The flexibility of electron scattering offers us the way to study in details these mechanisms and the corresponding from factors

There is a window where the longitudinal cross section dominates : when the pp pair is initially at rest and when the transfered energy is not too high (up to 500 MeV, below the Δ production threshold).

Fig. 13 - The total reduced cross section, when $\phi = 0$ is plotted against the four momentum of the virtual photon. The energy of the incoming electron and the kinematical coefficient [30] are also given on abscissa. The dashed curve corresponds to the plane wave treatment. The solid curve includes also meson exchange currents and final state interaction.

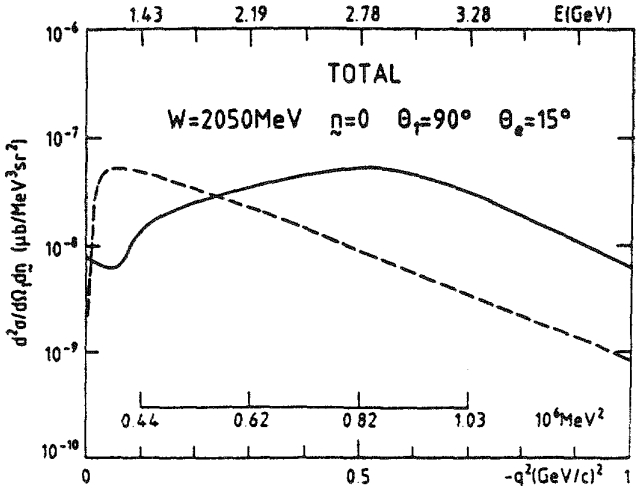

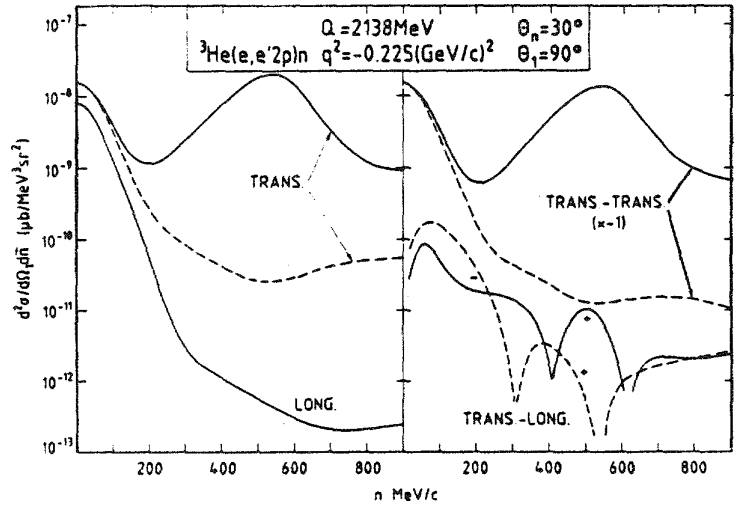

Fig. 14 - The various components of the reduced cross section of the $^3H(e,e'2p)n$ reaction are plotted against the momentum of the undetected neutron, which is emitted at $\theta_n = 30°$. The mass of the detected proton pair is kept constant at W = 2138 MeV, at the top of the Δ resonance. The dashed curves do not include three-body mechanism, which are included in the full curves.

This is the place where the two-body correlations should be studied : the final state interaction are sizeable, but they can be treated, at least in the few-body systems, with reliable methods.

The counting rates are reasonable but not very high : 10^{-8} μb.MeV^{-3}.sr^{-2} in figs. 11-12, corresponds to 20 counts/hour for a luminosity of 2.5 x 10^{36} cm^{-2}s^{-1} (100 mg/cm^2 and 10 μA), solid angles of 20 msr and momentum acceptance of 20 MeV/c.

The detection of three particles in coplanar or non coplanar kinematics is certainly an experimental challenge, but the issue is capital for the future of Nuclear Physics.

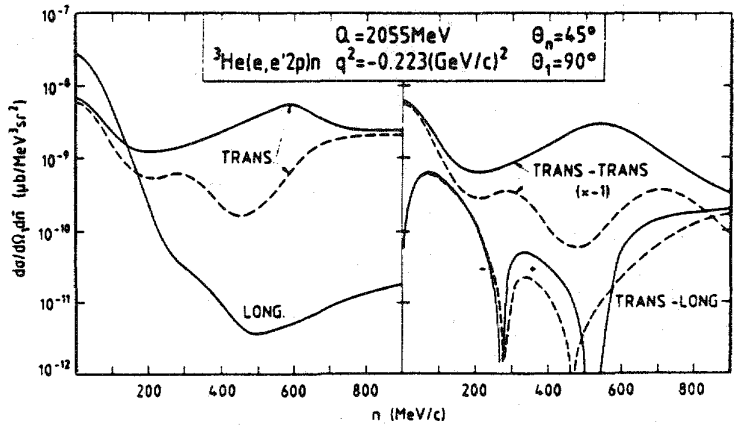

Fig. 15 - The same as in Fig. 14, but at the pion production threshold, when W = 2055 MeV.

References

[1] K. Gottfried, Ann. Phys. (NY) 21 (1963) 29 ;
Y.N. Srivastava, Phys. Rev. 135 (1964) 3612.
[2] B.H.J. McKellar, Lecture Notes in Physics, 260 (1986) 7.
[3] J.M. Laget, New Vistas in Electronuclear Physics, E. Tomusiak, H. Caplan and E. Dressler, Eds., Plenum Press, NY (1986) p. 361.
[4] J.M. Laget, Few body systems, supplementum 1 (1986) 271.
[5] J.M. Laget, Preprint DPhN-Saclay 2447 (1987)
Submitted to Phys. Lett.
[6] M. Bernheim, et al., Nucl. Phys. A365 (1981) 349 ;
S. Turck-Chièze, Phys. Rev. Lett. 142B (1984) 145.
[7] E. Jans, et al., Phys. Rev. Lett. 49 (1982) 974 ;
C. Marchand, et al., Saclay preprint DPhN Saclay n° 2428 (1986).
[8] P.H.M. Keizer, PhD Thesis, University of Amsterdam, (1985).
[9] N. D'Hose et al., 8ème session d'Etude Biennale de Physique Nucléaire, Aussois, J. Meyer ed., LYCEN 8502 (Lyon University), (1985) p.S10.1.
G. Tamas, Nucl. Phys. A463 (1987) 295c.
[10] J.M. Laget, Phys. Lett. 151B (1985) 325.
[11] Ch. Hajduk and P.U. Sauer, Nucl. Phys. A369 (1981) 321.
[12] R. Schiavilla, V.R. Pandharipande and R.B. Wiringa, Nucl. Phys. A449 (1986) 219.
[13] C. Ciofi Degli Atti, E. Pace and G. Salme, Phys. Lett. 141B (1984) 14.
[14] R.A. Brandenburg, Y.E. Kim and A. Tubis, Phys. Rev. C12 (1975) 1368.
[15] J.M. Laget and J.F. Lecolley, Phys. Lett. (in press).
[16] J.M. Laget, preprint DPhN Saclay 2459 (1987), Submitted to Phys. Lett.

[17] J.M. Cameron, et al., Phys. Lett. 103B (1981) 317 ;
J.M. Cameron, Lecture Notes in Physics 260 (1986) 366.
[18] D. Kielczewska, et al., contributed paper to the 10th Int. Conf. on Few Body Problem in Phys. (Karlsruhe, Germany, August 21-27, 1983),p.213.
[19] N.M. O'Fallon et al., Phys. Rev. C5 (1972) 1926.
[20] P.E. Argan et al., Nucl. Phys. A237 (1975) 447.
[21] H.J. Gassen et al., Z. Phys. 303 (1981) 303 ;
J. Arends et al., Nucl. Phys. A412 (1984) 509.
[22] D.I. Sober et al., Phys. Rev. C28 (1983) 2234.
[23] C.A. Heusch et al., Phys. Rev. Lett. 37 (1976) 405 ;
37 (1976) 409 ; 37 (1976) 960(E).
[24] J.M. Cameron et al., Nucl. Phys. A424 (1984) 549.
[25] W.J. Briscoe et al., Phys. Rev. C32 (1985) 1956).
[26] J.M. Laget, Second Workshop on Perspective in Nucl. Phys. at Intermediate Energies, S. Boffi et al., Eds. World Scientific, Singapore (1986) p. 247.
[27] J.M. Laget, Phys. Rep. 69 (1981) 1.
[28] J.M. Laget, preprint DPhN Saclay 2454 (1987), Submitted to Phys. Lett.
[29] G. Backenstoss et al., Phys. Rev. Lett 55 (1985) 2782.
[30] J.M. Laget, Phys. Rev. C35 (1987) 832.

Appendix

The four structure functions of the D(e,e'p)n reaction, in the third Saclay kinematics which is shown in Fig. 1, are depicted here. They are defined according to eg. 23 of ref. [3]. The dashed curves are the result of the IWIA treatment (including the neutron exchange pole diagram). The dot-dashed curves include FSI. The full curves include also MEC and are the result of the full calculations. Note that MEC do not contribute to the longitudinal response function but dominate the Transverse and the Transverse-Transverse response functions.

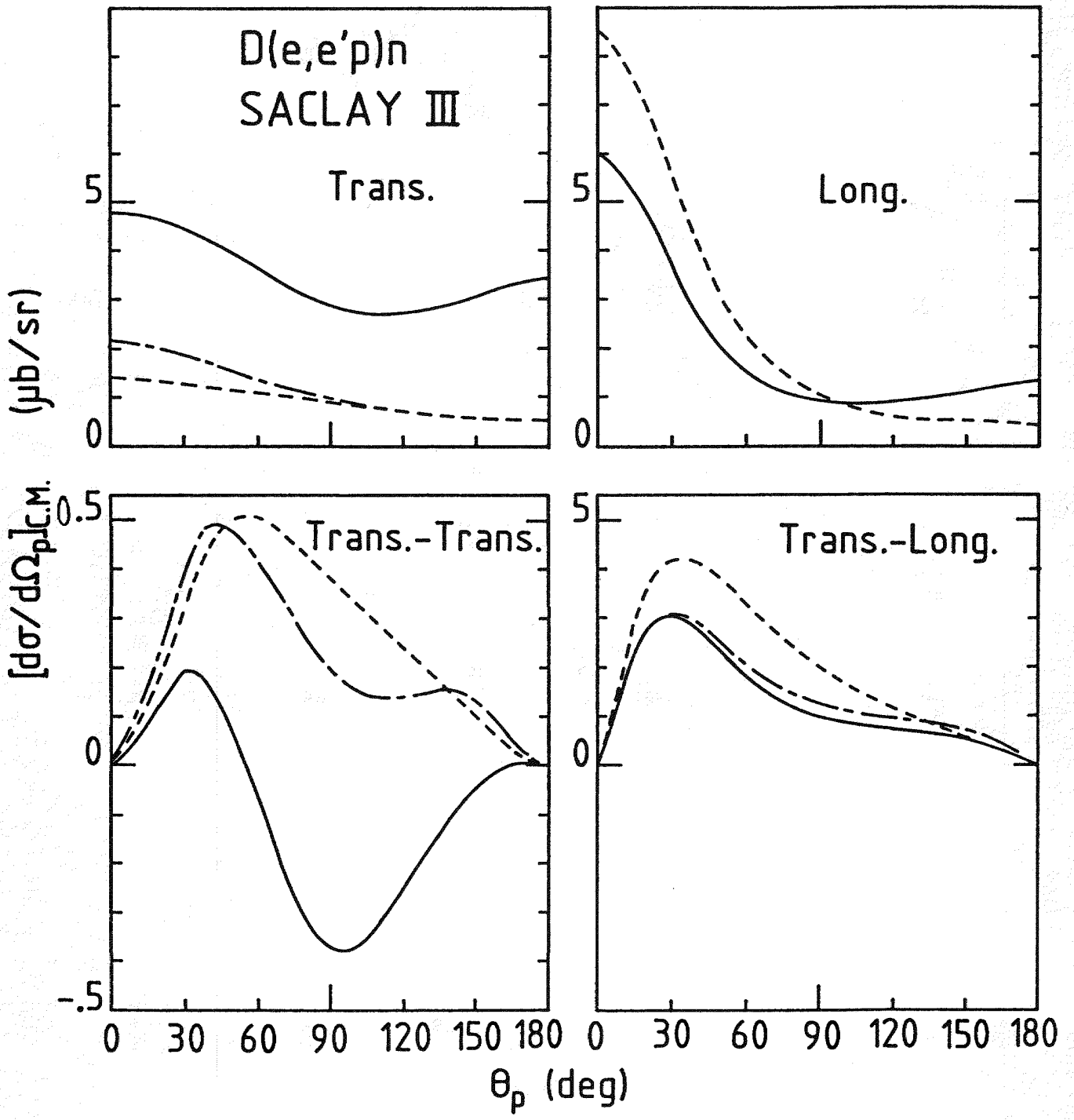
D(e,e'p)n
SACLAY III
Trans.
Long.
Trans.-Trans.
Trans.-Long.
(μb/sr)
[dσ/dΩp]c.m.
5
0
0.5
-.5
0 30 60 90 120 150 180
θp (deg)

HADRONS,Q.C.D., AND ALL THAT.

Gabriel KARL
Department of Physics
University of Guelph
Guelph, Ontario, N1G 2W1, Canada

In a few years, CEBAF, the new electron accelerator facility, will be ready to do experiments. These experiments will have a bearing on the physics of hadrons. My aim in this talk is to sketch the landscape in hadron physics when CEBAF will start to take data. This landscape is changing all the time. When I went to graduate school, nucleons were thought to be elementary particles, as were the other known hadrons, the pion, the kaon, the P33 resonance (which I shall call the delta in this note). As you know, this is no longer the case. All the above particles, and many others, are now understood to be composites of quarks. The changes in our notions about the physics of hadrons are illustrated by the fact that in the 1950's and 60's this field was part of high energy physics, while in the 1970's it became part of intermediate energy physics, and in this decade appears more often to be part of nuclear physics. One is tempted to extrapolate and guess that by the year 2000 hadron physics will be part of chemistry. This is not as ridiculous as one might think, since the main problems of theoretical chemistry and of hadron physics are similar in the sense that in both cases the underlying theory is known and one is faced with the difficulties of connecting the underlying basic theory to the world of experimental data.

In the case of hadrons, the underlying theory is Quantum Chromo Dynamics, abbreviated as QCD. This is the theory of quarks and gluons, which is a nonabelian analog of quantum electrodynamics. Instead of electrons, we have quarks and instead of the photon, we have gluons. Quarks are triplets under a color SU3 group while gluons are color octets. These are the correct degrees of freedom at short distances inside hadrons themselves. This pecular situation makes hadron physics very different from the physics of leptons, in which the bound states, like positronium, are very loosely bound.

At short distances, the understanding of quark and gluon degrees of freedom in perturbative QCD is in relatively good shape. The phenomenon of confinement, however, is nonperturbative and the precise connection between the physics at short distances and the physics at larger distances is not very well understood. Because of this, we don't yet know with any certainty whether, in addition to the well-known hadrons, the mesons (quark-antiquark) and baryons (tri-quark), there are also exotic states like gluonia (zero quark), mesic molecules (diquark-antidiquark), five quark (like cbarsuud) or six quark dibaryons (like lambda-lambda).

The theoretical connections between the world of QCD and the world of hadrons are still under persistent exploration. There are

many models that are being investigated like bag models, potential models, string models, skyrmion models, sum rule models. None of these spans by itself the wide gap between QCD and the world of hadrons. A very promising avenue of research is the connection between lattices, strings, potentials and spectroscopy. I tend to think that this path will solidify in the future as the "right" connection between QCD and spectroscopy. However, at the moment, none of the links are definitive and we may still be missing some of the important physics.

In potential models, the main ingredients are the confining potential, which is generally believed to be predominantly Lorentz scalar, and is usually taken to have some simple analytic form in the interquark distance like linear or quadratic. In addition to this spin independent force, the main spin dependent forces are the color magnetic interactions, which consist of 'contact' forces and dipole-dipole forces. The color magnetic forces are believed to stem from single gluon exchange between quarks and represent many aspects of hadron spectroscopy very well. In particular, the dipole-dipole force explains the mixings between S-wave and D-wave states to which we shall return later.

We turn now to discuss the simplest way in which experiments at CEBAF will be able to illuminate the field of hadron physics. In my opinion, this will proceed by studying the electroproduction of nucleonic resonances. We shall only discuss the easiest of all examples, the electroproduction of the P33 resonance. The coupling of the virtual photons to these resonances gives us constraints on the motion of constituents in the initial and final state. It is conceptually easier to think of the decay of the resonance into a nucleon and a virtual photon:

$$P_{33} \longrightarrow N\gamma$$

As the angular momentum and parity of the P33(3/2+) and the nucleon N(1/2+) are well known, the photon can only have angular momentum and parity 1+(magnetic dipole) or 2+(electric quadrupole).

In terms of quarks, the P33 consists of three quarks with their spins coupled to total spin S=3/2, while the nucleon has the three quarks coupled to total spin S=1/2; in both cases, the orbital angular momentum of the quarks is zero. This implies that the transition P33$\longrightarrow$ N involves the flip of a quark spin and therefore it is a magnetic dipole transition. This rule E2 = 0 is called the Morpurgo selection rule. Using the nucleon magnetic moments for normalization, the transition amplitude can be estimated in fair agreement with experiment. Of course, the prediction E2/M1 = 0 is only valid in the approximation of neglecting D-wave mixing in the nucleon and P33. If we allow for color magnetic interactions, we can predict the small amount of D-wave mixing and therefore the amplitude of the E2/M1. The strength of the color magnetic interactions is normalized by the splitting between the nucleon and P33 and the resulting D-wave mixing is apparently confirmed by the E2/M1 ratio evaluated by Mukhopadyay to be in the range -0.003 to -0.007. Other models can also fit this ratio, such as a relativistic model recently discussed by Weber, but one should

emphasize that the D-wave mixing was predicted unambiguously in potential models.

At large momentum transfers, perturbative QCD ought to be valid as stressed at this workshop by Carlsson. In this limit, he predicts that E2/M1 = 1.73 for the P33 to nucleon+virtual gamma transition. This prediction comes from the dominance of helicity conserving amplitudes at large momentum transfer. In that limit, therefore, only the helicity states + or - 1/2 of the P33 can decay or be produced. On the other hand, we have just seen that in photoproduction the helicity states + or - 3/2 are easily excited. Therefore, perturbative QCD is not valid for real photons. Therefore, we have the prediction that the helicity structure in the transition nucleon to P33 changes significantly with momentum transfer as the momentum transfer increases. It is not yet known whether this is the case. This would be an important topic of research at CEBAF, as it would illuminate our understanding of the nucleon and its excited state. Carlsson discussed at the workshop a possible escape hatch for this prediction of perturbative QCD, if the dominant helicity amplitude would vanish accidentally. This is a real possibility for certain wavefunctions of the nucleon and P33 and would provide constraints for other perturbative computations.

The P33 resonance is only the simplest example of many possible excitations of the nucleon, and similar studies may be performed in other cases. The first example of a predicted change in the helicity structure in the electroproduction of a resonance was made some time ago by Close and Gilman for the D13 resonance and it is now believed that this prediction is supported by the experimental data. Clearly, such studies are very important as they connect the behaviour of quarks at very short distances, prescribed by perturbative arguments to their properties at longer distances, the confinement scale described by wavefunctions.

At even larger distances, we can consider nuclei where the role of quarks is more controversial. Traditionally, nuclei are considered bound states of nucleons. This is an excellent approximation. From a more modern point of view, it is a great mystery why this approximation is so good when we know that nucleons are composite objects which overlap significantly in the nucleus. Why does the nucleus look so much like a gas of noninteracting nucleons? A related question is what happens to this picture at higher densities - will there be a phase transition to a quark-gluon plasma?

Even though the approximation of free nucleons in the nucleus is very good, we should not forget that it is an approximation and, therefore, we should investigate its limitations. As far as I know, Noble was the first to point out, on the basis of inelastic electron scattering data, that the nucleon has a larger effective size in the nucleus than a free nucleon. More recently, the EMC collaboration found deep inelastic scattering data which can be interpreted in that way.

A related conclusion is that the magnetic moment of a bound nucleon is also increased relative to the magnet moment of a free nucleon. Data on the magnetic moments of Helium three, Carbon thirteen, and Oxygen fifteen all indicate that a bound neutron has

a magnetic moment which is about -2.1 nuclear magnetons to be compared with -1.9 nuclear magnetons for a free neutron. There are similar data on tritium, nitrogen thirteen and fifteen which indicate a similar inflation in bound proton moments.

It has been noted by Ericson and Richter that much of the increase in nucleon moments is due to pion exchange currents in the nucleus, and the remainder is rather small. This point of view which allows for simultaneous quark contributions and pion contributions is rather dangerous in my opinion, because of the mixing of different length scales. One should either consider as a basis nucleons+mesons, or quarks+antiquarks. If we consider both at the same time, namely quarks and pions, we are in danger of a certain amount of double counting. If we separate a pion contribution then it seems to me that further talk of quark contributions is futile.

It was brought to my attention by R.D. McKeown that the effective increase in radius of a nucleon in Helium three is at most about 3.6% on the basis of electron scattering data. This is much less than the 10% change in magnetic moments discussed above. In the bag model, the two changes have to be identical, but in fact the constraints of the bag model need not hold for the effective nucleons in nuclei. Thus one should try to analyze the data allowing for both an effective size and an effective magnetic moment for the bound nucleon, without imposing a constraint between the two.

Of course, we want to understand in a physical way why the bound nucleon becomes larger and the magnetic moment increases when it is immersed in a nucleus. There are many attempts in this direction. For example, Oka et al show generally that if the nucleon-nucleon force is attractive (as it is), then the effective size will increase (as it does). In a bag model, the superposition of two bags of three quarks each leads to a single bag of six quarks which has a larger radius than the three quark bag. Similarly in string models, Noble has pointed out that the overlap of two strings leads in the overlap region to a thicker, swollen string.

In summary, then, nuclear physics now covers a larger spread of distances than in the past. At short distances, the relevant degrees of freedom are quarks and gluons, while, at longer distances, the relevant degrees of freedom are nucleons and mesons. The matching between these two sets of degrees of freedom will be an important task of the subject. CEBAF will provide useful experimental hints in this task.

ACKNOWLEDGEMENTS: I am indebted to the organizers of this workshop for the invitation to give this talk and for their support and hospitality. I also acknowledge useful conversations with C. Carlson, H. Weber, Vladimirov, T. Oka, R. McKeown and V. Burkert.

REFERENCES:

1) For general issues see:
N. Isgur and G. Karl, Physics Today, vol. 36, no. 11, p36 (1983)

2) For potential models see:
D. Gromes in The Quark Structure of Matter, Proceedings of the Yukon advanced Study Institute, N. Isgur, G. Karl and P.J. O'Donnell editors, World Scientific 1984.
3) For the radiative decay of the P33 resonance and related matters see:
C. Becchi and G. Morpurgo, Phys.Letters 17, 352 (1965)
F. Close and F.J. Gilman, Phys.Letters 38B, 541 (1972)
N. Isgur, G. Karl and R. Koniuk, Phys.Rev. 25D, 2394 (1982)
H. Weber, Charlottesville preprint, 1987
C. Carlsson, these proceedings
4) For the modification of nucleon properties in nuclei see:
J. Noble, Phys.Rev.Letters 46, 412 (1981)
Nucl.Phys. A368, 477 (1981)
G. Karl, G.A. Miller and J. Rafelski, Phys.Letters 143B, 326 (1984)
T.E.O. Erickson and A. Richter, Phys.Letters 183B, 249 (1987)
R.D. McKeown, Phys.Rev.Letters 56, 1452 (1986)
M. Oka and R.D. Amado, Phys.Rev. C35, 1586 (1987)

****

RELATIVISTIC HEAVY ION COLLISIONS

M.J. TANNENBAUM

Brookhaven National Laboratory*
Upton, N.Y. 11973

ABSTRACT

Some of the objectives and observables of Relativistic Heavy Ion Physics are presented. The first experimental results from oxygen interactions at CERN, 200 GeV/c per nucleon, and BNL, 14.5 GeV/c per nucleon are shown. The data indicate more energy emission than was originally predicted.

INTRODUCTION

High energy collisions of nuclei provide the means of creating nuclear matter in conditions of extreme temperature and density. At large energy density, or baryon density, a phase transition is expected from a state of nucleons containing confined quarks and gluons to a state of "deconfined" (from their individual nucleons) quarks and gluons covering the entire volume of nuclear matter, or a volume that is many units of the characteristic length scale. This state is expected to be in thermal and chemical equilibrium. In the terminology of high energy physics, this is called a "soft" process, related to the QCD confinement scale

$$\Lambda_{QCD} \approx 0.1 \text{ GeV} \approx (2 \text{ fm})^{-1}$$

This state is called the Quark-Gluon-Plasma (QGP) [1]

A schematic drawing of a relativistic heavy ion collision is shown in Figure 1. Two energy regimes are discussed for the QGP[2]. At lower energies, typical of the AGS, the colliding nuclei are expected to stop each other, leading to a Baryon-Rich system. This will be the region of maximum baryon density. At very high energy, 100 to 200 GeV per nucleon pair in the center of mass, the nuclear fragments will be well separated from a central region of particle production. This is the region of the Baryon-Free or Gluon plasma.

* This research has been supported in part by the U.S. Department of Energy under Contract DE-AC02-76CH00016

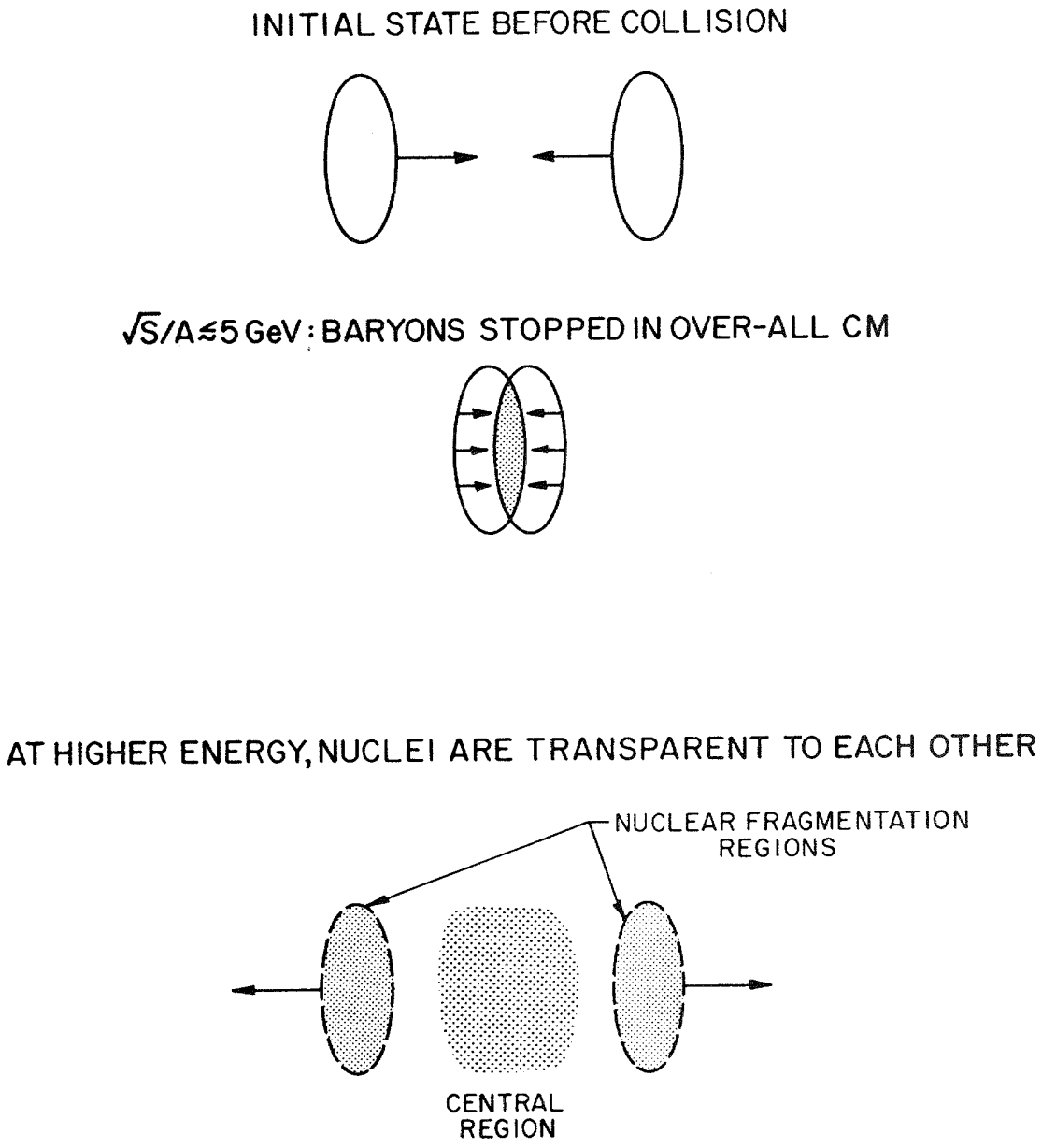

FIGURE 1. Schematic of Relativistic Heavy Ion Collision from RHIC Conceptual Design Report BNL 51932(1986)

There has been considerable work over the past few years in making quantitative predictions for the QGP. A recent calculation of a phase diagram for "isentropic expansion trajectories for a hadronizing QGP" [3] is shown below (Figure 2). The transition temperature from a state of hadrons to the QGP varies from Tc=140 MeV at zero baryon density to zero temperature at a critical baryon density ~6.5 times the normal nuclear density:

$$\rho_o = 0.15 \text{ nucleons/fm}^3 \approx 0.15 \text{ GeV/fm}^3$$

Predictions for the transition temperature are constrained to a relatively narrow range 140 < Tc < 250 MeV, while the critical baryon or energy density is predicted to be 5 to 20 times the normal density.[4]

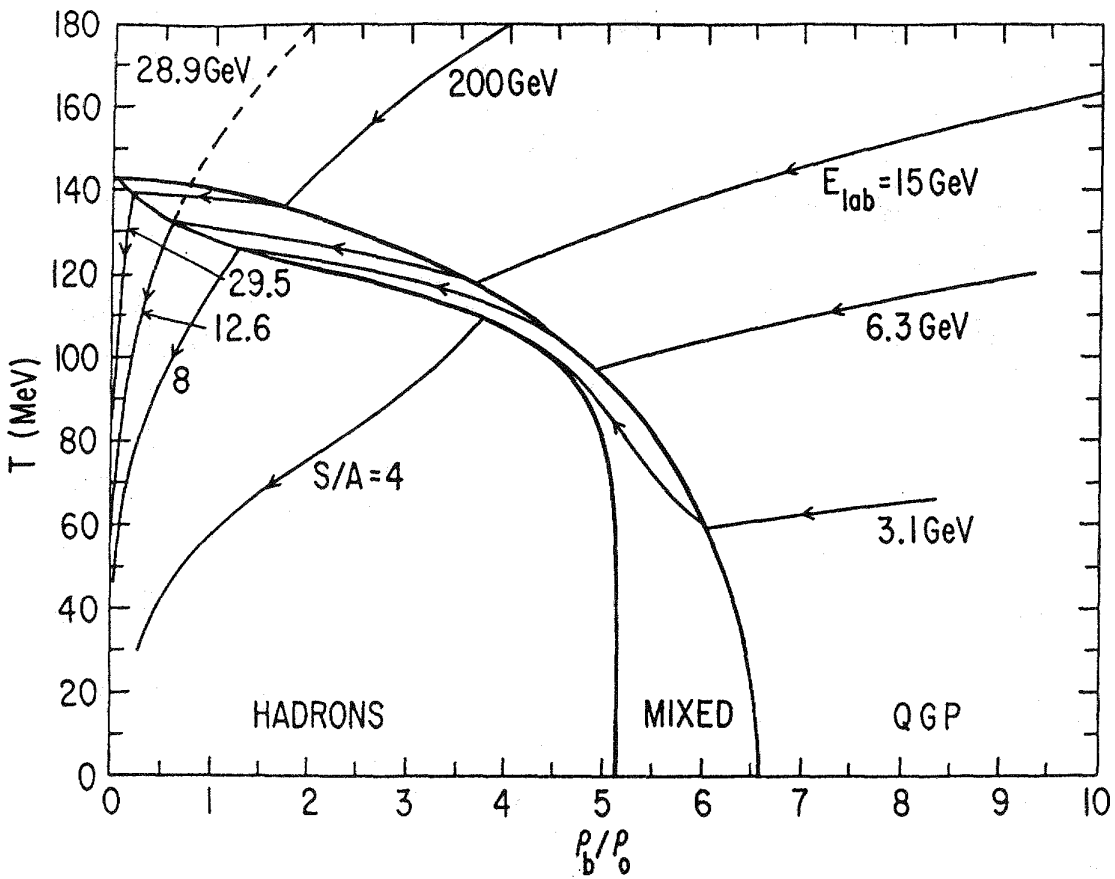

FIGURE 2

From the point of view of an experimentalist there are two major questions in this field. The first is how to relate the thermodynamical properties (temperature, energy density, entropy...) of the QGP or hot nuclear matter to properties that can be measured in the laboratory. The second question is how the QGP can be

detected.

OBSERVABLES

The challenge of RHI collisions can be understood from Figure 3, which is a streamer chamber photograph of a 200 GeV/u oxygen projectile colliding with a lead nucleus. It would appear to be a daunting task to reconstruct all the particles in such events. Consequently, it is more common to use single-particle or multi-particle inclusive variables to analyze these reactions.

NA 35 ^{16}O + Pb SEPTEMBER 1986

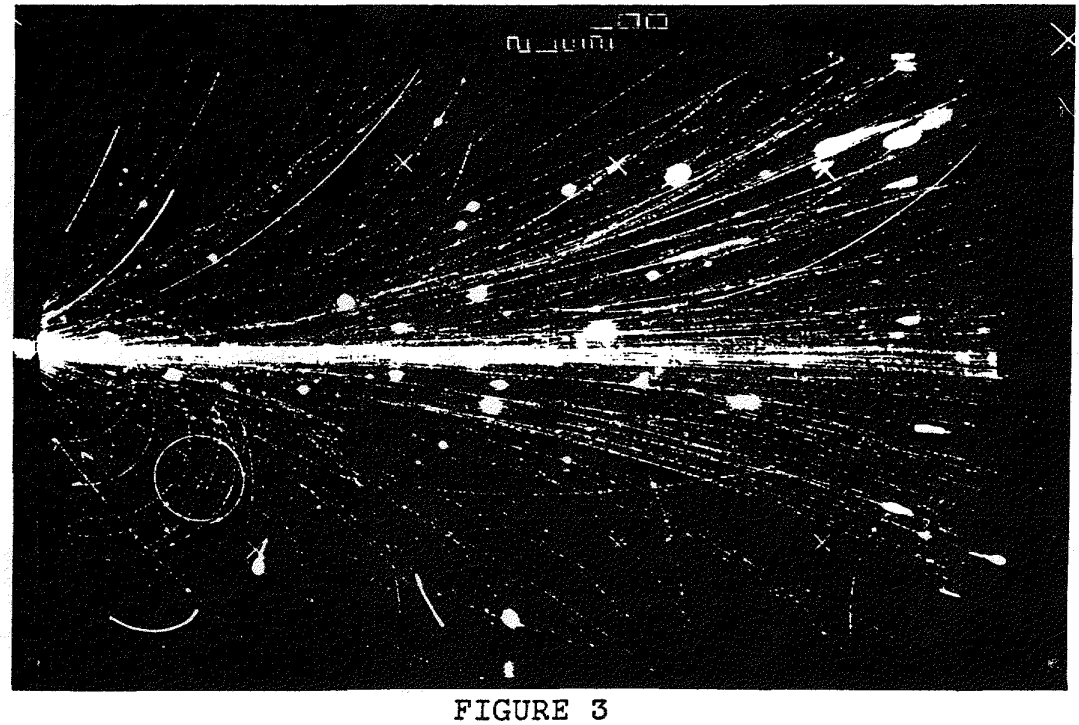

FIGURE 3

For any particle, the momentum can be resolved into transverse (Pt) and longitudinal (Pl) components, and in many cases the mass (M) of the particle can be determined. The longitudinal momentum distributions are conveniently expressed in terms of the rapidity (y):

$$y = \ln[(E+Pl)/Mt] \rightarrow \eta = -\ln \tan \theta/2 \qquad \text{as } M \rightarrow 0$$

$$\cosh y = E/Mt \qquad \sinh y = Pl/Mt$$

where $$Mt = \sqrt{Pt^2+M^2} \text{ and } E = \sqrt{Pl^2+Mt^2}$$

The transverse momentum distributions can be determined for the different particles, and typically the average transverse momentum, ‹Pt› is taken as a measure of the temperature, T. The charged particle multiplicity, either over all space, or in resricted intervals of rapidity, is taken as a measure of entropy

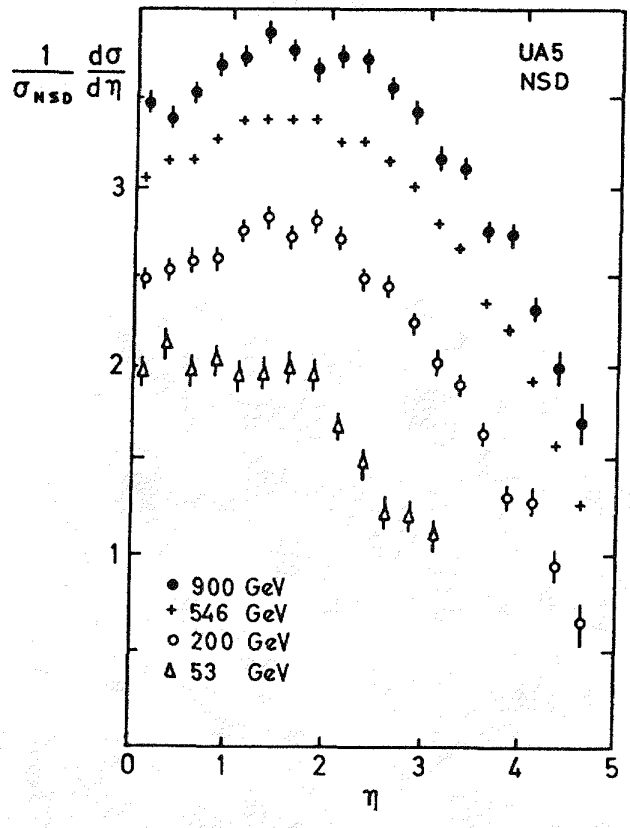

FIGURE 4. Eta is the pseudorapidity (M-->0) [Ref 1,p148c]

A convenient description of high energy collisions is provided by the charged particle density in rapidity, dn/dy (Figure 4). Regions of nuclear fragmentation take up the first 1-2 units around the projectile and target rapidity and if the center-of-mass energy is sufficiently high, a central plateau is exhibited. Another, similar variable is the transverse energy density in rapidity or dEt/dy ≃ ‹pt›*dn/dy. This is thought to be related to the co-moving energy density in a longitudinal expansion, and according to Bjorken [5] is proportional to the energy density in space ε:

$$\varepsilon = \frac{dEt/dy}{\pi R^2 \tau}$$

where τ is the formation time ~ 1 fm.

SIGNATURES OF THE QUARK-GLUON-PASMA

One of the more interesting signatures proposed for the QGP is that it could trigger a catastrophic transition from the metastable vacuum of the present universe to a lower energy state, " a possibility naturally occurring in many spontaneously broken quantum field theories " [6]. A more likely outcome is that the existence of the QGP will be inferred from a comprehensive and systematic set of experimental data exhibiting several striking features or "anomalies", "which can be interpreted in a unified way as manifestations of QGP production" [7]. Examples of the features expected for the QGP and signatures to find them are given below:

a) CHARACTERISTIC TEMPERATURE ENTROPY CURVE: [8]

FIGURE 5

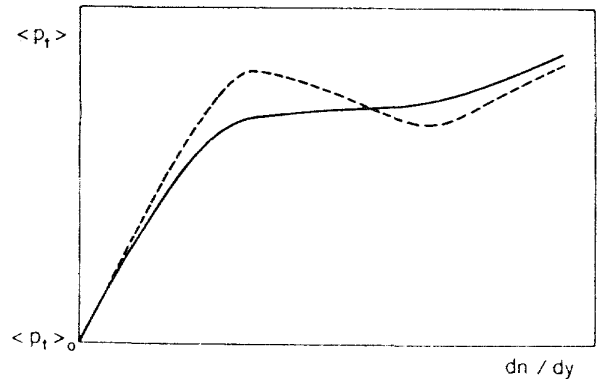

Note that this curve has the features of a phase transition with which we are all familiar. The ‹Pt›, acting as temperature, increases with increasing entropy (dn/dy); then as the phase transition takes place (e.g. water changing to steam) the temperature remains constant and begins rising again when the transition to the new phase is complete.

b) PLASMA DROPLETS CAUSED BY DEFLAGRATION: [9]
These would be manifested by large fluctuations in dn/dy or dEt/dy covering a range of ~1 unit on an event by event basis. The hope would be to observe the other plasma signatures only in the region of the fluctuation and not in the other regions.

c) THERMAL EQUILIBRIUM:
One of the best probes of thermal equilibrium is lepton pair production [10]. There are two characteristic

features of thermal production of lepton pairs. The number of lepton pairs per unit of rapidity is proportional to the square of charged particle density, and furthermore this ratio is proportional to the transition temperature Tc:

$$\frac{dN\mu^+\mu^-/dy}{(du/dy)^2 x 10^{-7}} = 15\ Tc\ (GeV)$$

Also, the Pt and mass dependence of the cross section are not independent but depend only on the transverse mass Mt. This means that at any fixed value of M, the ‹Pt(M)› is linearly proportional to M.

d) VOLUME OF THERMAL MATTER:
The size of the thermal source is thought to be measured by identical particle interferometry using the GGLP effect [11]. When two identical pions occupy nearly the same coordinates in phase space, the amplitudes interfere constructively due to the symmetry of the wave-function imposed by Bose-Einstein statistics. The characteristic momentum difference leading to decorrelation in momentum space can be measured, and is taken to be the fourier transform of the size of an extended source in position space. It should be noted that dynamical effects due to final state interactions can be large, and make the interpretation of such measurements a very specialized subject [12].

e) CHEMICAL EQUILIBRIUM [13,14]:
In the QGP there will be gluons, quarks and anti-quarks. They will continuously react with each other via the QCD subprocesses:

$$gg \rightarrow q\bar{q} \quad q\bar{q} \rightarrow gg \quad q\bar{q} \rightarrow q'\bar{q}'$$

where q' represents a different flavor quark (u,d or s). After several interactions have taken place, the reaction rates and the abundances of the gluons and the different flavor quarks (and anti-quarks) will become equilibrated, so that they no longer change with time. This is called chemical equilibrium. Since the transition temperature Tc is comparable to the strange quark mass ~150 MeV, the strange quarks $s,\bar{s}$ should have the same abundance as the $u,\bar{u}$ and $d,\bar{d}$ in the gluon plasma. In the baryon-rich plasma, the $s,\bar{s}$ will be enhanced compared to u and d since $u,\bar{u}$ and $d,\bar{d}$ are "Pauli" blocked by valence u and d quarks.

The principal probe of chemical equilibrium is the

particle composition. For instance, the abundance of strange mesons and baryons as well as anti-baryons should be quite different in a QGP than in a hadron gas or in an ordinary nuclear collision

f)DECONFINEMENT :

It has recently been proposed [15] that J/Psi production in A+A collisions will be suppressed by Debye screening of the quark color charge in the QGP. The J/Psi is produced when two gluons interact to produce a c,c pair which then resonates to form the J/Psi. In the plasma the c,c interaction is screened so that the c,c go their separate ways and eventually pick up other quarks at the periphery to become "open charm". This would be quite a spectacular effect since the naive expectation is that J/Psi production, being a pointlike process, should go like A*A in an A+A collision, and thus would be enhanced relative to the total interaction cross section, which increases only as A**2/3.

EXPERIMENTAL TECHNIQUES

Each of the probes of the QGP tends to have a different experimental technique associated with it. In all cases the multiplicities in nuclear collisions are so large that all the detectors used are very highly segmented. For measuring the charged multiplicity or dn/dy a segmented multiplicity detector is used, usually an array of proprotional tubes with pad readout, or a silicon pad array. For measuring transverse energy flow, dEt/dy, a hadron calorimeter is used. Some groups use an electromagnetic shower counter for this purpose. This has the advantage of being smaller, cheaper and higher in resolution than a full hadron calorimeter; but has the disadvantage of being biased, since only pizero and eta-zero mesons are detected (via their two photon decay). Nuclear fragmentation products are detected by calorimeters in the projectile direction and by E, dE/dx scintillator arrays in the target fragmentation region. The particle composition and transverse momentum distributions are measured using magnetic spectrometers with particle identification. Typically, time-of-flight, gas and aerogel Cerenkov counters, and dE/dx are used to separate pions from kaons, protons, deuterons, etc. Drift chambers are generally utilized for charged particle tracking, although streamer chambers and time projection chambers (TPC) are also in use. Lepton pair detectors are very specialized, and usually combine

magnetic spectrometers with lepton identification (muons by penetration, and electrons by "gas" and "glass").

One of the specific problems in this field is how to detect, with minimum bias, when a nucleus-nucleus collision has taken place. Two techniques are used. The first is to put a calorimeter at zero degrees to determine whether the projectile has the full beam energy or has lost some energy. The second uses a so-called bullseye counter downstream of the target, sized just large enough to detect all the beam particles. The bullseye also measures the charge of the beam particles since the pulse height is proportional to Z**2. If a particle misses the bullseye, or the charge changes, this is taken as an indication of a nuclear interaction.

With that quick overview of the experimental techniques, the following "photo album" of the first round of experiments at CERN and Brookhaven should be easier to comprehend. The CERN heavy ion program provides oxygen beams at 60 and 200 GeV/u and will eventually improve the source to provide sulfur and possibly lead beams. There are 5 major experiments: WA80 (Figure 6), NA34 (Figure 7), NA35 (Figure 8), NA36 (Figure 9), and NA38 (Figure 10). The BNL heavy ion program has provided oxygen and silicon beams at 14.5 GeV/c per nucleon and is scheduled to accelerate gold beams in 1989. A major improvement is planned for 1995 when RHIC is scheduled to begin operation. RHIC will provide colliding beams, covering the full mass number spectrum, with center-of-mass energies from 5 to 200 GeV per nucleon pair. At present, there are 3 major RHI experiments at the BNL-Tandem-AGS: E802 (Figure 11), E810 (Figure 12) and E814 (Figure 13).

FIRST EXPERIMENTAL RESULTS

CERN had a very successful oxygen run in the fall of 1986, and already one experimental result has been published [16]. At BNL, some time was made available for physics during machine studies with oxygen in the fall of 1986 and routine running began in the spring of 1987 with a silicon beam. No results are available yet from the silicon run, but a small test experiment using the oxygen beam will be reported [17]. Results on heavy ion collisions from cosmic rays [18] and from the Bevalac [19] have also been published this year but are beyond the scope of this article.

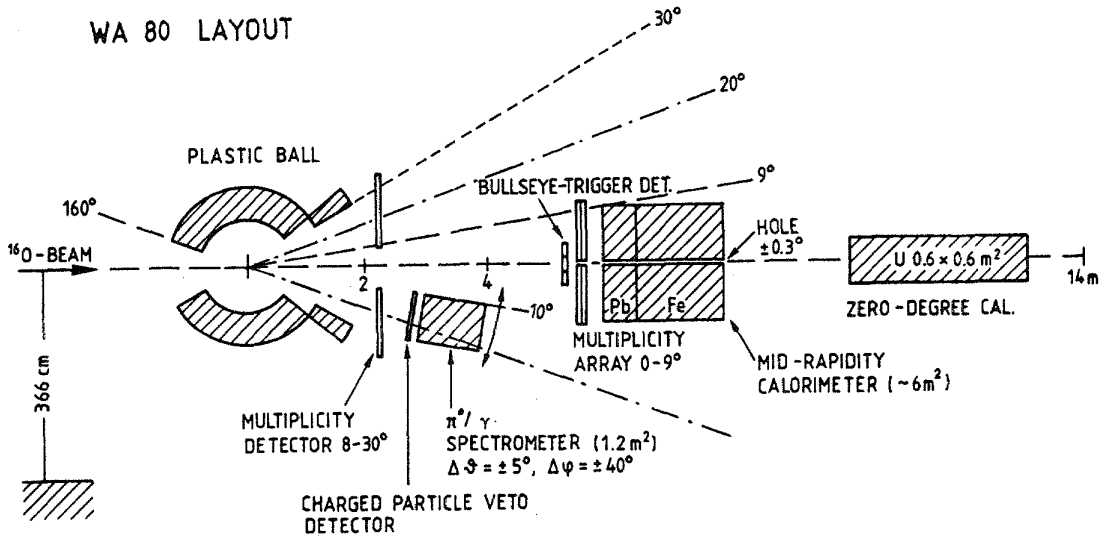

Experiment WA80: Study of Relativistic Nucleus-Nucleus Collisions at the CERN SPS

FIGURE 6

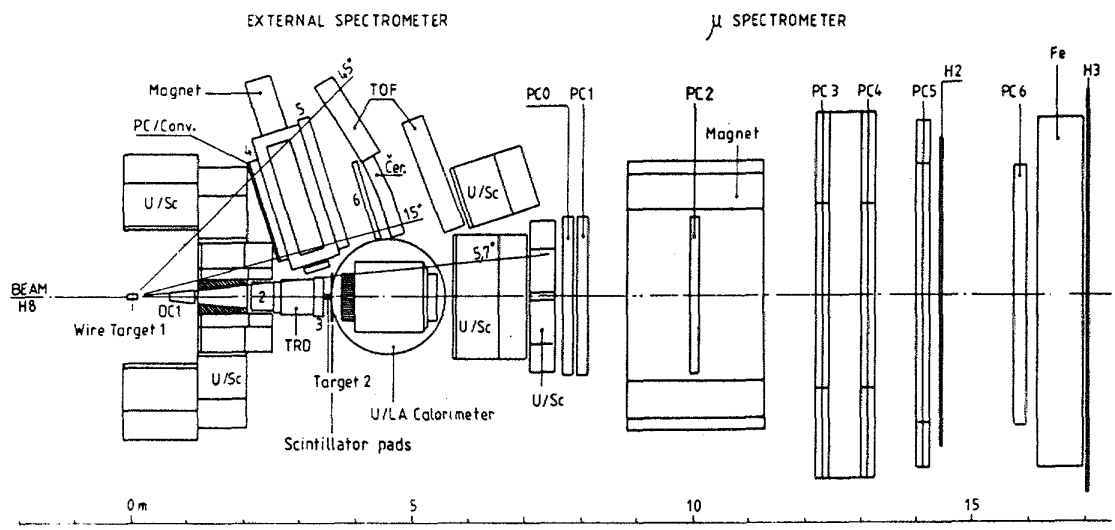

Experiment NA34/2: Study of High Energy Densities over Extended Nuclear Volumes via Nucleus-Nucleus Collisions at the SPS

FIGURE 7

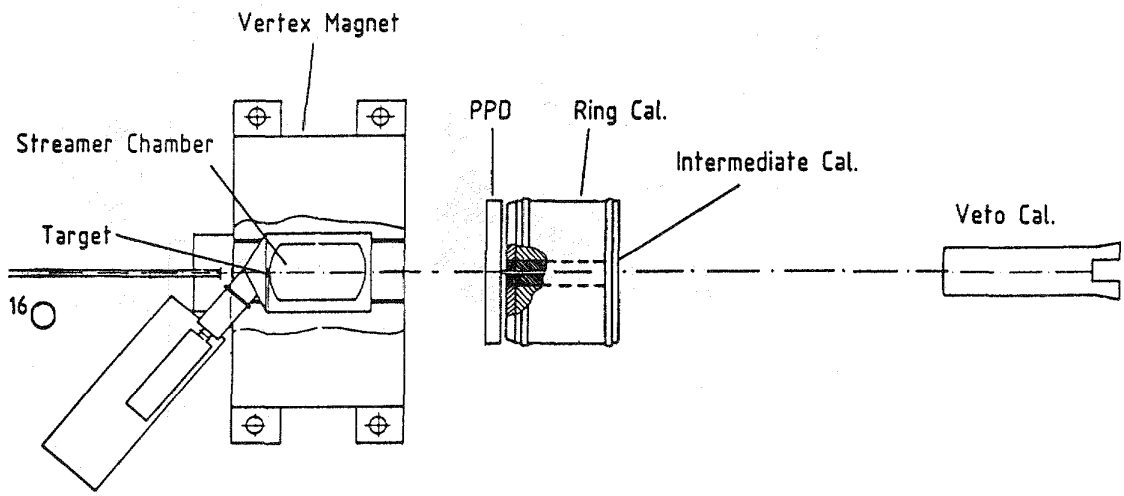

Experiment NA35: Study of Relativistic Nucleus-nucleus Collisions

FIGURE 8

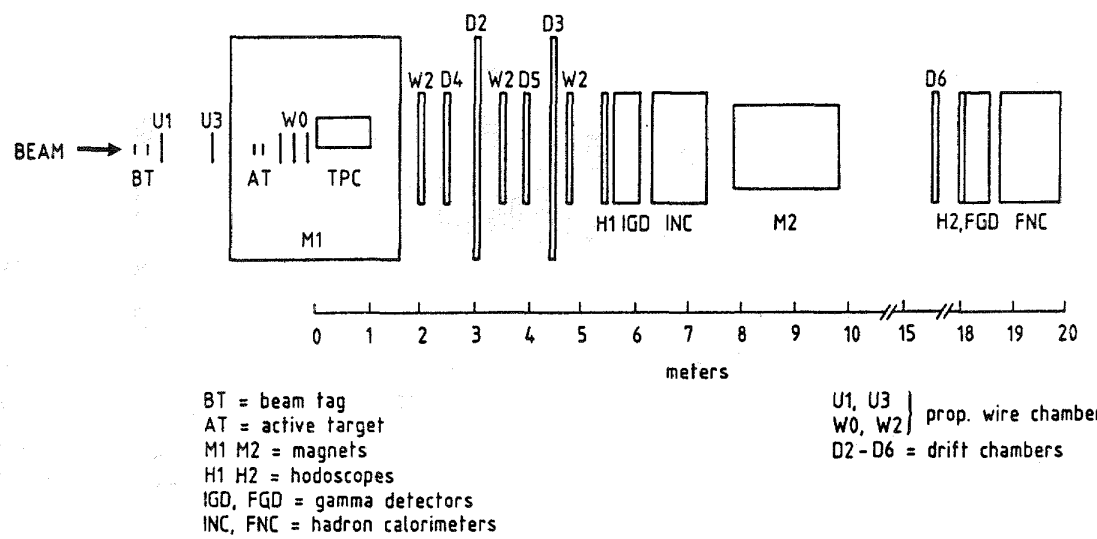

Exepriment NA36: Production of Strange Baryons and Antibaryons in Relativistic Ion Collisions

FIGURE 9

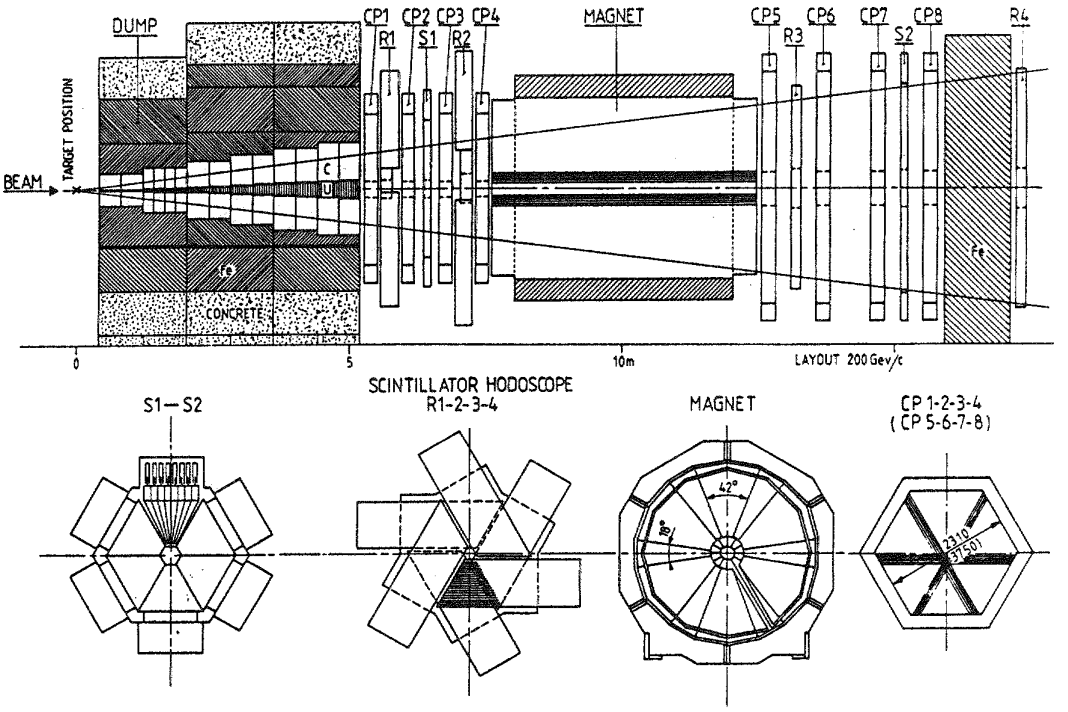

FIGURE 10. NA38 Study of High-Energy Nucleus-Nucleus Interactions with the Enlarged NA10 Dimuon Spectrometer

BNL-TANDEM-AGS PROGRAM

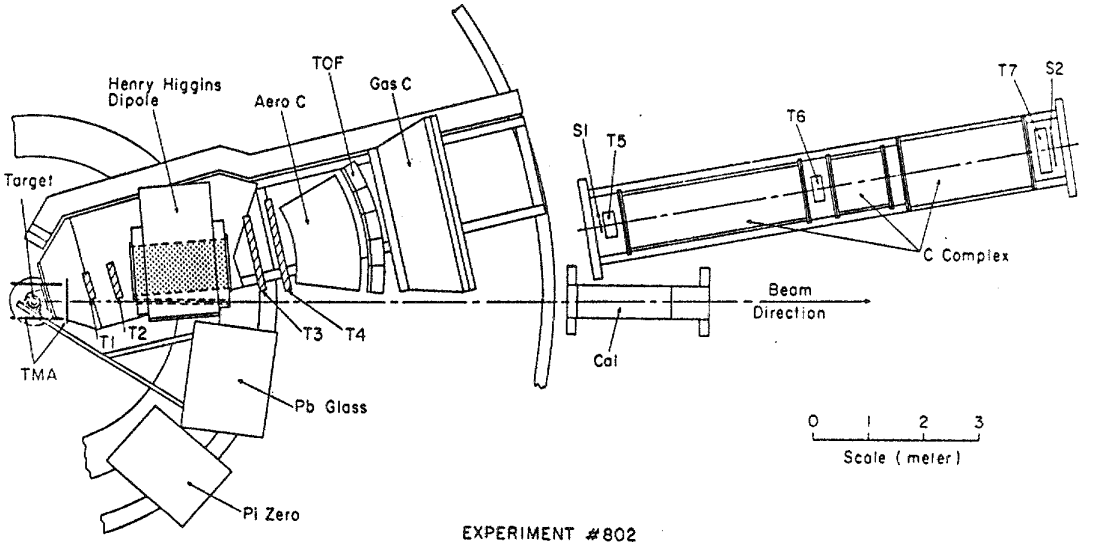

FIGURE 11. E802 Studies of Particle Production at Extreme Baryon Densities in Nuclear Collisions at the AGS

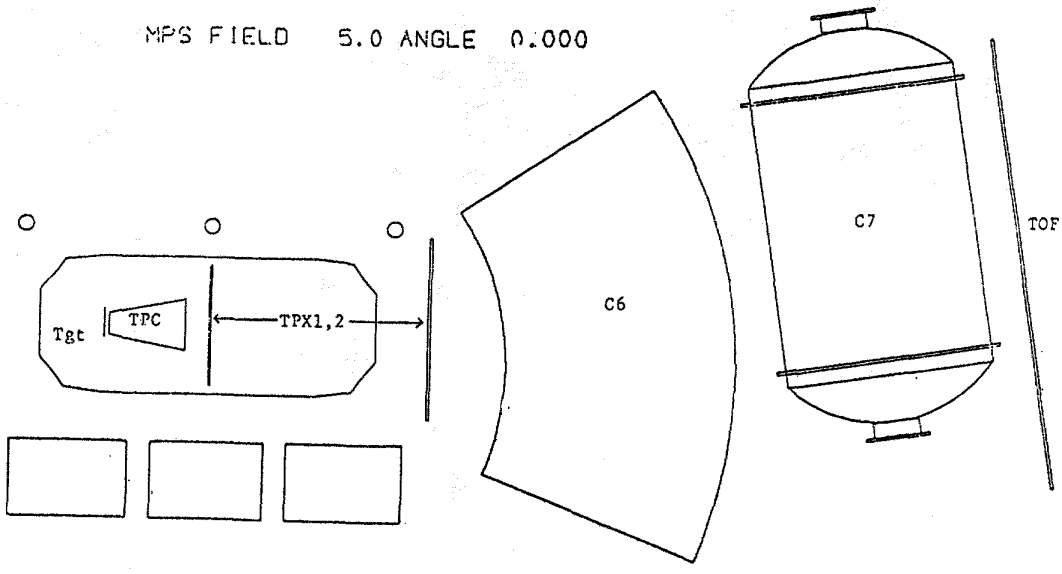

FIGURE 12. E810 A Search for Quark Matter (QGP) and other New Phenomena Utilizing Heavy Ion Collisions at the AGS

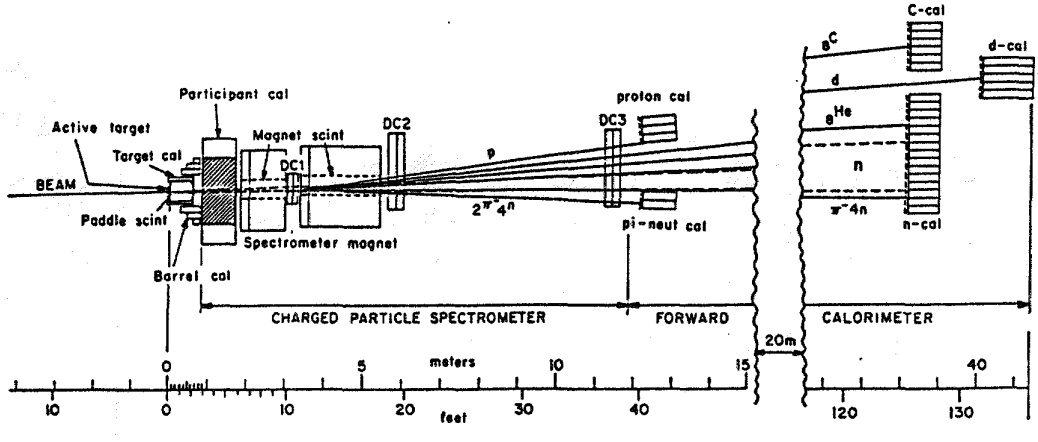

FIGURE 13. E814 Study of Exotic Nuclear States Via Coulomb or Diffractive Projectile Excitation

The NA35 experiment (Figure 8) uses a streamer chamber to detect all the charged particles emerging from an interaction as well as the neutral strange particles that decay inside the chamber. A ring-shaped hadron calorimeter and a shower counter (PPD) are used to measure the transverse energy in the lab rapidity interval $2.2<y(lab)<3.8$, corresponding to approximately $-0.8<y<+0.8$ in the nucleon-nucleon c.m system. The energy degradation of the oxygen projectile is measured using a zero degree veto calorimeter, which is also used for triggering. A streamer chamber photograph from this experiment was already shown above (Figure 3). Measurements of the mean charged particle multiplicity (for angles forward of 60 degrees) are shown in figure 14 as a function of the energy observed in the veto calorimeter. As the energy observed in the veto calorimeter decreases, the mean charged particle multiplicity increases, reaching a value of 260.

Very striking results have been obtained from the differential spectrum in transverse energy observed in the ring-calorimeter and PPD. In figure 15 the Et spectrum from the interactions of 200 GeV/u oxygen in a lead target is shown together with the Et spectrum from 200 GeV proton interactions in an Au target measured with the same setup. A most interesting feature of this data is that the 16-fold convolution of the measured p+Au spectrum beautifully reproduces the high energy edge of the O+Pb spectrum. This observation has been confirmed by the E802 collaboration at Brookhaven.

As one of the first major experiments scheduled at the Tandem-AGS, E-802 took data with a silicon beam in spring 1987 in the configuration shown in Figure 11. In addition, during the machine development run in the fall of 1986, a small test experiment was assembled from components of E802, and measurements were made using an oxygen beam of momentum 14.5 GeV/c per nucleon. The setup of the test experiment is shown in a photograph (figure 16). An array of 96 lead glass blocks (PbGl) was placed 1 meter downstream of the target. The array was 10 blocks wide by 10 high with a 2 by 2 block hole in the center for the beam to pass through. The PbGl array measured the electromagnetic energy emitted in a laboratory polar angular interval from 10 to 32 degrees, with full azimuthal coverage. In the nucleon-nucleon center of mass reference frame, this corresponds to a rapidity coverage of $-0.5<y<0.7$ for massless particles. Triggers were provided by a bullseye counter or by an

FIGURE 14

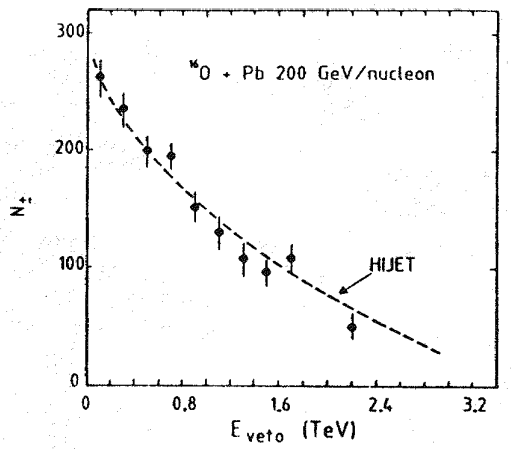

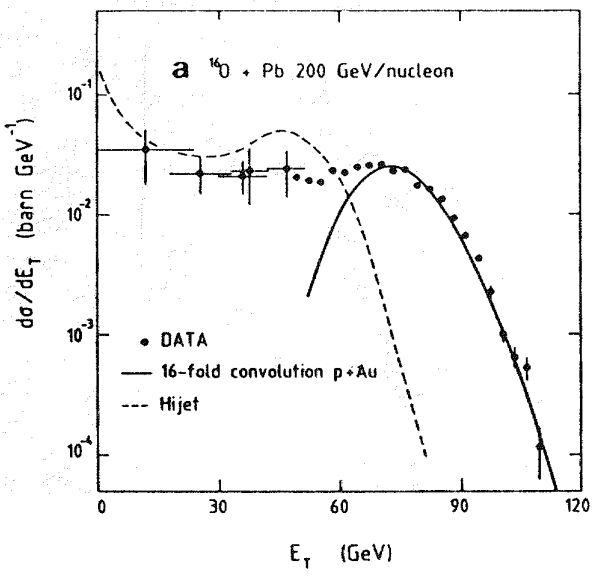

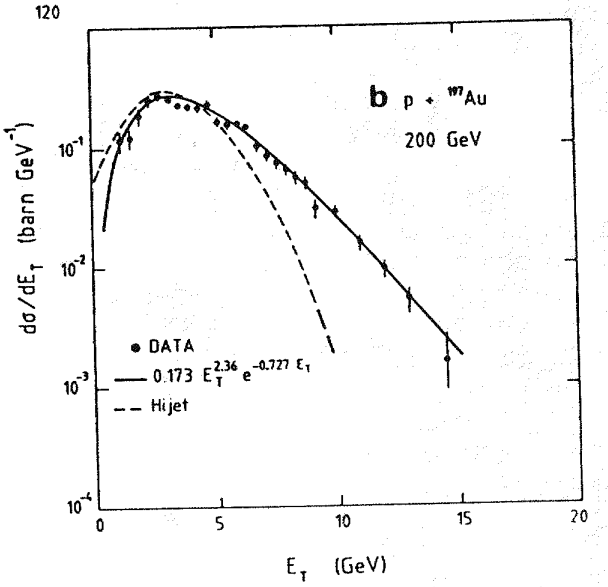

FIGURE 15. NA35 Et spectra for O+Pb and p+Au at 200 GeV/u

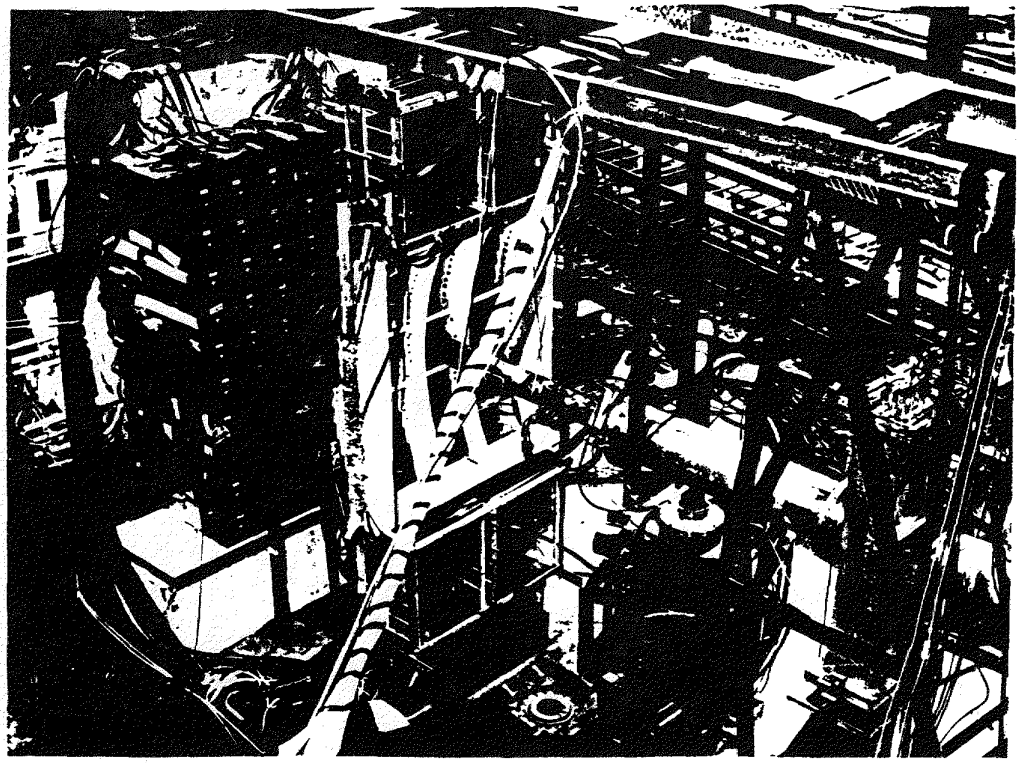

FIGURE 16. E802 test setup for oxygen runs.

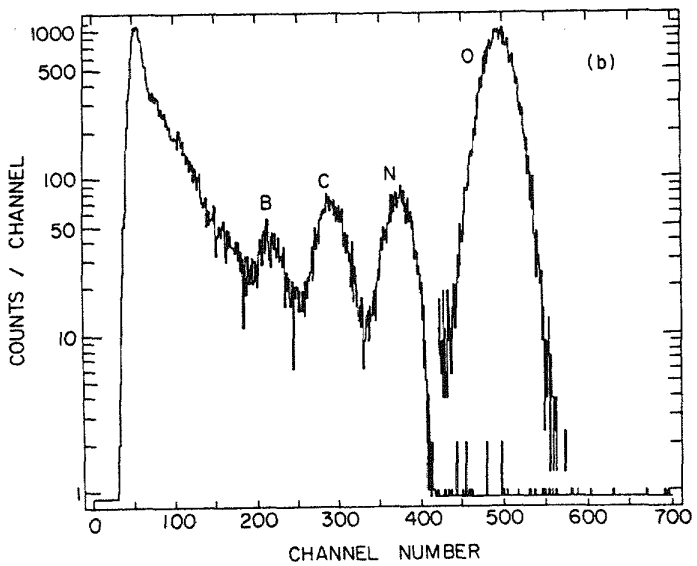

FIGURE 17. E802 Spectrum in Bullseye counter.

analog sum of the outputs of the 96 PbGl photomultipliers, corresponding to the total energy recorded with no transverse weighting. The pulse height specrum observed in the bullseye counter is shown in figure 17. The oxygen peak is obtained from a sample of non-interacting beam particles, and superimposed onto the data from the PbGl triggers. When energy is observed in the PbGl, the oxygen peak vanishes and is replaced by peaks corresponding to nitrogen, carbon and boron as well as a dominant continuum.

The spectrum of energy observed in the PbGl is shown in figure 18 for oxygen interactions in on Au, Cu, and mylar targets and proton interactions on an Au target , all measured at 14.5 GeV/c per nucleon in the same setup. The observed energy is denoted Etot since it is primarily the result of production of multiple neutral mesons, pizero and eta-zero, which are detected via their two-photon decay. Relativistic charged hadrons also emit Cerenkov light in the PbGl, approximately 500 MeV per particle, and contribute, on the average, about 50% of the observed energy. The Etot spectrum for O+Au shows a peak centered at 40 GeV and then a sharp drop-off until the yield runs out at ~70 GeV. The O+Cu data also show evidence of considerable energy emission, even though the maximum thickness of a Cu nucleus is only ~2/3 that of Au. It is of particular interest that the edges of the O+Au and O+Cu spectra become virtually identical above 50 GeV if the Cu cross section is multiplied by a factor of ~6.

These features can be described by a simple, geometrical model, based on the observation made at CERN (Figure 15) that the high energy edge of the O+Au (Pb in their case) is just the 16-fold convolution of the p+Au spectrum. This model can be extended to describe the entire O+Cu and O+Au spectra. The observed p+Au spectrum is convoluted from 1 to 16 times, with weights for the n-fold convolutions obtained from a geometrical calculation which averages over the impact parameter of the nucleus-nucleus collision to obtain the distribution in the number of projectile nucleons which interact at least once in the target. Woods-Saxon densities are assumed for both the projectile and target nuclei and a p-p inelastic cross section of 30 mb is used, corresponding to a nucleon-nucleon mean free path of ~2.2 fm.

Surprisingly good representations of both the O+Cu

FIGURE 18
E802 Data

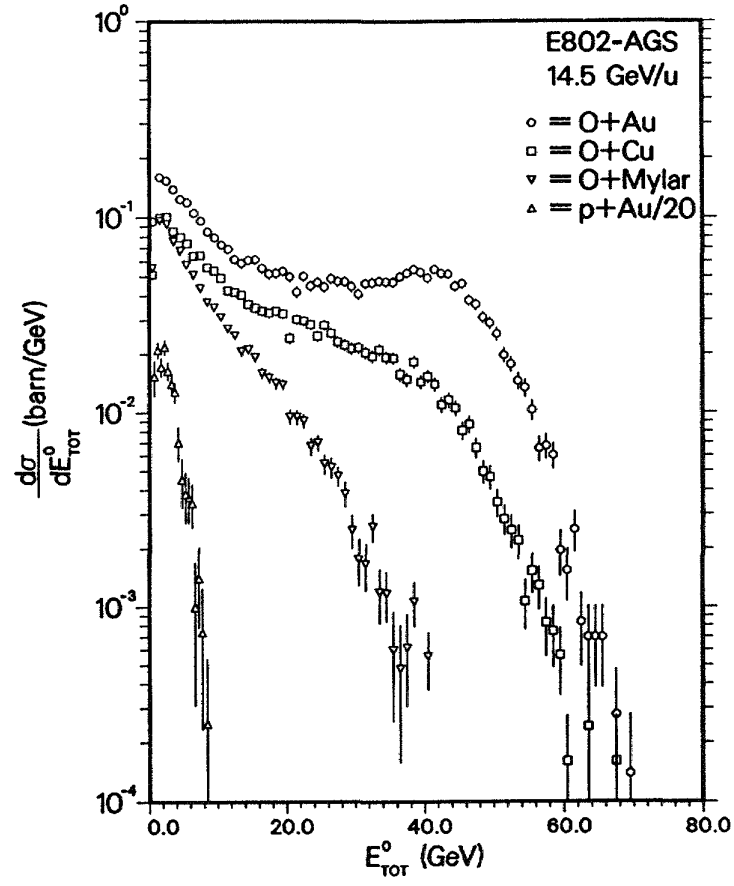

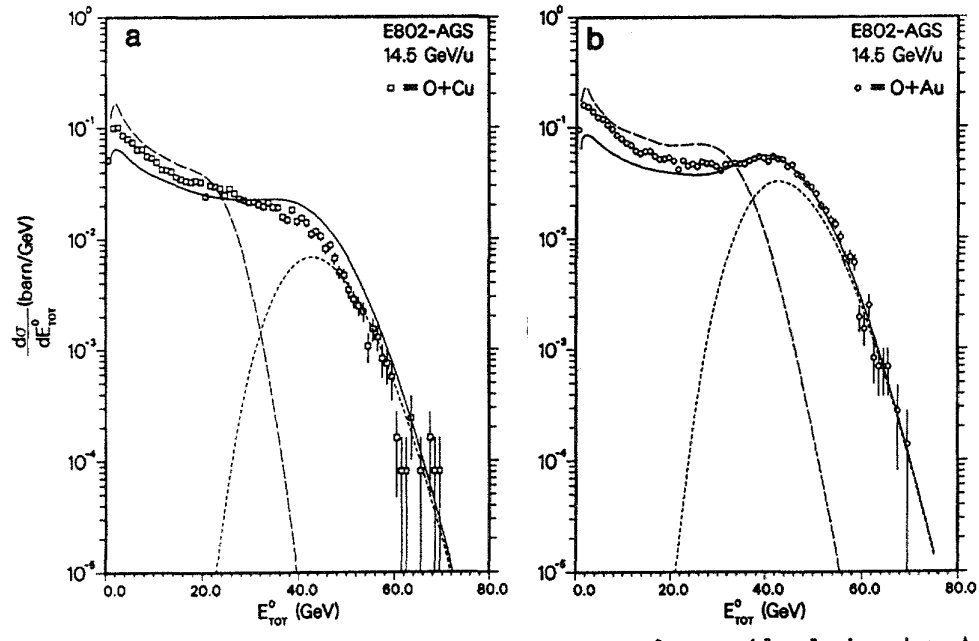

FIGURE 19. E802 Data with Fits as described in text.

and O+Au spectra are obtained from this "wounded-projectile-nucleon" model (Figure 19, solid lines). It then becomes clear that the peak in the O+Au spectrum and the identical shape of the high-energy edges of the O+Au and O+Cu spectra arise from events in which all 16 projectile nucleons interact in the target (Figure 19, dotted lines).

While seemingly reasonable, this naive model is in severe contradiction with the understanding of relativistic nuclear interactions gleaned from proton-nucleus collisions. When a proton passes through a nucleus, it can make several successive interactions. However, the observed dn/dy in p+A collisions is not simply proportional to the number of collisions but increases much more slowly. For instance, in a p+Au collision there are on the average 4.2 nucleon-nucleon interactions but the observed multiplicity density increases only by a factor of 2. Most of the effort in theories of the collisions of protons with nuclei has gone into trying to understand how the effects of the successive interactions are suppressed [20,21].

In general, the models for this suppression contain the same common features. When a relativistic nucleon interacts, it becomes an excited nucleon, and remains in that state inside the nucleus because time dilation prevents it from fragmenting into particles until it is well outside the nucleus. This feature immediately eliminates the possibility of a cascade in the nucleus from reinteraction of the secondary fragments. Furthermore it is usually assumed 1) that the excited nucleon interacts with the same cross section as an unexcited nucleon and 2) that the "fragmentation stage is independent of the number of interactions involved in the first stage" [20,22].

These features are epitomized in the wounded nucleon model (WNM) [23,24]. In this model the number of nucleons struck in a collision is computed geometrically (as above); but a nucleon contributes only once to the production of particle no matter how many times (>1) it is successively struck. Another model called HIJET [25] is frequently discussed. HIJET suppresses the effect of successive collisions by allowing only the leading baryon from an excited nucleon to interact sequentially. The suppression occurs because the leading baryon loses ~1/2 of its energy per interaction, so that the available energy is reduced on each successive interaction. Both

these models work well for p+A collisions, but fail to describe the first results for 160 collisons in nuclei (Figure 15, broken line, HIJET), (Figure 19, broken line, WNM). The failure is particularly striking for the O+Cu data from E802.

It is not difficult to understand the reason for the failure of these models in nucleus-nucleus collisons. The effect of projectile nucleons making successive collisions in the target has been suppressed, based on the proton-nucleus data. By the same token, the effect of target nucleons making successive collisions with projectile nucleons is also suppressed in these models, leading to a prediction of much lower energy emission in O+Au collisions than is actually observed. The naive model discussed above overcomes this problem by allowing a seeming contradiction: the effect of successive interactions of projectile nucleons in the target is suppressed (by utilization of the observed p+Au spectrum), whereas the case when target nucleons are successively struck by multiple nucleons from the projectile is not suppressed, but the effect is taken as linear in the number of interactions, as apparently indicated by the measurements.

This is all very exciting. The seeming contradictions will have to be sorted out by the theorists. Meanwhile, the experimentalists will take more data and find new contradictions. The opportunities for discovery are large, as befits a new field of research. To get a feeling for the state of the field, I quote the conclusion given by Tatsuo Matsui in a recent seminar at BNL: "The study of ultrarelativistic heavy ion collisions is a tremendously exciting and rich subject. It addresses a deep and fundamental question in the physical world; and requires an integrated use of expertise from many disciplines in Physics. It is a challenging and thrilling new frontier of Nuclear Physics. We need RHIC"

REFERENCES

[1] Proceedings of the Fifth International Conference on Ultra-Relativistic Nucleus-Nucleus Collisions, Quark Matter '86, Nucl. Phys. A461,1c-538c (1987); and previous proceedings in this series.
[2] R.Anishetty, P.Koehler & L.McLerran, Phys. Rev. D22,2793(1980)
[3] U.Heinz et al, Phys. Rev. Lett. 58,2292(1987)
[4] G.Baym & S.A.Chin, Phys. Lett. 62B,241(1976); G. Chapline & M.Nauenberg, Phys. Rev. D16,450(1977); H.Satz, Ann. Rev. Nucl. Part. Sci. 35,245(1985)
[5] J.D.Bjorken, Phys. Rev. D27,140(1983)
[6] P.Hut, Nucl. Phys. A418,301c(1984)
[7] L.Van Hove, Ref. 1,pp 3c-10c.
[8] L.Van Hove, Phys. Lett. 118B,138(1982)
[9] L.Van Hove, Z.Phys. C21,93(1983)
[10] R.Hwa & K.Kajantie, Phys. Rev. D32,1109(1985); K.Kajantie, J.Kapusta, L.McLerran & A.Mekjian Phys. Rev. D34,2746(1986)
[11] G.Goldhaber, S.Goldhaber, W.Lee & A.Pais, Phys. Rev. 120,300(1960)
[12] M.Gyulassy, Phys. Rev. Lett. 48,454(1982)
[13] J.Rafelski & B.Muller, Phys. Rev. Lett. 48,1066(1982)
[14] T.Matsui, B.Svetitsky & L.McLerran, Phys. Rev. D34,2047(1986)
[15] T.Matsui & H.Satz, Phys. Lett. B178,416(1986)
[16] NA35 Collab., A.Bamberger et al, Phys. Lett. B184,271(1987)
[17] E802 Collab., T.Abbott et al, submitted to Phys. Lett.
[18] T.H.Burnett et al, Phys. Rev. Lett. 57,3249(1986)
[19] J.W.Harris et al, Phys. Rev. Lett. 58,463(1987)
[20] P.M.Fishbane & J.S.Trefil, Phys. Rev. D9,168(1974); Phys. Lett. 51B,139(1974); K.Gottfried, Phys. Rev. Lett. 32,957(1974)
[21] W.Busza et al, Phys. Rev. Lett. 34,836(1975)
[22] S.Date, M.Gyulassy & H.Sumiyoshi, Phys. Rev. D32,619(1985)
[23] A.Bialas, A.Bleszynski & W.Czyz, Nucl. Phys. B111,461(1976)
[24] H.Brody, S.Frankel, W.Frati & I.Otterlund, Phys. Rev. D28,2334(1983)
[25] T.W.Ludlam, BNL Report 51921,373(1985)

FEW NUCLEON STUDIES WITH POLARIZED PROTON AND DEUTERON BEAMS AT THE SATURNE NATIONAL LABORATORY (SACLAY)

Yves Terrien
Service de Physique Nucléaire - Moyenne Energie
CEN Saclay, 91191 Gif-sur-Yvette Cedex, France

ABSTRACT

Experiments involving polarized p or d beams are reported. Based on a few examples of reactions involving a few nucleons, one shows that measurements of spin observables allow deeper physical analysis of the role of the Δ and N* resonances and of the existence of 3-body forces.

INTRODUCTION

The availability of intense and highly polarized p and d beams at intermediate energies opens up very large possibilities for studying structure of nuclei. In particular, the spin 1, isospin 0 characters of the deuteron make this beam to be an ideal tool to investigate the spin-flip $\Delta S=1$, $\Delta T=0$ resonances in nuclei by doing inelastic scattering. These resonances are very poorly known, and Saturne can provide decisive knowledge in this field. The Gamow-Teller $\Delta S=1$, $\Delta T=1$ resonances can also be studied by the (d,2p) reaction and also, of course, by the (^{3}He,t) reaction using a non-polarized beam. The well-known quenching of these states and their possible coupling with Δ-hole state can then be investigated. This physics is very active at the Saturne National Laboratory (LNS).

I would like, however, to concentrate my talk on the subject of the study of the few-body systems by reactions involving polarized beams. Indeed, with such few-body system, one faces relatively simple problems for which fully microscopic calculations can be done with good control of the mechanisms involved. This is true especially when spin observables are available, since the number of constraints on the theory is larger and, in same cases, sufficient to fully determine the reaction amplitudes. How does the nucleon-nucleon behave as a function of energy, can we know better the role of the Δ and N* resonances, does it exist three-body forces? All these questions are not new but fundamental, and with the experiments done or in progress at Saturne, we hope to shed light on them.

After having reviewed the main beam facilities that we have at Saturne, I will speak of the nucleon-nucleon (N-N) system, then I will give some results and present some projects on physics involving 3-nucleon system.

POLARIZED BEAMS FACILITIES AT SATURNE

Intense and highly polarized beams are available at Saturne. Their properties are summarized in table 1.

Table 1

Polarized beams at Saturne (intensity will be multiplied by ~ 10 with the new injector MIMAS)

Particle	Maximum kinetic energy (GeV)	Polarization (%)	Intensity/burst
$\vec{p}$	3	~ 90 (1 GeV) ~ 65 (2 GeV)	10^{10}
$\vec{d}$	2.4	~ 60 (vector) ~ 90 (tensor)	2×10^{10}
$\vec{n}$	1.2	~ 55	~ 10^6

Due to the existence of depolarizing resonances, some discrete energies are forbidden for the extracted proton beam. This is not the case for deuterons, which makes the polarization of these beams extremely stable over long periods of runs.

In both cases, the state of the polarization of the beam (up or down in the case of vector polarization and all states of tensor polarization) can be changed at every burst (i.e. every 1-4 second), which allows to avoid systematic errors in the measurement of asymmetries since, them, it does not require 2 separate runs.

The principle of the neutron beam is very simple. Polarized deuterons are broken up on a light target, followed by a magnetic field which sweeps the charged particles (protons from the break-up or residual deuterons) ; then a several meter long iron collimator of a small diameter set at 0° selects the "spectator" neutrons which constitute the beam. This has been shown[1] to provide a rather monoenergetic beam (the energy width is mainly due to the Fermi momentum of the neutron in the deuteron), with good intensity (the yield of neutrons obtained per unit of incident deuteron beam intensity is a few 10^3 better than that obtained by a knock-out reaction with proton beams on a deuterium target). For incident deuterons polarized at P percent in any direction, the neutrons at 0° remain polarized with practically the same percentage in the same direction. Fig. 1 shows a schematic picture of the neutron beam made or the IKAR experiment, where, with the diameter of the iron collimator restricted to 1.5 cm to get a well defined beam, we could obtain 10^6 neutrons for the 2×10^{10} deuterons available at SATURNE before the current installation of the new injector MIMAS. An original method of calibration of the neutron beam intensity based on the comparison between the n-^{4}He and

p-^{4}He elastic differential cross sections[2] has been used to obtain the absolute normalization of the cross sections presented in the following section.

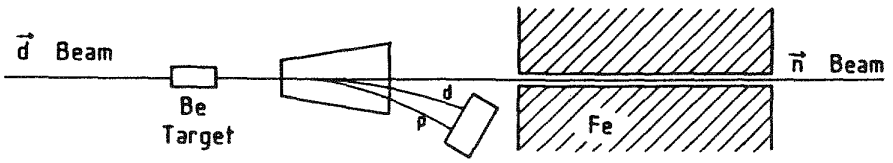

Fig. 1 - Polarized neutron beam.

THE STUDY OF THE ELEMENTARY N-N INTERACTION

The interest in studying the proton-proton interaction has been renewed a few years ago by the observation at Argonne of large structures in the variation with the incident energy of the parallel- and antiparallel-spin total cross section differences $\Delta\sigma_L$ and $\Delta\sigma_T$. One can say that the elementary proton-proton interaction at intermediate energies is now rather well known after the extensive measurements of spin observables made at Saturne[3] these last years. They have brought very interesting results, since through Phase-Shift Analyses (PSA) [refs.[4-6]], resonance-like behavior has been seen for the $^1D_2$ and may

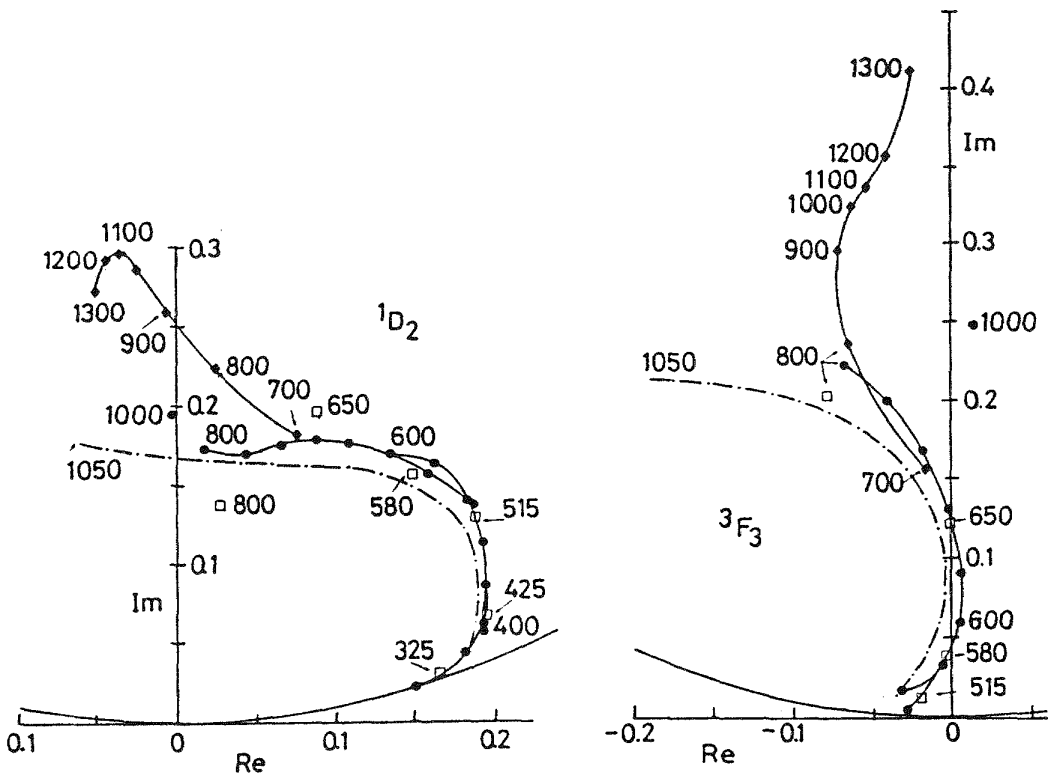

Fig. 2 - Argand plot for the $^1D_2$ and $^3F_3$ waves in pp scattering.

be $^3F_3$ waves in elastic scattering (see Fig. 2). It is commonly suggested that the observed behavior is governed by the excitation of the Δ_{33} resonance which largely dominates the proton-proton interaction from 400 to 800 MeV.

The situation is different for the neutron-proton interaction, which is isospin-mixed I=0,1 instead of I=1 only for p-p. Indeed, for the I=0 part, the excitation of the Δ is forbidden by the isospin conservation law, which means that other features could emerge in this I=0 component of the nucleon-nucleon interaction, which are not visible in the Δ-dominated I=1 p-p channel. Thus it is of great interest to undertake a detailed study of the n-p interaction in this energy domain, and also above, where the excitation of the I=1/2 N* resonances is expected to play a role in both the I=0 and I=1 components of the N-N interaction. The experimental situation is much worse in the case of the n-p interaction than in the case of the p-p interaction. Data are scarce : the spin-averaged total cross section σ_t is known, but, for elastic scattering, the differential cross section and analyzing power are poorly known (especially at small transfers) and very few spin observables have been measured. For inelastic channels, only a very limited set of data is available. Moreover, existing experiments have often been done by quasi-free scattering of neutrons bound inside a deuteron (beam or target) instead of using a free neutron beam. We thus have begun a program at Saturne to study the n-p interaction, using our polarized free neutron beam.

The first experiment, now finished, consisted of measurements of the $\vec{n}$-p elastic differential cross section and analysing power at small transfer, where there is no data. Analysing powers[7] and absolute differential cross sections[8] are presented in Figs. 3 and 4 respectively, together with PSA. It must be noted that our data, useful for PSA, are also essential to fix the free n-p amplitude, which is an important input in any miscroscopic calculation of nuclear reactions. The agreement of our data with the PSA predictions indicates a good experimental consistency between our normalization and those of the experiments giving σ_t. Also, the analysis of the physical data shows that the observables measured to not differ significantly in the p-p and n-p cases. This means that the I=0 component, which makes the difference between the p-p and n-p interactions, is negligible or has the same behavior for these observables. However, more experimental studies are needeed, especially at energies around one GeV or above, where the excitation of N* resonances becomes possible.

The second current experiment using the polarized free neutron beam consists of the measurement, by the transmission method, of the spin dependent total cross section differences $\Delta\sigma_L$ and $\Delta\sigma_T$, between 0.6 and 1 GeV. The free neutron beam with a polarization oriented either along the vertical or the longitudinal dirctions was transmitted through the 35 mm thick, 40 mm wide and 49 mm high polarized proton target of frozen-spin type, which can be used here since there

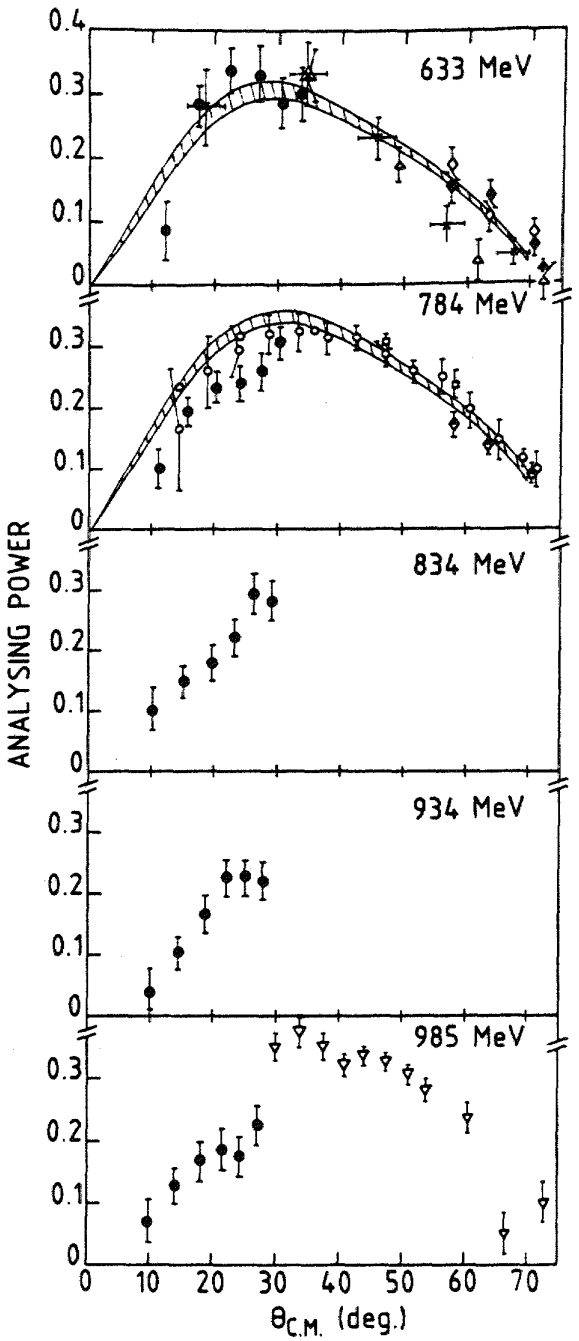

Fig. 3 - Analyzing power in $\vec{n}p$ elastic scattering (shaded area : PSA ref.[3]).

is no problem of beam intensity. These results for the isospin mixed I=0,1 n-p system together with the corresponding pure I=1 pp data yield two of the three spin dependent forward scattering amplitudes for isospin I=0.

The Fig. 5 shows the results of the present experiment. The Fig. 5b shows also other results calculated from data obtained at the ZGS (Argonne), by an experiment based on the transmission of polarized protons through a partially deuterated polarized target. Determination of the $\Delta\sigma$(np) from these data requires corrections for 3-body final state interactions which were calculated by Kroll. Our results obtained with free neutrons seem to disagree above 0.8 GeV with those of that quasi-free experiment.

Concerning inelastic channels, an interesting experiment has been done at Saturne for the $\vec{p}p \to d\pi$ reaction. Fig. 6 shows the angular distributions of the analysing power, for energies from 1.2 to 2.3 GeV. One clearly sees a large structure appearing at backward angles for a $\simeq$ 0. This means that same intermediate state at $\sqrt{s} \simeq 2.65$ GeV (see Fig. 7) seems to be excited. Is it a 6-quark effect or, more simply, the passage through the NN$^*_{688}$ intermediate state? It does not exist any calculation yet to answer this question, but it must be noted that the 2.65 GeV value is about equal to the pp invariant mass of the first of the two structures seen in $\vec{p}\vec{p}$ ($\Delta\sigma_L$) by Auer et al.[10].

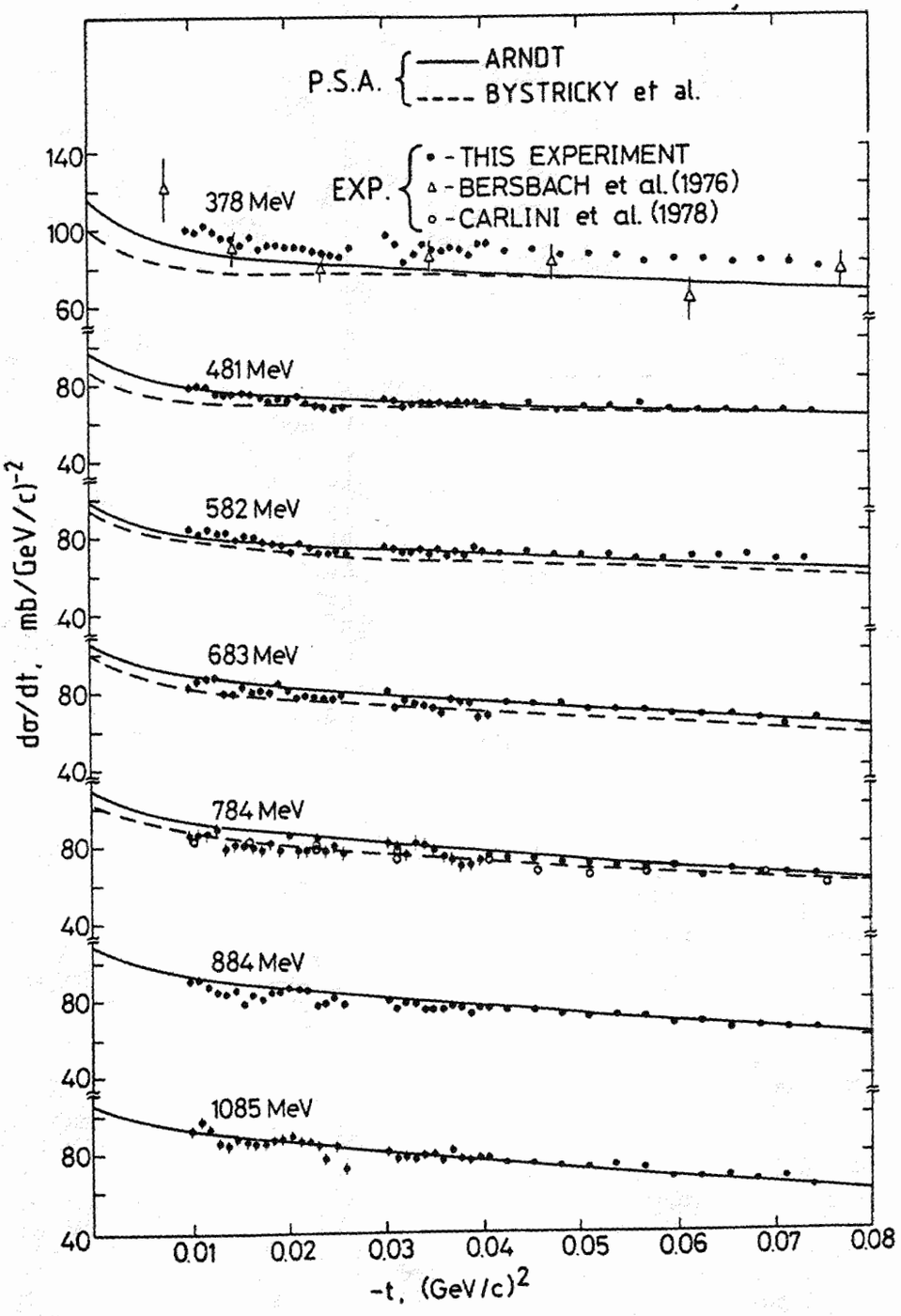

Fig. 4 - Differential cross sections in $\vec{n}p$ elastic scattering (solid line : PSA ref.[4] ; dashed line : PSA ref.[3]).

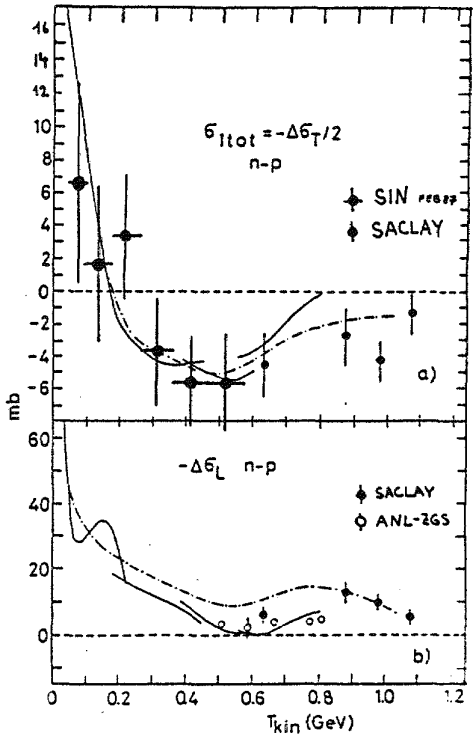

Fig. 5 - $\Delta\sigma_T$ and $\Delta\sigma_L$ for the $\vec{n}\vec{p}$ system (PSA solid line : ref.[4] ; dot-dashed line : ref.[4]).

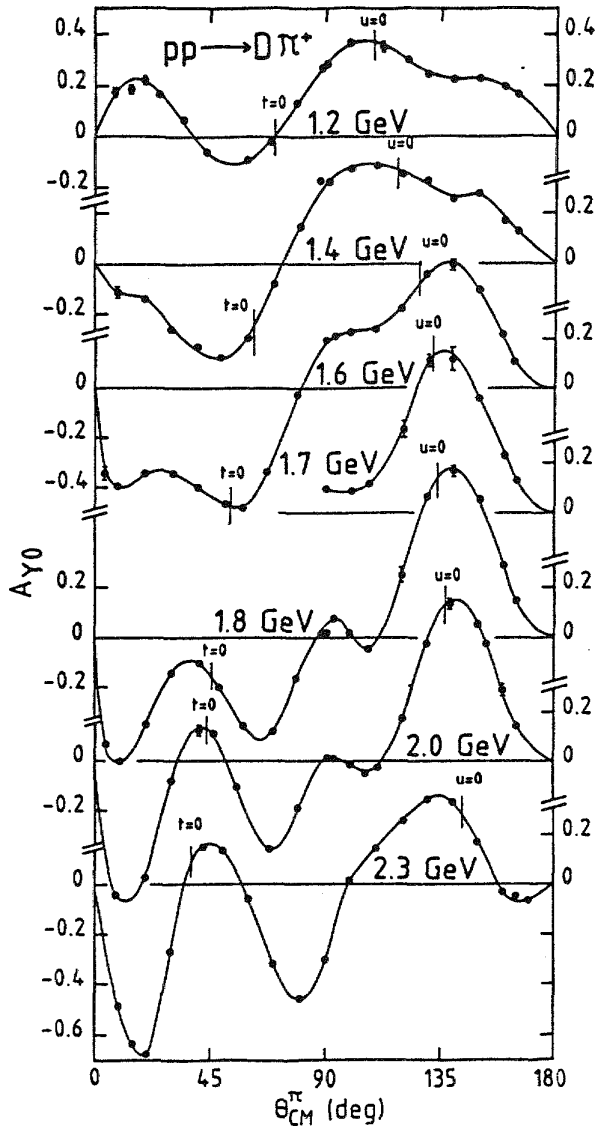

Fig. 6 - Analysing power angular distribution for the reaction $\vec{p}p \rightarrow d\pi^+$ between 1.2 and 2.3 GeV.

AN EXAMPLE OF REACTION INVOLVING 3-BODY SYSTEM

Two experiments have been done with simple 3 interacting nucleon systems, and the results, fully analysed, have shown very clearly the effect of 3-body forces. These are the measurement of the T_{20} asymmetry and of the differential cross section of the reaction $dp \rightarrow {}^3He\ \pi_0$ done at 0° and 180° with tensor polarized deuteron, at incident energies T_d ranging from the threshold to 2.2 GeV.

Experimental results[11] are shown in Fig. 8. Contrary to the rather smooth variation of the forward cross section, the backward values of this observable present two clear structures : one, around 1 GeV is at the place where the Δ_{33} excitation is expected to dominate, but the second at 2.2 GeV can correspond to various phenomena, like the excitation of $\Delta\Delta$ states and/or of various N* resonances.

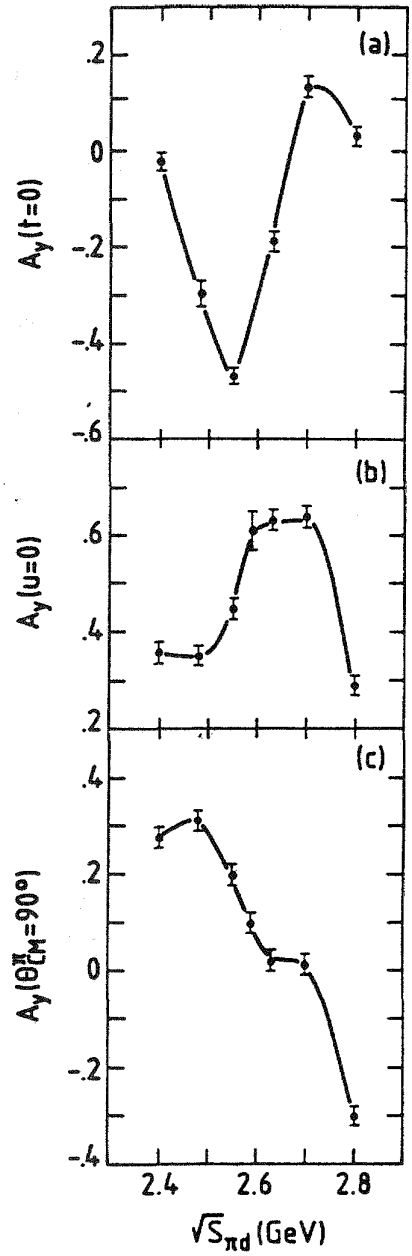

Fig. 7 - Analysing power for the reaction $\vec{p}p \to d\pi^+$: values for $t = 0$, $u = 0$, $\theta_\pi^{CM} = 0$, as a function of $\sqrt{s}$.

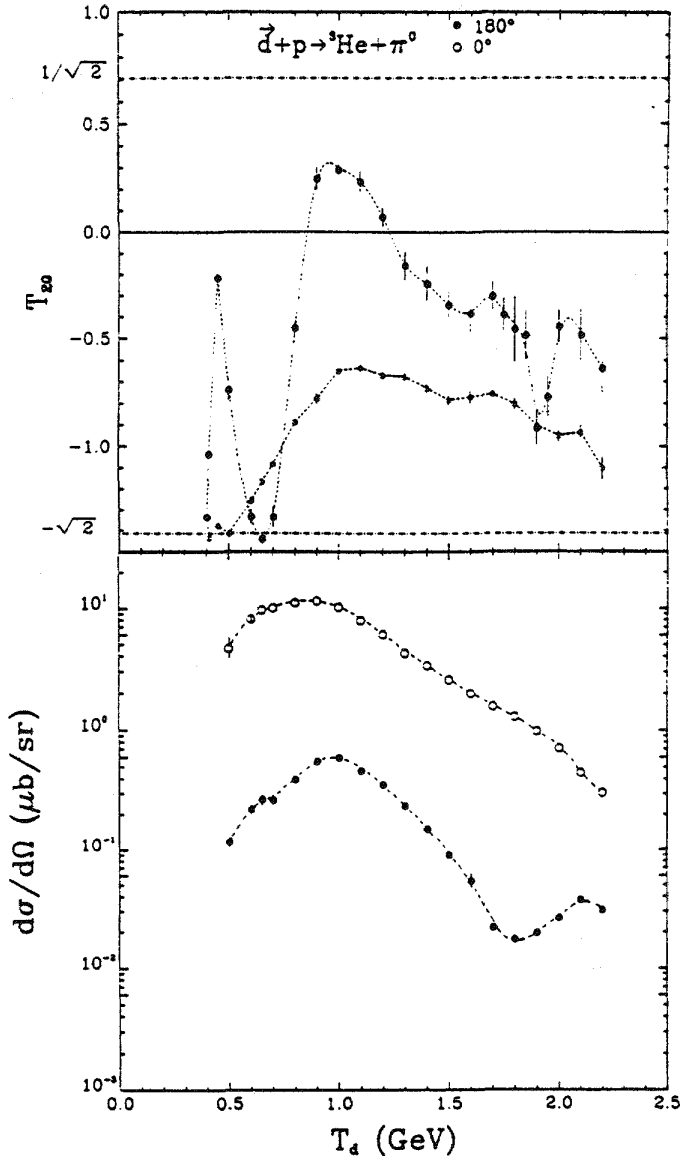

Fig. 8 - Excitation functions of the tensor analysing power T_{20} and of the differential cross section for the reaction $dp \to {}^3He\ \pi_0$ at 0° and 180°.

A first analysis of these data has been suggested by Germond and Wilkin[12,13], who have noted that, at 0° and 180°, two amplitudes only (central and spin-flip) are needed to describe the reaction and who have extracted them from the T_{20} and $d\sigma/d\Omega$ data. One can see in Fig. 9, which presents the two amplitudes as a function of T_d, that the narrow structure visible on $T_{20}(180)$ at 1.92 GeV is in fact the result of the interference of the two amplitudes having a

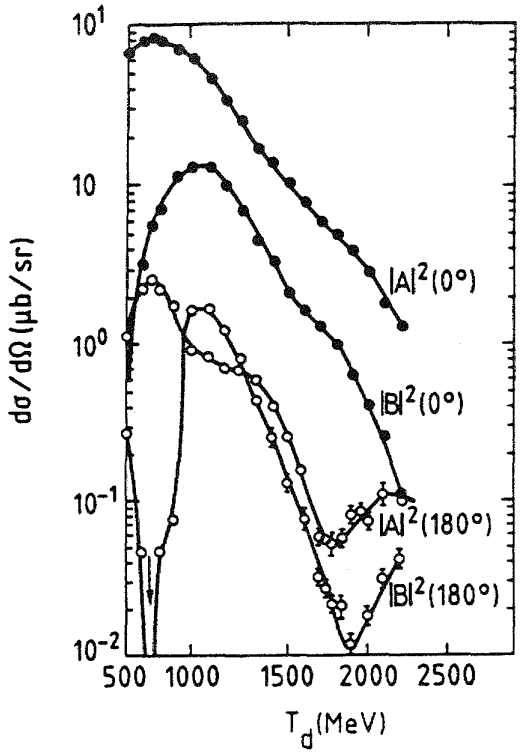

Fig. 9 - Central (A) and spin-flip (B) amplitudes for the reaction $\vec{d}p \to {}^3He\,\pi^0$ at 0° and 180°.

larger dip but at slightly different energies. Then these two amplitudes have been remarkably fitted in a calculation made by Ueda-[ref.[14]] including NNΔ and NΔΔ resonances predicted by models of the NΔ interaction. This is a good indication that 3-body forces must play a role here.

To go further in a more microscopic understanding of the process, the authors, in a very crude model involving simplified wave functions for d and t and phenomenological Lagrangians, have estimated[13] the importance of 2-nucleon graphs (1 and 2 ; Fig. 10) and 3-nucleon graphs (3, 4 and 5 ; Fig. 10). As expected, it is at 180°, where the momentum transfer is high, that these 3-nucleon graphs, which allow the transfer between nucleons to be shared, are important, even dominant above the Δ excitation region. More surprisingly, the excitation of N* plays a role at forward angle only (Fig. 11).

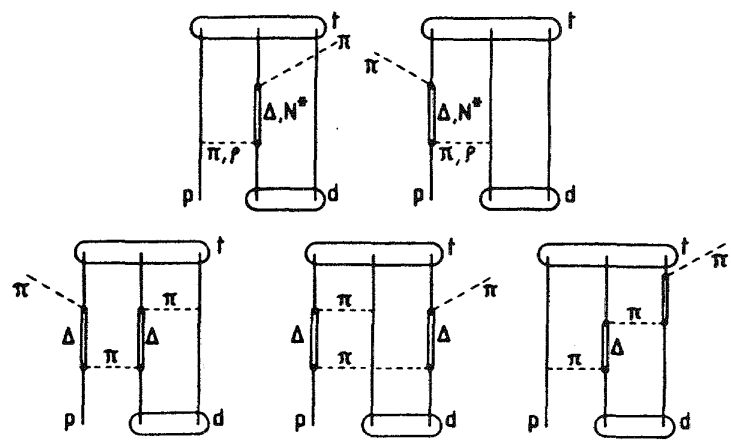

Fig. 10 - Two-body (1,2) and 3-body (3,4,5) graphs for the reaction $pd \to t\pi^+$ (or $pd \to {}^3He\pi_0$ which is equivalent).

A recent and more realistic calculation taking fully these 3-body effects into account has been made recently[15]. It can be seen in Fig. 12 that the inclusion of 3-body effects (solid line) gives a

good account of the observables measured, and, in particular, allows to explanation of the the second structure appearing in the excitation function of the 180° cross section above 1 GeV. It is interesting to note that the inclusion of 3-body graphs leads also to reproduce much better the angular distributions of the cross section for the reaction pd → $t\pi^+$ at 500 and 800 MeV (see the J.M. Laget's talk, this conference).

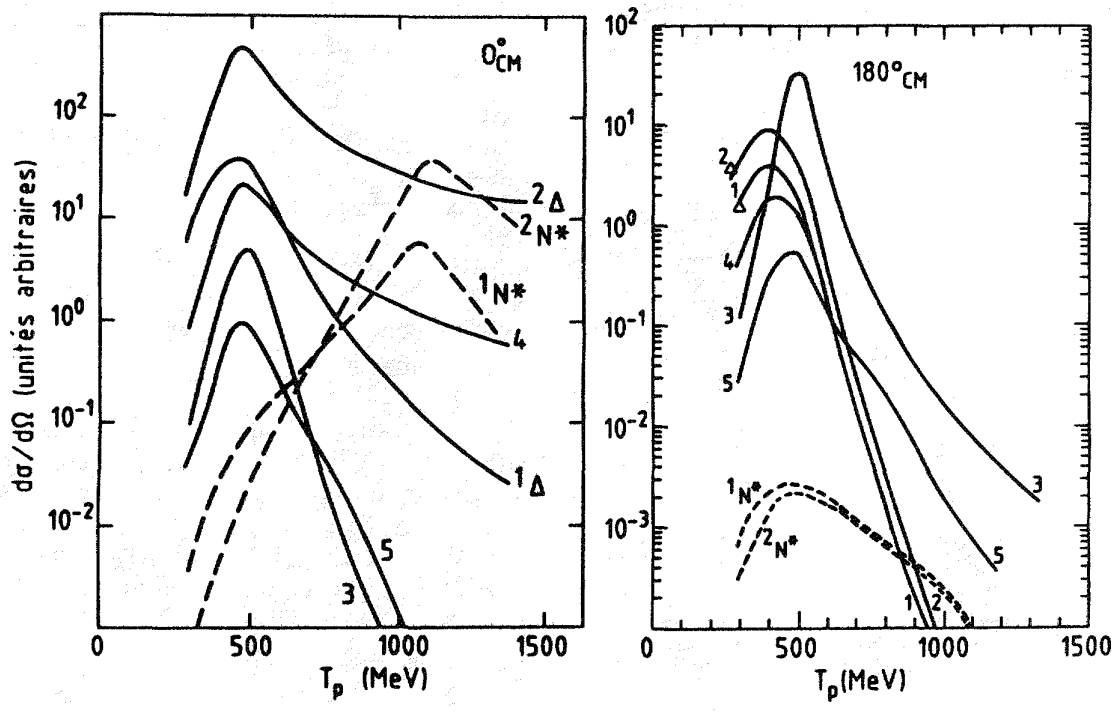

Fig. 11 - Estimation of the cross section of the pd → $t\pi^+$ reaction for the graphs of Fig. 10.

CONCLUSION

Through a few examples, I have tried to show that the measurement of polarization observables allows to go much deeper in the understanding of few-nucleon systems. Indeed, in some cases, complete description of the amplitudes involved can be given and full analysis can be done, with control of the description of the mechanism.

The experiments that we have done confirm the role of the excitation of the Δ and, maybe, of N* resonances. They also show the role of 3-body forces, may be through the existence of NNΔ or NΔΔ resonances. They could reflect the existence of sub-nucleonic degrees of freedom in the NN channel.

We want to continue these studies at Saturne, on some specific subjects, with the aim of being able to describe all reactions involving a few-body system in a coherent way. The main next steps in this

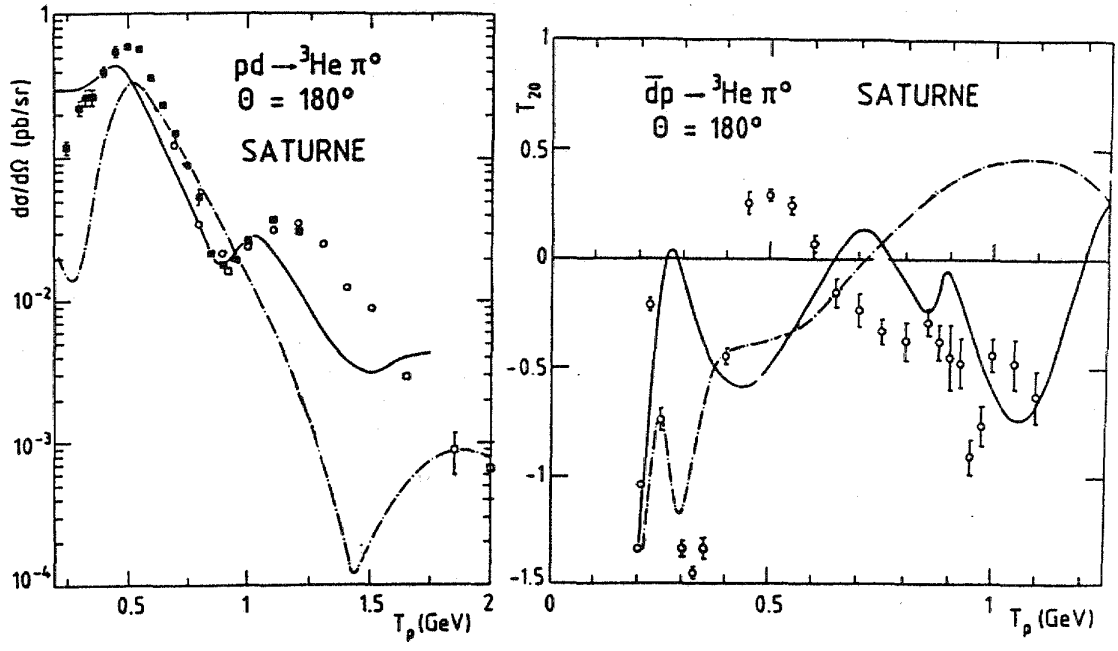

Fig. 12 - Full microscopic calculation[15] of $d\sigma/d\Omega$ and T_{20} with (solid line) or without (dot dashed line) 3-body graphs.

complete kinematics (to get the Δ/S ratio of the deuteron wave-function), the np → ppπ⁻ inelastic NN channel (to get the I=0 contribution), both experiment being planned in the coming months.

REFERENCES

1. G. Bizard et al., Nucl. Instr. Meth. 111, 451 (1973).
2. Y. Terrien and F. Wellers, J. de Phys. 46, 1873 (1985).
3. F. Lehar, J. Phys. Soc. Jpn. 55 suppl., 284 (1986).
4. R.A. Arndt, Phys. Rev. D28, 97 (1983).
5. J. Bystricky et al., J. de Phys. 48, 199 (1987).
6. Y. Higuchi et al., "1983 INS Symposium", Tokyo (1983).
7. G.A. Korolev et al., Phys. Lett. 165B, 262 (1985).
8. Y. Terrien et al., submitted to Phys. Rev. Lett.
9. R. Bertini et al., to be published ;
   RB. Mayer et al., Nucl. Phys. A437, 630 (1985).
10. I.P. Auer et al., PANIC 87, Kyoto (1987).
11. C. Kerboul et al., Phys. Lett. 181, 28 (1986) and PANIC 87, Kyoto (1987).
12. J.F. Germond and C. Wilkin, to be published.
13. C. Kerboul, Thesis, Université de Strasbourg (1987).
14. T. Ueda, submitted to Prog. Theor. Phys.
15. J.M. Laget and J.F. Lecolley, submitted to Phys. Lett. B ;
    J.M. Laget, contribution to this conference.

THREE-BODY FORCES AND THE TRINUCLEONS

J. L. Friar
Theoretical Division, Los Alamos National Laboratory
Los Alamos, NM 87545

ABSTRACT

Three-body forces are discussed in the context of classical, atomic, solid-state and nuclear physics. The basic theoretical ingredients used in the construction of such forces are reviewed. Experimental evidence for three-nucleon forces and an overview of the three-nucleon bound states are presented.

INTRODUCTION

Three-body forces play a minor role in most branches of physics, whether classical, atomic, solid-state, or nuclear physics. The archetype of a two-body, or pairwise, force is the classical gravitational force between particles or large composite objects, such as stars and planets. This long-range force is always attractive. The pairwise Coulomb force between charged particles, electrons and nuclei, has an identical functional form, but with the additional complication of a dependence on electrical charge. The longest-range force between neutral atoms is the pairwise Casimir-Polder[1] interaction ($\sim 1/r^7$), although the long-range van der Waals potential ($\sim 1/r^6$) is dominant. The familiar (two-body) semiphenomenological nucleon-nucleon force models in nuclear physics form the computation basis of our field. They contain the additional complexity of the spin and isospin degrees of freedom of the nucleon and incorporate a large amount of phenomenology. In analogy to the long-range atom-atom interactions, the form of the longest-range part of the two-nucleon force (the one-pion-exchange potential) is determined by general principles.

These pairwise forces are dominant, and a description of nature using such forces alone ranges from good to excellent. Finding small effects due to additional forces of fundamentally different type is not an easy task and often founders on an inadequate ability to solve the many-body problem. Making a small error in treating the dominant force can mask a smaller interaction. This is the reason why simple systems are the traditional hunting ground for small, exotic effects. Examples are the one-electron and two-electron ions in atomic physics and the two- and three-nucleon systems in nuclear physics. Interpretability depends on calculational precision, and simple systems are the best place for this. The recent experiment[2] on the Lamb shift in Helium-like Uranium ions depends heavily on detailed theoretical calculations in order to unravel the physics. Similarly, the two- and three-nucleon systems provide the best opportunity for detecting and detailing the properties of "small" nontraditional mechanisms in nuclear physics,[3]

such as meson-exchange currents, relativistic effects, and three-body forces.

THREE-BODY FORCES

Are three-body forces necessary in all circumstances? The answer is usually no, in principle, but, yes, in practice. In order to elucidate this obscure answer, we must provide a proper definition for such a force, and this is best done by example. If the nonlinearities of general relativity are ignored, the classical gravitational interaction between two elementary bits of matter is the radially-directed pairwise force assumed by Newton. Any additional particles interact via the same mechanism. Newton invented integral calculus so that he could linearly superimpose the elementary interactions in two or more composite systems. Such a superposition rules out elementary three-body forces which would exist if the interaction between one pair of particles depended on the presence of a third particle.

CLASSICAL THREE-BODY FORCES

Newton's superposition assumption does not rule out three-body forces between composite objects, however. Imagine that two such objects are the earth and the moon, which are assumed for the moment to be spherical and rigid. The radially directed force between them has been calculated by generations of physics students, and behaves as if the earth and moon were pointlike, with their masses concentrated at their geometric centers. Adding a third object, such as a satellite orbiting the earth, does not increase the complexity, because the force on that object is the sum of its simple pairwise interactions with the moon and the earth. The water in the earth's oceans is not rigid, however, and is deformed by the moon's attraction to produce tides. This tidal deformation changes the gravitational force on the satellite, which now depends on the relative orientations of the earth and moon in a complicated way, as illustrated in Figure 1. The satellite feels a weak (tidal) three-body force in addition to the (much stronger) pairwise interactions with the solid part of the earth and with the moon, which we have assumed are unaffected by their mutual presence.

This simple example is the archetype for most three-body forces in nature, including the nuclear ones. Such forces typically share common traits: (1) they are the result of treating the interactions of composite objects, since the elementary interactions between particles were assumed to be two-body in nature (i.e., it's a theorists' game); (2) alternatively, freezing out degrees of freedom (e.g., 3 bodies vs. 10^N bodies) leads to such forces; (3) they have a strong orientation (angular) dependence, just as the force on the satellite depends crucially on its orientation with respect to the tidal bulge, positioned by the moon; (4) we have discussed only the long-range part of the force (far from the earth's center), which is generally the easiest part to calculate in any area of physics; (5) distortion (change of shape) is often the origin of such forces.

The tidal three-body force effect on a satellite is observable, because the latter's position can be determined with great precision.

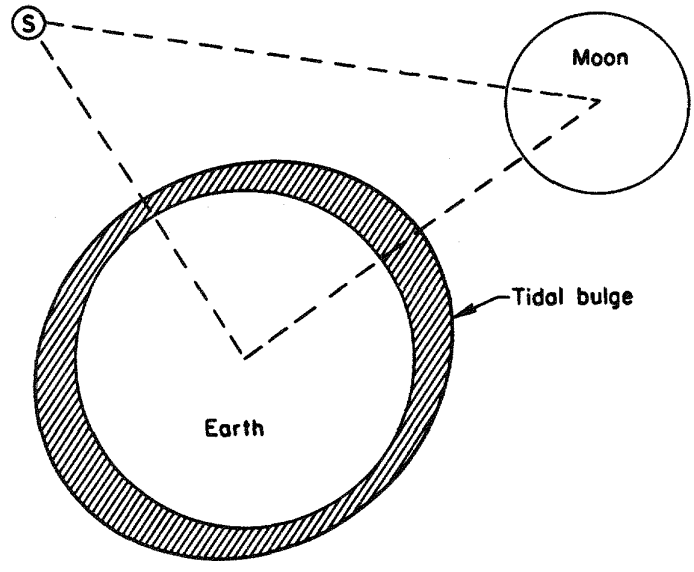

Fig. 1. Classical three-body force arising from tides.

THE THREE-NUCLEON FORCE

The pion is the lightest of all observed hadrons. It mediates the longest-range part of both the two-nucleon (OPEP) and three-nucleon (2π3NF) forces. Because the two- and three-nucleon systems are not deeply bound, and hence the nucleons lie relatively far apart, OPEP, V_π, plays a very important role, particularly through its tensor force. One might expect the corresponding importance of the 2π3NF, mediated by the exchange of two pions and illustrated in Figure 2. The first nucleon in (2a) emits a virtual pion which scatters (off-shell) from the second nucleon and is ultimately absorbed by the third nucleon. This virtual scattering contains a variety of physical mechanisms (2b-2f), not all of which are "real" three-body forces. Just as our classical example contained a small three-body force (the tidal bulge) in addition to two-body forces (from the solid earth and moon), the sequential interaction of OPEP in the triton is just part of solving the Schrödinger equation with two-body forces. Such a process is depicted graphically in Figure (2b), and is not a true three-body force. Eliminating this diagram in a consistent calculation is somewhat tricky, however, and has only been accomplished recently.[4]

We note that the Δ-mediated force[5] is a "distortion" of a nucleon, like our previous example. The Axilrod-Teller[6] three-atom force which is generated by the same mechanism (dipole distortion) that produces the pairwise van der Waals interaction is analogous to the 3-Δ force in nuclei. The "pair" process in (2d) is analogous to the Primakoff-Holstein[7] 3-electron force in atoms. The pion in (2e) and (2f) scatters from other virtual mesic constituents of the triton. The latter graphs are the analogues of the intermediate energy nuclear scattering processes in Figure 3, where pion-nucleus scattering in (3a) can proceed via π-π scattering[8] and proton-nucleus scattering in (3b) has a distinctive signature produced by nucleon-antinucleon "pair" correlations in the Dirac approach.[9]

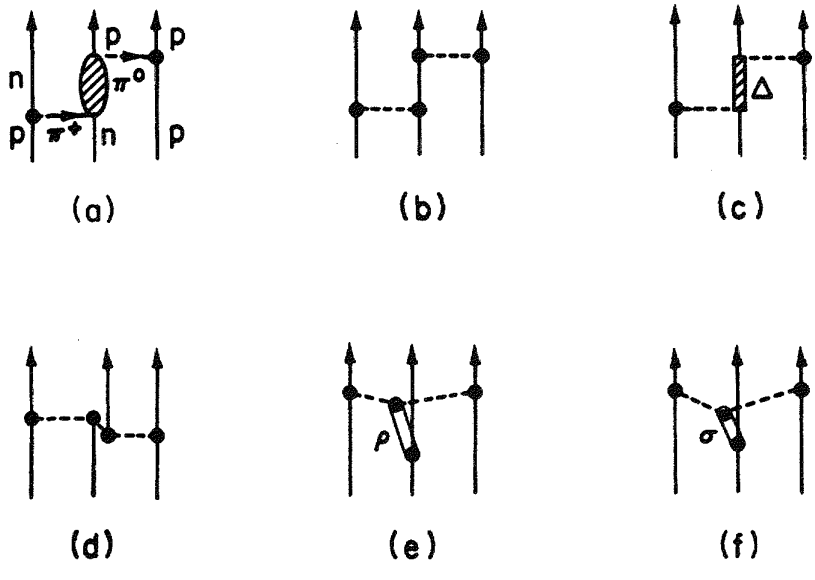

Fig. 2. Components of the 2π3NF in (a) are decomposed in (c) - (f).

The multiple charge states of the pion and the characteristic spin-dependent pion-nucleon vertex generate a rich spin and isotopic spin dependence. Moreover, because the two-body potential energy in a nucleus naively depends quadratically on the density and the three-body energy varies cubically, the relative effect of the three-body forces could change dramatically between spin-saturated and unsaturated systems, or between the diffuse triton and denser nuclear matter.[10]

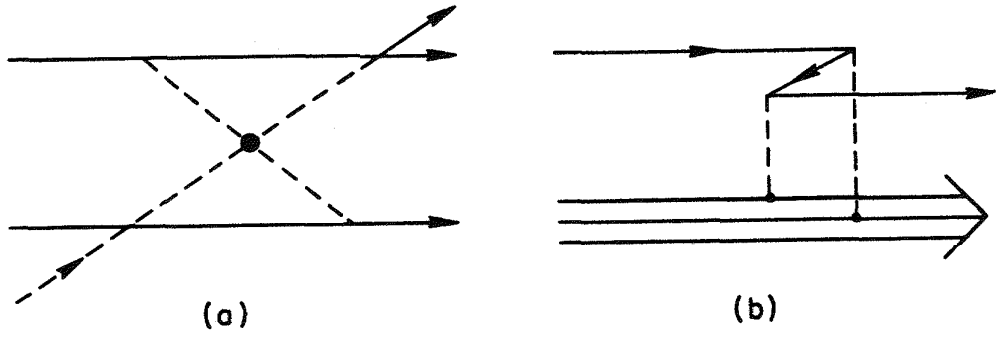

Fig. 3. Three-body forces in pion- and proton-nucleus scattering.

SIZE SCALES

A representative component of the 2π3NF has a schematic form expressible in terms of OPEP (V_π) and the nucleon rest energy: V_π^2/Mc^2, typical of one class of relativistic corrections. Using $\langle V_\pi \rangle$ ~30 MeV leads to an estimate of 1 MeV, or 2 percent of the rough value of the total[11] potential energy: 50 MeV. This is also commensurate with other naive estimates[3] of relativistic corrections.

TWO- AND THREE-BODY FORCE CALCULATIONS

Recently there has been substantial progress in our ability to solve the Faddeev equations[12] for the three-nucleon problem. These equations are exactly equivalent to the Schrödinger equation, but are written[13] in such a way that boundary conditions are much easier to implement. This technique currently represents the most accurate way to solve the triton problem for realistic potentials, although there has been substantial progress using many different computational methods: hyperspherical harmonic expansions[14-15], Green's function Monte Carlo techniques[16-18], and the Rayleigh-Ritz variational approach[19-21]. Large-basis triton Faddeev calculations[22,23] can be performed with an accuracy of approximately 10 keV out of a total binding energy of roughly 8 MeV. Cases which have been treated include two-body forces only, and two-body plus three-body forces.

Two-body force results for "realistic" potentials with strong tensor forces include: Reid Soft Core[24] (RSC) [-7.36 MeV], Argonne[25] V_{14} (AV_{14}) [-7.68 MeV], Super Soft Core (C)[26] [-7.53 MeV],

de Tourreil-Rouben-Sprung[27] (B) [-7.57 MeV], Paris[28] [-7.64 MeV], and Bonn[29] [-8.33 MeV].[30] All of these results follow from large basis calculations,[22,31] and with the exception of the Bonn result[32,33] have a binding deficiency of approximately 1 MeV.

The latter potential has at least 3 salient features. The configuration space version has a momentum dependence of the form $\{p^2,\phi(r)\}/M$, in common with the Paris[28] and Nijmegen[34] potentials. By itself, therefore, this feature cannot account for the difference. A second feature is the fact that, in common with the AV_{14} potential and unlike the others, the T=1 potential is fit to np scattering results. This will always enhance the binding, as the following argument[35] shows. Because the angular momentum barrier[11] suppresses higher partial waves, s-wave forces and the concommitant tensor-coupled d-waves dominate the triton binding. There are 3 pairs of forces, one T=1 pair between the two neutrons, V_{nn}, and two np forces which are 3/4 S=1 (T=0) and 1/4 S=0 (T=1) by statistical spin weighting. Thus the triton potential is $V = \frac{3}{2} V_{np}(T=0) + \frac{3}{2}\left(\frac{2}{3}V_{nn} + \frac{1}{3}V_{np}(T=1)\right)$, and the effective T=1 potential is a $\frac{2}{3} - \frac{1}{3}$ weighting of nn and np forces, of which the latter is the stronger. Using a pure $V_{np}(T=1)$ force will overbind, while using V_{nn} alone tends to underbind. Crude estimates[35] indicate that each 1/3 costs about 100 keV, or using V_{nn} alone underbinds by 100 keV and using V_{np} alone overbinds by 200 keV. The third salient feature is the weak tensor force in the Bonn potential. This has been known for two decades to increase the triton binding. The reason is that the tensor force dominates the binding in both the deuteron and triton. It is most effective in the deuteron, however, where virtually all of the potential energy is associated with the tensor force. The obvious requirement that realistic forces reproduce the deuteron binding energy means that weakening the tensor force must be compensated by an increase in the (attractive) central force. The latter is more effective in the triton and this leads to an increase in the binding. Simple (but unphysical) models[35] without a tensor force overbind the triton. Whether the tensor force in the Bonn model is more physical than those of the older forces remains to be determined in the future. Nucleon-nucleon scattering data which are sensitive to the tensor force are of rather low quality. Recent efforts have begun to improve this situation, but the required experiments are very difficult.

Given that the triton binding energy is too low, will three-body forces improve the situation in a convincing fashion? A variety of models have been developed which incorporate two-pion-exchange three-body forces. The Tucson-Melbourne force[36] is the oldest which incorporates chiral constraints with good phenomenology

for "soft" pion-nucleon scattering. The Brazilian approach[37] uses phenomenological Lagrangians rather than current algebra, but is quite similar. The Urbana-Argonne model[10] is purely phenomenological, but is also based on two-pion exchange.

An additional approach is the Hajduk-Sauer (HS) isobar model.[38] This model is distinct from the others in that it incorporates the isobars via the triton wavefunction explicitly, rather than incorporating them implicitly into the two- and three-body forces. The additional complexity required by this approach makes the HS calculation a *tour de force* and unique among trinucleon calculations. Nevertheless, this model is also based primarily upon two-pion-exchange.

The common ingredient in all of these models is the long-range behavior. Using the most common short-range behavior suggested by the phenomenology of chiral symmetry breaking in the pion-nucleon interaction[36] produces a near unanimity of results for the first three models. The additional binding[22,31] is approximately 1.5 MeV, which would overbind all of the previously discussed two-body models. However, reasonable alternative modifications of the short-range behavior associated with the range of the pion-nucleon form factor can lead to much less, or much more, binding. The purely pionic forces are very sensitive to the assumed short-range behavior. The fourth model of Hadjuk and Sauer is very different in approach and technical development. It leads to approximately .3 MeV additional binding. However, because this calculation is unique and its physics development very different from the others, it has not proven possible to trace the difference in binding to any particular difference in physical assumptions. Thus, although the techniques used in solving the triton Faddeev equations have been extended in principle and practice to include three-body forces, the results of such calculations are problematical at this time.

SCALING OF OBSERVABLES

If the binding energies of two-body or two-body plus three-body force models are in disagreement with experiment, can the other observables associated with each of these calculations be trusted? The answer is no, in general. With a little additional care,[39] however, we can make predictions which are much more reliable. The trick is to recognize that the triton, like the deuteron, is a weakly bound system ($E_B/A<3$ MeV) and for much of the time the nucleons will be outside of each other's force range. Thus, much of the environment in the triton for each of these models should be determined by the binding energy, which sets the size scale. In addition, the longest-range component of all realistic force models is OPEP.[40] We need to recall that in the deuteron the asymptotic

form of the wavefunction is given by $\exp(-\kappa r)/r$, where $\kappa \sim E_B^{1/2}$; an analogous but more complicated form holds for the triton.[13]

If this argument holds, scaling may result. That is, observables for a given force model may depend primarily on the binding energy for that model, and not on the details of the force other than common, physically constrained ingredients such as OPEP. This hypothesis is easy to test if one uses the many combinations of two- and two- plus three-body force models which have been solved recently, and plot each observable versus the corresponding model binding energy. If a narrow band is obtained over the rather wide range of energies of the various models, we say that "scaling" holds; that is, there is only a single effective independent variable: the binding energy. Extrapolation to the physical binding energies of ^{3}He and ^{3}H is then a rather simple operation. Examples of scaling are the Phillips' line[41] for n-d doublet scattering lengths and the Tjon line[42] for the alpha particle binding energy.

A good example of this process is the rms charge radius. Schematic trinucleons are depicted below in Figure 4. The protons are shaded. If all NN forces were identical we would have the equilateral configuration in (4a). The rms charge radius is the (mean) distance from the trinucleon center-of-mass (CM) to any one of the protons. Because the pp or nn force is weaker than the np

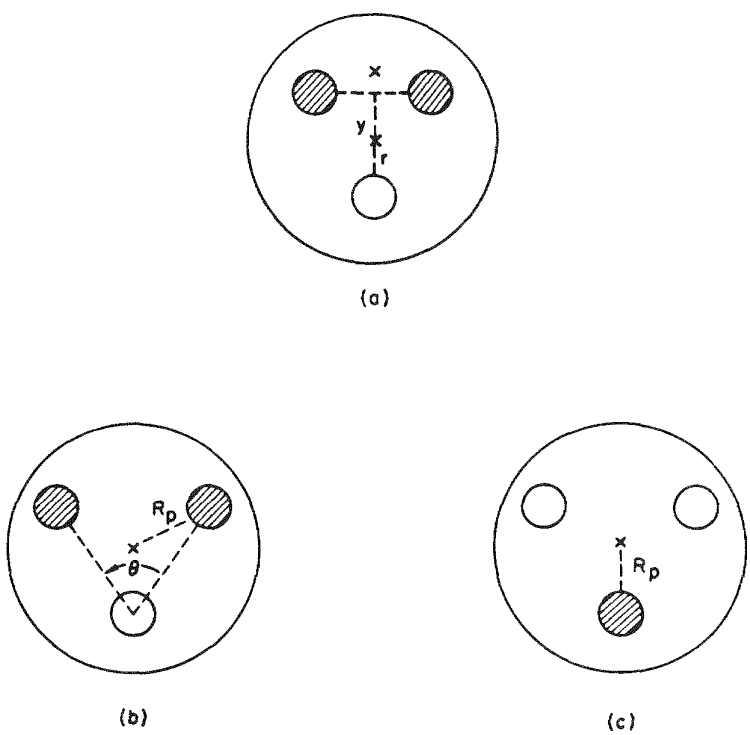

Fig. 4. Schematic trinucleons with coordinates.

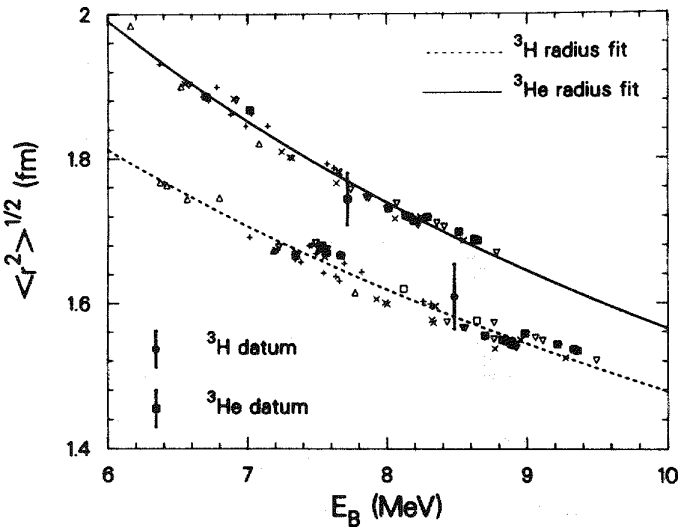

Fig. 5. Scaling plot of rms charge radii calculations with fits and data.

force, the like particles actually lie further from the CM than the remaining unlike particle. Qualitatively, the angle θ in Figure (4b) is greater than 60° and the equilateral configuration (S-state) in (a) becomes isosceles in (b). The deviation of the isosceles from the equilateral configuration is a measure of the mixed symmetry S'-state. The geometry clearly indicates that the charge radius of ^{3}He is greater than that of ^{3}H. This is shown in Figure 5, a "scaling plot" of the rms charge radius $\langle r^2 \rangle^{1/2}$ versus E_B for our theoretical data set. A point Coulomb interaction is included in the ^{3}He calculations.[43] The data from a Saclay[44] analysis are in good agreement with the simple fits.

The qualitative behavior can be easily understood. The mean-square radius is a matrix element which heavily weights the asymptotic portion of the wavefunction, which is determined by $\kappa \sim (E_B)^{1/2}$. Assuming that the entire wavefunction is given by the asymptotic form and performing the quadratures leads to $\langle r^2 \rangle^{1/2} \sim E_B^{-1/2}$. The isoscalar combination of rms radii $[(2\langle r^2 \rangle_{He} + \langle r^2 \rangle_H)/3]^{1/2}$, does indeed vary in this fashion, while the difference component, which is largely determined by the S'-state, decreases more nearly as E_B^{-1}. The latter behavior can be traced to the rapid decrease of the probability of the S'-state, $P_{S'} \sim E_B^{-2}$, as a function of binding. This trend has a large spread and does not manifest scaling as clearly as the rms radii.[39]

Although not specifically included on our plot, the Bonn result[30] falls on the ^{3}H curve.

The weak pp Coulomb force produces two competing effects[43] on the ^{3}He charge radius. The Coulomb interaction lowers the binding energy and this increases the radius. In addition the asymptotic form of the wavefunction is changed from a Hankel function (exponential) to a Whittaker function, which falls more rapidly at large separations, thus lowering the rms radius. These two effects are seen clearly in Figure 6.

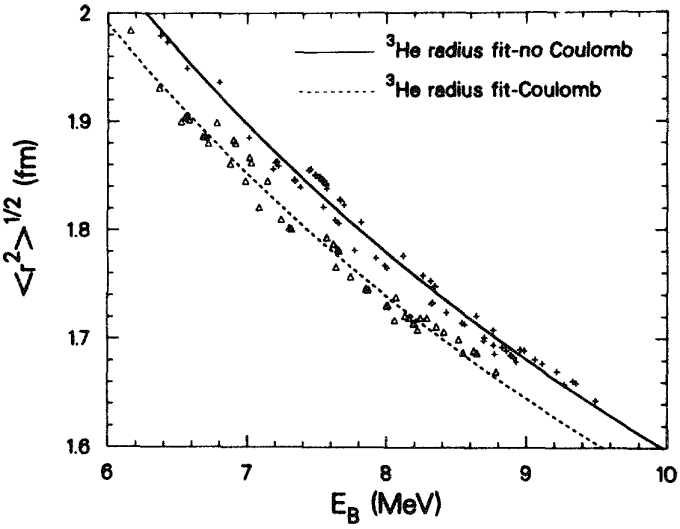

Fig. 6. Scaling plot of ^{3}He rms charge radius calculations, with and without a Coulomb interaction.

The Coulomb energy of ^{3}He has long been known to be smaller than the 764 keV binding energy difference of ^{3}He and ^{3}H. The first quantitative demonstration of this was given by Fabre de la Ripelle[45] and Friar[46], who derived a simple approximation to the Coulomb energy which allowed experimental electron scattering data to be used to estimate that energy. The simplest version of that formula can be derived from Figure 4. The (point-nucleon) Coulomb potential in Figure (4a) is α/x, where α is the fine structure constant. If the trinucleons are primarily in an equilateral configuration, we can replace x by $\sqrt{3}r$, which in effect replaces the two-body correlation function by the charge density: $E_c \equiv \langle \alpha/x \rangle \simeq (\alpha/\sqrt{3}) \int d^3 r \rho_{ch}(r)/r$. This simple approximation can be extended to include mixed-symmetry wave function components and the proton's charge distribution. It can be demonstrated[43] to work at the 1% level by calculating both sides of the relationship. If experimental data are used for ρ_{ch} one finds $E_c = 638 \pm 10$ keV. A

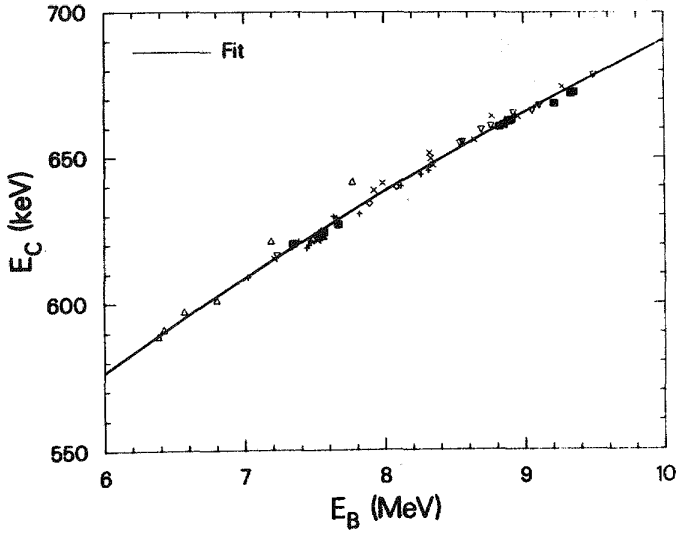

Fig. 7. Scaling plot of ^{3}He Coulomb energy.

scaling plot of E_c versus E_B, taking account of the proton's charge distribution, is shown in Figure 7. It produces $E_c \simeq 652$ keV at $E_B = 8.48$ MeV. The slightly larger number results from the inability of theoretical wave functions to reproduce the inner portion of $\rho_{ch}(r)$, which leads to a small increase in E_c. The additional 100 keV which is needed is due to other direct and indirect charge-symmetry-breaking mechanisms.

Another important set of observables is the asymptotic normalization constants[30,47]. If one stretches the triton until a deuteron is outside the force range of the remaining neutron, the wave function becomes proportional to an exponential (~exp(-βy), where y is the relative coordinate of the two systems and β is the wave number for the deuteron-triton binding energy difference). The proportionality constant is the asymptotic normalization. Because of the NN tensor force, there are actually 2 constants, one for s-wave (C_S) and one for d-wave (C_D), and their ratio, $\eta = C_D/C_S$. There has been considerable recent interest in these constants for the analogous deuteron problem[40]. Because the wave number β increases as triton binding increases, the asymptotic wave function becomes steeper and probability decreases in the exterior region. It becomes easier for the asymptotic wave function to match smoothly onto the interior portion if the asymptotic normalization constant increases as the binding increases. Each constant (C_S, C_D and η) increases with energy, as illustrated by η in Figure 8. Both ^{3}H and ^{3}He (with a Coulomb interaction) are shown together with data.

The scattering of a nucleon from a deuteron at very low energies leads to two scattering lengths: doublet (a_2) and quartet

(a_4). The latter is not very interesting, being primarily sensitive to the deuteron binding energy. The former, however, reflects the underlying dynamics of the triton[41], but perhaps in a trivial way[48]. Figure 9 shows the results of n-d and p-d doublet scattering length calculations at Los Alamos[49] for a variety of realistic and unrealistic two-body and three-body force models, plotted versus the corresponding ^{3}H or ^{3}He binding energy. The n-d case scales according to the "Phillips line" and passes through the datum. The p-d case does not and is controversial because of the existence of

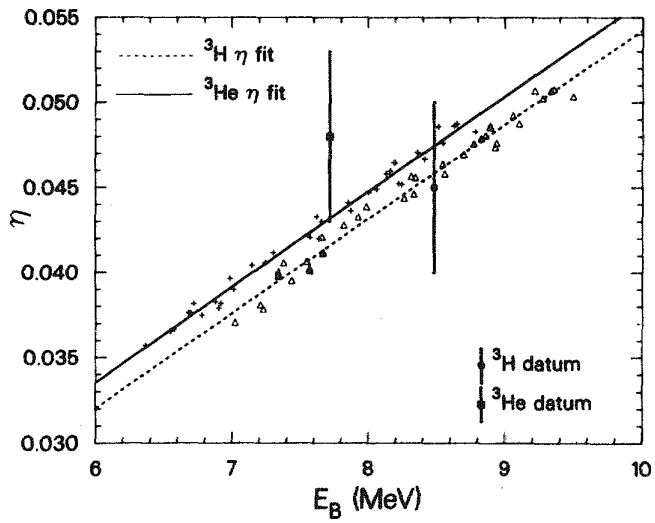

Fig. 8. Scaling plot of the asymptotic D/S ratio, with fits and data.

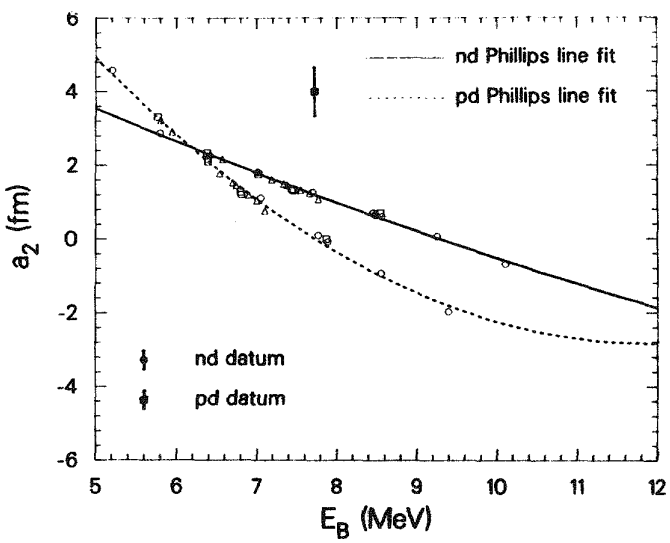

Fig. 9. Phillips' curve for Nd doublet scattering lengths, with fits and data.

extremely weak, long-range polarization forces ($\sim 1/r^4 + \ldots$), which nevertheless affect the definition of the scattering length. Recently it has been shown that a proper treatment of these long-range forces should produce a negligible change in a_2, although some care needs to be exercised[50,51]. There is still an unresolved discrepancy between the results of Refs. 49 and 52, and those of Ref. 53.

SUMMARY

There has been much progress in our understanding of ^{3}He and ^{3}H recently. Faddeev calculations of high accuracy are now possible for binding energies and other observables. This has led in some cases to both quantitative and qualitative descriptions. We still have an incomplete knowledge of the triton binding at the level of roughly 1 MeV, but our understanding of certain trinucleon observables is much better.

REFERENCES

1. H. B. G. Casimir and D. Polder, Phys. Rev. 73, 360 (1948).
2. C. T. Munger and H. Gould, Phys. Rev. Lett. 57, 2927 (1986).
3. J. L. Friar, B. F. Gibson, and G. L. Payne, Ann. Rev. Nucl. Part. Sci. 34, 403 (1984).
4. S. A. Coon and J. L. Friar, Phys. Rev. C34, 1060 (1986).
5. J.-I. Fujita and H. Miyazawa, Prog. Theor. Phys. 17, 360 (1987).
6. B. M. Axilrod and E. Teller, J. Chem. Phys. 11, 299 (1943).
7. H. Primakoff and T. Holstein, Phys. Rev. 55, 1218 (1939).
8. E. Oset, D. Strottman, M. J. Vicente-Bacas, and Ma Wei-Hsing, Nucl. Phys. A408, 461 (1983).
9. J. Tjon, in "Perspectives in Nuclear Physics at Intermediate Energies," Proceedings of ICTP Workshop, Trieste, 1987 (to be published).
10. J. Carlson, V. R. Pandharipande, and R. B. Wiringa, Nucl. Phys. A401, 59 (1983).
11. J. L. Friar, B. F. Gibson, and G. L. Payne, Phys. Rev. C (in press).
12. L. D. Faddeev, Zh. Eksp. Teor. Fiz. 39, 1459 (1960).
13. G. L. Payne, Lecture Notes in Physics 273, 64 (1987).
14. Yu. A. Simonov, Yad. Fiz. 3, 630 (1966).
15. M. Fabre de la Ripelle, Lecture Notes in Physics 273, 283 (1987).
16. J. Carlson, LA-UR-87-1372, Los Alamos Preprint.
17. K. E. Schmidt, Lecture Notes in Physics 273, 363 (1987).
18. M. H. Kalos, Phys. Rev. 128, 1891 (1962).
19. R. B. Wiringa, Few-Body Systems (Suppl. 1), 130 (1986).
20. Y. Akaishi, Few-Body Systems (Suppl. 1), 120 (1986); Lecture Notes in Physics 273, 324 (1987).
21. C. Ciofi degli Atti and S. Simula, Nuovo Cim. 41, 101 (1984).
22. C. R. Chen, G. L. Payne, J. L. Friar, and B. F. Gibson, Phys. Rev. C31, 2266 (1985); C33, 1740 (1986).
23. C. Hajduk and P. U. Sauer, Nucl. Phys. A369, 321 (1981).
24. R. V. Reid, Ann. Phys. (N.Y.) 50, 411 (1968).

25. R. B. Wiringa, R. A. Smith, and T. A. Ainsworth, Phys. Rev. C29, 1207 (1984).
26. R. de Tourreil and D. W. L. Sprung, Nucl. Phys. A201, 193 (1973).
27. R. de Tourreil, B. Rouben, and D. W. L. Sprung, Nucl. Phys. A242, 445 (1975).
28. M. Lacombe, et al., Phys. Rev. C21, 861 (1980); D12, 1495 (1975).
29. R. Machleidt, K. Holinde, and C. Elster, Phys. Repts. 149, 1 (1987).
30. T. Sasakawa, Nucl. Phys. A463, 327c (1987).
31. S. Ishikawa and T. Sasakawa, Few-Body Systems 1, 143 (1986); 1, 3 (1986).
32. R. A. Brandenburg, et al., LA-UR-86-3700, Los Alamos Preprint.
33. J. Haidenbauer and Y. Koike, Phys. Rev. C34, 1187 (1986).
34. M. M. Nagels, T. A. Rijken and J. J. de Swart, Phys. Rev. D17, 768 (1978).
35. J. L. Friar, B. F. Gibson, and G. L. Payne, Phys. Rev. C (in press).
36. S. A. Coon, et al., Nucl. Phys. A317, 242 (1979).
37. H. T. Coelho, T. K. Das, and M. R. Robilotta, Phys. Rev. C28, 1812 (1983).
38. C. Hajduk, P. U. Sauer, and W. Streuve, Nucl. Phys. A405, 581 (1983).
39. J. L. Friar, B. F. Gibson, C. R. Chen, and G. L. Payne, Phys. Lett. 161B, 241 (1985).
40. T. E. O. Ericson and M. Rosa-Clot, Ann. Rev. Nucl. Part. Sci. 35, 271 (1985).
41. A. C. Phillips, Rep. Prog. Phys. 40, 905 (1977).
42. J. A. Tjon, Phys. Lett. 56B, 217 (1975); Phys. Rev. Lett. 40, 1239 (1978).
43. J. L. Friar, B. F. Gibson, and G. L. Payne, Phys. Rev. C35, 1502 (1987).
44. F.-P. Juster, et al., Phys. Rev. Lett. 55, 2261 (1985).
45. M. Fabre de la Ripelle, Fizika 4, 1 (1972).
46. J. L. Friar, Nucl. Phys. A156, 43 (1970).
47. J. L. Friar, B. F. Gibson, D. R. Lehman, and G. L. Payne, Phys. Rev. C25, 1616 (1982); and to be published.
48. V. Efimov and E. G. Tkachenko, Phys. Lett. 157B, 108 (1985).
49. C. R. Chen, G. L. Payne, J. L. Friar, and B. F. Gibson, Phys. Rev. C33, 401 (1986).
50. Gy. Bencze, et al., Phys. Rev. C35, 1188 (1987).
51. A. I. L'vov, Preprint 14, Moscow, FIAN (1987).
52. G. H. Berthold and H. Zankel, Phys. Rev. C34, 1203 (1986).
53. A. A. Kvitsinskii, Pis'ma Zh. Eksp. Teor. Fiz. 36, 375 (1982).

DEUTERON FORM FACTORS IN THE SKYRME APPROACH

Ebbe M. Nyman*
Department of Physics, University of Helsinki, SF–00170 Helsinki, Finland

ABSTRACT

The electromagnetic form factors of the deuteron are calculated in the Skyrme model, where the structure of the nucleons is due to their origin as topological solitons of meson fields. In addition to this, the structure of the deuteron is represented by a non-relativistic wave function. The form factors are obtained as matrix elements of an isoscalar current operator, which is determined from a fit to the isoscalar electric form factor of the nucleon. The magnetic form factor is dominated by the exchange-current contribution and can, depending somewhat on the isoscalar form factor used as input, be brought into agreement with the empirical value over the entire range where data are available ($q^2 \leq 70$ fm^{-2}). There are also large exchange-current contributions to the charge and quadrupole form factors. The predicted tensor polarization is similar to that obtained with conventional meson-exchange current mechanisms.

INTRODUCTION

In this talk I shall discuss a very challenging problem – one of the main questions that the CEBAF scientific progran sets out to solve:

- How can the dynamics of quark confinement be best described and modeled (solitons, bags, fluxtubes, potentials)? How is this confinement modified by the presence of another nucleon, such as occurs in the deuteron?
- How is the structure of the nucleon modified in the deutreron?
- How are the elementary processes, such as e-p scattering, modified in the deuteron? How do quarks hadronize in the deuteron?

This talk deals with only one particular aspect of the above, which is find out to what extent the Skyrme's soliton description of the nucleon can account for those changes in the nucleonic structure which are observed in electron-deuteron scattering. Therefore, I have taken the liberty of modifying the original Ref. 1 by replacing phrases such as "nuclear matter" or "nuclear medium" by "the deuteron" or "another nucleon".

The Skyrme model is based on a single SU(2) field U that contains a scalar (σ) and a pseudoscalar isovector ($\vec{\pi}$) component:

$$U = (1/f_\pi)(\sigma + \mathrm{i}\vec{\tau}\cdot\vec{\pi}), \qquad \sigma^2 + \pi^2 = f_\pi^2. \tag{1}$$

The anomalous baryon current operator has the form

$$B^\mu = \frac{\epsilon^{\mu\nu\alpha\beta}}{24\pi^2}\mathrm{Tr}\{U^\dagger\partial_\nu U U^\dagger\partial_\alpha U U^\dagger\partial_\beta U\}. \tag{2}$$

*Supported in part by the Academy of Finland

This current operator, which is conserved independently of the form of the lagrangian, carries the baryon number as a topological charge (winding number). In the more general versions of the Skyrme model, where strangeness is included, the topological current would be generated by the Wess-Zumino action,[2] which is explicitly propoprtional to the number of quark colors. Thus, the anomalous current is all that is left of the underlying chromodynamic theory where the nucleons are made up out of quarks. The realization that boson fields such as (1) can carry baryon number is due to Skyrme,[3] but in more modern thinking this would be the "smoking gun" that signals the existence of the quarks. This frequently also goes under the name of the Cheshire cat picture, as illustrated in Fig. 1.

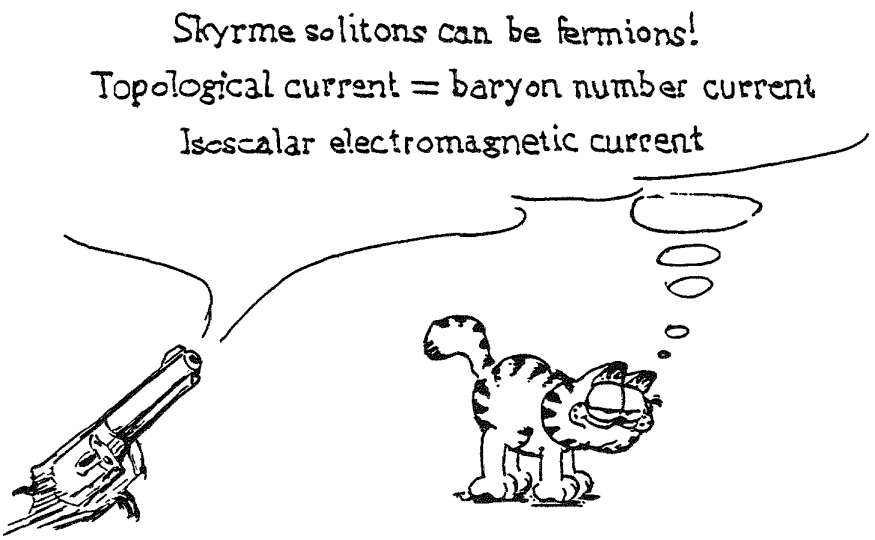

Fig. 1. The smoking gun and the Cheshire cat.

The isoscalar electromagnetic current operator J^μ is, in the absence of vector mesons, the following:

$$J^\mu = \tfrac{1}{2} B^\mu \,. \tag{3}$$

For single nucleons the topological soliton field U has the hedgehog form

$$U(\vec{r}\,) = \exp[\mathrm{i}\vec{\tau} \cdot \hat{r}\, \theta(r)]. \tag{4}$$

To avoid the use of an explicit lagrangian model we shall here determine the chiral angle θ directly from the electromagnetic structure of the nucleon and then use the result to predict the other isoscalar variables.

In order to obtain the proper spin-isospin structure for the isoscalar current operator the soliton field U must be allowed to rotate, corresponding to the substitution:[4]

$$U(r) \longrightarrow A(t) U(r - R(t)) A^\dagger(t). \tag{5}$$

Here $A(t)$ is a time-dependent SU(2) matrix, the elements of which are coordinates of the wave function of the quantized rotation. In order to express the current operator in terms of the conventional Pauli spin and isospin matrices, we evaluate matrix elements with respect to wave functions that correspond to

the correct spin and isospin ($\frac{1}{2}$) of the nucleons. This is achieved by means of the projection theorem:[5]

$$\langle \mathrm{N}'|A\vec{\tau}A^{\dagger}|\mathrm{N}\rangle = -\tfrac{1}{3}\langle \mathrm{N}'|\vec{\sigma}^{\,\mathrm{N}}\vec{\tau}\cdot\vec{\tau}^{\,\mathrm{N}}|\mathrm{N}\rangle\,. \tag{6}$$

Here N and N′ represent the single-nucleon states with respect to which the matrix elements have been evaluated, and $\vec{\sigma}^{\,\mathrm{N}}$ and $\vec{\tau}^{\,\mathrm{N}}$ are the spin and isospin operators for the single nucleon.

By substituting the rotating hedgehog field (5) into (2) and using the projection theorem one obtains the isoscalar charge and current operators for the nucleon as:

$$\rho(r) = -\frac{1}{4\pi^2 r^2}\sin^2\theta(r)\theta'(r), \tag{7}$$

$$\vec{J}(\vec{r}) = -\frac{1}{4\pi^2 r^2}\sin^2\theta(r)\theta'(r)\frac{\vec{P}}{M} - \frac{1}{8\pi^2\lambda r^2}\sin^2\theta(r)\theta'(r)\vec{\sigma}\times\vec{r}. \tag{8}$$

Here $\vec{P}$ is the momentum operator, M the mass and λ the moment of inertia of the soliton. Both the mass and the moment of inertia can be calculated from the chiral angle, provided the lagrangian is known. If the lagrangian is not specified, they appear as parameters. We shall here make the natural choice of using the experimental nucleon mass (939 MeV) and choose λ such as to obtain the correct isoscalar nucleon magnetic moment (0.88 n.m.). This corresponds to $\lambda = 0.0060\ \mathrm{MeV}^{-1}$, not far from the value obtained from the N–Δ mass difference ($0.0051\ \mathrm{MeV}^{-1}$).

The isoscalar electric and magnetic form factor of the nucleon are obtained from the Fourier transforms of the current operators (7) and (8) and are

$$G_{\mathrm{E}}^{\mathrm{S}}(q) = -\frac{2}{\pi}\int_0^{\infty}\mathrm{d}r\, j_0(qr)\sin^2\theta(r)\theta'(r)\,, \tag{9}$$

$$G_{\mathrm{M}}^{\mathrm{S}}(q) = -\frac{2m_{\mathrm{N}}}{\pi\lambda q}\int_0^{\infty}\mathrm{d}r\, r\, j_1(qr)\sin^2\theta(r)\theta'(r)\,. \tag{10}$$

Here we have interpreted the Fourier transform of (7) as $G_{\mathrm{E}}^{\mathrm{S}}$. Since, in the usual phenomenological representation of the current and charge operators of the nucleon, the convection current is proportional to F_1^{S} and as in the present approach the charge density equals the density of the convection current, one could have maintained that (9) represents F_1^{S} rather than $G_{\mathrm{E}}^{\mathrm{S}}$. At low and intermediate values of the momentum transfer the distinction between these two form factors is, however, relatively insignificant.

The chiral angle $\theta(r)$ may be determined from $G_{\mathrm{E}}^{\mathrm{S}}$ by inverting the Fourier transform (9). This yields the following transcendental equation for $\theta(r)$:

$$\theta(r) - \tfrac{1}{2}\sin 2\theta(r) = \pi - 2\int_0^{\infty}\frac{\mathrm{d}q}{q}G_{\mathrm{E}}^{\mathrm{S}}(q)\left(\sin(qr) - qr\cos(qr)\right)\,. \tag{11}$$

In the special case where the electric form factor is represented by the well-known dipole fit $\left(1 + q^2/\Lambda^2\right)^{-2}$, the equation for θ becomes[6]

$$\theta(r) - \tfrac{1}{2}\sin 2\theta(r) = \pi\, e^{-\Lambda r}\left(1 + \Lambda r + \tfrac{1}{2}\Lambda^2 r^2\right) . \tag{12}$$

The chiral angle is then found from a numerical solution to (12), or in general to (11). In Fig. 2 we compare the values of θ determined in this way from the dipole fit (using $\Lambda^2 = 0.71$ GeV^2) and also from two more modern fits to the data.[7, 8] We include for comparison also the result for θ obtained with the Skyrme model with a pion mass term.[9]

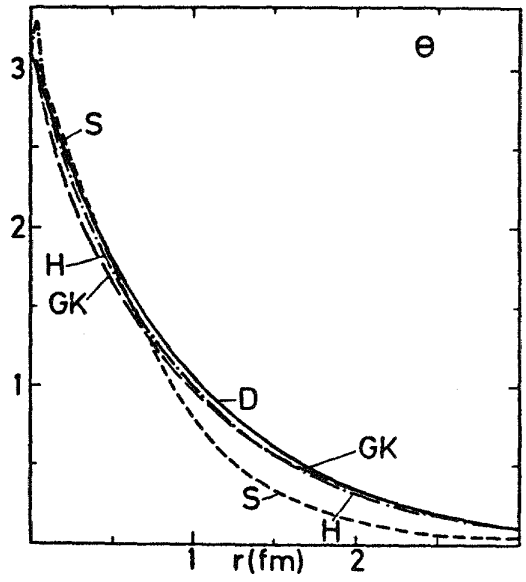

Fig. 2. The chiral angle as determined from the isoscalar electric form factor: dipole parametrization (D), parametrization of Ref. 7 (H) and of Ref. 8 (GK). The curve S is the result obtained from the lagrangian of the Skyrme model.[9]

APPLICATION TO THE DEUTERON

To construct the isoscalar current operator for the two-nucleon system we use the product ansatz[10]

$$U(\vec{r}_1, \vec{r}_2; \vec{r}) = U(\vec{r} - \vec{r}_1)U(\vec{r} - \vec{r}_2) \tag{13}$$

for the soliton field with baryon number 2. Here $\vec{r}_1$ and $\vec{r}_2$ are the coordinates of the centers of the two solitons and $\vec{r}$ is the point of interaction with the electromagnetic field. With this ansatz the isoscalar current splits into a sum of two single-nucleon current operators and an exchange-current operator:

$$J^\mu(\vec{r}_1, \vec{r}_2; \vec{r}) = J^\mu(\vec{r} - \vec{r}_1) + J^\mu(\vec{r} - \vec{r}_2) + J^\mu_{\rm ex}(\vec{r}_1, \vec{r}_2; \vec{r}). \tag{14}$$

Here $J^\mu(\vec{r} - \vec{r}_1)$ and $J^\mu(\vec{r} - \vec{r}_2)$ are the isoscalar currents of the single nucleons considered above and $J^\mu_{\rm ex}$ is an irreducible two-body exchange-current operator.

It is worth noting that this decomposition, while very natural and convenient, requires use of the the product ansatz (13). In the general case, a distinction between single-nucleon and exchange-current contributions would be difficult to obtain.

The spatial part of the exchange current operator $\vec{J}_{\rm ex}$ may be brought into the form[5]

$$\begin{aligned}\vec{J}_{\rm ex}(\vec{r}_1,\vec{r}_2;\vec{r}) =& \frac{1}{16\pi^2}\nabla\times{\rm Tr}\{\dot{U}_1^\dagger U_1 U_2\nabla U_2^\dagger - \dot{U}_2 U_2^\dagger U_1^\dagger\nabla U_1\}\\ &+\frac{1}{16\pi^2}{\rm Tr}\{(\nabla\dot{U}_2 U_2^\dagger+\nabla U_2\dot{U}_2^\dagger)\times U_1^\dagger\nabla U_1\\ &-(\nabla\dot{U}_1^\dagger U_1+\nabla U_1^\dagger\dot{U}_1)\times U_2\nabla U_2^\dagger\},\end{aligned} \tag{15}$$

where we have used the abbreviation

$$U_k\equiv U(\vec{r}-\vec{r}_k),\qquad (k=1,2). \tag{16}$$

The usual spin and isospin behaviour of the exchange current operator (15) is obtained by rotating each soliton independently according to eq. (5). This is an approximation, in the spirit of the product ansatz, which becomes exact in the limit of well separated solitons. It is therefore justified at least in the deuteron, where the average interparticle separation is large. When the projection theorem (6) is applied to each nucleon, the Fourier transform of the exchange current takes the form:

$$\begin{aligned}\vec{J}_{\rm ex} =& -\frac{\rm i}{72\pi^2\lambda}\vec{\tau}_1\cdot\vec{\tau}_2\,\exp[\tfrac{1}{2}{\rm i}\vec{q}\cdot\vec{r}]\vec{q}\int{\rm d}^3R\exp[{\rm i}\vec{q}\cdot\vec{R}]\sin^2\theta(|\vec{R}+\vec{r}|)\\ &\times\left\{\left[\alpha(R)+\tfrac{1}{3}\gamma(R)\right]\vec{\Sigma}+\gamma(R)\left[\vec{\Sigma}\cdot\hat{R}\,\hat{R}-\tfrac{1}{3}\vec{\Sigma}\right]\right\}\end{aligned} \tag{17}$$

for the exchange-current operator. Here we have used the abbreviation $\vec{\Sigma}=\vec{\sigma}^{\,1}+\vec{\sigma}^{\,2}$ and introduced the functions

$$\begin{aligned}\alpha(R) &= \frac{1}{2R}\sin 2\theta(R),\\ \gamma(R) &= \theta'(R)-\frac{1}{2R}\sin 2\theta(R),\end{aligned} \tag{18}$$

which were also used in Ref. 5.

The charge and quadrupole form factors of the deuteron are obtained as the matrix elements of the spin-scalar and spin-tensor parts of the time component of the isoscalar current operator. The matrix element of the charge operator for the deuteron has the general form

$$\langle\rho\rangle = F_{\rm C}-\tfrac{1}{12}q^2 S_{12}(\hat{q})F_{\rm Q}(q)\,, \tag{19}$$

where $F_{\rm C}$ and $F_{\rm Q}$ are the charge and quadrupole form factors, respectively. Here $S_{12}(\hat{q})$ is the spin-tensor operator

$$S_{12}(\hat{q}) = 3\,\vec{\sigma}^{\,1}\cdot\hat{q}\,\vec{\sigma}^{\,2}\cdot\hat{q}-\vec{\sigma}^{\,1}\cdot\vec{\sigma}^{\,2}. \tag{20}$$

In the impulse approximation, in which only the two single-soliton charge operators of the form (7) are taken into account, the charge and quadrupole form factors are obtained[11] as

$$F_{\rm C}(q) = G_{\rm E}^{\rm S}(q) \int_0^\infty {\rm d}r j_0(\tfrac{1}{2}qr) \left[u^2(r) + w^2(r)\right] , \tag{21}$$

$$F_{\rm Q}(q) = \frac{12}{q^2} G_{\rm E}^{\rm S}(q) \int_0^\infty {\rm d}r j_2(\tfrac{1}{2}qr) \left[\sqrt{\tfrac{1}{2}}\, u(r) - \tfrac{1}{4} w(r)\right] w(r) . \tag{22}$$

Here, u and w are the usual deuteron wave functions.

The charge component of the exchange current operator $J^\mu_{\rm ex}$ (3.2) has the form[5]

$$\rho_{\rm ex} = \frac{\rm i}{16\pi^2}\, \vec{\rm q} \cdot \int {\rm d}^3{\rm r} \exp[{\rm i}\vec{\rm q}\cdot\vec{\rm r}]\, {\rm Tr} \left\{ {\rm U}_1^\dagger \nabla {\rm U}_1 \times {\rm U}_2 \nabla {\rm U}_2^\dagger \right\} . \tag{23}$$

The notation is the same as used in eq. (16). After rotating the two solitons independently according to eq. (5) and using (6) this operator takes the final form

$$\begin{aligned} \rho_{\rm ex} = & \frac{\rm i}{24\pi^2}\, \vec{q} \cdot \int {\rm d}^3 R \frac{\sin^2\theta(r_2)}{r_2} \Big\{ \alpha(r_1) \left[\vec{\sigma}^{\,2}(\vec{\sigma}^{\,1}\cdot\hat{r}_2) + \vec{\sigma}^{\,2}\cdot\hat{r}_1 - 2\hat{r}_2\right] \\ & + \gamma(r_2) \left[\vec{\sigma}^{\,1}\cdot\vec{r}_1\vec{\sigma}^{\,2}(\hat{r}_1\cdot\hat{r}_2) + \vec{\sigma}^{\,2}\cdot\vec{r}_2\vec{\sigma}^{\,1}(\hat{r}_1\cdot\hat{r}_2) - 2\vec{\sigma}^{\,1}\cdot\hat{r}_1\vec{\sigma}^{\,2}\cdot\hat{r}_1\hat{r}_2\right] \Big\} \end{aligned} \tag{24}$$

The functions α and γ are defined in eq. (18). The variables $\vec{r}_1$ and $\vec{r}_2$ are defined as

$$\begin{aligned} \vec{r}_1 &= \vec{R} - \tfrac{1}{2}\vec{r} , \\ \vec{r}_2 &= \vec{R} + \tfrac{1}{2}\vec{r} , \end{aligned} \tag{25}$$

where $\vec{r}$ is the internucleon separation.

RESULTS

It is clear, of course, that in order to be able to account for the form factors of the deuteron with any accuracy at all, one must at some stage build in information that corresponds to the essentially known wave function of the deuteron. Using the above results as two-body operators, it is straightforward to incorporate *e.g.*, the wave function corresponding to one of the modern potential models of the interaction.[12, 13] The full details of the calculations will be reported elsewhere.[14]

In Fig. 3 we have plotted the predicted magnetic form factor of the deuteron using the wave functions corresponding to the Paris potential[12] and the dipole form (12) for the chiral angle. The predicted form factor values are in exceedingly good agreement with the empirical values, which have been taken from Refs. 15, 16. The results obtained using the wave functions that correspond to the Reid soft-core potential[13] are almost indistinguishable from those in Fig. 3. There is, however, a rather strong sensitivity to the single-nucleon form factor through the predicted chiral angle.

In Fig. 4 we show the same quantities as in Fig. 3, but using the chiral angle calculated from the parametrization for the isoscalar nucleon form factor of Ref. 8. We note that the sensitivity of the results to the isoscalar form factor used as input is far greater than to the model for the deuteron wave function. This insensitivity to the wave-function model is largely due to the fact that the calculated form factor is dominated by the exchange current contribution, which is known to be rather insensitive to the wave function model.

We also show for comparison, in Fig. 3, the prediction for the magnetic form factor using the chiral angle given by the original Skyrme model, augumented by a pion-mass term.[9] This represents a considerable overprediction of the magnetic form factor in comparison with the empirical values.

The value for the deuteron magnetic moment in the impulse approximation is ≈ 0.845 n.m. for all the models considered above. The exchange-current correction to this value is ≈ 0.04 n.m. so that the total predicted magnetic moment is ≈ 0.885 n.m. This value is larger by some 0.03 n.m. than the empirical

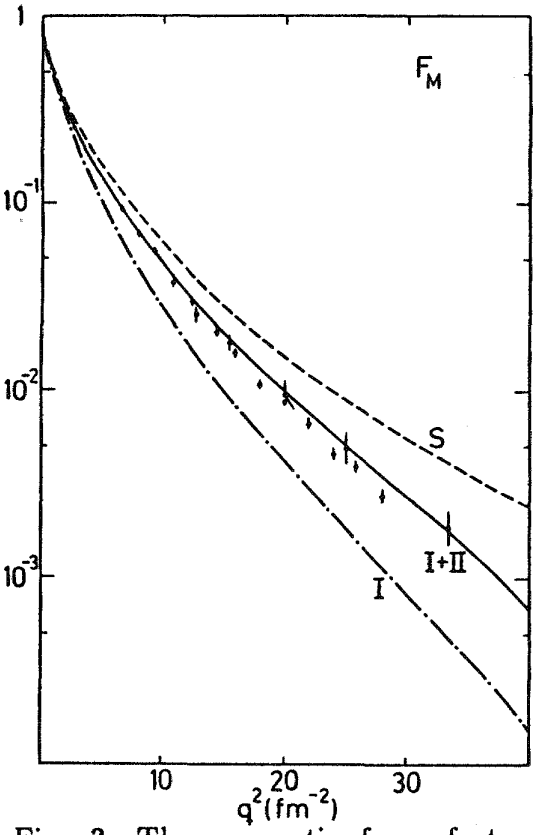

Fig. 3. The magnetic form factor of the deuteron. The curves I and I+II are obtained using the chiral angle given by the dipole parametrization for G_E^S with (I+II) and without (I) the exchange-current contribution. The curve S is the result obtained with the chiral angle given by the Skyrme-model lagrangian.[9] The experimental data points are from Refs. 15 and 16.

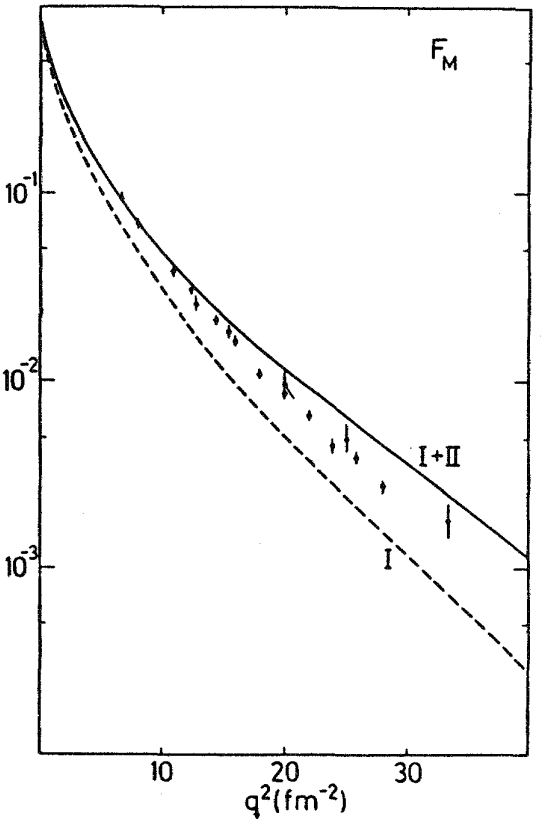

Fig. 4. The magnetic form factor of the deuteron as obtained using the chiral angle determined from the Gari-Krümpelmann[8] parametrization for G_E^S. The curve I represents the result of the impulse approximation. The experimental data points are from Refs. 15 and 16.

value, 0.857 n.m., but a large part of the overprediction ($\approx$ 0.02 n.m.) may be explained by the additional exchange-current correction that is associated with the velocity-dependent terms in the nucleon-nucleon interaction.[17, 18]

In Fig. 5 we show the predicted charge form factor as obtained with the deuteron wave functions corresponding to the parametrized Paris potential[12] and using the chiral angle given by the dipole form factor 12. The exchange-current contribution has, in agreement with conventional meson-exchange calculations,[19, 20] the opposite sign to that of the impulse approximation at low values of the momentum transfers. Therefore, the zero in the form factor is drawn towards smaller momentum transfers. In Fig. 5 the charge form factor values as obtained with the deuteron wave functions that correspond to the Reid soft core potential[13] are also shown. The difference between the values for the two potentials gives a measure of the uncertainty caused by the wave functions. We note that the general size of the uncertainty caused by the wave functions is

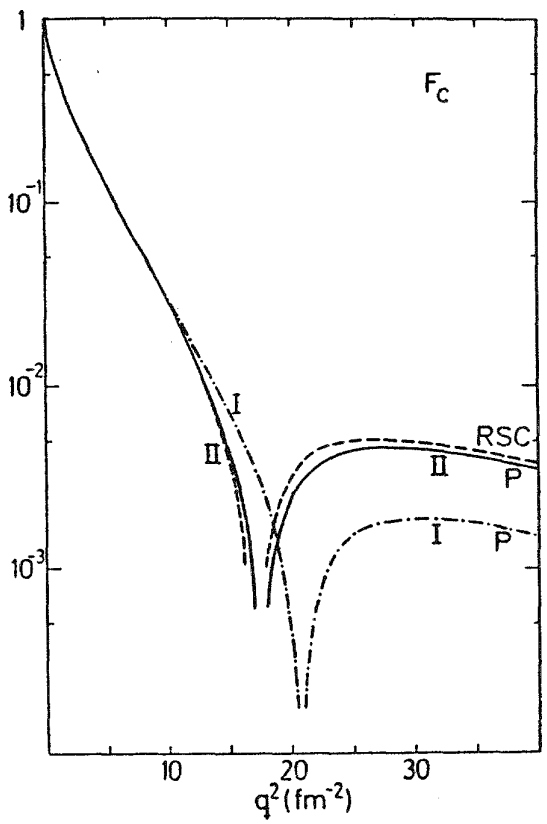

Fig. 5. The charge form factor of the deuteron using the chiral angle given by the dipole form for G_E^S. The curves I and II are the impulse approximation and complete results as obtained with the Paris-potential deuteron wavefunctions. The curve RSC is the result obtained with the Reid soft-core potential wavefunctions.

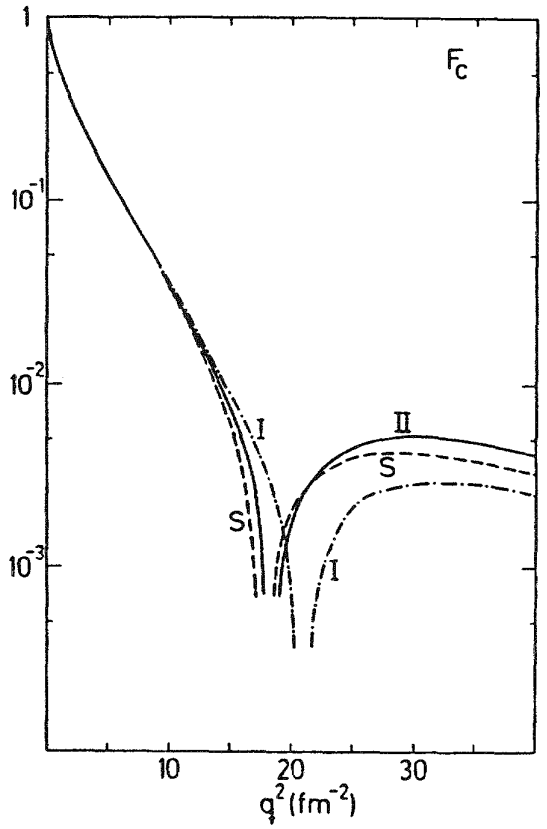

Fig. 6. The charge form factor of the deuteron as obtained with the chiral angle given by the Gari-Krümpelmann parametrization[8] for G_E^S. The curves I and II are the results of the impulse approximation and full calculation, respectively. The result obtained using the chiral angle obtained from the Skyrme-model lagrangian[9] is denoted S.

smaller than the exchange-current contribution. In Fig. 6 we show the charge form factor predicted when using the Gari–Krümpelmann parametrization for the nucleon isoscalar electric form facto[8] to determine the chiral angle, again using the Paris potential deuteron wave functions. The results are rather similar to those obtained with the chiral angle that corresponds to the dipole form for G_E^S (Fig. 5). In Fig. 6 we also show the charge form factor that is obtained when using the Skyrme model (with a pion-mass term) to determine[9] θ. The spread between the predictions in Figs. 5 and 6 gives an estimate of the theoretical uncertainty of the results. Evidently, we may conclude that the uncertainty is small.

The predictions for the quadrupole form factor are given in Figs. 7 and 8. In Fig. 7 we have plotted the quadrupole form factor as obtained when using the chiral angle that corresponds to the dipole form for G_E^S and the deuteron wave functions that correspond to the Paris potential.[12] The result obtained

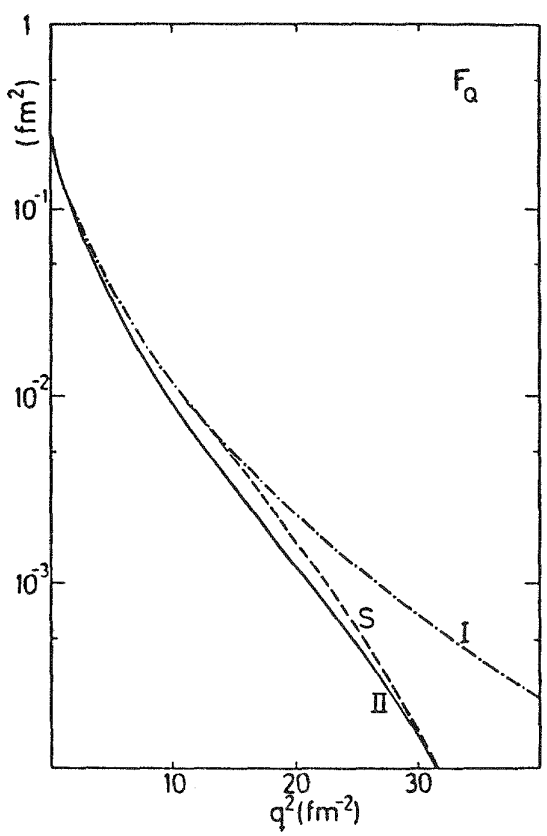

Fig. 7. The quadrupole form factor as obtained using the chiral angle given by the dipole form for G_E^S. The curves I and II are the results of the impulse approximation and full calculation, respectively. The curve S is the result obtained with the chiral angle of the Skyrme model.[9]

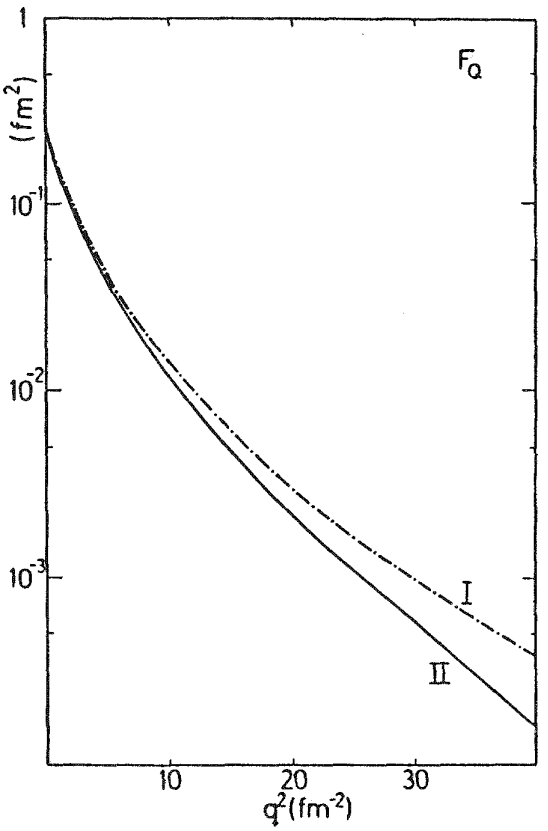

Fig. 8. The quadrupole form factor as obtained using the chiral angle given by the Gari-Krümpelmann[8] parametrization for G_E^S. The curves I and II are the results of the impulse approximation and full calculation, respectively.

with the chiral angle of the Skyrme model[9] is also shown. In Fig. 8 we show the quadrupole form factor as obtained when using the chiral angle that corresponds to the Gari-Krümpelmann parametrization[8] for G_E^S . The results in Figs 7 and 8 are very similar, although the fact that the Gari-Krümpelmann parametrization for G_E^S falls off at a slower rate than the other ones is reflected in the slower falloff rate of the predicted quadrupole form factor. It is interesting to note that the exchange-current contribution to the quadrupole form factor in this approach is negative, a result that is opposite to that obtained from simple meson-exchange current mechanisms.[19, 20]

The value predicted for the quadrupole moment of the deuteron in the impulse approximation is $\approx 0.275\,\mathrm{fm}^2$ with the models above. This is slightly lower than the empirical value $0.2860 \pm 0.0015\,\mathrm{fm}^2$. The exchange-current contribution is negative and of the order of $-0.01\,\mathrm{fm}^2$, thus increasing the disagreement with the empirical value. Whether the disagreement with the empirical value is due to wave function or to the current operator of the Skyrme model is not clear.

Although the charge and quadrupole form factors have not been measured separately, their incoherent sum is known from the invariant form factor $A(q)$, which is defined as

$$A(q) = F_C^2(q) + \tfrac{1}{18}\, q^2\, F_Q^2(q) + \tfrac{1}{6\, m_N{}^2}\, q^2\, F_M{}^2(q)\,. \qquad (26)$$

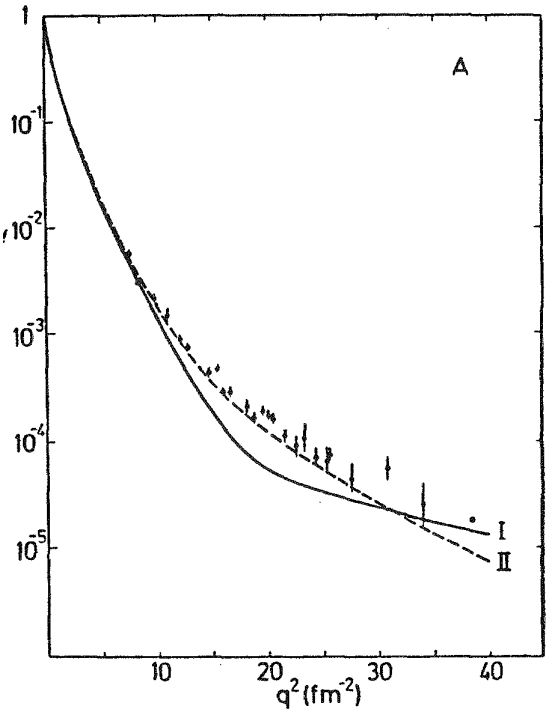

Fig. 9. The form factor A as obtained using the chiral angle given by the dipole form for G_E^S. The curves I and II are the results of the impulse approximation and full calculation, respectively. The experimental data are from Refs. 16 and 24–28.

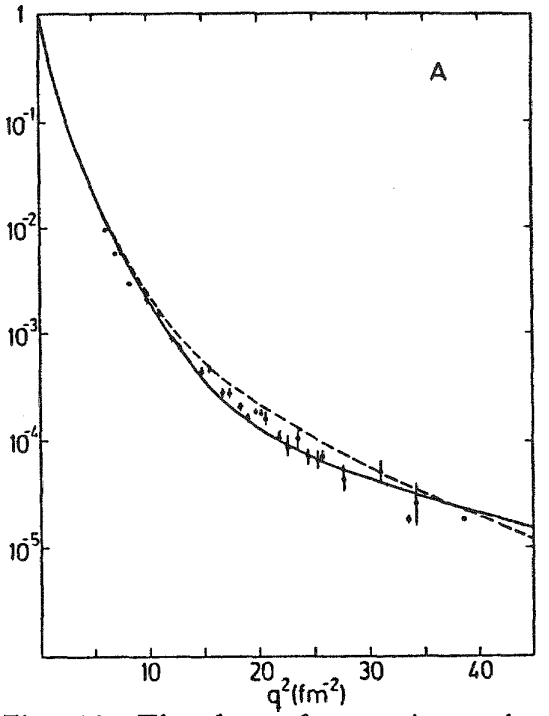

Fig. 10. The form factor A as obtained using the chiral angle given by the Gari-Krümpelmann parametrization for G_E^S. The curves I and II are the results of the impulse approximation and full calculation, respectively. The experimental data are from Refs. 16 and 24–28.

In Figs. 9 and 10 we compare the predicted values for A with the empirical values from Refs. 24 and 25–28. The predictions in Fig. 9 correspond to the chiral angle given by the dipole form for G_E^S and those in Fig. 10 to the Gari-Krümpelmann parametrization[8] for G_E^S The latter predictions are clearly in better agreement with the empirical values in the region of q^2 around 20 fm^{-2}, where the form factor (26) is small because of the zero in the charge form factor. The underprediction around $q^2 = 20$ fm^{-2} in Fig. 9 is related to the large negative exchange correction to the quadrupole form factor.

The charge and quadrupole form factors may be separated empirically if the tensor polarization is measured in addition to the invariant form factor A. It is essentially equal to (the negative of) the quantity P, defined as

$$P = \tfrac{1}{3}\sqrt{2}\, q^2 F_Q(q) \frac{F_C(q) + \frac{1}{12} q^2 F_Q(q)}{F_C^2(q) + \frac{1}{18} q^2 F_Q^2(q)}, \qquad (27)$$

So far, the tensor polarization has only been measured at two relatively low values of momentum transfer where discrimination between models cannot be done. In Figs. 11 and 12 we have plotted the predicted values for P as well as the two available data points.[29] The results in Fig. 11 correspond to using the dipole form factor for G_E^S to determine the chiral angle and those in Fig. 12 to using the Gari-Krümpelmann parametrization[8] for G_E^S to determine the chiral angle. The exchange-current corrections to the tensor polarizations are large and similar to those obtained using meson-exchange mechanisms.[30] Noting that the best prediction for the form factor A is obtained with the Gari-Krümpelmann

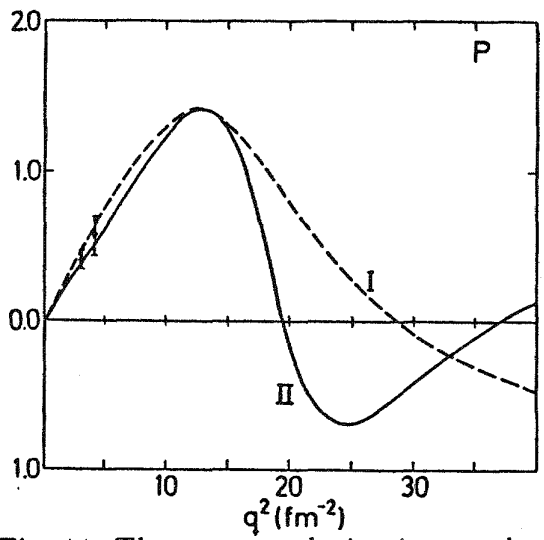

Fig. 11. The tensor polarization as obtained using the chiral angle given by the dipole form for G_E^S. The curves I and II give the results of the impulse approximation and complete calculation, respectively. The experimental data are from Ref. 29.

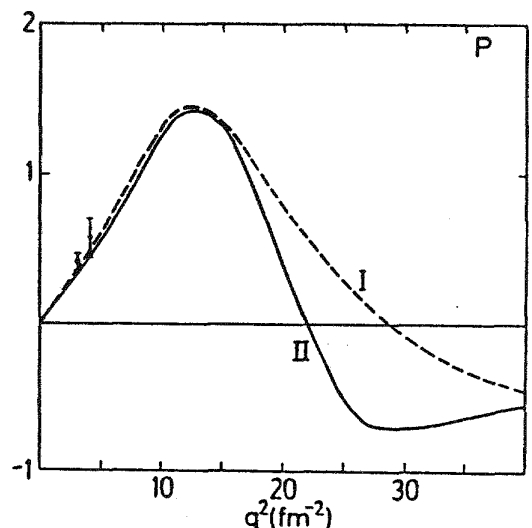

Fig. 12. The tensor polarization as obtained using the chiral angle given by the Gari-Krümpelmann parametrization for G_E^S. The curves I and II give the results of the impulse approximation and complete calculation, respectively. The experimental data are from Ref. 29.

form for θ, one may expect that the prediction for P with that chiral angle (Fig. 12) will also be the most realistic one.

At values of momentum transfer above 1 GeV/c the present predictions for the magnetic form factor begin to differ from those obtained with the typical meson-exchange mechanisms. This becomes clear from Fig. 13 where we have plotted the predicted magnetic form factor up to $q^2 = 70\,\mathrm{fm}^{-2}$ both using the chiral angle given by the dipole form factor and that using the Gari-Krümpelmann parametrization[8] for G_E^S. For comparison we have also in Fig. 13 plotted the prediction for F_M obtained using the conventional impulse approximation with the exchange correction implied by the spin-orbit interaction corresponding to Ref. 12, using the Gari-Krümpelmann parametrizations[8] for G_E^S and G_M^S as well as the prediction obtained when the contribution form the $\pi\rho\gamma$ exchange-current mechanism (Fig. 13) has been added. While the last prediction admits no zero in the form factor, the other predictions do predict a zero. The conventional impulse approximation leads to a zero already at $q^2 = 40\,\mathrm{fm}^{-2}$, which does not appear to be consistent with the empirical values. The Skyrme-model predictions suggest that F_M has a zero between $50\,\mathrm{fm}^{-2}$ and 60 fm^{-2}, depending somewhat on the input data. In Fig. 13 we also show the most recent data[21] on F_M. These indicate that the magnetic form factor has a zero near $50\,\mathrm{fm}^{-2}$, in agreement with our theoretical results. This is quite remarkable in view of the fact that the model is only believed to correspond to the large-color limit of QCD at low energies, and hence the model should not a priori be expected to be reliable above the confinement momentum scale.

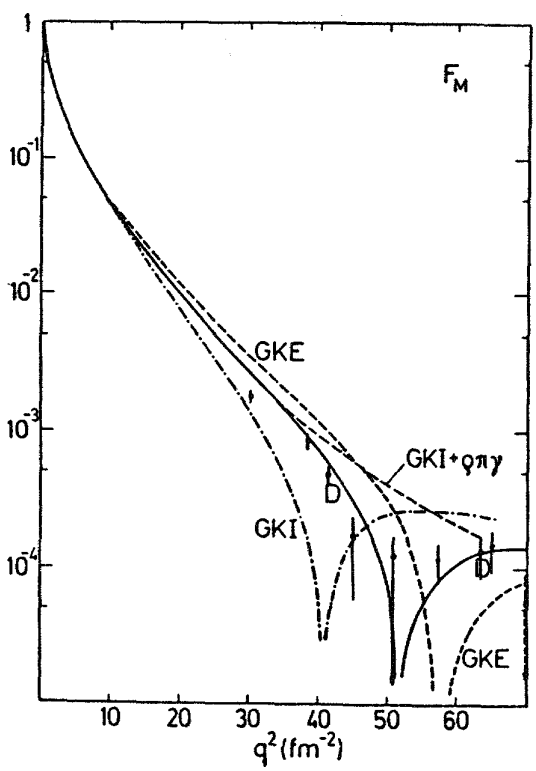

Fig. 13. The magnetic form factor for momentum transfers up to 70 fm^{-2}. The curves D and GKE are obtained using the chiral angle given by the dipole (D) and Gari-Krümpelmann[8] (GKE) parametrizations for G_E^S. The curve GKI is the conventional impulse approximation result including corrections from the velocity-dependent interaction using the Gari-Krümpelmann fit to the nucleon form factors. The curve GKI+$\pi\rho\gamma$ is the same result with corrections from the $\pi\rho\gamma$ exchange-current mechanism included. The experimental data points have been obtained from Ref. 31. (The last point should be at $71\,\mathrm{fm}^{-2}$.)

DISCUSSION

The reasonably good agreement with the empirical deuteron form factors that was achieved above with the topological soliton approach indicates that this approach can provide a good starting point for analyzing nuclear electromagnetic isoscalar observables. The main advantages of the description of the isoscalar current operator in terms of the anomalous baryon current are the large degree of model independence, absence of free parameters and the underlying link to QCD.[31] In the present work we have, however, applied the model only in its simplest form, essentially equating the anomalous baryon current operator with the isoscalar electric current. The topology of the mapping represented by the SU(2) field U in (2.1) dictates the form of (2.2) for the topological baryon-number current, but terms containing higher derivatives may turn out to be important in the Lagrangian. Such terms would play a role above the confinement scale (≈ 1 GeV)

According to the vector-meson dominance model, all isoscalar couplings should be mediated by (in the isoscalar case) ω-mesons. As it is known how to incorporte such couplings into the present model,[22, 23] we have tested the sensitivity to such a modifiction. According to preliminary results, the good agreement between theory and experiment will persist in this case.

REFERENCES

1. F. Gross, Proceedings of the 1986 CEBAF Summer workshop, p. 11, ed. F. Gross. and R. Minehart (CEBAF, 1986).
2. J. Wess and B. Zumino, Phys. Lett. **37B**, 95 (1971).
3. T.H.R. Skyrme, Proc. Roy. Soc. **A260**, 127 (1961).
4. G.S. Adkins, C.R. Nappi and E. Witten, Nucl. Phys. **B228**, 552 (1983).
5. Ebbe M. Nyman and D.O. Riska, Nucl. Phys. **A454**, 498 (1986).
6. Ebbe M. Nyman and D.O. Riska, Phys. Rev. Lett. **57**, 3007 (1986).
7. G. Höhler *et al.*, Nucl. Phys. **B114**, 505 (1976).
8. M. Gari and W. Krümpelmann, Phys. Lett. **173B**, 10 (1986).
9. G.S. Adkins and C.R. Nappi, Nucl. Phys. **B233**, 109 (1984).
10. T.H.R. Skyrme, Nucl. Phys. **31**, 556 (1962).
11. T.A. Griffy and L.I. Schiff, High Energy Physics, Vol. **1**, p. 341 ed. E.H.S. Bishop, (Academic Press, New York, 1967).
12. M. Lacombe *et al.*, Phys Rev. **C21**, 861 (1980).
13. R.V. Reid, Ann. of Phys. **50**, 411 (1968).
14. Ebbe M. Nyman and D.O. Riska, Nucl. Phys. (to be published)
15. S. Auffret *et al.*, Phys. Rev. Lett. **54**, 649 (1985).
16. R. Cramer *et al.*, Z. Phys. **C29**, 513 (1985).
17. D.O. Riska and M. Poppius, Phys. Scripta **32**, 581 (1985).
18. D.O. Riska, Phys. Scripta **31**, 107 (1985).
19. M. Gari and H. Hyuga, Nucl. Phys. **A264**, 409 (1976).
20. A.D. Jackson, A. Lande and D.O. Riska, Phys. Lett. **55B**, 23 (1975).
21. R.G. Arnold *et al.*, Phys. Rel. Lett. **58**, 1723 (1987).
22. M. Bando *et al.*, Phys. Rev. Lett. **54**, 1215 (1985).

23. Ulf-G. Meissner, Norbert Kaiser, Andreas Wirzba and Wolfram Weise, Phys. Rev. Lett. **57**, 1676 (1986).
24. C. Buchanan and M. R. Yearian, Phys. Rev. Lett. **15**, 303 (1965).
25. J.E. Elias *et al.*, Phys. Rev. **177**, 2075 (1969).
26. S. Galster *et al.*, Nucl. Phys. **B32**, 221 (1971).
27. R.G. Arnold *et al.*, Phys. Rev. Lett. **35**, 776 (1975).
28. F. Martin *et al.*, Phys. Rev. Lett. **38**, 1320 (1977).
29. M.E. Schulze *et al.*, Phys. Rev. Lett **52**, 594 (1984).
30. D.O. Riska, Interaction studies in nuclei, ed. H. Jochim and B. Ziegler, p. 815 (North-Holland, Amsterdam 1975).
31. E. Witten, Nucl. Phys. **B72**, 445 (1978).

MANY-BODY THEORY AND ELECTRON SCATTERING

M. Jaminon and C. Mahaux
Institut de Physique B5, Université de Liège, B-4000 Liège 1 (Belgium)
H. Ngô
Division de Physique Théorique, Institut de Physique Nucléaire,
F-91406 Orsay (France)

ABSTRACT

Recent electron scattering experiments have been interpreted in terms of occupation probabilities of shell-model orbits, spectroscopic factors and radial shape of single-particle states. We describe some of the information that many-body theory yields on these quantities.

INTRODUCTION

In the present paper we limit ourselves to a "traditional" description in which nuclei contain structureless nucleons which obey the laws of nonrelativistic quantum mechanics. We often consider the case of nuclear matter, which presents the great simplification that single-particle states are known : they are plane waves $|k\rangle = \exp(ik.r)$ where k denotes the nucleon momentum. For simplicity, we drop arrows on vectors and omit physically irrelevant factors.

OCCUPATION PROBABILITIES

In nuclear matter, the Fermi momentum k_F is related to the density ρ by $\rho = 2\, k_F^3/3\,\pi^2$. In the free Fermi gas approximation, the interactions between the nucleons are neglected. Then, the momentum states $|k\rangle$ are fully occupied for $k < k_F$ and completely empty for $k > k_F$. The corresponding occupation probabilities are thus given by the step function $\vartheta(k_F-k)$, which is represented by the dashes in Fig. 1.

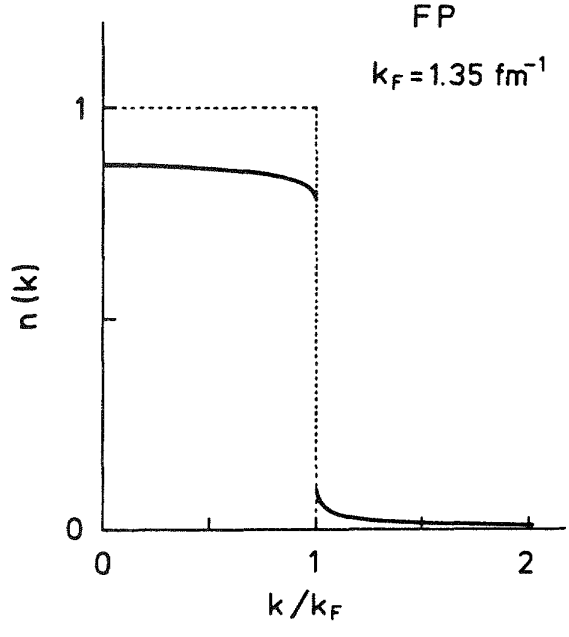

Fig. 1. Taken from ref. 1. Occupation probabilities in nuclear matter. The dashed lines correspond to the uncorrelated case; the solid curves take the nucleon-nucleon interaction into account (ref. 2).

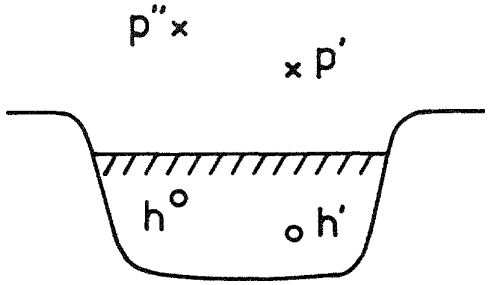

Fig. 2. A two particle-two hole configuration admixed in the correlated ground state.

Henceforth, we denote by $h,h',\ldots$ the momenta of "hole" states $(h,h',\ldots < k_F)$, by $p,p',\ldots$ the momenta of "particle" states $(p,p',\ldots > k_F)$; we limit ourselves to second order perturbation theory. When the nucleon-nucleon interaction v is turned on, two nucleons with momenta h,h' which lie within the Fermi sea can exchange energy and jump in particle states p',p''. This gives rise to two particle-two hole admixtures in the correlated ground state (Fig. 2). The occupation probabilities are then given by

$$n(h) = 1 - \sum_{h',p',p''} \frac{\langle h,h'|v|p',p''\rangle^2}{[e_{p'} + e_{p''} - (e_h + e_{h'})]^2} \quad , \qquad (1a)$$

$$n(p') = \sum_{h,h',p''} \frac{\langle h,h'|v|p',p''\rangle^2}{[e_{p'} + e_{p''} - (e_h + e_{h'})]^2} \quad , \qquad (1b)$$

where e_k is the average nucleon energy. The summation indices are different in eqs. (1a) and (1b), with the consequence that $1-n(k_F-0)$ differs from $n(k_F+0)$.

The momentum distribution in the correlated ground state is represented by the solid curves in Fig. 1. We shall see below that its discontinuity at the Fermi surface, i.e.

$$Z(k_F) = n(k_F-0) - n(k_F+0) \quad , \qquad (2)$$

is intimately related to the spectroscopic factor. Calculations of $n(k)$ are surveyed in ref. 1. The results are quite sensitive to the prescription adopted for the nucleon energy e_k and to the detailed nature of the nucleon-nucleon interaction. One typically finds $n(k_F-0) \approx 0.75 \pm 0.15$, $n(k_F+0) \approx 0.15 \pm 0.10$.

In a nucleus, the energy denominator on the right-hand side of eq. (1a) is larger than the shell gap, while when $h \approx k_F$ it can become arbitrarily small in nuclear matter. Therefore, the depletion of states close to the Fermi surface is expected to be somewhat smaller in nuclei than in nuclear matter, but a fifteen to twenty per cent depletion should not be unexpected. How could one detect this depletion ? Two types of experimental data have been used.

(i) The radial dependence of the difference between the charge density distribution of ^{206}Pb and ^{205}Tl is proportional to what would be expected if these two nuclei only differed by a $(3s_{\frac{1}{2}})$ proton, except for a 0.7 reduction factor.[3] The simplest explanation would be that the occupation probability of the $(3s_{\frac{1}{2}})$ proton orbit in ^{206}Pb is only equal to 0.7 .[4] The reliability of this simple interpretation has been disputed,[4] in particular because it neglects configuration mixing in ^{205}Tl . An improved interpretation has recently been given in terms of sum rules,[5,6] with the resulting estimate[6] $n_{3s_{\frac{1}{2}}}(^{208}Pb) \approx 0.82 \pm 0.09$.

(ii) Inelastic electron scattering which excites states with a predominant one particle (p)-one hole (h) nature are quenched by a factor 0.6 as compared to the shell-model estimate.[7] Core polarization and exchange current corrections only account for part of this large quenching. An additional quenching factor is given by the product of the occupation probability of the hole state and of the depletion probability of the particle state,[7,8] i.e. by $n(h)\,[1 - n(p)]$. For $n(h) \approx 0.8$ and $n(p) \approx 0.1$, this additional quenching is approximately equal to 0.7 , in good agreement with experimental evidence.[7,8]

We now turn to theoretical estimates of the depletion. The many-body theory of the mean field enables one to relate the occupation probability of a single-particle orbit $|n\ell j\rangle$ to the imaginary part $W(r;E)$ of the optical-model potential.[9] In the case of hole states, one has

$$n_{n\ell j} = 1 + \frac{1}{\pi} \langle n\ell j | \int_{E_F}^{\infty} \frac{W(r;E')}{(E'-E)^2}\, dE' \, |n\ell j\rangle \quad , \qquad (3)$$

where E_F denotes the Fermi energy. Occupation probabilities calculated from this expression are represented in Fig. 3. There, the two

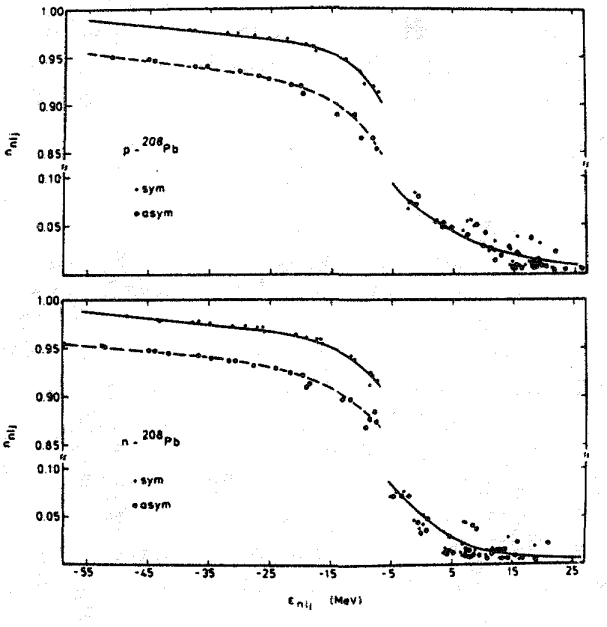

Fig. 3. Taken from ref. 9. Occupation probabilities versus single-particle energies in the case of protons (top) and neutrons (bottom) in ^{208}Pb , as calculated from eq. (3). The Fermi energy is located at - 6 MeV .

sets of points correspond to two different assumptions on the high energy behaviour of $W(r;E)$, which in turn reflect the amount of short range correlations introduced in the calculation. The full dots (solid curves) correspond to a case in which short range correlations are suppressed; the depletion is then quite similar to that calculated in the framework of the random phase approximation[10] and reaches about ten per cent near the Fermi surface. The open circles (dashed curves) include the effect of short range correlations; these are seen to increase the depletion by about five per cent. An additional five per cent increase may arise from tensor correlations. Hence, the depletion close to the Fermi surface is expected to be close to twenty per cent, in good agreement with the experimental evidence outlined above.

MEAN FIELD

In nuclear matter as well as in nuclei the mean field can be identified with the so-called "mass operator" or "self-energy". Here we only consider its real part in nuclear matter, and terms of first and second order in the strength of the nucleon-nucleon interaction v. The mean field felt by a nucleon with momentum h and energy E then reads[1]

$$V(h;E) = V_H(h) + V_P(h;E) + V_C(h;E) \quad , \tag{4}$$

where

$$V_H(h) = \sum_{h'} \langle h,h'|v|h,h'\rangle \quad , \tag{5}$$

$$V_P(h;E) = \sum_{h',h'',p''} \frac{\langle h,p''|v|h',h''\rangle^2}{E + e_{p''} - (e_{h'} + e_{h''})} \quad , \tag{6}$$

$$V_C(h;E) = \sum_{h',p',p''} \frac{\langle h,h'|v|p',p''\rangle^2}{E + e_{h'} - (e_{p'} + e_{p''})} \quad . \tag{7}$$

The quantity $V_H(h)$ is the familiar Hartree-Fock contribution. It is static, i.e. independent of energy.

The physical origin of the quantity $V_P(h;E)$ is the following (Fig. 4). Because of the residual interaction the hole configuration $|h\rangle$ is coupled to two hole-one particle configurations $|h',h'',p''\rangle$. Hence, V_P accounts for configuration mixing in the $(A-1)$ system; it is sometimes called the "polarization" contribution to the mean field.

The physical origin of the contribution $V_C(h;E)$ is the following. Because of the existence of two hole-two particle admixtures in the ground state of the (A) system, the hole state h is empty part of the time (Fig. 2 and eq. (1a)). Hence it is not always possible to take out a nucleon with momentum h, i.e. to create the hole state $|h\rangle$. This gives rise to the contribution $V_C(h;E)$, which is

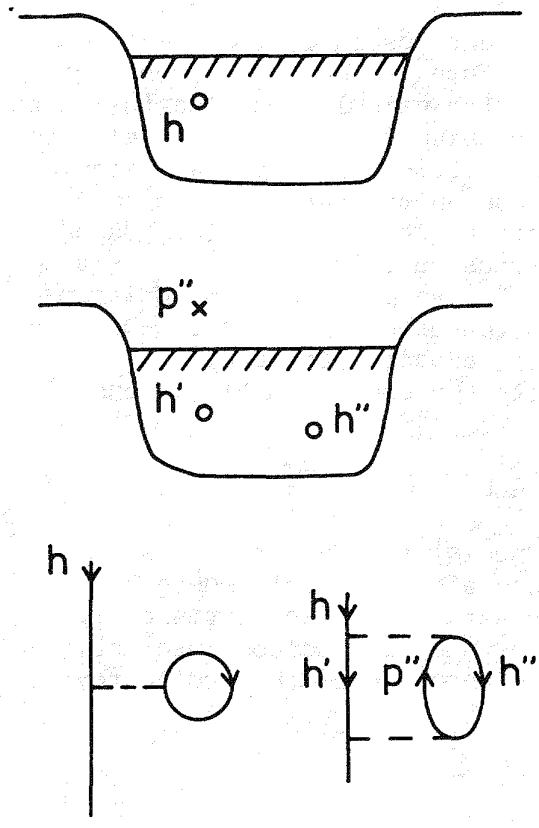

Fig. 4. In the Hartree-Fock approximation, the hole state configuration $|h\rangle$ is stable (top). When the interaction is turned on, the configuration $|h\rangle$ is coupled to two hole-one particle configurations $|h',h",p"\rangle$ (middle). The bottom drawings represent the corresponding contributions $V_H(h)$ (left) and $V_P(h;E)$ (right) to the mean field, see eqs. (5) and (6).

sometimes called a "correlation" correction since it arises from correlations in the ground state of the (A) system. This suggests that $V_C(h;E)$ is intimately related to the depletion probability of the momentum state $|h\rangle$. This is confirmed by the comparison between eqs. (1a) and (7), which shows that

$$1 - n(h) = - \left[\frac{\partial}{\partial E} V_C(h;E)\right]_{E=e_h} . \qquad (8)$$

The relation (3) then follows from the following "dispersion relation" which connects $V_C(h;E)$ to the imaginary part of the mean field :

$$V_C(h;E) = \pi^{-1} \int_{E_F}^{\infty} \frac{W(h;E')}{E' - E} dE' . \qquad (9)$$

QUASIPARTICLE STRENGTH AND SPECTROSCOPIC FACTOR

The energy e_k of a quasiparticle with momentum k is the root of the following energy-momentum relation :

$$e_k = k^2/2m + V(k;e_k) . \qquad (10)$$

The quasiparticle strength is given by

$$Z(k) = 1 + \left[\frac{\partial}{\partial E} V(k;E)\right]_{E=e_k} . \qquad (11)$$

From eqs. (4)-(11) one finds

$$Z(h) = n(h) - \sum_{h',h'',p''} \frac{\langle h',h''|v|h,p'\rangle^2}{[e_h + e_{p''} - (e_{h'} + e_{h''})]^2} \quad . \qquad (12)$$

This leads to the following physical interpretation of $Z(h)$. The quasiparticle strength is the joint probability of (i) being able to create the hole h in the (A) system (first term on the right-hand side of eq. (12)), (ii) finding that the residual $(A-1)$ system has the energy e_h (second term on the right-hand side of eq. (12)). This shows that $Z(h)$ is intimately related to the spectroscopic factor.

The second term on the right-hand side of eq. (12) accounts for configuration mixing in the $(A-1)$ system (Fig. 4). Note that eqs. (1a), (1b) and (12) yield eq. (2). The denominator in the last term in eq. (12) can vanish. In nuclear matter this implies that one should be careful when defining the value of the corresponding sum (actually a multifold integral). In nuclei this implies that this term varies a lot from one microscopic calculation to another, because it sensitively depends on the closeness of e_h to the energy of some two hole-one particle configurations $|h',h'',p''\rangle$.

As we mentioned above, calculations in nuclear matter typically yield $Z(k_F) \approx 0.60 \pm 0.25$. In nuclei the value of the spectroscopic factor near the Fermi surface should be expected to be somewhat larger than $Z(k_F)$ because of shell effects.

Figure 5 shows the value of the spectroscopic factors in ^{208}Pb , as calculated in the framework of a dispersion relation approach[9] based on eq. (9) and on a similar equation for $V_p(k;E)$. The comparison between Figs. 3 and 5 shows that near the Fermi energy one has typically

$$Z_{n\ell j} \approx n_{n\ell j} - 0.10 \quad . \qquad (13)$$

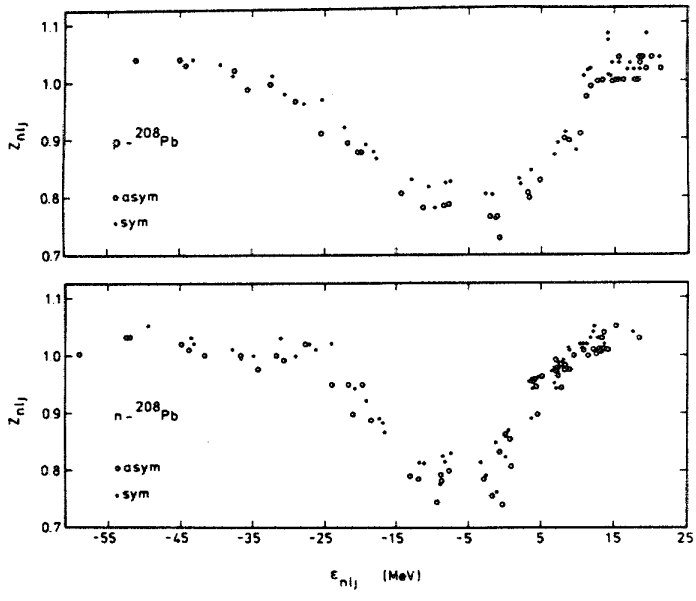

Fig. 5. Taken from ref. 9. Single-particle strengths versus single-particle energies in the case of protons (top) and neutrons (bottom) in ^{208}Pb , with the same convention as in Fig. 3.

Our previous discussion of the occupation probabilities then suggests that the spectroscopic factors should be close to 0.70 in the vicinity of the Fermi surface. Note that away from the Fermi surface the single-particle strength should be associated with the sum of the spectroscopic factors of the many states of the (A-1) system over which the hole state $|n,\ell,j\rangle$ is spread (ref. 1).

Empirical determinations of the "absolute" spectroscopic factor are extremely difficult. In view of eq. (2), near the Fermi surface it is approximately equal to the difference between the occupation probabilities of hole and particle states. In first order in the depletion, this difference is equal to the product $n(h)\,[1 - n(p)]$ of which we have seen above that it contributes to the quenching of one particle-one hole excitations in inelastic electron scattering. This quenching has been estimated to be close to 0.7 (ref. 7). Another estimate of the spectroscopic factor is provided by the quenching of single-particle magnetic form factors, e.g. in ^{207}Pb ;this again approximately yields 0.7 ± 0.1 for the spectroscopic factor of levels which are usually considered to be "almost pure" one hole configurations (ref. 11). These empirical values are seen to be in fair agreement with the theoretical estimates.

SHELL-MODEL ORBITS

Let us denote by $\Psi(1,\ldots,A)$ the exact wave function of the ground state of the (A) system. Because of the strength of the nucleon-nucleon interaction, Ψ is a very complicated many-body wave function, whose overlap with <u>any</u> Slater determinant is smaller than $(0.9)^A \approx 10^{-10}$; here, the number 0.9 is an average occupation probability derived from the calculations surveyed above. Hence, finding the appropriate definition of "the" shell-model orbits is by no means a trivial problem. Note that occupation probabilities

$$n_\alpha = \langle\Psi|a_\alpha^+ a_\alpha|\Psi\rangle \qquad (14)$$

are well defined for <u>any</u> set of single-particle wave functions $\{\alpha(r)\}$. One should therefore specify the definition of $|\alpha\rangle$ when one quotes values of n_α . At least two model-independent definitions have been proposed, as we briefly outline below. They both present the merit of being fully specified by the many-body Hamiltonian H , while most "single-particle wave functions" used in the literature, e.g. Hartree-Fock wave functions, are model dependent.

(i) The "<u>natural orbitals</u>" (ref. 12) are the eigenstates of the exact one-body density matrix

$$\rho(r;r') = \langle r'|\rho|r\rangle = \langle\Psi|a^+(r')\,a(r)|\Psi\rangle \quad . \qquad (15)$$

They form a complete orthogonal set, say $\{\nu(r)\}$. The one-body density matrix can be written in the form

$$\rho(r;r') = \sum_{\nu} n_{\nu}\, \nu(r)\, \nu(r') \quad , \tag{16}$$

where n_{ν} are the occupation probabilities of the natural orbitals. Note that the latter are fully defined by the ground state wave function of the (A) system : they contain no information on its excited states, nor on the eigenstates of the (A+1) and (A-1) systems.

The sum over ν in eq. (16) runs over an infinite number of natural orbitals. An "optimal" independent-particle approximation can be defined by selecting the A largest eigenvalues n_{ν} to define the "Fermi sea" ($\nu \in F$) and by writing

$$\rho_o(r;r') = \sum_{\nu \in F} \nu(r)\, \nu(r') \quad . \tag{17}$$

This definition of the Fermi sea is optimal for two reasons [13] : (a) It retains the largest eigenvalues of ρ , i.e. minimizes the depletion of the Fermi sea. (b) The quantity

$$\sigma = A^{-1}\, \mathrm{trace}(\rho - \rho_o)^2 \tag{18}$$

is smaller for the definition (17) of ρ_o than for any other independent-particle approximation ρ'_o . The "mean square deviation" σ is determined by the exact ground state wave function Ψ and is thus model-independent. Theoretical estimates (ref. 14) yield $\sigma \approx 0.02$-0.03 in the case of realistic nucleon-nucleon interactions. Note that σ involves both diagonal and off-diagonal elements of the one-body density matrix. The existence of a minimum value of $\mathrm{trace}(\rho-\rho'_o)^2$ implies that if some Slater determinant exactly reproduces the diagonal elements $\rho(r) = \rho(r;r')$ of the one-body density matrix (i.e. the radial density distribution) it cannot exactly reproduce its off-diagonal elements; in particular, the momentum distribution will not be correctly reproduced (refs. 15, 16).

(ii) The "overlap functions" (refs. 17, 18) are defined as follows. Let $\Phi_{\lambda}(1,\ldots,A\pm1)$ denote the exact (many-body) wave function of the excited state λ of the (A±1) system. The overlap orbitals $\lambda(r)$ are defined by the following equations

$$\lambda^{(\pm)}(r) = [S_{\lambda}^{(\pm)}]^{-\frac{1}{2}}\, \varphi_{\lambda}^{(\pm)}(r) \quad , \tag{19}$$

$$\varphi_{\lambda}^{(+)}(r_{A+1}) = (\Phi_{\lambda}(1,\ldots,A+1)|a^{+}(r_{A+1})|\Psi(1,\ldots,A)\rangle \quad , \tag{20a}$$

$$\varphi_{\lambda}^{(-)}(r_{A}) = (\Phi_{\lambda}(1,\ldots,A-1)|a(r_{A})|\Psi(1,\ldots,A)\rangle \quad , \tag{20b}$$

$$\langle\lambda^{(\pm)}(r)|\lambda^{(\pm)}(r)\rangle = 1 \quad . \tag{21}$$

In eqs. (20a), (20b), the rounded bra indicates that in the matrix elements the integrals run over all the variables except that which appear in the creation or annihilation operator. The "spectroscopic factors"

$$S_\lambda^{(\pm)} = \langle \varphi_\lambda^{(\pm)}(r) | \varphi_\lambda^{(\pm)}(r) \rangle \qquad (22)$$

are specified by the normalization condition (21).

The overlap functions are eigenstates of the single-particle Hamiltonian formed by adding the mass operator to the kinetic energy operator (ref. 19). It immediately follows (see e.g. ref. 20) that the overlap functions form a complete set when weighted by the spectroscopic factors :

$$\sum_{\lambda(+)} S_\lambda^{(+)} |\lambda^{(+)}\rangle \langle\lambda^{(+)}| + \sum_{\lambda(-)} S_\lambda^{(-)} |\lambda^{(-)}\rangle \langle\lambda^{(-)}| = 1 , \qquad (23)$$

and that the spectroscopic factors are identical to those introduced in eq. (11) above.

One consequence of eq. (23) is that the one-body density matrix can be written in the form

$$\rho(r;r') = \sum_{\lambda(-)} S_\lambda^{(-)} \lambda^{(-)}(r) \lambda^{(-)}(r') \quad . \qquad (24)$$

This expression is formally analogous to eq. (16), but its interpretation is quite different (ref. 19). In particular, $S_\lambda^{(-)}$ cannot be interpreted as an occupation probability because the overlap functions are not orthogonal to one another. Futhermore the energy spacing associated with the overlap functions is the same as that between the excited states (with given angular momentum and parity) of the $(A\pm1)$ systems. Hence the overlap functions should not be identified with shell-model orbits. This identification can be done only after introducing some approximations, e.g. after assuming that several $\lambda^{(-)}(r)$ have the same radial shape; the approximate validity of this assumption is supported by recent $(e,e'p)$ experiments, see e.g. ref. (21). Likewise, sum rules associated with any single shell-model orbit only have an approximate validity. This should be kept in mind when evaluating the accuracy of recent applications of such sum rules in order to determine the occupation probability of "the" $(3s\frac{1}{2})$ proton orbit in ^{208}Pb , see e.g. refs. 5, 6.

CHARGE AND MOMENTUM DISTRIBUTIONS

From the estimates surveyed above one expects that the depletion of an orbit located near the Fermi surface is approximately equal to twenty per cent, of which about ten per cent are due to long range correlations. The problem then arises of estimating the effect of this depletion on ground state observables, in particular on the charge and momentum density distributions. It is necessary to consider at least these two observables simultaneously. Indeed, one of them (e.g. the charge density distribution) can be very accurately reproduced within a Hartree-Fock model (in which it is assumed that no depletion exists) provided that the single-particle orbits are chosen purposedly (ref. 22). However, a Hartree-Fock model will not be able to accurately reproduce both the charge and the momentum distributions.

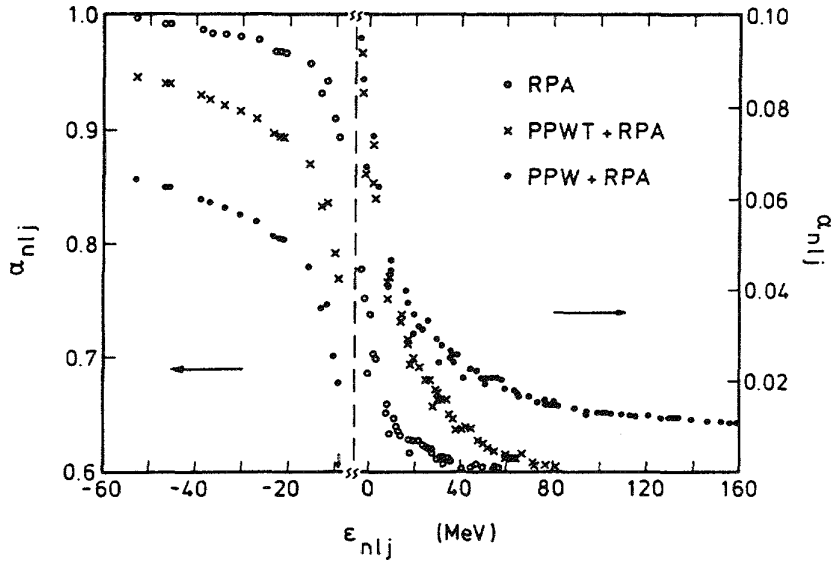

Fig. 6. Taken from ref. 23. Occupation probabilities of proton natural orbitals in ^{208}Pb . The open circles include the effect of long range correlations as evaluated in the RPA, ref. 10. The full dots add results calculated in nuclear matter to those derived from the RPA (ref. 7). The crosses are obtained from the full dots by decreasing the depletion by five per cent.

Figure 6 shows three sets of occupation probabilities which have been considered in refs. 14, 23, 24. The open circles have been calculated from the random phase approximation (RPA) and therefore only include the effect of long range correlations. The effect of the latter is not large : the calculated root mean square radius increases by only 0.03 fm as compared to the Hartree-Fock approximation if one retains the same set of (Hartree-Fock) single-particle wave functions (ref. 23). Note, however, that these Hartree-Fock wave functions are expected to be different from the natural orbitals which would be obtained from a self-consistent calculation within the RPA.

The full dots in Fig. 6 represent a set of occupancy probabilities which had been suggested in ref. 7; the corresponding depletion is obtained by adding the RPA depletion to that due to short range and tensor correlations as estimated from nuclear matter calculations. This set of occupation probabilities yields a large (0.24 fm) increase of the charge root mean square radius if one retains the same (Hartree-Fock) single-particle basis. In this case, however, it appears likely that the correlations are so large that the natural orbitals are quite different from the Hartree-Fock orbitals. The latter are even ill-defined. In other words, it is not consistent to introduce a large depletion without, at the same time, taking into account the effect of the correlations on the natural orbitals. It is mainly, for this reason, that it is quite difficult to identify effects of the depletion of the Fermi sea in analyses of experimental charge density distributions. The origin of this difficulty lies in the fact that the single-particle orbits (more specifically the natural orbitals)

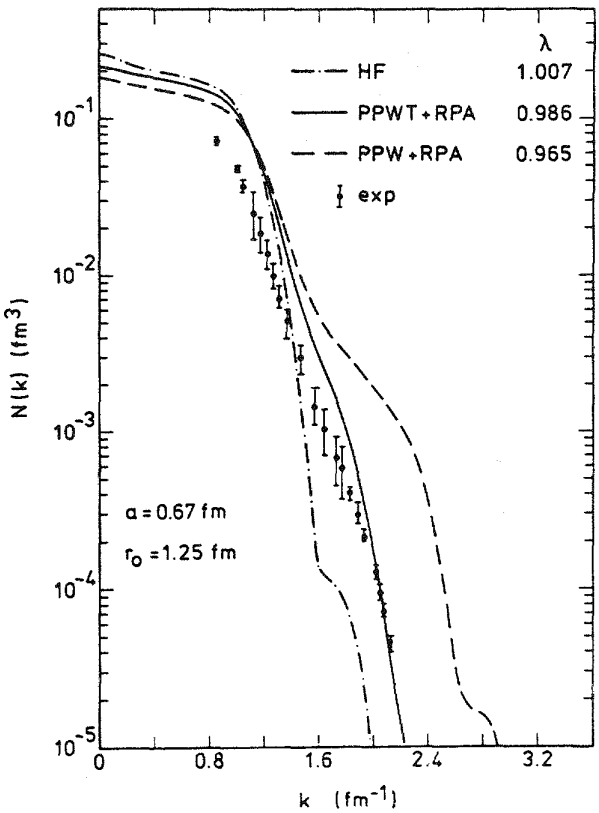

Fig. 7. Taken from ref. 14. Momentum distribution of nucleons in ^{208}Pb. The dash-one dot curve is associated with the open circles of Fig. 6, the solid curve with the crosses, and the long dashes with the full dots of Fig. 6. In the present figure, the full dots are empirical values (refs. 25, 26) derived from analyses of quasi-elastic backward inclusive cross sections of 642 MeV electrons and 200 MeV protons on ^{12}C and ^{58}Ni.

are not known.

As suggested in ref. 15 the effect of the depletion of the Fermi sea could be more unambiguously identified if one would have experimental information on off-diagonal as well as one diagonal elements of the one-body density matrix, for instance on both the momentum and charge density distributions. Figure 7 exhibits the fact that the momentum distribution is quite sensitive to the depletion of the Fermi sea and, correspondingly, to the repletion of single-particle states located outside the Fermi sea. Forthcoming measurements of (e,e') and (e,e'p) cross sections should be able to yield detailed information concerning the momentum distribution. This will be most valuable since the present empirical information is derived from processes which involve strong interactions, and whose analysis is therefore questionable.

DISCUSSION

Recent measurements and analyses of (e,e), (e,e') and (e,e'p) cross sections exhibit limitations of the mean field approximation. In particular, information is becoming available on occupation probabilities of shell-model orbits and on "absolute" spectroscopic factors. In order to exploit the information content of these and of forthcoming experiments, renewed theoretical effort should be devoted to the proper definition of these quantities and of the shell-model orbits themselves. In particular one should try to avoid using model-dependent quantities which are ill-defined and whose flexibility may blur the identification of deviations from the independent-particle model; in particular this warning applies to the use of Hartree-Fock single-particle wave functions. We discussed two possible model-independent definitions of the shell-model orbits, namely :

(a) The natural orbitals, which are eigenstates of the one-body density matrix. These orbits form a complete, orthonormal set. They are quite convenient for the discussion of the charge density distribution and provide an "optimal" independent particle approximation (Slater determinant). However, it is not clear whether they can be constructed from a single-particle potential. Furthermore, and more importantly in the present content, they are not related to the levels of the (A±1) system and, correspondingly, to the concept of spectroscopic factors.

(b) The overlap functions, which are defined in terms of overlap integrals between the wave function of the ground state of the (A) system and of those of the ground and excited states of the (A±1) systems. They are intimately related to the spectroscopic factors. They present the difficulty of being nonorthogonal and linearly dependent. However, they can be constructed from a single-particle potential, namely the mass operator.

It appears unlikely that it will be possible to calculate overlap functions and spectroscopic factors from the bare nucleon-nucleon interaction, since the latter is very strong and complicated. However, the many-body theory can be very helpful in establishing relationships between quantities which are at first sight of a quite nature. An example is provided by eqs. (8), (9) which express the occupation probabilities of hole states in terms of the imaginary part of the optical-model potential. Likewise, similar dispersion relations are helpful in relating the shell-model to the optical-model potential. This is important because much more empirical information is available on the latter than on the former. This has given rise to recent and rather successful attempts to calculate the shell-model potential from an extrapolation of the optical-model potential (refs. 27, 28, 29). The results exhibit the feature that the lack of orthogonality of the overlap orbit does not only arise from the energy dependence of the depth of the mean field, but also from the energy dependence of its radius. The latter feature is the dominant one in the vicinity of the Fermi surface and might therefore have to be taken into account in the interpretation of recent electron scattering data.

REFERENCES

1. C. Mahaux, P.F. Bortignon, R.A. Broglia and C.H. Dasso, Phys. Reports, **120** (1985) 1
2. S. Fantoni and V.R. Pandharipande, Nucl.Phys. **A427** (1984) 473
3. J.M. Cavedon, B. Frois, D. Goutte, M. Huet, Ph. Leconte, C.N. Papanicolas, X.-H. Phan, S.K. Platchkov, S. Williamson, W. Boeglin and I. Sick, Phys.Rev.Lett. **49** (1982) 978
4. J. Friedrich, Phys.Rev. **C33** (1986) 2215
5. H. Clement, P. Grabmayr, H. Röhm and G.J. Wagner, Phys.Lett. **183B** (1987) 127
6. E.N.M. Quint, B.M. Barnett, A.M. van den Berg, J.F.J. van den Brand, H. Clement, R. Ent, B. Frois, D. Goutte, P. Grabmayr, J.W.A. den Herder, E. Jans, G.J. Wagner, J.B.J.M. Lanen, L. Lapikás, H. Nann, G. van der Steenhoven, G.J. Wagner and P.K.A. de Witt Huberts, Phys.Rev.Lett. **58** (1987) 1088

7. V.R. Pandharipande, C.N. Papanicolas and J. Wambach, Phys.Rev. Lett. **53** (1984) 1133
8. T. Suzuki and H. Hyuga, Nucl.Phys. **A402** (1983) 491
9. C. Mahaux and H. Ngô, Nucl.Phys. **A431** (1984) 486
10. J. Dechargé and L. Sips, Nucl.Phys. **A407** (1983) 1
11. C.N. Papanicolas, L.S. Cardman, J.H. Heisenberg, O. Schwentker, T.E. Milliman, F.W. Hersman, R.S. Hicks, G.A. Peterson, J.S. McCarthy, J. Wise and B. Frois, Phys.Rev.Lett. **58** (1987) 2296
12. P.O. Löwdin, Phys.Rev. **97** (1955) 1474
13. D.H. Kobe, J.Chem.Phys. **50** (1969) 5183
14. M. Jaminon, C. Mahaux and H. Ngô, Nucl.Phys. A (submitted)
15. O. Bohigas and S. Stringari, Phys.Lett. **95B** (1980) 9
16. M. Jaminon, C. Mahaux and H. Ngô, Phys.Lett. **158B** (1985) 103
17. T. Berggren, Nucl.Phys. **72** (1965) 337
18. C.F. Clement, Nucl.Phys. **A213** (1973) 493
19. M. Jaminon, C. Mahaux and H. Ngô, to be published
20. J.P. Blaizot and G. Ripka, "Quantum Theory of Finite Systems" (MIT Press, Cambridge, Massachusetts, USA, 1986), p. 495
21. J.W.A. den Herder, J.A. Hendriks, E. Jans, P.H.M. Keizer, G.J. Kramer, L. Lapikás, E.N.M. Quint, P.K.A. de Witt Huberts, H.P. Blok and G. van der Steenhoven, Phys.Rev.Lett. **57** (1986) 1843
22. M. Gaudin, J. Gillespie and G. Ripka, Nucl.Phys. **A176** (1971) 237
23. M. Jaminon, C. Mahaux and H. Ngô, Nucl.Phys. **A440** (1985) 228
24. M. Jaminon, C. Mahaux and H. Ngô, Nucl.Phys. **A452** (1986) 445
25. B. Harradi, Master's Thesis, University of Clermont-Ferrand II, 1986
26. M. Avan, J. Baldit, M. Bernheim, J. Fargeix, H. Fonvielle, P. Force, A. Gérard, J.L. Guelau, B. Harradi, H. Jackson, A. Magnon, C. Marchand, J. Morgenstern, J. Picard and P. Vernin, Annual Saclay Report 1985-1986, page 17
27. C. Mahaux and R. Sartor, Phys.Rev.Lett. **57** (1986) 3015
28. C. Mahaux and R. Sartor, Nucl.Phys. **A468** (1987) 193
29. C.H. Johnson, D.J. Horen and C. Mahaux, Phys.Rev. C (submitted).

WORKSHOP SUMMARY

John Domingo
SIN, 5432 Villigen, Switzerland

I should first of all warn you that I have absolutely no qualification to summarize a workshop on electromagnetic interactions. First my experimental background is entirely in the field of strong interactions and secondly I have reached the age where most of my time is spent worrying about budgets, manpower, and applied psychology. My only experience with lepton probes is my slight involvement in the high energy muon scattering experiment NMC at CERN. In fact the only reason I am standing here wasting your time is that when Franz Gross called me to ask if I would give the summary I was in the midst of a direction meeting and it is much quicker to say yes than to explain why it is impossible. I am beginning to feel like the gal in *Oklahoma* who couldn't say no – the result is roughly the same!

As any of you who ever tried it will agree, giving an interesting conference summary is extremely difficult unless you prepare it in advance and tell the speakers what they should have said! In the case of this workshop it was especially difficult due to the many parallel working groups. I will therefore have to confine myself to a few points which I found particularly interesting (perhaps just particularly easy for me to understand) in the plenary sessions and the limited number of working groups I was able to attend. My selection should certainly not be interpreted as being in any way a priority list.

Let me start by posing what I believe will be the central question for nuclear physics in the 90's and perhaps beyond:

How can we reconcile our old well tested picture of a nucleus consisting of individual nucleons moving in an average central potential with our present belief that the nucleons consist of an assembly of three quarks and the size of this assembly compared to the average internucleon separation is such that the nucleons must overlap to an appreciable degree.

It is clear that the nucleon-meson picture of the nucleus must have a large amount of validity since it is able to explain such a large body of data, but from the quark description it is not obvious how this can be. Since the quark picture appears to work well at very high momentum transfers and the classical nucleon-meson description at the transfers available with present nuclear electromagnetic facilities, one expects a transition region somewhere and we hope CEBAF will be able to see indications of this.

There has been a great deal of heat and very little light shed on the question of at what Q^2 one can begin to apply perturbative QCD. I certainly have nothing to add to this discussion except to point out that I believe the question is not when one will be able to apply perturbative QCD but rather at what sort of Q^2 one will begin to see significant deviations from the predictions of the standard nucleon-

meson theories. Clever theoreticians will almost certainly be able to patch up the nucleon-meson models with more parameters so that they will continue to fit the data; the question is whether at some Q^2 the explanation will become simpler in the quark picture. I think even without the existence of a "smoking gun" this will be an extremely interesting field of investigation in which CEBAF will certainly be able to make a major contribution.

In addition to the quark description, one has the many successes of the Skryme model as discussed yesterday by Nyman. But before I am forced to think about "combed spinning hedgehogs", I will continue to hope that Migdal's observation at the Kyoto conference that everything that is mathematically beautiful isn't necessarily present in nature covers this case.

Let me briefly review some of the experimental investigations mentioned here which deal with the central question:

How Are Hadrons Modified When Placed In A Nucleus?

I Probably the best known experimental result dealing with possible modifications is the original EMC result comparing the structure function of iron with that of deuterium. After several years of controversy between various experimental groups, the basic features of the modification are now agreed upon. A comparison between the BCDMS and SLAC results for the Fe/D^2 ratio and new preliminary EMC results for the Cu/D^2 ratio is shown[1] in Figure 1. One can see that all the data now shows a deviation form the original EMC result which indicated a continuous rise in the ratio at small x. There clearly seems to be a maximum at around x=0.1 and a drop to below 1 for smaller x. Just what this low x data will tell us about the rather murky question of shadowing must await future experiments such as those planned by the NMC collaboration. I am sure most of you have heard at least 20 different explanations of the effect ranging from nucleon binding to color conductivity; clearly much more experimental data is needed before one can begin to eliminate most of the theories and approach a reasonably small subset. It is clearly much too early to say whether CEBAF can contribute to this type of experiment, but the possibility of having a final energy considerably higher than 4 Gev makes it worth considering.

II Another question frequently discussed dealing with hadron modification is that of deeply bound lambda shell model states in heavy hypernuclei. Here the question is two fold:

First whether deeply bound shell model states really exist in the simple form our model calculations indicate. Secondly whether the lambda (or other strange hadron) continues to behave as a spatially confined indentifiable particle (distinct from nucleons) or whether the Pauli principle operating at the quark level leads to a partial deconfinement so that only the strange quark is allowed to occupy the deeply bound levels.

Clearly these questions will only be answered by combining many experimental techniques from level spectroscopy to a detailed study of the bound lambda's wavefunction. The first piece of the puzzle was shown here by Crien as a preliminary result from the (π,K) experiments at Brookhaven. Figure 2 shows these results for $^{89}_{\Lambda}$Y and indicates a series of lambda-neutron hole states the first of which supposedly corresponds to the lambda in the lowest s shell. I think it is important that the organizers of the workshop have included not only talks dealing with electromagnetic but also hadronic probes. If we are to make significant progress in these difficult questions, we will need all the data we can obtain. We need to think of nuclear physics as a whole and not divide ourselves into separate groups depending upon the probe we use. I see several people in the audience who come from the same background as myself; clearly using an electromagnetic probe is going to involve considerable recalibration of one's intuition – not particularly easy at my age, but it is certainly good for one to change techniques occasionally and hopefully even for the field.

I hope CEBAF will have a lot to contribute to the hypernuclear questions through detailed studies of the bound lambda's wavefunction via (e,e'K) reactions. Clearly there are count rate problems, but I think some of the ideas brought up in the working session may go a long way toward alleviating them.

III A question where CEBAF should certainly be able to contribute greatly is in the electro production of nucleon resonances and how these are modified in a nucleus. The case discussed in this workshop is that of the E_2/M_1 ratio for the ($\gamma N \rightarrow \Delta$) reaction. I think this is an excellent case illustrating that one wants to study only a few selected resonances where the information is of particular interest; not to devote one's life to resonance chasing. In the case of the idea is particularly simple since on the basis of the simplest quark models there should be no E_2 amplitude since the nucleon has the three quarks in an S state and the transition to a Δ just involves a quark spin flip. The E_2 amplitude must arise via a d wave admixture to the wavefunction either due to the color hyperfine interaction of some other mechanism. Recent analysis[2] of the data yields a E_2/M_1 ratio in the range –0.5 to –1.5 % although the exact value is somewhat uncertain due to the difficulty of extracting the non resonant background. This value seems to be roughly that predicted by the quark model calculations, but it has also been explained by non quark effects[3]. It is of interest to note that the value given by perturbative QCD is $\sqrt{3}$ [4] so we clearly are a long way from the region where it is valid – if it ever is. The large difference between these values make it interesting to think about the possibility of trying to look at the reaction at high momentum transfers. Since this would seem to necessitate producing the Δ far off shell, it probably would be extremely difficult, however, one could perhaps see the value moving or even changing sign. This may not be an experiment for CEBAF – or anywhere – but it is worth thinking about.

IV Another currently hot topic is the question of the πN sigma term and what it implies about the $s\bar{s}$ content of the nucleus. As most of you probably know the present experimental data indicates that the $\Sigma\pi$N is roughly 60 Mev whereas chiral perturbation theory predicts a value almost a factor of 2 smaller. One possible interpretation[5] of this difference is that "in some sense" roughly 20-30 % of the quarks in the proton are strange. This explanation seems the most straightforward in spite of this unexpectedly large value; the problem is the term "in some sense". The strange quark content may just represent the difference between the content of the perturbation vacuum and the true vacuum – whatever that may mean! Since it is very hard for me to picture the quarks being outside the bag in the "true vacuum" I am very uncertain about what we would be measuring in experiments like (e, e'K) or (e, e'π) but perhaps they could shed some light on this puzzle.

V Finally let me come to y scaling; I find it difficult to understand why it apparently works so well. Figure 3 was shown on Wednesday by Posted and presents preliminary data from SLAC which seems to indicate that scaling works not only at very forward angles but also at 180°. Since the usual interpretation of y scaling is that it is telling us about the momentum distribution of the nucleons, I find it truly amazing that it appears to be independent of Q^2 even for extremely high nucleon momentum where I would expect all sorts of other effects to be important. I don't understand why it works, but we can surely use it to learn something about nuclei.

FACILITY QUESTIONS

Finally let me come to more specific questions about the experimental facilities which have occurred to me during this week. Again if some of them seem to be rather naive you can attribute it to the fact that my experience has been in another field so my intuition is badly calibrated for electromagnetic interactions.

1. The first question that occurred to me was whether one really needs 100 Kev resolution at 4 Gev. Most of the discussion at the workshop has involved few nucleon systems where the level spacing is much larger; so why work so hard to get this fantastic resolution? The best reason I have heard during the workshop was that given by Bertozzi that one will need this type of precision in energy determination in order to extract various parameters with the desired accuracy. Of course another gut feeling we probably all share is that good resolution never hurts and if you don't do it at the beginning you never will. Unfortunately high resolution at these energies is very expensive.

2. My second question is whether one really needs to work so hard on achieving spectrometer acceptance for a 20 cm target length. I realize the cross section at

these high momentum transfers will be extremely small (neutrino like), but one will have a very high beam current. For most targets the 10 cm length would seem to be adequate; is it really worth sacrificing something else to gain a factor of 2? Murphy and Liouville will certainly be hard at work to make sure you have to give up something valuable to attain the 20 cm acceptance.

3. It was clear in the sessions and the report this morning of the (e, e'K) working group that one would like to be able to reach a much smaller angle between the electron and hadron spectrometers than is possible in the present design. I think the suggestion of incorporating a septum magnet at the entrance of the spectrometers is worth investigating with detailed optical studies. It was also suggested that these septums might consist of a first stage of iron and copper acting as a beam shield for a second superconducting stage. Finally there is the question of constructing a much shorter hadron spectrometer for use with K's. The problem here would seem to be achieving the desired resolution with a much shorter design since there are general theorems relating the resolution at a given momentum to the spectrometer length; of course the exact relation depends on the type of spectrometer. The other important question is whether one can afford a special K spectrometer; it would certainly be valuable to have a shorter one if an acceptable design can be found. I personally don't see much chance of having a second high resolution electron spectrometer so the K spectrometer would also have to be in area A.

4. My next question is what type of facility should be foreseen for the third area and when should it be installed? There was considerable discussion in the working sessions about the desirability of having some type of facility midway between the high resolution relatively small solid angle spectrometer of hall A and the large acceptance moderate resolution facility of hall B. Just what this should be clearly depends upon the final design of the other two facilities and the type of physics one wants to do with it. Extrapolating from the start up period at SIN I am afraid the in-house groups at CEBAF are going to have about all they can handle trying to get halls A and B equipped at beam turn on. But there are a lot of spectrometer magnets lying about and a number of users interested in such a facility so why don't they take this one on more or less by themselves. This could be just the preliminary facility and if it really turns out to be in high demand CEBAF could design an optimum facility at a later date.

5. Finally as we have learnd the prototype cavities are performing extremely well so that it seems likely that one will be able to raise the energy from 4 to 6 Gev or even higher. The users should seriously start thinking about what energy they would like to see the facility running at and what this would entail in additional experimental facilities. Also what they would be willing to give up or postpone to achieve this increase in energy. This last point raises a question that I think is

extremely important for the nuclear community seriously start considering:

What Facility Will You Be Willing To Close To Get Something New?

Clearly the nuclear physics budget is not necessarily a zero sum game; as Herman happily pointed out on Monday – but it isn't an infinitely expanding one either! If the field wants something new it will have to be willing to give up some existing facility to get it, and it is much better that the community decides the priorities rather than letting them be set by a power struggle between lab directors and politicians.

GENERAL POINTS

Finally let me make some general remarks about issues which I think will be important to the scientific success of CEBAF. On Wednesday there was a discussion concerning how one should go about requesting proposals and whether one should have definite or generic proposals. I feel strongly that one should request real proposals as soon as possible certainly by fall of 88. Having one's name attached to a definite proposal will wonderfully concentrate the mind since the damned thing has to be ready to run in 1993. It will force the users to make a real commitment to the facility and not just a virtual show of interest. It will also have the effect of fixing the required parameters of the various instruments rather than having to rely on wish lists and general statements from the PAC. Of course one doesn't want to have a tremendous backlog of experiments as was the case in the early days of Lampf or Lear, but a little overbooking is probably good for the political health of the laboratory. Also any PAC worth its salt will give the budding Nobel prize experiment priority over the bread and butter ones still on the books.

I realize that there is a justified concern by the various groups that if they spend too much of their effort during the next few years on building up a new facility their published output is bound to drop and the granting agencies and university deans will frown on this. However, if the granting agencies and their review boards aren't willing to consider the facility building period as necessary and potentially much more productive than just cranking out the same old stuff then they are really crazy to build new accelerators let alone start new laboratories! The academic overseers may be a little more tricky, but here I would think a little pressure from the higher ranks of the agencies or some other prestigious body should be helpful. **Someone has to build up these facilities for the discipline can't make any real progress through the "Butterflies" who flit from existing apparatus to existing apparatus.**

A tentative suggestion for the first proposal would be:

Letters of Intent	PAC Spring 88
Definite Proposals	PAC Fall 88

Finally let me make a plea to the "senior" members of the user's community. I know from being involved in the early days of SIN that there are going to be a great many facility questions which will seem rather secondary and not terribly important; however, in the long run many of these will have a large effect on the success of the laboratory. Questions like: What should be in the general stockroom, how large should the electronics pool be and how should it be booked, what type of 24 hour cantine service does one need, how large and of what quality should the guest house be? One doesn't want to occupy the young people with these secondary problems, but for those of you senior enough to have years of experience working at other user facilities it will be extremely helpful if you can give CEBAF the benefit of this experience either by making suggestions or serving on various committees. As someone said when asked about the preliminary SIN beam layout "Oh you can live with anything". Of course you can but if the wrong decisions are made for lack of input you will have to live with it for a long time. My closing comment is therefore:

GET INVOLVED WITH CEBAF NOW
OR DON'T BITCH IN 93 !

References:

[1] D. von Harrach, Proceedings of the Eleventh Int. Conf. on Particles and Nuclei (Panic 11), Kyoto 1987 (to be published)

[2] M. Bourdeau and N.C. Mukhopadhyay, Proceedings of the 1986 CEBAF Summer Study Group pg. 135

[3] J. Bienkowska and Z. Dziembowkski, Proceedings of the 1986 CEBAF Summer Study Group pg. 111

[4] C.E. Carlson, Theoretical and Experimental Investigations of Hadronic Few-Body Systems, 1986, edited by C. Giofi degli Atti, O. Benhar, E. Pace, and G. Salme, Springer Verlag Wien New York pg. 473

[5] J. Donoghue and C. Nappi, Phys.Lett. 168B, 105 (1986)

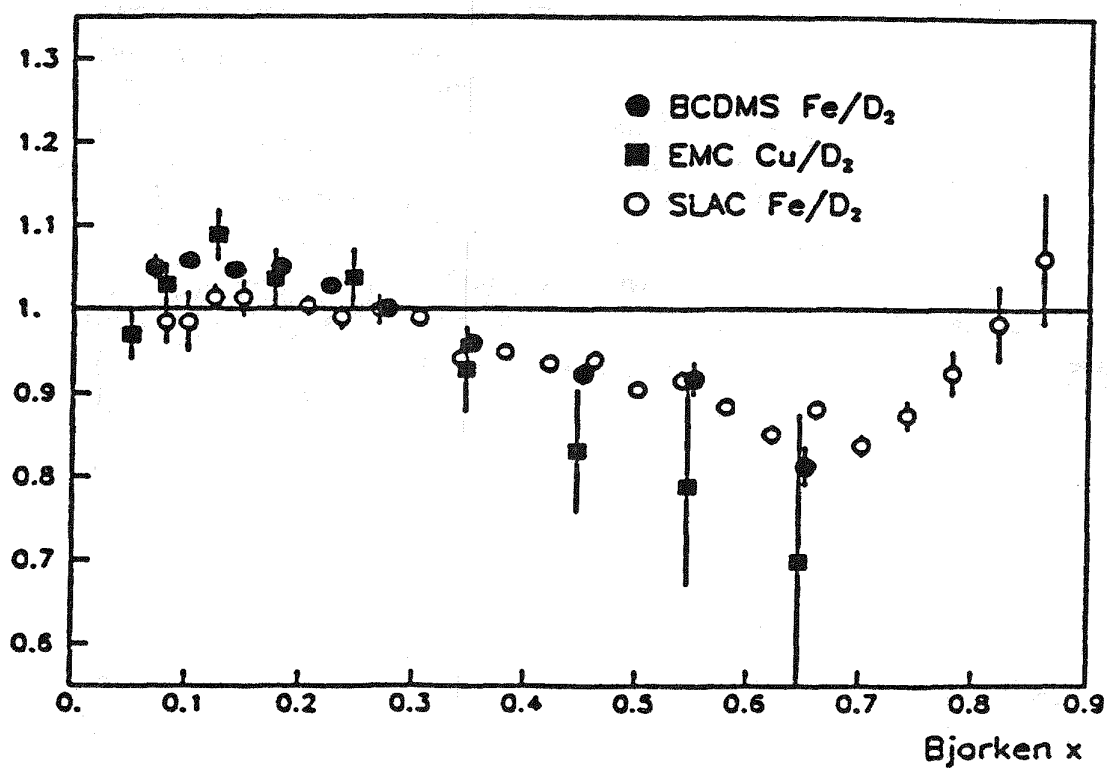

Fig. 1 Ratio of the structure function Fa(x) for Fe/D^2 from BCDMS and SLAC and for Cu/D^2 from EMC

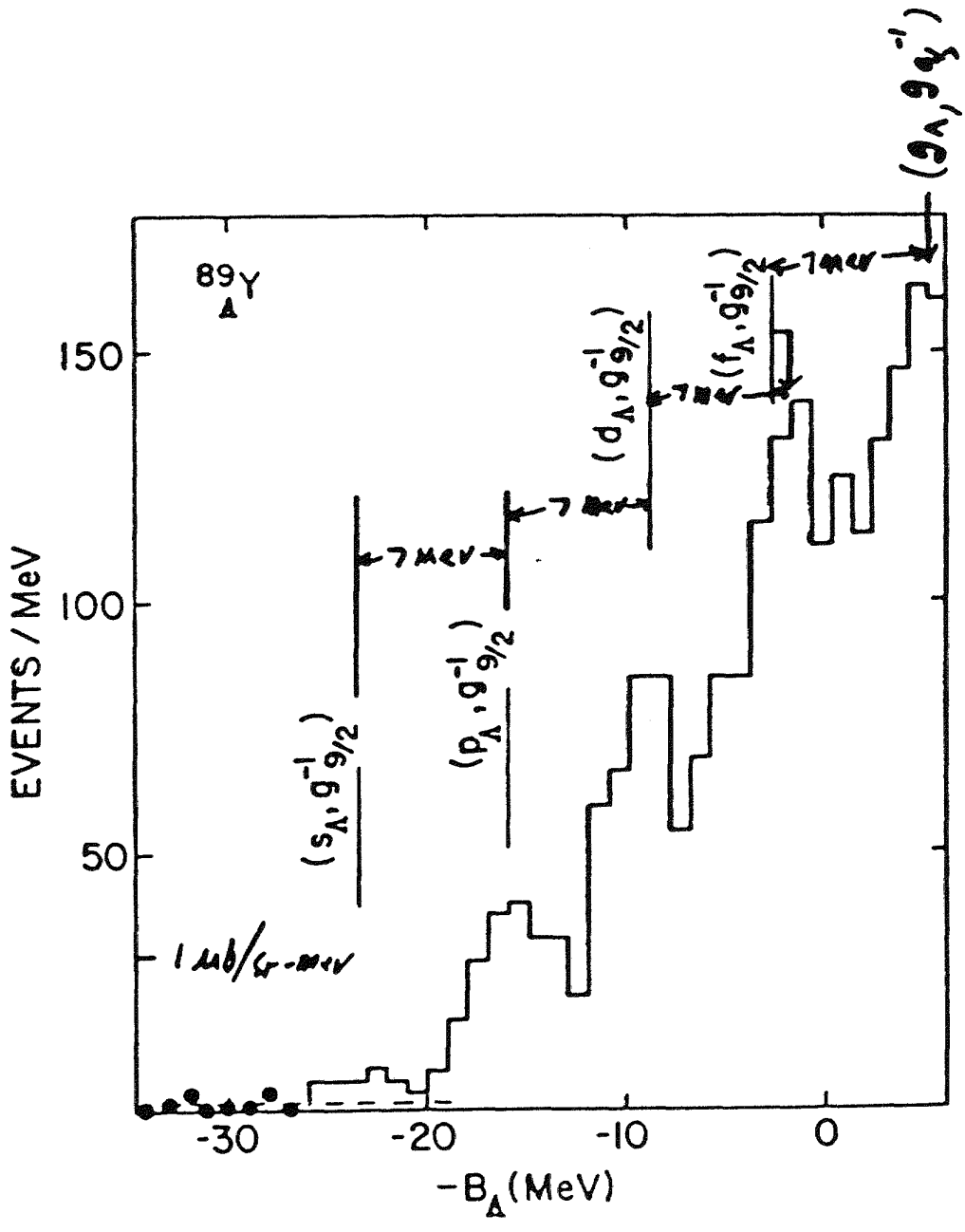

Fig. 2 Binding energies for ${}^{89}_{\Lambda}$Y states as derived from the (π^+, K^+) reaction on ^{89}Y in the Brookhaven experiment 798 (Preliminary data)

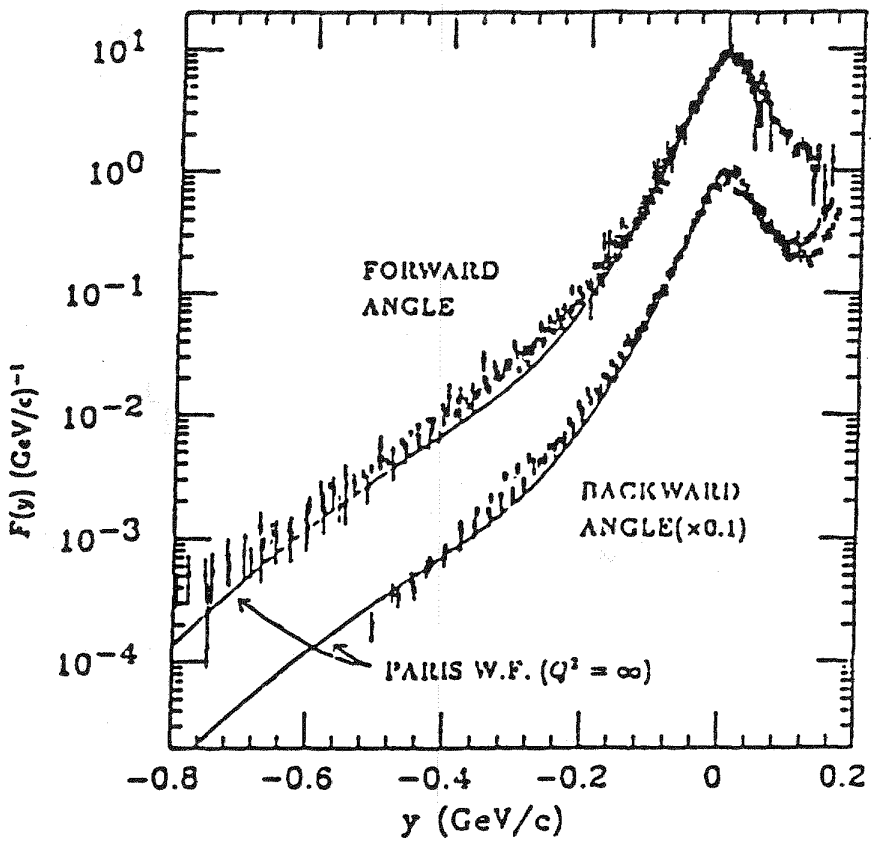

Fig. 3 Data from SLAC indicating that y scaling is valid for data taken at 180° as well as at very forward angles.

FORM FACTORS OF SIMPLE SYSTEMS

Richard Madey
Kent State University, Kent, OH 44242

ABSTRACT

The primary discussions at the Physics Collaboration Meetings on "Form Factors of Simple Systems" centered around three experiments to extract the electric form factor of the neutron. These three experiments and some of their principal features are described. The importance of the electric form factor of the neutron warrants measurements of this fundamental quantity by alternate methods.

INTRODUCTION

This report summarizes the Physics Collaboration Meetings on "Form Factors of Simple Systems". Discussions included the electric form factor of the neutron, the electric form factor of the proton, and electric and magnetic form factors of the deuteron, the triton, ^{3}He, and ^{4}He. Most interest centered around experiments for extracting the electric form factor of the neutron.

The electric form factor G_{En} of the neutron is a fundamental quantity needed for the understanding of both nucleon and nuclear structure. The dependence of G_{En} on Q^2, the square of the four-momentum transfer, is determined by the charge distribution of the neutron. Also the Q^2-dependence of G_{En} tests the spatial symmetry of the neutron wave function under quark permutation. The electric form factor G_{En} is small and poorly known for all Q^2 except $Q \approx 0$.

THE ELECTRIC FORM FACTOR OF THE NEUTRON

Three experiments to extract the electric form factor of the neutron are being planned at the present time. All three require a longitudinally-polarized electron beam; two use polarized targets (viz., ^{3}He and solid ND_3), and one uses an unpolarized liquid deuterium target and a neutron polarimeter. In the polarized-target experiments, the asymmetry in scattering is measured; in the unpolarized target experiment, the polarimeter measures the polarization of the outgoing neutron.

The experimental arrangement with the polarized ^{3}He gas target is sketched in Fig. 1. With the ^{3}He target placed in the large-acceptance-spectrometer (LAS), the scattering asymmetry is measured for polarizations of the incident electron beam parallel and antiparallel to the momentum of the electrons. This configuration takes advantage of the large solid angle available with the LAS. In preliminary design calculations, McKeown[1] estimates the following angular intervals can be used: $\Delta\phi \approx \pm 30°$, $15 \leq \theta$ (deg) ≤ 30, and $43 \leq \theta_q$ (deg) ≤ 30. Another advantage of this configuration is that a large range of Q^2 can be observed. A disadvantage of using the LAS is the low luminosity of typically 10^{33} cm^{-2} sec^{-1}.

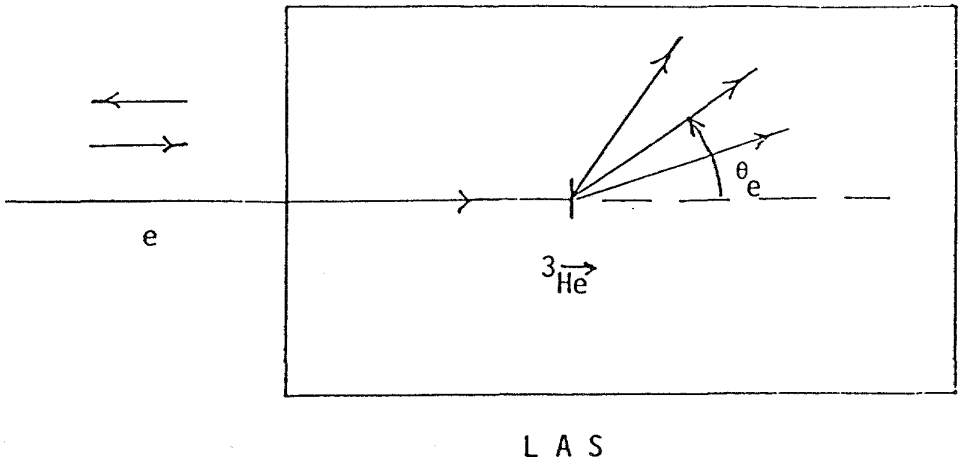

Fig. 1. Experimental arrangement with a polarized $^3\vec{He}$ target.

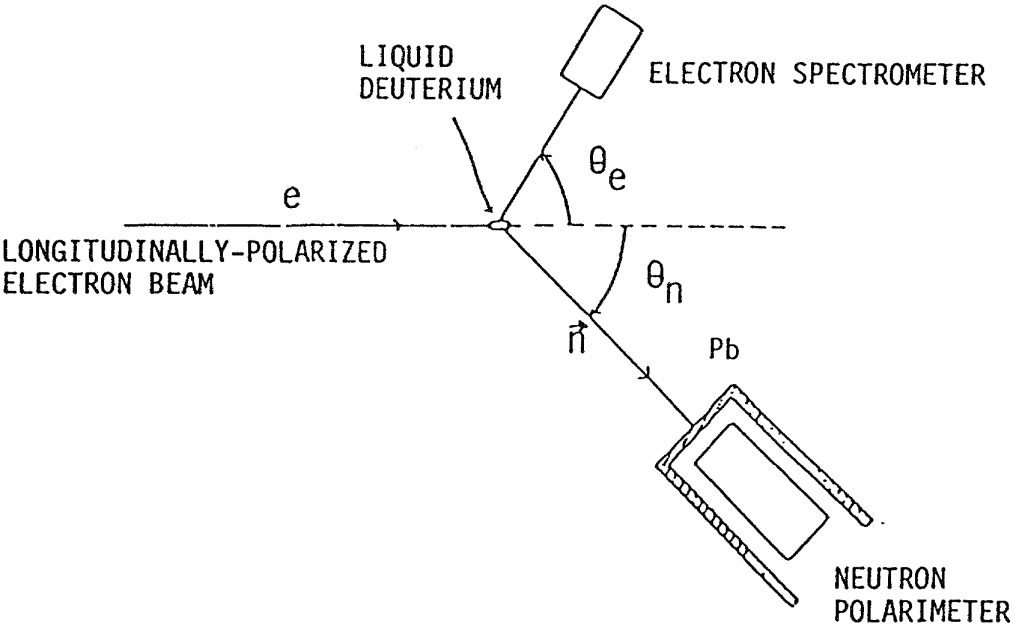

Fig. 2. Experimental arrangement with a D_2 target and polarimeter.

The group from California Institute of Technology is constructing the polarized ^3He target.

The experimental arrangement with a liquid deuterium target and a neutron polarimeter is shown in Fig. 2. A longitudinally-polarized electron beam is incident on a liquid-deuterium target. A neutron polarimeter measures the transverse polarization p_s, of the recoil neutron at an angle t_n after quasi-elastic scattering of the longitudinally-polarized electron from an unpolarized neutron in deuterium. A magnetic spectrometer measures the momentum of the electron scattered at an angle t_e. The electron is measured in coincidence with the recoil neutron.

By surrounding the neutron polarimeter with lead, the scintillation counters are protected from the gamma flash that occurs when the electron beam strikes the target. For neutrons above about 100 MeV, the mean-free-path is about 18.4 cm in lead. Lower-energy neutrons have shorter mean-free-paths. The neutron mean-free-path in lead (and in steel) are plotted in Fig. 3 as a function of neutron energy. The radiation length of a high-energy gamma ray is about 0.56 cm in Pb. Thus a solid Pb shield with a thickness of 12.75 cm would reduce the photon energy by a huge factor ($= 1.3 \times 10^{-10}$) to a value below the threshold of the detector, whereas the transmission of neutrons would be 0.50.

The Proceedings of the CEBAF 1984 Summer Workshop contains a description of the configuration, principle, properties, and performance of the neutron polarimeter developed at Kent State University (KSU).[2] A primary advantage of the polarimeter and unpolarized target arrangement is that high luminosities of the order of 5×10^{38} cm^{-2} sec^{-1} are possible. Such luminosities can be achieved either with the high-resolution-spectrometer (HRS) and a 10-cm long liquid deuterium target or with a medium-resolution-spectrometer (MRS) and a 20-cm long liquid deuterium target.

An experimental arrangement with a solid polarized deuterium target ($\vec{ND}_3$) and a neutron detector is sketched in Fig. 4. This experiment measures the asymmetry of the scattered neutrons in coincidence with scattered electrons. A lead shield can be used to protect the neutron detector from the gamma flash when the electron beam strikes the target. The lead shield attenuates the neutrons by a factor of about two. Shown ahead of the neutron detector in Fig. 4 is a medium-resolution spectrometer (MRS), which can be used to detect protons simultaneously. Thus, a primary advantage of this experimental arrangement is the ability to make simultaneous measurements of the asymmetry of neutrons and protons scattered from deuterium. Then by comparing the proton asymmetry measured from a deuterium target with that from a polarized $\vec{NH}_3$ target, it is possible to obtain a measure of the effect of the binding of the proton and the neutron in deuterium.

CONCLUSIONS

The following two conclusions were reached in the group discussions on "Form Factors of Simple Systems":

1. The importance of the electric form factor of the neutron warrants measurements of this fundamental quantity by alternate methods.

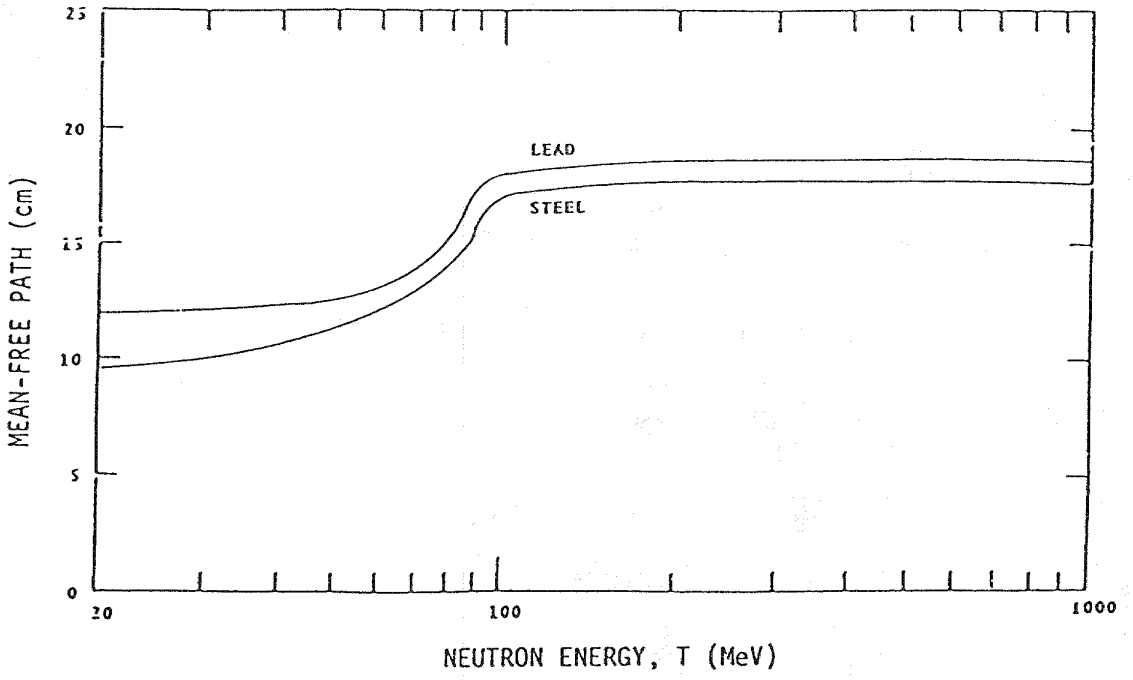

Fig. 3. Neutron mean-free paths.

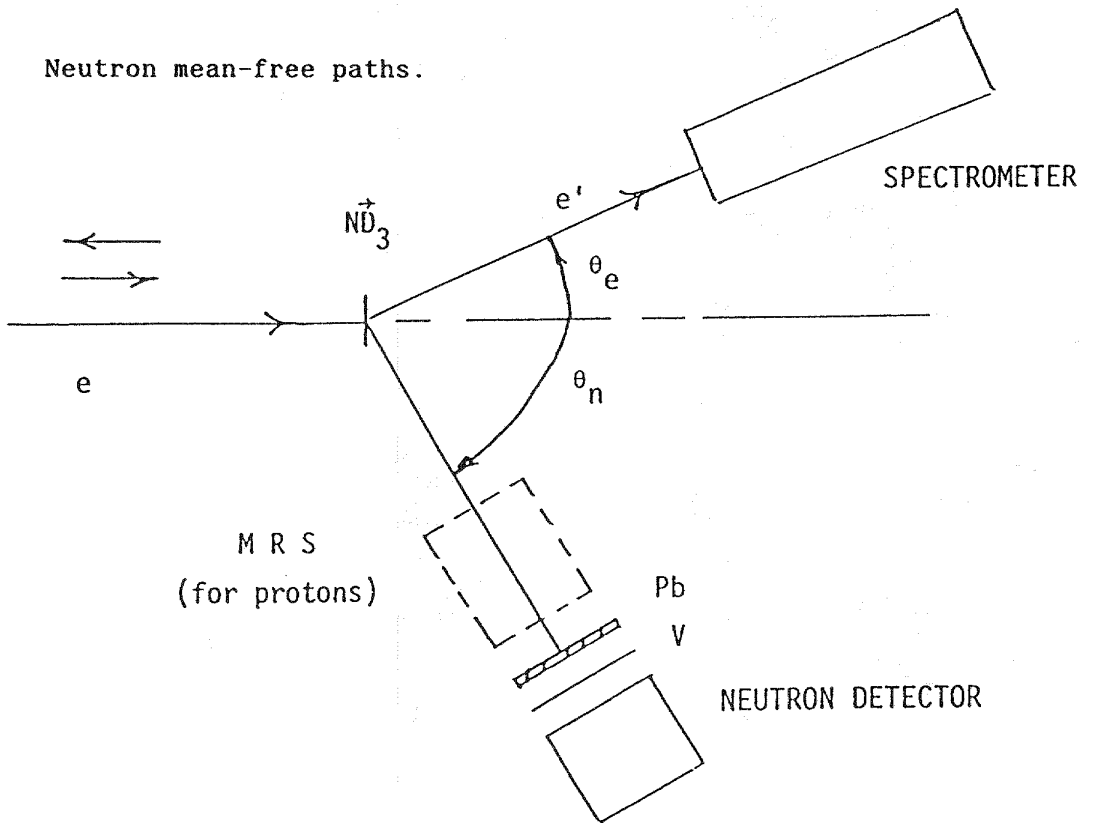

Fig. 4. Experimental arrangment with a polarized target and a neutron detector. A medium-resolution spectrometer (MRS) permits a simultaneous measurement of the proton asymmetry.

2. Preliminary proposals (or letters of intent) for measuring G_{En} by the three methods described here will be prepared and submitted to CEBAF:

Experiment	Preparer
$^3\vec{He}$ + LAS	R. McKeown, California Institute of Technology
$\vec{ND}_3$ + Neut Detector	J. McCarthy, University of Virginia
D_2 + Polarimeter	R. Madey, Kent State University

REFERENCES

1. R. McKeown, Private Communication.

2. R. Madey, J.W. Watson, B.D. Anderson, A.R. Baldwin, and P.J. Pella, Proc. CEBAF 1985 Summer Workshop, eds. H. Crannell and F. Gross, CEBAF, Newport News, VA (1985) pp 290-314.

SUMMARY - (e,e'2N) AND MULTIHADRON REACTIONS

J.W. Lightbody Jr.
National Bureau of Standards
Gaithersburg, MD 20899

In this report I attempt to summarize the activities of the (e,e'2N) and Multihadron Reaction Working Group co-chaired by B. Mecking and myself. The subject of this work is one of the higher priority core programs at CEBAF. The group addressed specific experimental research proposals using the LAS and conventional spectrometers proposed for CEBAF. Figure 1 gives a list of the participants in this working group and also a list of those talks presented at our meetings. In this summary, we have selected for discussion only a few of the talks as representative of current thinking.

Multihadron knockout is a new field of study for most of us in electromagnetic nuclear physics, made possible by the advent of cw accelerators, and made interesting by the high energy beam capability to be provided at CEBAF. High energy and momentum transfers provide a means to study short range cooperative phenomena and reaction mechanisms involving several nucleons. This thought is central to current interest in nuclear physics because we do not yet understand the explicit dynamics of interacting nucleons in the nuclear medium, the role of many-body forces, or the extent to which quark degrees of freedom are manifest. There remains the issue of whether phenomena in our energy domain (several GeV) can be described by using the currently accepted picture of free, non-static nucleons interacting via π, ρ, and ω meson exchange, or whether the quarks in nucleons suffer partial deconfinement (modified nucleons) in the nuclear medium, in which case extrapolation of our understanding of on-shell phenomena introduces substantial uncertainty in our understanding of many-body systems. To what extent is this latter deconfinement concept related to the presence of 3-, 6-, 9-,$\cdots$, 3N-quark bag components in the nuclear many-body wave function ?

In order to probe deeper into these issues we must look at multi-hadron final states. For this reason the LAS facility and a conventional spectrometer set-up with at least three spectrometers on a common pivot are essential. The LAS detector is important in order to make a survey of what type and level of multi-particle correlations exist. In addition, detection of more than two hadrons in the final state using conventional magnetic spectrometers gives unacceptably low rates. However, since we expect that there will be some level of

correlation in the case of pairs of ejected nucleons, from kinematic focus arguments alone, we must also be prepared to make measurements in a much more restricted kinematic range, where we can suppress the possibly paralyzing torrent of single hadron events or other backgrounds. For this purpose a conventional large acceptance spectrometer set-up is also essential. There are differences of opinion at this time regarding the values of the conventional spectrometer acceptances (both momentum and solid angle), the degree of kinematic flexibility that they provide in terms of scattering angle range and out-of-plane angular range, and the extent to which high resolution spectrometers are important.

The beginning organizational discussion touched on several interesting questions. First, the LAS detector is to be used as an electron-hadron coincidence facility. In order to function properly a shower counter will most certainly be required in the electron detector. Then, in order to realize the proposed counting rate gains of the LAS over conventional spectrometers, the electron detector must have full 360° coverage about the beam direction, not just a small sector. In addition, interest was expressed in having electron detection capability within the 15° electron scattering cone called for in the current planning. (e,e'2N) counting rates, even for the LAS facility, will be very low unless we can operate in the far forward cone. This latter point is not a new thought and earlier discussions focussed on the need for a specialized forward angle electron detector. Although these capabilities are planned, budgetary constraints may compromise their realization. Such an action would be contrary to the strong initial motivation for the LAS.

Another aspect of the LAS facility planning concerns the photon tagging system. In view of the PAC review of the core CEBAF physics program, it is not clear that the tagger should be built first, or the extended electron detector mentioned above. Little emphasis was placed on tagger experiments in the PAC report, and a great deal of emphasis was placed on the LAS electron detection capability and extending the upper-end luminosity with which the LAS can be used. It would, therefore, seem logical for the laboratory to place highest priority on completing the full electron detection system.

Many of us are going to be relying heavily on successful operation of the LAS and extending the LAS operating luminosity to of order 10X that of the LAME detector, also referred to as the 'existence-proof' facility, constructed at Cornell ($L=2.4\times10^{32}$ $cm^{-2}sec^{-1}$).

Great effort and attention must be assigned to this endeavor. Just as a strong part of the raison-d'etre for having a 4-GeV, high resolution spectrometer was to match the raw beam properties, we need to have a device capable of exploiting the cw character of the beam. This is one of the primary motivations behind CEBAF - to be able to make coincidence measurements with multi-particle final states. Some thought should be given to providing insurance against the prospect of the LAS not operating at high luminosity. This means that triple spectrometers with large acceptances and great kinematic flexibility (both in- and out-of-plane) on a single pivot should be provided early in the CEBAF operating schedule. Obviously, such a system must have another very strong motivation. We already discussed this above. This type of set-up is used when one wishes to examine a very specific part of the overall multi-hadron phase space, which may be revealed as interesting in a LAS survey experiment.

Before turning to a brief description of the talks presented at our meetings, let me make one final remark of the overview type concerning experiments with the LAS. Hopefully, this will not be taken as a gratuitous remark. How does one compare data with theory ? Generally, theorists will make a calculation, or series of calculations, with well defined kinematics. Data will then be placed on these curves, comparisons made, and conclusions drawn. The virtue of the LAS is that data will be collected simultaneously at many angles. This feature supposedly makes up for the low luminosity employed in the LAS compared to a spectrometer set-up (perhaps a factor 10^4 lower). What then does one do with low statistical precision data in comparing to theory computed at a few well defined scattering and reaction plane angles ? It would appear that we need a global way of looking at the entire experimental phase space and comparing this to theory. I don't know how to do this, and think that some thought should be given to this question before drawing conclusions about the relative merits of using the LAS and conventional magnetic spectrometers in multihadron studies.

We turn now to discussion of several of the talks (indicated by asterisks in figure 1) presented at our meeting. Richard Sealock of the UVA group presented his ideas about using the LAS to perform a survey type (e,e') experiment such as the recent NPAS experiment NE5, which looked at the quasifree knockout, dip, and Δ-resonance regions and focusses on y-scaling and A-dependence of the response functions. Figure 2 shows preliminary results for the $^{12}C(e,e')$ cross sections for differing primary beam energies, at the same scattering angle. The data

have not been radiatively corrected. These data show the substantial variation in form factors across the region spanning the QF and Δ-peaks. Figure 3 draws a comparison between the running time for the SLAC 1.6 GeV spectrometer used in NE5, and the LAS, using exactly the same kinematic range. The NE5 vertical acceptance is replaced by the full cone of revolution in the LAS. This accounts for a gain in LAS of a factor of 50 in rate. We achieve another factor of 13 because the LAS covers the entire momentum range of interest in one field setting rather than the 13 used in NE5. The net result is that the two systems require essentially the same running time. With a more extensive electron detection capability, LAS could take an enormously larger θ range than the 34 mrad used here. Also the LAS luminosity was assumed to be the same as that achieved at Cornell's LAME detector set-up. It is hoped that at least an order of magnitude increase in this upper-end luminosity can be achieved at CEBAF. Much more detailed single arm (e,e') survey experiments than those performed at NPAS will therefore be achievable. Of course, at the same time we will be able to examine the partial channels that make up the inclusive results, including their energy and angular distributions. Considering that months of NPAS beam time are involved in the relatively sparse data that we have on hand now, in the same time frame at CEBAF we shall be able to complete a vastly more detailed survey including Rosenbluth separations and exclusive partial channel decompositions.

The next subject is two-nucleon emission (which I addressed in our meetings). Figure 4 shows further NPAS (e,e') data. These data for ^{4}He were provided by Donal Day, also of the UVA group. The feature of this figure which I wish to focus on is the apparent break in the data near X=2. If 6-quark bags exist in the nuclear ground state, as suggested by Pirner and Vary and others, one manifestation would be a quasielastic scattering response at precisely X=2. Alternatively, this same tail on the response function may be due to complex, short range NN correlations which introduce high momentum components into the one-body momentum distribution. No explicit calculations of one-body momentum distributions can reproduce this feature. Data is needed in the (e,e'N) and (e,e'2N) channels to help examine the question if one or two nucleons are involved in this region of the response function.

Figure 5 shows results of a calculation by Laget (see contribution to these Proceedings by J.M. Laget) of the ^{3}He(e,e'2N) reaction at CEBAF energies. The longitudinal 2p cross section (dashed curve) represents the contribution to the total (e,e'2p) cross section from

ground state correlations. These effects are obviously masked by final state and MEC effects which bring the dashed curve up to the solid curve. The 90° cm cross section is important because it is least sensitive to rescattering effects. These cross sections are small (of order picobarns) and even with the planned CEBAF magnetic spectrometers, rates on the order of 10-100 counts per hour are what we can achieve with luminosities of order 10^{36}. In order to achieve some level of confidence in calculations, data should be taken spanning the entire energy loss region shown, where there is a transition from more sensitivity to final state interactions at lower energy loss, to a sensitivity more to initial state correlations at larger energy loss.

Figure 6 reminds us of an important point relating to kinematic flexibility. In order to span the energy loss range indicated in figure 5, we see that there is a region where magnetic spectrometers will mechanically overlap. The sausage shaped curves represent the position of the two proton spectrometers, and are taken to have the same angular width as the electron spectrometer. In-plane measurements are precluded in the 200 to 600 MeV energy loss range (for 90° cm angle) and we must have out-of-plane capability if we are to study this region at all. This same out-of-plane capability will also make it possible to disentangle the longitudinal part of the cross section, which is the most sensitive to correlation effects. From Laget's work the TT interference term is very nearly equal to the direct transverse term. This makes isolation of the direct longitudinal cross section practical without resort to Rosenbluth separations, a very important point considering how fast counting rates fall off with scattering angle.

We have discussed to some extent (e,e'), (e,e'N), and (e,e'2N) reactions. We turn now to possible photoreaction studies in hypernuclear physics. The reaction $\gamma+p \Rightarrow K^{+}+\Lambda$ is the basic process in such hypernuclei reaction studies. Louis Wright of Ohio University discussed some of his work relating to lambda polarization. It turns out that the elementary production operator contains several rather poorly determined coupling constants. Figure 7 indicates some of relevant points. From the known properties of the weak lambda decay one can write down the form of the angular distribution of decay protons (shown in figure 7). By measuring the proton distribution above and below the γ-K reaction plane, one can then determine the lambda production polarization (P). Figure 8 indicates the status of present data for P. The curves represent various background and pole terms in the production

process. The data clearly do not provide overwhelming evidence for or against the various models indicated. It would clearly be important to have a better understanding of this process if hypernuclear studies are to make significant new advancements. The reason that we discussed this reaction in the context of multihadron final states is that K-p coincidence measurements are required in such studies.

In a related study, Greg Franklin of Carnegie-Mellon discussed the photo-production of strange dibaryons. In contrast to the fundamental process discussed above where one starts with protons, starting with deuterons one can examine the process where a lambda produced on the proton interacts with the neutron to form a strangeness (S)=-1 dibaryon. This is indicated in figure 9. The dibaryon mass spectrum shown in figure 10 indicates two dibaryon masses at roughly 2100 and 2150 MeV expected based on model calculations. There is some evidence for at least one such state in $K^-+d \Rightarrow \pi^-+(\Lambda p)$ data. This is shown in figure 11. In particular, the small excess cross section near a cm energy of 2140 MeV. The shape and position of the 'cusp' peak at 2125 MeV is reasonably well understood. Its cm angular distribution shown at the bottom of figure 10 is also understood. The excess cross section at 2140 MeV is not understood, nor is the angular distribution understood, and this is the reason for making a high precision study in the photoproduction channel.

The last subject we have singled out is $(e,e'\pi N)$ reactions at CEBAF. Paul Stoler of the RPI group discussed this subject in the context of Δ-resonance production, propagation, and decay. The point of this work was to draw a comparison of counting rates obtained for the $^4He(e,e'\pi p)$ reaction using the different CEBAF facilities, with a 2.5 GeV beam and electron scattering angle of 14°. The experimental conditions for the different set-ups are given in figure 12. The results of this comparison are shown in figure 13. The reaction considered is the quasi-free process, hence there is a strong kinematic correlation between the pion and nucleon. The case for the VAS type spectrometers in this type of reaction study is very strong. Stoler drew the same conclusion asserted earlier, that for 3 or more charged hadrons ($\pi\pi N$ from N^* decay, for example), the LAS has great advantage over any of the conventional spectrometer set-ups. For very specific one- or two-hadron final states such as the Δ-decay, VAS type systems are much more efficient than the LAS.

In conclusion, a number of very interesting experiments have been proposed in the multihadron area.

The important issues concern which facilities are best suited to the proposed experiments. Luminosity limitations for the LAS weigh heavily in this concern. Also, highly correlated final states are probably best addressed by conventional spectrometer set-ups. A forward angle electron spectrometer appears to be essential for the LAS and should be given a high priority in order to pursue even survey multihadron reaction studies. Large out-of-plane angles are important to the multihadron studies. When there is strong correlation between pairs of hadrons, for example the (e,e'2p) studies, large out-of-plane angles for the separate spectrometers are essential. Finally, neutron detection remains an important part of the multihadron program, and heavy emphasis should be placed on development of suitable neutron detectors, be they recoil type or time-of-flight devices. As with the LAS, luminosity limitations to the neutron detectors should be carefully studied.

LIST OF PARTICIPANTS

(e,e'NN) and Multihadron Emission Working Group

J. Arends
D. Beck
B. Berman
W. Bertozzi
C. Bingham
W. Boeglin
P. Bosted
G. Chang
L. Dennis
J. Domingo
D. Doughty
K. Egijan
R. Eisenstein
M. Finn
G. Franklin
J. Heisenberg
J. Jourdan
E. Klempt
S. Krewald
J. Lightbody
R. Lindgren
R. Lourie
P. Martin
R. McKeown
B. Mecking
R. Minehart
R. Miskimen
S. Nanda
C. Papanicolas
C. Perdrisat
G. Peterson
R. Robinson
R. Sealock
P. Stoler
G. Tamas
M. Tannenbaum
S. Thornton
P. Ulmer
R. Varner
T. Walcher
C. Williamson
L. Wright

LIST OF TALKS

J. Arends: Large Acceptance Detectors at ELSA

G. Chang: Hadronic Final States in Deep Inelastic Scattering

J.M. Finn: (e,e'p) and Two-body Currents

G. Franklin: Search for Strange Dibaryons (*)

E. Klempt: Search for New Particles

R. Minehart: Nuclear Physics at PEP

R. Sealock: Electroproduction of δ's in Nuclei (*)

P. Stoler: (e,e'πN) in the δ-Region (*)

L. Wright: Hyperon Photoproduction (*)

J. Lightbody: (e,e'NN) Experimental Problems (*)

G. Tamas: Saclay Large Acceptance Detector

FIGURE 1

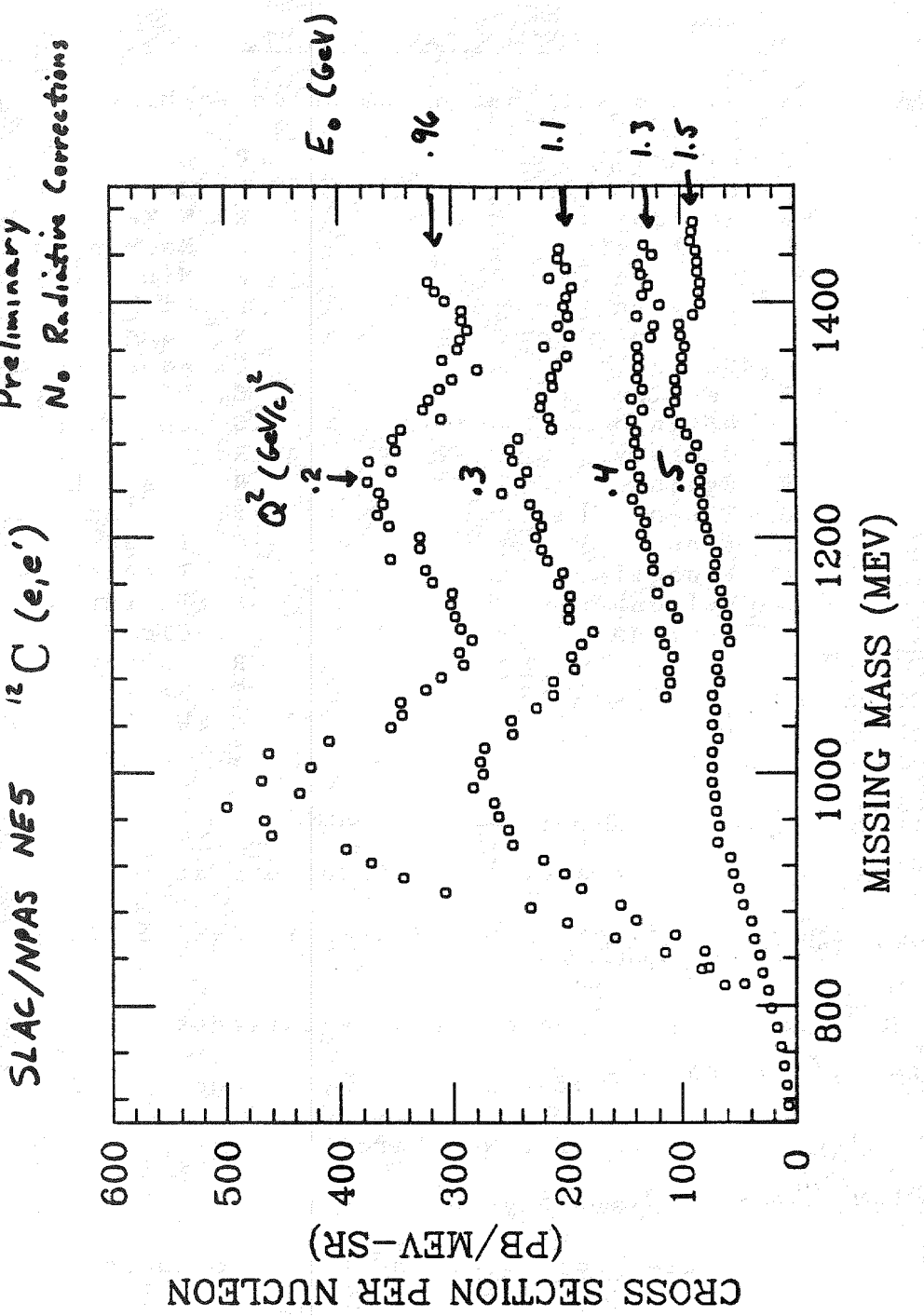
SLAC/NPAS NES
^{12}C (e,e')
Preliminary
No Radiative Corrections
E_0 (GeV)
.96
1.1
1.3
1.5
Q^2 (GeV/c)^2
.2
.3
.4
.5
CROSS SECTION PER NUCLEON
(PB/MEV-SR)
MISSING MASS (MEV)
0
100
200
300
400
500
600
800
1000
1200
1400

FIGURE 2

^{12}C at $E_0 = 1.1$ GeV

$\theta = 37.5°$, $\Delta\theta = 34$ mrad

momentum range 300 – 1000 MeV/c

	NES	LAS
luminosity ($cm^{-2}s^{-1}$)	2.4×10^{35}	3×10^{32}
$d\Omega$ (msr)	2	104
momentum settings	13	1
count rate (H_z)	20	18
run time (hrs)	6	6

FIGURE 3

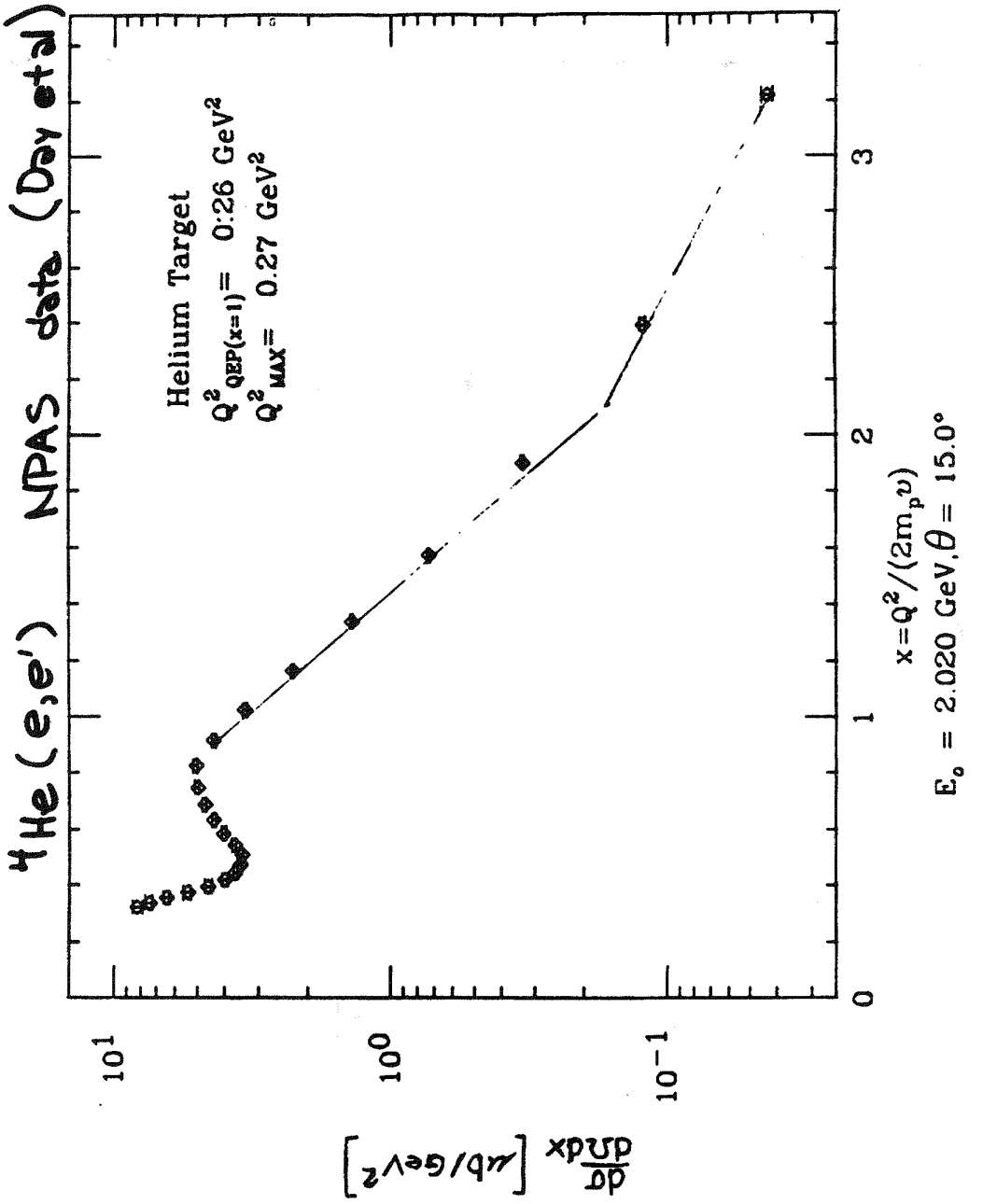
4He (e,e') NPAS data (Day et al)
Helium Target
$Q^2_{QEP(x=1)}$ = 0.26 GeV^2
Q^2_{MAX} = 0.27 GeV^2
E_o = 2.020 GeV, θ = 15.0°
$x = Q^2/(2m_p\nu)$
$\frac{d\sigma}{dnd x}$ [nb/gev^2]
10^1
10^0
10^{-1}
0
1
2
3

FIGURE 4

Laget calculation: (J.M. Laget, PR C35, 832 (1987))

$$\frac{d\sigma}{d\Omega_e dE_e dp_1 d\Omega_1 d\Omega_2} = \Gamma_v \left[\frac{p_1^2 p_2}{E_1}\left(\frac{Q}{P}\right)_{cm}\right] \times \left\{\sigma^T + \epsilon\sigma^L + \epsilon\sigma^{TT}\cos 2\phi + f(\epsilon)\sigma^{LT}\cos\phi\right\}$$

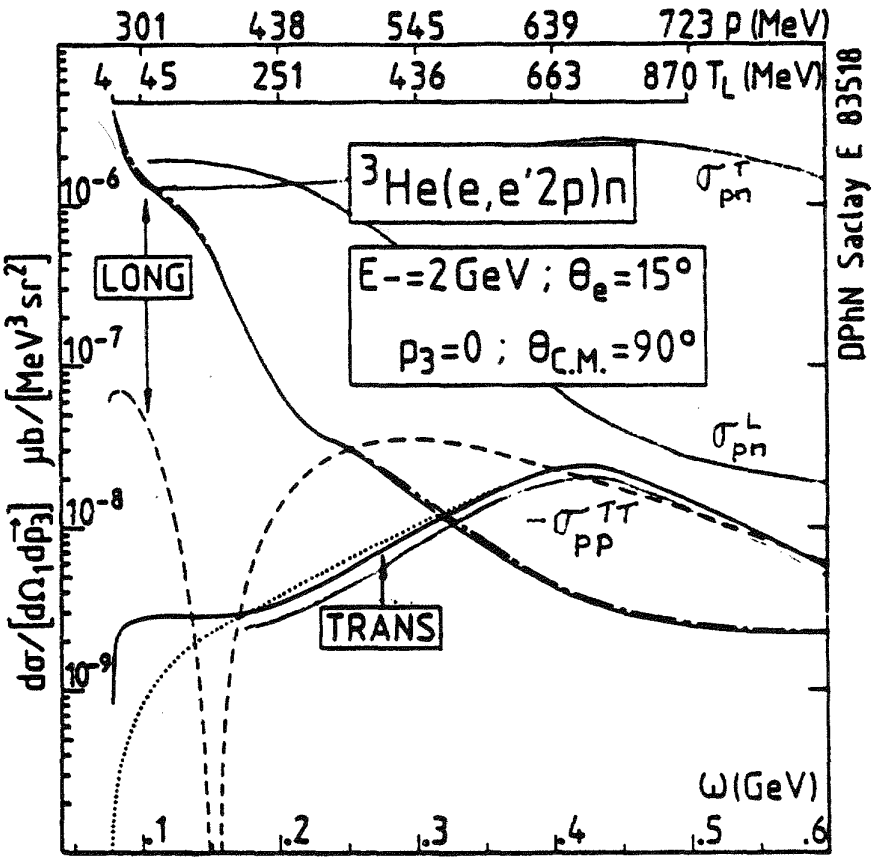

(---) PW
(·····) PW + MEC
(-·-·-) PW+MEC+pp rescatter.
(——) PW+MEC+all rescatter.

FIGURE 5

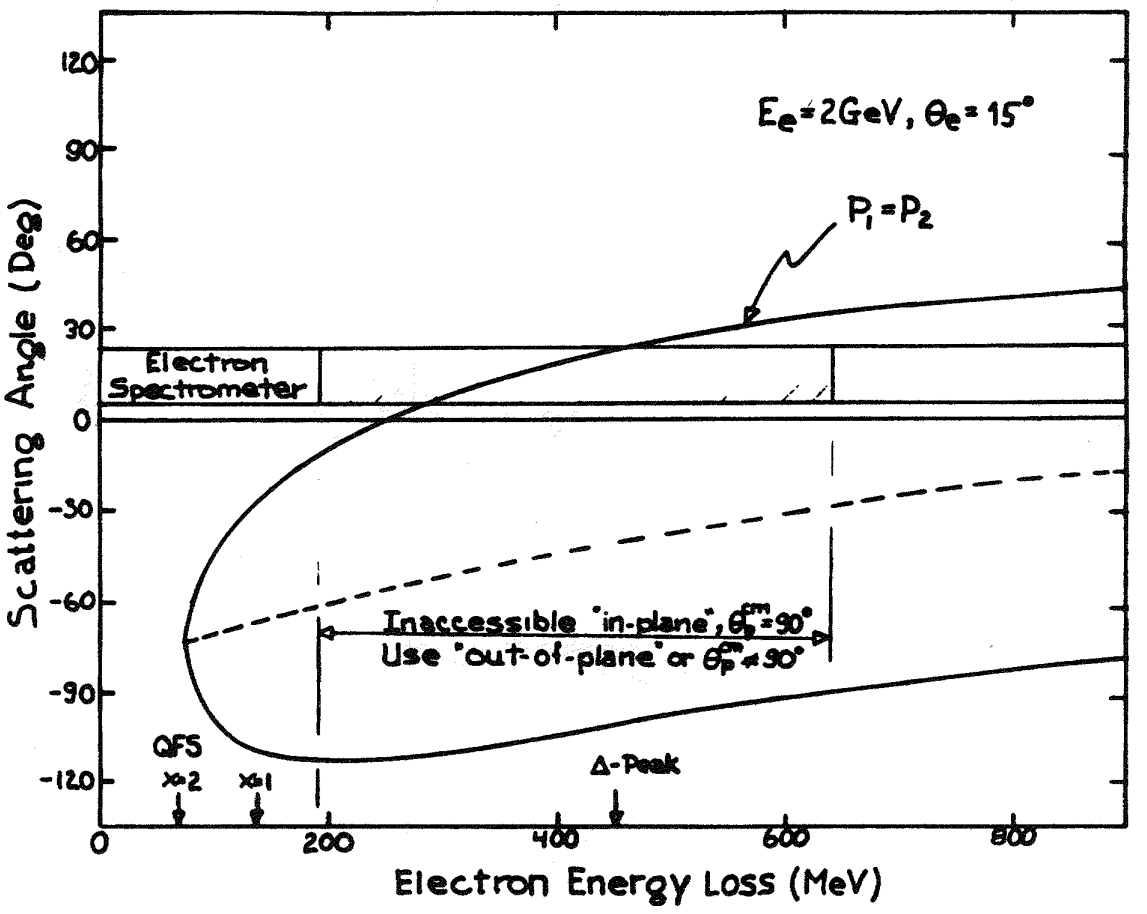
E_e=2GeV, θ_e=15°
$P_1=P_2$
Electron Spectrometer
Inaccessible "in-plane", θ_p^{cm}=90°
Use "out-of-plane" or $\theta_p^{cm}\neq$90°
QFS
x=2
x=1
Δ-Peak
Scattering Angle (Deg)
Electron Energy Loss (MeV)
120
90
60
30
0
-30
-60
-90
-120
0
200
400
600
800

FIGURE 6

Λ - Polarization in $\gamma + p \to K^+ + \Lambda^\circ$

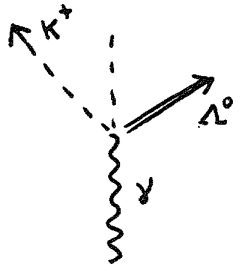

1. Polarization must be along $\hat{P}_\gamma \times \hat{P}_K$ since parity is conserved in the production process.

2. Λ°-decay

$$\Lambda^\circ \to \begin{cases} p + \pi^- & 64.2\% \\ n + \pi^\circ & 35.8\% \end{cases}$$

($\Delta I = 1/2$ or minimal violation of isospin rule.)

Λ° has spin $1/2$ $\therefore$ in its rest frame p and π^- have relative s and p waves. and since the decay violates parity conservation they interfere.

It follows that the angular distribution of the decay protons is

$$dN(\theta) = \frac{N}{4\pi}\left(1 + \alpha P \cos\theta\right) d\Omega$$

where α = s-p interference $= 0.642 \pm 0.014$

$$\cos\theta = \hat{P}_p \cdot \left(\hat{P_\gamma \times P_K}\right)$$

N = # of protons

$\therefore$ By measuring N above and below the production plane, one can find αP.

In Λ rest frame

$$\alpha P \sin\beta = \frac{N_{above} - N_{below}}{N_{above} + N_{below}}$$

β = $\measuredangle$ above the production plane

FIGURE 7

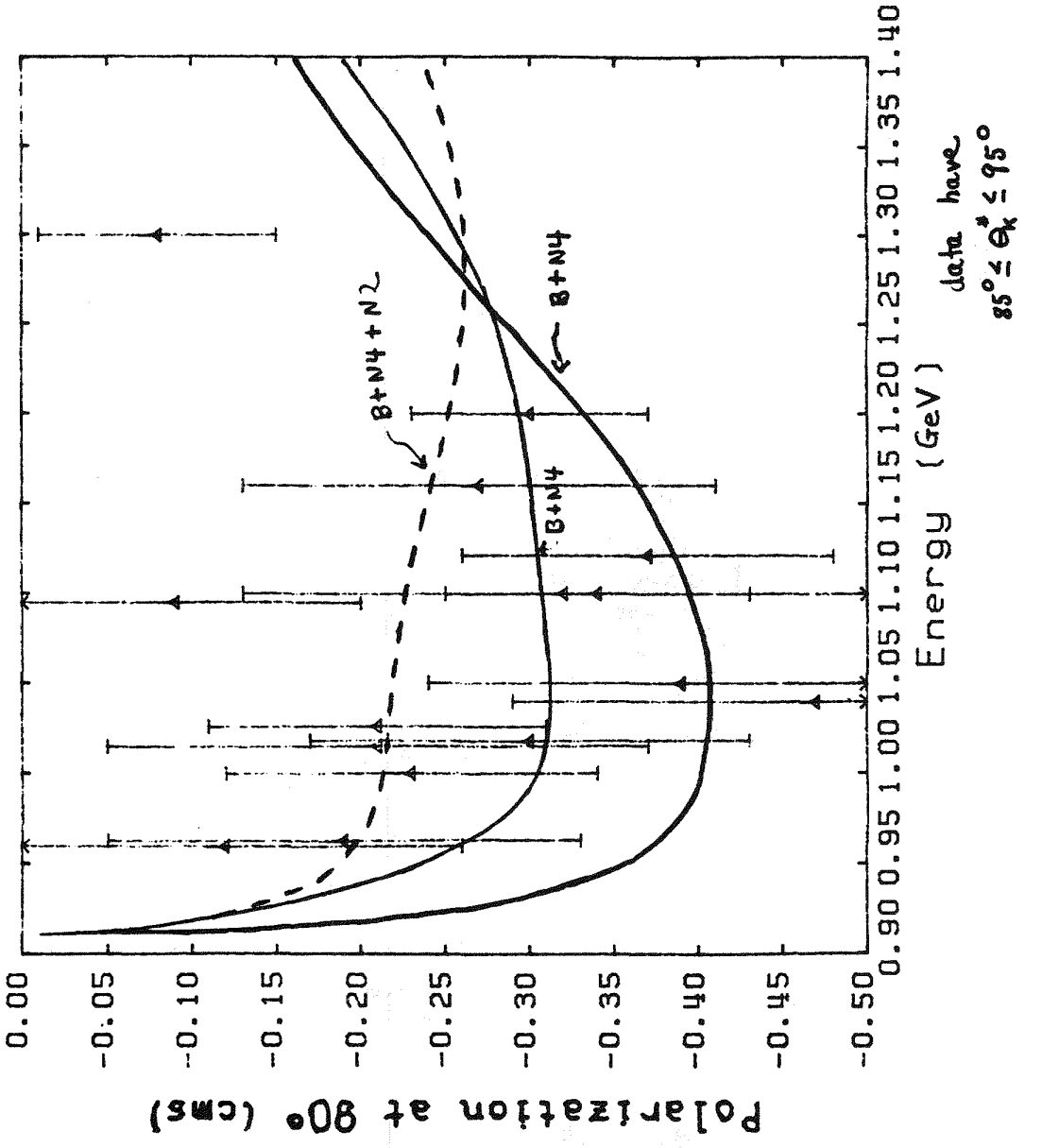
Polarization at 90° (cms)
0.00
-0.05
-0.10
-0.15
-0.20
-0.25
-0.30
-0.35
-0.40
-0.45
-0.50
0.90 0.95 1.00 1.05 1.10 1.15 1.20 1.25 1.30 1.35 1.40
Energy (GeV)
data have
$85° \leq \theta_k^* \leq 95°$
B+N4+N2
B+N4
B+N4

FIGURE 8

Kaon Experiments at CEBAF

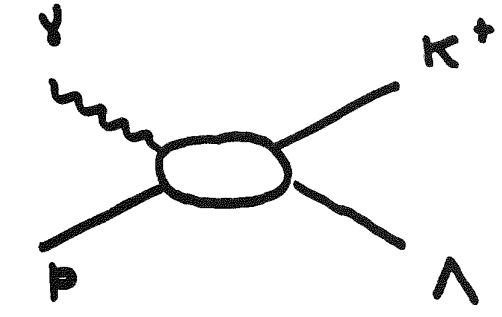

; Interaction vertex includes kaon pole term, and various resonance terms ...

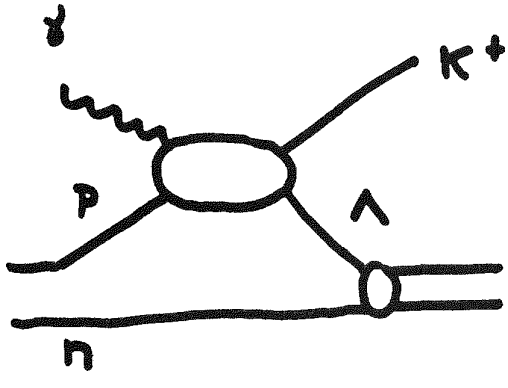

; Strange dibaryons

FIGURE 9

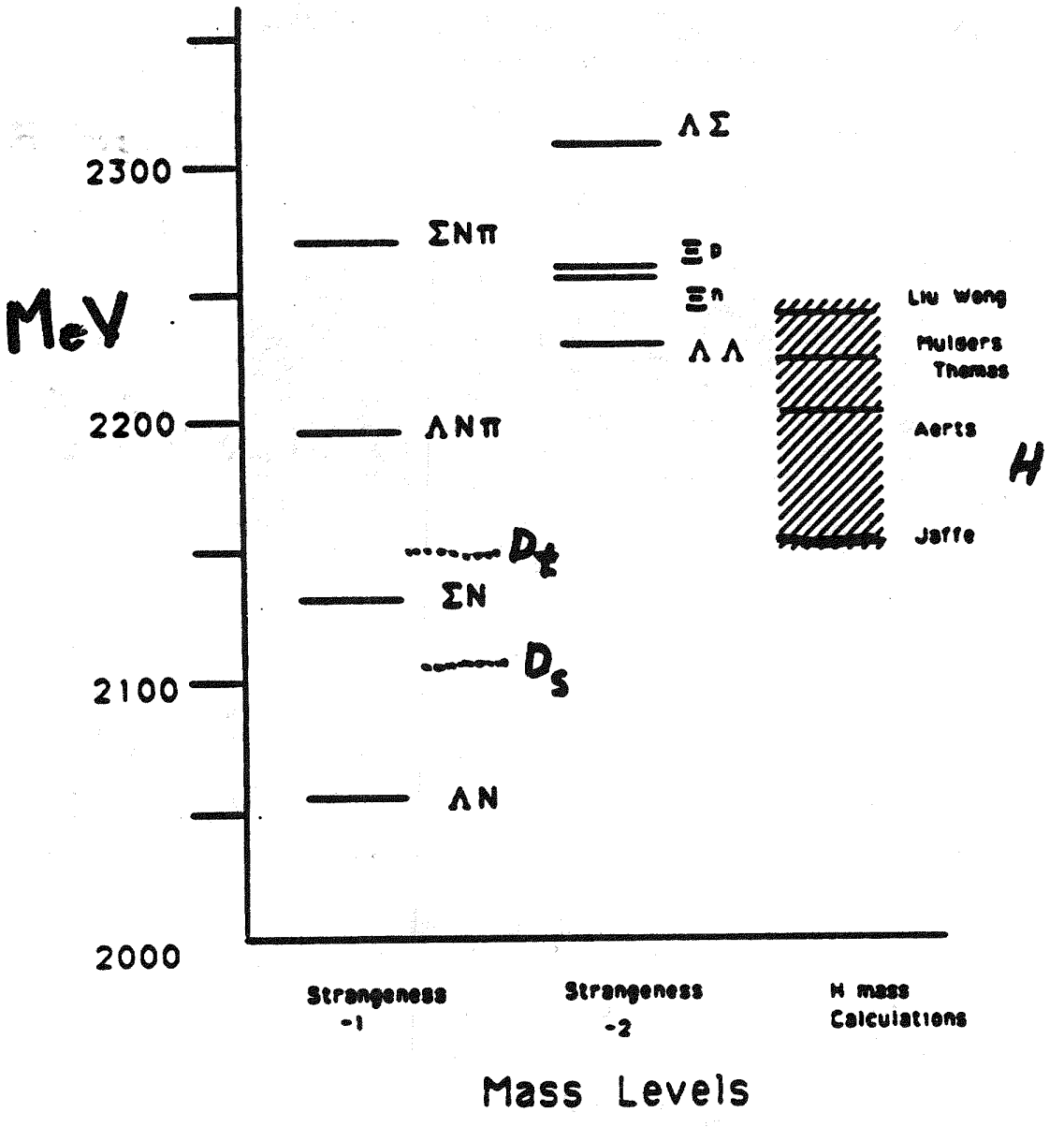

Mass Levels

FIGURE 10

S = -1 $K^- + d \rightarrow \pi^- + (\Lambda p)$

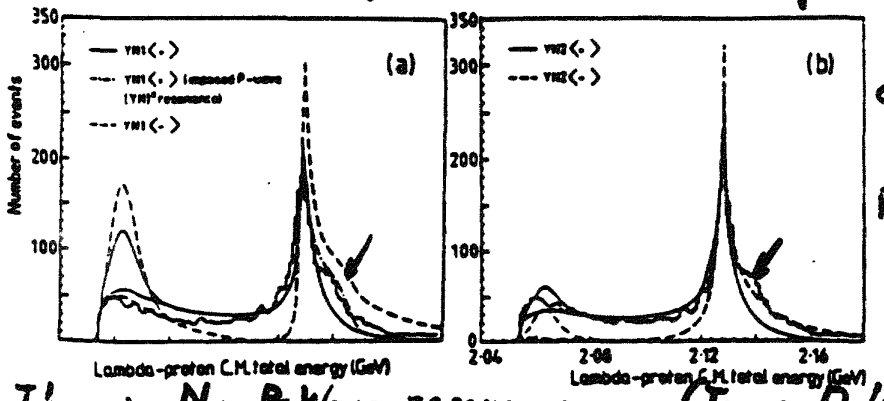

Stopped K^-

Data: Tan

Theory: No P-Wave resonance. (Torres, Dalitz, Deloff)

Fig. 1. The m(Λp) spectra for the models YN1<-> and YN2<-> are compared with the data of Tan[1]. Below 2080 Mev, the lower branch of each curve gives the rate when only events with proton recoil momenta ≥ 75 Mev/c are counted. The effect of an imposed YN resonance is shown for YN1<->.

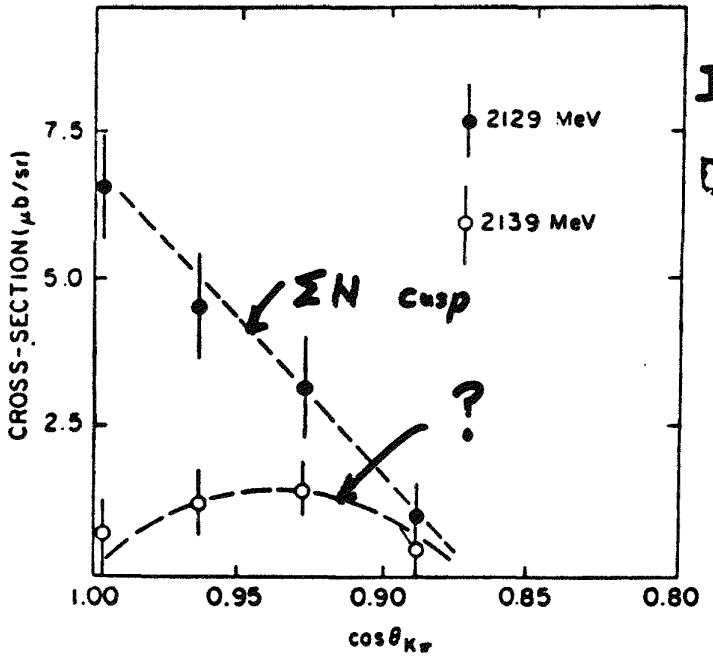

In flight

Data: Pickup et al

D_T ?

FIGURE 11

SPECTROMETER CHARACTERISTICS

VAS

$\Omega_e = 10$ msr $\quad \Omega_\pi = \Omega_p = 40$ msr

$l_\pi = 6$ m

$I_e = 7\,\mu A \quad X_{TGT} = 10$ cm

$L = 2 \times 10^{37}$

LAD

$L = 1 \times 10^{33}$

$\epsilon_\pi = .73 \quad \epsilon_p = .62$

HALL A

$\Omega_e = \Omega_H = 10$ msr $\quad l_H = 18$ m

$\Omega_{H2} = 40$ msr $\quad l_{H2} = 6$ m

$L = 2 \times 10^{37}$

FIGURE 12

$^4He(e\,e'p\pi^-)X$ QUASIFREE

M-C FREE FERMI GAS

PION F S I

VAS $\dot{N}_\pi = 1.8 \times 10^4$ /hr

$\dot{N}_{\pi p} = 1 \times 10^3$ /hr

LAD $\dot{N}_\pi = 1$ /hr

$\dot{N}_{\pi p} = 1$ / 20 hrs

$\Phi_e = 2\pi$ $\dot{N}_{\pi p} = 3$ /hr

$\Phi_\pi = 2\pi$ $\dot{N}_{\pi p} = 100$ /hr

9 FOC. PL. $\dot{N}_{\pi p} = 1 \times 10^3$ /hr

HALL A $\dot{N}_\pi = 1 \times 10^3$ /hr

$\dot{N}_{\pi p} = 100$ / hr

FIGURE 13

The (e,e'N) Program at CEBAF: A Summary of (e,e'N) Working Group Meetings

John M. Finn
Department of Physics
College of William and Mary
Williamsburg, VA 23185

ABSTRACT

The (e,e'N) program meetings drew strong user participation and the discussions were intellectually vigorous. A consensus was reached calling for a broad based program of studies covering the kinematical domain of the CEBAF facility. Working groups were formed to explore critical issues. Two problem areas requiring further study by the summer study group were identified: out-of-plane measurements and kinematical sensitivities.

INTRODUCTION

The (e,e'N) program has played a key role in the development of CEBAF. Early work in (e,e'p) spectroscopy in the 1960's and 70's demonstrated the significance of the probe for determining single particle nucleon densities and was one of the driving forces for a high duty factor electron facility in the one to two GeV range. Experimental developments in recent years have expanded our view of this reaction and it is becoming recognized as a general tool for attacking a broad range of physical issues. For example, among the topics currently being explored with existing facilities are questions of the extent of nucleon modification by the nuclear mean field, inclusive signatures for short-range two-nucleon currents, the significance of scaling behavior observed in the negative y region, and fundamental measurements such as the electric form factor of the neutron. Hadronic and electromagnetic spin degrees of freedom, as yet largely unexplored, are expected to become an important part of the program as the new high duty factor facilities come on line. CEBAF, with its unique combination of high energy, high resolution and high duty factor, is expected to play a critical role in developing our understanding of this probe and the underlying physics.

The large turn out for the (e,e'N) working group meetings is a reflection of an active community with ongoing programs at all major medium energy facilities with sufficient energy to carry out such measurements. Because

the participants came prepared to work, and because there is already a good understanding among members of the community of the requirements and potential for extending this program to CEBAF energies, substantial progress was made during the week of the workshop. Table I gives a partial list of participants in the working group meetings. Some individuals expressing interest in the (e,e'N) program had conflicting obligations to other committees and could not join in our discussions.

It was recognized that the primary purpose of this workshop is to get timely user advice on the planned experimental facilities. In particular, a couple of laboratory milestones are approaching that will have significant impact on the future (e,e'N) program: In October the laboratory hopes to freeze the out-of-plane capability of Hall A and, in January, the high resolution spectrometer conceptual designs are to be frozen. Therefore the working group concentrated its efforts on identifying critical issues that needed to be explored in more detail over the course of the summer study. To this end subcommittees were formed to study the physics issues involved in a number of areas and to make specific recommendations for items requiring further study this summer. Subcommittees were formed to explore the following topics: Many Body Problems and Nucleon Modification, Two-Nucleon Currents, Spectroscopy, Out-of-Plane Measurements, Spin Physics, and (e,e'n) Reactions. Members of these subcommittees are listed in Table II.

A secondary purpose of the working group is to form a users community interested in carrying out (e,e'N) experiments at CEBAF and in assisting with the development of the experimental facilities required to carry out this program. The first step to forming an active community is to start a dialogue that addresses the scope of the program, the experimental facilities required for the program and the organization of the community's efforts. Because of limited time the last point was not discussed in our meetings but deferred to later in the summer. To begin this dialog, most of the actual meeting time of the group was set aside for short contributions by the participants followed by vigorous discussion. In general the talks were structured in such a way that general theoretical issues were examined first, followed by discussion of experimental data, with detailed technical methods discussed last. A list of contributors with some general indication of the topic covered is given in Table III.

In my summary of the working group meetings I will restrict myself to conveying the general flavor of the

Table I: Participants in 1987 (e,e'N) working group:

Fred Bertrand	ORNL
J.M. Lambert	Georgetown
Paul Ulmer	William & Mary
Mike Finn	William & Mary
Robert Lourie	MIT
J.W. Van Orden	Maryland
Arun Saha	CEBAF
Eamon Harper	George Washington
Bill Thompson	North Carolina
Paul Boberg	Maryland
Kim Egiyan	Yezevan Phys. Inst. USSR
Reiner Neuhausen	Mainz
V. Dmitrasinovic	William & Mary
Herbert Funsten	William & Mary
Franz Gross	William & Mary
Carrol Bingham	Tennessee
Alireza Mokhtari	George Washington
Carl Shakin	Brooklyn College
Werner Boeglin	MIT
John Watson	Kent State
Sirsh Nanda	CEBAF
John Wisnant	South Carolina
John LeRose	CEBAF
Jean Mougey	CEBAF
William Bertozzi	MIT
Costa Papanicolas	Illinois
K.K.Seth	Northwestern
Chris Lyndon	William & Mary
Omar Benhar	INFN, Rome
Larry Zamick	Rugers
J.M. Laget	Maryland
C. Predrisat	William & Mary
Peter Dunn	CEBAF

Table II: (e,e'N) Sub-Committee Membership

A. **Many Body Effects**

*Van Orden
Saha

B. **Two-body components**

Shakin
*Lourie
Saha
Mahktari

C. **Spectroscopy**

Bertozzi
*Ulmer
Saha
Watson

D. **Out-of-plane Measurements**

*Boeglin
Mougey
Papanicolas
Saha
Lerose
Mahktari

E. **Spin Physics**

*Nanda
Perdrisat
Saha
Makhtari

F. **(e,e'n) Reactions**

*Watson
Makhtari
Lerose

* Reporter

Table III: short contributions to (e,e'N) working group

[Tues. 2-5 PM]

A. Many Body Effects

W. Van Orden	Relativistic Treatment of (e,e'p)
C. Shakin	Dynamical Properties of Nucleon in medium

B. Two Body Effects

J.M. Laget	Quasi-deuteron model
Mougey	Saclay results on ^{3}He
R. Lourie	Bates explorations of continuum

C. Spectroscopy

Klerwalt	Coupled channel analysis
P. Ulmer	Rl/Rt and Q dependence

D. Out-of-plane Measurements

J. Mougey	Beam Swinger Technique
W. Boeglin	Need for Accuracy

E. Spin Physics

S. Nanda	Focal Plane Polarimeters

[Weds 4:30-5:30 PM]

F. (e,e'n) Reactions

J. Watson	(e,e'n) spectroscopy

Other Reports

K. Egiyan	Work in USSR
R. Neuhausen	Mainz spectrometers

meetings and will report on new developments, points of general consensus and committee recommendations. I refer the reader to other papers in these proceedings for a review of the field, and in particular to the review of (e,e'N) experiments by Bertozzi[1].

Although there was some interest expressed in carrying out initial survey experiments with the LAS, it was clear the the vast majority of the discussion involved experiments requiring the high resolution capabilities of the Hall A spectrometers.

RECENT DEVELOPMENTS

A number of new experimental and theoretical results were presented which will be outlined in more detail under the appropriate topic heading. (The present experimental situation is also reviewed in these proceedings by Bertozzi.) Theoretical advances in relativistic calculations were reported by Van Orden, in coupled channel calculations, by Klerwald, and in nucleon behavior in the medium, by Shakin. Laget reviewed the quasi-deuteron model as well as presenting the latest Saclay results on ^{3}He. Other experimental results were presented by Egiyan (USSR) and by members of the Bates collaboration (Bertozzi, Boeglin, Lourie, and Ulmer.) Neuhausen was scheduled to report on the spectrometer plans for Mainz, but graciously yielded his time to others.

A number of technical issues were debated as well. Mougey reported on plans for a beam swinger apparatus , Boeglin discussed the kinematical sensitivity of out-of-plane measurements, Nanda reported on focal plane polarimeters and Watson discussed neutron detection techniques. Some of the issues discussed overlapped the interests of other working groups, especially the (e,e'2N) and (e,e'n) groups.

MANY BODY EFFECTS AND NUCLEON MODIFICATION

A topic of intense interest is the question of whether the nucleon is modified in the nuclear medium. Usually the issue is put in the context of whether the nucleon "swells" in the nuclear interior. Shakin pointed out that in any fundamental approach studying nucleon propagation in the nuclear environment the nucleon mass must be treated as a dynamical quantity. Not only may the nucleon mass be modified but the electromagnetic form factors may also be modified in an observable way. His soliton model,[2] predictions of which are shown in Figure 1, is one way of trying to develop a more fundamental picture

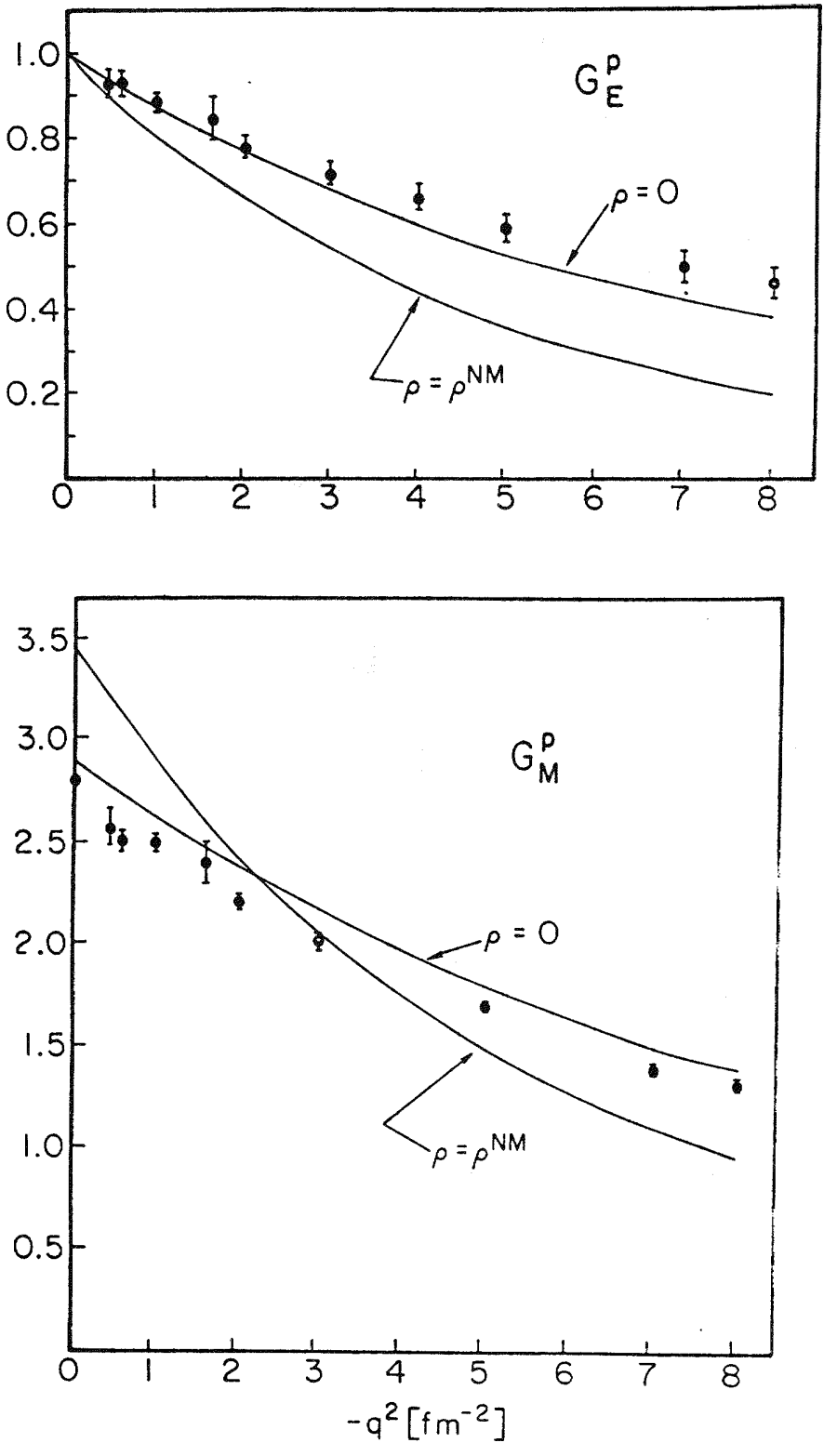

Figure 1. Soliton model predictions for $G_{E,M}$ in nuclear matter.[2]

of the nucleon in terms of the quark degrees of freedom. It is also known that straight forward dynamical effects can also affect the nucleon response.[3] Van Orden cautioned that such many body effects cannot be studied in isolation from other contributions to the reaction process. There was general agreement that to separate out competing processes a broad kinematical range must be sampled and that this clearly required a machine with the energy range of CEBAF. It was understood that for genuine progress to be made complete self-consistent calculations would have to carried out and compared to a broad systematic body of data.

In this context I would like to point out that although claims have been made both favoring and opposed to nucleon swelling on the basis of existing (e,e'p) data[4-6] (see Figures 2 and 3), those claims are probably not statistically significant. The existing data, in addition to covering too limited a kinematical range for this purpose , are also of limited precision, which is a direct reflection of the low energies and low duty factors of current facilities. The value of the present data is in the development of the general techniques, the establishment of general trends, and in the demonstration of the importance of separating the various electromagnetic amplitudes. There is a strong need to improve the accuracy of follow-up experiments.

TWO-BODY CURRENTS

Initial explorations using the (e,e'p) reaction at Bates[7] and Saclay[8] indicate that two-body currents play a larger role in the elementary (e,e') reaction process than generally recognized. The first studies were in the dip region between the quasi-elastic and delta resonance structures where MEC's and other two-body currents have long been suspected of being a major ingredient in filling in the valley between these structures. Both the Bates and Saclay results in this region strongly support the presence of a second reaction channel. Laget has made progress in interpreting the ^{3}He results from Saclay in a quasi-deuteron model(see Figure 4).[8] More recent work from Bates, shown in Figure 5,[9] follows the development of this channel into the delta resonance region in ^{12}C and finds a kinematical dependence consistent with the two-nucleon knockout hypothesis based the gamma production experiments of Homma et al.[10] and Kanazawa et al.[11] In the (e,e'N) reaction, unlike the (e,e') measurements, the pion production channels are kinematically well separated from the one- and two-nucleon knockout channels. The Bates work of Ulmer et al.[12] shows a signature for a second channel of

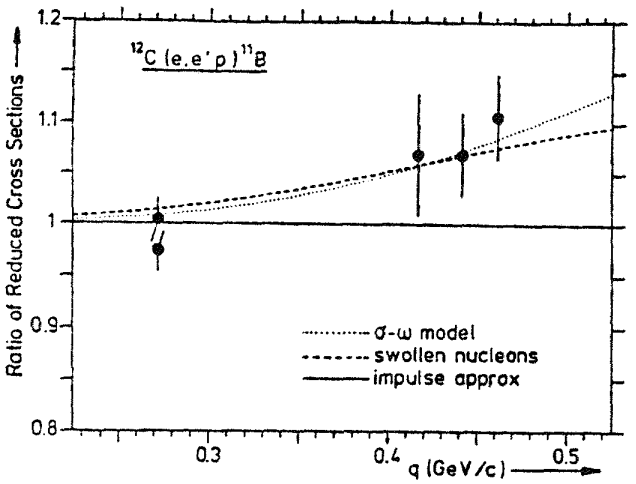

Figure 2. Ratio of backward to forward reduced cross section as a function of three-momentum transfer q for the $^{12}C(e,e'p)^{11}B_{g.s.}$ from NIKHEF experiments.[4]

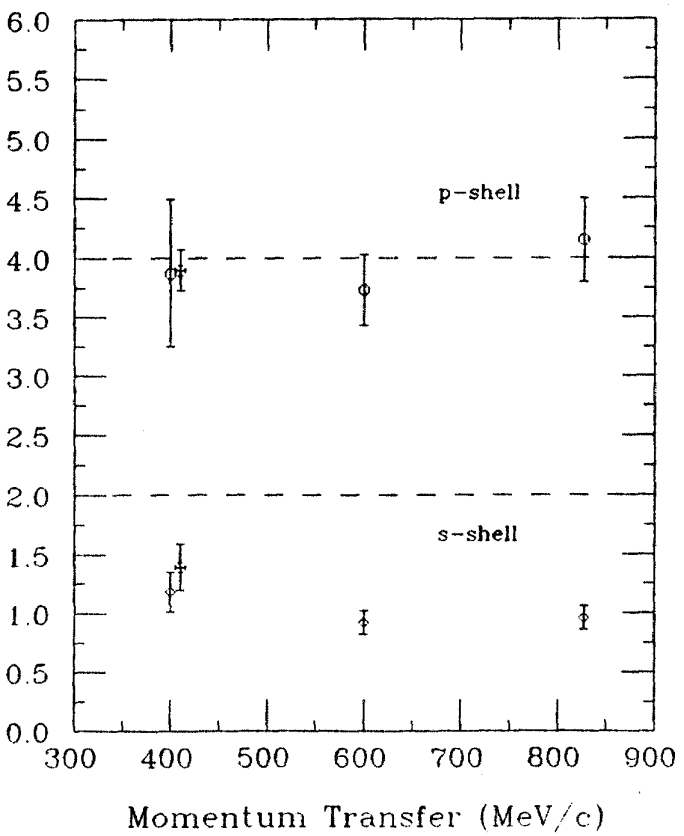

Figure 3. Priliminary ratios of measured p- and s- shell cross sections to DWIA predictions from Bates experiments.[5]

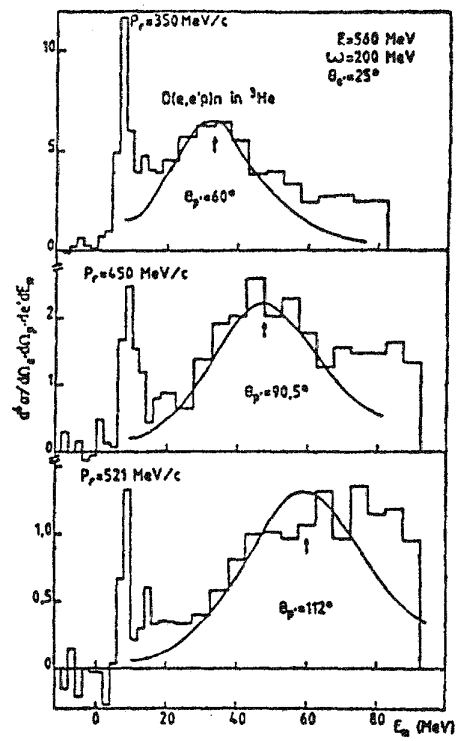

Figure 4. Missing energy spectra from $^{3}He(e,e'p)$ in the dip region measured at Saclay.[8] Curve shows two-nucleon knockout calculation by Laget.

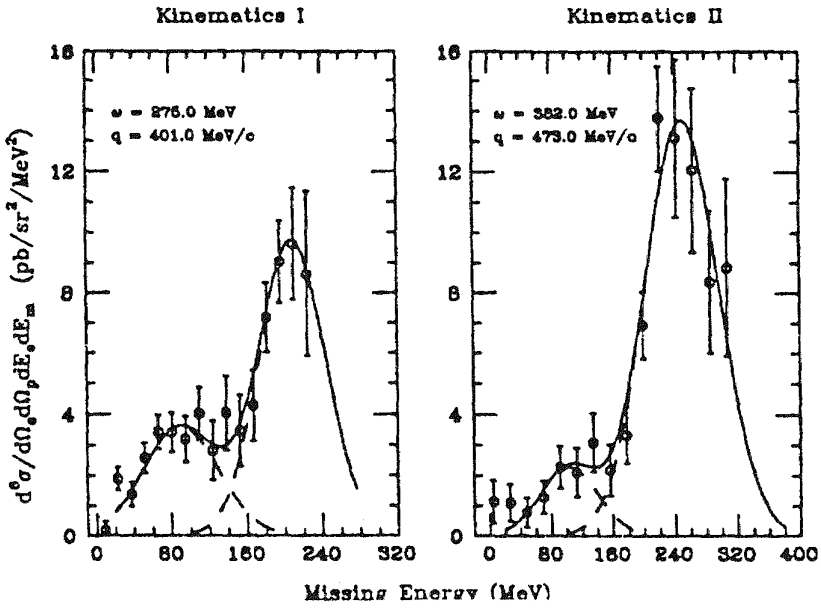

Figure 5. Missing energy spectra obtained from $^{12}C(e,e'p)$ measurements at Bates. Kinematics I corresponds to a point halfway between the dip and delta regions while Kinematics II is at the maximum of the delta peak. Curves are guassian fits.

transverse character that contributes significantly even in quasi-elastic kinematics (see Figure 6). Present experimental plans at Bates call for extension of these measurements into the negative y region to suppress MEC degrees of freedom and perhaps enhance initial state correlations.

It is clear that with a machine of the capabilities of CEBAF the natural extension is to measure two-body currents directly via (e,e'2N) experiments. The counting rates for such triple coincidence measurements will be low however, so that there will still be interest in performing more comprehensive, albeit inclusive, measurements with the (e,e'N) reaction. At present only a few, almost random, measurements have been performed out of a vast kinematical domain available for exploration.

SPECTROSCOPY

Recent measurements at NIKHEF have demonstrated once again the importance of high resolution for determination of spectroscopic factors. Figure 7 shows a typical high resolution (e,e'p) spectrum from NIKHEF.[4] With a resolution of 100 to 200 keV they can measure the single nucleon-hole content of even weak excited states in the the residual A-1 spectator system, and begin determining orbital configurations for these states. These measurements will benefit from higher energy and momentum transfers with the ideal kinematics having a knockout nucleon with a kinetic energy of 200 to 400 MeV, where the nucleus is most transparent. Although these kinematics can be reached by a one GeV machine, longitudinal and transverse separations will benefit from using a higher energy beam and more forward scattering angles. The benefit is two fold in that higher energies allow both larger longitudinal polarizations and higher counting rates. Strong interest was expressed in extending these separations up to the highest momentum transfers possible at CEBAF at least for the few body system and several other sample nuclei spanning the periodic table.

One of long standing[13] and, as yet, unresolved problems in spectroscopy is the issue of missing spectroscopic strength observed in (e,e'p) and other one body probes. It was felt that more theoretical progress is needed to determine if indeed strength has been redistributed and, if so, into which channels. Van Orden pointed out that his relativistic calculations[14] indicate stronger optical potential effects than traditional non-relativistic calculations. He also pointed out that complex optical potential calculations fail to conserve flux and that,

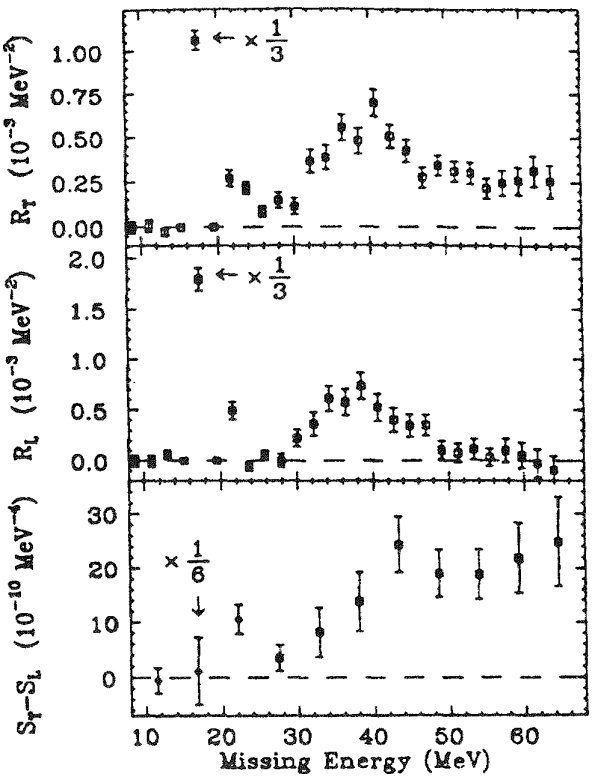

Figure 6. Separated $^{12}C(e,e'p)$ response functions and their difference.[12]

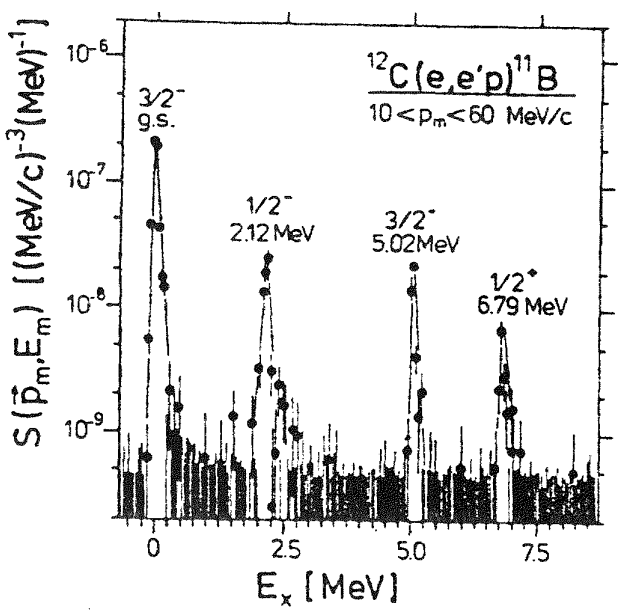

Figure 7. High resolution $^{12}C(e,e'p)$ spectrum from NIKHEF.[4]

while they are useful for estimating the flux removed from the elastic channel, they don't give any insight as to which inelastic channels are being fed. It was felt that coupled channel calculations might be more useful in describing the continuum missing energy strength, and there was considerable interest in Klerwald's calculations. Of course, if the nucleon form factor is modified significantly in the medium, this would have relevance for the interpretation of spectroscopic strengths.

Bertozzi pointed out the complementary roles played by (e,e') and (p,p') probes of single body densities and the benefits that have come for a unified study of these reactions.[15] He surmised that a similar situation might occur in (e,e'p) and (p,2p) studies.

OUT-OF-PLANE MEASUREMENTS

Mougey[16] presented plans illustrating the laboratory's preferred method for making out-of-plane measurements and asked for user input, pointing out that the laboratory needs to freeze this option at an early date (October) since it impacts on the civil construction plans. An out-of-plane measurement capability is needed to measure the fifth structure function which is dependent on the beam helicity and requires a polarized beam as well. It is also necessary for a complete decomposition of the other four structure functions as well as for the determination of various target and recoil nucleon polarization projections. Donnelly[17-19] among others[20-23] has been working on the classification and physical significance of these elementary observables. Measurements of these observables can provide sensitive tests of the reaction mechanism. Fabian and Arenhovel,[20] for example, as indicated by Figure 8, have shown that the transverse-transverse interference amplitude in the case of the deuteron may change sign in the presence of MEC and IC contributions while the direct transverse response changes only slightly. The fifth structure function, being time reversal odd, vanishes in the absence of final state interactions or some other complexity in the reaction channel.[17-18]

There is no easy way to make out-of-plane measurements given the large size of the HAll A spectrometers. The possibility of a straight forward approach, moving the hadron spectrometer to sweep out a cone about the virtual photon direction, seems full of technical difficulties. The plan favored by the laboratory is to deflect the beam in a vertical plane as shown in Figure 9.[16] This plan has the advantage of clearly being technically achievable,

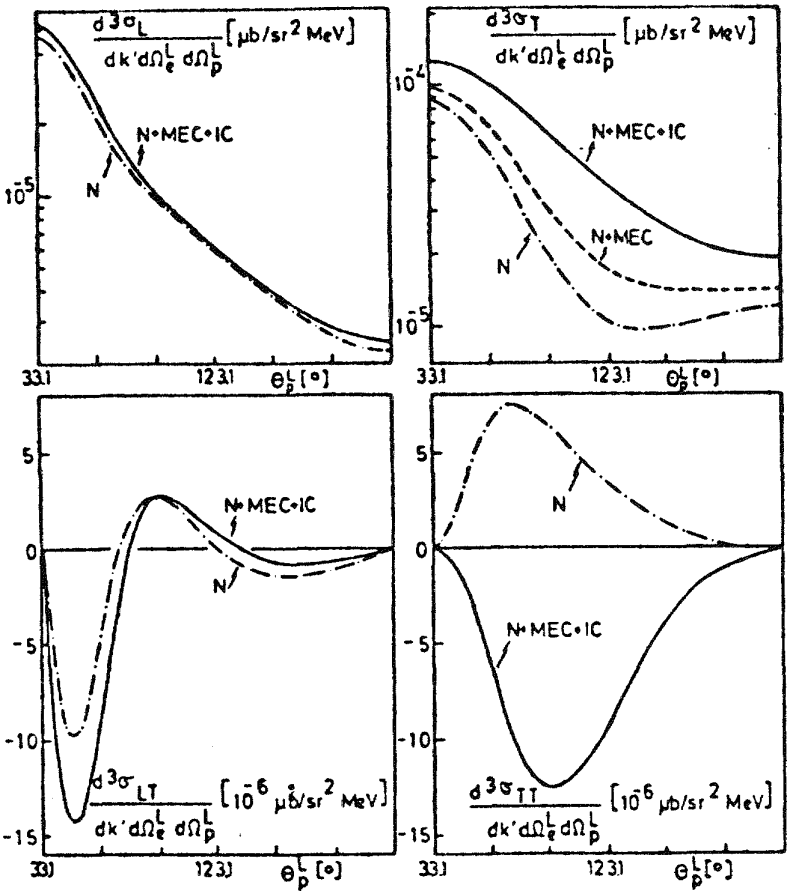

Figure 8. Calculation of EM interference amplitudes for D(e,e'p)n Reaction near pion production threshold.[20]

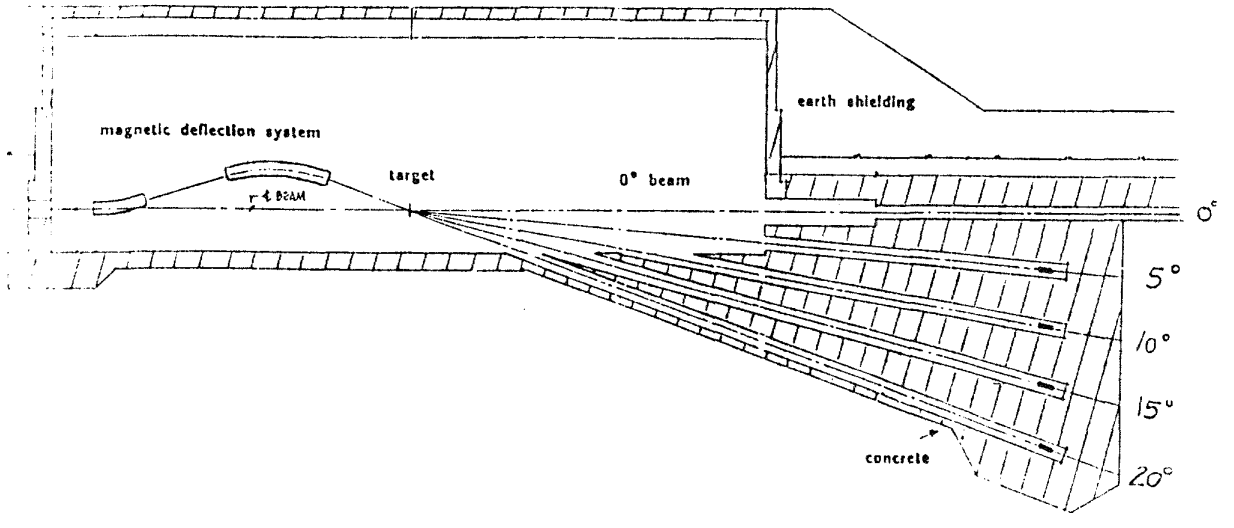

Figure 9. Beam Swinger technique for out-of-plane measurements.[16]

although expensive. If the electron spectrometer is restricted to small angles with respect to the beam, this method has the added advantage of magnifying the effective out-of-plane angle that can be reached. To avoid radiation safety problems it is proposed that only four discrete bend angles be provided, each having its own dump. (These secondary beam dumps might be limited in luminosity.) In order to maintain constant kinematics, both spectrometers will have to moved as well as the beam deflected. This situation leads to the maximum experimental complications. It was agreed that the out-of-plane issue needs to be studied in more detail over the summer study period.

A related problem is the report by Boeglin indicating surprising strong kinematical sensitivities found for out-of-plane experiments planned on the deuteron at Bates. It was felt that a detailed analysis of expected kinematical sensitivities for CEBAF conditions needs to be carried out as part of the summer study effort.

SPIN PHYSICS

Under this heading one can consider all the possible polarization experiments that can be performed in the (e,e'N) reaction: one can determine the contribution from the various virtual photon helicity amplitudes, one can polarize a target with nonzero spin, one can measure the polarization state of the recoiling nucleon, or one can can consider measurements involving a combination of the above techniques. The result is a large number of physical observables that have been studied in some systematic detail by Donnelly,[17-19] Van Orden[21,22] and Boffi.[23] Sample results from the work of Boffi and his collaborators are shown in Figure 10.

In the deliberations of the working group, it was assumed that a polarized beam would be available and that the laboratory would have the capability to measure the EM interference amplitudes, so that this point was not raised as a separate issue apart from its applicability to specific physical problems. [If it were necessary to justify such measurements it should be sufficient to note the important contributions that longitudinal and transverse separations have played throughout the entire history of single arm electron scattering. Recent experiments at Bates, NIKHEF, and Saclay are beginning to document a similar importance for the equivalent coincidence observables.] It was understood that meaningful measurements of these amplitudes would make exacting demands on the accuracy of the experimental equipment.

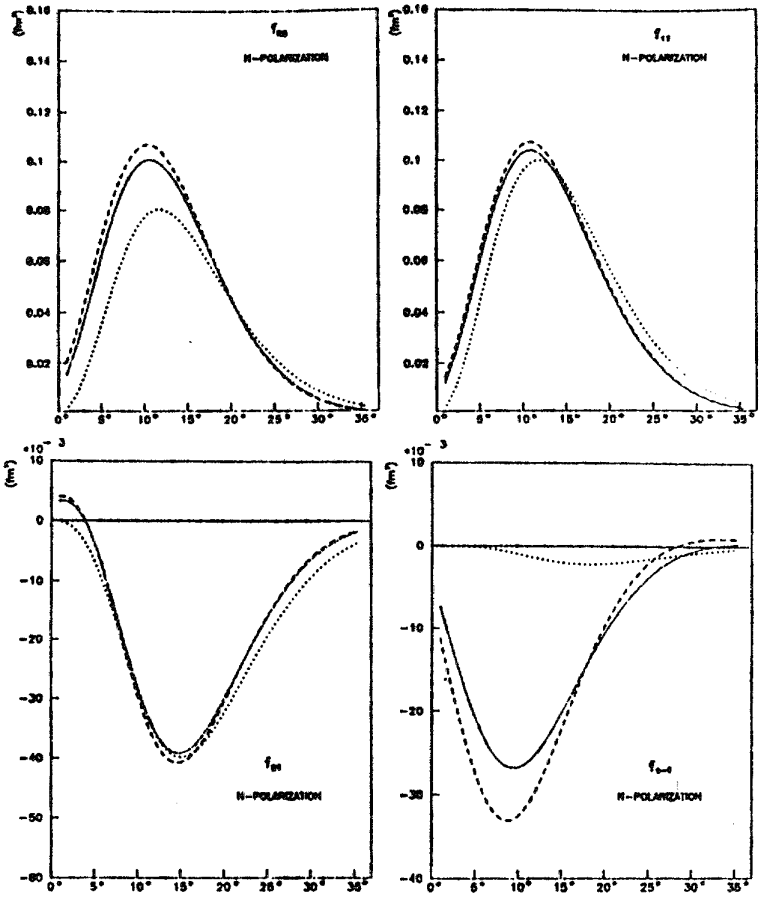

Structure functions for the $p_{3/2}$ hole in N-polarized ^{7}Li vs. γ. The final proton energy is 144 MeV and q=2.6 fm^{-1}. Bound state from ref. 23, optical model from ref. 21 (solid line) and from ref. 22 (dashed line); dotted line for PWIA.

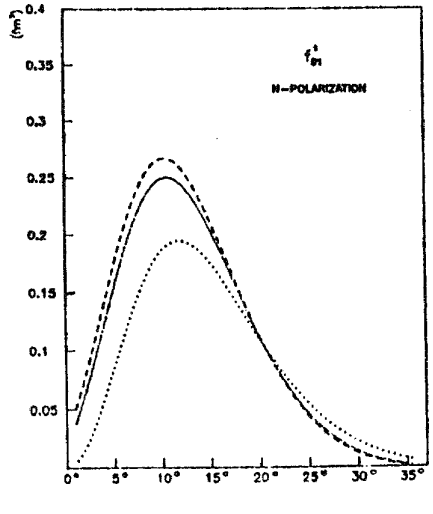

The fifth structure function $f_{51}^{\prime}$ for $p_{3/2}$ hole in ^{7}Li

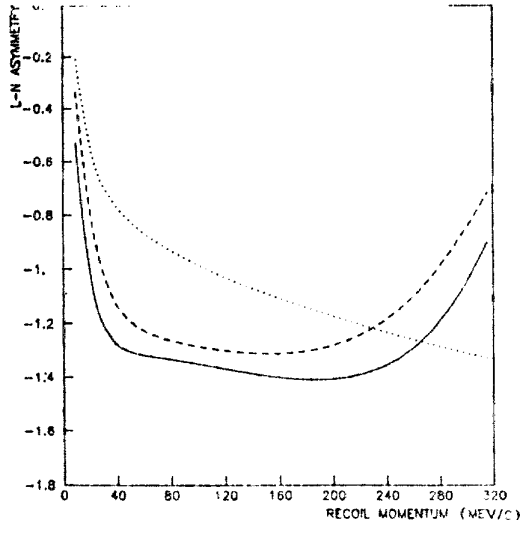

Asymmetry $(E^{\uparrow}-E^{\downarrow})/E_0$ for $p_{3/2}$ hole in ^{7}Li

Figure 10. Sample results for polarized (e,e'p) measurements from a polarized Li target.[24]

Only a few isolated measurements of hadronic spin observables have been made with electromagnetic probes, such as the measurement of T_{20} from elastic scattering off of the deuteron with measurement of the recoil deuteron polarization.[24] A complementry measurement, using a polarized deuterium target in the reaction D(e,pn)e' has recently been published.[25] With the advent of high duty factor machines and polarized electron beams, these type of experiments should become a growing part of the program. The experience of proton machines have shown that measurements of analyzing powers, polarization transfers, and target and recoil nucleon polarizations are extremely important for understanding the hadronic currents in the nucleus.

Although target and recoil nucleon polarizations may yield equivalent information in some special cases, in general both types of measurements need to be performed to completely specify all possible measurables. Target polarization measurements tend to give information about the polarization of the outermost valence nucleon, while recoil polarization measures the polarization of the knockout nucleon, which may originate from a inner orbital.

Nanda reported on the properties of carbon focal plane polarimeters like those used in the HRS at LAMPF. These polarimeters can have relatively high efficiencies (a few percent) for proton energies in the 200 to 800 MeV range. Figure 11 shows a schematic of the LAMPF proton focal plane polarimeter. [26] Such polarimeter designs can be directly copied for use at CEBAF and would be suitable for most (e,e'p) spectroscopy measurements. Above about 1.2 GeV/c, analyzing powers of potential polarimeters have not been calibrated.

(e,e'n) EXPERIMENTS

Although (e,e'p) and (e,e'n) experiments study the same physics, the techniques required for measurements of neutrons are very different than that for protons. For this reason some of the physicists interested in (e,e'n) studies have formed a separate working group to explore this reaction in more detail. Therefore I will be brief in summarizing our deliberations on this topic. I will assume that the (e,e'n) working group will discuss the important special case of measurement of the electric form factor of the neutron in some detail and I will limit myself to complimentary measurements of spectroscopic factors using the (e,e'n) reaction.

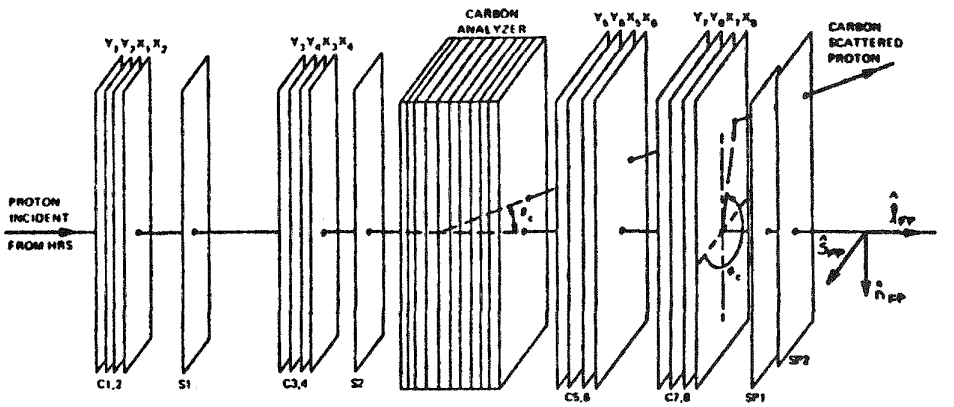

Figure 11. LAMPF HRS focal plane polarimeter layout.

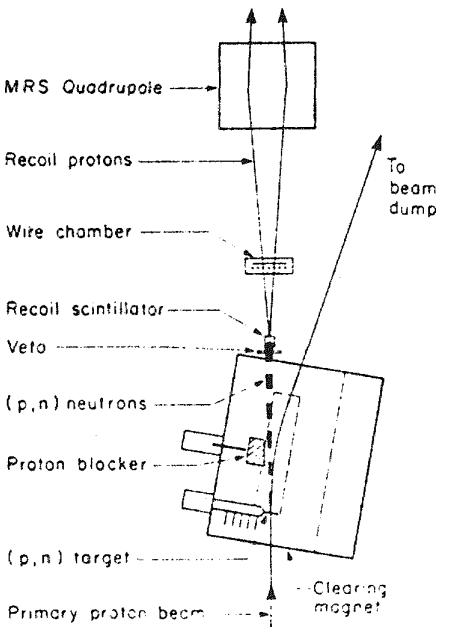

Figure 12. A schematic diagram of the TRIUMF (p,n) facility using the medium resolution spectrometer.[20]

Although (e,e'n) measurements are more difficult than (e,e'p) measurements and required resolutions are harder to achieve, it was thought that even a limited program, comparable in scope to the first generation of (e,e'p) experiments of the last decade, would provide valuable information.

Typically the neutron energy is determined by time-of-flight techniques. For example. the (p,n) group at Kent State obtains about 300ps FWHM timing resolution in a large neutron detector consisting of scintillator slabs viewed by two mean-timed phototubes. For neutrons in the energy range of 80 to 200 MeV, energy resolutions of a few hundred keV are obtained with flight paths on the order of a hundred meters.[27] Such long flight paths are not economically feasible within the present budgetary constraints at CEBAF but TOF measurements came be made within the 30 M radius of the scattering halls. An alternative method is to scatter the neutron in a Hydrogen target and to measure the scattered proton in a spectrometer. Watson reported on his experience with this technique at TRIUMF. A schematic of this aparatus is shown in Figure 12.[28]

SUMMARY

After consultation with members of the subcommittees it was decided to recommend two items as critical for further study during the summer: 1) the best means for carrying out out-of-plane experiments in Hall A and 2) a detailed analysis of kinematical sensitivities in the (e,e'N) reaction.

The severe accuracy requirements needed for this program have been repeatedly a cause for concern.[29,30] To quote from last years working group:[30]

> "Some counting rates and accuracy estimates have been given by Mogenstern[ref 29] in the case of Deuterium. They showed that it is not easy to achieve a good accuracy in extracting σ_L and σ_T, even with a 2% accuracy in the cross-section measurement."

There is also a strong sense that the program requires extensive and systematic explorations to pin down the various components of the reaction process, and that this will require the full kinematical capabilities of CEBAF. A corollary to this point is that more complete and self-consistent theoretical calculations will be required, and that this would require an increased level of theoretical

support. These conclusions are consistent with conclusions reached by previous working groups.[30]

The working group also agreed that we should begin discussions this summer to build a well defined users' group of physicists interested in pursuing a program of (e,e'N) reactions at CEBAF and in participating in the development of the required facilities.

In writing up this summary from a perspective of late summer, it is gratifying to note that progress has been made on all the major objectives of the working group. The laboratory has formed a task group led by Franz Gross to examine the out-of-plane issue and this group has had the benefit of serious user input. Kinematical sensitivities of the (e,e'N) process have also been explored in some detail as part of the above effort and the results transmitted to the spectrometer design group. Informal conversations held by users over the course of the summer has led to a general letter to the community inviting them to a (e,e'N) collaboration meeting to be held at William and Mary in September. Topics on the agenda include discussion of letters of intent and the selection of appropriate user representatives for the program as a whole.

In general times have never been better for those interested in this reaction and the physical problems that this probe studies. The reaction is a well established component of the CEBAF core program, and it is reasonable to foresee a long term systematic development of the program capable of supporting the training of a number of young physicists. There is already a vigorous community in place pursuing a number of "hot" topics at existing laboratories. One can expect that a number of highly competitive programs will be undertaken in this area as the one GeV, high duty cycle, machines come on line in the next few years. CEBAF, because of its higher energy, is in a unique position to complement these efforts by addressing those aspects of the program that are not accessible to these machines.

ACKNOWLEDGEMENTS

I would like to recognize the efforts of the many participants in this year's working group whose names are listed in Table I. I apologize to those whose contributions I failed to acknowledge explicitly in this summary, and I thank the many people that assisted me in preparing this report.

REFERENCES

1. W. Bertozzi, R.W. Lourie and J.M. Finn, "Coincidence Measurements from Nuclei", in these proceedings.

2. C.S. Celenza, A. Rosenthal, and C.M. Shakin, Phys. Rev. C 23, 232 (1985).

3. S. Fantoni and V.R. Pandharipande, " Dynamical Structure Functions in Nuclear Medium", in proceedings of 1986 CEBAF Summer Workshop. page 169.

4. G. van der Steenhoven, Phys. Rev. Lett. 58, 1727 (1987) and 57, 182 (1986). see also Phys. Lett. B, to be published.

5. J.M. Finn, W. Bertozzi and R.W. Lourie, "The (e,e'p) Coincidence Program at Bates and CEBAF", in proceedings of the Workshop on Perspectives in Nuclear Physics at Intermediate Energies, Trieste, Italy, May (1987).

6. A. Gerard, "Nuclear Medium Effects on Nucleon Properties", in proceedings of 1986 CEBAF Summer Workshop, p289.

7. R.W. Lourie et al., Phys. Rev. Lett. 56, 2364 (1986).

8. J. Mogenstern, in proceedings of the Fourth Miniconference NIKHEF-K, Nucl. Phys. **A446**, 301c (1985).

9. H. Baghaei et al., to be published.

10. Homma et al., Phys. Rev. Lett. **45**, 706 (1980).

11. M. Kanazawa et al., Phys. Rev. C 35, 1828 (1987).

12. P. Ulmer et al., submitted to Phys. Rev. Lett.

13. S. Frullani and J. Mougey, "Single Particle Properties of Nuclei through (e,e'p) Reactions", Adv. Nucl. Phys. **14**, ed. J.W. Negele and E. Vogt (Plenum, NY, 1984)

14. J.W. Van Orden, preliminary results presented to working group.

15. W. Bertozzi and J.J. Kelly, " the Common Ground between Hadronic and Electromagnetic Probes", in proceedings of the Conf. on New Horizons in Electromagnetic Physics, Charlottesville VA (1982).

16. J. Mougey, private comm.; see also J. Mougey and C.C. Chang , report on Hall A experimental program, in these proceedings.

17. T.W. Donnelly, "Coincidence and Polarization Measurements with High Energy Electrons, "Proceedings of the CEBAF workshop, June 1984.

18. T.W. Donnelly, "Super-Rosenbluth Physics", BUTG Workshop: Nucleon and Nuclear Structure and Exclusive Electromagnetic Reaction Studies, MIT, July 1984.

19. T.W. Donnelly and A.S. Raskin, Ann. Phys.(N.Y.), to be published.

20. W. Fabian and H. Arenhovel, Nucl. Phys. **A314**, 253 (1979).

21. A. Picklesimer, J.W. Van Orden, and S.J. Wallace, Phys. Rev. C **32**, 1312 (1985).

22. A. Picklesimer and J.W. Van Orden, Phys. Rev. C **35**, 266 (1987).

23. S. Boffi, "New Physics from the (e,e'N) Reaction", in proceedings of 1986 CEBAF Summer Workshop, p133.

24. M.E. Shulze et al., Phys. Rev. Lett. **32**, 597 (1984).

25. M.V. Mostovoy et al., Phys. Lett B **188**, 181 (1987).

26. S.K. Nanda, Ph.D. Thesis, Rutgers Univ., LANL pub. LA-10368-T and UC-34C issued May 1985.

27. J.W. Watson et al., Phys. Rev. Lett. **55**, 1369 (1985).

28. W.P. Alford et al., Phys. Lett B **179**, 20 (1986).

29. J. Morgenstern, Report on the 1985 CEBAF Summer Study Group.

30. A. Gerard, "Report on Working Group on Single Particle Emission", in Proceedings of the 1986 CEBAF Summer Workshop.

NUCLEON RESONANCES AND MESON PRODUCTION

Volker Burkert

Continuous Electron Beam Accelerator Facility
12070 Jefferson Avenue
Newport News, Virginia 23606

This parallel session attracted many of the CEBAF users. More than forty individuals participated in this session with an average attendance of twenty-five to thirty. The list of participants and the list of oral presentations at this session is given at the end of this report.

This report summarizes the discussion during this session that dealt with resonance physics and meson production from free nucleons. The discussion on nucleon resonances in nuclei is summarized in the report by P. Stoler.

Introduction

Of the many baryon resonances, only the $\Delta(1232)$ (or $P_{33}(1232)$) has played a major role in electro- and pion nuclear physics. The reason being the limitation in energy of the accelerators which have been used in nuclear physics experiments in the past. With the 4 (or 6) GeV, high current CW electron beams at CEBAF, the entire nucleon resonance region will be accessible in a large range of the four-momentum transfer Q^2 (Figure 1).

The ultimate goal in studying electroexcitation of free nucleons is to obtain information on the transition form factors $A^T_{1/2}$, $A^T_{3/2}$ and $A^S_{1/2}$ for individual nucleon resonance, where 1/2 and 3/2 refer to the total helicity of the initial $\gamma_v N$ system, and T and S refer to transverse and scalar coupling of the photon, respectively. Because there exist many broad resonances in close proximity to each other, inclusive measurements are not sufficient to extract this information. To identify spin/parity and isospin of the respective nucleon state (only non strange baryon resonances have been discussed during this session) the hadronic final state has to be identified and analyzed in terms of partial waves in the angular distribution of the decay particles.

Many of the lower mass resonances have a sizeable branching ratio into the πN and ηN channels which are experimentally the most convenient channels to study. The process $\gamma_v p \rightarrow \eta p$ selects directly final states with isospin 1/2 and is of

particular relevance for studying the $S_{11}(1535)$ and the $P_{11}(1710)$ resonances, both of which have a large branching ratio into the ηN channel.

The single pion production channel does not correspond to a well defined isospin state. It will therefore be important to study final states with different isospin content to enable complete isospin decomposition of the transition amplitudes. The reactions $\gamma_v p \rightarrow p\pi^o$, n π^+ and $\gamma_v n \rightarrow \pi^- p$ will provide such a complete isospin information.

Physics Aspects of N* Electroproduction

The knowledge of the transition form factors over a large Q^2 range appears essential for testing microscopic models of the nucleon and of properties of the photon-nucleon coupling. In measuring the nucleon transition form factors, many details of the wavefunction of the excited state can be obtained, which provide information on the interaction of light quarks in confined systems. This interaction is expected to be governed by the theory of strong interaction, QCD. At the present time QCD is making contact with baryons in the form of more or less sophisticated quark models which employ ingredients from QCD. The confrontation of prediction of these QCD 'inspired' quark models with experiments provides information on how to connect baryons to the fundamentals of QCD (G.Karl).

Of special interest is the $\Delta(1232)$. The natural explanation of the magnetic character of the $\gamma N \rightarrow \Delta(1232)$ transition in SU(6) quark models as a simple spin flip indicates that quarks indeed play an important role in the resonance excitation. Small non-magnetic contributions due to electric and scalar quadrupole transition appear to be sensitive to tensor forces from the one-gluon exchange (G. Karl) as well as from residual non-resonant pion effects (H. J. Weber).

The very small value of $E_{1+}/M_{1+} \simeq$ -0.01 found in analyses of photoproduction data is in sharp contrast to the perturbative QCD prediction $E_{1+}/M_{1+} = 1$ at $Q^2 \rightarrow \infty$ (C. Carlson).It would be very interesting to see whether or not such a dramatic departure from the almost complete magnetic dominance at small Q^2 can indeed by seen at high Q^2.

At high momentum transfer dynamical quark models predict dominant resonance excitation by helicity coupling in the initial γ_vN system, which is in accordance with predictions from perturbative QCD (C. Carlson). For some of the higher resonances like the $D_{13}(1520)$ and the $F_{15}(1688)$ the switch from helicity 3/2 dominance at Q^2=0 to helicity 1/2 dominance at high Q^2 has indeed been found

experimentally (Figure 2). The switch from helicity 3/2 to helicity 1/2 dominance occurs at relatively small Q^2 which indicates that at high Q^2 helicity 1/2 may indeed be the only contributing resonance.

Another interesting resonance is the $S_{11}(1535)$ which is most conveniently studied in the $\gamma_v p \rightarrow p\eta$ reaction (K. Giovanetti). The total η-production cross section appears to be largely dominated by the transverse photon coupling in the lower Q^2 range ($\leq$ 1.5 $(GeV/c)^2$). The helicity amplitude $A^T_{1/2}$ exhibits an unusually slow fall off with Q^2. At $Q^2 = 3$ $(GeV/c)^2$ its magnitude has decreased by only 50% as compared to its value at $Q^2 = 0$, if the scalar coupling is assumed to be negligible. This behavior is not well accounted for in non-relativistic quark model calculations. Relativistic effects may be important. Under CEBAF conditions it will be possible to study this resonance much more accurately and at higher Q^2.

Previous Measurements

Previous experiments which studied electro excitation of nucleon resonances have been performed at the electron synchrontrons at Bonn, DESY and NINA.

All analyses of exclusive electroproduction data generally suffer from the lack of sufficiently detailed measurements. For example, not a single coincidence experiment has been performed with polarized beams or polarized targets, nor has the recoil polarization been measured in any of these experiment. It is quite clear that many aspects of nucleon resonance production can be studied in a more sensitive way if polarization observables are measured (R. Eisenstein, R. Minehart, V. Burkert). Many of the weaker resonant amplitudes can be studied more efficiently in polarization experiments due to strong interference effects with the larger amplitudes.

Most of the measurements have been performed with relatively low luminosities of typically[2] 10^{35} cm^{-2} sec^{-1} with spectrometers having relatively small acceptances. Also, the possibilities to perform out-of-plane measurements were very limited which consequently limited the capability to separate the various structure functions in the exclusive cross sections.

Complete Measurements at CEBAF

In single pion electro-production from nucleons 11 independent measurements are needed at a given kinematical point Q^2, W, θ^*_π in order to nail down all amplitudes of the process $\gamma_v N \rightarrow N'\pi$ in a model independent fashion. Complete

determination of the transition amplitudes in pion and eta production would provide the data base for a phase shift analysis of the nucleon resonance region which need not make use of results from πN scattering analysis. Such a program may be considered as a long term goal of nucleon resonance physics with electromagnetic probes at CEBAF.

Unpolarized experiments allow measurement of 4 structure functions. With a polarized electron beam one additional structure function can be measured. Measurement of polarization asymmetries with polarized targets or recoil polarimeter will be very important. In either case, 8 structure function can be measured. Using a polarized beam in conjunction with a polarized nucleon target or with a recoil polarimeter enables the measurement of 5 additional structure functions.

Not all of the structure functions contain independent information. In particular only 4 of the structure functions which can be measured with polarized targets are different from the ones measured with recoil polarimeters. In many applications the two methods can be quite competitive (H. Funsten). This allows one to choose the more convenient techniques to measure a specific polarization structure function.

Many of the limitations of previous experiments can be overcome at CEBAF if the experimental equipment for such a program is carefully planned. In order to separate the various structure functions, experiments will have to be done in such a way that the hadrons can be measured out of the electron scattering plane. A full fledged program using polarized hydrogen and deuterium targets will be feasible owing to recent advances in polarized target technology. With the emergence of NH_3 and ND_3 as radiation resistent target materials for polarized protons and deuterons, polarized solid state targets can now be used in intense electron beams. Luminosities ranging from $\simeq 10^{34}$ to $\simeq 5.10^{35}$ $cm^{-2}sec^{-1}$ for target temperatures between 0.3 to 1.K can be achieved (J. McCarthy). This requires that the experimental equipment be designed in such a way to accommodate the high magnetic field which is needed to maintain the polarization during operation in an intense electron beam. Also spectrometers with large angle and momentum acceptance are desirable which can be used with such luminosities. In addition, intense polarized electron sources have come into operation over the past ten years which can efficiently be used in the nucleon resonance program at CEBAF.

Short Term Goals for CEBAF

The primary interest in nucleon resonance physics at CEBAF for the first round of experiments will naturally focus on the more prominent states like the $P_{33}(1232)$, $S_{11}(1535)$, $D_{13}(1520)$, and $F_{15}(1688)$, to extract the transition form factors in a large range of Q^2. Precise measurements of these transition form factors may have a strong impact on the development of more realistic inter-quark potentials and in general on the implementation of QCD to baryons. In the region of the $P_{33}(1232)$, precise measurements of small multipoles E_{1+} and S_{1+} will be feasible if polarized beams and polarized targets/recoil polarimeters are available. Beside the resonant multipoles in the $P_{33}(1232)$ region, low energy theorems can be tested by precisely measuring the electromagnetic multipoles near pion threshold (G. Tamas).

Of particular interest in the lower mass region is the 'Roper' $P_{11}(1440)$ resonance which has not been well studied in electron scattering experiments. Recently, the $P_{11}(1440)$ has attracted some attention due to indications of a possible strong longitudinal coupling. Polarized target experiments may be particularly sensitive in studying the longitudinal coupling of this resonance in electron scattering (Figure 3).

In the higher mass region the QCD improved Quark Shell Model of Isgur & Karl[2] predicts nucleon states which have not been observed in πN scattering. Many of these states may in fact decouple from the πN channel but may be excited by real or virtual photons. Some of these channels are predicted to have a large branching ratio into the ωN and ρN channels. In a detailed partial wave analysis of these channels it should be possible to isolate the resonant contributions in the respective partial waves (M. Manley).

Although the discussion in this working group has focused on the strangeness=0 states, there is clearly also an interest in studying Λ and Σ resonances at CEBAF (P. Bertin). In cases where rare events have to be detected, special experimental techniques may be required to identify the respective decay channels with good signal/background ratio.

In summary, the electroproduction of excited baryons at CEBAF is a crucial aspect of the program of establishing connections between the fundamental theory of QCD and hadron physics. Only very few nucleon resonances have been studied in some detail in previous electron scattering experiments. With the intense CW electron beams at CEBAF, a broad experimental program to study the transition

form factors of many nucleon resonances will be feasible. In this program, use of intense polarized electron beams, polarized hydrogen and deuterium targets, as well as nucleon recoil polarimeters will play an important role. It is also essential that hadrons can be measured out of the electron scattering plane over the full polar angle range of the detected meson or nucleon.

All these aspects have to be taken into account in designing experimental equipment that would allow to collect the data base which is sufficiently detailed for a subtantial improvement of our present knowledge of the electromagnetic interaction of nucleons.

List of Participants

G. Adams	J. Arends	B. Berman	P. Bertin
V. Burkert	C. Carlson	H. Crannell	J. Domingo
J. Dubach	R.A. Eisenstein	H. Funsten	K. Giovanetti
E. Harper	J. Heisenberg	D.J. Horen	G. Karl
J. Kelly	J.M. Lambert	L. Tiator	M. Manley
J. McCarthy	B. Mecking	R. Minehart	A. Mokhtari
G.S. Mutchler	M. Oka	B. Preedom	B. Ritchie
N. R[illegible]ning	A. Saha	K.K. Seth	C. Smith
C.E. [illegible]ronach	G. Tamas	S. Thornton	K. von Reden
H.J. Weber	H.T. Williams	J. Wood	L.E. Wright
M. Yamazaki	W. Ziegler		

List of Oral Presentations

1. G. Karl: "Remarks about Helicity Amplitudes of Resonances"
2. J. Schiffer: "Comments about Delta Interactions in Nuclei" Studies at CEBAF"
3. H. J. Weber: "Electric Quadrupole Transitions of the $\Delta(1232)$"
4. R. Eisenstein: "$\Delta(1232)$ - Low and Intermediate Energy Prospects"
5. C. Carlson: "Nucleon Resonances and Perturbative QCD at High Q^2"
6. J. McCarthy: "Polarized Proton and Deuteron Targets for CEBAF"
7. R. Minehart: "Sensitivity of Polarization Measurements of Pion Production Amplitudes"
8. K. Giovanetti: "Study of the $S_{11}(1535)$"
9. M. Manley: "Rho Meson Production in the Resonance Region"
10. H. Funsten: "Recoil Polarization in N* Production"
11. P. Stoler: "Nucleon Resonances in Nuclei - an Experimental Program for CEBAF"
12. G. Tamas: "Pion Photoproduction at Threshold"
13. J. Dubach: "(e,e'Nπ) Reaction on Nuclei"
14. P. Bertin: "Experimental Techniques in Rare Event Detection"
15. V. Burkert: "Experimental Aspects of Nucleon Resonance

References

1. F. Foster, G. Hughes; Program in Physics, Vol. 46, 1445 (1983)
2. N. Isgur, G. Karl; Phys. Rev. D23, 817 (1981)
3. B. Boden, G. Kroesen; Report of the 1986 CEBAF Summer Study Group, June 2-August 29, 1986, pg. 121.

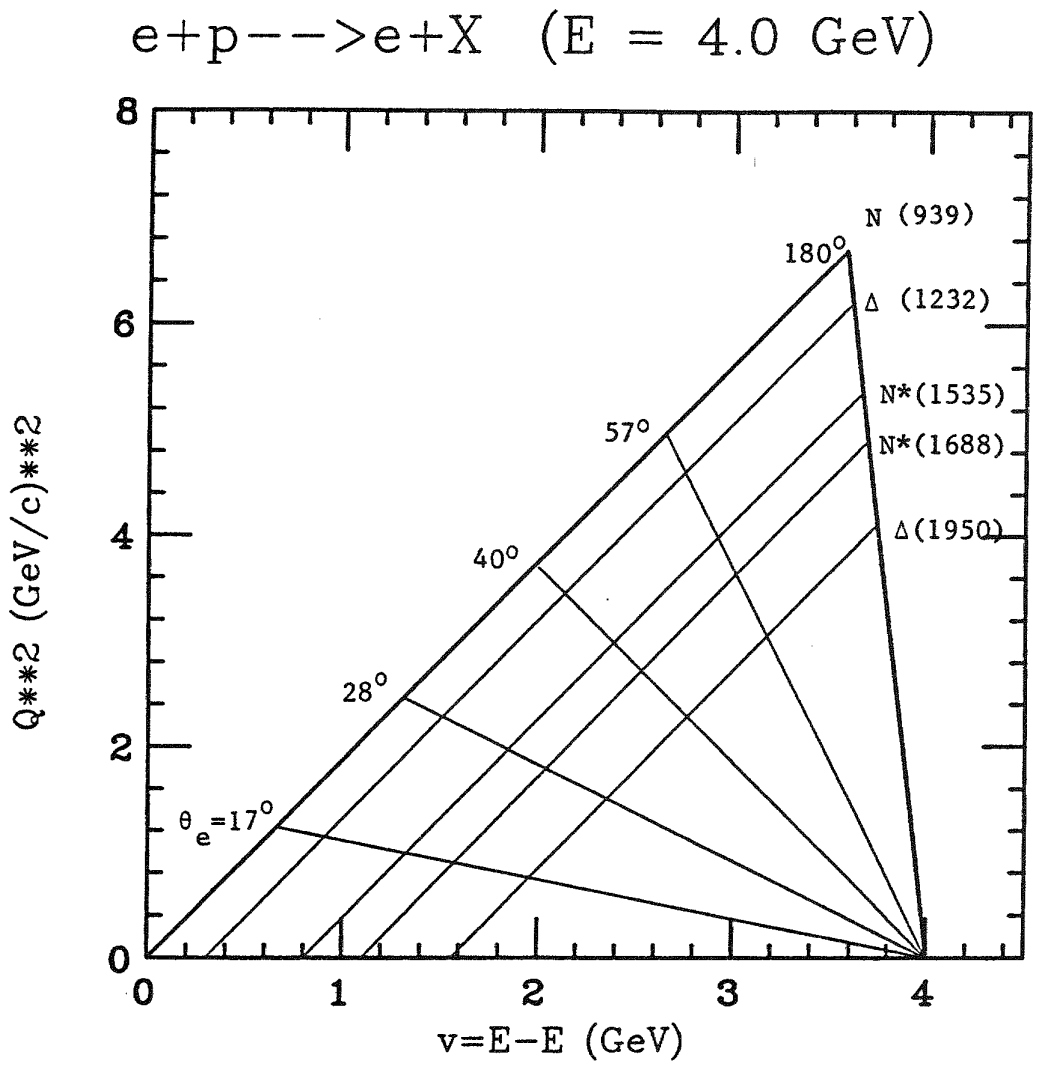

Figure 1 Kinematical Q^2 - ν region accessible with a 4 GeV Electron Beam.

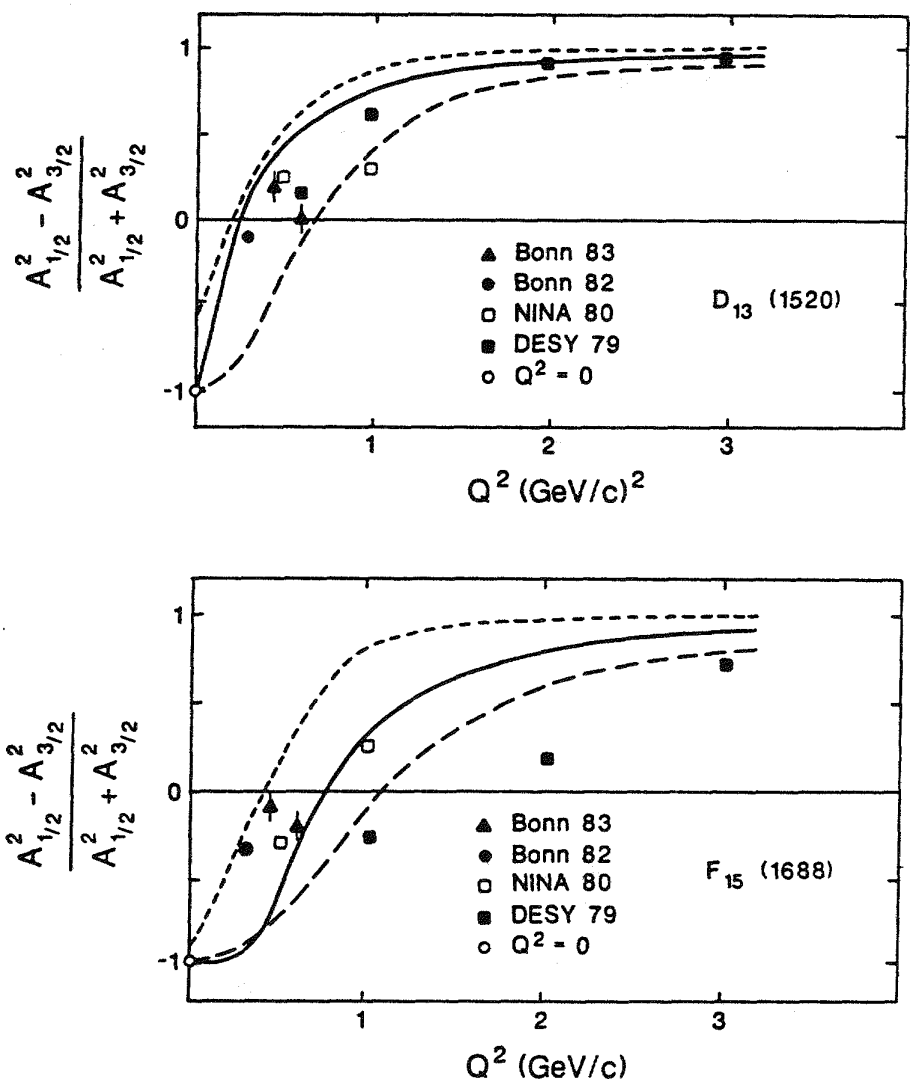

Figure 2 Helicity asymmetries for the D_{13} (1520) and F_{15}(1688).

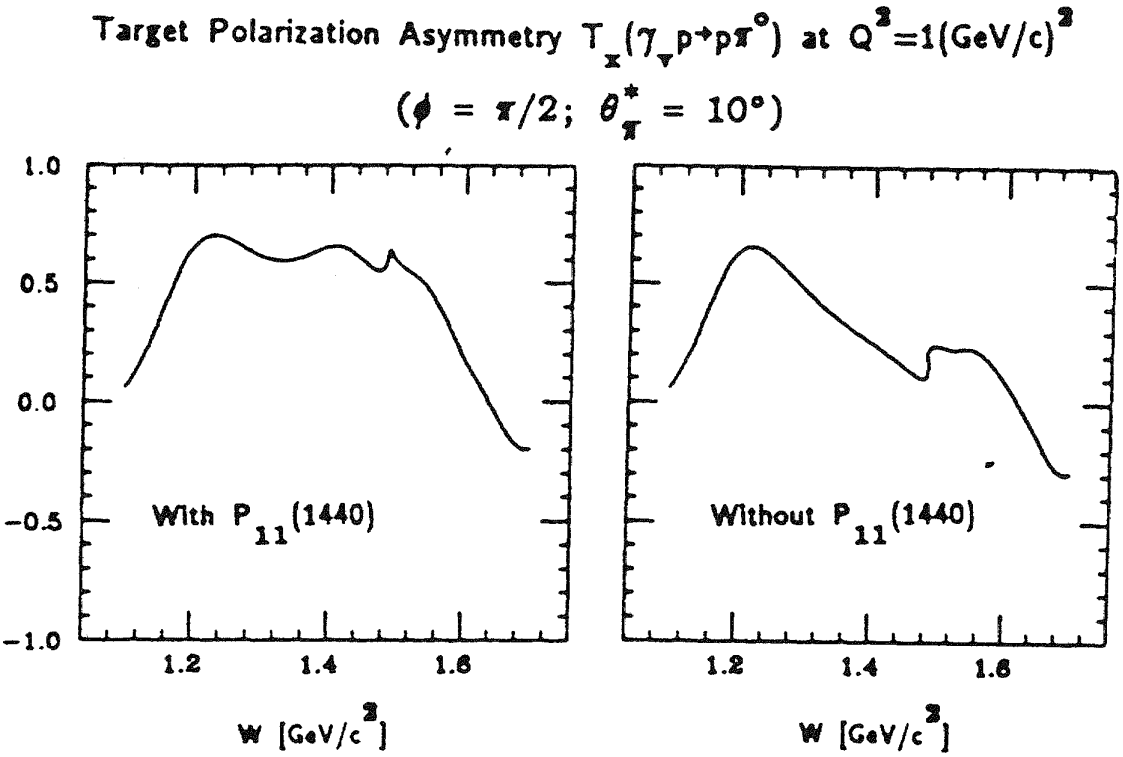

Figure 3 Polarized target asymmetry $T_x(\gamma_v p \to p\pi^o)$ for a specific kinematical situation. The target protons are polarized perpendicular to the virtual photon direction, in the electron scattering plane. Results of a recent analysis[3] have been used to predict the asymmetry (l.h.s.). To illustrate the sensitivity to the longitudinal coupling of the P_{11} the expected asymmetry is shown if the P_{11} were not excited (r.h.s.)

BARYON RESONANCES IN NUCLEI

Paul Stoler
Physics Dept., Rensselaer Polytechnic Institute, Troy, NY 12181

INTRODUCTION

Baryon resonances play an important role in a variety of nuclear reactions which transcend the interests of several CEBAF physics collaborations, including "(e,e'N)", "multihadron production", and "baryon resonances and meson production". Of specific interest to the present collaboration is how the nuclear environment affects the production, propagation, absorption, and decay of nucleon resonances, as well as their interference with non-resonant backgrounds in meson production processes.

In comparison with the program of studying the properties of resonances in nucleons, the additional complications associated with the nuclear medium requires us to carefully consider the types of experiments which are most likely to answer some of our questions in the framework of tractable and interpretable theoretical calculations. Considerable input from our theoretical colleagues will be essential. On the experimental side we must assess the feasibility of potential experiments in terms of parameters such as counting rates and background levels in the context of the presently planned or alternative experimental facility programs.

WORKSHOP HIGHLIGHTS

The initial collaboration workshop showed that we are at an early stage on both accounts. Among the 42 participants, 10 indicated a specific interest in resonances in nuclei. In addition, there were participants in other collaboration workshops such as "multi-hadron production" with similar physics interests. Most of the discussions focussed on the delta, since it is the lowest energy, most prominant and often studied resonance. Another attractive feature is that it decays solely into the two hadron final state.

Imbedded in a nucleus an important mode of interaction with the other nucleons may lead to the non-mesonic absorption of the delta with the subsequent emission of two nucleons. Another interesting process involving delta absorption is one in which an N-Δ interaction could lead to a Δ-Δ state, which disappears with the emission of 4 nucleons (Sh-86).

The reaction A(e,e'Nπ)X will be sensitive to the production and propagation of deltas in the nucleus. Due to the large effects of final state interactions, and the complications of many body systems one has to carefully select experiments which are meaningfully interpretable.

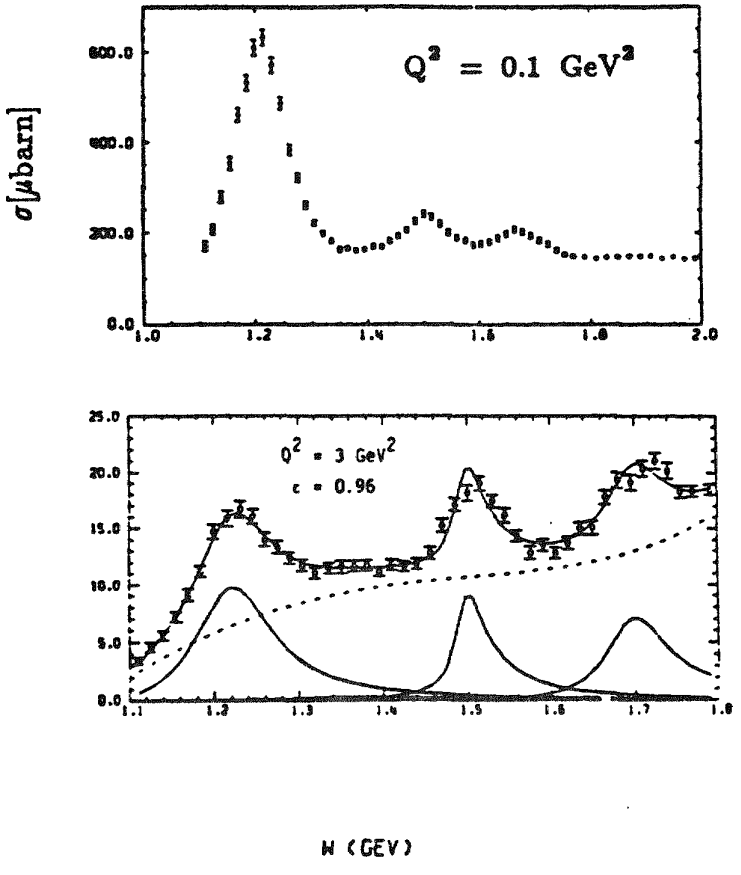

Figure 1. The reaction H(e,e')X showing the dominant delta and $D_{13}(1520)$, $S_{11}(1535)$, and $F_{15}(1688)$ resonances.

An initial round of experiments would involve light nuclei, such as ^{2}H, ^{3}He, and ^{4}He, in which the initial virtual (or real) photon is tuned to produce a delta of some initial momentum. The final pion and nucleon state is also fixed to a delta invariant mass. Several possible experiments are discussed in St-86.

At higher excitations most of the resonances have relatively small amplitudes, strongly overlap, and exhibit a variety of multi-meson decay modes. Furthermore, in meson production, especially charged mesons, they are overwhelmed by a large non-resonant background, so that their effects in the complicated environment of a nucleus probably cannot be studied. However, in addition to the delta, as seen in figure 1 three resonances stand out clearly above the rest, which may make them accessible to study in a nucleus. They are the $D_{13}(1520)$, $S_{11}(1535)$ and the $F_{15}(1688)$. The S_{11} is of particular interest since its form factor remains anomolously high at large Q^2, and it is the only strong resonance which has a large branching ratio to the η channel. Thus, η production really selects this resonance.

The π^{o} and η channels are especially interesting to measure because the non-resonant backgrounds are much smaller than in the case of charged mesons. However, experience has shown that detecting η's and π^{o}'s, especially from nuclear targets, is not easy. A discussion of this problem is given in a contribution to this workshop by M. Yamazaki (Ya-87).

A list of potential experiments which may be carried out at CEBAF is shown in Table I. The experiment A(e,e'4N)X which was mentioned above, is added to this list.

In order to interprete these experiments it will be very important to have a good knowledge of the elementary nucleon resonance amplitudes, at least for the dominant resonances. For example, Wi-86 have shown this to be a prerequisite in the interpretation of photopion data in the exclusive reaction $^{14}N(\gamma,\pi^{+})^{14}C$ in the region of the delta resonance. Thus, a vigorous program of measurement of large resonance amplitudes on nucleons will have important ramifications for the nuclear case as well.

To estimate experimental feasibility, counting rates were projected for the experiment A(e,e'Nπ)X using three potential detector facility; the LAS-Hall B, the HRS-hall A, and three hypothetical medium resolution, medium acceptance spectrometers (MARS). It was found that LAS and MARS can be quite complementary, in that MARS would be far superior for experiments in which the kinematics are well defined, whereas LAS can be used in more 'global' type survey experiments involving the possibility of

simultaneously detecting hadrons at all angles. The maximum counting rates with MARS is about 1000 per hr in favorable low Q^2 delta kinematics. Incidentally, it is very important to use extended targets dispersed in the beam direction. This allows rejection of accidental background which do not come from the reaction vertex. Also, significant increase in the LAS maximum luminosity above 10^{33} would considerably increase its potential for these type experiments.

EXAMPLES OF REACTIONS

Reaction	Physics
(e,e'NN)	Resonance absorption; $\Delta + N \rightarrow N + N$
(e,e'NNNN)	$\Delta + N \rightarrow \Delta + \Delta$; $\Delta + N + \Delta + N$
(e,e'Nπ^0)	Resonance formation, propagation;
(e,e'pπ^-)	relative role of resonant and
(e,e'nπ^+)	non-resonant contributions.
(e,e'pη)	Study of $S_{11}(1535)$; special.
A(e,e'$\pi^{0+/-}$)A	Coherent; nuclear structure effects.
All of the above with real photons.	

Table I. Examples of reactions which may be used to study the effects of resonances in nuclei.

References

(Sc-85) J.P. Schiffer, Comments, Nucl. Part. Phys., 14 15 (1985).
(St-87) P. Stoler, Research Program at CEBAF (II), SURA 261 (1987).
(Wi-86) R. Wittman and N.C. Mukhopadhyay 57, 1113 (1986).
(Ya-87) M. Yamazaki, contribution to CEBAF Summer Workshop (1987).

HADRONIC PROPERTIES OF VIRTUAL PHOTONS

R. Roy Whitney
CEBAF
12070 Jefferson Avenue
Newport News, Virginia 23606

Introduction

Determining the hadronic properties of the virtual photon is critical for the full understanding of the physics of electron scattering. The dominant hadronic contribution to the virtual photon comes from vector mesons (ρ, ω, ϕ) which have the same quantum numbers as the photon.

In the passage of a virtual photon through a nucleon or nucleus, the hadronic component is contributing to the interaction. One of the important aspects of the interaction is the amount of time (or equivalently the distance) the photon spends (or travels) as a meson. If the distance is short, the hadronic component is less important.

Figure 1 gives the formation length for ρ^0 mesons vs. kinematic variables. For a 6 GeV incident electron beam, the region of formation length can be explored for energy loss, ν, less than ~5 GeV. This means that at CEBAF the formation length can be varied from a fraction of the size of a nucleon to roughly the inter-nucleon distance in the nucleus.

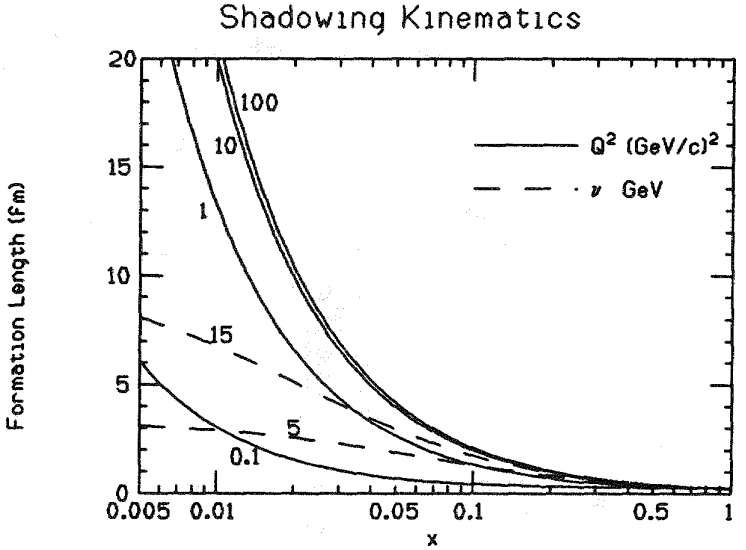

Figure 1. $x = \frac{Q^2}{2M_n\nu}$ is the Bjorken variable. The equation for the formation length, d, is:

$$d = \frac{1}{\sqrt{\nu^2 + Q^2 + M^2} - \nu}$$

where M = mass of ρ^o, Q^2 is the four momentum transfer squared and M_n the mass of the nucleon. For x = 1, d ~ .25 fm almost independent of Q^2.

The results of varying the formation length in a nucleus have been observed in shadowing experiments. A discussion of these experiments for CEBAF is presented in Reference 1. This discussion will focus on another aspect. The exclusive production of ρ^0 meson from the proton;

$$e + p \rightarrow e' + p' + \rho^0 \searrow \pi^+ + \pi^-$$

This reaction provides a sensitive test of assumptions made for the hadronic properties of the virtual photon[2,3,4] and the experiments can be extended to include nuclear targets.

Results to Date

The knowledge of the reaction at the present time can be summarized as follows:

1) For low t:
   a) The cross-section falls like e^{-bt}, where t = (Q-P)^2, P is the four momentum of the ρ^0 meson and b is a parameter equal to roughly 1/2 ($R^2_{\rho^o} + R^2_A$), the R being the radii of the scattered and target particles.[1] The vector dominance model VDM predicts the result.
   b) The helicity of the photon is transfered to the ρ^0 meson. This is known as s-channel helicity conservation, SCHC.
2) For t $\geq \sim$0.5 GeV^2, VDM and SCHC break down. The cross-sections do not decrease as fast as the exponential behavior indicated for low t. This indicates that VDM has broken down.

The breakdown of SCHC is observed when the exclusive production of vector means is analyzed in terms of a spin density matrix.[3] There are 26 independent matrix elements if the available polarizations are included. Only a few of the elements have been measured in existing experimental results. The regions of kinematics covered are limited and in general, the statistics are very low. Shown in Figure 2 is the helicity transfer matrix element coming from the angular distribution of the ρ^o in the center of mass system, CMS, when no polarizations are observed in the experiment. The angular distribution is

$$W(\theta,\varphi,\Phi) \Rightarrow W(cos\theta) = 3/4\left(1 - r^{04}_{00} + (3r^{04}_{00} - 1)cos^2\theta\right)$$

where θ is the polar angle and φ the asimuthal angle of the π^+ in the ρ^0 CMS. Φ is the asimuthal angle between the ρ^0 production plane and the electron scattering plane. The φ and Φ angles have been integrated out. The interpretation is:

$$r^{04}_{00} = 0, \quad \text{helicity} = \pm 1, \quad W \propto \sin^2\theta$$

$$r^{04}_{00} = 1, \quad \text{helicity} = \quad 0, \quad W \propto \cos^2\theta$$

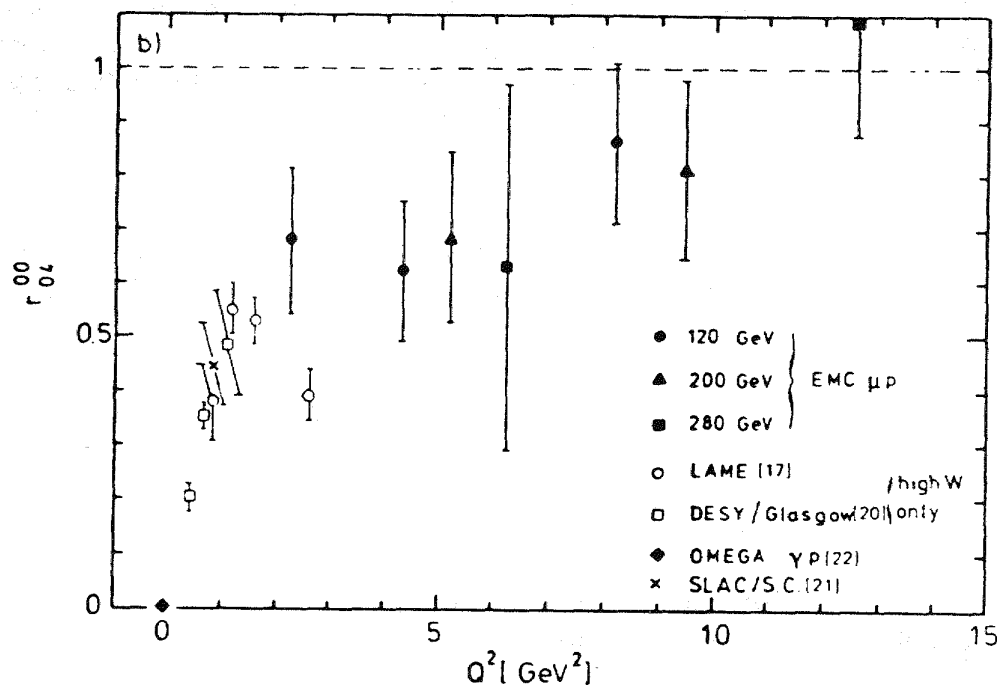

Figure 3. ρ^o density matrix element r_{00}^{04}[6]. Results from various experiments are shown: EMC[6], LAME[7], DESY-Glasgow[8], SLAC[9], EMEGA[10].

From the rapid variation of r_{00}^{04} with Q^2, it is concluded that the virtual photon's hadronic properties are rapidly varying. SCHC has broken down. The combined breakdown of VDM and SCHC indicate that the virtual photon appears more a point-like or bare object exhibiting a hard scattering process.

Experiment

To greatly improve on the existing results for ep $\rightarrow$ epρ^0, additional ϕ and Φ angular dependencies need to be measured and polarized targets and beams need to be employed. Initial experimentation could take place with the LAS[11] only and at 4 GeV incident beam energies. It is very important to add coverage of the forward angle. The kinematics favor having at least one forward going particle at small angles. The addition of shower counters will be essential when ω meson production is investigated.

The desired experiment is a quality measurement of cross sections and $W(\theta,\varphi,\Phi)$ for all the appropriate spin orientations as a function of the kinematic variables including formation length. Backgrounds from the reactions $ep\rightarrow e\pi^-\Delta^{++}$ and $ep\rightarrow \pi^+\Delta^0$ are more easily removed if the detector covers enough of the available phase space. Calculations of the phase space indicate that final state pions can be produced at all angles and cover a broad range of momenta. Counting rates for $ep\rightarrow ep\rho^0$ are given in Table I assuming a luminosity of $10^{33}/cm^2$-sec which is 10^{10} electrons/sec incident on a 0.16 gm/cm^2 hydrogen target. The LAS should be able to use this luminosity.

Table I

Events per day including detector efficiency for the LAS plus forward toroid for the process $ep\rightarrow ep\rho^0$. The luminosity has been taken as $10^{33}/cm^2$-sec for the full range of Q^2.

W (GeV) = $p\rho^0$ total energy in their CMS

$Q^2(GeV/c)^2$	2.0 – 2.5	2.5 – 3.0	3.0 – 3.5
0. – .5	267,000	285,000	279,000
.5 – 1.	34,000	37,000	35,000
1 – 1.5	11,000	11,000	11,000
1.5 – 2	5,000	5,000	5,000
2 – 2.5	2,400	2,400	2,400
2.5 – 3	1,200	1,200	1,200
3 – 3.5	700	700	700
3.5 – 4	400	400	400

The experiment is clearly do able at CEBAF. The event rates will be roughly 100 times higher than in previous experiments. The statistics will be adequate to determine the spin density matrix elements over important ranges of kinematic variables. The measurements can be expanded to include ω and ϕ mesons as well as inelastic channels and nuclear targets other than A=1.

Conclusion

The proposal for CEBAF is to measure with much higher statistics more of the spin density matrix elements in $ep\rightarrow ep\rho^0$ so as to better determine the hadronic properties of the virtual photon. The kinematic regions available at CEBAF are of interest. The formation length can be varied from less than the size of the nucleon to the internuclear spacing. The counting rates are adequate and the required experimental techniques will be available.

References

1. E. Paul, "Physics in the Transition Region from Soft to Hard Processes", Research program at CEBAF (II), CEBAF, Newport News, VA 23606, (1987).
2. F. Janata "Hadron Production in Charged Lepton Scattering",
3. K. Schilling and G. Wolf, Nuc. Phys. B61, 381 (1973)
4. T. H. Bauer, et al., Rev. Mod. Phys. 50, 261 (1978)
5. I. Cohen, et al., Phys. Rev. D, 25, 634 (1982).
6. EMC, J. J. Aubert et al., Phys. Lett. 161B, 203 (1985)
7. D. G. Cassel et al., Phys. Rev. D26, 1 (1982)
8. P. Joos et al., Nucl. Phys. B113, 53 (1976)
9. C. del Papa et al., Phys. Rev. D19, 1303 (1979)
10. D. Aston et al., Nucl. Phys. B209, 56 (1982)
11. B. Mecking, "Large Acceptance Magnetic Spectrometor for CEBAF", Report to the February 13–15, 1987 CEBAF Program Advisory Committee and private communication.

HADRONIZATION OF QUARKS AT CEBAF ENERGY

C. C. CHANG
Department of Physics and Astronomy
University of Maryland, College Park, Maryland 20742

ABSTRACT

Using the Lund Monte Carlo codes as a guide, the exclusive hadron production on a hydrogen target at 6 GeV incident electron energy is investigated. The study shows that the features of jet production similar to those observed at high energies are present even at CEBAF energy.

I. INTRODUCTION

The first evidence for the existence of point-like constituents (partons) in the nucleons was made in the late 1960s via the deep inelastic electron-nucleon scattering.[1] The observed energy and angular distributions of the inelastically scattered electrons were consistent with the assumption that each electron scatters from a charged parton that is essentially free. What happened to the struck parton after the collision was not an important factor in reaching this conclusion.

On the other hand, studying the properties of the hadronic system produced following the deep inelastic scattering (the so-called hadronization process) is of great interest for the following reasons. The production of hadrons may give information on the mechanisms by which the nucleon's partons rearrange themselves into the observable hadrons after the primary scattering. These mechanisms must be related to the forces that bind partons into the original nucleon, and may give the reason why no parton has yet been observed as a separate entity.

Recently, nuclear medium effects on the nucleon structure function have been demonstrated by the EMC effect,[2] i.e., the structure function of the nucleon embedded in the nucleus is different from the one measured on a free nucleon. One important question to ask is how does the nuclear medium affect the hadronization process. The use of nuclear targets is interesting because the kinematics of the reaction can be set up so that the distance over which the fragmentation takes place (the hadronization length) can be made to be comparable to the nuclear size. The information on this subject is rather limited. With CEBAF's high duty factor electron beam, it would be possible to study the exclusive hadron production on nuclear targets.

To aid us in investigating the feasibility of studying the jet fragmentation processes at CEBAF's energies on a proton target, we

use the Lund Monte Carlo codes.[3] The Lund string model is one of the phenomenological tools that is routinely used by high-energy physicists to describe hadronization in quark and gluon jets. The applicability of this model at the beginning of the scaling region has been studied by Dietrich and Johnson,[4] and was found to be useful.

In order to avoid the resonance region, we limit all the calculations in the following to have a value of W greater than 2 GeV. It is therefore essential to have an electron beam energy which is greater than or equal to 6 GeV. A Q^2 vs. x kinematic plot for 6 GeV incident electron energy is shown in Fig. 1. For the following discussions, we choose the limits $1.75 \leq E' \leq 1.85$ GeV and $26^\circ \leq \theta \leq 30^\circ$ which give values of Q^2 centered around 2.5 $(GeV/c)^2$ and x centered around 0.3. The results for other values of Q^2 and x are similar.

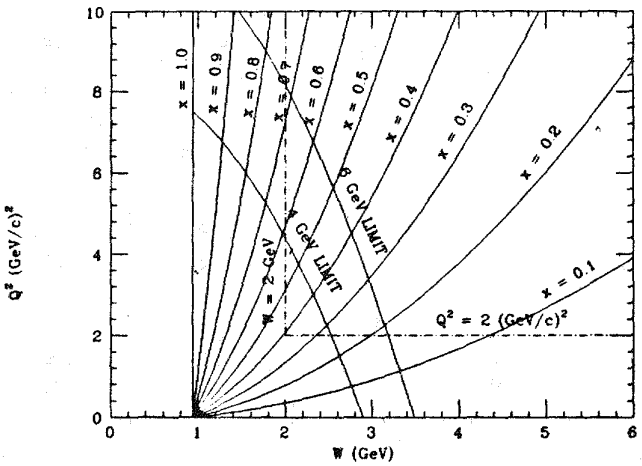

Fig. 1. Q^2 vs W kinematic plot.

Figures 2-5 show the Feynman-x distributions for π^+, π^-, K^+, and proton fragments with and without unstable particle decays included. One question one would like to answer is whether the fragments from the struck quark (current jet) and the target diquark (target jet) can be separated at low energy. The Lund-model calculations with particle decays included suggest that there are some indications of the forward-backward peaking (in the lepton-nucleon c.m. system) in proton and K^+ distributions while there is no clear evidence for double-peaking structure in π^+ and π^- productions. The reason is that π^+ and π^- yields are "contaminated" by unstable particle decays. Figures 2-5 also show the primary pion production yields, i.e., by suppressing the unstable particle decays. The forward-backward peaking is now obvious. The peak at negative x_F is due mainly to the target diquark while the peak at positive x_F is composed mainly of the current jet. This is because it is easier to produce a baryon from the diquark system than from a single quark, thus enhancing the peak at negative x_F for proton. Because of baryon number conservation there must always be a baryon in the final state. Since this happens preferentially among the target fragments, it leaves less energy for meson production at negative x_F.

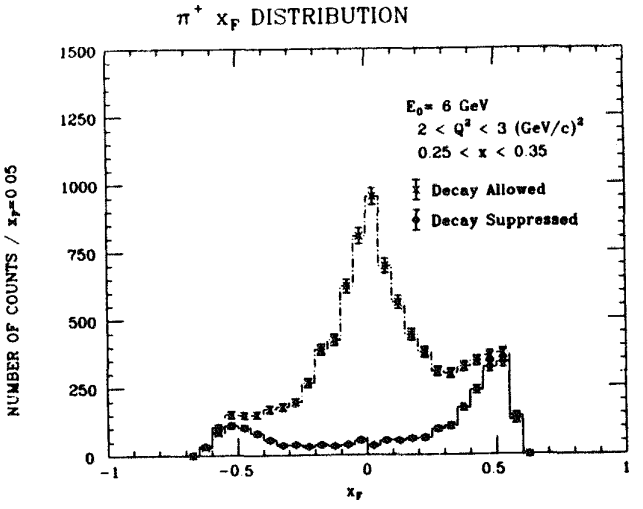

← Fig. 2. The Feynman-x distribution for π^+ fragments from proton.

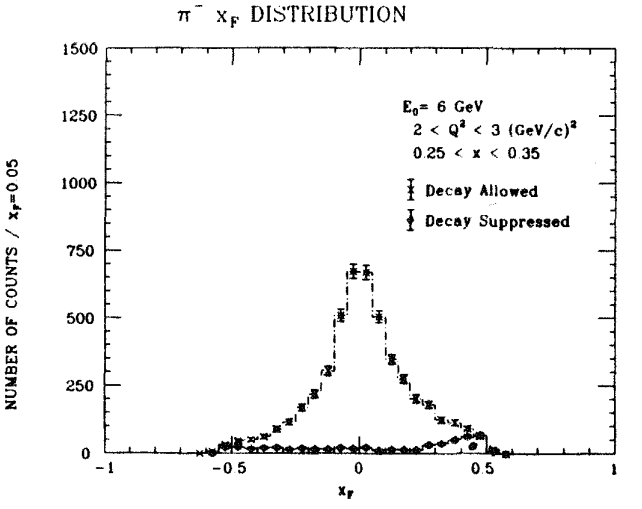

Fig. 3. The → Feynman-x distribution for π^- fragments from proton.

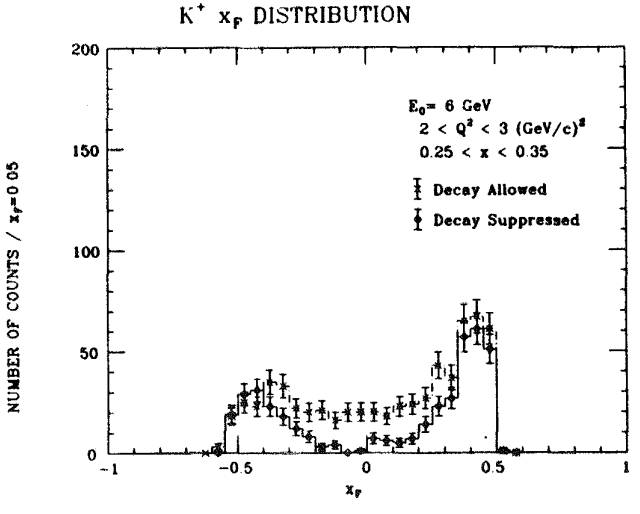

← Fig. 4. The Feynman-x distribution for K^+ fragments from proton.

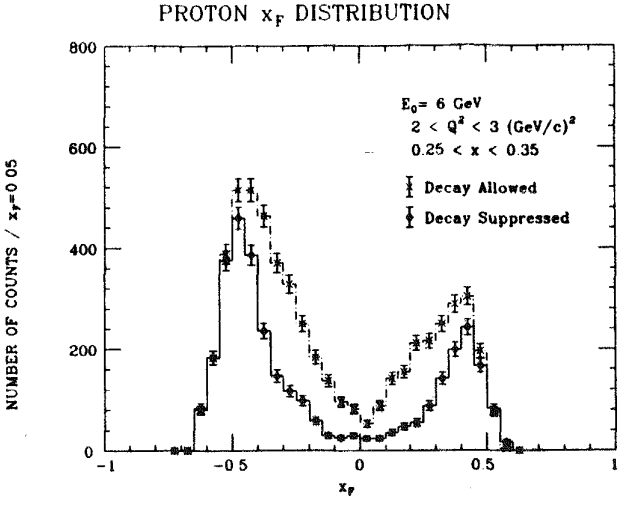

Fig. 5. The → Feynman-x distribution for proton fragments from proton.

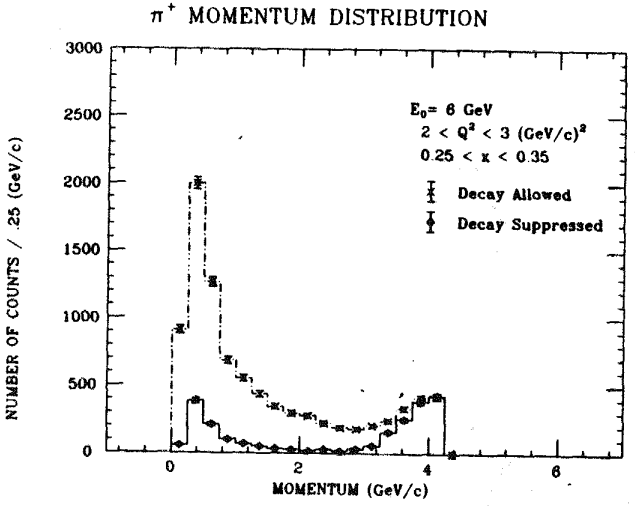

← Fig. 6. The momentum distribution for π^+ fragments.

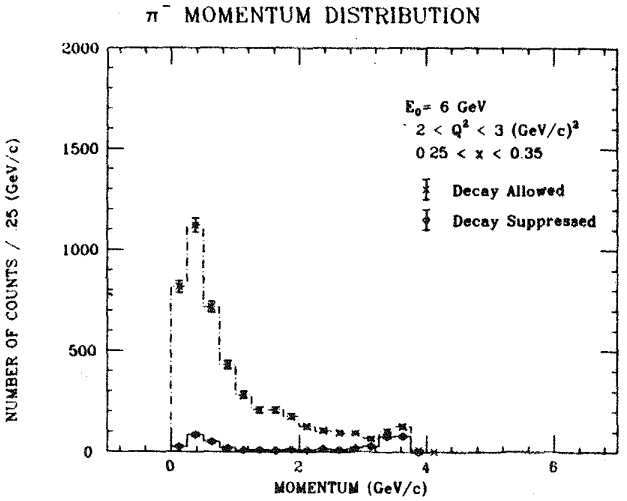

Fig. 7. The → momentum distribution for π^- fragments.

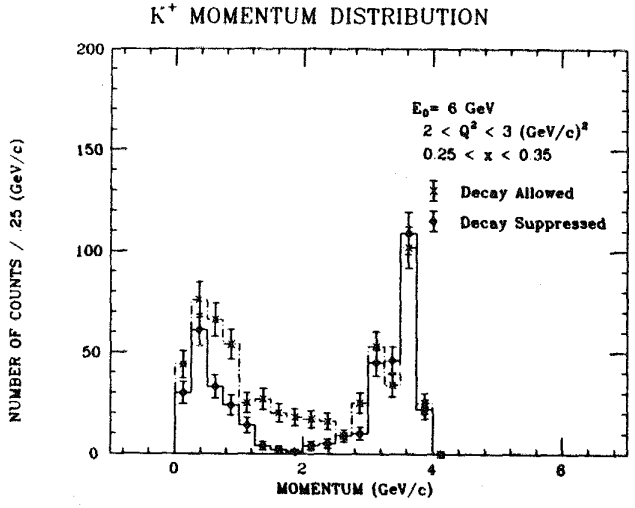

← Fig. 8. The momentum distribution for K^+ fragments.

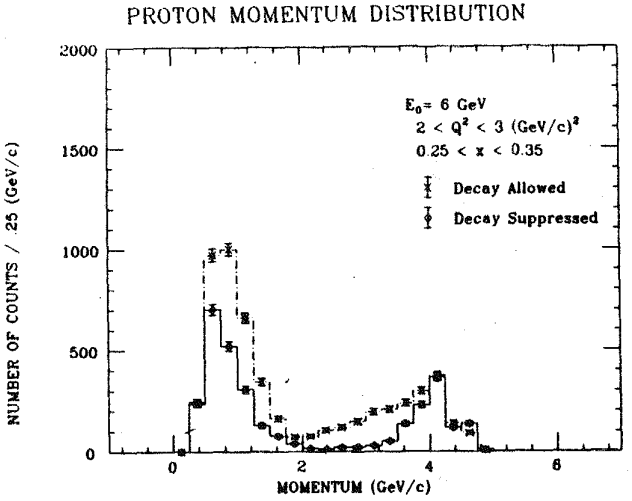

Fig. 9. The → momentum distribution for proton fragments.

Figures 6-9 show the momentum distributions for π^+, π^-, K^+, and proton. It is obvious from these figures that a device capable of detecting hadrons with momentum up to 5 GeV/c is required.

Figure 10 shows the proton fragment angular distribution in the laboratory system for 100 simulated events. It is interesting to note that the size of the cone for proton fragments is resonable.

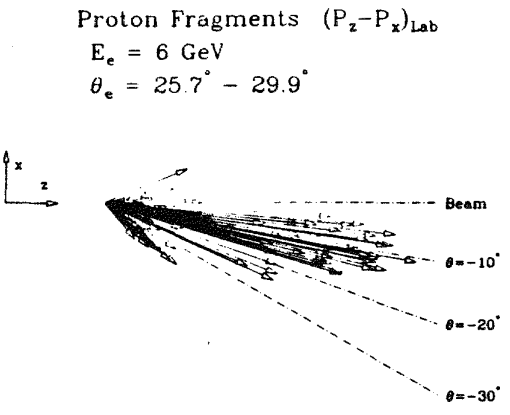

Fig. 10. The angular distribution for 100 simulated proton fragment events.

In conclusion, it is possible and is of interest to study the hadronization of quarks on protons and on nuclear targets at CEBAF. For hadrons, it is necessary to have a device capable of detecting particles with momentum up to about 5 GeV/c and with good particle identification. A possible device would be the LAS as proposed by Mecking[5] coupled with a forward-angle spectrometer.

REFERENCES

1. R. E. Taylor, Proc. 4th Symp. on Electron and Photon Interaction, Liverpool, 1969, Daresburg Nucl. Phys. Lab., p. 251.
2. J. J. Aubert *et al.*, Phys. Lett. 123B, 275 (1983).
3. T. Sjöstrand, Comput. Phys. Commun. 39, 347 (1986).
4. F. S Dietrich and C. W. Johnson, Proc. of the 1986 CEBAF Summer Study, RPAC II, p. 389.
5. B. A. Mecking, Proc. of the 1985 CEBAF Summer Study, PRAC I, pp. 3-20.

NEUTRON DETECTION AT CEBAF

J. W. Watson
Kent State University, Kent, OH 44242

ABSTRACT

The options for neutron detection at CEBAF are discussed, with emphasis on the resolution obtainable with available technology. Recommendations are made about provisions for flight paths for neutron time-of-flight measurements. Possible new technologies are discussed.

INTRODUCTION

This paper is a summary of the discussions of a working group on the needs for neutron detection capability at CEBAF organized at the 1987 CEBAF Summer Workshop. This group was chaired informally by the author and by Richard Lindgren of the University of Virginia. We discuss, in order, techniques for photon suppression, time-of-flight measurements and proton recoil detection. We present recommendations for provisions for longer flight paths. Finally, we discuss possible new technologies for neutron detection.

PHOTON SUPRESSION

A potential problem that must be dealt with in planning for neutron detection in an electron accelerator laboratory is the intense flux of photons produced by the beam passing through the target. A possible way of removing this flux without severely attenuating the flux of neutrons is a Pb "filter." A moderate thickness of Pb (~10 cm) will attenuate the photon flux by several orders of magnitude, but will attenuate the flux of medium-energy neutrons by typically less than 50%. This approach has apparently been successful in recent exploratory measurements at the Bates Laboratory of M.I.T. and at NIKEF in Amsterdam.

TIME-OF-FLIGHT TECHNIQUES

The time-of-flight method utilizing fast organic scintillators has been the standard technique for neutron spectral measurements for nearly three decades. The detectors described by Madey, et al. in Ref. 1 are representative of the state-of-the-art. In a time-of-flight measurement the fractional kinetic-energy resolution ($\Delta T/T$) can be approximated as

$$(\Delta T/T) = \gamma(\gamma + 1)[(\Delta t/t)^2 + (\Delta x/x)^2]^{1/2} \qquad (1)$$

where $\gamma = (1 - (v/c)^2)^{-1/2}$, t and x are the time-of-flight and the flight path, Δt is the combined time resolution of the detector

and the time reference (beam pickoff, conjugate particle detection, etc.) and Δx is the flight path uncertainty introduced by the finite dimensions of the neutron detector.

If we assume Δt = 300 ps, Δx = 10 cm (typical values from Ref. 1) and x = 30 m, which is about the maximum flight path available in Hall A, we obtain the energy resolutions in Table I. In Table II we present the flight paths required for 1 MeV neutron energy for various neutron energies.

Table I: Neutron Energy Resolution at 30 m

T(MeV)	ΔT(MeV)
100	0.8
200	2.0
300	3.6
500	7.8
1000	26.7

Table II: Flight Path for 1 MeV Resulution

T(MeV)	x(m)
100	25
200	60
300	105
500	235
1000	805

From Tables I and II it is clear that if one needs resolution on the order of one MeV, for example for (e,e'n) spectroscopy, one will be severely restricted in the energy range of neutrons that one can observe by the time-of-flight method. Even the construction of underground tunnels for neutron flight paths will only allow one to measure neutrons up to perhaps 300 MeV at best while maintaining 1 MeV resolution, because of the prohibitive cost of tunnels. Unless there are specific physics motivations calling for improvement in resolution in the 100 to 300 MeV range only, there appears to be little utility in installing underground tunnels for neutron flight paths, given the availablilty of other techniques.

PROTON RECOIL TECHNIQUES

The measurement of proton recoil energies from n-p collisions was one of the standard techniques for neutron energy measurements prior to the development of fast organic scintillators. This technique has recently been revived[2] for medium energy neutron detection at TRIUMF, which has the same situation as CEBAF with the accelerator and experimental halls being below grade. At TRIUMF the large acceptance "medium resolution spectrometer" (MRS) has been adapted for proton recoil detection. The "converter" is an organic scintillator typically 2 cm thick (~20 MeV energy loss for 200 MeV protons). By combining the energy loss of the recoil proton in the converter scintillator with the energy measured with the MRS, an overall energy resolution < 1 MeV is achieved even though the converter is relatively thick. This technique has been used successfully from 200 to 450 MeV with ΔT_n < 1 MeV, and there is no reason to believe that the technique could not be extended to substantially higher energies. Thus either of the spectrometers in Hall A at CEBAF could be adapted for good

resolution proton recoil detection for a broad range of neutron energies, provided that the converter scintillator is shielded by a "photon filter" as described above.

RECOMMENDATIONS FOR NEUTRON FLIGHT PATHS

The recent successful development of the proton recoil technique for medium-energy neutron spectrometry at TRIUMF, coupled with the limited benefits of flight paths up to even 100 m, led the working group to refrain from making a blanket request for underground tunnels for neutron flight paths. We did recommend, however, that the truck access tunnels for each experimental hall be aimed at the target so that limited options for longer flight paths would be available, should this become important.

POSSIBLE NEW TECHNOLOGIES

The principle advantage that time-of-flight techniques typically have over proton-recoil techniques is larger counting rates due to larger products of efficiency and solid angle. The numbers in Tables I and II were obtained from Eqn. (1) assuming Δx = 10 cm and Δt = 300 ps, numbers characteristic of the detectors in Ref. 1. There has been little motivation to date to improve upon these values, because accelerators such as the IUCF have beam pulse widths on the order of 300 ps. Both Δx and Δt could in principle be dramatically improved by using segmented detectors, and by using fast, high-density materials such as BaF^3. This could allow one to take advantage of the much smaller beam pulse widths at CEBAF and obtain values of ΔT_n much better than those in Table I.

1. R. Madey, J.W. Watson, M. Ahmad, B.D. Anderson, A.R. Baldwin, A.L. Casson, W. Casson, R.A. Cecil, A. Fazely, J.N. Knudson, C. Lebo, W. Pairsuwan, P.J. Pella, J.C. Varga and T.R. Witten, Nucl. Instrum. and Meth., 214, 401 (1983).
2. W. P. Alford, R.L. Helmer, R. Abegg, A. Celler, O. Hausser, K. Hicks, K.P. Jackson, C.A. Miller, S. Yen, R.E. Azuma, D. Frekers, R.S. Henderson, H. Baer and C.D. Zafiratos, Phys. Lett. B178, 20 (1986).
3. R. Madey, R.M. Sellers, A.R. Baldwin, B.D. Anderson, M. Plumley and J.W. Watson, Bull. Am. Phys. Soc., in press (1987).

REPORT OF THE PHOTONUCLEAR PHYSICS COLLABORATION

Hall Crannell
The Catholic University of America
Washington, D.C. 20064

Abstract

The members of the Photonuclear Physics Collaboration recommend than plans for a high intensity photon beam be included in the development of Hall C.

Report

A small group of about 15 participants at the CEBAF Summer Workshop met for two hours to consider the physics that requires real photons and the nature of the facilities that are planned to provide these photons. While it was clear that given a choice of only one kind of probe, the more kinematically flexible virtual photon would be selected, experiments with real photons offer additional information not obtainable in other ways. The group concluded that the facilities at CEBAF should provide for studies of interactions with both real and virtual photons.

Intermediate energy photons can most easily be made with electron beams, and there are a variety of techniques that have been developed for doing this. Facilities for producing photon beams using channeling radiation, laser backscattering, positron annihilation, bremsstrahlung, and photon tagging have been developed. Each of these techniques has its advantages and disadvantages. The Photonuclear Physics Collaboration members briefly reconsidered various options for CEBAF. For reasons of initial cost or general unsuitability to the design of

CEBAF, options using channeling radiation, laser backscattering, and positron annihilation appear not to be appropriate at this time.

A bremsstrahlung tagging facility has been considered as a resource to be place in Hall C, and is currently included in preliminary budget planning. This is certainly the most reasonable location for a tagged photon beam. The relatively low intensity of tagged photons ($\sim 10^7$/sec) necessitates the use of large solid angle detectors for most experiments in order to achieve adequate counting rates. The motivation for many experiments using tagged photons with the large aperture spectrometer has been presented in a number of CEBAF workshop and research reports and the members of this collaboration were unaware of any recent developments that have ameliorated the need for these facilities.

The collaboration members spent some time discussing the potential need for more intense photon beams than can be provided with tagging. The intensity of the photon beam can be increased by a factor in excess of 10^4 over that obtained with tagging by using the full electron beam intensity. In this case tagging can no longer be employed and direct information on the photon energy is lost. Nevertheless there appears to be several experiments where the increased photon intensity will be critical for the success of the experiment. These include those with modest energy resolution where the usual bremsstrahlung subtraction methods can be used, studies of the few (usually two) body photodisintegration where the cross sections are low but the photon energy can be reconstructed from the kinematics of the decay products {such as ^{4}He(γ,dd)}, and those cases where the target density is low such as in the use of polarized gas targets.

The use of polarized targets is predicted to be an important tool in developing an understanding of nucleon resonances, and in fact is a major consideration in selecting the design parameters of the large aperture detector. For example, calculations presented at this workshop show that the production of the S_{11} resonance N*(1650) is sensitive to the polarization state. It will be very difficult, and probably impossible, to disentangle the contributions from all of the resonances without the use of spin variables. The use of low density polarized targets will require higher intensity photon beams.

For all of the reasons mentioned above the members of the collaboration feel that it is very important to consider carefully the requirements for a high intensity photon beam and to plan the facilities so that such a beam may be installed when needed. We therefore recommend that the plans for a beam dump associated with a high intensity photon beam be included in the designs for Hall C.

An important consideration in the design of any photon beam is the installation of a well shielded electron beam dump. This is non trivial problem since most of the power remains in the electron beam after the radiator, and the radiator, and hence the beam dump, must be located near the target. These problems are roughly proportional to the beam power and thus will be much more serious for a high intensity beam.

Dumping the beam downward into a hole in the floor is a popular option since it provides considerable shielding from the earth. Such a dump will have to be provided for the tagged photon beam. It seems logical to consider making this dump capable of handling the full power of the

beam so that a full intensity bremsstrahlung beam may be installed when appropriate.

The members of the collaboration had no information on the cost of implementing this recommendation, and thus have no knowledge of the negative impact it might have on initial operations. Clearly more study of the cost and benefits are needed. The members did not seriously deliberate the need for photon beams in other than Hall C. These considerations are left for the future.

Present Status of the High Resolution Spectrometers

Jean Mougey
Continuous Electron Beam Accelerator Facility
12070 Jefferson Avenue
Newport News, VA 23606

1. Introduction

The Hall A spectrometer set up is designed primarily for the part of the CEBAF program which requires energy resolutions comparable to the designed value for the beam energy spread ($4\sigma_E = 10^{-4}$). It deals mainly with completely exclusive experiments in which the nuclear (bound) final state has to be fully specified. Typical values for the required missing mass resolution range from $\sim$ 1 MeV in light systems (d $\longleftrightarrow$ np separation) to $\sim$ 100 KeV in heavy nuclei, or for hypernuclear spectroscopy. High accuracy in the definition of the particle emission angles is also required to achieve the missing mass resolution and to allow absolute determination of cross sections to the level of 1%. Discussions on these points can be found in many contributions to this workshop, as well as in the proceedings of the previous CEBAF Summer Workshops and Summer Study Meetings.

Moreover, following the recommendations of the CEBAF Program Advisory Committee, design modifications are being studied to accommodate extended targets, with more moderate resolution. This would allow to accomplish a significant fraction of the few nucleon studies, including single arm (e,e') experiments. The need for out-of-plane capabilities in Hall A has been reemphasized, and the best strategy to achieve this goal has to be defined very soon. Modifications required to accommodate polarized hydrogen and deuterium targets have also to be examined.

The major requirements for Hall A spectrometers, derived from kinematics and cross section evaluations of some typical experiments are given in Table I. In addition, the two spectrometer set-up should allow to operate at high luminosity values ($\geq 10^{38}$ cm^{-2} sec $^{-1}$). The hall configuration should make possible the future implement of a third spectrometer, likely to be with $p_{max} \leq 1.5$ GeV/c, larger momentum and angular acceptances and shorter optical length. Such spectrometer could be used to detect kaons, pions, backscattered electrons and/or to perform triple arm experiments. Neutron detection capabilities should also be implemented.

Table I

Major Requirements for Hall A Spectrometers

	Electron Spectrometer	Hadron Spectrometer
Maximum momentum	4 GeV/c, upgradeable to 6 GeV/c	3GeV/c
Momentum acceptance	$\sim 10\%$	$\geq 10\%$
Solid angle	$\sim$ 10 msr	$\geq$ 10 msr
Angular range	$\leq 10^{\circ}$, 130°	$\leq 10^{\circ}$, 130°
Angular position accuracy	$\sim$ 0.1 mr	$\sim$ 0.1 mr
<u>Thin target mode</u>		
Momentum resolution δp/p	$\leq 5.10^{-5}$ optimized at 2 GeV/c	$\leq 10^{-4}$
Angular resolution $\delta\theta = \delta\phi$	$\sim$ 1 mr	$\sim$ 1 mr
Transverse position resolution δy	$\sim$ 0.3 mm	$\sim$ 0.3 mm
<u>Extended target mode</u>		
Target length acceptance (at 90°)	$\sim \pm$ 5 cm	$\sim \pm$ 5 cm
Momentum resolution	$\leq 3.10^{-4}$	$\leq 3.10^{-4}$
Angular resolution	$\leq$ 1 mr	$\leq$ 1mr
Transverse position resolution	$\sim$ 1 mm	$\leq$ 1 mm

2 - Hall A Configuration

The proposed spectrometer arrangement in Hall A is shown in Figure 1. The Hall itself is a circular underground building, 175' inner diameter, clearspan (no column), with 51' total height under crane hook, the beam height being 9' above floor. A 20 ton crane with maximum coverage will be permanently installed, while a mobile one (50 tons) will be used for initial spectrometer assembly and on demand. Truck access to end station floor for heavy loads will be possible through a hoistable platform (50 tons, 60' long). The off-centered location of the spectrometer pivot allow to reduce the room diameter, thus, in particular, the cost of the roof, without significantly hampering the angular motion of the spectrometers. The choice of the spectrometer configuration – one horizontal, one vertical – is discussed thereafter. Both spectrometers can separately reach a 10° forward angle (defined at the center of their acceptance), while the minimum angle between the two will be around 30°.

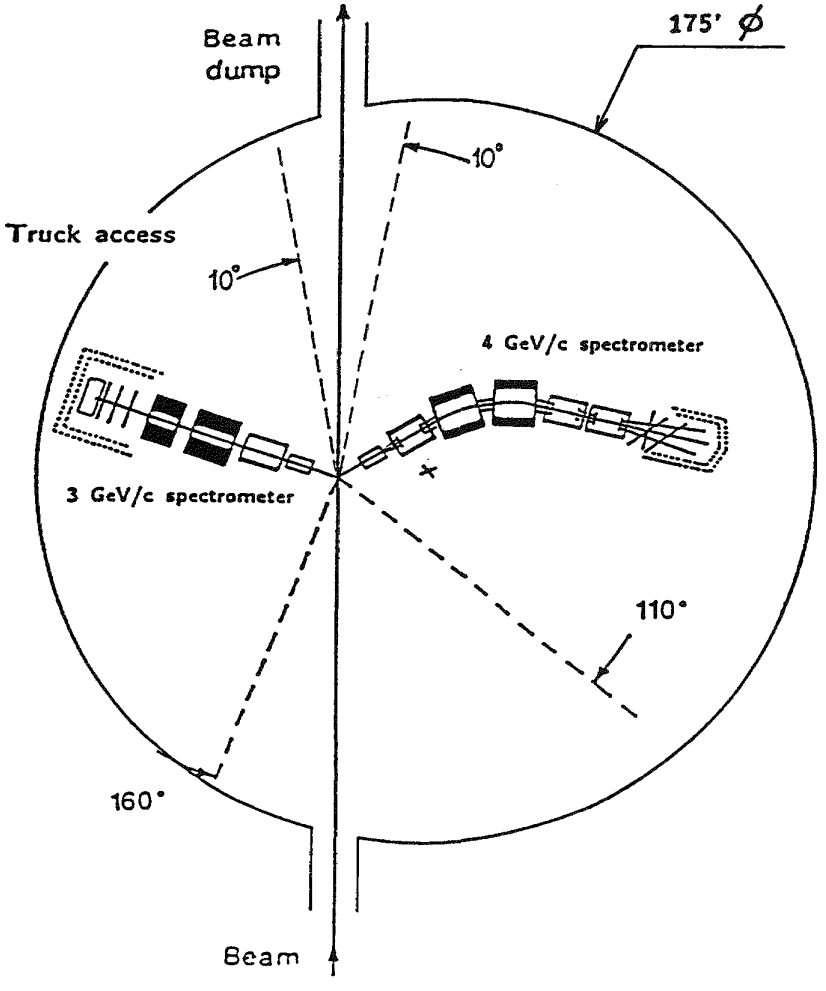

Figure 1 Spectrometer Arrangement in Hall A

As shown in Figure 2, the proposed scenario for out-of-plane measurements is to move the beam in the vertical plane, in one among five channels with angular spacings such as to provide sufficient overlap with the $\pm$ 5° ($\pm$ 2°) vertical acceptance of the electron (proton) spectrometer. In that scheme, by using discrete channels, one avoids the radiation problems created when bending the beam back to the 0° dump, due to bremsstrahlung and energy-degraded electrons. Moreover, it makes the system totally free of any mechanical motion. However, as the auxiliary beam dumps are closer to the end station roof, their power rating may have to be limited to $\sim$ 10% of the main dump one.

At present, the solution of moving the beam rather than lifting one spectrometer – namely the hadron one – is preferred, considering technical difficulties, costs and the high accuracy required for these experiments. I shall come back later on kinematical implications of this scenario.

3. Electron Spectrometer

The basic design for the 4 GeV/c electron spectrometer is shown in Figure 3, as it was defined about a year ago.[1] The main characteristics are listed in Table II. It is a QQDDQQ, essentially symmetric design, with a total bending angle of 45°, and a first order resolving power of 47000 for a beam spot size of 0.2 mm. Without changing distances between the various elements, it can be reconfigured to a 30° bending angle, 6 GeV/c spectrometer. With the same optical length, the radial length is increased by 0.8 mm, and the resolving power decreases to 31000. The spectrometer is bending horizontally. This allows to make optimal use of the dipole apertures while having an angular acceptance which is smaller in the plane of scattering, in which the cross section varies rapidly with angle. Its optical properties are shown in Figure 4, through the first order characteristic trajectories. Point-to-point imaging in both planes, to second order, is obtained along a 45°inclined focal plane by a sextupolar field component built inside the third quadrupole (Q3/M3). In between the two dipoles, the first order conditions $<y|\phi> = <\theta|\theta> = 0$ are realized. The transverse cross-over ensures modest dipole gaps (30 cm) in view of the large $\pm$ 90 mr angular acceptance, while the radial condition $<\theta|\theta> = 0$ makes optimum use of the pole width to build up resolving power. The drawbacks of this attempt to combine high resolution and large acceptances in a short, weakly bending, economical design are a large $<y|y>$ term in the last dipole and quadrupoles, and important higher order couplings

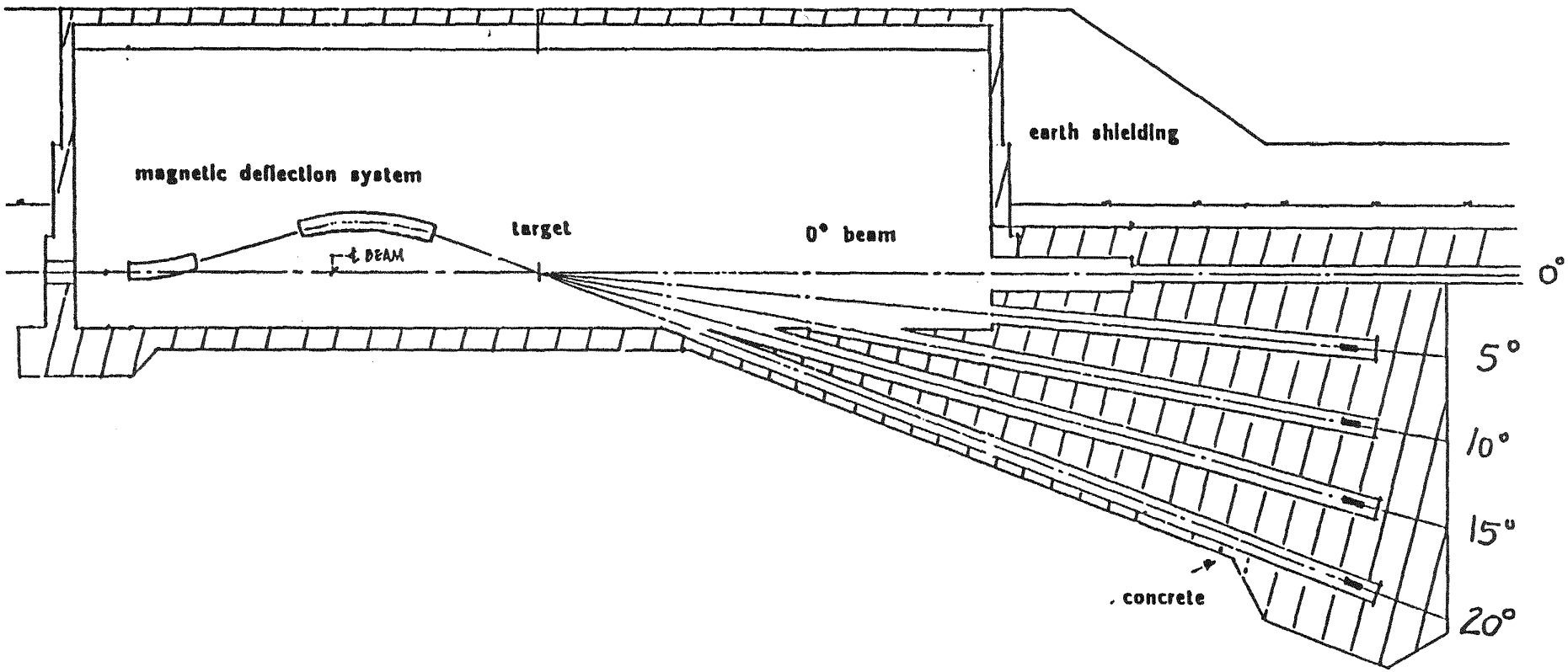

Figure 2 End Station A Out-of-plane set up. Only one of the entrance magnetic systems is represented, for sake of clarity.

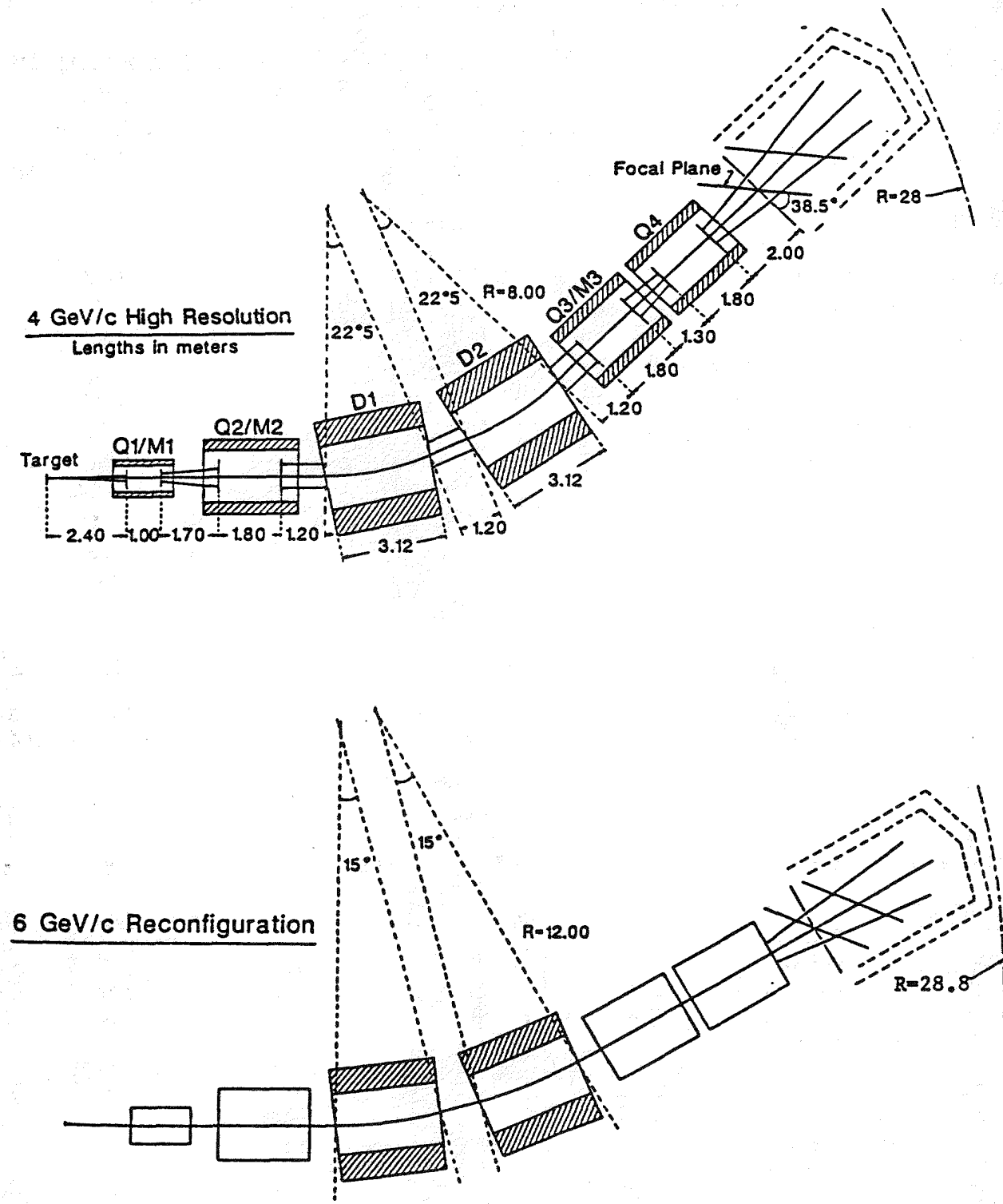

Figure 3 Schematic lay-out of the high resolution electron spectrometer for Hall A.

Main Design Parameters for Hall A Spectrometers

General Parameters	Electron Spectrometer*	Hadron Spectrometer
Type	QQDDQQ	QQDD
Bending	horizontal, 45° (30°)	vertical, 60°
Physical length (m)	23.7	18.0

Optical Parameters

Maximum momentum	4 GeV/c (6)	3 GeV/c
Momentum acceptance (%)	± 5	± 7.5
Solid ang (msr)	10.8	10.8
Angular acceptance horiz.	± 30	± 75
(mr) vert.	± 90	± 36
Momentum dispersion (cm/%)	9.94	6.97
Transverse focusing	point to point	point to point
Linear magnification horiz.	- 1.064	- 6.380
vert.	0.993	- 1.148

Technical Parameters

Dipoles	D1	D2	D1	D2
Magnetic length (m)	3.12	3.12	3.12	3.12
Physical aperture	160 x 30	160 x 30	160 x 30	160 x 40
Bending radius (m)	8	8	6	6
Maximum field	1.67	1.67	1.67	1.67
Bending angle (deg.)	22.5° (15°)	22.5° (15°)	30°	30°
Amp x turns (x 10^6)	0.48	0.48	0.48	0.64
Stored energy (MJ)	2.8	2.8	2.8	4.8

Quadrupoles	Q1	Q2	Q3	Q4	Q1	Q2
Magnetic length (m)	1	1.8	1.8	1.8	1	1.8
Warm bore diameter (m)	0.44	0.8	0.8	0.8	0.44	0.8
Inner coil diameter (m)	0.5	1	1	1	0.5	1
Maximum quadrupole strength (T/m)	8. (12.)	2. (3.)	2.1 (3.2)	4.8 (7.2)	6.2 (9.3)	2.3 (3.5)
Designed value	12	7.5	7.5	7.5	12	7.5
Maximum sextupole strength (T/m^2)	0	0.3 ( )	0.3 ( )	0		
Maximum octupole strength (T/m^3)	2.9	0.14 ( )	0 ( )	1.4 ( )		
Quad. amp x turns (x 10^6)	2.4	7.2	7.2	7.2	2.4	7.2
Stored energy (MJ)	1.5	5.3	5.3	5.3	1.5	5.3

*All parameters are for 4 GeV/c maximum momentum. Numbers under parenthesis are the corresponding values for 6 GeV/c, when different

between transverse and radial planes generated by the strongly focusing entrance doublet. Such higher order terms will have to be corrected by software.

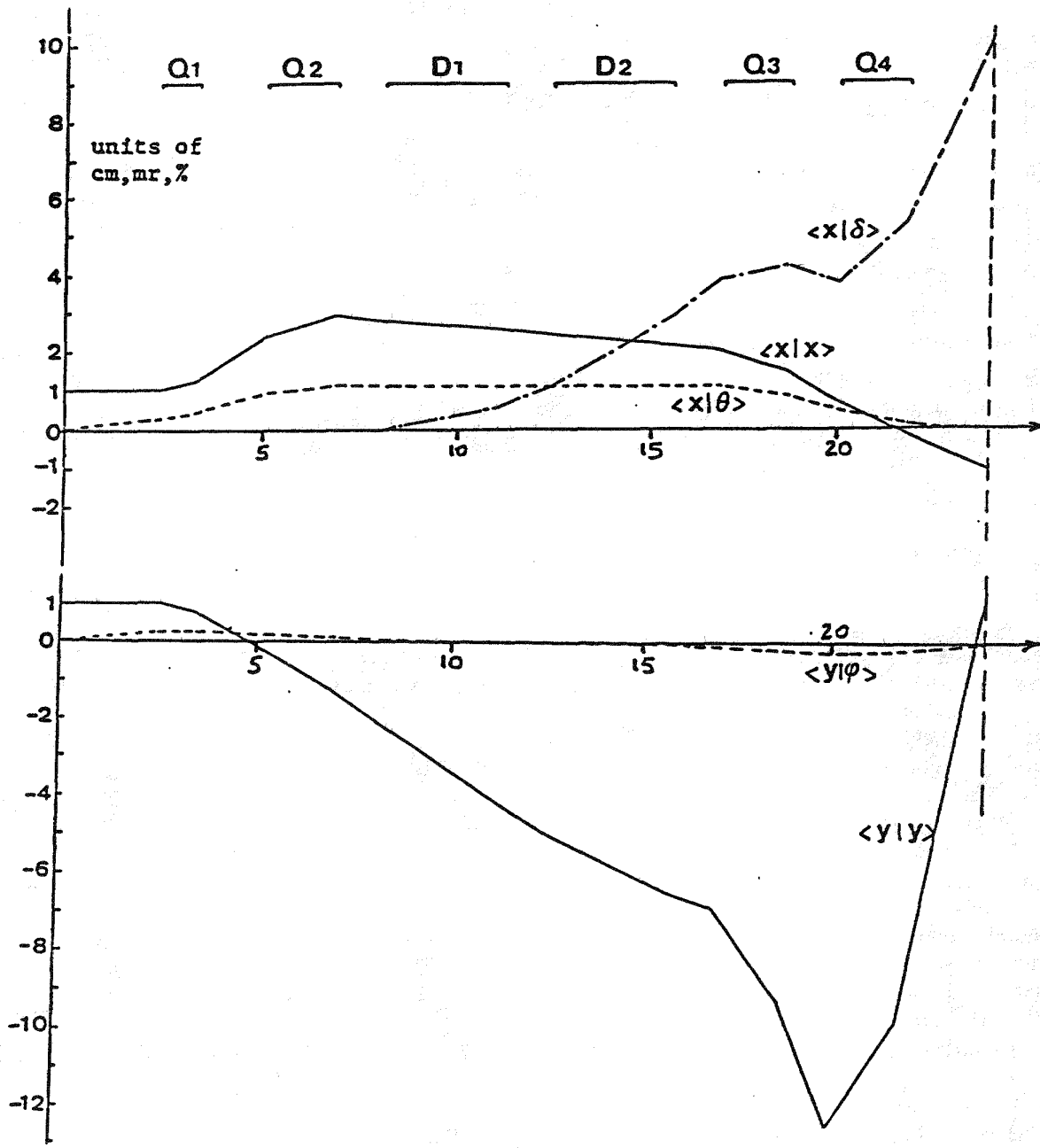

Figure 4 Characteristic ion-optical trajectories (first order) through the 4 GeV/c electron spectrometer.

The optical properties have been studied in the thin target mode of operation using raytracing (RAYTRACE, SNAKE) and multidimensional fitting (MUDIFI) computer codes. Prior to the software backtracing of the trajectories, the design has been optimized through third order by including sextupolar and octupolar fields in the quadrupole elements. Models were used to define dipole and quadrupole fringe fields, as the geometry of the magnetic elements is not yet fully finalized. Using a beam spot size of $\delta x_o = \pm$ 0.1 mm, $\delta y_o = \pm$ 0.1 mm, and the full spectrometer acceptances, $\Delta p/p = \pm$ 5%, $\Delta\theta = \pm$ 30 mr, $\Delta\phi = \pm$ 85 mr, 2000 trajectories have been selected randomly, traced through the spectrometer and used to define a set of coefficients allowing to trace back θ_o, y_o, ϕ_o and the relative momentum deviation δ_o at the target location. Using another set of 2000 random trajectories, the resolution of the spectrometer was obtained by comparing the true and traced back intital trajectory coordinates. For that purpose, finite detector resolutions were introduced by modifying randomly the final trajectory coordinates within the following limits:

$$\delta x = \delta y = \pm 0.1 \text{ mm} \qquad \delta\theta = \delta\phi = \pm 0.5 \text{ mr}$$

With such procedure, the following figures for the resolutions (FWHM) are obtained (see also Figure 5).

$$\delta p/p = 2.5\ 10^{-2} \qquad \delta y = 0.44 \text{ mm}$$
$$\delta\theta = 1 \text{ mr} \qquad \delta\phi = 0.9 \text{ mr}$$

As already explained, the spectrometer is planned to be built out of a few "modular" elements: Q2, Q3, Q4 are identical cos 2θ quadrupoles, with superconducting coils and warm iron yokes. An appropriate coil geometry (3 sectors) allows to eliminate the dominant higher order multipoles, and to make optimal use of the aperture. The front quadrupole Q1 has half inner coil diameter and a cold bore at liquid N_2 temperature, to allow small angles with the beam. Additional layers of conductors, powered independently, can be used to produce sextupole or higher order multipole fields which can be tuned either to correct spectrometer aberrations, or to compensate for unwanted high order multipole contributions coming from fringe fields, misalignments,...

4. Hadron Spectrometer

A layout of the design for the 3 GeV/c hadron spectrometer which was considered at the time of the Workshop is shown in Figure 6. It consists in a QQDD, 60°

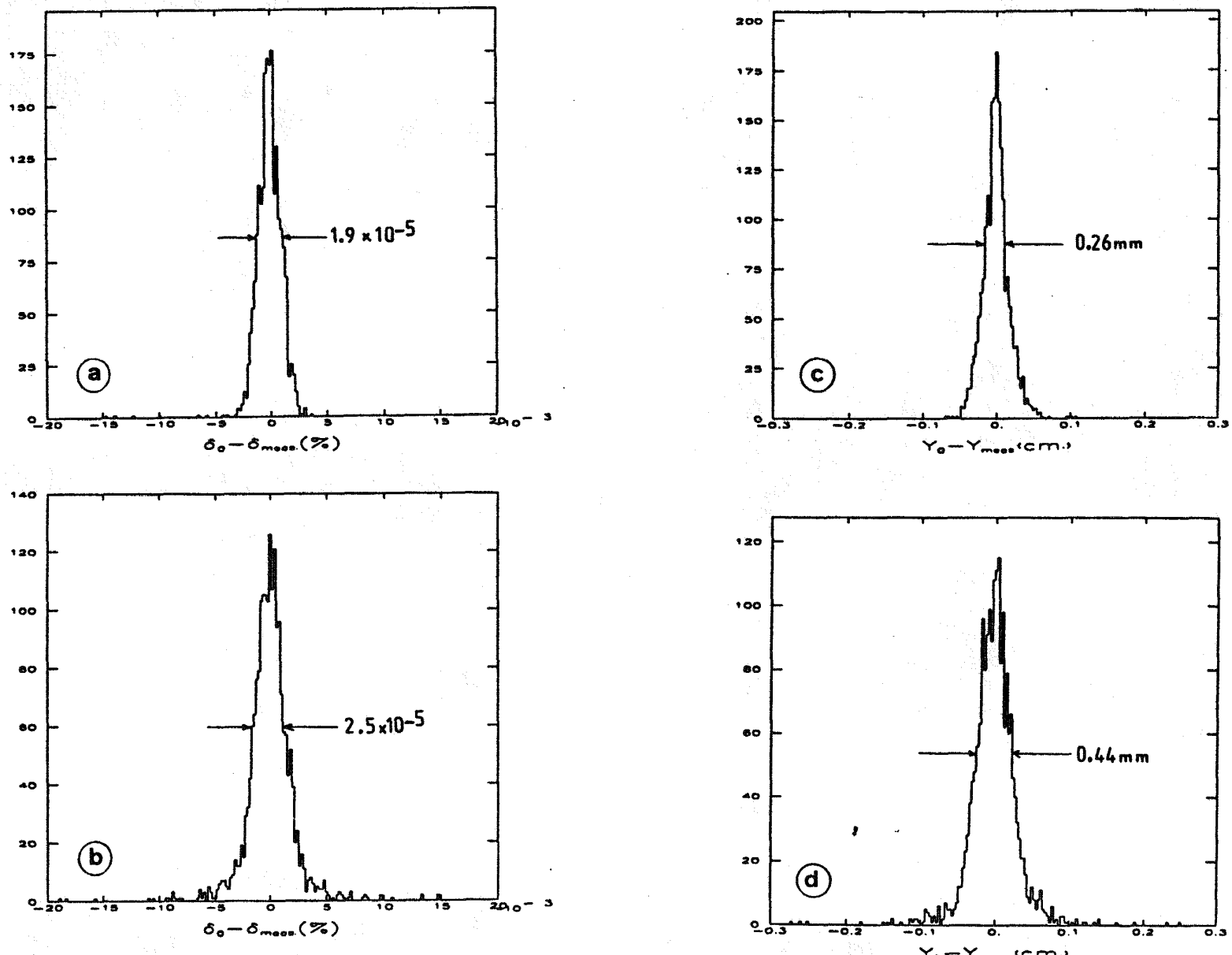

Figure 5 Computed momentum (a and b) and transverse position (c and d) resolutions in the 4 GeV/c spectrometer, without (a and c) and with (b and d) finite detector resolution (see text).

bend, 18m long vertical spectrometer, which makes use of the same basic modules as the electron spectrometer. Its main characteristics are given in Table II. The first order optics is shown in Figure 7, in terms of the usual characteristic trajectories. Here the spectrometer is tuned to be point-to-point focusing in the transverse plane. The large <y|y> term allows very precise reconstruction of the reaction point, even at small forward angles. This data is needed for trajectory reconstruction in the electron spectrometer when coincidence experiments are performed on extended targets. The counterpart is small target length acceptance ($\sim \pm 2$ cm) unless one increases the dipole gaps substantially. Moreover, the $< \phi|\phi >$ term is small ($= 1/<y|y>$), resulting in a rather poor angular resolution of ~ 3 mr in the horizontal plane.

The resolving power for a 0.2 mm beam spot size is 30000. The small <x|x> and $<x|\theta >$ terms in the last dipole allow for a resonably large momentum acceptance of $\pm$ 7.5%. However, the use of "standard" dipoles makes that all the focusing occurs in the front doublet. Together with the small bending angle and the short distance from last dipole to focal point, it leads to serious difficulties when trying to bring the focal plane to a reasonable angle, as well as to correct from aberrations. One possibility is to insert a sextupole element – with conventional coils – between the two dipoles.

5. Use of Extended Targets

Experiments on few nucleon systems call for liquid or high pressure gas targets extending along the beam over 10 cm or more. Compared to the ~1 mm source dimension one expects from thin solid targets, it represents two orders of magnitude increase in the required spectrometer acceptance, if one wants to keep the same solid angle value. Moreover, if one realizes that the present designs involve already magnetic elements with very large apertures relative to their lengths, and object and image distances very small compared to the bending radii, one foresees that modifying the designs to accommodate longer targets will not be an easy task.

For single arm experiments – like the measurement of few nucleon form factors – using the electron spectrometer, an additional position measurement in the dispersive plane, somewhere inside the spectrometer, is needed to determine the target reaction point along the beam. As it has to be inside the dispersive part of the spectrometer, the most natural location is in between the two dipoles (Figure 8a). In the standard optics tuning, trajectories are parallel to the spectrometer axis, so

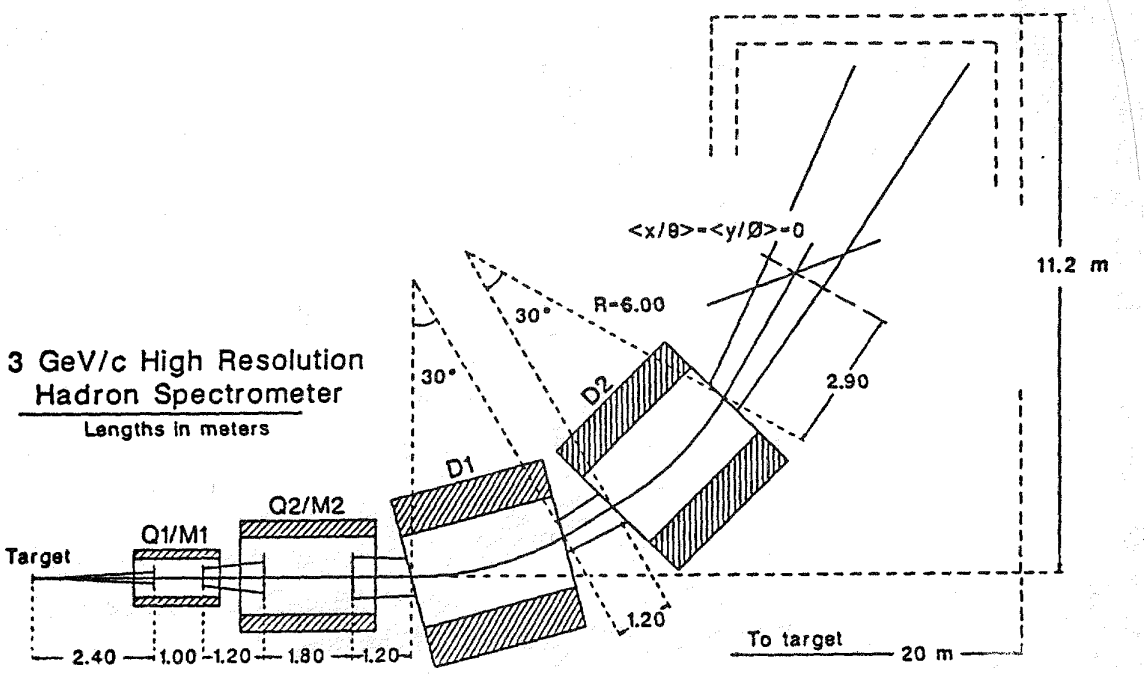

Figure 6 Schematic lay-out of the high resolution hadron spectrometer for Hall A.

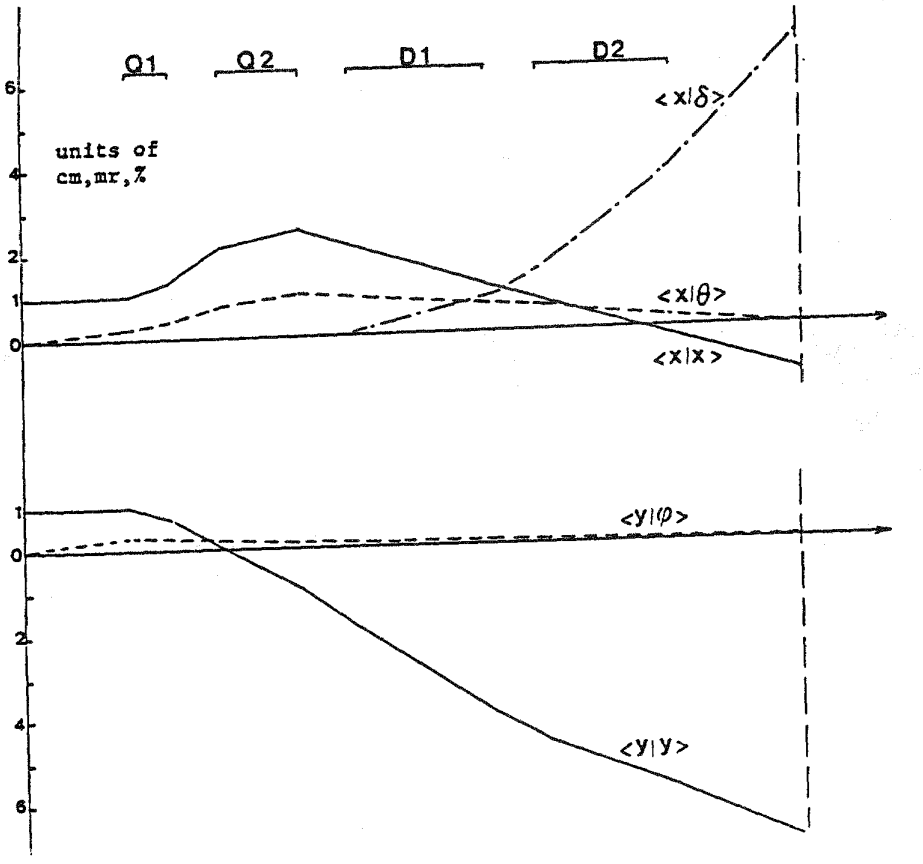

Figure 7 Characteristic ion-optical trajectories (first order) through the 3 GeV/c hadron spectrometer.

multiple scattering effects are maximized. Nevertheless, with a 20 mg/cm^2 detector thickness, their contribution to the resolution is 0.5 MeV (roughly independent of energy) which is still acceptable. However, due to the point-to-parallel first order transformation at this point, the position on target x_o is very badly determined by a position measurement x_1. This completely destroys the resolution. An angular measurement is needed, which can be done by adding a second detector, for instance after the second dipole (Figure 8b). To first order, one has:

$$\delta = 0.4\ x_f + 1.18\ (x_1 - x_2)$$

$$x_o = 2.82\ x_f + 11.0\ (x_1 - x_2)$$

which give x_o and δ with 3 mm and 3.4 10^{-4} resolution respectively. Multiple scattering effects in the first detector are eliminated by the second position measurement, but have dominant contributions to the resolutions (δx_o = 13 mm, $\delta p/p$ = 8.10^{-4} at 2 GeV/c) in the second one. Unless the second detector can be made much thinner than 20 mg/cm^2, the resolution will be about 2 MeV. Another possibility is to tune the spectrometer in a re-imaging mode (Figure 8c) by producing an intermediate focus in the dispersive plane. Due to the symmetric design, the whole spectrometer becomes achromatic. The target position and the momentum are determined using:

$$x_f = \langle x_f | x_o \rangle x_o \qquad = 1.07 x_o$$

$$x_1 = \langle x_1 | x_o \rangle x_o + \langle x_1 | \delta \rangle \delta \qquad = -0.47 x_o - 0.875$$

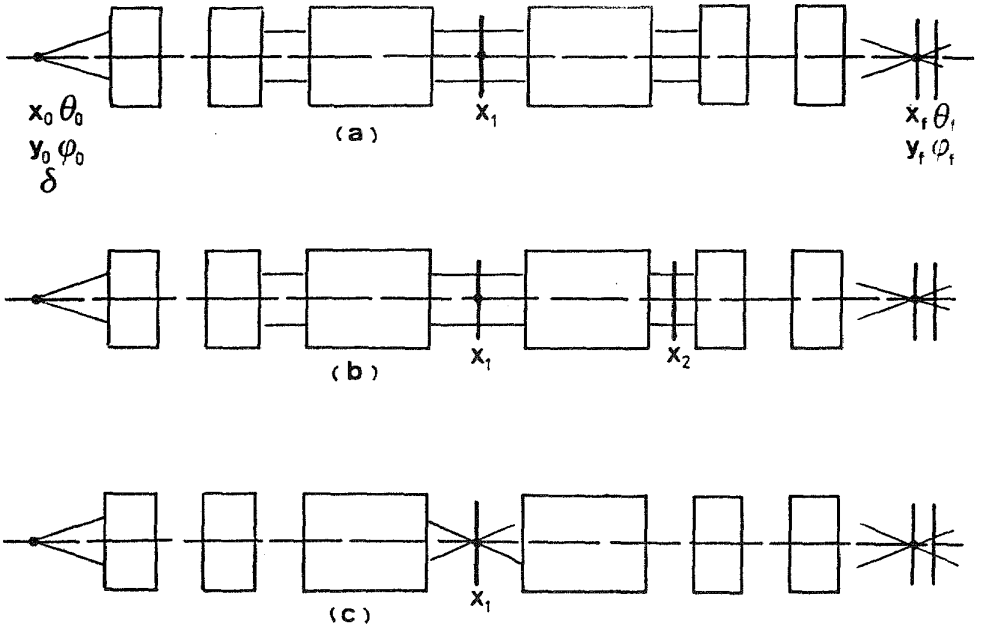

Figure 8 Possible schemes for operating the horizontal electron spectrometer with targets extending along the beam (see text).

With 0.2 mm position resolution, one can achieve $\delta p/p = 2.10^{-4}$ i.e. $\sim$ 1MeV at 4 GeV. Multiple scattering do not contribute to first order, and a target length of $\sim$ 15 cm can be accepted. The increase in field gradient values in the quadrupoles, needed to obtain the intermediate focus, is manageable. However the intermediate "focal plane" is laying at a very small angle (4.5°) with no possibilities to rotate it, due to the very small available distance between the dipoles. This gives rise to large aberrations in both the radial and transverse plane, which, even if they could be corrected by software, would hamper seriously the acceptancies, and increase the detector sizes.

For coincidence experiments, one can use the hadron spectrometer (bending vertically) to determine the reaction point along the beam. At very forward angle, $\theta_p = 10^o$, one can still achieve 1.2 10^{-4} resolution in the electron arm when $\theta_e = 90^o$, which in most cases will correspond to a scattered electron momentum below 2 GeV/c.

However, the present design for the hadron spectrometer suffers from a small target length acceptance due to the large <y|y> term at the end. Modified designs have been considered during the 1987 Summer Study Meeting. Although more work is needed before drawing definite conclusions, a more promising solution is a QDDQ design in which focusing strength in the radial plane is provided by tilted pole faces in the dipoles. By adding a third, weakly focusing, conventional coils quadrupole in front, one can decrease the <y|y> term down to about 3 in the last dipole, which would allow close to $\pm$ 5 cm long targets without increasing the dipole gaps, and with only a slight reduction ($\sim$ 8 msr) in solid angle. The same addition to the electron spectrometer improves its optics also, by decreasing both the <x|x> and <y|y> terms by nearly a factor of 2, at the expense of an increase in length of about 1.5m.

6. Out-of-Plane Experiments

Coincidence measurements under non coplanar kinematics are needed to isolate some of the interference structure functions which enter in the general expression of the coincidence cross sections. As mentioned earlier, an analysis of required accuracies, technical difficulties and costs favors moving the beam rather than a spectrometer. One examines here some implications of the proposed scheme.

Figure 9 shows the kinematics for a (e,e'X) reaction. The beam makes an angle α relative to the (horizontal) plane in which both spectrometers move; ϕ is the angle

between the scattering plane (scattering angle θ) and the particle X emission plane; γ is the angle between X and the momentum transfer $\vec{q}$. One has

$$tan\gamma = \frac{e.sin\alpha.sin\theta}{q\sqrt{cos^2\alpha - cos^2\theta}.sin\phi + sin\alpha(ecos\theta - e')cos\phi}$$

Moreover, one has

$$cos\theta = cos\theta_e cos\alpha$$

where θ_e is the (horizontal) electron spectrometer angle.

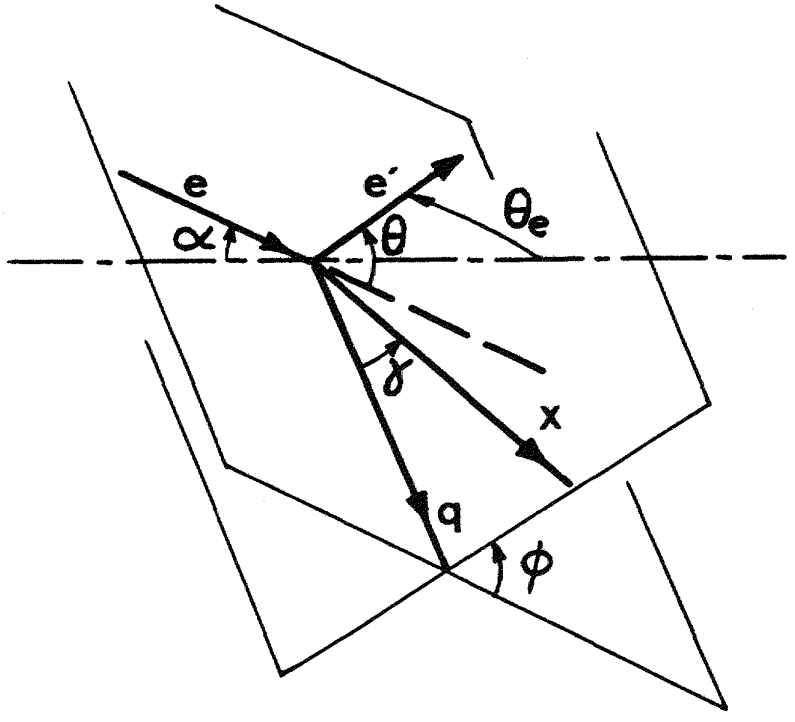

Figure 9 Noncoplanar (e,e'X) kinematics.

Figure 10a shows θ as a function of θ_e for discrete value of α. One sees that, for $\alpha = 20^o$, the minimum scattering angle is 20^o for θ_e=0, or 22.27^o for $\theta_e = 10^o$, which is an obvious limitation of this scenario. Figure 10b shows the values of γ one can reach for $\phi = 90^o$, $\theta = 22.27^o$, e = 2.56 GeV and q = 1 GeV/c under quasielastic kinematics (x = 1). One has roughly $\gamma = (2.5 \div 3)\phi$. For $\phi \neq 90^o$, γ is larger for the same α value. Under other kinematics with x $\neq$ 0, $\delta\gamma/\delta\phi$ is always much larger than unity. Therefore, the limitation to $\alpha = 20^o$ looks reasonable in this scenario. A practical limit in any attempt to move the hadron spectrometer is likely to be $\gamma = 30^o$. It is clear that experiments for which values of γ larger than 60^o are needed cannot be performed by moving either the beam or any of the large Hall A spectrometers. On Figure 10c, q is varied while keeping $\phi = 90^o$, $\alpha = 20^o$ and the quasi-elastic kinematics condition. The maximum value of γ one can achieve is given at low q by the minimum electron angle $\theta_e = 10^o$, and at high q by the maximum incident energy e = 4 GeV. One sees that, as long as the limitation does not come from the beam energy, γ_{max} is almost independent of q.

7. Use of Polarized Targets

An important fraction of the few nucleon physics program deals with polarization experiments, in particular the use of polarized proton, deuterium and helium targets. Most often, these targets require the presence of a magnetic field in the target volume during the measurement time. The possibility of using such targets together with a pair of focusing, limited acceptance high resolution spectrometer has been investigated. Two kinds of targets were considered.

a. Gas jet targets

An example is the ^{3}He target[2] which is planned to be used for G_E^n measurement through $^3\vec{H}e(\vec{e},e')$ inclusive measurements at the quasi elastic peak. The method used to polarize ^{3}He nuclei is a direct optical pumping technique of a 1 torr cell of ^{3}He gas by an infrared laser beam. It has been demonstrated that a high polarization rate of 70% can be achieved, with a sample thickness of 10^{19} atoms/cm^2. As the beam intensity has to be limited to a few $10^{14}e^-$/sec to control the depolarization rate, the luminosity values are not larger than a few 10^{33} cm^{-2}sec^{-1}. These figures are too low for Hall A spectrometers, and the LAS will be a preferred set up for such measurements.

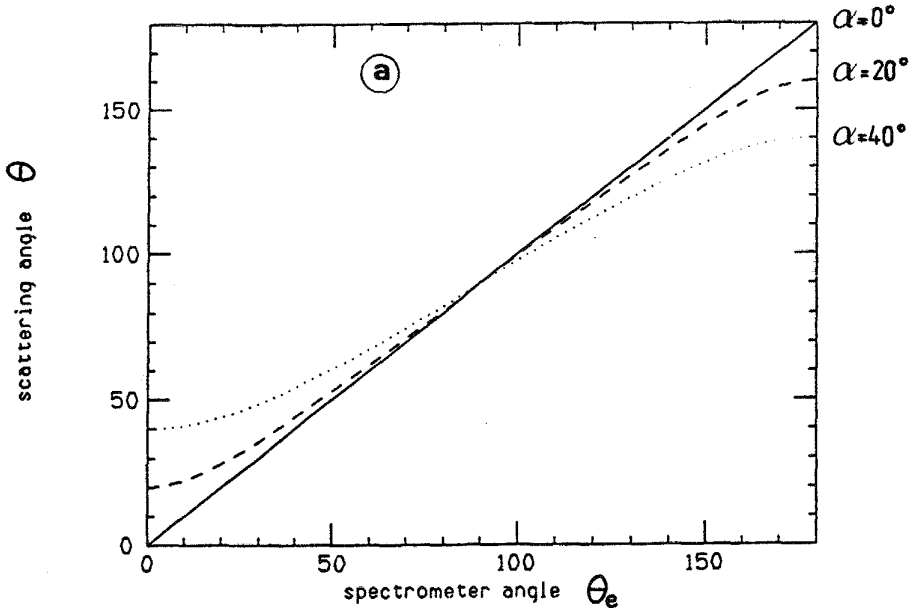

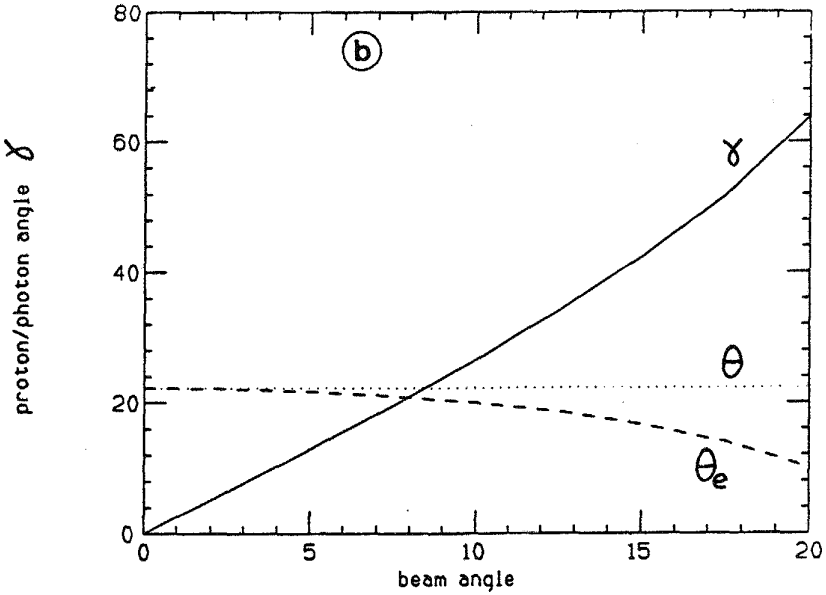

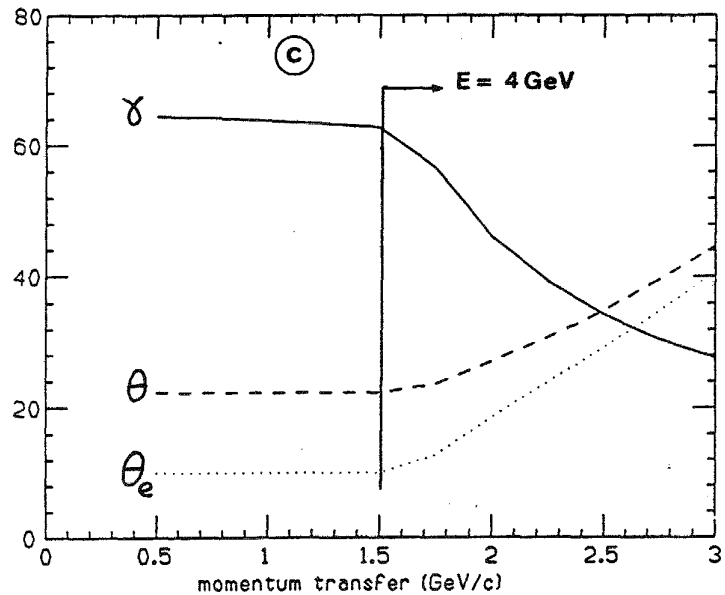

Figure 10 Angular relations and ranges for non-coplanar (e,e'X) kinematics: a) electron scattering angle θ_e; b) proton/photon angle & as a function of the beam angle α off the horizontal plane; c) maximum proton/photon angle as a function of the momentum transfer q. [A quasi-elastic kinematics is considered for b) and c) (see text).]

b. Solid targets

A major breakthrough for the possibility of using polarized solid state targets on external beams has been the development of very low temperature NH_3 and ND_3 targets[3], which have enhanced resistance to radiation damage and high polarization percentages. The dynamical polarization process requires very high magnetic fields (2.5 - 5T) to be applied continuously. To get the required homogeneity of $\sim 10^{-4}$ over a few cm^3 volume in a possible scheme for CEBAF[4], integrated field values $\int \vec{B}.d\vec{l}$ of up to 1 Tm may be experienced by the incoming and outgoing particles. This means $\sim 18^o$ deflection angles for $\sim$ 1 GeV/c particles. This, together with a few cm lateral displacement, is almost incompatible with in-plane, relatively small solid angle spectrometers. However, there are a few cases for which such targets may be envisaged in Hall A[5]. One is the measurement of G_E^n through coincidence (e,e'n) studies with a longitudinally polarized electron beam and a polarized deuteron target. In this case, the target is oriented in the scattering plane, perpendicular to the momentum transfer $\vec{q}$, i.e. at small angle relative to both the incident and scattered electrons. Particle trajectory simulations using the raytracing code SNAKE show that the experiment can be performed in the momentum transfer range $0.5 < Q^2 < 2$ $(GeV/c)^2$, using the 4 GeV/c electron spectrometer. The reduction in solid angle is never higher than 30%, as shown in Table III (preliminary).

Table III

Solid Angle Variation for a $\vec{d}(\vec{e}, e'n)p$ experiment using the 4 GeV/c Electron Spectrometer

Momentum transfer Q^2 $(GeV/c)^2$	0.45	0.95	1.54	2.02
Beam Energy (GeV)	4.	4.	4.	4.
Scattering angle	10^o	15^o	20^o	24^o
Polarization angle				
- re. beam	24.7^o	34.7^o	42.8^o	48.2^o
- re. scattered electron	14.7^o	19.7^o	22.8^o	24.2^o
Fractional solid angle	0.92	0.87	0.80	0.73

8. Magnet Design Studies

As mentioned earlier, the present designs for the spectrometers rely on combinations of a few modular elements. This has been considered simplify magnet studies, permit interchangeability and optimize costs and schedule.

Iron-dominated dipoles with essentially rectangular pole faces, uniform fields ($B_{max} \leq 1.7T$) have been chosen as dispersive elements. The field is expected to be homogeneous to one part in 10^4 within a 100 cm (width) x 30 cm (gap) x 312 cm (length) volume. Superconducting coils have been considered to be efficient[6] in reducing weights and costs, although the use of conventional water-cooled copper coils is not completely ruled out. Several geometries are being studied (see Figure 11). The window frame design allows to reduce the physical aperture, thus the total iron volume. But it implies "saddle-shaped" coils, difficult to realize when superconducting. Lateral forces on the coils which are closer to the high field region are very large. Moreover, as space is needed for cryostat and thermal shields, the coils are far from filling the gap height, which, in turn, makes that one loses the advantage of a high field homeogeneity in such solution. Solutions with separated poles, with tapered filtering gaps and anti-saturating profiles are also studied, either with racetrack coils (11b) or saddle-shaped coils (11c). Although the coil shape is more complicated in the last scheme, the possibility for the coil to be even higher than the gap leads to the best results in terms of field homogeneity and field map stability as a function of the nominal field (which is intended to vary between 0.17 and 1.7T). Detailed field and force calculations as well as an optimization of the end geometries are in progress.

The quadrupole elements have been chosen to be current-dominated, cos 2θ-type superconducting magnets, as large apertures and high field gradients are necessary to accomodate the large acceptances and the high particle momenta. Fields at coil positions reach $\sim$ 4T. A field gradient homogeneity of $\sim 10^{-3}$ is required within $\sim 3/4$ of the inner coil diameter. Each "pole" is defined by three coils winded on the same cylinder, with widths and spacing adjusted so as to cancel higher order multipoles (see Figure 12a). The windings are surrounded by an iron shield, located outside the cryostat. Two kinds of dimensions will be used, the front quadrupole being smaller to allow small forward angles. As the ratio between the effective magnetic length and the coil diameter is very small (1.8 for the large quadrupole, 2 for the small one), 3-dimensional studies are necessary. They are performed using both iron-free codes and the non-linear 3D program TOSCA allowing to study the

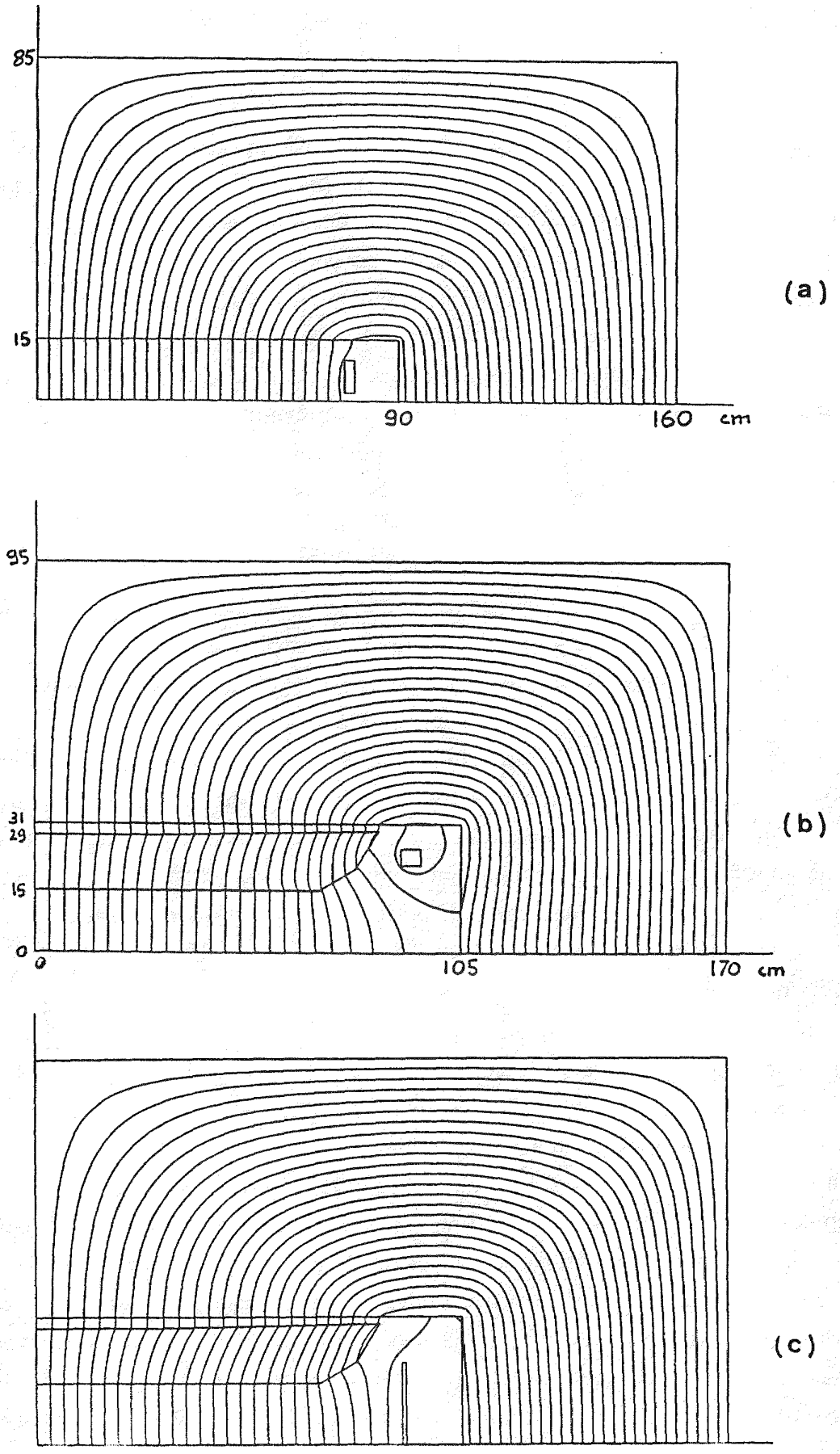

Figure 11 Possible configurations for the superconducting dipole elements. (a) window frame with saddle coils; (b) H-type frame with racetrack coils; (c) H-type frame with saddle coils.

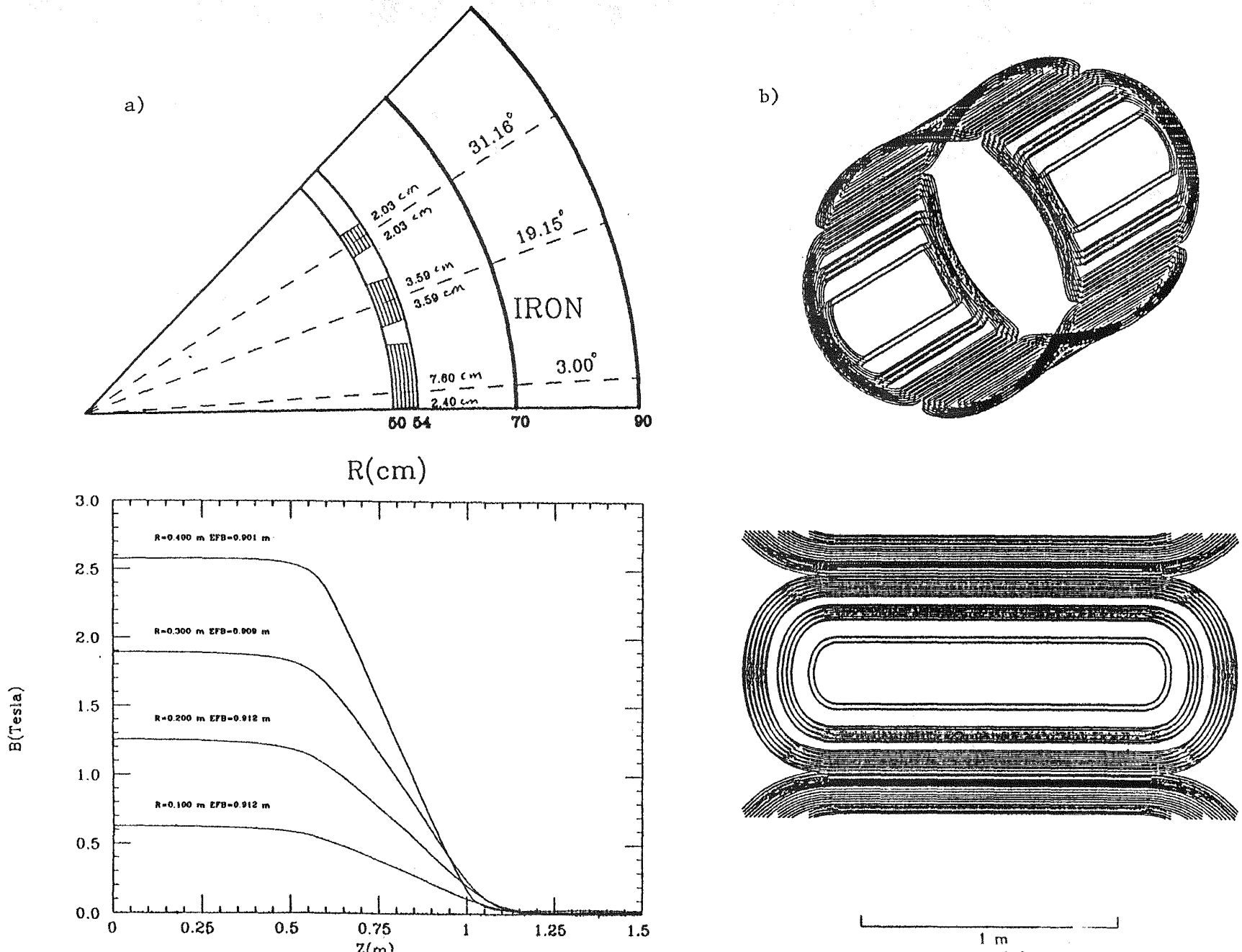

Figure 12 Superconducting cos 2θ quadrupoles (a) coil and iron configuration (b) possible solution for the end coil geometry and corresponding field distribution in the y=0 symmetry plane at various distances from the quadrupole axis.

geometry of the iron shield. Special attention is given to the shape of the coil ends. Standard "constant perimeter" ends tend to exaggerate the already poor aspect ratio. A modified version of them is shown in Figure 12b.

9. Conclusion

Although much work is still to be done, both on spectrometer optics and in design optimization of the magnetic elements, the high resolution spectrometers are gradually taking shape. The optics designs are going to be frozen by the end of September, and the main concepts for the design of the magnetic elements should be defined by the end of the year. A few key questions have to be answered soon, some being extensively discussed during the 1987 Summer Study Meeting. They include:

- Choice of the best scenario for out-of-plane experiments. The physics requirements for each experimental program have to be clearly defined, as well as the needed kinematical ranges and accuracies.
- Extended target capability. Define realistic requirements and tolerances, as well as possible compromises.
- Use of polarized targets: what can – has to – be done in Hall A?

As emphasized also in Costas Papanicolas' contribution, this is certainly an appropriate time for the potential uses of Hall A to express their own views regarding the designs of their future experimental set up. Many opportunities are offered to user collaborations to make actual contributions to the project, in particular (but without limitation) in detection systems, targets and target chambers, aperture defining slits,... which can be defined as fairly independent tasks.

References

1. J. Mougey, Proceedings of the 1986 CEBAF Summer Workshop, p. 45.
2. R.G. Milner, Proceedings of the 1986 CEBAF Summer Study Meeting (RPACII), p. 685.
3. E. Schilling, Proceedings of the 1986 CEBAF Summer Study Meeting (RPACII), p. 693.
4. V. Burkert, Proceedings of the 1985 CEBAF Summer Study Meeting (RPAC), p. 11-54
5. A. Mokhtari and J. LeRose, Contribution to the CEBAF 1987 Summer Study Meeting, to be published.
6. Proceedings of "Workshop on CEBAF Spectrometer Magnet Design and Technology," CEBAF, 7-11 April, 1986.

Report of the CEBAF High Resolution Spectrometers Program Collaboration

C. N. Papanicolas
Nuclear Physics Laboratory and Department of Physics
University of Illinois, Urbana, IL 61801

Abstract

The highlights, tentative conclusions, and broad issues addressed by the High Resolution Spectrometers Program Collaboration are summarized. Particular emphasis is placed on issues that may affect the design parameters of CEBAF End Station A.

1 INTRODUCTION

The detailed design report of End Station A, presented by J. Mougey[1] defines to a large degree the scope of the physics that can be pursued in that experimental Hall. The parameters that led to this design derived from the physics program that our community has identified as being "outstanding". The most recent restatement of these priorities and objectives can be found in the report of the 1^{st} CEBAF Program Advisory Committee,[2] which has been presented to this workshop by J. Schiffer[3]. The deliberations of the physicists participating in this Program Collaboration is then nothing else but the latest iteration in the loop:

$$\text{(physics objectives)} \Longleftrightarrow \text{(definition of Experimental facilities)}.$$

The significance of this latest iteration hinges on the fact that it is the last major deliberation before design parameters of crucial importance get frozen.

2 Capabilities and Limitations

Like every other realistic design, the one presented to us by J. Mougey, offers numerous possibilities but also a number of limitations. I will try to summarize here the physics program that can be pursued in Hall A, given the constrains of the current design, identify its potential handicaps and make its implicit compromises explicit. Last and most important try to identify the questions and tasks that need immediate attention, before the civil construction begins and before the design of the spectrometers gets frozen.

A detailed description of experimental Hall A and the proposed instrumentation can be found in Mougey's[1] article. Only the key parameters of this experimental hall are restated here, to facilitate the discussion:

Experimental Hall

- Circular building, 54m diameter.
- Beam line off Center.
- Allowed Radiative Power Dissipation in the room 40W.

4 GeV/c Electron Spectrometer (QQDDQQ)

- Horizontal bend; $\Delta\Omega = 10msr$; $\Delta p/p = 10\%$
- Energy Resolution: Better than 10^{-4}; In energy loss mode $2.5\text{x}10^{-5}$
- Angular Range: $10^0 < \theta_e < 130^0$ **3 GeV/c Hadron Spectrometer**

(QQDD)

- Vertical Bend; $\Delta\Omega = 10msr$; $\Delta p/p = 15\%$
- Flight path: 15m
- Angular Range: $10^0 < \theta_x < 160^0$

These parameters indicate some obvious kinematic restrictions but also some that are not so easy to detect. For instance the radiative power dissipation limit implies that the beam must be dumped very efficiently. This may be very hard to achieve in the case of polarized targets and when a beam swinger is used to bring the beam off axis in order to achieve "out-of-plane" kinematics.

Also few issues remain unresolved. The most serious one concerns out-of-plane detection capabilities. Two options have been considered. The first involves the conventional approach, getting the hadron spectrometer (approx. 500 ton) off the floor. Obviously, this is not easy (expensive too), given that accurate alignment is essential and that substantial out-of-plane angular range is desired. The second option is that of a multichannel beam swinger, discussed extensively by J. Mougey[1]. In this scheme the spectrometers stay in the plane of the floor but the beam impinges on the target from a direction that does not lie in the plane defined by the axes of the spectrometers. Its advantages are ease of angle changes (turning magnets on/off), reproducibility, and accuracy. The big disadvantage is that it does not offer a complete angular coverage excluding small angles.

The overall design of the experimental Hall and the proposed instrumentation are optimized for high resolution, high luminosity experiments. It is also obvious, that these parameters have been traded for solid angle. Experiments ben-

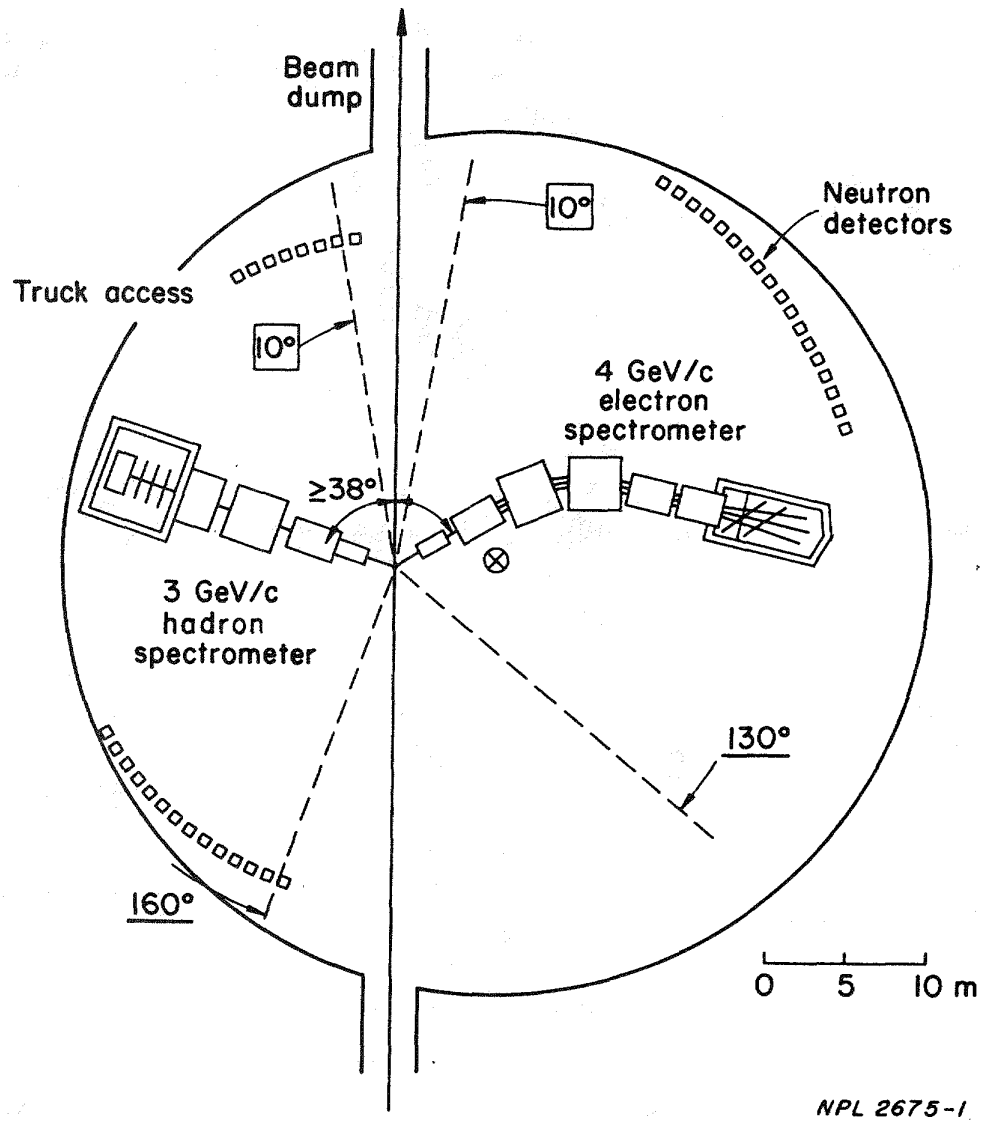

Figure 1: The most recent design plan for CEBAF experimental Hall A. The two spectrometers and possible locations for neutron detectors are also shown.

efiting from the conjugate choice of parameters are to be pursued in Experimental Hall B (or C).

Before examining the various components of the physics research program that can be pursued in Hall A, we shall briefly review the kinematic flexibility offered in the proposed facility. In a typical (e, e'x) experiment, the direction and energy of the emitted decay product is being detected, in addition to the familiar kinematic determination of the electron scattering variables. Figure 2 shows the geometry of the process and our choice of axes, suitable for discussion in the plane

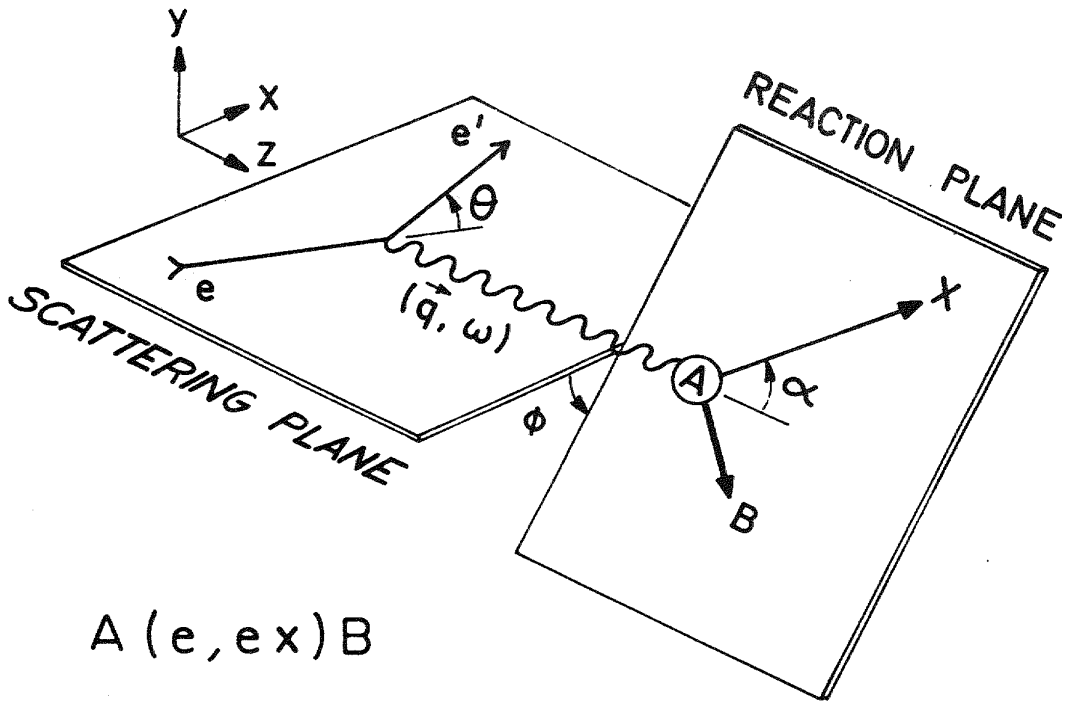

Figure 2: Geometry of the scattering process A(e, e'x) .The choice of axes ($\vec{q}$ oriented) is appropriate for a PWBA discussion.

wave Born approximation (PWBA). The familiar form for the coincident electron scattering cross section involves the five coincident structure functions[4,5]:

$$\frac{d^4\sigma}{d\Omega_x d\Omega_e d\omega dE_x} = \sigma_{Mott}\left(\frac{\Gamma_x}{\Gamma_{Tot}}\right)\{V_L R_L(q,\omega) + V_T R_T(q,\omega) + V_{TL}cos\phi_x R_{TL}(q,\omega) + V_{TT}cos2\phi_x R_{TT}(q,\omega) + h\tilde{V}_{TL}sin\phi_x \tilde{R}_{TL}(q,\omega)\} \quad (1)$$

where σ_{Mott} is the Mott cross section, and h is the helicity of the beam. $\left(\frac{\Gamma_x}{\Gamma_{Tot}}\right)$ gives the probability that the state of interest will decay by emitting a product x. The factors V_L, V_T, V_{TL},V_{TT} and $\tilde{V}_{TL}$ depend only on kinematic variables, the "knobs" of the experimentalist. All nuclear structure information is contained in the structure functions $R(q,\omega)$.

Figure 2 helps to define most of the kinematic variables in the above expression. The kinematic flexibility in the electron scattering angle θ_e, the reaction product angles α and ϕ, the "out of plane angle", is essential to disentangle the five structure functions. Most familiar is the separation of the longitudinal $R_L(q,\omega)$ from the transverse response $R_T(q,\omega)$ through the Rosenbluth method, which requires maximum dynamic range in θ. A casual examination of the parameters listed above may lead to the conclusion that this is a non-issue. But note that at 4 GeV and at 130^0 q=39 fm^{-1}. Even at 500 MeV incident Energy at this backward scattering angle one obtains q=4.5 fm^{-1}. In other words it may be that the

geometrical flexibility is available but in an uninteresting (or severly restricted) dynamic regime, especially for heavy nuclei. Clearly, instincts developed at low energy facilities may be misleading!

Evidently, a careful mapping of the interference responses at forward scattering angles will be required for a complete experimental determination of the physics of interest. Forward scattering angles offer the advantage of maximizing count rates due to the rapid increase of σ_{Mott}. At the same time this very rapid variation signifies the high sensitivity of the measurements to systematic error, and a low tolerance for finite acceptances and spreads. As we will show in subsequent sections, there is a real possibility that such limitations may wash out the desired signal in a number of measurements, unless utmost care is taken in the design of the experimental equipment.

Two issues then emerge as deserving further and very careful study:

1. The adequacy of the kinematic flexibility offered in the proposed facility. Are the smallest angles accessible to the spectrometers (10^0), the minimum angle of proximity between the two instruments (38^0) adequate? What flexibility is needed for out-of-plane detection? Is a beam swinger an acceptable alternative to an out of plane spectrometer?

2. The assessment of the sensitivity of the various proposed experiments to systematic error, and their needs for monochromaticity, extreme angular precision (instrumental, within the broad hardware bites) needs immediate study. Little experience is available at such high incident energy, and what little experience there is at low energy coincidence experiments, indicates that we will be facing a difficult situation.

Instead of trying to address these issues abstractly, I will attempt to examine them in the context of the proposed physics program. I will therefore try to offer an incomplete and biased summary of the conclusions of the various physics collaborations. It is biased in the sense that only the aspects of the program that can be carried in Hall A, are mentioned with exclusive emphasis on their experimental requirements.

3 The Physics Program

In the subsections that follow I present in arbitrary order the requirements of the various physics collaborations, as I have tried to record them during their deliberations. This anthology is bound to be incomplete. I hope it will help in highlighting the issues that need immediate attention.

3.1 Form Factors of Few Body Systems

The study of the form factors of few body systems constitutes a very rich physics program that has been carefully explored and has provided much of the justification for the demand of high energy high duty factor electron beams. Experiments such as the measurement of the G_{En}, the Electric form factor of the neutron, the exploration of the Tensor Polarization of the deuteron at high momentum transfers, the deuteron breakup and the form factors of ^{3}H, ^{3}He, ^{4}He are driving this program.

It is however interesting that alternative reactions can access the same physics. For instance the measurement of G_{En} can be achieved either through the $\vec{d}(e,e'n)$ or the $d(e,e'\vec{n})$ reactions. Similarly the tensor polarization of the deuteron (T_{20}) can be performed either through the $\vec{d}(\vec{e},e'd)$ or the $d(\vec{e},e'\vec{n})$ reaction. The difficulties associated with the implementation of a polarized target facility and the instrumentation of recoil polarimeters are quite different. A detailed study of the advantages and disadvantages of these two options is rather urgently needed, given that both present formidable technical problems and they may affect conventional construction.

The capability for out-of-plane detection has invariably manifested itself in almost every experiment discussed in this program. A detailed study by Boeglin and Bertozzi[6] of the sensitivities to finite acceptances, beam spread, and systematic error, in the measurement of the responses of the deuteron in an $(e,e'p)$ measurement has brought home the difficulty of such measurements. The amplification of the error in the Transverse-Transverse response f_{-11}, can be appreciated with the help of Figure 3. A miniscule uncertainty (even worse, systematic error) in the measured cross section is sufficient to wipe out the desired signal. The very high priority program of studies of few-body systems can be effectively pursued in the proposed design[1] of Hall A. Certain requirements of the program, most notably the need for polarized targets and out-of-plane detection are not yet resolved, and they need to be addressed most urgently.

3.2 Hypernuclear Physics

A big and exciting $(e,e'K)$ program has been articulated for CEBAF. However, its realization requires rather specialized equipment which in certain cases approaches the limits of our technological know-how. Its full implementation requires the following experimental facilities:

- An electron spectrometer capable of reaching very forward scattering angles ($\theta < 5^0$), for "virtual photon tagging".
- Extremely high resolution in (e,e'), ideally tens of KeV but certainly not worse than hundreds of KeV, in order to distinguish nuclear final states.

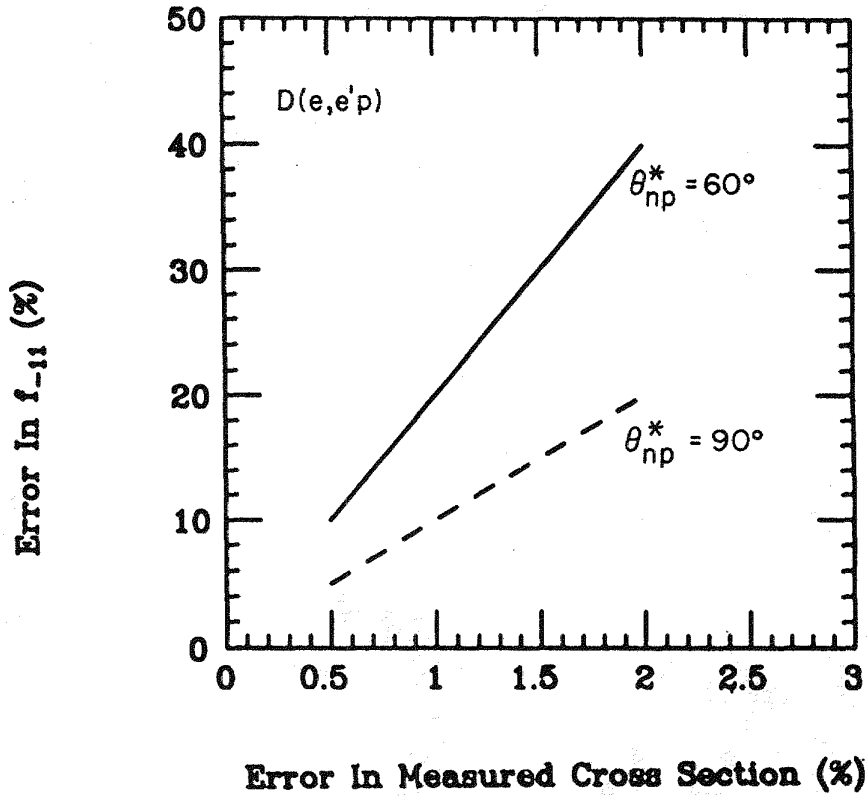

Figure 3: The magnification of error in the f_{-11} response of the deuteron, is indicative of the need for the extreme care needed in controlling instrumental and systematic error.

- A hadron spectrometer for K detection with short flight path, ideally in the range of 10-15m.

Clearly these capabilities will not be met by the first generation equipment intended for Hall A. We need therefore to assess what portion of the $(e, e'K)$ program can be carried with the proposed equipment or with modest modifications to it.

In order to achieve scattering angles smaller than 10^0, the front quadrupole(s) of the 4 GeV spectrometer need to be modified. This is certainly feasible and a study of the possible options (Panofsky quads, septa of various kinds) is needed. At this point I would like to raise the question of finite acceptance. At very forward angles the slope characterizing most dynamic variables is extremely steep. Is, for example, the angular definition of 1 msr of the electron spectrometer adequate? With what precision should the equipment be aligned before the measurements get dominated by instrumental uncertainties? The resolution of the electron spectrometer, in the energy loss mode, is projected to be 2.5 x 10^{-5} which corresponds

to 100 KeV at 4 GeV, adequate for all but the most demanding measurements in heavy nuclei. The flight path of the 3 GeV hadron spectrometer is 18 m, longer than the one desired for an optimized K-spectrometer, but still quite reasonable for a first generation program.

It appears that a significant part of the $(e, e'K)$ program can be pursued with the start-up equipment of Hall A, provided that the electron spectrometer can be designed so it can achieve the very small scattering angles required by $(e, e'K)$.

3.3 $(e, e'p)$ and $(e, e'n)$

The design of Hall A was to a large degree driven by the requirements dictated by the $(e, e'p)$ program. It is not surprising then that $(e, e'p)$ experiments can be pursued very effectively in Hall A. Out of the deliberations of the physicists interested in pursuing $(e, e'p)$ and $(e, e'n)$ studies the following issues have emerged.

- Out-of-place detection capability is of paramount importance. Maximum kinematic freedom is essential. Resolution of this issue is most urgent.
- Proton polarimeter(s) need to be installed in the focal plane of the hadron spectrometer. A preliminary design is needed in order to insure that the required space for its implementation is provided.
- Various schemes for neutron detection have been explored for the purposes of pursuing the $(e, e'n)$ reaction. Medium resolution TOF channels can be built within the perimeter of the building (see Figure 1). The use of the hadron spectrometer for neutron detection (using a 180^0 (n,p) reaction) appears feasible even attractive. However if resolution exceeding 1 MeV is required time of flight (TOF) channels much be designed and incorporated into civil construction plans. Clearly this is an urgent matter.

3.4 Nucleon Resonances

A big program for the study of nucleon resonances has been articulated but it appears to be largely incompatible with the optimization path followed for Hall A. Such a program can be best pursued with instruments of not so high resolution but with larger solid angle and momentum bite. Extreme kinematic flexibility, especially concerning out-of-plane detection capabilities is required. The need for polarized targets is also essential and not easy to address in Hall A.

This program can be best pursued with the equipment contemplated for Hall C. However, its demands show that Hall A can become a far more versatile and "general purpose" area if the out-of-plane detection capability is implemented

in a maximal fashion, and a way to handle the high intensity magnetic fields associated with polarized targets is found.

3.5 $(e, e'2N)$ and Short Range Correlations

As in the case of baryon resonances, the optimal equipment needed to pursue $(e, e'2N)$ studies cannot be found in either Hall A and Hall B. The physics interest in obtaining direct evidence on nuclear two-body densities is very high. Unfortunately, there is very little experience in this very difficult, triple coincidence reaction channel. Kinematic flexibility is very important, but the three arms tend to get in the way of each other.

The recommendation of the CEBAF-PAC was to pursue survey$(e, e'2p)$ measurements using LAS, taking advantage of the huge solid angle of this device. The case of the$(e, e'pn)$ channel is different. There the first exploratory measurements may be taken in Hall A, as an outgrowth of both the $(e, e'p)$ and $(e, e'n)$ programs.

3.6 Emerging issues and tasks

The brief review of the requirements of the various physics programs that can be pursued in Hall A reveals that certain outstanding issues are common: all physics programs demand complete and precise angular coverage. Extensive out-of-plane detection capability is required. We have also seen that very high accuracy is essential in order to reduce systematic error to acceptable levels. In addition, polarized targets appear to be highly desirable, and in certain areas, essential. Additional, but not as crucial issues have also been identified. Among them most pressing is the evaluation of the need for long neutron TOF channels since they affect civil construction. Last, but not least, is the question of the desirability and the definition of the characteristics of a third spectrometer. A third spectrometer is allowed in the conceptual design of Hall A. Let me offer a few comments on these issues.

In many cases the overall accuracy and in particular the instrumental error may prove to be the limiting factors. Certainly the very high quality of the CEBAF beam will help, but a number of "typical" measurements need to be simulated in order to ascertain their sensitivities. These simulations will provide valuable guidance for the refinement of the spectrometer designs. Experience from low energy coincidence measurements[7] has shown that a significant reduction of systematic error can be achieved by the simultaneous measurement of several coincident cross sections. It is impractical to contemplate the construction of multiple hadron spectrometers for CEBAF. However, the multiple "out-of-plane" injection channels, discussed by J. Mougey, may offer such a possibility. If a kicker magnet is

installed at the end of the switchyard, it will be possible to obtain five coincident cross sections simultaneously. I believe that this option may prove very useful, and deserves further consideration.

The resolution of the out-of-plane detection issue has emerged as the most important item, affecting almost every aspect of the program. The multiple, out-of-plane entrance channels, address the problem, but only partially. The inaccessibility of small angles is problematic. On the other hand, endowing the hadron spectrometer with out of plane capabilities is very difficult for large angles. Given the significance of maximum kinematic freedom, is the hybrid solution, having both, out of the question?

Experiments with polarized targets appear to be problematic. Such experiments are important, but no solution has been suggested. It is however the consensus of the collaboration that every effort should be made to improve the facility and to make it as polarized-target-friendly as possible.

Finally let me touch upon the issue of the maximum length of extended targets that can be accommodated by the spectrometer pair. The current design allows targets as long as 8 cm. The question whether targets as long as 20 cm should be allowed was raised during the PAC deliberations. To do so, a major redesign of the spectrometers is needed. Given that this will necessarily compromise other parameters of the design, while improving count rates by less than a factor of 3, the overwhelming feeling was that such a modification is unwarranted.

4 Conclusion

The design of Hall A and the associated instrumentation successfully meets most of the requirements of experiments requiring high luminocity and high resolution. The out-of-plane capability is crucial and various schemes for its successful implementation have been suggested. The availability of polarized targets is also important and every effort should be made to accommodate them.

Acknowledgements It is a pleasure to acknowledge extensive and fruitful discussions with J. Mougey. I would like to thank the CEBAF staff and physicists for their warm hospitality during the week of the workshop. Support is provided in part by the National Science Foundation under grant NSF PHY 86 10493.

REFERENCES

1. J.Mougey, These Proceedings.
2. Report of the Program Advisory Committee for CEBAF, CEBAF, March, 1987.
3. J. Schiffer, These proceedings.
4. T. DeForest, Jr., Ann. Phys. **45**, 365 (1967).
5. T.W. Donnelly and A. S. Raskin, Annals of Physics **169**, 247, (1986).
6. W. Bertozzi, These proceedings.
7. C. N. Papanicolas, S. E. Williamson, H. Rothhaas, G. O. Bolme, L. J. Koester, Jr., B. Miller, R. Miskimen, P. Mueller and L. S. Cardman, Phys. Rev. Lett. **54**, 26 (1985).

Program Collaboration Report for the Large Acceptance Spectrometer

R. D. McKeown

W. K. Kellogg Radiation Laboratory
California Institute of Technology
Pasadena, CA 91125

In this report, various issues relating to the Large Acceptance Spectrometer (LAS) that were raised in the program collaboration meeting as well as the physics collaboration meetings will be discussed. During the course of the workshop, several users made concrete suggestions about the present plan for equipping Hall B and an enthusiastic group of users expressed interest in collaborating on the development and construction of the LAS and associated hardware. We are hopeful that this represents the beginning of a working association with a larger group of users who will participate in bringing this device online at CEBAF.

Physics Interest

It is becoming quite clear that there is very broad interest in the community in the capability of the LAS to perform a wide variety of physics experiments. Many discussions in the physics collaboration meetings at this workshop involved the use of the LAS and some users are beginning to evaluate specific physics experiments with the general parameters of the existing design. As an indication of the breadth of the discussion, we will briefly mention some topics that were covered in the physics collaboration meetings which were relevant to the LAS.

Due to the low momentum resolution and its large acceptance, the LAS appears well-suited for use in experiments with two or more energetic hadrons in the final state. A

particularly useful feature is that excellent out-of-plane capability is naturally available.

J. Lightbody (NBS) discussed the possible use of the LAS in studying the $(e, e'2N)$ to extract the two-body density. Using calculations by Laget[1], rates were calculated for some particularly favorable kinematics where the two-nucleon correlation effects are important. It appears that the particular solid angle and momentum bites that were chosen would favor using three spectrometers in Hall A for such measurements. Since the implementation of deploying individual spectrometers with versatile out-of-plane capability is certainly difficult, it would appear that further effort in exploring the use of the LAS for these experiments is warranted.

P. Stoler (RPI) analyzed the possibility of using the LAS for studying resonance electroproduction by observing $N\pi$ final states. In this case, using the LAS appeared quite favorable compared to individual spectrometers in Hall A.

There were also discussions of ρ production (R. Whitney from CEBAF) and hadronization in deep-inelastic scattering (G. Chang from U. Maryland). These experiments require detection of final-state hadrons over a wide range of angles and so are well-suited to LAS. Experiments with real photons are, of course, a major use of this device. Polarized target experiments are often limited in achievable luminosity due to target technology. The large acceptance of the LAS allows recovery of useable count rates for performing form-factor measurements in quasi-elastic scattering as well as resonance production. There was much discussion about measuring the neutron electric form-factor, and experiments using polarized deuterium and ^{3}He targets would benefit from using the LAS.

Detector Concept

This device is a new challenge for the electromagnetic nuclear physics community. It is a technical project that is rather different from the usual spectrometers and detectors employed in nuclear physics. Clearly, there are many technical issues that need to be addressed. A technical review of the present concept will take place in August of this year.

Perhaps more relevant to potential users is the fact that the LAS will require substantially different conceptual thinking in the design and evaluation of experiments. This was becoming evident in the physics discussions at this workshop which were mentioned above, where some people were attempting to compare the relative merits of the LAS versus more standard spectrometer concepts. Usually the useful solid angle is defined by the spectometer that is available, and then estimating the count rate is rather straightforward. For the LAS, the physicist chooses the solid angle appropriate to the experiment. Often one can choose annular solid angles by integrating over azimuthal angles (this does not preclude analyzing the azimuthal angle dependence of the cross-section). One can often measure quantities over a range of Q^2 simultaneously. These various tricks allow one to recover much or all of the rate lost by the luminosity limitation of the LAS. As an example, a calculation of the expected statistical precision of a measurement of the neutron electric form-factor using quasi-elastic scattering from a polarized ^{3}He target is shown in figure 1. The luminosity was assumed to be $1 \times 10^{33} \mathrm{cm}^{-2}\mathrm{sec}^{-1}$, with beam and target polarizations of 50% each. The angular range for the scattered electrons was $15° \leq \theta \leq 45°$ in 3° steps, and $-45° \leq \phi \leq 45°$. A measurement with very good precision is possible in a single 30 day run, and all of the different Q^2 points are obtained simultaneously in one run. In this

particular case, use of the LAS is favored over the electron spectrometer in hall A, but that would not be so clear if one considered only one Q^2 measurement.

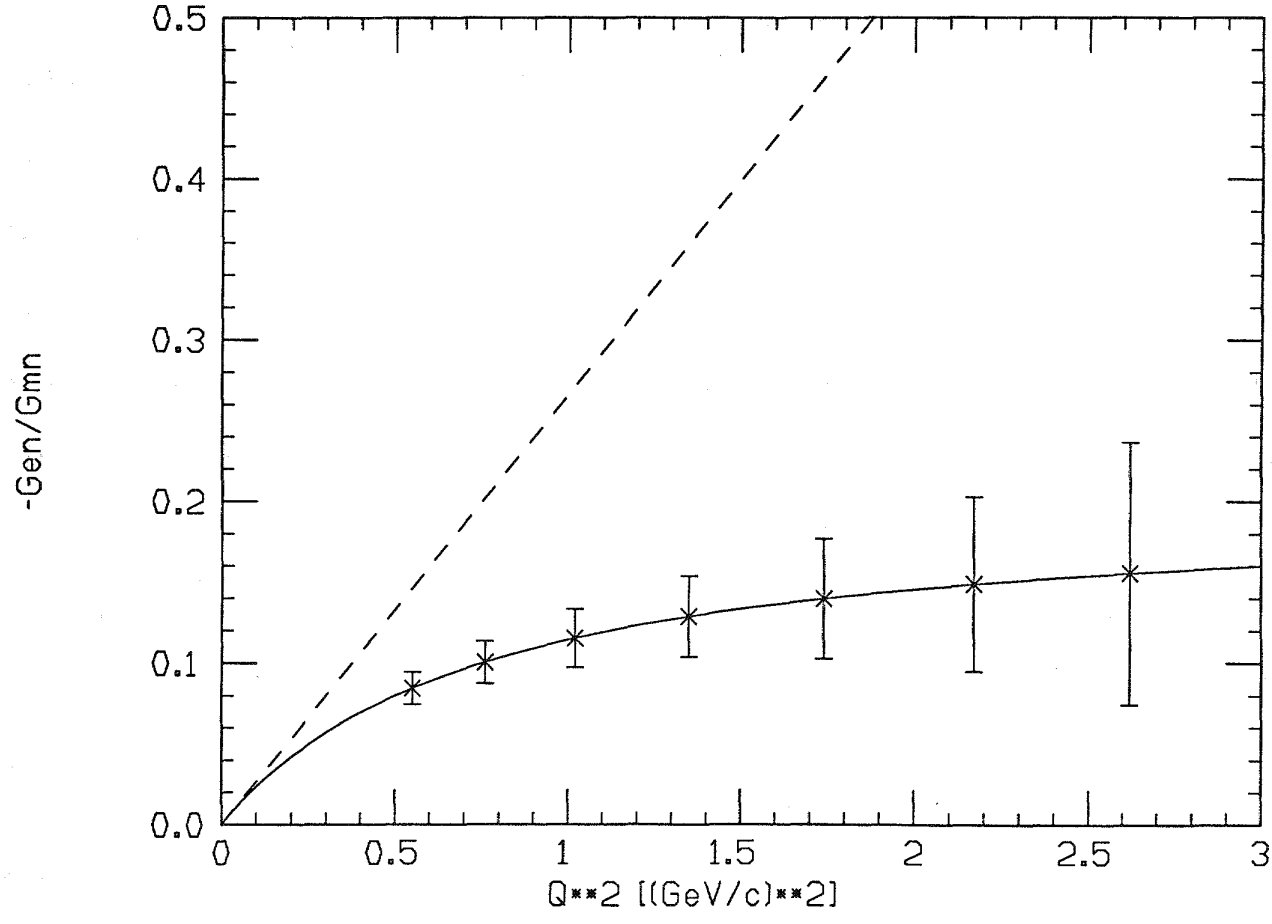

Figure 1. Attainable statistical precision for a single 30 day run for the neutron electric form-factor as a function of the momentum transfer. The ratio to the magnetic form-factor is plotted, and the solid line is a standard parametrization used in reference 2 while the dashed line is a recent prediction from reference 3. The target spin was at 45° with respect to the beam direction and approximately perpendicular to $\vec{q}$.

The statistical precision of this measurement could be substantially improved by either efficient detection of the recoiling neutron, or possibly by vetoing events with energetic

protons in the $\vec{q}$ direction. This would reduce the contribution of scattering from protons to the data sample and thereby increase the size of the measured asymmetry by about a factor of 3. Of course, the effects of final state interactions must be understood, particulaly for coincidence measurements.

Data acquisition is also going to be more sophisticated than with the usual nuclear physics sp trometer. Effective use of the LAS will require rather elaborate trigger processors to select the events of interest. It may often be possible to perform several different experiments at once. Data reduction and analysis will not only require substantial computing resources, but new and imaginative concepts for displaying and digesting large amounts of data. The LAS will be a workhorse for general survey experiments, and the physicist (theorist and/or experimentalist) must decide how to reduce the large amount of information in the multiply differential cross-sections to simple plots of physical quantities that demonstate particular concepts. Much thinking needs to be done in this area.

User Input

This is certainly an appropriate time for users to make their views known regarding the design of the LAS and other aspects of Hall B. During the workshop, several opinions were expressed in this area.

It was pointed out that it would be useful to have a high-intensity bremsstrahlung beam in hall B. The generation of such a photon beam would be accomplished by installing a sweep magnet in the entrance to Hall B with a high intensity beam dump (probably down into the ground). This is an item that would clearly be better implemented from the start rather than added later.

Several physics programs require detection of particles in the region $\theta < 15°$. These include experiments with real photons, ρ production, and hadronization in deep-inelastic scattering. This could potentially affect the priority given to outfitting the small scattering angle region with detectors or a supplemental spectrometer. Perhaps the first generation of these studies could be accommodated by offsetting the target upstream so the LAS covers angles down to $\theta < 10°$. This would imply losing magnetic analysis capability in the backward hemisphere, which may not be serious in this context. The feature of the present LAS design which arranges normal incidence of scattered particles from the target is also compromised, and some loss in ϕ acceptance would result.

Another area that needs further consideration is neutron detection capability in the LAS. It was mentioned that neutron converters could be installed that would give very good energy resolution. Such a capability would be useful for real photon experiments, $(e, e'\mathrm{n})$, $(e, e'\mathrm{np})$, and neutron form-factor measurements. Clearly, this is an area that could use much further work.

User Participation

An interesting aspect of the LAS is there is potentially much opportunity for users to actually participate in the development of this instrument. There are many sub-systems and different facets which are relatively decoupled from each other. Clearly, there are many ways to divide up such a task. Figure 2 shows one option that is certainly less than optimal.

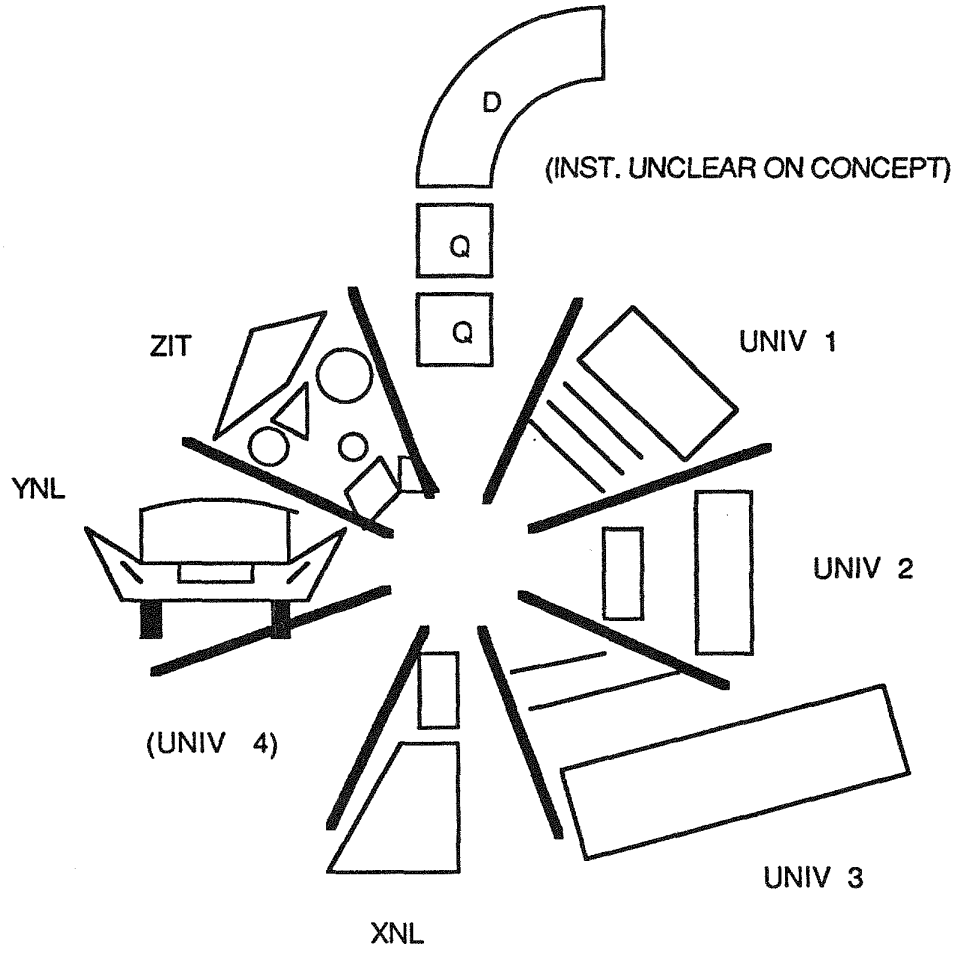

Figure 2. A possible plan for LAS user participation.

A very enthusiastic group of physicists attended the program collaboration meeting held at this workshop. Many expressed the view that they are ready to go to work! We are presently still working out how to organize this collaboration, and will develop a plan this

summer. In the short term, there are several things that interested users can do. Firstly, they can spend some time working out their physics ideas with the current design. This will strengthen the physics case and give guidance in adjusting the design. Secondly, they can send a short note to one of us expressing their interest and suggesting an area in which their expertise may be particularly valuable. We will begin compiling lists of interested users and will probably begin setting up some regular meetings to facilitate some actual work on the project by users in the near future.

References

[1] L. M. Laget, invited talk at this workshop.

[2] S. Galster *et al.*, Nucl. Phys. **B32**, 221 (1971).

[3] M. Gari and W. Krumpelmann, Phys. Lett. **B173**, 10 (1986).

THE CEBAF LARGE ACCEPTANCE SPECTROMETER

Bernhard A. Mecking
CEBAF, 12070 Jefferson Avenue, Newport News, Virginia 23606

ABSTRACT

The present status of the CEBAF Large Acceptance Spectrometer project is described. The spectrometer will be used for the investigation of electron- and photon-induced nuclear reactions.

INTRODUCTION

The scientific program for the CEBAF 4 GeV electron accelerator concentrates on the study of the structure and the motion of the nuclear constituents. The proposed experimental equipment consists of two focusing magnetic spectrometers with high momentum resolution ($\delta p/p \leq 10^{-4}$) but relatively small acceptances ($\Delta\Omega \simeq 10^{-3} \cdot 4\pi$, $\Delta p/p \simeq 10\%$) and a large acceptance magnetic spectrometer. In the following report, the physics motivation and the general design criteria for a large acceptance spectrometer at CEBAF will be discussed. Technical details and the status of the proposed design will be given.

PHYSICS MOTIVATION

Electron scattering experiments have provided us with information on the electromagnetic structure of ground states and excited states of nuclei (explored in (e,e') experiments) and about some aspects of the nuclear single-particle structure (explored in (e,e'p) experiments). Very little is known about the many-body aspects of the nucleus, like e.g. the structure of bound nucleons, the origin of short-range correlations or the propagation of mesons or nucleon resonances in the nuclear medium. The reason for this limitation is largely due to the technical features of the experimental facilities that are presently available:

a) The low duty-cycle of existing electron accelerators limits coincidence experiments to a narrow kinematical region where sufficient signal-to-noise ratio can be achieved. It also makes the operation of large acceptance detectors inefficient because their counting rates are limited by the high instantaneous background rates.

b) High accuracy in charged particle detection can only be achieved in small acceptance magnetic spectrometers.

This picture is presently changing dramatically due to technical developments:

a) Electron accelerators with 100% duty-cycle are being built.
b) The quality and versatility of large acceptance detectors has improved dramatically.

At CEBAF, there are two categories of experiments that require a large acceptance detector: the detection of multiple particle final states and measurements at limited luminosity. Examples will be given for both categories:

1. Multiple Particle Final States

For reactions involving several particles in the final state, high detection efficiency can only be achieved by using a detector with a wide coverage of the angular and energy range for all outgoing particles. Examples for reactions which are of special interest for CEBAF are:

a) Hadronic final states in inclusive electron scattering off nuclei. Single arm electron scattering and (e,e'p) coincidence experiments have generated puzzles which can only be solved by a detailed investigation of the hadronic final state. Using a large acceptance detector, a bias-free investigation can be carried out by triggering on the scattered electron only. In the off-line analysis, the inclusive scattering cross section can then be decomposed into its hadronic channels. With increasing energy loss for the electron, the following phenomena can be studied:

(1) Electron scattering at large negative y (y= momentum component of the struck nucleon parallel to the direction of the virtual photon $\vec{q}$) yields higher cross sections than expected from standard nuclear models. The excess cross section can either be explained by high momentum components in the nuclear wave function (which would lead to the emission of a single nucleon) or by interaction of the virtual photon with quark clusters[1)] (which would lead to the emission of nucleon pairs or nucleon clusters like deuterons etc.). These two possibilities can be distinguished by detecting the hadronic final state.

(2) quasi-free electron scattering off bound nucleons (requiring the hadronic final state to contain a recoiling nucleon around the direction of $\vec{q}$). A long-standing problem is the failure of the experimental Coulomb sum rule to account correctly for the number of protons in the nucleus. This has been interpreted as a change of the nucleon form factor in the nuclear medium or as evidence for a direct interaction of the virtual photon with a quark confined in a six-quark bag. Again, the observation of the hadronic final state will allow to distinguish the different models.

(3) multi-nucleon emission (requiring the hadronic final state to contain ≥2 nucleons). Two nucleon emission is thought to be responsible for filling the dip between the quasi-free peak and the Δ-peak; there should also be strength in the Δ-region due to Δ-excitation with a subsequent Δ+N → N+N interaction.

(4) production and propagation of non-strange (Δ and higher nucleon resonances) and strange (Λ, Σ and their excited states) 3-quark objects in nuclei (requiring the hadronic final state to be a πN, ηN, $\pi\pi$N, KΛ etc. system in the appropriate mass range). Modifications of the properties of these resonances in the nuclear medium can be studied.

b) Photo- and electro-excitation of the nucleon resonances.
The harmonic oscillator quark model with QCD motivated additions (like a one-gluon exchange term) describes successfully the properties of the nucleon resonances that are known from elastic π-nucleon scattering. However, the model predicts many additional states which have not been observed. A plausible explanation[2] is that these states decouple from the πN channel and can, therefore, not be excited in elastic πN scattering. Since, on the other hand, the photocoupling is still strong, photoexcitation is the only promising production mechanism. Predicted decay channels are:

$$\gamma\ N \rightarrow N^* \rightarrow \pi\ \Delta \rightarrow \pi\ \pi\ N$$
$$N^* \rightarrow N\ \rho \rightarrow \pi\ \pi\ N$$
$$N^* \rightarrow N\ \omega \rightarrow \pi\ \pi\ \pi\ N$$

c) Photo- (and electro-) excitation of vector mesons: γ N → V N ($V = \rho,\omega,\phi$). An important goal of this program is to measure the γ-V coupling constant to get information on the hadronic content of the photon[3] and its variation with Q^2. In addition, the vector meson coupling to the nucleon can be determined. In boson exchange models of the nucleon-nucleon interaction, this quantity is of fundamental importance for the short range part of the NN-interaction.

d) Hyperon production and interaction: γ N → K Λ (Σ)
The basic cross sections and coupling constants for these reactions have to be known for the analysis of the electromagnetic excitation of hypernuclei. A tagged low intensity hyperon beam can be generated using the outgoing kaon to determine the Λ kinematics. The production rates are large enough so that the decay and the interaction of the produced hyperon can be studied in the following reactions:

(1) Λ p → Λ p (elastic scattering)
Because of the short decay length, the interaction of low momentum Λ's is best studied in the production target. Using the γp → $K^+\Lambda$ reaction for Λ production, about 500 Λ scattering events

can be observed per day in a large acceptance spectrometer.

(2) $\gamma\, d \to K^+ \Lambda\, n$
This reaction also allows to study the ΛN interaction. Especially interesting is the search for long-lived S=-1 dibaryons; the masses of these objects have been predicted to be around the Σ-cusp[4].

(3) radiative hyperon decay: $\Lambda^*(1520) \to \gamma\, \Lambda$ and $\Lambda^*(1520) \to \gamma\, \Sigma$.
The radiative decay width yields a sensitive test of the quark structure of these systems. Using a tagged photon beam, about $5 \cdot 10^5$ $\Lambda^*(1520)$ can be produced per day.

e) Exclusive photoreactions on few-body systems

$\gamma\, d \to N\, N\, \pi$ $\qquad$ $\gamma\, {}^3He \to p\, p\, n$
$\to \Delta\, \Delta \to N\, N\, \pi\, \pi$ $\qquad$ $\to \pi$ (3N)

The basic properties of bound 3-quark systems are best studied in few-body nuclei because the nuclear structure can be calculated exactly (at least in the framework of a non-relativistic potential model). Interesting questions are the off-shell behavior of the γNN^* vertex, the structure of the N^*N interaction, the existence of dibaryons[5] and of 3-body forces in ^3He [6].

f) Interaction parameters of unstable particles.
The measurement of the A-dependence of total production cross sections for unstable particles can be used to determine their total hadronic cross sections. In contrast to hadronic production reactions, the electromagnetic production offers the big advantage that the interaction of the incident projectile is so weak that the A-dependence of the cross section can be interpreted directly in terms of the interaction of the produced particle. Especially interesting is a comparison of the hadronic interaction of the $\eta(549)$ and $\eta'(958)$ which are supposed to be different mixtures of the same SU(3) states. The large η' mass is attributed to a sizeable exotic (gluonic or hybrid) component; this should show up as a difference in the hadronic behavior of η and η' [7].

A comprehensive study of the reactions b) - e) requires the use of polarized beams (longitudinally polarized electrons, linearly and circularly polarized photons) and polarized targets (polarized protons, vector- and tensor-polarized deuterons).

2. Limited Luminosity

The luminosity (target density • beam intensity) limitation can be due to the target or due to the beam.

a) Limitation due to the beam intensity.
Experimental programs using secondary particle beams (real γ, μ, π, K) need large acceptance coverage to collect sufficient count rate, independent of the number of particles in the final state. Especially important are tagged photon beam experiments where the intensity has to be limited to $\simeq 10^7$ tagged γ/sec to keep accidental coincidences small.

b) Limitation due to the use of a polarized target.

(1) polarized solid state hydrogen and deuterium targets.
For present state-of-the-art solid state polarized targets (NH_3 or ND_3) the luminosity has to be kept low in order to avoid a reduction of the polarization due to beam heating and radiation damage ($\simeq 10^{33} cm^{-2} sec^{-1}$ for tensor-polarized deuterium, $\simeq 10^{35} cm^{-2} sec^{-1}$ for polarized hydrogen).

(2) polarized gas targets.
The disadvantages of polarized solid targets (high magnetic fields, nuclear background, low temperatures, limited to hydrogen and deuterium) can, in principle, be avoided by using a low density polarized gas target in combination with a high intensity electron beam. A dedicated electron storage ring would clearly be ideal for these experiments. However, the rapid progress in polarized gas target technology will make experiments in the CEBAF external electron beam possible.

Polarized gas target experiments in the CEBAF external beam will have lower luminosity than a storage ring. However, there are also some important advantages using an external beam:
(a) there are no difficulties to achieve longitudinal electron polarization
(b) the vacuum requirements are modest → less differential pumping will be required.
(c) there is greater flexibility in the arrangement of the experimental apparatus
(d) since the beam passes through the target only once, the beam stay clear area is much smaller → very small diameter openings for bottle targets can be used.

These features should make it possible to achieve higher target density than in a storage ring. A minimum density of $\simeq 10^{15}$ atoms/cm^2 is necessary to give reasonable counting rates. At this luminosity ($\simeq 10^{30} cm^{-2} sec^{-1}$), the combination of a polarized gas target and a large acceptance spectrometer will be useful for the investigation of reactions induced by quasi-real photons.

For ^{3}He, the densities already reached[8] give a luminosity of

several $10^{32}cm^{-2}sec^{-1}$. This luminosity will allow an extensive nuclear physics program to be carried out with a large acceptance detector. Polarized ^{3}He targets can be used as a source of polarized neutrons and to investigate the structure of the 3-body system. The following experiments are of special interest:

(a) $^3\vec{He}(\vec{e},e'n)pp$ to determine the electric form factor of the neutron G_e^n.

(b) $^3\vec{He}(\vec{e},e'\Delta^\circ)pp$ to determine the C2/M1 ratio for the $n\to\Delta^\circ$ transition.

GENERAL DESIGN CONSIDERATIONS

A large acceptance detector at CEBAF should be suitable for a broad range of photonuclear experiments using electron and photon beams. Therefore, it should have the following properties:

1. Homogeneous coverage of a large angular and energy range for charged particles, for photons (total absorption counters) and possibly neutrons.

2. Good momentum and angular resolution (→ magnetic analysis for charged particles).

3. Good particle identification properties in the momentum range of interest (→ combination of magnetic analysis and time-of-flight).

4. No transverse magnetic field at the beam axis (to avoid sweeping e^+e^--pairs into the detector).

5. No magnetic field in the target region to provide for the installation of polarized (solid state or gaseous) targets requiring their own guiding field or other complicated equipment (cryogenic or track sensitive targets, vertex detectors etc.).

6. Symmetry around the beam axis to facilitate triggering and event reconstruction.

7. To account for the Lorentz-boost the $\int\vec{B}\cdot d\vec{l}$ should increase with decreasing particle emission angle.

8. High luminosity and count rate capability. The detector should operate in the difficult background environment encountered in electron scattering experiments. The background caused by a tagged bremsstrahlung photon beam ($N_\gamma \simeq 10^7$/sec) is much lower and will give no additional constraints.

9. Open geometry for the installation of a long time-of-flight path for neutron detection.

The consequences of these requirements for the choice of the magnetic field configuration have been studied. Transverse dipole, longitudinal solenoidal and toroidal fields have been considered. In all cases, the target has been assumed to be inside the magnetic field volume. The results are summarized in table I. To fulfill requirements #2 and #3, a large $\int B \cdot dl$ and a long time-of-flight (ToF) path is necessary. This can be achieved by all field configurations. The transverse dipole field is ruled out by #4 in combination with #8; it also violates #6. The solenoid which has become the standard magnetic field configuration at e^+e^- colliders violates requirements #5, #7 and #9. The only configuration that fulfills all requirements is the toroidal magnetic field. Since the ϕ-range for magnetic analysis is limited due to the coils, the detection efficiency for high multiplicity (> 4) final states will be low. However, in view of the CEBAF program (which does not feature high multiplicity reactions), it seems to be important that the detector can extend and complement the physics program carried out by the standard spectrometer set-up.

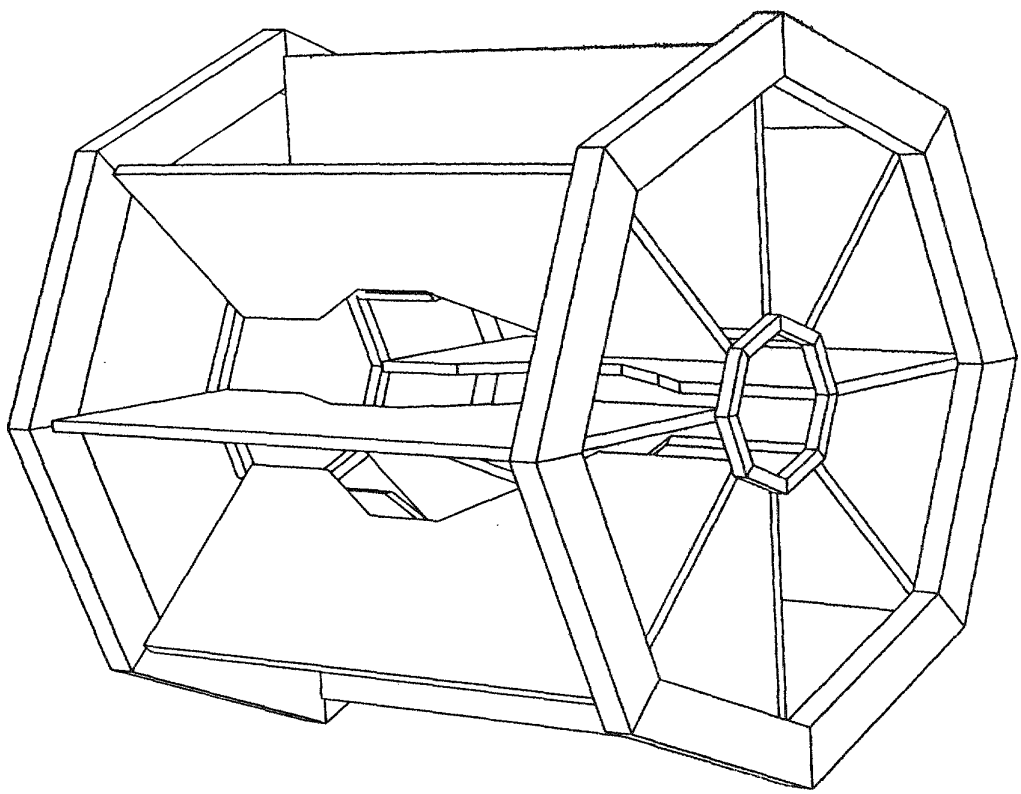

Fig. 1 Perspective view of the toroidal magnet.

THE LARGE ACCEPTANCE SPECTROMETER

The solution that has been proposed for the CEBAF Large Acceptance Spectrometer (LAS) is a superconducting toroidal magnet equipped with drift chambers, scintillation counters and shower counters. A description of the main features of the LAS will be given below.

1. Toroidal Magnet

The magnet consists of 8 superconducting coils arranged around the beam line to produce essentially a magnetic field in ϕ-direction. Size and shape of the coil were determined on the basis of the physics requirements (see table II for details). A perspective view of the magnet is shown in fig. 1, the coil shape is given in fig. 2. Each coil is embedded in a rigid coil case (about 4 meter long and 2 meter wide). For the magnetic field calculations, the finite size of the coil was simulated by adding up the contributions of 4 discrete conductor loops (as indicated in fig. 2). The r-dependence of the magnetic field is given in fig. 3 for different z-positions. In a cylinder of 50 cm diameter around the axis the magnetic field is $\lesssim$10 Gauss. As demonstrated in fig. 4, the field lines are essentially circles (corresponding to a pure ϕ-field) with important deviations close to the coils. Figure 5 gives the integral over the ϕ-component of the field as a function of the particle emission angle θ. For forward going particles, the integral is about twice as high as for particles going sideways.

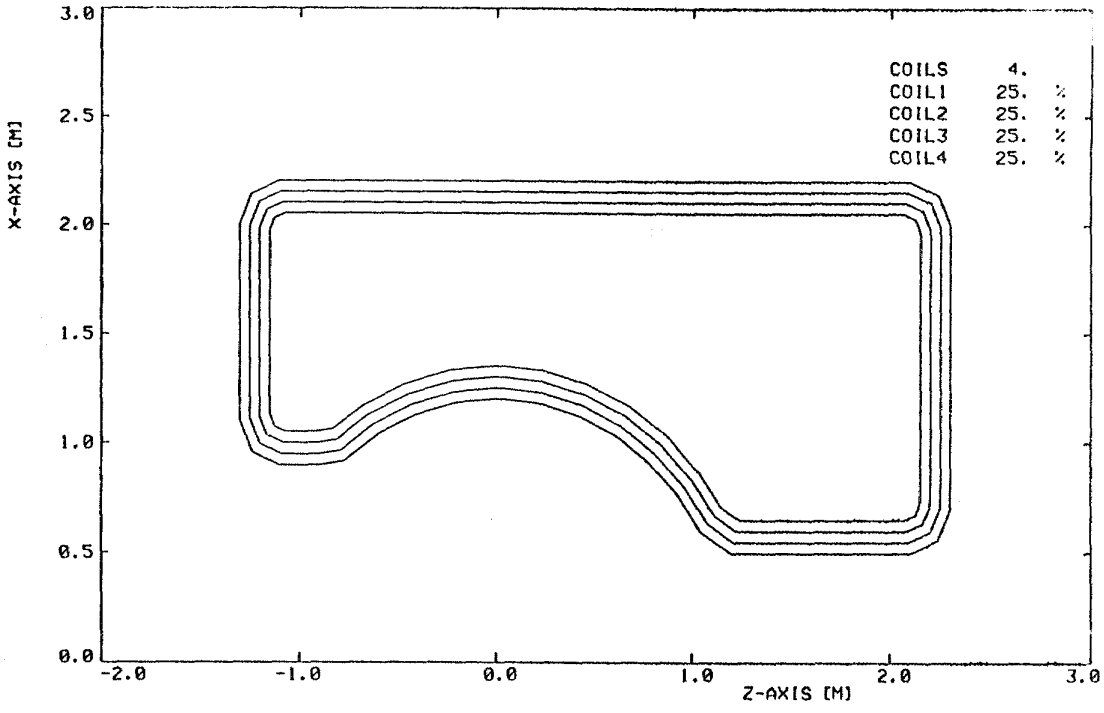

Fig. 2 Coil shape. The conductor is represented by 4 current loops.

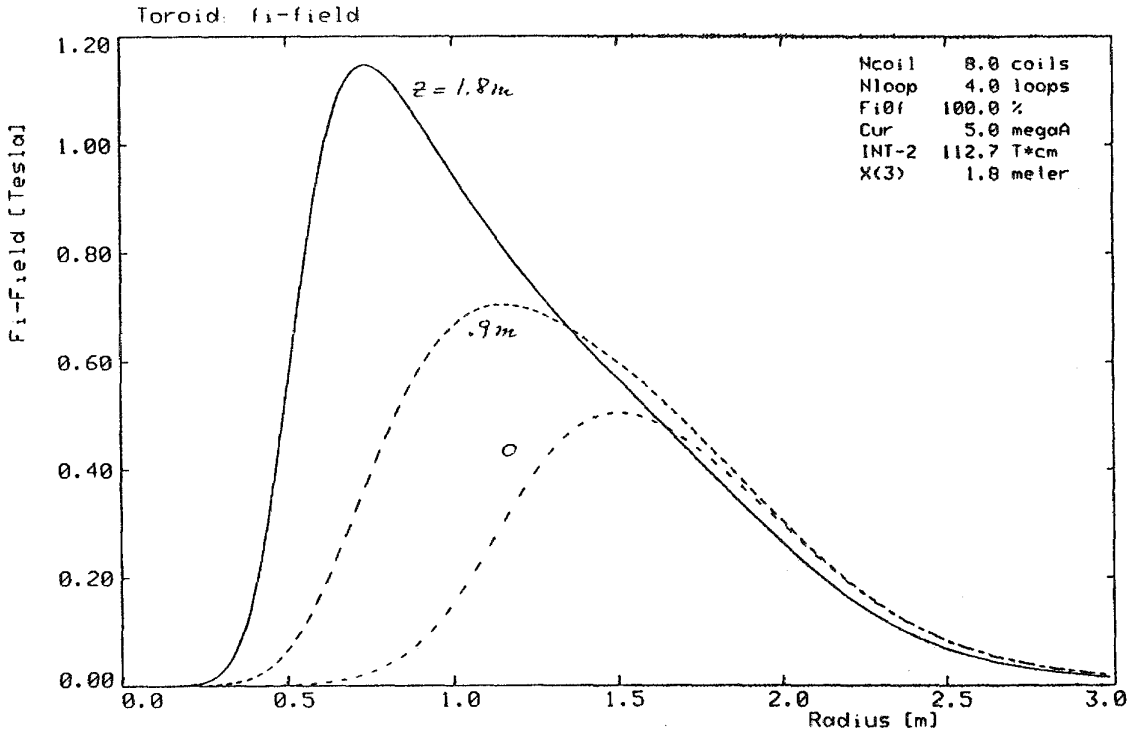

Fig. 3 Radial dependence of B_ϕ for z=0, 0.9 m and 1.8 m (z=0 corresponds to the target position) and ϕ=0 (corresponding to the mid-plane between two coils).

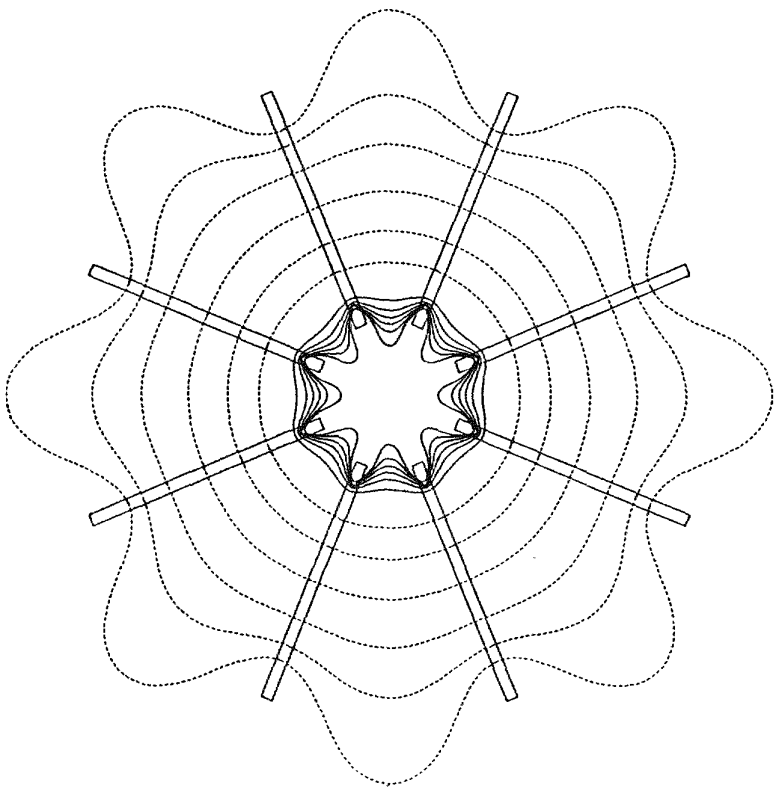

Fig. 4

Field lines (giving the direction of the magnetic field) for z=1.8m (forward part of the magnet.

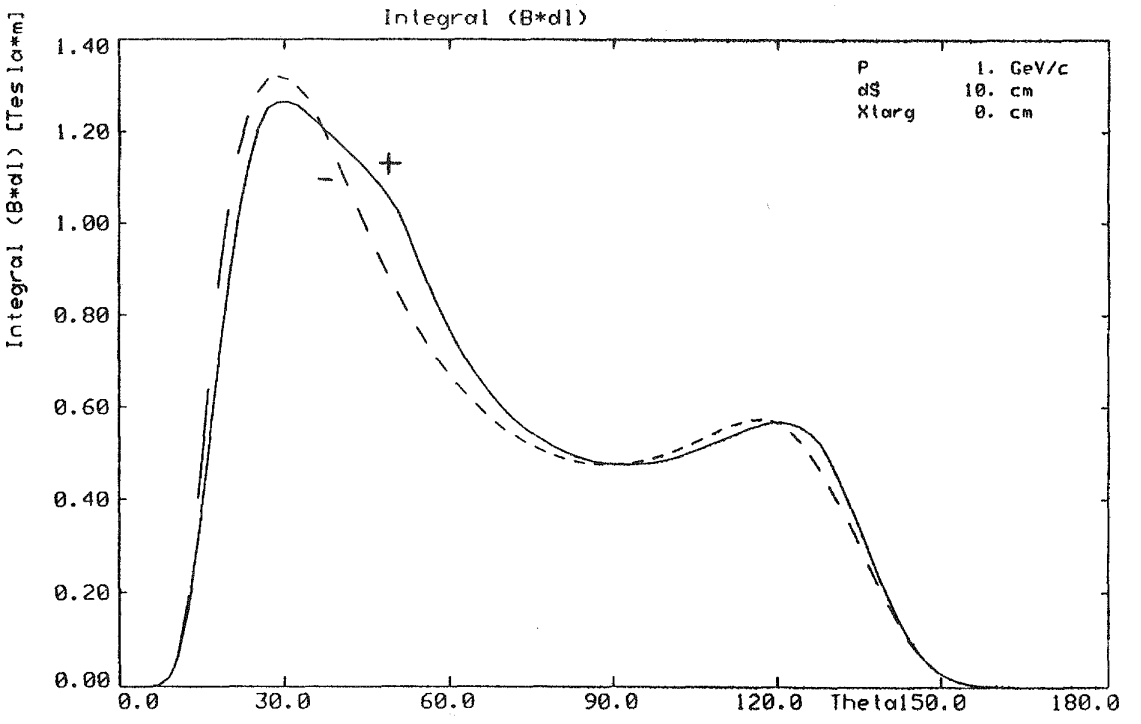

Fig. 5 θ-dependence of $\int B_\phi \cdot dl$ integrated along the particle trajectory. θ is the particle emission angle relative to the axis; the target has been assumed to be at z = 0 m. Particle momentum 1 GeV/c, both polarities.

The inner section of the coil is circular to avoid transverse (in ϕ-direction) motion of those outgoing particles that do not form a 90° angle with the conductor. This is demonstrated in fig. 6a for a rectangular coil shape (the current has been adjusted to make the total bend angle the same as for the circular coil). The transverse deflection depends on the angles θ (relative to the axis), ϕ (azimuthal angle) and on the particle momentum and polarity. The resulting loss of events will be difficult to correct. By using a circularly shaped coil, the angle of incidence can be kept normal to the coil, independent of θ. As shown in fig. 6b, the transverse particle motion is very much reduced.

2. Particle detection system

The proposed particle detection system consists of drift chambers to determine the track of charged particles, scintillation counters for the trigger and for time-of-flight, and shower counters to detect photons. A side view of the detection system is given in fig. 7, a cut in the target region in fig. 8. Note that all 8 segments are individually instrumented to form 8 independent magnetic spectrometers. This will facilitate pattern recognition and track reconstruction in a large background environment.

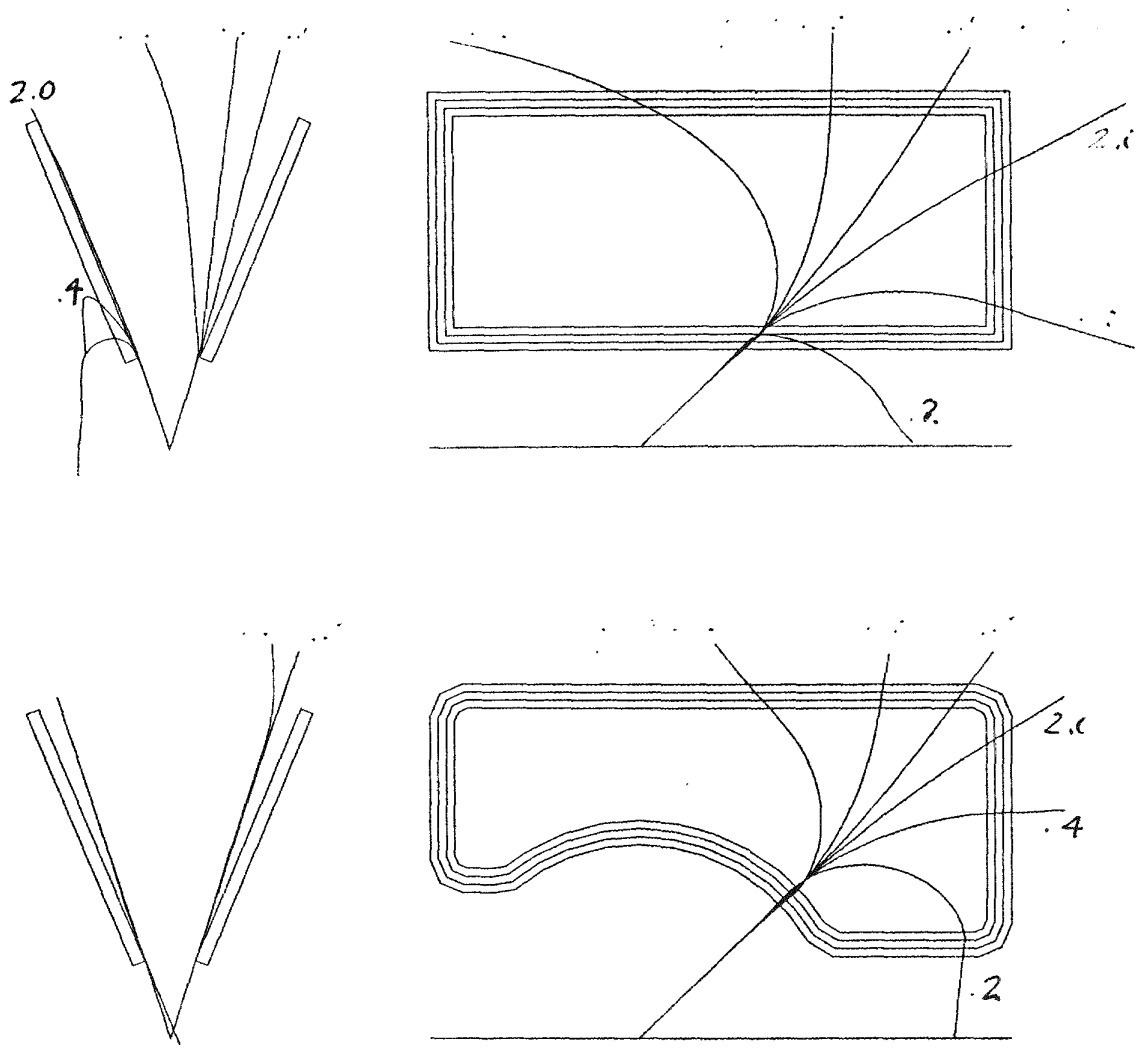

Fig. 6 Transverse particle deflection in toroidal magnets for particles with θ=45°, p= 0.2, 0.4 and 2.0 GeV/c and ϕ=±18° (ϕ=0 corresponds to the mid-plane).

a) rectangular coil shape. Particles that are deflected away from the axis by the ϕ-component of the field are bent back to the mid-plane; particles that are deflected towards the axis are bent towards the coils and are lost.

b) coil with a circular inner section. Note that there is no transverse motion at inner edge of the coil.

2.1 Tracking chambers

Charged particles are tracked by planar wire chambers. Each planar chamber consists of 4 layers of sense wires stretched in ϕ-direction. The position of the hit along the sense wire can be determined by stereo layers or by charge division.

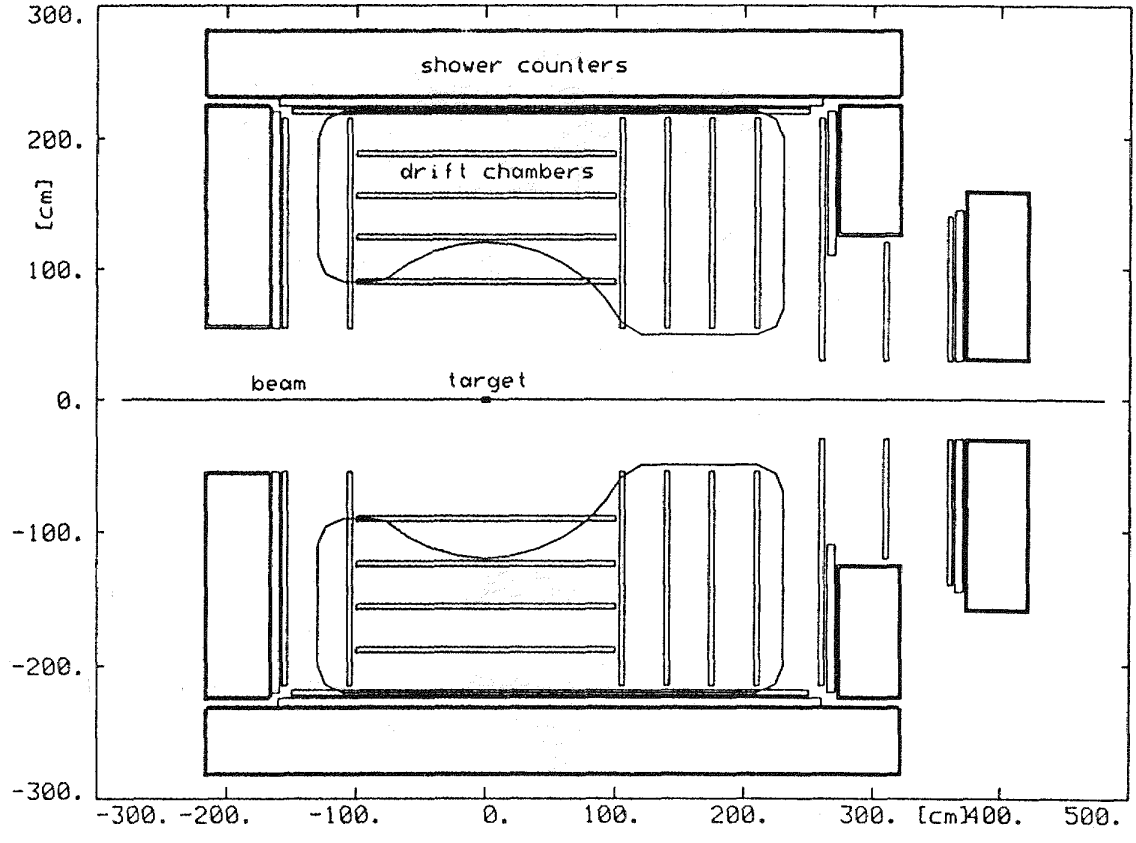

Fig. 7 Transverse view of the proposed particle detection system

2.2 Scintillation Counters

The drift chamber is surrounded by scintillation counters. The counters serve the double purpose of providing the trigger and the time-of-flight information. (Also, a fraction of the high energy neutrons ($\simeq$5%) will interact in the scintillation counters and will thus be detected.) Each counter is approximately 20 cm wide and 5 cm thick and is viewed by 2" phototubes at both ends for improved timing and position resolution. The counter covers the full ϕ-range corresponding to one segment but only a small θ-range thus facilitating triggering on a given event pattern.

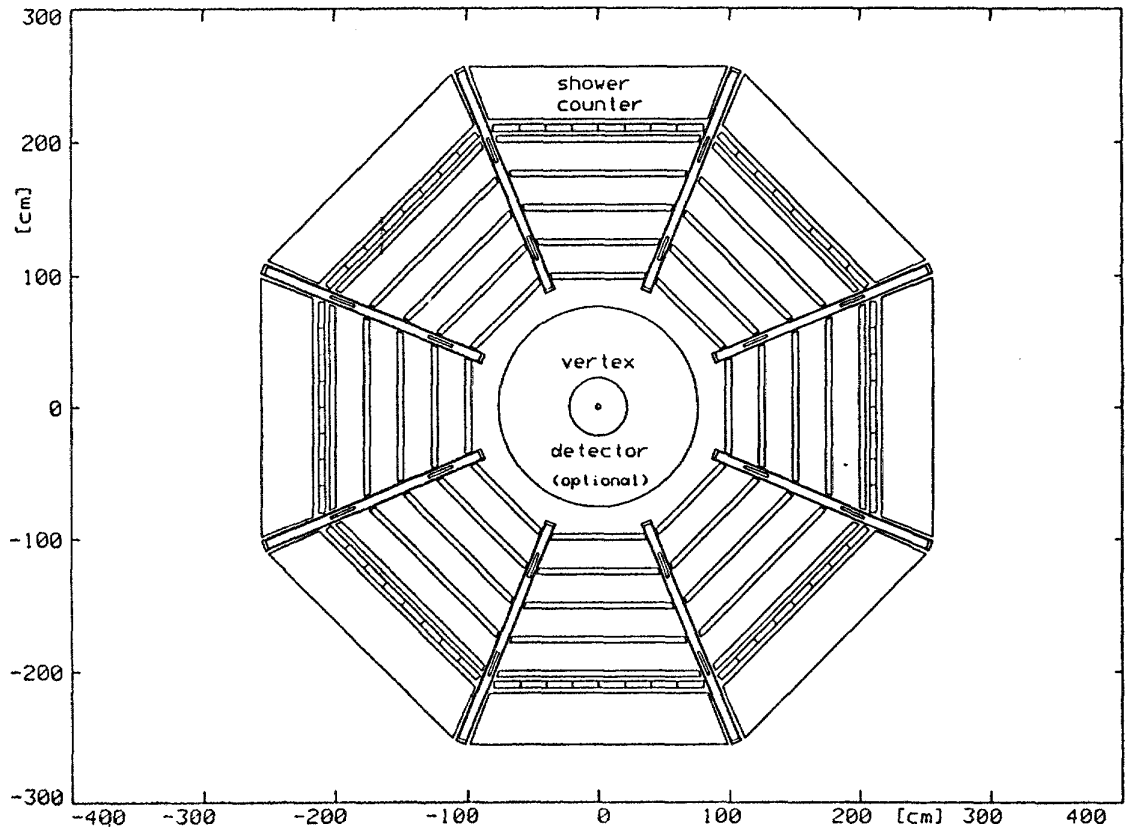

Fig. 8 View of the detection system in the direction of the beam for z=0 (target position)

2.3 Shower Counter

The detector is surrounded by shower counters for the identification of electrons (in electron scattering experiments) and the detection of high energy photons from the decay of hadrons like π^0, η, η' etc. Due to the size of the counter ($\simeq$80 m^2), relatively inexpensive materials and construction techniques have to be used (e.g., a sandwich of lead plates interleaved with active material like scintillating fibers or gas detectors). The anticipated energy resolution is $\sigma/E_\gamma \leq .13/\sqrt{E_\gamma}(GeV)$.

3. Maximum Luminosity

In an electron beam, the main background is caused by electron-electron scattering and wide angle bremsstrahlung. At a luminosity of $10^{33} cm^{-2} \cdot sec^{-1}$, the rate of Møller scattered electrons is estimated to be of the order of $5 \cdot 10^7 sr^{-1} \cdot sec^{-1}$. Since the energies are low, the electrons are bent back even by the small magnetic fringe field. A

fraction of the electrons will, however, radiate photons that will subsequently generate spurious signals in the chambers. The total integrated flux of photons due to wide angle bremsstrahlung has been estimated to be of the order of $10^6 sr^{-1} \cdot sec^{-1}$ (luminosity $10^{33} cm^{-2} \cdot sec^{-1}$, E_o = 2 GeV, ^{12}C target, all photons above 10 keV). Compared to these electromagnetic background rates, the hadronic rates are nearly negligible. The total rate of electrons scattered into the angular range $15° \leq \theta \leq 150°$ due to hadronic processes is less than 1000/sec. The total hadron rate (mainly produced by by quasi-real photons) is $\simeq 5 \cdot 10^4$/sec. On the basis of these counting rate estimates and also due to past operating experience of a large acceptance detector at an electron accelerator[9], one can safely expect that the detector can be operated at a luminosity of $\simeq 10^{33} cm^{-2} \cdot sec^{-1}$ (corresponding to a 1 μA electron beam on a 1 mg/cm^2 target).

There will be no difficulties to operate the detector at tagged photon beam intensity ($\simeq 10^7 \gamma$/sec). (At this photon beam intensity, the hadronic production rate is about the same as in electron beam with a luminosity of $10^{32} cm^{-2} sec^{-1}$; however, due to the lack of Møller scattered electrons the background rate is much lower.)

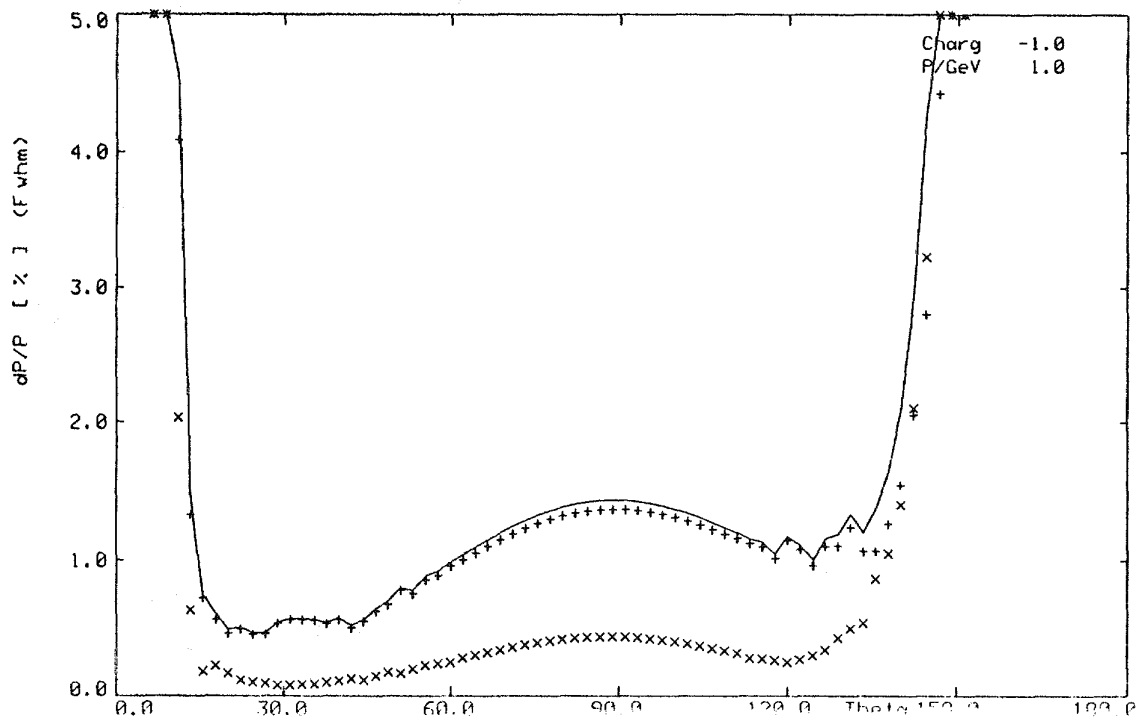

Fig.9 Momentum resolution $\delta p/p$ (FWHM) as a function of the particle emission angle θ for p = 1 GeV/c. The vertex is assumed to be known with an accuracy of 120 μm (FWHM).
x contribution of the chamber position resolution
\+ multiple scattering contribution
-- sum of both contributions.

4. Track Resolution

The track resolution has been calculated taking the position resolution of the chambers and multiple scattering into account. The momentum resolution $\Delta p/p$ for known vertex position is shown in fig. 9 for 1 GeV/c particles as a function of the particle emission angle θ. The momentum resolution reaches 0.6 % in the forward direction; in the central part, it drops to 1.5 % due to the decreasing $\int B \cdot dl$. For known vertex position, $\Delta p/p$ is dominated by multiple scattering; therefore, it is nearly constant in the whole momentum range of interest. The initial angle can be determined with an uncertainty $\Delta\theta \leq$ 1 mrad for 1 GeV/c particles (2 mrad for 0.2 GeV/c).

5. Particle Identification

The combination of momentum and time-of-flight (a r.m.s. time resolution of $\Delta\tau$=200 psec was assumed) gives clean particle identification over a wide momentum range. In the forward direction, pions can be separated from kaons up to 1.5 GeV/c, the limit for kaon/proton separation is 2.5 GeV/c. π/e, π/μ and μ/e separation can be achieved by using the pulse height in the shower counter in addition.

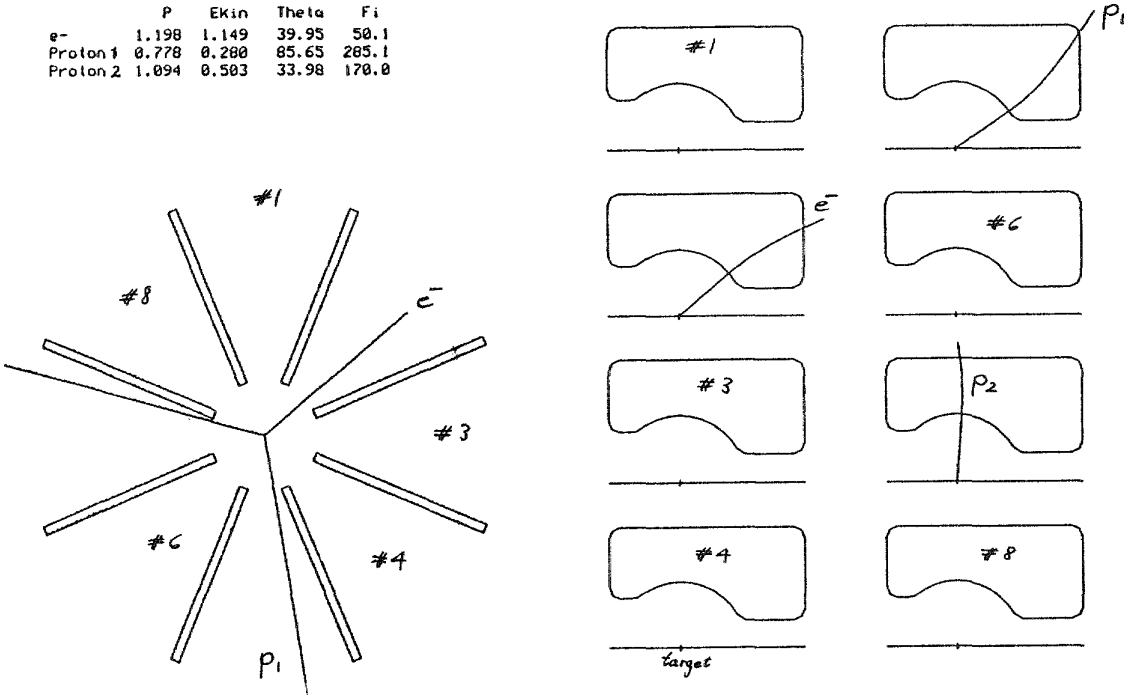

Fig. 10 Single event display for a Monte Carlo generated event from the reaction (e,e'pp). E_e = 2 GeV, θ_e =40°. The left hand side of the display shows a view of the event in the direction of the beam, the r.h.s. presents the tracks in the 8 individual segments.

6. Acceptance

Using a Monte Carlo technique, random multiple particle events were generated to determine the acceptance. Examples for single events as they would be reconstructed and displayed on-line by the detector single-event display are presented in figs. 10 and 11. For the calculation of the acceptance, the θ-range of the detector was taken to be $15° \leq \theta \leq 150°$, 20% of the ϕ-range was assumed to be obstructed by the coils. In addition, cuts in the kinetic energy of the emitted particles were applied to account for detection thresholds: $T_{\pi} \geq 40$ MeV and $T_p \geq 50$ MeV. For the process $\gamma\, p \rightarrow F35(1975) \rightarrow \pi^- \Delta^{++} \rightarrow \pi^- \pi^+ p$ about 60% of the all $\pi^- \pi^+ p$ events are accepted if only θ and T_{min} cuts are used. The addition of the ϕ-cuts reduces the total detection efficiency to 30%.

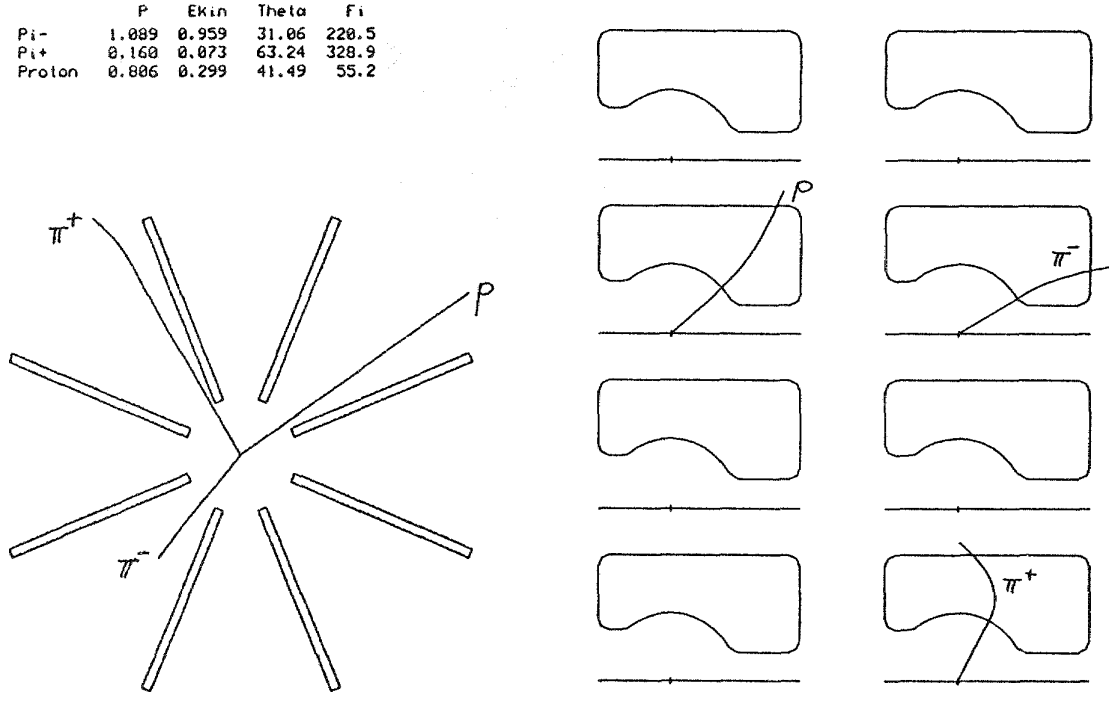

Fig. 11 Single event display for a Monte Carlo generated event from the reaction $\gamma\, p \rightarrow N^* \rightarrow \pi^- \Delta^{++} \rightarrow \pi^- \pi^+ p$ induced by real photons. $E_\gamma = 1.6$ GeV.

7. Counting Rate Examples

a) (e,e'X)
The counting rate has been estimated for $^{12}C(e,e')$ at $E_e = 2$ GeV and $\theta_e = 15°$. A luminosity of $10^{33} cm^{-2} sec^{-1}$ (per nucleon) and 80% ϕ-

coverage have been assumed. The total rate of electrons scattered into the angular interval 14°-16° and the energy interval (1.3-2.0) GeV is ≃100/sec.

b) photon induced reactions
Combining a tagged photon beam with an intensity of 10^7 γ/sec and a hydrogen target of 0.5 g/cm^2 (≃7 cm liquid) results in a total hadronic production rate of ≃400 events/sec (E_o = 2 GeV, σ_{tot} = 140 μb).

8. Layout of End Station B

The LAS will be located in end station B; the layout is shown in fig. 11. The end station and the beam dump are fully shielded to allow for experiments using a high intensity beam on a thin gas target (this also allows a second high intensity experiment to be mounted in this area). For photon experiments, a vertically deflecting tagging spectrometer is located in an enlarged tunnel section.

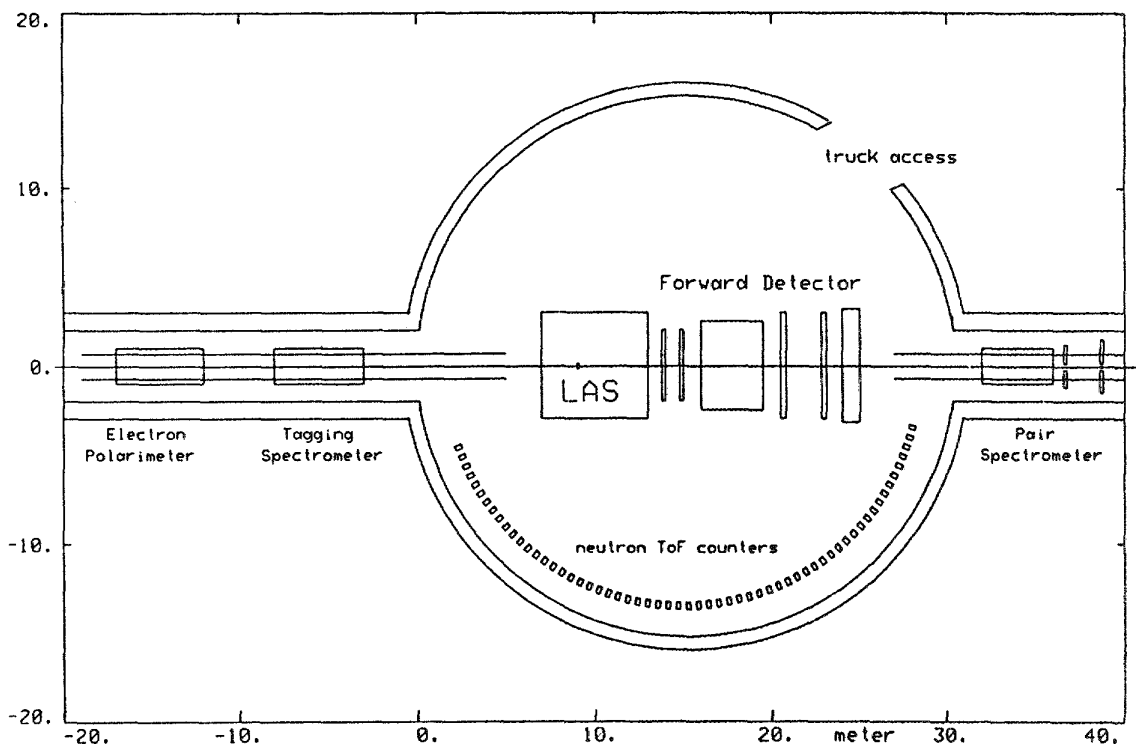

Fig. 12 Proposed layout of end station B

SUMMARY

A large acceptance magnetic spectrometer has been proposed for the investigation of electron- and photon-induced nuclear reactions at CEBAF. The magnetic field is generated by superconducting toroidal coils. Charged particles are tracked using drift chambers and scintillation counters; high energy photons are detected by shower counters. The spectrometer will be indispensable for the investigation of multiple particle final states from (e,e'X) reactions and from the decay of excited $q\bar{q}$ and qqq-states. It will also provide high counting rates for experiments in which the luminosity is limited due to low target density or low beam intensity.

REFERENCES

1) H.J. Pirner et al., Phys. Rev. Lett. 46 (1981) 1376

2) N. Isgur, Proc. of the 1984 CEBAF Summer Workshop, Newport News, Virginia, ed. by F. Gross and R. R. Whitney, p. 199

3) T.H. Bauer et al., Rev. of Mod. Physics, 50 (1978) 261

4) M.E. Sainio, AIP Conf. Proc. 150 (1986) 886

5) M.P. Locher et al., Adv. in Nucl. Phys., Vol. 17 (1986) 47

6) I. Sick, Lecture Notes in Physics 260 (1986) 42

7) F. Lenz, Nucl. Phys. B279 (1987) 119

8) R.D. McKeown and R.G. Milner, 1985 CEBAF Summer Study, RPAC I, p. 12-45

9) L.A. Ahrens et al., Nucl. Instr. Meth. 173 (1980) 537.

Table I: Evaluation of magnetic field configurations for a large acceptance spectrometer to be used for electron- and photon-induced reactions (+ denotes advantage, - drawback)

	Dipole	Solenoid	Toroid
Large solid angle	(+)	+ +	(+)
No field transverse to beam line	- -	+	+
No field at the target position	- -	- -	+
ϕ-symmetric field configuration	-	+ +	+
Open mechanical structure	(+)	-	+
Large $\int B \cdot dl$ at small angles	+	- -	+
High luminosity capability	(-)	+	+

Table II: Design considerations for the toroidal magnet

1) Size
   time-of-flight path required for particle identification via momentum and β
   $L \geq 2$ m for particles going sideways
   $L \geq 3$ m for particles going forward
   → diameter $\simeq$ 4 m, total length $\simeq$ 4 m

2) Field level
   a) small destabilizing forces → low magnetic field
   b) good momentum resolution → high magnetic field
   → compromise solution: $\int B \cdot dl \geq .5$ T•m

3) Number of coils
   a) large number of coils to reduce ϕ-dependence of the field
   b) small number of coils to reduce obstruction of the ϕ-range due to the coils
   → compromise solution: 8 coils

4) Coil shape
   a) no transverse particle motion due to r- and z-components
   → circular inner coil shape
   b) large $\int B \cdot dl$ in the forward direction
   → asymmetric coil shape with longer forward part

THE (γ,K) PROGRAM: A NEW CEBAF INITIATIVE FOR THE STUDY OF NUCLEAR STRANGENESS

R. E. Chrien
Brookhaven National Laboratory, Upton, New York, 11973

E. V. Hungerford
University of Houston, Houston, Texas, 77004

ABSTRACT

This paper is a summary of the CEBAF working group discussions on electromagnetic production of strangeness in nuclear systems. A review of the recent BNL results in (π,K) is presented as representative of the physics questions that could be addressed with the CEBAF facility. Recommendations of the working group concerning the necessary experimental apparatus for a (e,e',K) program are presented.

There are two questions to answer before considering whether to proceed with a (γ,K) program at CEBAF.

1) Is strangeness production in nuclei a field of significance for future development of nuclear physics?

and

2) Is (γ,K) a reaction that is a practical method and justifiable for a facility such as CEBAF?

If the answer to both of these questions is affirmative, then one should proceed with all possible speed to allocate the resources necessary to initiate such studies. Beam and spectrometer design for the laboratory will be fixed in the near future, so time is short and quick action is required.

To answer the first question--the significance or utility of strangeness in nuclei--we briefly summarize the current state of the field, with particular emphasis on some very recent developments in the BNL program which we believe are especially relevant to CEBAF and the planning here.

For about the last ten years the dominant or preferred method for producing hypernuclei has been strangeness exchange[1], shown in Fig. 1 as analogous, ignoring the dissimilar quark masses, to the familiar charge exchange reaction,

$$K^- + n \rightarrow \Lambda + \pi^- \ .$$

This reaction at forward angles strongly favors the population of so-called substitutional states in which the Λ occupies the same orbital as the neutron it replaces. It is characterized by a small momentum transfer and, because of the strong absorbtion of the kaon and pion, it is extremely peripheral. The reaction is virtually useless for populating bound states of heavier hypernuclei. Because

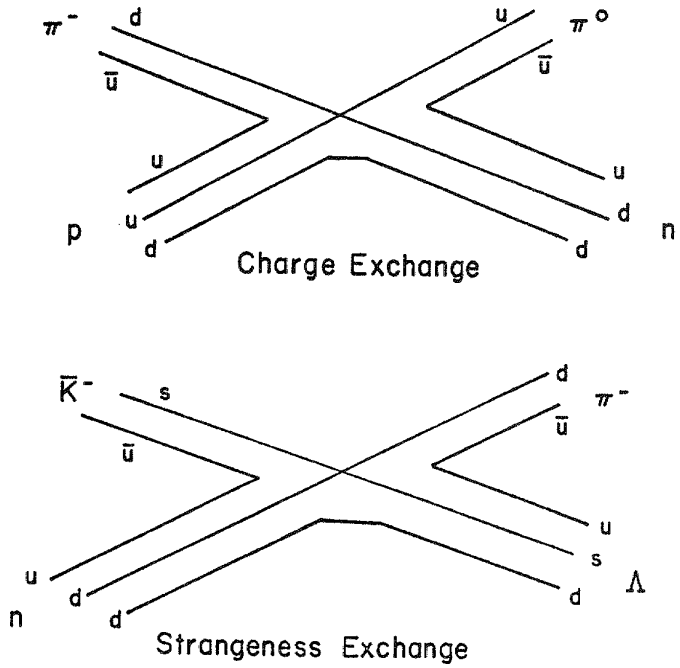

Fig. 1. The diagram for strangeness exchange and its analog, charge exchange.

the single-particle well depth of the Λ is only about one-half that of the nucleon, the valence substitutinal states are typically unbound. Bound states, which consist of a Λ in the successive s, p, d, f... shells coupled to a neutron hole in the valence shell, tend to be of higher angular momentum and are not strongly populated by 0° (K,π) reactions. The situation is graphically displayed in Fig. 2, which shows a series of (K,π) 0° spectra obtained by the Heidelberg-Saclay collaboration[2]. The bulk of the reaction strength lies above the Λ-bound region.

Recently the use of stopped kaons has been advocated as a possible complement to in-flight techniques. The method has been augmented with the use of various decay-signal tags for suppression of background[3]. Several spectra obtained at KEK with this technique[4] are shown in Fig. 3. We shall see that in comparison with spectra shown below, the stopped kaon method is markedly inferior for producing Λ hypernuclei. Furthermore, little benefit has been demonstrated by tagging[5].

We assert here that the reaction of choice for the study of hypernuclear bound states is the associated production reaction,

$$\pi^+ + n \rightarrow \Lambda + K^+ ,$$

originally suggested by H. A. Thiessen[6] of Los Alamos and subsequently analyzed by Dover, Walker, and Ludeking[7]. This reaction

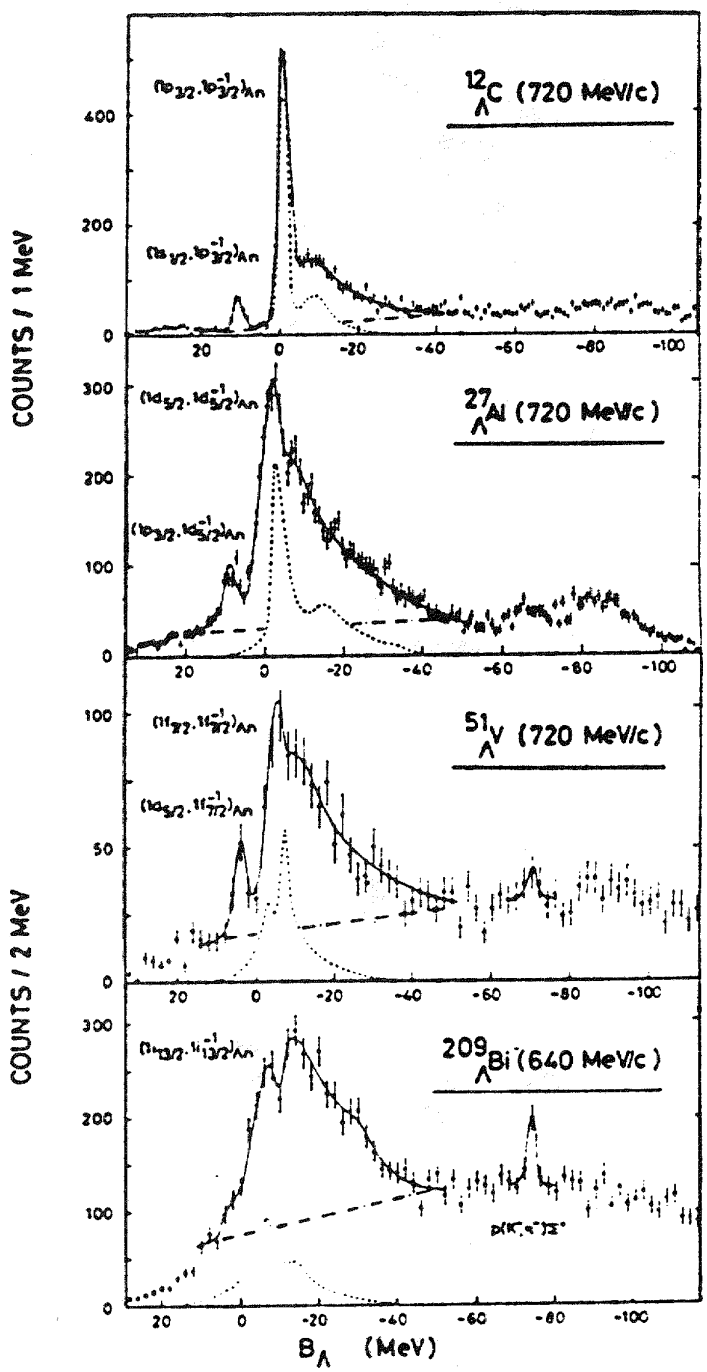

Fig. 2. An early survey of the (K^-,π^-) reaction.

produces a momentum transfer, q, ≈350 MeV/c at $p_\pi \approx 1050$ MeV/c, a maximum in the elementary cross section. In 1983 we did a test of this reaction for $_\Lambda{}^{12}$C, where typical cross sections for exciting the 1^- ground state and 2^+ excited states were about 5.0 μb/sr. Figure 4 shows recent data from BNL on the production of those states[9]. They should be compared to the $_\Lambda{}^{12}$C data of fig. 3. This test encouraged us to try to answer the crucial question: will

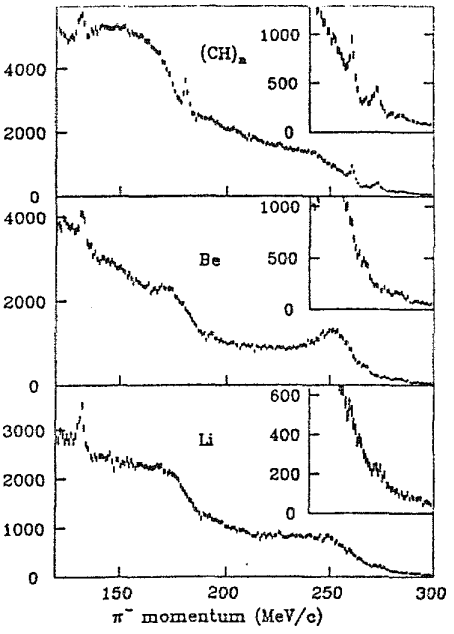

Fig. 3. Examples of spectra obtained from stopped K^-. These data are taken from ref. 4 where they are marked "preliminary".

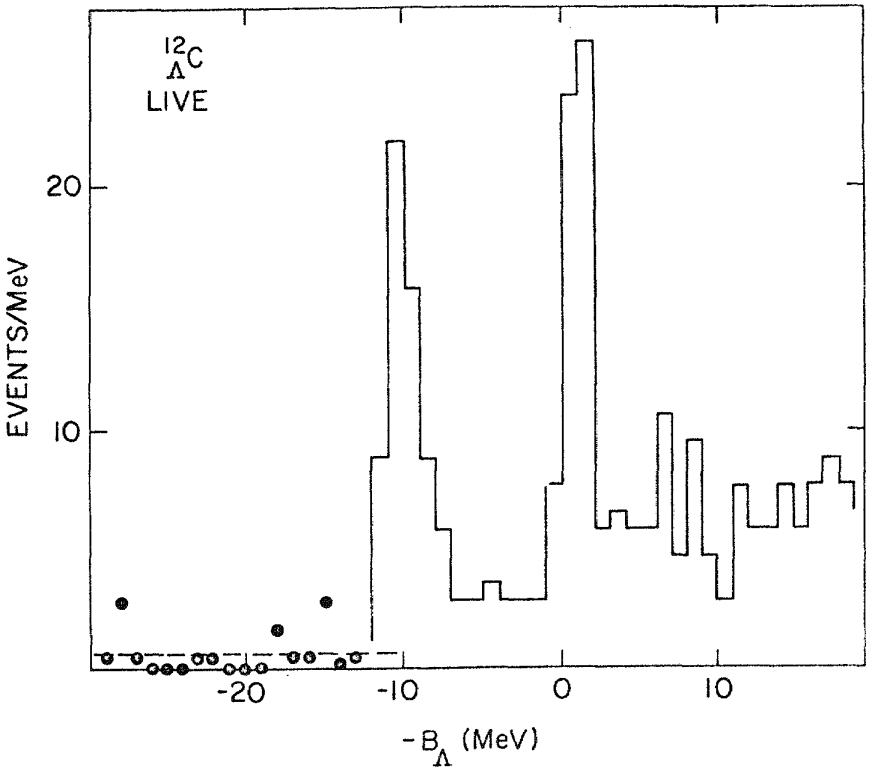

Fig. 4. A (π^+,K^+) spectrum of $^{12}_{\Lambda}C$, obtained at BNL. The effect of hypernuclear tagging suppresses the quasi-free contribution in this spectrum.

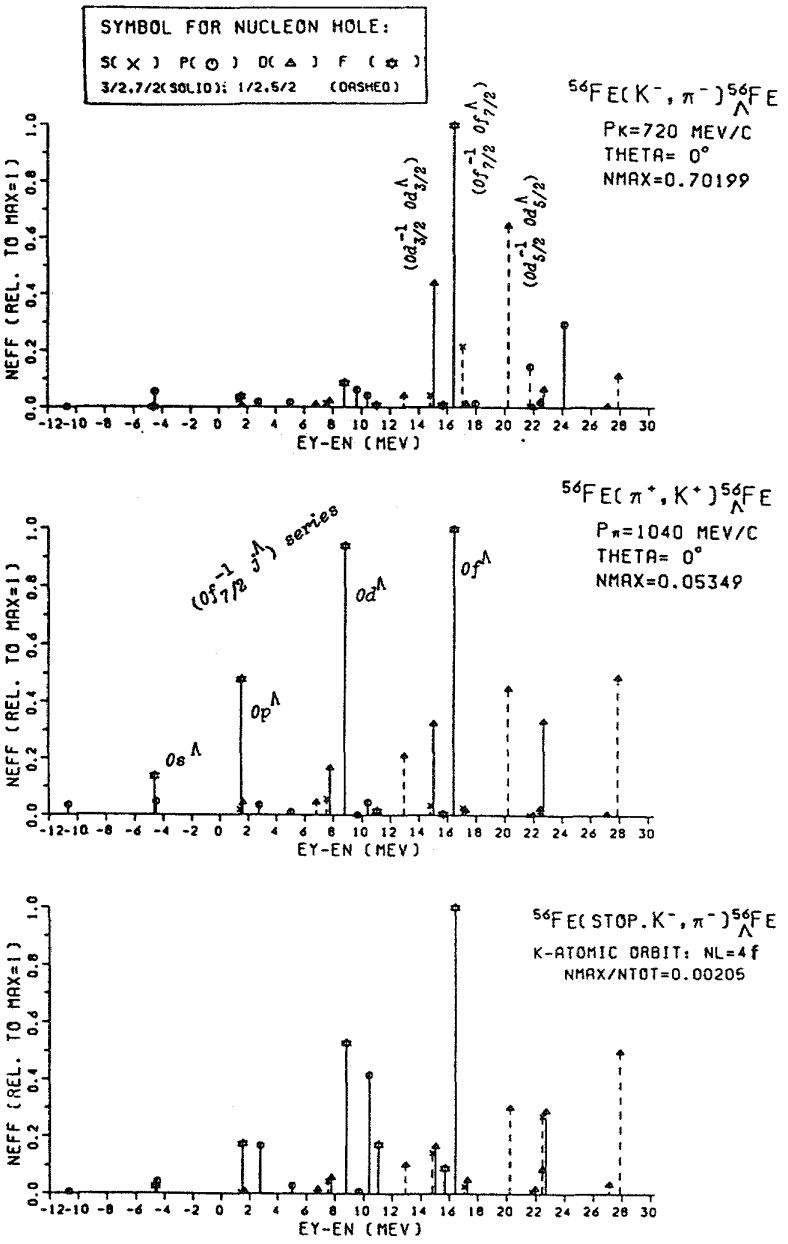

Fig. 5. A comparison of (K^-,π^-), (π^+,K^+) and stopped K^-,π^- as calculated with a DWIA code.

the (π^+,K^+) reaction allow us to examine Λ bound states of hypernuclei beyond the p-shell?

Remember that when the reaction transforms a neutron to a Λ we have a Λ-particle coupled to a neutron hole state. For low energy excitation this hole will lie in a valence shell, which for nodeless wave functions will have progressively higher ℓ as we move up in the periodic table, p, d, f, g, h... The Λ will drop into various shell

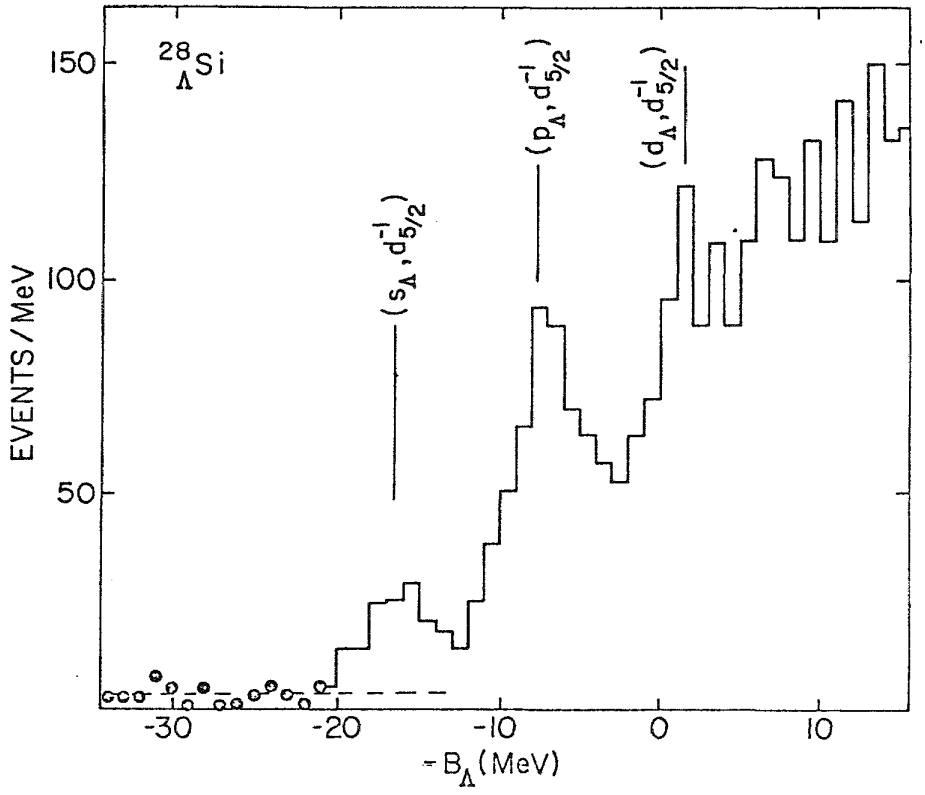

Fig. 6. A spectrum of (π^+,K^+) for $_{\Lambda}^{28}$Si showing the s, p and d shell Λ peaks.

model orbitals coupled to those valence hole states. Figure 5 shows a calculation by Bando[10] which displays the spectra produced by the reactions (K^-,π^-), (π^+,K^+) and (K^- stopped, π^-) on a target of ^{56}Fe. The (π^+,K^+) reaction gives a beautifully distinct series of states above a small background of weaker excitations.

Two of the experimental spectra obtained earlier this year at the Brookhaven AGS are shown in Figs. 6 and 7: $_{\Lambda}^{28}$Si and $_{\Lambda}^{89}$Y. The data clearly demonstrate the existence of deeply-lying shell model orbitals. The shell model series based on the $d_{5/2}$ hole and the $g_{9/2}$ hole are seen rather clearly, in a way reminiscent of atomic spectroscopy, like the Balmer series for hydrogen. It is an exciting, comforting, and still surprising fact that the nuclear shell model works for deeply-lying orbitals as well as for orbitals near the Fermi surface.

Let us now pursue the question of relevance to CEBAF, remembering that the (π,K) reaction is the hadronic first cousin to (γ,K). Each reaction features rather high momentum transfer and favors states containing high momentum components. This is just what is needed for bound states of heavy hypernuclei! Some of the important physics questions to be addressed by a (γ,K) program at CEBAF are enumerated below.

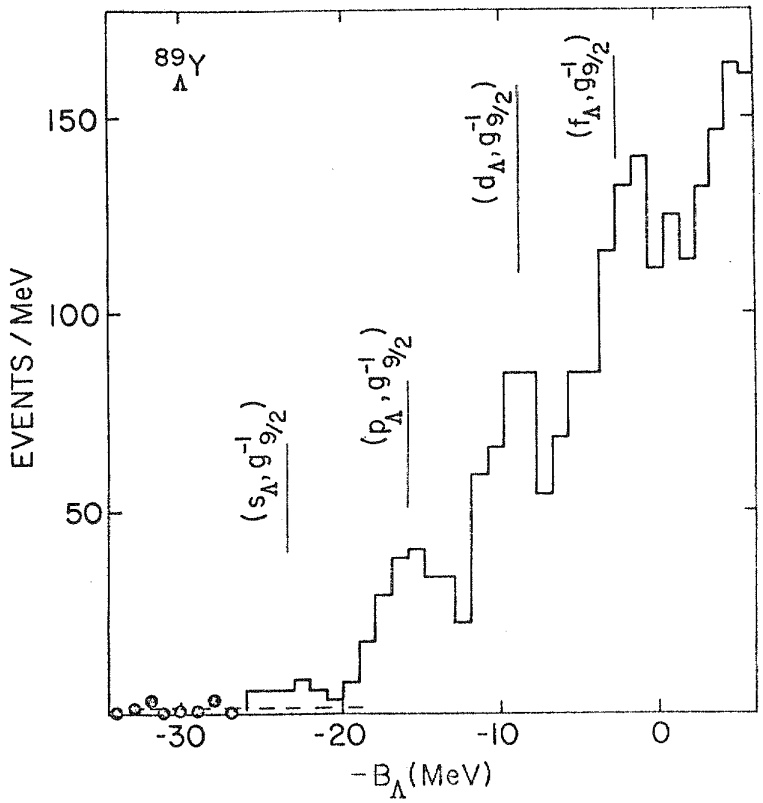

Fig. 7. A spectrum of (π^+,K^+) for $_\Lambda{}^{89}$Y showing s, p, d, and f shell Λ peaks.

1) Do the single particle level positions giving us any information on quark deconfinement? If we assume a distinguishable Λ hyperon in a nuclear potential, a set of single particle levels can be readily calculated. If, however, we assume the validity of a shell model at the quark level, then the Λ may be subjected to a repulsive Pauli pressure in the nuclear medium due to the fact that it contains two non-strange quarks. The effect of this Pauli pressure will affect the level positions, particularly for the heavy systems.

Dover has calculated the binding energies of the Λ single-particle states[11], and these are shown in Fig. 8, in which a Saxon-Woods potential is assumed with the following parameters: V_0 = 29.34 MeV, r_0 = 1.08 fm, a = 0.6 fm, and ξ = 0.427 fm^2. In the folding model $\langle r^2_v\rangle = \langle r^2\rangle_p + \langle r^2\rangle_{\Lambda N}$ and $R = r_0 A^{1/3}\,(1+\xi/(r_0A^{1/3})^2)$. The fits to the experimental data of ref. 9, shown as filled circles on Fig. 8, are excellent.

Dover points out that it is instructive to view the effect of Pauli pressure in the following way: for distinguishable particles (like a Λ hyperon) in a potential well, an expansion for the s-p shell spacing may be written in powers of mass number A, as follows:

a) $\Delta sp \propto (A^{-2/3} + kA^{-1} + \ldots)$

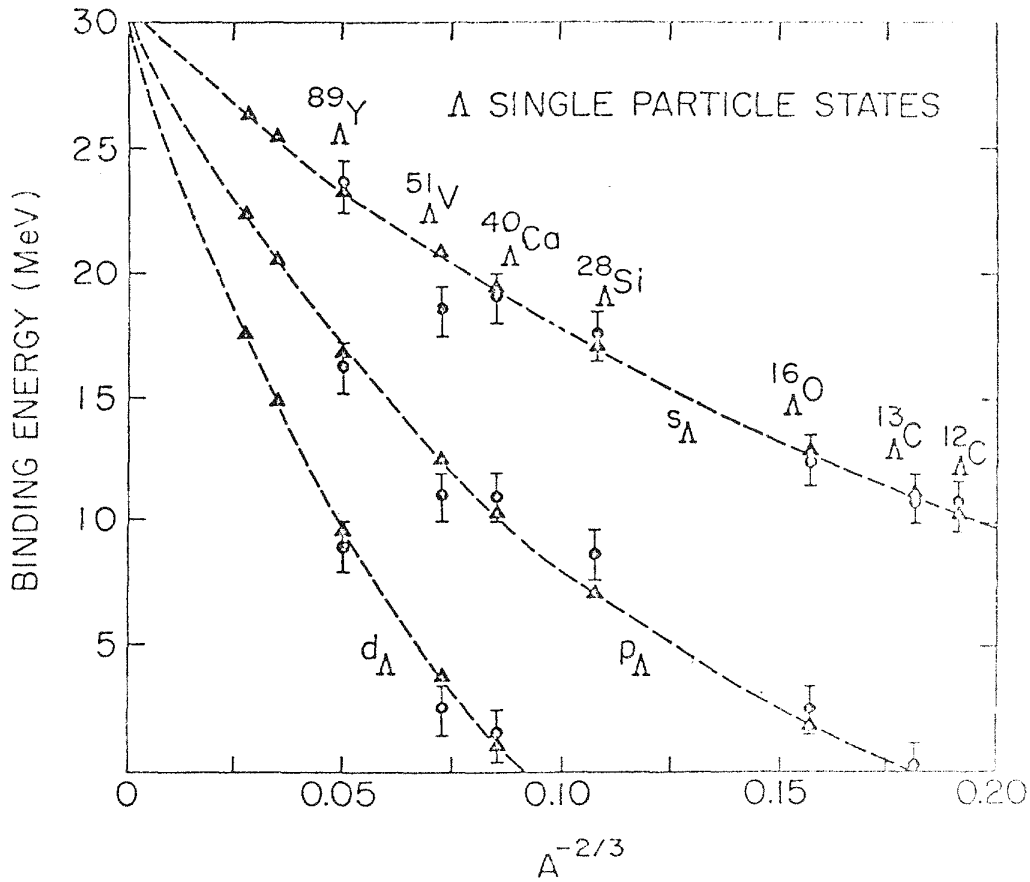

Fig. 8. A global plot of Λ single particle states compared to recent BNL data.

In contrast, for indistinguishable particles (nucleons), the expansion is different

b) $\Delta sp \propto (A^{-1/3} + k'A^{-1} + \ldots)$

The $A^{-1/3}$ term above may be viewed as an indication of Pauli pressure. If we view the Λ hyperon--made up of u, d, and s quarks--as part of "quark shell model", it is only 1/3 distinguishable. Thus one can imagine that in an expression such as

c) $\Delta sp \propto (k''A^{-1/3} + A^{-2/3} + kA^{-1} \ldots)$

The coefficient k" represents a measure of quark deconfinement. The different between expressions 1) and 2) is ≈1.5 MeV for ^{208}Pb, and this should be measurable with present techniques. Thus some measure of quark deconfinement (or a limit) may be achievable by measuring energy level spacings in Pb.

The effect remains to be assessed, but it is clear that a map of such levels up to and including Pb needs to be produced. Resolution is important so that CEBAF clearly can play an important role in this work.

2) Some of the peaks in our (π^+,K^+) spectra look broader than our experimental resolution. Furthermore, these peaks appear to be superposed on a steeply rising continuum as the excitation energy increases.

Several questions then arise: are we seeing the spreading width of these states? How much strength is dispersed into the many multiparticle-multihole states which are present? Better resolution is clearly needed to answer these questions.

3) A distorted-wave impulse analysis has been successful in predicting (K,π) and (π,K) cross sections for exciting hypernuclear states in p-shell nuclei[12]. Distortion effects must be calculated in applying this analysis, and these effects are very pronounced in heavy nuclei. In (π,K) both pion and kaon distortions are important, while in (γ,K) only K^+ distortions need be invoked. How do they vary with momentum? Does the summed strength predicted by the DWIA calculations exhaust the strength observed in the experiment?

4) Spin-flip transitions are not significant in (π,K). In (γ,K) reactions, however, both parity-favored and parity-unfavored states are accessed. We know that Λ-spin multiplets are very closely spaced. In some cases we have set significant limits (for example, in $^{9}_{\Lambda}$Be) on the Λ spin-orbit splitting[13]. In (γ,K) with improved resolution, we may be successful in determining such splittings.

5) In (γ,K) reactions, form factor measurements may be successful in determining the charge distributions for these deeply-lying shell model states. Clearly, adequate counting rate and resolutions are required to attach these interesting problem areas.

The discussions in the workshop sessions on hypernuclei were centered on the second question posed in the opening paragraph. Is it feasible to undertake an experimental program in (e,e',K) at CEBAF? One can consider such a program divisible into two parts, although these parts can be attacked in parallel because they involve different instrumentation.

On one hand, we need to develop information on the elementary interactions $\gamma + p \rightarrow \Lambda + K^+$. Our knowledge of this reaction is displayed in Fig. 9[14]. The data are sparse and need to be better determined. It appears that high count rate at modest resolution is required. The consensus of opinion at the workshop is that a program of elementary kaon production probably can be carried out at the large acceptance spectrometer (LAS). Such a program, we feel, should be an important segment of the CEBAF effort.

On the other hand, the investigation of the (e,e',K) reaction to discrete hypernuclear final states requires quite a different set of instruments. The spectrometers, for example, must be capable of operating at extremely forward angles and achieving the best possible resolution. Coupled with this is the necessity for count rates sufficient to determine the transition form factor. Count rates of a few per hour to discrete states may not seem large, but they might allow detailed studies if the final states are sufficiently well separated in the spectrum.

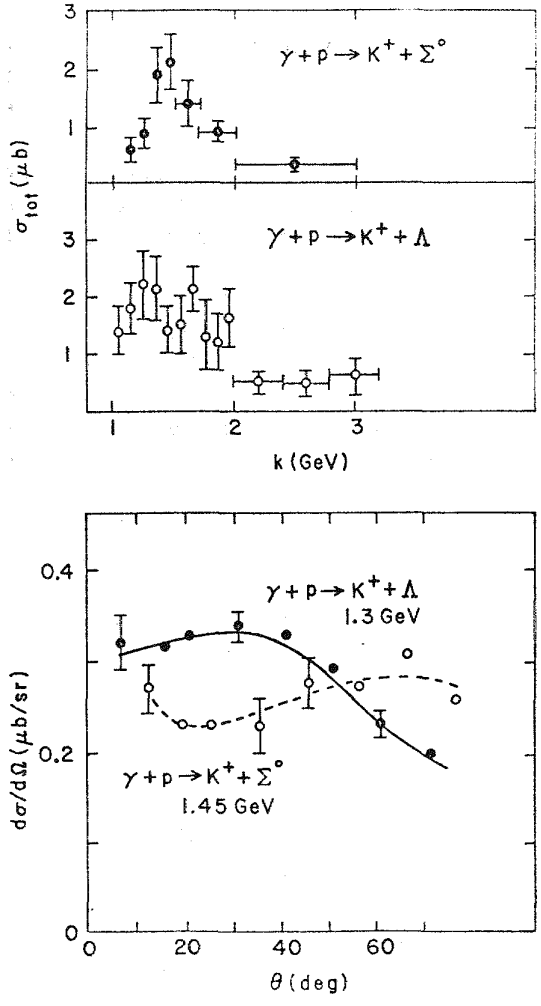

Fig. 9. The elementary cross sections for Λ and Σ photoproduction.

Figure 10 shows some calculated differential cross sections[15] for the population of the 1^- ground state of $_{\Lambda}{}^{12}B$. Note that the cross section reaches 80% of its maximum value by 1.5 GeV/c, and that for energies above this value, the kaon production is strongly forward peaked. Figure 11 shows that the virtual photon production is concentrated in a narrow forward cone for the emerging electrons, as is the bremsstrahlung background[16]. Figure 12 shows the relative production of the parity unfavored 2^- member of the doublet compared to the 1^- member, and again demonstrates the forward peaking[17]. Figure 13 shows the form factor of the $_{\Lambda}{}^{16}N$ 2^- member of the ground state doublet as a function of electron scattering angle θ_e. Again small values of both θ_e and θ_K are indicated[18].

These figures show what features are essential to the operation of a successful hypernuclear facility using the (e,e',K) reaction. Such a facility could be termed a "Fine Resolution e, e',K" facility, or "FREEK".

The FREEK program needs an electron spectrometer operating near 0 degrees. The virtual photon flux peaks very strongly at 0°

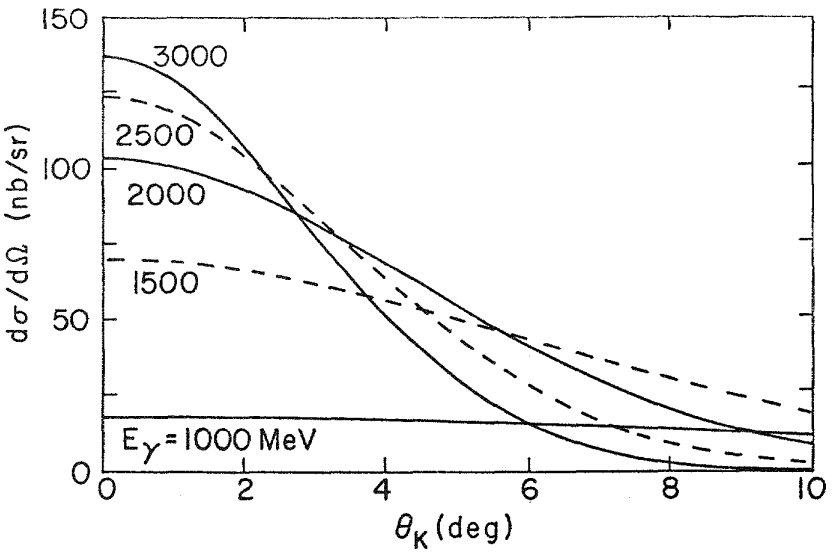

Fig. 10. Differential cross sections for the production of the 1^- $\Lambda^{12}B$ ground state as a function of E_γ and of θ_{K^+}.

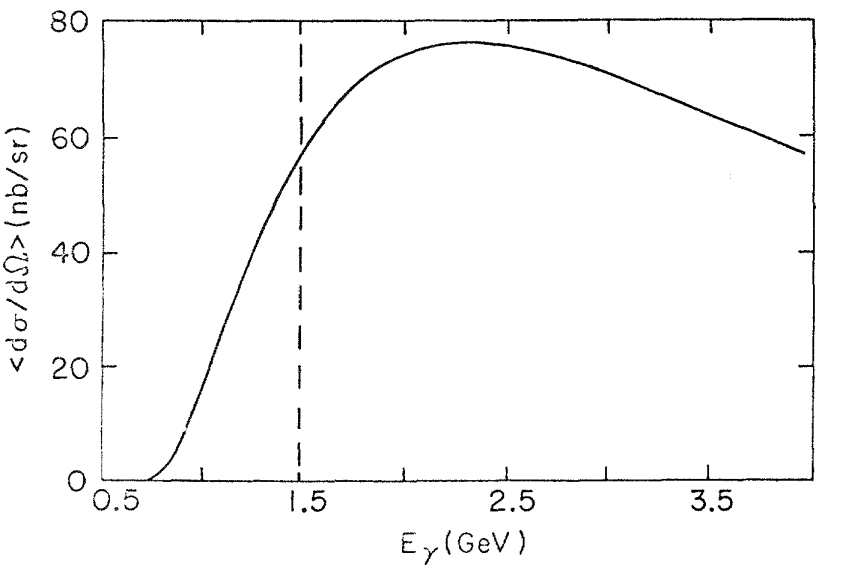

electron scattering, and falls rapidly away from 0. The singles rate which the electron spectrometer arm can handle sets the maximum luminosity at the target. The hadronic background in the kaon spectrometer arm can be very low, however.

The electron spectrometer singles rate cannot exceed 3×10^8/ sec. This rate is determined by the necessity to correlate an electron event with a detected kaon; the beam structure gives electron bunches separated by 2 ns. A forward angle electron spectrometer concept was suggested by Mike Finn.

The second "FREEK" requirement is a high-quality kaon spectrometer. There are many possible designs for such a spectrometer. A prototypical design may possibly be found in the Bates

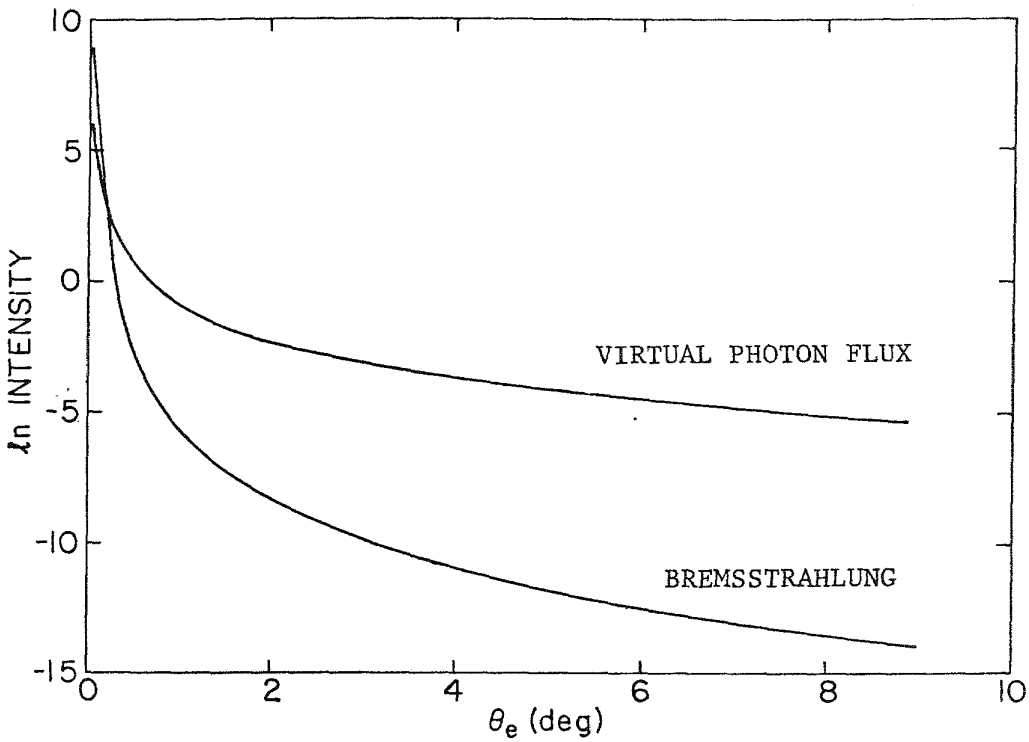

Fig. 11. The virtual photon flux as a function of electron scattering angle. The ln flux is plotted, and the ln bremsstrahlung flux is also plotted for comparison.

design of Bertozzi et al.[19] or in the BNL "Moby Dick" spectrometer[20]. It is essential to maintain high resolution with as short a path length as possible so that kaon decay is reduced to a minimum.

Because of the high singles rates envisioned in the electron spectrometer, considerable discussion within the working group centered on possible tricks to avoid this limitation. It had been pointed out earlier by P. Y. Bertin[21] and subsequently by B. Mecking[22] that dispersing the beam perpendicular to the bend offers several advantages. The dispersion would serve to decouple electron and kaon spectrometers from the electron accelerator beam spread and instabilities. Furthermore, were it possible to track the emitted particles back to the target, the luminosity could be increased without losing the necessary correlation between the electron and the kaon. Since the necessary tracking could easily be done to a precision of better than one millimeter, dispersing the beam over a centimeter allows a luminosity increase of better than a factor of 10.

Among the features of a facility incorporating a forward angle electron spectrometer, we note the following:

a) thin samples and low luminosity, leading to good resolution;
b) separated isotopes, feasible because of small target size and thickness;

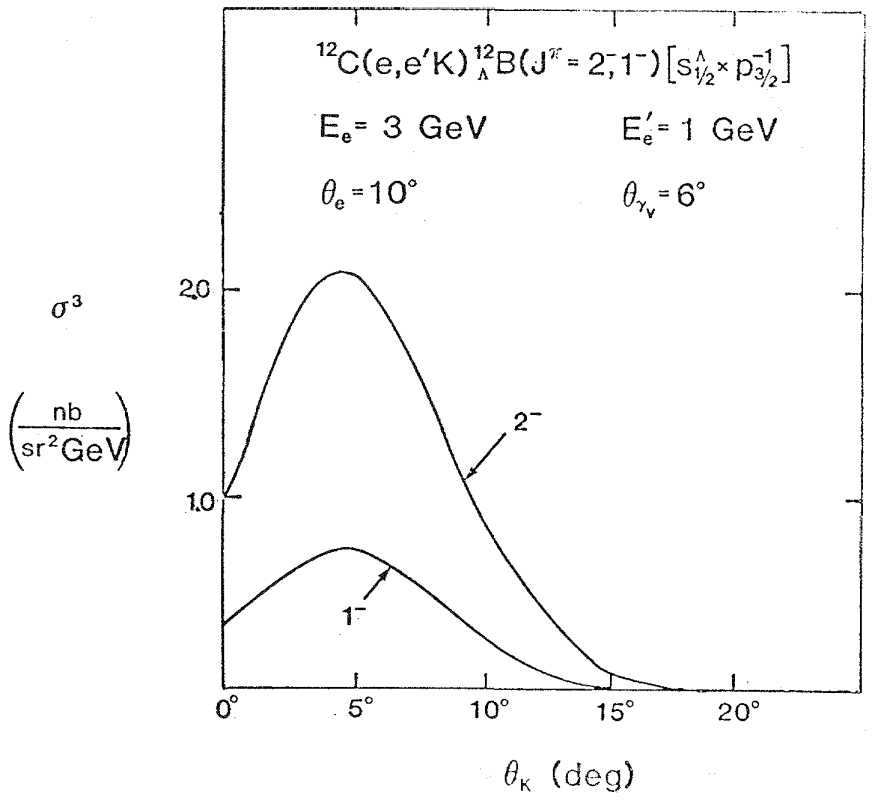

Fig. 12. Population of the 1^- and 2^- ground state doublets of $\Lambda^{12}B$ by (e,e',K^+).

c) beam dispersion to improve count rate, stability, and resolution;
d) a low hadronic background, allowing hypernuclear decay measurements and the use of decay tags for background and quasi-free suppression.

With these considerations, the suggested parameters for the "FREEK" spectrometers are given in Table I.

Table I. Fine Resolution (e,e'K) Facility

	Electron Arm (or Leg)	Kaon Arm
Pmax	≈ 0.5 GeV/c	≈1.2 GeV/c
θ	near 0°	5-20°
dΩ	≈1 msr	10 msr
Momentum Bite	0.4	0.1
Resolution	10^{-4}	0.5×10^{-4}
Length	--	≈9m

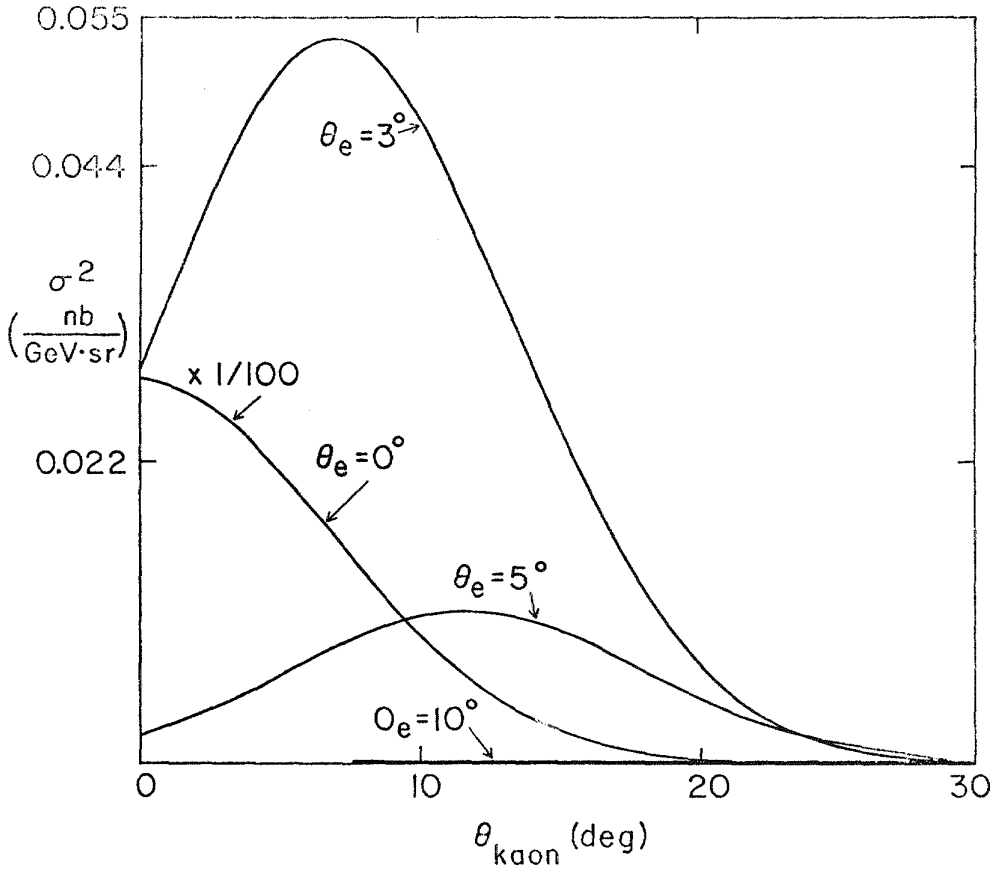

Fig. 13. The population of the $_{\Lambda}{}^{16}$N 2^- level at 3.6 MeV for various θ_e, θ_K angles, in (e,e',K^+). The calculation assumes a solid angle, $\Delta\Omega e$, of 2.2 msr, an electron momentum of 4 GeV and E_γ = 1.2 GeV.

We advocate the choice of (γ,K) on ^{12}C leading to the 1^- and 2^- states of $_{\Lambda}{}^{12}$B as an initial experiment. Besides providing a verification of the count rates and spectrometer performance, important information on the spin dependence of the Λ-hyperon-nucleon potential in a nuclear medium is obtained, if sufficient resolution permits the splitting of this doublet. Table II lists the parameters and rates of this experiment. With the beam dispersed in y to form a strip on target 100μ wide by 1 cm high, an estimate of the count rates can be made.

Table II. Count Rates @ E_0 = 1.7 GeV/c; $\theta_e = 0°$

γ flux	6.0×10^7 photons/MeV*/sec
I_0	1μA*
$d\sigma/d\Omega$	55 nb/sr
$(\Delta p/p)e$	0.4
$(d\Omega)K$	10 msr
εK survival	0.4
target	100 mg/cm^2
εff	0.7

$^{12}C(\gamma,K^+)\Lambda^{12}B$

1^- state	30/hr.*
2^- state	90/hr.*
Total to GS doublet	120/hr.*

*Beam Dispersion Factor = 10

In summary, we recommend:

- A study of elementary (e,e'K) amplitudes over a broad range of Q^2 (4-momentum transfer). This could presumably be done at the Large Acceptance Spectrometer, provided that a forward angle spectrometer is added to that device.

- The establishment of a high quality, forward angle, (e,e'K) system featuring high resolution and high rates through use of a dispersed beam on target.

- A test of the system with the reaction $^{12}C(\gamma,K^+)_\Lambda{}^{12}B$ leading to the $1^-,2^-$ ground state doublet.

Finally, we believe that the answer to both questions--is it significant to do γ,K? and is it practical to do γ,K at CEBAF? is a resounding

YES!

ACKNOWLEDGEMENT

Research has been performed in part under contract DE-AC02-76CH00016 with the United States Department of Energy.

REFERENCES

1. For a reasonably recent review of the hypernuclear field, see the collection of papers contained in Nucl. Phys. A450 (1986).
2. R. Bertini et al., Nucl. Phys. A360, 315 (1981).
3. T. Yamazaki, ref. 1, p. 1.
4. H. Tamura et al., post deadline contribution to XIth Intern. Conf. on Particles and Nuclei, "PANIC87", Kyoto, Japan, April, 1987.
5. R. S. Hayano, invited talk at XIth Intern. Conf. on Particles and Nuclei, "PANIC87", Kyoto, Japan, April, 1987.
6. AGS Experiment 758 proposal, March, 1980.
7. C. B. Dover, L. Ludeking, and G. E. Walker, Phys. Rev. C22, 2073 (1980).
8. E. C. Milner et al., Phys. Rev. Lett. 54, 1237 (1985).
9. R. E. Chrien, et al., XIth Intern. Conf. on Particles and Nuclei, "PANIC87", Kyoto, Japan, April, 1987.
10. H. Bando and T. Motoba, Prog. Th. Phys. 76, 1321 (1986).
11. C. B. Dover in "Kaon-Nuclear Reactions and Hypernuclei", invited talk at the Intern. Symp. on Medium Energy Physics, Beijing, 1987.
12. E. H. Auerbach et al., Ann. of Phys. 148, 381 (1983).
13. M. May et al., Phys. Rev. Lett. 51, 2085 (1983).
14. H. Genzel, P. Joos, and W. Pfeil, quoted by A. Bernstein, Proc. of the Intern. Conf. on Hypernuclear and Kaon Physics, Heidelberg, MPIHV20, 411 (1982).
15. Bernhard A. Mecking, "Experimental Aspects of Hypernuclear Physics at CEBAF", unpublished, 1987.
16. L.-G. Tang and L. Xu, private communication.
17. S. R. Cotanch and S. Hiao, Nucl. Phys. A450, 433c (1986).
18. S. R. Cotanch, private communication, 1987.
19. W. Bertozzi et al., Nucl. Instrum. & Meth. 162, 211 (1979).
20. P. H. Pile in Intersections between Particle and Nuclear Physics, AIP Conf. Proc. 123, 813 (1984).
21. P. Y. Bertin, "Photo-et Electro-Production de Meson K", contribution aux Journées d'Études de Physique Nucleaire sur la Photoproduction et l'Électroproduction de Mesons sur le Nucleon et les Noyaux (Clermont-Ferrand, 1986).
22. B. Mecking, private communication, 1987.

(e,p) Parity Violation Program at CEBAF

R. Carlini
Los Alamos National Laboratory, Los Alamos, NM 87545

R. Siegel
College of William & Mary, Williamsburg, VA 23185

PHYSICS MOTIVATION

All existing weak interaction data is consistent with the standard model to the level of present experimental accuracy. However, it is generally felt that the minimal standard model is incomplete and new physics could appear at a mass scale as low as a few hundred GeV. A high precision, low q^2, measurement of $\sin^2\theta_W$ in the quark sector, together with such measurements in the electromagnetic and lepton sectors will provide as complete as possible a constraint on higher mass Z's and other phenomena. Measurements are required in all sectors because theoretical extensions to the standard model allow new physics to manifest itself somewhat differently in the three sectors. In addition, a trinity of experiments is essential to verify and/or uncover any bad measurements.

The goal of a next generation (CEBAF) polarized (e,p) program is to do high precision measurements with the hope of:

- Measuring $\sin^2\theta_W$ to a new accuracy .This requires an (e,p) asymmetry measurement to a few % in order to obtaint $\Delta\sin^2\theta_W/\sin^2\theta_W$ to better than 1%.
- At the 1% level, the measurement is sensitive to radiative corrections and higher-order charged and neutral-current corrections. This tests assumptions about the renormalizability of the Standard Model. No complete analysis of these corrections exists, but they probably modify the q^2 dependence of the general relations. Low q^2 measurements of $\sin^2\theta_W$ complement high q^2 measurements and are needed to yield quantitative information on these corrections.
- Setting a strong lower mass limit on a second Z .
- Is the Standard Model correct in the low-energy strong coupling regime of strong interactions?
- How accurate are some of the most basic assumptions of nuclear physics, such as CVC, the lack of second class currents, and isospin invariance?
- Measure weak neutral structure functions $F_1^{(0)}$, $F_2^{(0)}$, and $F_A^{(0)}$. These test some of the basic assumptions of the Standard Model. For example, if both proton and neutron structure functions are measured to determine the isovector part, one should find;

$$[F_1^{(0)}]_{\text{isovector}} = (1-2\sin^2\theta_W) \bullet [F_1^{em}]$$

  at all q^2, which follows from CVC.
- Perhaps uncovering new physics?

IN THE E6 MODEL

What will a high precision low q^2 (e,p) parity violation experiment contribute to the mass limit on a Z' within an E6 Framework? Lykken[1] has done as estimate having assumed that null limits will be obtained from the high precision experiments listed below:

- M_Z measured at SLC and LEP to $\pm$ 50 MeV.
- M_W/M_Z measured at CERN with ACOL or Tevatron combined with the above experiments gives M_W to $\pm$ 200 MeV.
- AFB, forward/backward asymmetry in $e^+e^- \Rightarrow Z^\circ \Rightarrow \mu^+\mu^-$ to be measured at LEP with accuracy of $\pm 2 \times 10^{-3}$.
- R, measured at the Los Alamos LCD to $\pm 2 \times 10^{-2}$.

One must also assume that the top quark is found and Higgs mass not too big, so standard model radiative corrections can be accurately calculated. For this discussion we will ignore atomic parity violation experiments since their theoretical interpretation is difficult. We will, also, ignore semileptonic experiments which have theoretical uncertainty of $\pm$ 3%.

Definition of Parameters $M_{Z'}, \theta_1, \theta_2$, and λ in E_6 Model

$M_{Z'} \equiv$ Mass of Second Z
$\theta_2 \equiv$ mixing angle between Z° and Z'.

$$M^2_{Z^\circ} - M^2_{Z'} = (M^2_{Z'} - M^2_{Z^\circ}) \tan^2 \theta_2$$

M_{Z° = measured mass

$$\lambda \equiv \tilde{g}_2 / \tilde{g}_3$$

$\theta_1 \equiv$ mixing angle between hypercharge eigenstates.

$$Z' \Rightarrow \ddot{Y} = \cos \theta_1 \, Y' - \sin \theta_1 \, Y''$$

The Tevatron could produce Z' directly if $\lambda M_Z < 300$ GeV. Note if $\lambda << 1$ then Tevatron limit may be poor at certain hypercharge mixing angles θ_1. If any of these experiments shows evidence for another Z, then information concerning its manifestation in each sector becomes of critical theoretical importance. Figure 1 shows the results of Lykken's calculation on the effect an (e,p) parity violation experiment (at a $\theta_2 = .2$) would have on the lower mass limit of a Z' with and without the Los Alamos LCD, respectively. The conclusion is that the limit set, within the E6 model, by a 1% (e,p) experiment is somewhat stronger at all θ_1 than can be set by the proposed Los Alamos LCD experiment.

Lower Bound on Mass of Z'

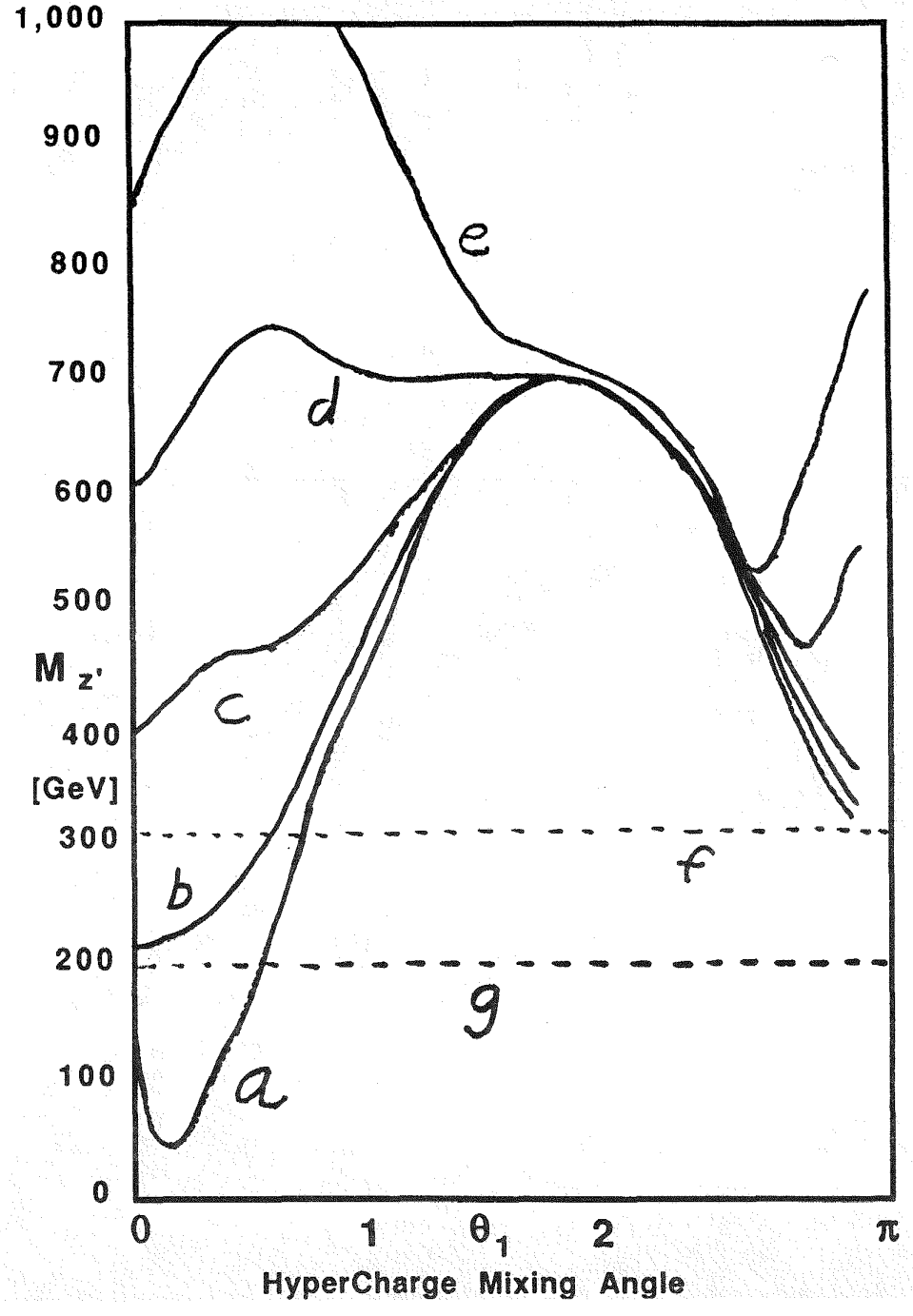

Lower bounds on mass of Z' in E_6 model with:
$\sin^2\theta_W = 0.225$, $\theta_2 = 0$, $\lambda = 1$
Assumes null results on all experiments.

Curves:

(a) Expts. are: M_Z measured to ±50 MeV
M_W measured to ±200 MeV
Forward/backwards assymetry
in $e^+e^- \Rightarrow \mu^+\mu^-$ to ±0.2%

(b) As above but including LCD measuring R to ±2%.

(c) As in (a) but including (e,p) results assuming both $a_e(2V_u - 1/2V_d)$ and $V_e(2a_u - 1/2a_d)$ are extracted to ±5%.

(d) As in (c) but (e,p) accuracy to ±2%.

(e) As in (c) but (e,p) accuracy to ±1%.

(f) Upper bound on what Tevatron can see assuming integrated luminosity $10pb^{-1}$, Z' decays only into standard fermions.

(g) As above, but assuming Z' decays into full 27's of fermions and superpartners.

INTERPRETATION OF THE DATA

The parity violating asymmetry can be expressed in terms of q^2, electron energy, electron scattering angle and structure functions as given below.

$$A_p \equiv [d\sigma\Uparrow - d\sigma\Downarrow] / [d\sigma\Uparrow + d\sigma\Downarrow] = -Gq^2/\sqrt{2}(4\pi\alpha)\xi \bullet \{$$

$$\cos(\theta/2) \bullet [\; F_1^{\gamma,P} \bullet [(1-4\sin^2\theta_W)\, F_1^{\gamma,P} - F_1^{\gamma,N}] \; + q^2 F_2^{\gamma,P} \bullet [(1-4\sin^2\theta_W) F_2^{\gamma,P} - F_2^{\gamma,N}] \;]$$

$$+2\sin^2\theta/2 \bullet (q^2/4M^2) \bullet G_M^{\gamma,P} \bullet [(1-4\sin^2\theta_W) G_M^{\gamma,P} - G_M^{\gamma,N}]$$

$$-\sin^2\theta/2 \bullet (\varepsilon_1 + \varepsilon_2) / M \bullet G_M^{\gamma,P} \bullet (1-4\sin^2\theta_W) \bullet F_A^{(0),P} \}$$

Where,

$$\xi = \cos^2\theta/2 \bullet [(F_1^{\gamma})^2 + q^2 (F_2^{\gamma})^2] + 2\sin^2\theta/2 \bullet [q^2/4M^2] [F_1^{\gamma} + 2MF_2^{\gamma}]^2$$

$G_M \equiv F_1 + 2M\, F_2$
ε = Electron initial / final energy
q^2 = 4 Momentum
θ = Scattering Angle
F_1^{γ} = Charged Structure Function
F_2^{γ} = Weak Magnetism
P = Proton
N = Neutron
$\Uparrow$ = Polarization Direction

As A_P is very sensitive to θ, E, q^2 and the target (LH_2 or LD_2) an experimental separation of the various contributions is possible, and by varying the q^2 at which the measurements are taken different terms can be isolated and extracted. This provides the experiment with internal cross checks that allow detection of any fundamentally wrong physics assumptions, such as the effect of strange quarks.

A critical question is how accurately can $\sin^2\theta_W$ be extracted from the observable scattering asymmetry. Pollock[2] has done an analysis of the uncertainties introduced by each of the terms in the expression above at a q^2 of .2 GeV^2, and has concluded that the existing

experimental uncertainty in the neutron form factor G^N_E will be the limiting systematic uncertainty in the extraction of $\sin^2\theta_W$. Fortunately, one of the major goals of the CEBAF program is to measure basic form factors to better accuracies. Even with todays very poor knowledge of the neutron form factor the systematic error it contributes to $\sin^2\theta_W$ is only ±2.6%. With conservative assumptions about improved measurements we can contemplate an $\Delta\sin^2\theta_W/\sin^2\theta_W$ measurement having well under 1% systematic uncertainty.

ACCELERATOR RELATED REQUIREMENTS

A stable reliable polarized source is essential to conduct this program of research. Present sources can achieve approximately 40% polarization, but even this is non-trivial. However, this is sufficient with a 2 GeV electron beam current of 100 μA . There is, also, the possibility of new polarized electron sources that might provide 80% polarization.

A continuous precision measurement of the beam energy and a servo system to apply a correction signal to the Klystrons supplying power to the rf cavities wil be required. Laser backscattering is the likely choice to provide this continuous beam energy monitoring. Its advantages include:

- Laser technology is currently sufficient,
- Valuable to entire CEFAF program,
- Non-destructive to beam.

Figure 2 shows a schematic of a possible apparatus. A suitable location must be selected to allow maximum benefit for all users. Fortunately, high beam quality is intrinsic to superconducting linacs. This includes little or no beam halos, large apertures, and stable operation. In order to take maximum advantage of these features it is essential to interface the experiment to the accelerator at an early stage. This will result in the least effort and expense, and will not require the experiment to work around, usually with great difficulty, what at a early stage might be some arbitrary or minor machine design criteria.

BEAM MONITORS AND CONTROLS

It will be necessary to monitor and control beam intensity variations and apply a correction signal to the polarized source. Control systems for beam motion, phase space, and residual transverse polarization will, also, be required. Generally, such systems exist within

Laser Back Scattering

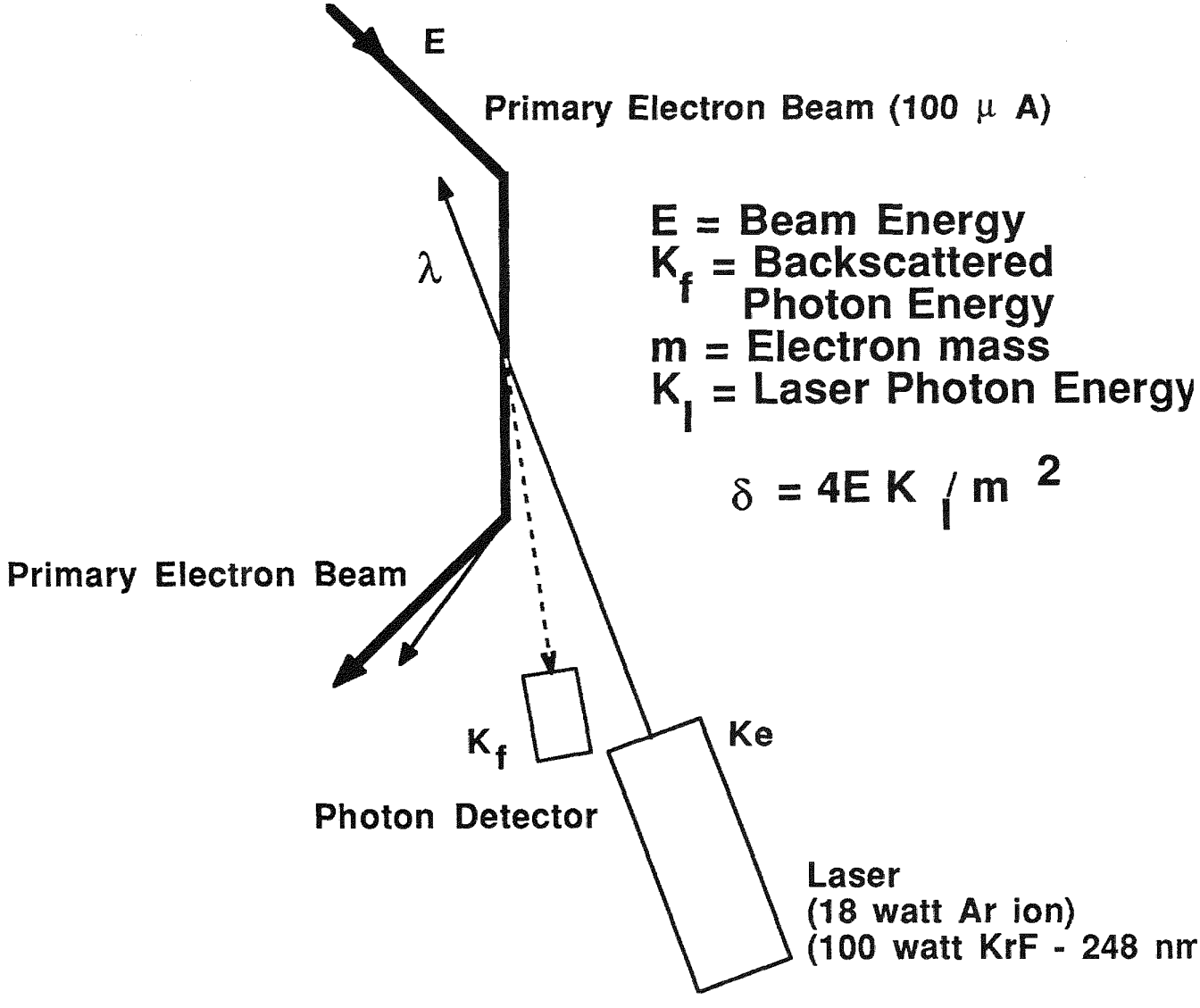

E(GeV)	$\lambda(K_I)$ (nm)	δ	$K_{f(max)}$ (MeV)
0.25	500	0.01	002.5
1.00	500	0.04	038.0
4.00	500	0.15	520.0
1.00	196	0.10	087.0

accelerators, but parity experiments usually require greater accuracies than equipment designed to serve solely as accelerator diagnostics.

It will be necessary to determine an optimum helicity reversal rate in order to minimize the intrinsic noise spectrum of the beam. Several philosophies exist on this subject, and the final decision can be made only after studying the properties of the actual beam. A rapid reversal (KHz) of the beam helicity has the advantage that the experimental conditions will not change significantly between helicity reversals. However, the statistical sampling is poorer. A slower reversal rate (1 sec) provides the great advantage that a much wider band-width for all servo systems can be used, and this technique is readily applicable to non-pulsed machines, such as CEBAF.

TARGET CONSIDERATIONS

A LH_2 or LD_2 target 10 to 20 cm in length to be used with 100 μA of 2 GeV electrons appears possible based on extrapolation of existing SLAC and BATES target. Such targets are limited by peak current local heating and the CEBAF target will probably require a vertical flow path for the cryogenic liquid.

POSSIBLE DETECTORS

A focusing toroid spectrometer, shown in Fig. 3, is one candidate detector for the parity violation program. Its advantages include:

- Strong gradient fields ⇒ Short focal length,
- Large $\Delta\Omega$ for a given q^2 range,
- Large ϕ range,
- Highly symmetric detector - which is critical for systematics,
- Sufficient momentum resolution to exclude unwanted processes (i.e. Inelastic),
- Pb glass detectors compatible with either counting or analog current integrating techniques.

Focusing Toroid for e + p ⇒ e + p

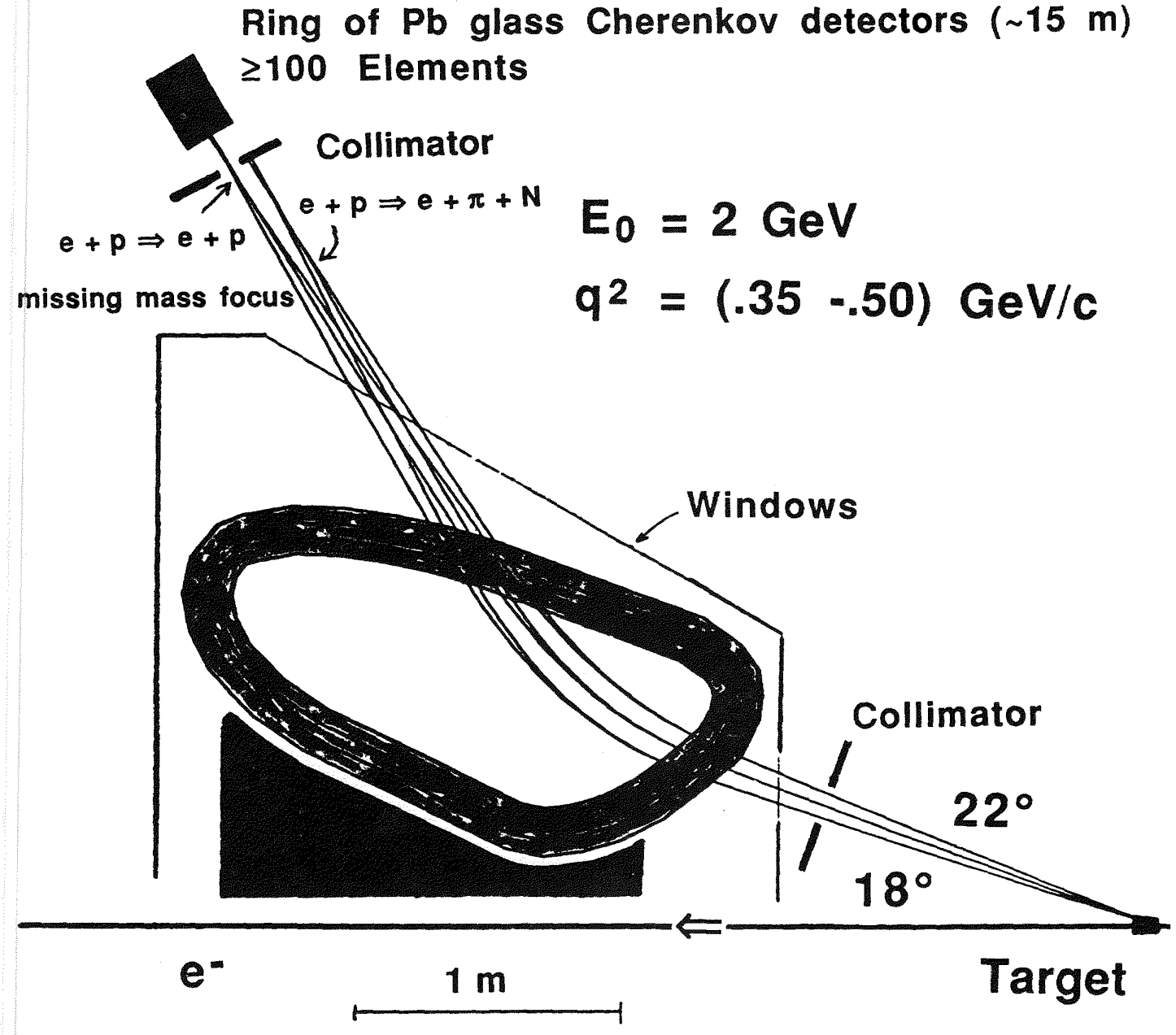

An experiment based upon this detector would have the following characteristics:

Beam Energy: (Limited by practical fields)	2.0 GeV Maximum
Luminosity: (100 μA on a 10 cm LH_2 target)	2.5×10^{38} cm^{-2} sec^{-1}
ϕ - Coverage:	60%
Beam Time: 1,000 hours at ($q^2 = .3$)	$A_p = -.3 \times 10^{-4} \bullet q^2$
Nominal Precision:	$\Delta A_p = \pm 4 \times 10^{-7}$

The beam time required for ancillary systematic measurements is typically Inverse to the figure of merit $= A_p^2 \bullet d\sigma/d\Omega$, and nominally is equal to the measurement time.

Another exciting detector concept would be to employ a true (e,p) elastic coincidence detector. The kinematics of the reaction appear to make such a detector attractive. The elastic scattered electron is at 16 degrees in the lab frame, while the proton is at approximately 80 degrees, and has a non-relativistic kinetic energy nominally of 150 MeV. The micro-structure of the CEBAF beam should prove useful in separating protons from the background produced by the gamma flash. This detector concept is in it's infancy, but could significantly reduce the cost and running time of such measurements.

DATA COLLECTION PHILOSOPHY

Parity violation experiments require high statistics and two techniques have been traditionally employed to measure the asymmetries. Scattered particles can be counted or the analog currents in detectors, which are proportional to the number of particles, can be measured to record the data. There are advantages (+) and disadvantages (-) to each approach. These are summarized below:

Counting Scattered Particles:

- \- Dead time effects have to be carefully handled,
- \+ Easy separation of elastic events.

Analog Current Integrating Techniques:

- \+ No dead time problems,
- \+ Simpler overall electronics,
- \- Depends on magnetic/geometrical selection of elastic events.

At a continuous beam accelerator either or both techniques should be applicable for these experiments.

PARITY VIOLATION SCHEDULE

As a result of the 1987 CEBAF summer workshop a tentative experiment schedule was generated. This is given, below, as a function of calender year.

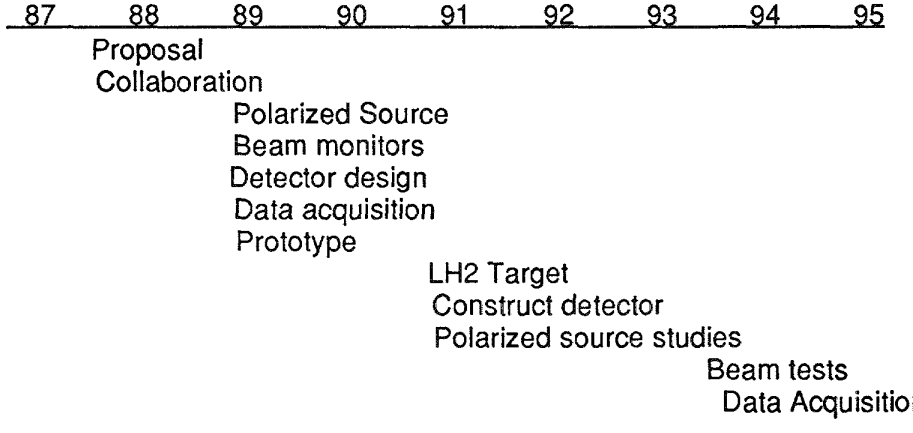

CONCLUSION

A major accomplishment in physics in the last fifteen years has been the success of the electroweak model of Glashow, Weinberg, and Salam in describing the unification of the electromagnetic and weak forces. The CEBAF parity violation program will constitute a major test of the validity of, and extensions to the standard model of electroweak unification.

REFERENCES

1. J. Lykken, Los Alamos National Laboratory, private communications.
2. S. Pollock, Stanford University, private communications.

A Program Collaboration for Hall C

Donal Day
Institute of Nuclear and Particle Physics
University of Virginia

Prior to and during this workshop members of the CEBAF users community have discussed a Program Collaboration for Hall C. The motivation for these discussions has been the fact that some of the highest priority physics have experimental requirements that are not met by devices presently planned for Hall A or Hall B. In addition the laboratory has encouraged the formation of user initiated program collaborations by the set aside of 5M dollars for experimental equipment in Hall C and by the organization of this workshop itself.

This paper is a summary of our discussions.

High Priority Physics

When the future of our field was being studied, the experimental requirements of several classes of experiments were written down so as to determine the necessary machine requirements in terms of the energy, current, and duty factor. The machine being designed and constructed today will have the capability of providing very high average currents into the experimental halls. When the electrons arrive in the end stations the experimental quantities of greatest interest are the rate handling capability of the spectrometers, their particle identification ability, the luminosity, and the solid angle.

It is useful to write down now some of the physics areas we believe are representative of the highest priority physics and their critical experimental needs.

Baryon Resonances

- High Luminosity
- Large $\Delta\Omega$
- Large $\Delta p/p$
- Polarized Targets
- Long targets and large out of plane angles
- Small θ_e and out of plane measurements
- Polarized beams
- Moderate Resolution, $\Delta E/E \sim 10^{-3}$

Two Body Currents

- High Luminosity
- Small θ_e

- Large $\Delta\Omega$
- Neutron TOF
- Long Targets and out of plane measurements
- Moderate Resolution, $\Delta E/E \sim 5.10^{-4}$

N^* in Nuclei

- Multihadron (=2) detection
- Long Targets
- High Luminosity
- Polarized Beams and Targets
- Moderate Resolution

Form Factors of Simple Systems

- Polarized Targets
- High Luminosity when not using polarized targets
- Large $\Delta\Omega$
- neutron detection

Few will argue that the above list constitutes a large part of the physics motivation for this laboratory. The question that we have addressed is whether this physics can be done with the facilities presently planned for Hall A and Hall B. Based on initial studies it appears that additional facilities are required. For example, if one compares my short list of requirements with the expected capabilities of the LAS, we find that it is generally unsuited for experiments that require a high luminosity, and the 4π solid angle is not useful when studying reactions with correlated final states. Improving the luminosity of the LAS might be possible through design changes, as can it's electron identification properties. I believe it would be unwise to force this burden on the LAS. An attempt to make the LAS do what every physics program needs, would produce a device that is not optimized for any.

The spectrometers in Hall A are being designed for high resolution and have small solid angles, a limited $\Delta p/p$, and present intractable problems for a polarized target with a B field perpendicular to the beam. Of course, a frozen spin target could be used but the combination of low power dissipation (meaning small average currents on target) and the small solid angles would preclude any experiment with low count rates.

What is To Be Done?

The laboratory has already given its approval to the LAS and the high resolution spectrometers in Hall A. The reasons for this decision are clear. Those devices will allow a

substantial portion of the most interesting physics to be done; survey experiments and real photon scattering in the LAS and high resolution (e,e'p) work in Hall A. The Program Collaboration we have been talking about must study in detail the capabilities of those devices in regard to the physics we find interesting and motivating. Can acceptable changes in the designs of Hall A and Hall B spectrometers we made that would preclude the advantages of addtional faciltities.? At the present stage this does not appear to be possible. We should proceed with a concerted effort to detail the common needs of the physics we outline and design an excellent facility for Hall C.

Hall C Experimental Facilities

A Program Collaboration is defined by the experimental facilities necessary to complete experiments, though they may have widely different physics goals. The first question we must answer is whether theres exist a common demoninator of experimental requirements among the physics classes listed above. It appears that there is. Based on discussions at this Workshop and work done previously we believe that it would require two spectrometers in Hall C of moderate resolution. One possible configuration would be an electron spectrometer should with a solid angle of 10 msr and a $\Delta p/p$ of 0.5 and a hadron spectrometer subtending 50 msr and accepting a wide range in momenta, $p_{max}/p_{min} > 2$.

A crucial element of the experimental facilities for Hall C would be flexiblity. We must design a system that would allow neutron detection, additional detectors (e.g. silicon strip detectors) to be added, and the ability to go to small electron scattering angles and out of plane at the same time.

Conclusion

The facilities presently designed for Hall A and Hall B are exciting and promise to produce important results. We believe that there is some very high priority physics for which those devices are not well suited. A serious effort must be made to evaluate the need for additional facilities to be built in Hall C.

The worst thing that could happen is that attempts be made to make the Hall A HRS spectrometers and the LAS in Hall B become something they are not. Promises about perfomance are easily made, and much harder to realize. What is worse is that this course could to the loss of Hall C itself.

A UNIFIED THEORY OF PHOTO-PION REACTIONS IN FEW-NUCLEON SYSTEMS

M. Araki
Institut für Kernphysik, Universität Mainz, 6500 Mainz, FRG

ABSTRACT

We present a unified theory of photo-pion reactions in two-nucleon systems ($\gamma d \to pn$, $\pi^0 d$, and πNN) and NN bremsstrahlung ($NN \to NN\gamma$) by taking into account two- and three-body unitarity. The input to this theory is the two-body amplitude resulting from a coupled channel theory for $\pi B \to \pi B$ and $\gamma B \to \pi B$, where B=N or $\Delta(1232)$. This formulation is carried through in the framework of the gauge and chiral invariant Lagrangian, which is obtained from the chiral bag model Lagrangian. In this way, the N and Δ are treated on equal footing as three-quark states.

INTRODUCTION

At low and intermediate energies, pions and isobars play significant roles in nuclear reactions, in particular, photo-pion reactions where exchange currents have an important role. Hence we need to include the interactions of the photon with nucleons, pions and isobars. At the same time, the pion rescattering and the vertex and mass renormalization need to be included in a self-consistent way to maintain unitarity. This can be achieved by applying the classifaction method of J.G. Taylor[1] for deriving equations that satisfy unitarity using the last-cut lemma. This lemma has been used to formulate equations for pion-nuclear reactions in few-nucleon systems: i.e., πB-πB[2] and BB-πBB.[3]

THEORY

We have applied a similar method, for the first time, to photo-pion reactions in single nucleon systems: i.e., $\gamma N \to \pi N$[4] and $\gamma N \to \gamma N$.[5] In these analyses the B-$\bar{B}$ pair contribution is excluded since the vertices are far off-shell and would suppress the contribution. In Ref.5, however, the quark-antiquark pair contribution[6] is incorporated, in a minimal way, into the equations for $\pi N \to \pi N$, $\gamma N \to \pi N$ and $\gamma N \to \gamma N$. The resulting equations for $\pi B \to \pi B$ and $\gamma B \to \gamma B$ can be written in the form of the Lippmann-Schwinger (L-S) equation, in the standard two-channel formalism with obvious notations:

$$t_{\pi\pi} = V_{\pi\pi} + V_{\pi\pi}\, G_0\, t_{\pi\pi}$$

$$t_{\pi\gamma} = V_{\pi\gamma} + t_{\pi\pi}\, G_0\, V_{\pi\gamma}$$

We find that two-body (πB) unitarity requires that the vertices and masses of $V_{\pi\pi}$ and $V_{\pi\gamma}$ in the S-channel be unrenormalized quantities, while those in the other channels are renormalized ones by a further requirement of three-body ($\pi\pi$B) unitarity. This renormalization is carried out consistently with the requirement of unitarity to give correct pole structures to the amplitudes. The second Born terms (i.e., $V_{\pi\pi}\, G_0\, V_{\pi\pi}$ and $V_{\pi\pi}\, G_0\, V_{\pi\gamma}$) generate, in the S-channel, mass and vertex renormalization terms and rescattering terms.

We will now apply the same technique to derive equations for $\gamma d \to pn$, $\pi^0 d$, πNN amd $NN \to NN\gamma$.[7] All of the two-body amplitudes in this theory are derived from the coupled L-S equation as described above. We will show how the equations for $\gamma d \to pn$ and $NN \to NN\gamma$ can be derived in a consistent manner. We denote the amplitudes as follows: for BB$\leftarrow$BB by $T^{(n)}$; BB$\leftarrow\pi$BB, $F^{(n)}$; BB$\leftarrow\gamma$BB, $\tilde{F}^{(n)}$; πBB$\leftarrow$BB, $M^{(n)}$; πBB$\leftarrow\gamma$BB, $\tilde{M}_A^{(n)}$; γBB$\leftarrow\gamma$BB, $\tilde{M}_B^{(n)}$. The number in the parentheses in the superscript, represents the irreducibility of the amplitude, i.e., one less than the minimum number of particles in any given intermediate state for the diagrams which contribute to the amplitude. Using the last-cut lemma we can write the amplitude $\tilde{F}_C^{(1)\dagger}$ as

$$\tilde{F}_C^{(1)\dagger} = \tilde{F}_C^{(2)\dagger} + T^{(1)}\, G^{(1)}\, \tilde{F}^{(2)\dagger}$$

where $T^{(1)}$ and $G^{(1)}$ are the BB scattering amplitude and the BB propagator, respectively, and where the subscript C indicates thatonly the connected diagrams are taken into account. The connected part of $\tilde{F}^{(2)\dagger}$ can be decomposed, using the last-cut lemma, in order to expose the three-body (πBB) unitarity cut. The full three-body (πBB) dynamics are taken care of by the AGS amplitude[8] which is directly related to $M_C^{(2)}$, which is contained in $\tilde{F}_C^{(2)}$. The physical amplitude for $\gamma d \to pn$ can be derived by taking the residue of $\tilde{F}_C^{(1)\dagger}$, in the initial state at the deuteron pole, while the amplitude for $NN \to NN\gamma$ results from the conjugate amplitude, $\tilde{F}_C^{(1)}$. The amplitudes for $\gamma d \to \pi^0 d$ and πNN can be similarly derived from $\tilde{M}_{A,C}^{(1)}$. In this way, we have obtained all photo-pion reaction amplitudes both in single and two-nucleon systems. The final equations can be written in the compact form in terms of the amplitudes for BB-πBB.[3] Readers are referred to Refs.4, 5, and 7 for details.

ACKNOWLEDGEMENT

The author is grateful to Dr.I.R. Afnan for collaboration on this topic and for providing him with the details of the work cited in Refs.2 and 3. He also thanks Professor D. Drechsel for collaboration regarding Ref.5 and for discussions on Ref.6. The Australian Research Grant Scheme and the Deutsche Forschungsgemeinschaft are acknowledged for their financial support.

REFERENCES

1. J.G. Tayler, Nuovo Cimento, Suppl.1, 934 (1963).
2. B. Pearce and I.R. Afnan, Phys.Rev. C34, 991 (1986); I.R. Afnan and B. Pearce, ibid., C35, 737 (1987).
3. I.R. Afnan and B. Blankleider, Phys.Rev. C32, 2006 (1985); References cited therein, in particular, Y. Avishai and T. Mizutani, Phys.Rev. C27, 312 (1983).
4. M. Araki and I.R. Afnan, to be published in Phys.Rev.C (1987).
5. M. Araki and D. Drechsel, manuscript in preparation.
6. S. Scherer, D. Drechsel and L. Tiator, to be published in Phys.Lett.B.
7. M. Araki and I.R. Afnan, manuscript in preparation.
8. E.O. Alt, P. Grassberger and W. Sandhas, Nucl.Phys.B2, 167 (1967).

ΛN INTERACTION IN $\gamma+d \rightarrow K^+ + \Lambda^\circ + n$

R.A. Adelseck and L.E. Wright
Department of Physics and Astronomy, Ohio University
Athens, Ohio 45701

INTRODUCTION

The knowledge of the hyperon-nucleon interaction is an essential supplement to the nucleon-nucleon force, since the additional degree of freedom introduced by strangeness will help with our understanding of the strong interaction by probing parts of the interaction not accessible to conventional NN calculations and experiments. The presence of a strange quark heavier than the u/d quarks also allows the study of quark effects in the nuclear force.

The experimental sources for the lambda-nucleon interaction are basically: i) study of hypernuclei, ii) lambda-proton scattering, and iii) final state interactions. In this paper we focus our attention on the third possibility. In order to extract detailed information from final state interactions, we need a well understood initial state, intermediate interaction (production process) and final state (except for the interaction of interest itself). Such a situation can be found in the photoproduction process of kaons from the deuteron whose wavefunction is described by realistic potentials such as the Reid[1] or Paris[2] potential. The production channel of the lambda proceeds via the $p(\gamma,K^+)\Lambda^\circ$ reaction, which has been formulated covariantly by diagrams representing the exchange of p, Λ°, Σ° and their resonances in the s and u channels and of the K and K^* mesons in the t channel. The coupling constants are determined phenomenologically by an analysis of the existing data in the energy range of interest. In the final state there are three very different particles interacting with each other making it possible to distinguish their respective interactions. The $K\Lambda$ interaction is completely taken care of through the elementary production operator which leaves only the KN and ΛN interactions and since the K^+-nucleon interaction is very weak, we neglect kaon distortions to lowest order.

We find measurable final state interaction effects in the inclusive (γ,K^+) reaction as well as in the coincidence cross section $(\gamma,K^+\,\Lambda^\circ)$.

METHOD

For the production process we take the proton to be on its mass shall ($E^2 = M^2+p^2$) and for the neutron we use the spectator nucleon model,[5] which requires low neutron

momenta. However, this is guaranteed because large cross sections occur only for low momentum components in the deuteron wavefunction, which we calculate from the Paris potential as described in reference 2. The cross section in the rest frame of the deuteron (lab system) can be written in the form

$$d\sigma = \left(1 + \frac{|\vec{p}_n|}{E_n} \cos\theta_n\right) |\psi(\vec{p}_n)|^2 \, d^3 p_n \, d\sigma_{el} \qquad (1)$$

$$d\sigma_{el} = (2\pi)^4 \frac{M_p M_\Lambda}{4 E_\Lambda E_K p_\gamma \cdot p_p} \bar{u}(\vec{p}_\Lambda) \, T_{\gamma K} \, u(p_p) \, \delta^{(4)}(p_p + p_\gamma - p_K - p_\Lambda) \frac{d^3 p_K d^2 p_\Lambda}{(2\pi)^6}$$

where $p_i = (E_i, \vec{p}_i)$ is the four momentum of particle i, $\psi(\vec{p}_n)$ is the deuteron wavefunction in momentum space ($\vec{p}_n = -\vec{p}_p$) and $T_{\gamma K} = \sum_{i=1}^{4} A_i M_i$ is the elementary production operator given in many references.[3,4] Since we are mainly probing the low momentum components of the wavefunction, we are only sensitive to the peak of the s-wave part and thus our results are not very sensitive to the potential used for the deuteron.

For the ΛN interaction potential we consider a Yukawa form with a cut-off at short distances[6] and the type 3 potential of Verma and Sural[7] which is a superposition of an attractive and repulsive Gaussian shape potential (Figure 1).

$$V_1 = \begin{cases} 0 & \text{for } r < d \\ -V_A \exp(-\nu r)/\nu r & \text{for } r > d \end{cases} \qquad (2a)$$

where ν is the two-pion range 1.3992 fm^{-1}, and

$$V_2 = -V_A \exp(-r^2/\lambda_A^2) + V_R \exp(-r^2/\lambda_R^2) \qquad (2b)$$

Both potentials are fitted to reproduce the experimental values for the singlet and triplet scattering length and effective range parameters. Furthermore, V_2 reproduces the binding energy of the hypertriton. The low energy parameters used in both papers differ slightly because of the poor experimental data but are comparable. The singlet and triplet parameters used are given in Table 1. Using a given interaction potential we calculate the distorted wavefunction of the relative Λ-n motion by numerically solving the Schroedinger equation.

DISCUSSION

Although a previous report[8] on the hyperon-nucleon interaction in the deuteron photodisintegration only considered the s-wave interaction, we find it necessary to

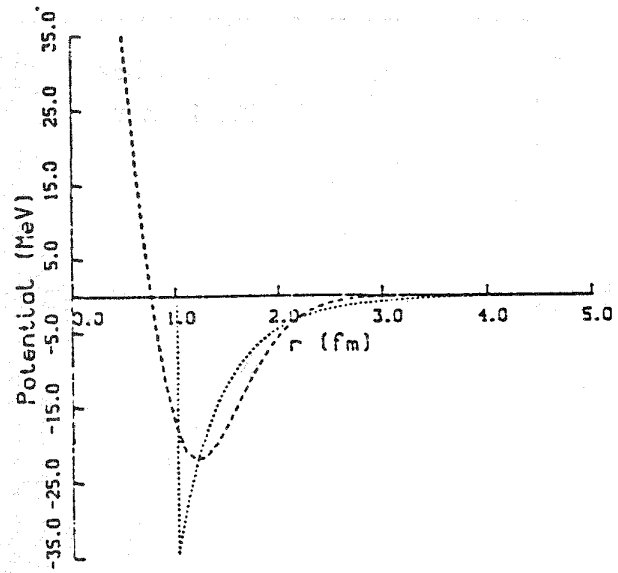

Fig.1 Comparison of the singlet potentials for V_1 (dotted curve) and V_2 (dashed curve)

Table 1

Potential parameters used in the current calculations, see eq. 2a,b

		d (fm)	V_a (MeV)	λ_a (fm)	V_r (MeV)	λ_r (fm)
V_1	singlet	1.017	204.1			
	triplet	1.180	223.3			
V_2	singlet		167.34	1.10	246.80	0.82
	triplet		132.41	1.10	181.68	0.82

include the lowest four partial waves. The s-wave interaction does provide much of the strength but it only accounts for about 80% of the total effect. It is not clear if reference 9 includes higher partial waves.

Figure 2 shows an angular distribution of the Λ° in a (γ, KΛ) coincidence experiment. The photon and kaon have been taken to be parallel to obtain maximum cross sections. The final state interaction is responsible for an enhancement of the cross section by about a factor of 10 near the threshold for the given kinematical variables. In the forward direction one finds an increase of about 20%. This same trend can also be seen in Figure 3 which shows the inclusive (γ, K^+) cross section. Again the kaon has been taken to be in the forward direction. In general the ΛN interaction considerably enhances the cross section near threshold while suppressing it at higher energies. Both potentials produce about the same cross section which is not surprising since they have been chosen to give the same low energy parameters and hence the same s-wave contribution. However, the d(γ, K^+)Λ°n process does have some contribution from higher partial waves and hence may be capable of distinguishing different ΛN potentials.

This work was supported in part by DOE Contract No. DE-AC02-79ER10397-08.

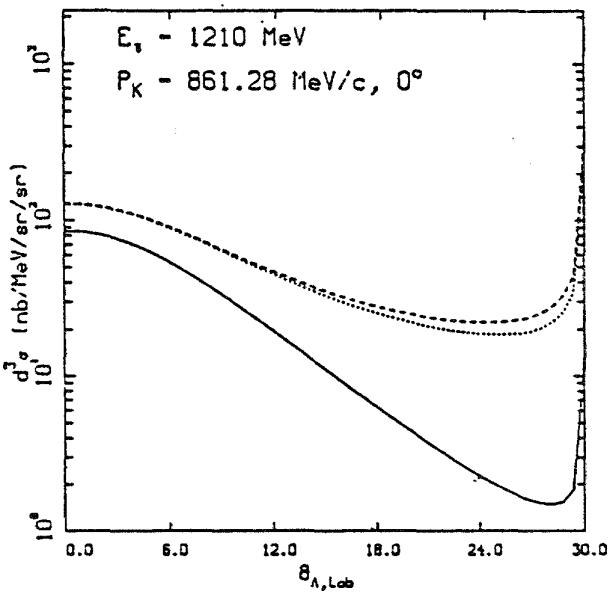

Fig.2 Angular distribution of the exclusive cross section (γ,KΛ). The solid curve is a calculation without any final state interaction, the dotted (dashed) curve has been calculated using V_1 (V_2).
($d^3\sigma = d^3\sigma/dp_K/d\Omega_K/d\Omega_\Lambda$)

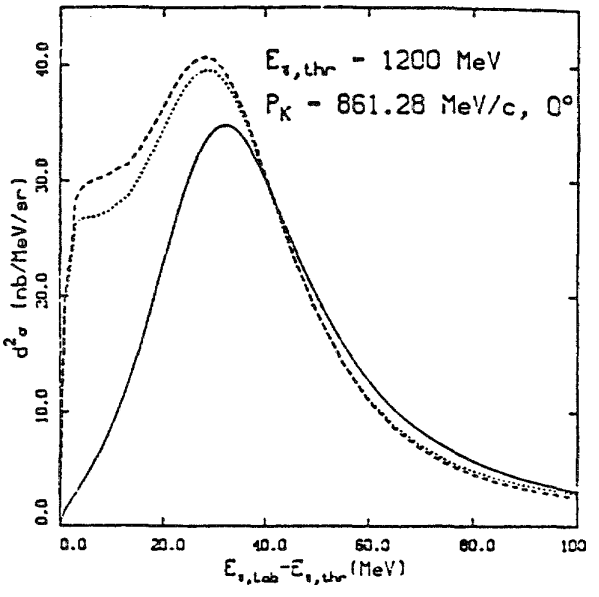

Fig.3 Comparison of the energy dependence of the two potentials. The same coding as in Fig.2 has been used.
($d^2\sigma = d^2\sigma/dp_K/d\Omega_K$)

REFERENCES

1) R.D. Reid, Ann. of Phys. 50 (1968) 411.
2) M. Lacombe et al., Phys. Rev. C21 (1980) 861.
3) R.A. Adelseck, C. Bennhold, L.E. Wright, Phys. Rev. C32 (1985) 1681.
4) H. Thom, Phys. Rev. 151 (1966) 1322.
5) J.M. Laget, Phys. Rep. 69 (1981) 31.
6) R.K. Bhaduri, Y. Nogami, W. van Dijk, Phys. Rev. 155 (1967) 1671.
7) S.P. Verma, D.P. Sural, Phys. Rev. C22 (1980) 229.
8) F.M. Renard, Y. Renard, Phys. Lett. 24B (1967) 159; Nucl. Phys. B1 (1967) 389.
9) Stephen R. Cotanch, Shian S. Hsiao, Nucl. Phys. A450 (1986) 419.

THE EXPERIMENT OF APPLYING PLASMA CHEMICAL REACTION AND NON-PLASMA CHEMICAL REACTION IN THE HIGH FREQUENCY ION SOURCE

BAI GUI BIN

Institute of low energy nuclear physics Beijing Normal University

Abstract

The experiment result of appling halogen plasma chemical reaction and non-plasma chemical reaction are different in the R.F.ion source[(I)(2)] the etching rate of the plasma for metal is higher than that of non-plasma.When the plasma chemical reaction is applied,the metal ion content proportion is larger in ion beam and the effect is very well, by reason mainly that there are much more high energy particles and activated particles presented in plasma.

I. The experimental structure and the working principle.

For comparing the difference of the plasma chemical reaction and non-plasma chemical reaction,condition of comparing them must be created,the structure used in this experiment is shown in Fig.I. Fig.I-I,I-2,I-3,I-4,I-5 are five tungsten sticks, they are cuted from a tungsten pole with same diameter,they are all put into a discharge chamber.I-I is exposed in the plasma,and is at a negative potential.I-2 and I-I are a pole,at a negative potential too, but it is shielded by a quartz glass tube with an internal diameter φ4mm. I-3 is shielded by a quartz glass tube with an internal diameter φ4mm, and freely set in the plasma region,it is not directly exposed in the plasma. I-4 is directly exposed in the plasma. I-5 is at a positive potential,it is not shielded too.

After the halogen family element (or the halide)enter the discharge chamber,it is ionized by a high frequency electromagnetic field,and the plasma is formed.chemical reaction is caused in it with five metals pole at the same time.The reaction is go on at certain entering gas quantity and under a same discharge power condition with the same time of beginning and ending.

2.The experimental results

2.I The comparision of the results of chemical reaction for the five metal poles with the halogen.

The changing rate of the diameter of the metal poles is measured in experiment for many time and the variation of them is different.The changing rate of diameter is the reduction quantity of the metal pole in diameter after the chemical reaction of the metal pole with the halogen during a definite time.The rate of I-3 is the least,it is used as a criterion for the datum,with which the rate of others is compared.Because I-2and I-3 are in a roughly similar condition, their change are indentical. I-4 is four to six time as large as I-3. I-5 is six to ten time as large as I-3. I-I is 3 more orders of magnitude than I-3.

2.2 The case of extracting matal ion by the use of the structure I-3 and I-4 respectively.

(I) The experimental results of using structure I-3 is showed in Fig.2 and Fig.3.

(2)The experimental results of applying structure I-4 is shown in Fig.4 , Fig.5 and Fig.6.

One can see from experimental results in both sase that when the plasma chemical reaction is applied,usefull metal ion content proportion is higher in the ion beam than that of non-plasma range chemical reaction.When form I-3 is used, Pd^+ smaller than IO % in total ion beam, Ag^+ makes up only 6 % and Ta^+ can not see in ion mass spectrum. Whereas when form I-4 is used, Ag^+ makes up 40 %, Ta^+ makes up 57 % and W^+ makes up 30 %.

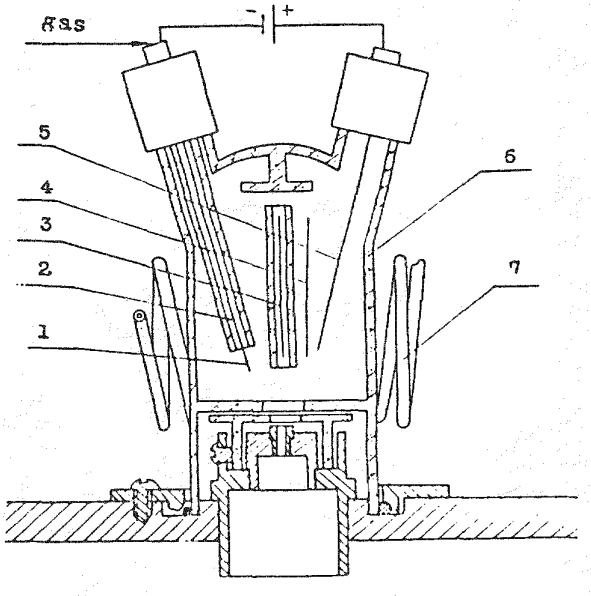

Fig.I The structure for processing plasma chemical reaction and non-plasma chemical reaction in the R.F.ion source.

(I)(2)(3)(4)(5)are tungsten poles; (6)the discharge chamber made of quartz glass; (7)the coil of the R.F. oscillater.

3. Discussion

The experimental results has showed that the etching rate of the metal exposed in plasma is higher than in quartz tube, therefor wanted the metal ion content proportion higher in ion beam.The reason is that ionizetion rate is higher in plasma than in quartz glass tube (or non-plasma range) and there are many favourable factors present, specially more high

energy particles and activeted particles.

3.I The higher energy of the electrons in plasma.

The electrons which constitute about one half of the amout of charged particles possess higher energy by I to 2 orders of magnitude[3][4] than the molecules, the atoms and the particles in glass tube in the same plasma. The electrons in plasma are the most active ones in all particles. The energy increase in the discharge chamber is essentially transfered by electrons which make the molecules resolved, the atoms and the molecules etc. activated and ionized.

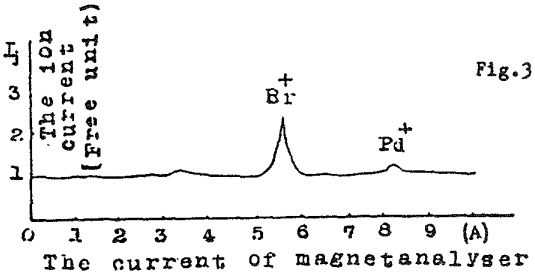

Fig. 2 The ion mass spectrum of $Pd + BB_{r3}$ by using structure I-3.

3.2 More activated particles.

(I)The gas molecules of the halogen family elements are resolved easily into atoms in the process of their collisiion with particles (or bombarded by particles) in plasma and will absorb energy.

For example, $B_{r2} \xrightarrow{I.97ev} B_r + B_r$,

$Cl_2 \xrightarrow{2.48ev} Cl + Cl$.

For two Bromine atoms the energy increases I.97ev which is more than that for one molecule (B_{r2}). For two chlorine atoms the energy increases 2.48ev which is more than that for one molecule (Cl_2). The chemical activety of atoms is more intensive than that of molecules and is liable to cause chemical reaction.

(2)The ionization rate in plasma range is much higher than in the tube shielded (non-plasma range). The atoms of the halogen are ionized into ions and electrons in the plasma. In this process, part of energy is increased again.

For example, $B_r \xrightarrow{II.8ev} B_r^+ + e$,

$Cl \xrightarrow{I3ev} Cl^+ + e$.

When a Bromine atom is ionized into an ion (B_r^+) and an electron (e) (a pair of ion and electron) the energy is increased by II.8 ev, while two atoms (be a molecule) are ionized into two ions and two electrons, the energy are increased by 23.6ev +I.97ev=25.57ev.

For the same reason, when a molecule (Cl_2) is ionized into two ions and two electrons (two pair of ion and electron), the energy are increased by 28.48ev.

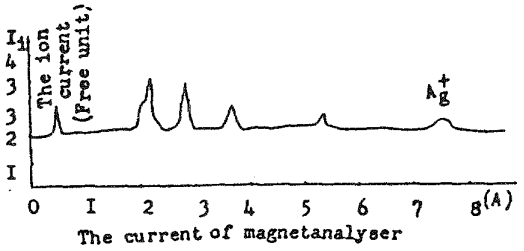

Fig.3 The ion mass spectrum of $Ag + BF_3$ by using structure I-3.

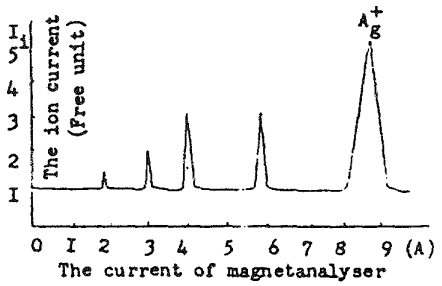

Fig.4 The ion mass spectrum of $Ag + BF_3$ by using structure I-4.

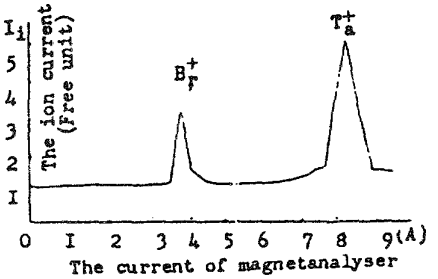

Fig.5 The ion mass spectrum of $Ta + BB_r$ by using structure I-4.

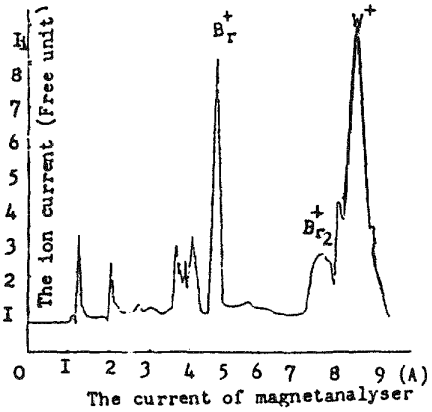

Fig.6 The ion mass spectrum of $W + BB_{r3}$ by using structure I-4.

The fact that ions join chemical reaction is a important charecteristic of the plasma chemical reaction. The ability of the ion acquiring electron are stronger than that of molecule and atom, so it is more easily to take place for the chemical reaction with the metal.

(3) There are much atoms (or molecules) in excited state in the plasma than in the non-plasma in discharge chamber.The excited atoms (or molecules) also possess more energy than the non excited ones. It can be calculated from formula $\mathcal{E}=h\frac{c}{\lambda}=h\nu$.

such as, T_a^*(excited state) 2.6ev energy more than T_a , Pd^*(excited state)$_{3.44}$ev energy more than Pd.

One can know that great quantity of the excited state particles are present by the plasma light. For the excited particles the chemical reaction is easily to take place than the non excited ones.

3.3 The duo-pole diffusion effect[5] is an inherent physical characteristic at the boundary between the plasma and the suspension metel. Owing to this nature, (I)An amount of the halogen contact with the metal is increased; (2)particles flowing to the surface of the metal from the plasma have definite energy which causes the physical and chemical sputtering at the surface of the metal.This is a factor of the fact that the plasma range chemicai reaction is faster than in the non-plasma range.

The duo-pole diffusion effect had bring into profitable play in the prossess of extracting metal ions from R.F. ion source when the plasma chemical reaction is applied.

Above mentioned factors and other beneficial factors existed in the plasma make the diameter changing rate of I-4 be 4 to 6 time as large as I-3, and make structure I-4 the extracted metal ion percentage in ion beam higher than form I-3.

3.4 To utilize advantageous condition in plasma more full, several theusand voltage difference is added between the I-5 (positive electrode) and the I-I (negative electrode) by outer power supply at the discharge chamber. (I) many positive ions of the halogen are forced to shoot towards I-I, make many electrons and negative ions flow to I-5, the contact number of the halogen element particles with the metal much more increased. (2) When the high energy particles bombard metals, the chemical reaction occures rapidly and the physical and chemical sputtering are more obvious. Therefore, the diameter changing rate of I-I is 3 more orders of magnitude than I-3, i.e. the diameter changing rate of I-I is 3 more orders of magnitude than I-2, but I-I and I-2 is at the same tungsten pole, only the I-2 is shielded by quartz glass tube. This explains that the conductance is no good in quartz glass tube, in other words, the ionizing rate is low. Although I-Iand I-2 is at the same pole and at the same negative potential, the result have authentically 3 order difference of magnitudes.

The techniques of the plasma chemical reaction and the sputtering adopted in R.F. ion source are very effective for extracting the high melting point metal ions. The ions have been extracted are : R_e^+,W^+,Mo^+,Ta^+,Au^+, Pt^+, Ag^+, Y^+, Pd^+, Cr^+, Ti^+ V^+, Fe^+ Cu^+ Al^+ Si^+ Be^+ Bi^+ In^+ Ga^+ Nd^+ Ce^+, Li^+ and so on.

This two techniques had been applying in 400kev ion implanter at beijing Normal University.

4. Concluding remarks

The application of the plasma chemical reaction and the sputtering in R.F. ion source has its own merit, since for the R.F. ion source the quartz glass discharge chamber is used,while the chemical property of the quartz glass is more stable than that of metals and the metals that is no need to produce ion can be shielded, then the useful metal ion content is higher in the drawn ion beam. This method is simplicity and convenience. The noble metal can be economically used. This technoiogy can be used at equipments with R.F. ion source simply some improvements are being made. The technology can be used to conduct mass spectrum analysis for certain plasma polymer.

Reference

(I) Ma Mingxiu,IaoWei,BaiGuibin,ZhangTonghe, "An improved R.F. heavy ion source," Radiation effects, Vol$_{44}$ (I979)

(2) BaiGuibin,WangWeguo,MaMingxiu,ZhouFengsheng and HaoZhonghe, " The chemical synthesis and sputtering of working material in R.F. heavy ion source, " Journal of nature science of Beijing Normal University, No$_4$ (I982)$_{29}$

(3) J.R.Hollahan and A.T.Bell, "Techniques and application of plasma chemistry " New York (I974)$_{I-2}$

(4) HongMingfan,HUJianfang and Han Shuling, " The action of low temperature plasma to the material surface " Physics communication, No$_2$ (I984)$_{I2}$

(5) B.Grass,B.Gryca and K.Micklossy, "Plasma technology "(I968) Chinese edition.

QCD at Low and High Momentum Scales

L.S. Celenza, Chueng-Ryong Ji, and C.M. Shakin
Department of Physics and Center for Nuclear Theory
Brooklyn College of CUNY
Brooklyn, N.Y. 11210

An attempt is made to understand the interrelation between modern relativistic models of nuclear structure and QCD in the low-momentum domain, where quark and gluon condensates play an important role. We make use of the auxiliary (bilocal) field technique and also perform a Fierz rearrangement of the interaction, after integrating out the (gluon) gauge field. In the limit that the gluon (dynamical) mass which is generated by gluon condensate is large, we obtain the Lagrangian of the Nambu-Jona-Lasinio model, which is known to give a good account of the dynamics of chiral-symmetry breaking. The replacement of QCD by an effective theory involving various auxiliary fields ($\sigma, \pi, \rho, \omega \cdots$) is meaningful in the low-momentum scale where the dynamical masses, $M_i(Q^2)$, and the running coupling constant $\alpha_s(Q^2)$ can be approximated by constants. As the momentum scale Q^2 becomes larger, $M_i(Q^2)$ and $\alpha_s(Q^2)$ become smaller. Perturbative QCD may be valid in the regime where the higher-order contributions in $M_i^2(Q^2)/Q^2$ and $\alpha_s(Q^2)$ can be neglected. However, the recent perturbative QCD phenomenology for the proton Dirac form factor indicates that the nonperturbative effects from quark and gluon condensates and their consistent treatment are crucial to give agreement with the experimental data for the normalization and the Q^2 dependence of the form factor in the region 10 $(\mathrm{GeV/c})^2 < Q^2 <$ 30 $(\mathrm{GeV/c})^2$.

Because of the non-Abelian nature of QCD, i.e., the presence of cubic and quartic gluon interactions, the direct application of functional methods in QCD is limited. However a recent analysis of strongly coupled QED is suggestive:[1] The study of an approximate Schwinger-Dyson equation indicates that one may have a confining phase above a critical coupling constant ($\alpha > \alpha_c = \pi/3$). There is also a large body of work that deals with chiral symmetry breaking in QCD using an approximate Abelian theory.[2] Motivated by that work, we wish to introduce an effective theory appropriate at length scales where dynamical gluon mass generation is important:

$$S_{QCD}^{eff} = \int d^4x \int d^4y \left[\tfrac{1}{2} A_a^\mu(x) \, D_{\mu\nu}^{ab}(x-y)^{-1} \, A_b^\nu(y) \right] + \int d^4x \left[\bar{q}(x) \, i\not{\partial} \, q(x) + J_a^\mu(x) \, A_\mu^a(x) \right] , \tag{1}$$

where

$$D_{\mu\nu}^{ab}(x-y)^{-1} = \left[\left\{ g_{\mu\nu} \partial^2 - \left(1 - \tfrac{1}{\xi}\right) \partial_\mu \partial_\nu \right\} \delta^4(x-y) + \Pi_{\mu\nu}(x-y) \right] \delta_{ab} \tag{2}$$

(Here ξ is a gauge parameter and $\Pi(x-y)$ is the gluon self-energy arising from the coupling of the gluon to the gluon condensate.) Further,

$$J_a^\mu(x) = g\,\bar{q}(x)\gamma^\mu\frac{\lambda_a}{2}q(x). \tag{3}$$

After integrating out the gluon field, and making a specific gauge choice, Eq. (1) becomes

$$S_{QCD}^{eff} = -\tfrac{1}{2}\int d^4x\int d^4y\; J_a^\mu(x)\,D_{\mu\nu}^{ab}(x-y)\,J_b^\nu(y) + \int d^4x\;\bar{q}(x)\,i\not{\partial}\,q(x). \tag{4}$$

We substitute Eq. (3) into Eq. (4) and make a Fierz rearrangement of the interaction. For simplicity, we work in the Landau gauge and concentrate on the scalar-isoscalar term in the effective action. We have, after the Fierz rearrangement,

$$S_{eff} = \int d^4x\int d^4y\left\{\bar{q}(x)\,i\not{\partial}\,q(y)\,\delta^4(x-y) - \frac{g^2}{2}a\,\bar{q}(x)q(y)\,D(x-y)\,\bar{q}(y)q(x)\right\}, \tag{5}$$

where $a = 1/6$ and

$$D(x-y) = \int\frac{d^4q}{(2\pi)^4}\,\frac{e^{iq\cdot(x-y)}}{q^2\left[1-\pi(q^2)\right]} \qquad \left(\pi(q^2)\to m_g^2/q^2 \text{ as } q^2\to 0\right) \tag{6}$$

We now introduce the bilocal field $\sigma(x,y)$. Without changing the dynamics we can include a constant of the form

$$\int[d\sigma]\exp\left[i\int d^4x\int d^4y\left\{\tfrac{1}{2}\left[\sigma(x,y) - g\sqrt{a}\,D(x-y)\,\bar{q}(x)q(y)\right]\times D^{-1}(x-y)\left[\sigma(x,y) - g\sqrt{a}\,D(x-y)\,\bar{q}(y)q(x)\right]\right\}\right] \tag{7}$$

in the vacuum-to-vacuum amplitude, $\exp[iW]$. At this point, we have for the vacuum-to-vacuum amplitude,

$$e^{iW} = N\int[d\sigma][dq][d\bar{q}]\exp\left\{i\int d^4x\int d^4y \times\left[\tfrac{1}{2}\sigma(x,y)D^{-1}(x-y)\sigma(x,y) + \bar{q}(x)\left[\delta^4(x-y)\,i\not{\partial} - g_\sigma\,\sigma(x,y)\right]q(y)\right]\right\}, \tag{8}$$

where $g_\sigma = g\sqrt{a}$. Inclusion of a pion-like auxiliary field would yield the more general result,

$$e^{iW} = N\int[d\sigma][d\vec{\pi}][dq][d\bar{q}]\exp\left[i\int d^4x\int d^4y \times\left\{\tfrac{1}{2}\sigma(x,y)D^{-1}(x-y)\sigma(x,y) + \tfrac{1}{2}\vec{\pi}(x,y)D^{-1}(x-y)\vec{\pi}(x,y) + \bar{q}(x)\left[\delta^4(x-y)\,i\not{\partial} - g_\sigma\left\{\sigma(x,y) + i\vec{\pi}\cdot\vec{\tau}\gamma_5\right\}\right]q(y)\right\}\right] \tag{9}$$

Equation (9) exhibits a manifest chiral symmetry. It is also worth commenting upon the limiting case, where we take the mass of the exchanged gluon to be quite large. Let us write

$$D(x-y) \simeq -\delta^4(x-y)/m_g^2. \tag{10}$$

Then Eq. (5) becomes

$$S_{eff} = \int d^4x\left\{\bar{q}(x)\,i\not{\partial}\,q(x) + \frac{ag^2}{2m_g^2}\left[\left(\bar{q}(x)q(x)\right)^2 + \left(\bar{q}(x)\,i\gamma_5\vec{\tau}\,q(x)\right)^2\right]\right\}, \tag{11}$$

if we also include the pion-like order parameter, as in Eq. (9). Note that in the large-mass limit we obtain the Lagrangian of the Nambu-Jona-Lasinio model. If we include fields with the quantum numbers of the pion and the rho meson, as well as the scalar and vector fields, $(\sigma, \pi, \rho, \omega \cdots)$, we can create a phenomenological model which is highly successful indescribing nuclear properties. However, from the series of assumptions we have made, it is clear that the effective theory is only meaningful in the low-momentum region where the dynamical masses $M_i(Q^2)$ and the running coupling constant $\alpha_s(Q^2)$ are "frozen" at large constant values.

As the momentum scale Q^2 becomes larger, $M_i(Q^2)$ and $\alpha_s(Q^2)$ become smaller. Thus perturbative QCD may be valid in the regime where the higher order contributions in $\frac{M_i^2(Q^2)}{Q^2}$ and $\alpha_s(Q^2)$ can be neglected. For example, in the large Q^2 limit, an expression for a form factor may be factored and may be written (generically) as[4]

$$F(Q^2) = \int [dx][dy]\, \phi(y, Q_y^2)\, T_H(x, y, Q^2)\, \phi(x, Q_x^2). \quad (12)$$

Here the nonperturbative effects are summarized in the quark distribution amplitude $\phi(x,Q^2)$. The hard-scattering amplitude can be obtained by a perturbative calculation. However, it has been pointed out in the various analyses of the proton form factor that the nonperturbative effects are significant,[5] and $\phi(x,Q^2)$ should include the information concerning quark and gluon condensates (via QCD sum rules). Furthermore, the recent phenomenology also indicates that one should include various nonperturbative effects.[6] For example, one can use a "frozen" coupling constant even in the calculation of T_H to give agreement (both in the normalization and the Q^2 dependence) for the form factor with the experimental data $[10\ (\mathrm{GeV/c})^2 < Q^2 < 30(\mathrm{GeV/c})^2]$.

In conclusion, our work represents an attempt to relate nuclear physics to QCD in the low-momentum domain. At higher momenta one may undertake perturbative QCD calculations. However, it is essential to include nonperturbative effects in a consistent formalism.

References

1. T. Morozumi and H.So, Regoto University preprint RIFP-689 (1987).
2. R. Casalbunoni, S. DeCurtis, D. Dominici and R. Gatto, Phys. Lett. 150B, 295 (1985) and references therein. For a review, see H. Peshkin in Recent Advances in Field Theory and Statistical Mechanics, eds. J.B. Zuker and R. Stora (North Holland, Amsterdam, 1984).
3. Y. Nambu and G. Jona-Lasino, Phys. Rev. 122, 345 (1961).
4. S.J. Brodsky and G.P. Lepage, Phys. Scripta 23, 945 (1981); G.P. Lepage and S.J. Brodsky, Phys. Rev. D22, 2157 (1980); Phys. Rev. Lett. 43, 545 (1979); Erratum-ibid, 43, 1625 (1979); A. Duncan and A.H. Mueller, Phys. Lett. 90B, 159 (1988); Phys. Rev. D21, 1636 (1980); V.L. Chernyak, A.R. Zhitnitsky and V.G. Serbo, JETP Lett. 26, 514 (1977).
5. N. Isgur and C. Llewellyn-Smith, Phys. Rev. Lett. 52, 1080 (1984); V.L. Chernyak and I.R. Zhitnitsky, Nucl. Phys. B246, 52 (1984); Phys. Rep. 112, 173 (1984); M. Gari and N.G. Stefanis, Phys. Rev. D35, 1074 (1987); I.D. King and C.T. Sachrajda, Nucl. Phys. B279, 785 (1987).
6. C.-R. Ji, A.F. Sill and R.M. Lombard-Nelsen, SLAC-PUB-4068; to be published in Phys. Rev. D.

Hypernuclear Magnetic Moment Measurements at CEBAF: A Signature of Relativistic Nuclear Dynamics?*

JOSEPH COHEN AND R. J. FURNSTAHL

Physics Department and Nuclear Theory Center
Indiana University, Bloomington, Indiana 47405

Measurements of hypernuclear magnetic moments in systems with one Λ hyperon added to a closed-shell core of nucleons might distinguish between predictions of conventional nonrelativistic models and relativistic (σ–ω) mean-field models. These experiments are particularly suitable for the CEBAF hypernuclear program.

There has recently been an increasing interest in relativistic effects arising in models of the nucleus based on the Dirac equation with strong scalar and vector potentials. Of particular interest are observables for which relativistic predictions differ significantly from predictions in the traditional framework of nonrelativistic nucleons. However, unambiguous experimental signatures of relativistic dynamics have been difficult to find. We suggest that hypernuclei (and hypernuclear magnetic moments in particular) may provide a clear signature and that CEBAF is the natural place to carry out the relevant experimental measurements.

Relativistic models characteristically predict a reduced effective mass for the nucleon M_N^* which leads to enhanced single-particle convection currents. The long-standing problem of enhanced isoscalar magnetic moments in nuclei with one particle outside a closed-shell core [1] is a direct consequence of these currents. This problem has been resolved recently [2] in the context of the σ–ω (Walecka) model with the realization that the enhancement of the valence single-particle current does not imply an enhanced current for the nucleus; the response of the core to the valence nucleon generates a contribution to the baryon current that counterbalances the (M_N/M_N^*) enhancement of the single-particle current. The end result is a return to the simple nonrelativistic Schmidt moment predictions for the isoscalar nuclear magnetic moments.[2]

Although relativistic and nonrelativistic models yield similar results, there is a significant difference between these approaches. In the relativistic picture, the isoscalar Schmidt values are obtained after a strong cancellation between the valence convection current and the contribution from the modified core, while they arise directly from the valence current in the nonrelativistic shell model (isoscalar "core polarization" corrections are small in conventional nonrelativistic models). This distinction leads to different predictions for hypernuclear magnetic moments.

We consider the addition of a Λ hyperon to a closed-shell nucleus, and apply an extended σ–ω (Walecka) model in the mean-field approximation. † In this model,

* Contribution to the CEBAF 1987 Summer Workshop. Supported in part by the National Science Foundation and the Department of Energy.

† This model has also been suggested by J. V. Noble, Phys. Lett. **B89**, 325 (1980), and A. Bouyssy, Phys. Lett. **B99**, 305 (1981).

the Λ hyperons couple to the same scalar and vector fields as the nucleons, but with different coupling strengths. In this case, unlike regular nuclei, the relativistic core response does not cancel the enhancement of the single-particle current due to the Λ. Furthermore, only the core response contributes to the hypernuclear magnetic moment.

Since the Λ is neutral, the Λ single-particle contribution to the magnetic moment of the hypernucleus is due to its anomalous moment only. In the extreme single-particle shell model, this is the only contribution (for a Λ hyperon added to a closed-shell nucleus), and it gives rise to the "Schmidt value" $[-(j/j+1)\mu_\Lambda$ for the Λ in a state with $j = l - 1/2$ and μ_Λ for $j = l + 1/2]$. However, the modification of the nuclear core will produce *deviations from the Schmidt values*, which may be an experimentally measurable[3] effect. It could be an extremely interesting part of the hypernuclear program at CEBAF, where hypernuclear production by means of the $(e, e'K^+)$ reaction is advocated.[4]

The relativistic hypernuclear formalism is a direct extension of the nuclear formalism. We start with a mean-field lagrangian density for nucleons[2] and a Λ hyperon[5] in the presence of a scalar field ϕ_0 and a vector field $V^\mu = (V_0, \vec{V})$ [maintaining the three-vector component of V^μ is crucial in our discussion]:

$$\begin{aligned}\mathcal{L}_{MFT} = \overline{\psi}_N \left[\gamma_\mu (i\partial^\mu - g_v^N V^\mu) - (M_N - g_s^N \phi_0)\right] \psi_N \\ + \overline{\psi}_\Lambda \left[\gamma_\mu (i\partial^\mu - g_v^\Lambda V^\mu) - (M_\Lambda - g_s^\Lambda \phi_0)\right] \psi_\Lambda \\ + \text{purely mesonic terms},\end{aligned} \tag{1}$$

where the meson-baryon coupling constants for nucleons and hyperons may differ. To calculate the magnetic moments of the Λ hypernuclei,[5] we follow the same steps as in the corresponding nuclear (nucleons only) calculation.[2] In the absence of a self-consistent mean-field solution for the entire system (core + Λ), we use the core self-consistent solution as a starting point.

Using single-particle wave functions generated in the fields of the core to calculate the baryon current, we find an enhanced current due to the valence hyperon (because $M_\Lambda \to M_\Lambda^* = M_\Lambda - g_s^\Lambda \phi_0$). However, self-consistency requires that the effects of the valence particle on the core wave functions be taken into account. The core response contribution to the current[5] (which is as large as the valence particle contribution because all core nucleons are involved) is evaluated by summing the polarization insertions (RPA rings) computed with the nucleon propagator. We evaluate this linear response for an analogous system in nuclear matter (one Λ hyperon added to a filled Fermi sphere of nucleons in a large volume Ω) and apply the result to finite hypernuclei in a local density approximation.‡ In

‡ We have also evaluated the response directly for finite hypernuclei and find similar results to those presented here.

nuclear matter, the core response involves only the mixing of positive- and negative-energy wave functions; this is a static response that cannot occur in a nonrelativistic theory.

The result for the total baryon (convection) current is [5]

$$\Omega \vec{j}_B = U_\Lambda^\dagger(\vec{t},\lambda)\,\vec{\alpha}\,U_\Lambda(\vec{t},\lambda)\left\{1+\frac{g_v^\Lambda}{g_v^N}\frac{(g_v^N/m_v)^2\Pi_0}{1-(g_v^N/m_v)^2\Pi_0}\right\} \quad , \tag{2}$$

where $\Pi_0 = -\rho_N/E^{N*}_{k_F}$, $\rho_N = 2k_F^3/3\pi^2$, and $E^{N*}_{k_F} = [k_F^2 + M_N^{*2}]^{1/2}$. In Eq. (2), U_Λ is a positive-energy Dirac spinor, k_F is the Fermi momentum, and $\vec{t}$ is the momentum of the valence Λ. The first term is the enhanced valence-particle current ($\vec{t}/[\vec{t}^2 + M_\Lambda^{*2}]^{1/2}$ in nuclear matter). Unlike the nuclear case,[2] the core corrections do not entirely cancel the enhancement of $\vec{j}_B$ in hypernuclei, because the mass of the Λ and its couplings to the meson fields are different from those of the nucleon. *Thus, the effects of the strong fields in relativistic models might be observed by introducing a strange particle into the system.*

Furthermore, the effects of core modifications can be detected electromagnetically. The Λ single-particle convection current is not observed electromagnetically and the anomalous magnetic moment ($\mu_\Lambda = -0.613$ n.m.) is not modified in the present model. However, the core response modifies the electromagnetic current and magnetic moment; in the present work we include this effect in a local density approximation.[2] Applying Eq. (2), the total electromagnetic current is [5]

$$\begin{aligned}\langle \vec{J}(\vec{x})\rangle = {} & \frac{\mu_\Lambda}{2M_N}\vec{\nabla}\times\{U_\Lambda^\dagger(\vec{x})\beta\vec{\Sigma}U_\Lambda(\vec{x})\} \\ & -\frac{1}{2}U_\Lambda^\dagger(\vec{x})\vec{\alpha}U_\Lambda(\vec{x})\,\frac{g_v^\Lambda}{g_v^N}\left(1+\frac{m_v^2}{g_v^{N2}}\frac{E^{*N}_{k_F}(\vec{x})}{\rho_N(\vec{x})}\right)^{-1} .\end{aligned} \tag{3}$$

where $U_\Lambda(\vec{x})$ is the Hartree single-particle solution for the Λ in the meson fields of the closed-shell nucleus. Using this current, we calculate the magnetic moment of the hypernuclear system. The first term leads to the Schmidt values for the hypernuclear magnetic moments (within 1%) while the second term produces deviations proportional to the strength of the vector potential. (They also depend on M_N^*). Since the Λ is an isoscalar, these deviations are relatively free of ambiguities (*e.g.*, no pions), and additional corrections (*e.g.*, conventional core polarization) are expected to be small.

In this work we use the "finite Hartree" parameters from Ref. 6. To be consistent with good fits to available hypernuclear spectroscopic data,[7] we choose the Λ–meson couplings so that $g_s^\Lambda/g_s^N = g_v^\Lambda/g_v^N = 0.4$. (Note that the central Λ potential is weaker than the nucleon one and that the Λ spin-orbit splitting is very small in this model.) We emphasize that our results are not sensitive to the precise values of these couplings.

We have calculated magnetic moments for hypernuclei ranging from ${}^{17}_{\Lambda}$O to ${}^{209}_{\Lambda}$Pb for a Λ added in a variety of single-particle states. Here the results for the $1s_{1/2}$ Λ single-particle state, which is the most reasonable candidate for an experimental measurement, are compared with the nonrelativistic Schmidt values:

${}^{17}_{\Lambda}$O	${}^{41}_{\Lambda}$Ca	${}^{91}_{\Lambda}$Zr	${}^{209}_{\Lambda}$Pb	$A \to \infty$	Schmidt
−0.648	−0.665	−0.676	−0.681	−0.689	−0.613

(Results for the Λ in other single-particle states, where the deviations are larger, are given in Ref. 5.) Note that nearly the maximum possible effect on the $1s_{1/2}$ state is found in ${}^{209}_{\Lambda}$Pb.

In summary, we find that a relativistic mean-field model predicts $\gtrsim$10% deviations from the hypernuclear Schmidt moments predicted by nonrelativistic shell models and that the deviations are proportional to the size of the mean-fields. Thus the measurement of hypernuclear magnetic moments at CEBAF could put constraints on relativistic models as well as on the application of some QCD-motivated models to nuclei;* such experiments would provide interesting tests of different pictures of nucleons and nuclei.

REFERENCES

1. L. D. Miller, Ann. Phys. **91**, 40 (1975).
2. T. Matsui, Nucl. Phys. **A370**, 365 (1981); W. Bentz *et al.*, Nucl. Phys. **A436**, 593 (1985); J. A. McNeil *et al.*, Phys. Rev. **C34**, 746 (1986); R. J. Furnstahl and B. D. Serot, Nucl. Phys. A, to be published.
3. T. Yamazaki, Phys. Lett. **B160**, 227 (1985); Nucl. Phys. **A446**, 467c (1985).
4. T. W. Donnelly and S. Cotanch, in: RPAC 1985 (CEBAF, Newport News, VA, 1986), p. 7-1; B. Mecking, *ibid.*, p. 7-25; Joseph Cohen, in: RPAC 1986 (CEBAF, Newport News, VA, 1987), p. 305 and Phys. Rev. **C32**, 543 (1985); Joseph Cohen, M. W. Price, and G. E. Walker, Phys. Lett. **B188**, 393 (1987), and references therein.
5. Joseph Cohen and R. J. Furnstahl, Phys. Rev. **C35** (1987), to be published (no. 6, June, 1987).
6. B. D. Serot and J. D. Walecka, Adv. in Nucl. Phys. **16** (Plenum, New York, 1986).
7. C. E. Price, private communication (1985); G. E. Walker, Nucl. Phys. **A450**, 287c (1986).

* It has been suggested that this experiment will provide a direct test of changes in the properties of hadrons in nuclear matter.[3]

Neutral Pion Photoproduction on Proton Near Threshold

R. Davidson and Nimai C. Mukhopadhyay
Physics Department, Rensselaer Polytechnic Institute, Troy, NY 12180-3590

First experimental results[1] on neutral pion photoproduction from protons near threshold (NPPT), of fundamental interest as rigorous tests of corrections to the low-energy theorems (LET) and current algebra, and relevant in the context of understanding electroweak structure of hadrons, are in. Mazzucato et al.[1] extract the E_o+ amplitude at threshold to be (-0.5 ± 0.3), in strong disagreement with the value of -2.47 predicted[2] by the LET, and with the previously inferred[1] experimental value of (-1.8 ± 0.6), all in units of $10^{-3}/m_{\pi}+$. This is the first claim of experimental evidence for the large s−wave rescattering effects[2] suspected in the E_o+ amplitude.

We are primarily concerned here in examining uncertainties associated with the E_o+ prediction of the chiral Lagrangian theory[3,4], incorporating the LET and current algebra. We also look for possible inconsistencies in the analysis of Mazzucato et al.[1]

In an effective chiral Lagrangian theory[3,4], the pseudovector nucleon Born terms incorporate the LET (Table I). To this, we can add contributions from t-channel vector mesons (ρ, ω), s- and u-channel Δ and higher baryon exchanges, fitting extant multipoles for cm energies of 1100 and 1350 MeV. This theory yields real amplitudes at the tree level. Their unitarization is ambiguous; thus, these amplitudes can be taken as either a T or K matrix element, where $T = K\ (1 - iK)^{-1}$. With $T_{33} = \sin\delta\ \exp(i\delta)$, we have

$$T_{31} \approx \cos\delta\ \exp\ (i\delta)\ (K_{31} + iK_{32}K_{21}/(1 - iK_{22})), \tag{1}$$

where channels 1, 2 and 3 are γp, $\pi^+ n$ and $\pi^0 p$ respectively. We can either use the theory to compute $|T_{31}|$ and unitarize it by giving it the Watson phase δ, or compute T_{31} via (1). The latter produces the so-called "cusp effect" in the cross section[5].

Table I shows our theoretical predictions for the real part of the multipoles for NPPT, in the form $E_0+ = a/m_{\pi}+$, $M_1- = bqk/m_{\pi}^3+$, $M_1+ = cqk/m_{\pi}^3+$, q and k being the cm pion and photon momenta. We find the cusp effect to be only important for E_0+. P_{11} (1450) and S_{11} (1535) contribute less than 10% of each of these multipoles for NPPT. Thus, the chiral Lagrangian theory prediction of E_0+ remains in serious disagreement with the new value of E_0+ at threshold. However, its predictions for M_1+ and M_1- are in excellent agreement with experiment.

Two comments on the results of Mazzucato et al.[1] are now in order. First, given their fitted multipoles, we get the coefficient C to be always negative for E_γ between 146.5 MeV and 169.2 MeV, consistent with zero, in contrast to values given in their Table I. Second, fitting multipoles to their A, B, C's, we end up with b in M_1- significantly different from $(-2.0 \pm 1.5) \times 10^{-3}$, ours being close to -7×10^{-3}. However, we do agree with their E_0+ and M_1+ values. Thus, serious disagreement between LET and experiment for E_0+ still persists, and calls for an independent experiment confirmation.

We thank G. Adams for discussions. This research is supported by the U.S. Department of Energy (Contract #DE-AC02-83ER40114-A004).

References

1. E. Mazzucato et al., Phys. Rev. Lett. 57, 3144 (1986).
2. See, for example, G. Furlan et al. Nuovo Cim. LXIIA, 519 (1969).
3. M.G. Olsson et al., Phys. Rev. D17 2938 (1978) and references therein.
4. R. Davidson, N.C. Mukhopadhyay and R. Wittman, Phys. Rev. Lett. 56, 804 (1986), and to be published.
5. G. Fäldt, Nucl. Phys. A333, 357 (1980).

Table I: Various contributions to calculated values of multipoles for π^0 photoproduction near threshold in units of 10^{-3}. See text for definition of a, b, c. Cusp effect is shown for "Total" only.

	Nucleon Born	Delta	Vector Mesons	Total	Total with cusp effect	Expt.[1]
a	-2.47	0.35	0.08	-2.04	-2.86	-0.5 ± 0.3
b	-6.61	2.22	0.89	-3.48	-3.48	-2.0 ± 0.3
c	3.39	3.83	0.74	7.96	7.97	8.0 ± 0.3

DEEP INELASTIC PHOTO- AND ELECTRONUCLEAR REACTIONS

Egiyan K.Sh.

Yerevan Physics Institute, St. Markarian 2, Yerevan 375036, Armenia, USSR

Abstract: Some experimental data on deep inelastic photo- and electronuclear reactions are discussed, where the secondary protons are produced in a kinematically forbidden region for interaction with the nucleon.

Deep inelastic will be called the nuclear reactions which can not be considered as a sum of interactions of incident particles with quasifree nuclear nucleons. The production of the so-called cumulative particles is a classical example. Cumulative we mean to be particles the production of which is kinematically forbidden for interaction with a free stationary nucleon. In the present work some available experimental data on photo and electroproduction of cumulative protons and the possible development of this trend are discussed.

1. Inclusive Photoproduction of Cumulative Protons (CP)

Let us consider the inclusive process

$$\gamma + A \to p + X \qquad (1)$$

where X is the residual system. The conservation laws will read [1,2]

$$(p_\gamma + x_A p_A - p_p)^2 = p_X^2 = (x_A M_A - m_p)^2 \qquad (2)$$

where x_A is the fraction of four-momentum of nucleus A carried away by the system with which the collision took place (cluster, nucleon, quark). Solving (2) with respect to x_A one obtains

$$x_A = \frac{1}{A} x_N = \frac{1}{A} \cdot \frac{E_\gamma}{E_\gamma - T_p} \cdot \frac{E_p - p_p \cos\vartheta_p}{m_N} = \frac{1}{A} \frac{E_\gamma}{E_\gamma - T_p} \alpha_N \qquad (3)$$

where α_N is the so-called light-cone variable. The kinematical definition of cumulativeness is the cryterion $x_N > 1$ in (3).

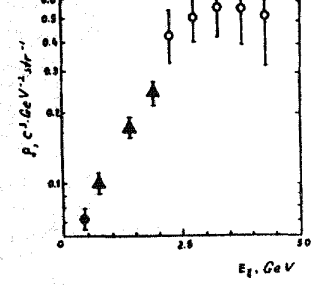

Fig.1 The dependence of $f_p(E_\gamma)$ on E_γ at $P_p = 0.53$ GeV/c and $\vartheta_p = 120°$. ▲ - [8] ● - [9].

Then the whole range of $\vartheta_p \geq 90°$ is cumulative for protons, independent of their energy. The main inclusive data on CP photoproduction are obtained at the Yerevan Electron Synchrotron in 1973-1981 [3-7]. There are some data from Kharkov [8] and Tokyo [9]. Let us consider the yields of CP in an invariant form

$$f_p(E_\gamma, \vec{P}_p, A) = \frac{1}{P_p^2} \cdot \frac{d^2\sigma}{d\Omega_p dE_p} = f_p(E_\gamma, x_p, P_\perp, A) \qquad (4)$$

First of all, dependences of $f(E_\gamma)$ on E_γ is measured at fixed $\vec{P}_p$ and for nuclei from ^{12}C (Fig.1) to ^{208}Pb. The main conclusions are: i) $f_p(E_\gamma)$ increases with E_γ in the range of $E_\gamma \leq 2$ GeV, and at $E_\gamma \geq 2.5$ it remains nearly constant. In CP photoproduction the regime of limiting (Yang) fragmentation sets in [10] much earlier at(lower energies) than at "ordinary" interactions with nucleons and if the limiting fragmentation is due to properties of the matter in the fragmentator, then these properties are different in the "ordinary" nucleon and in the intranuclear fragmentator emitting cumulative nucleons. ii) The behaviour of $f_p(E_\gamma)$ is the same for all nuclei, e.g. firstly, the CP production is a local process and, secondly, interactions of secondary leading photoparticles in nuclei do not make essential contribution to the CP production. iii) In the scaling regime ($E_\gamma \geq 2.5$ GeV) and at $T_p \leq 0.3$ GeV, $x_N = \alpha_N$(see (3)). iiii) To study the reaction (1) in the scaling regime, one may use the bremsstrahlung spectrum of γ-quanta of $E_\gamma^{max} > 2.5$ GeV, since the main contribution will make this very region. The inclusive data given below have been obtained at $E_\gamma^{max} = 4.5$ GeV. These data indicate, that the CP production is connected with the presence of states in nucleus which differ from the standard one-particle nucleon states. A natural question arises: can one get information about the structure function of these states from these data? Of course, the direct way to obtain the structure function of fragmentators still is the deep inelastic scattering of leptons. There are practically no such measurements up to now. There is only one work [11] on scattering of μ-mesons on ^{12}C at 200-280 GeV and $q^2 \geq 50(GeV/c)^2$. It is obtained that the structure function at $x_\mu > 1$ is so well described by an exponent $exp(-x_\mu/x_{\mu_0})$with $x_{\mu_0} = 0.14$. The experimentally measured value of $f_p(\alpha, P_\perp)$ in its most general form can be presented [12] as:

$$f_p(\alpha, P_\perp) = F(x, P_\perp) \cdot \sigma \cdot G(x, P_\perp) \qquad (4')$$

where $G(x, P_\perp)$ is the structure function of fragmentator, $F(x, P_\perp)$ is hadronization function, σ denotes the scale of the cross section. In cases when the registering particle is the same as before the collision (for instance, at electron scattering or when the registered nucleon was in the state of an intranuclear nucleon), evidently $F(x, P_\perp) = 1$. But if the scattering occurs on a quark and a fragment is registered, then $F(x, P_\perp)$ is a function of quark hadronization. At lepton scattering the meaning of σ is unambiguous - this is Mott's cross section. σ is unknown in the cumulative particle production. One must do an assumption. Let us consider [12] the spectator mechanism, when the cumulative particle results from the hadronization of the constituents(quark) of the fragmentator which do not participate in collisions of the incident particle with the fragmentator. In this case one may assume that $F(x, P_\perp) = const$ and $\sigma = const$, then $f(\alpha, P_\perp) \sim G(x, P_\perp)$ [12,13]. In Figs. 2 and 3 the dependences of inclusive yield $f_p(\alpha, P_\perp)$ on α at a number of fixed $P_\perp$ are presented for ^{12}C (Fig.2) [14], ^{63}Cu (fig.3b) and ^{208}Pb (Fig.3a) [15]. In the

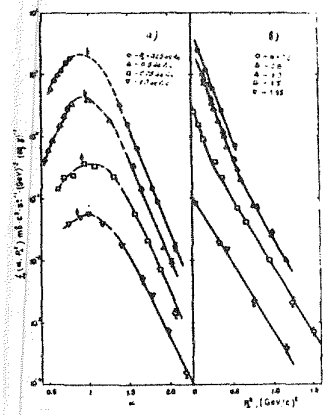

Fig.2 The dependence of $f_p(\alpha, p_\perp)$ for ^{12}C on α at $p_\perp$ = 0.25 (o), 0.5 (Δ), 0.75 (□) and 1.0 (▽) GeV/c (a); (б) on the $p_\perp$ at α = 0.5 (o), 0.8 (▲), 1.0 (Δ), 1.5 (□) and 1.95 (▽).

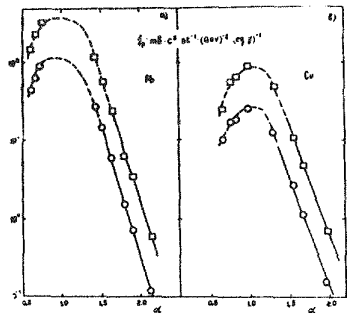

Fig.3 The dependence of $f_p(\alpha, p_\perp)$ on α a) for ^{208}Pb, b) for ^{63}Cu. (o) — $p_\perp$ = 0.25 (□) — $p_\perp$ = 0.5 GeV/c.

range of $\alpha > 1$ (the cumulative range) $f_p(\alpha)/p_\perp$ is sharply decreasing and at $\alpha \geq 1.8$ for all $p_\perp$ is well approximated by one exponent $f(\alpha)_{p_\perp = const} \sim exp(-\alpha/\alpha_0)$ with $\alpha_0 = 0.134 \pm 0.004$. Similar values of α_0 are also obtained for the cumulative production by incident hadrons [16]. Processing the available data on deep inelastic scattering of electrons on the lightest nuclei (e.g. ^3He) like it has been done at SLAC[7], then X_{e0} asymptoticly tends to the value of 0.14 beginning from $Q^2 \simeq 3$ (GeV/c)^2. Thus, all the data together testify, apparently, to the fact that right the structure function of an exotic state of nuclei fragmentating into cumulative particles is studied.

One can make one more conclusion from our data [15]. The ratio $R_A = f_p^A(\alpha, p_\perp)/f_p^C(\alpha, p_\perp)$ of structure functions of a given nucleus to the structure functions of carbon nucleus grows with α (Fig.4), which may be interpreted as enrichment of the fragmentator in nuclei by constituents (quarks) of high momenta. This is theoretically predicted in [13].

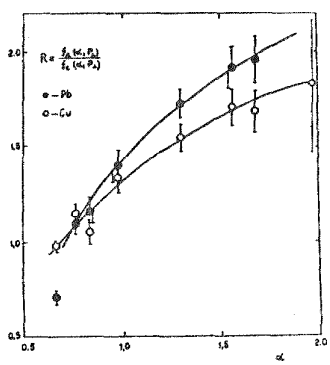

Fig.4 The dependences of $R = f_A(\alpha, p_\perp)/f_C(\alpha, p_\perp)$ on α . (o) — A = 63; (●) — A = 208.

2. Correlated Photoproduction of CP

Let us consider the semiinclusive process

$$\gamma + A \to \vec{p} + \vec{h} + X \qquad (5)$$

where „←" and „→" correspondingly indicate backward (cumulative) and forward (noncumulative) particles registered in coincidence. As forward hadrons have been chosen the π-meson and proton with momentum ~1.0 GeV/c at emission angle of 16°. These investigations have shown that ($\vec{p}, \vec{h}$) correlations do exist. In case of ($\vec{p}, \vec{p}$)-coincidence the chance for correlation is higher than in case of ($\vec{p}, \vec{\pi}$) one.(Fig.5).

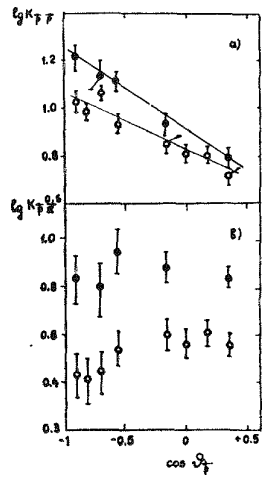

Fig.5 The dependences of correlation functions $K_{\vec{p}\vec{p}}$ (a)and $K_{\vec{p}\vec{\pi}}$ (b) on $\cos\vartheta_{\vec{p}}$. (o)— $p_{\vec{p}}$ = 0.4 GeV/c; (●)— 0.58 GeV/c.

Let us consider the structure function of nuclei in correlation measurements of CP, i.e. dependences of $f_{\vec{p}\vec{h}}(\alpha_{\vec{p}}, p_{\perp\vec{p}})$ on $\alpha_{\vec{p}}$. Since three yields of $f_{\vec{p}\vec{h}}$, $f_{\vec{p}}$, $f_{\vec{h}}$ have been measured in the experiment, one can determine the correlation function

$$K_{\vec{p}\vec{h}}(\alpha_{\vec{p}}, p_{\perp\vec{p}}) = \frac{f_{\vec{p}\vec{h}}(\alpha_{\vec{p}}, p_{\perp\vec{p}})}{f_{\vec{p}}(\alpha_{\vec{p}}, p_{\perp\vec{p}}) \cdot f_{\vec{h}}} \cdot \sigma_t^{\gamma A} \qquad (6)$$

where $f_{\vec{h}}$ is the yield of forward hadron. In Fig.6 the dependence of $K_{\vec{p}\vec{p}}(\alpha_{\vec{p}}, p_{\perp\vec{p}})$ and $K_{\vec{p}\vec{\pi}}(\alpha_{\vec{p}}, p_{\perp\vec{p}})$ on $\alpha_{\vec{p}}$ is shown at three values of $p_{\perp\vec{p}}$ =0.2; 0.3 and 0.4 GeV/c.

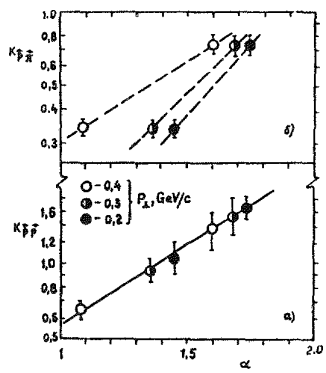

Fig.6 The dependences of $K_{\vec{p}\vec{p}}(\alpha, p_\perp)$ (a) and $K_{\vec{p}\vec{\pi}}(\alpha, p_\perp)$ (b) on α . (●) — $p_\perp$ = = 0.2; (⊙) — 0.3; (o) — 0.4 GeV/c.

It is seen that in both ($\vec{p}, \vec{p}$) and ($\vec{p}, \vec{\pi}$) correlations $K_{\vec{p}\vec{h}}$ grows with $\alpha_{\vec{p}}$. Then it follows from eq.(6) that the structure function $f_{\vec{p}\vec{h}}(\alpha_{\vec{p}}, p_{\perp\vec{p}})/p_\perp = const$ differs from the inclusive one of $f_{\vec{p}}(\alpha_{\vec{p}}, p_{\perp\vec{p}})/p_\perp = const$, i.e. in correlation measurements is investigated a higher-momentum component of fragmentator constituents. In case of ($\vec{p}\vec{p}$) correlations one can estimate the change in the hardness of the structure function. Indeed, all points of $K_{\vec{p}\vec{p}}(\alpha_{\vec{p}}, p_{\perp\vec{p}})$ for

all $P_{1\bar{p}}$ lie on one and the same line which is well described by the exponent $K_{pp} \sim exp(\alpha/\alpha_{0K})$ with $\alpha_{0K} = 0.726 \pm 0.05$. As it can be seen from Fig.2 [13,14], in the range of $P_{1\bar{p}} = 0.2 \div 0.5$ GeV/c and $\alpha_{\bar{p}} \geq 1.5$, $f_{\bar{p}}(\alpha_{\bar{p}}, P_{1\bar{p}})$ is factorized rather well, and $f_{\bar{p}}(\alpha)|_{Q=const} \sim exp(-\alpha/\alpha_{0\bar{p}})$ with $\alpha_{0\bar{p}} = 0.134 \pm 0.004$. It follows from the eq.(6) that $f_{\bar{p}\bar{p}}(\alpha_{\bar{p}}, P_{1\bar{p}})$ at $\alpha \geq 1.5$ is also factorized, and structure function $f_{\bar{p}\bar{p}}(\alpha_{\bar{p}}) \sim exp(-\alpha/\alpha_{0pp})$ with $\alpha_{0pp} = 0.165 \pm 0.06$.

3. Electroproduction of CP

In case of primary electrons, four classes of investigations may be carried out: i) Inclusive electron scattering at $x_e > 1$ and $Q^2 \geq 3$ (GeV/c) (scaling regime). The cross section of this process for $E_e \simeq 4.5$ GeV is changed in the interval of $10^{-36} \div 10^{-38}$ cm^{2}str^{-1} GeV^{-1} for $x_e = 1 \div 2$ ($Q^2 = 4 \div 6$ (GeV/c)^2). At such small cross sections investigations can succeed with intensive beams like the SLAC beam. ii) Inclusive electroproduction of CP at $x_p > 1$. As the secondary electron is undetected, this process is, in fact, the inclusive photoproduction ($Q^2 \to 0$), the results of which have been discussed above. iii) The next type of measurements involves correlation measurements of (e,e'N) at $x_e < 1$, but $x_N > 1$. N can be any particle. In case when N is a nucleon, $x_N > 1$ at all $\vartheta_N \geq 90°$. Such measurements can be carried out at our accelerator with its today's parameters. Below we shall discuss the available preliminary data. iiii) Finally, one must, and it is necessary to make plans for investigations (e,e'N) when $x_N, x_e > 1$. Only in this case will be obtained the most important results for understanding of the process of cumulative particles production. Our projects for such measurements will be realized after an essential reconstruction of the Yerevan Electron Synchrotron.

Let us consider those new, preliminary data obtained in (e,e'P) measurements at $x_e < 1$ and $x_p > 1$. Such data are extremely important in the determination of the CP production mechanism. For instance, there is expected a peak in the spectrum of secondary electrons from quasielestic scattering of both cumulative and non-cumulative protons (registered in coincidence with electrons) for the model of direct secondary rescatterings [18] and for the spectator variant of the few-nucleon correlation model [19]. In the first case this peak must not change its place with the increasing cumulativeness (e.g., detection angle) of protons, while in the second case the peak is expected to be shifted according to a certain law [19]. In Fig.7 the our measured yields of (e'P) coincidences on ^{12}C as functions of E'e for different angles (cumulativeness) of CP are shown. One can prove that when $\vartheta_p \geq 120°$ and $T_p \geq 85$ MeV ($x_p \geq 1.3$), there is no essential contribution from the quasielastic peak, i.e. it is hard to fit the experiment with the predictions of the theoretical models mentioned above. The experimental data do not exclude the few-nucleon correlation model predictions, but there concrete calculations are needed for one to make more unambiguous statements.

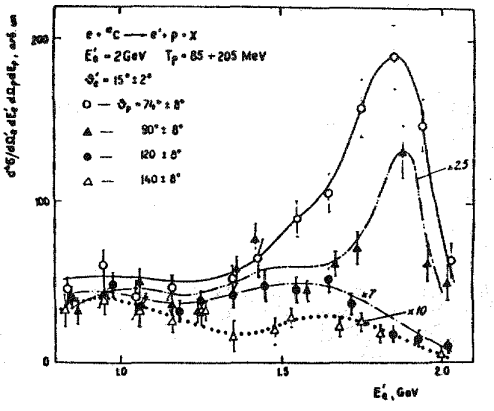

Fig.7 The spectra of secondary electrons in the reaction $e + {}^{12}C \to e' + p + X$. The curves through the experimental points are plotted "by eye". The experimental points are normalized relative to each other.

References

1. V.S. Stavinsky, preprint JINR P2-8037, Dubna, 1980 (in Russian).
2. A.M. Baldin et al., preprint JINR E1--82-172, Dubna, 1982.
3. K.V. Alanakyan et al., EPI-220(12)-77, Yerevan, 1977 (in Russian).
4. K.V. Alanakyan et al., Yad.Fiz., 5, 545 (1977) (in Russian).
5. K.Sh. Egiyan, Izv.AN Arm.SSR, Fizika, 16, iss.6, 421 (in Russian).
6. K.V. Alanakyan et al., Nucl.Phys., A367, 429 (1981).
7. R.O. Avakyan et al., EPI-424(31)-80, (1980) (in Russian).
8. Kuz'menko et al., Pis'ma v ZhETF, 23, 174 (1976) (in Russian).
9. K. Baba et al., Phys.Lett., 113B, 459 (1982).
10. G.A. Leksin, Proc. of the VIII Int. Conf. on High-Energy Phys., Tbilisi, 1976, 1, A-3.
11. I.A. Savin, Proc. of the VI Int. Seminar on Problems of High-Energy Physics, Dubna, 1984, 205.
12. A.M. Baldin, Proc. of the Int. Conf. on Extreme States in Nuclear Systems, Dresden, 1980, 2, 1.
13. L.A. Kondratyuk, M.Zh. Shmatikov, preprint ITEP-114, Moscow, 1983.
14. K.Sh. Egiyan, preprint EPI-525(12)-82, Yerevan, 1984.
15. K.V. Alanakyan et al., preprint EPI-889 (40)-86, Yerevan, 1986.
16. A.V. Efremov, Part. and Nucl., 13, No.3, 613 (9182) (in Russian).
17. S. Roch et al., SLAC-PUB-2838, 1981.
18. V.B. Kopeliovich, Phys.Rep., B9, No.2, 51 (1986).
19. L.L. Frankfurt and M.I. Strikman, Phys. Rep., 76, No.4, 215 (1981).

EXPERIMENTAL DATA ON DEEP INELASTIC HADRON-NUCLEUS REACTIONS AND SOME CRUTIAL EXPERIMENTS ON ELECTRON BEAM

V.B.Gavrilov

INSTITUTE OF THEORETICAL AND EXPERIMENTAL PHYSICS, Moscow, USSR

Now it is obvious that the interaction of a high energy hadron with a nucleus does not reduced to the sum of the interactions with quasifree nucleons. The cumulative particle production /I/ and the nuclear scaling /2/ are the most striking effects indicating to this. Let us consider the inclusive reaction

$$a + A \rightarrow b + X \qquad (I)$$

It is well established that the secondary particles "b" may be emitted into the kinematical region forbidden for aN interactions. The dependence of the invariant cross section on the energy of the particle emitted at fixed angle may be parametrized by the following expression:

$$f = \frac{E d\sigma}{d^3p} = C \exp(-T/T_0) \qquad (2)$$

Nuclear scaling means that the value of T_0 does not depend on the atomic weight of the target nucleus, and at the large initial energy both T_0 and $\rho = f/\sigma_{in}^A$ do not depend on the incident particle type and its energy. Fig.I shows $\delta T_0/T_0$ as a function of A for the cumulative protons /3/. It is seen that the relative variation of T_0 at the atomic weight increase is sufficiently smaller than the variations of such nuclear characteristics as the binding energy (ε) or Fermi momentum (p_F). This fact indicates to the locality of the process of cumulative particle production. It should be noted that the values of T_0 are the same for the incident antineutrinoes /4/, photons /5/ and hadrons /6,7/. For the cumulative particle production the strong A dependence of the cross sections (stronger than $f \sim A$) is characteristic /2/.

The angular dependences of the inclusive cross sections of proton production do not depend on the initial energy (Fig.2a), but they differ for different nuclei at the region $\vartheta \leq 90^0$ (Fig.2b) /8/. The excess of the forward emitted protons for the carbon nucleus may be naturally explained by the contribution of the quasifree processes which take place at the periphery of the nucleus. Because of the weak A dependence of the quasifree cross sections ($f \sim A^{4/3}$) the relative contribution of these processes decreases rapidly with the atomic weight increase. For the heavy nuclei the main contribution give the processes which take place in the inner part of the nuclei. These processes are called the deep inelastic hadron-nucleus reactions as an opportunity of the quasifree nuclear reactions.

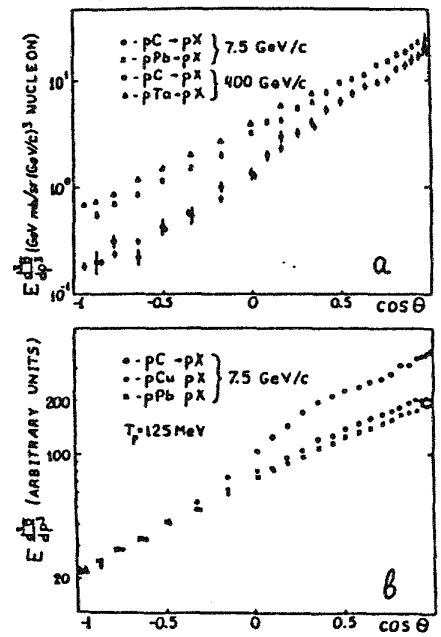

Fig.2

The deep inelastic hadron-nucleus reactions may be considered as successive local interactions of the incident hadron with nuclear matter as it is shown in Fig.3. These local interactions may be the interactions with short range nucleon correlations /9/ and with the quark bags /I0/, or any type of the interactions followed by the local heating of nuclear matter /II/. Sometimes the inclusive spectra of the particles produced in the deep inelastic hadron-nucleus reactions are connected immeduately with the quark-gluon nuclear structure function /I2/.

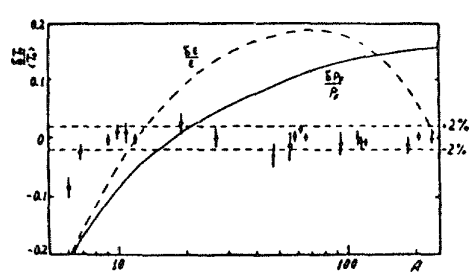

Fig.I

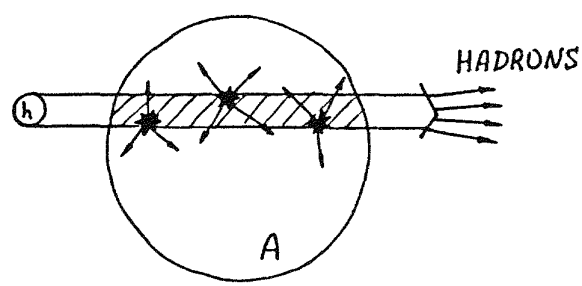

Fig.3

As it was noted above the independence of the cumulative particle spectra on the atomic weight of the target nucleus indicates to the locality of the mechanism of the deep inelastic hadron-nucleus reactions. The investigations of the correlations between two protons with small relative momenta /I3/ permit to speak about an alongated shape and the small transverse size ($r_1 \simeq I$ fm) of the region of the deep inelastic hadron-nucleus reaction. Finally, the studiing of the angular dependence of the coefficint of two-nucleon coalescence into a deuteron /I4/ suggests not only the elongated shape of the interaction region but also a successive knock-out of nucleons during propagation of the incident hadron through a nucleus.

Fig.4 shows the coalescence coefficient

$$\alpha(T,\vartheta) = \frac{\rho_d(T,\vartheta)}{N/Z\,[\rho_p(T/2,\vartheta)]^2} \qquad (3)$$

as a function of $\cos\vartheta$ for the interactions of the high energy hadrons with the heavy nuclei /I4/. For the isotropic emission of particles from a spherical region the value of α would not depend on the emitting angle. The curves in Fig.4 show the dependences $\alpha(\cos\vartheta)$ expected in the case of the successive emission of nucleons along the trajectory of the incident hadron during its propagation through a nucleus.

The space-time picture of the deep inelastic lepton-nucleus reaction (Fig.5) differs from that of the hadron-nucleus reaction. At large Q^2 virtual γ or W transfers locally its energy and momentum to a single quark which generates a quark-gluon jet propagating through the nucleus. The questions which we interest in the analysis of the lepton-nucleus interactions are the following:

I) What the exitation of nuclear matter does occur at the local scattering of lepton by quark ?

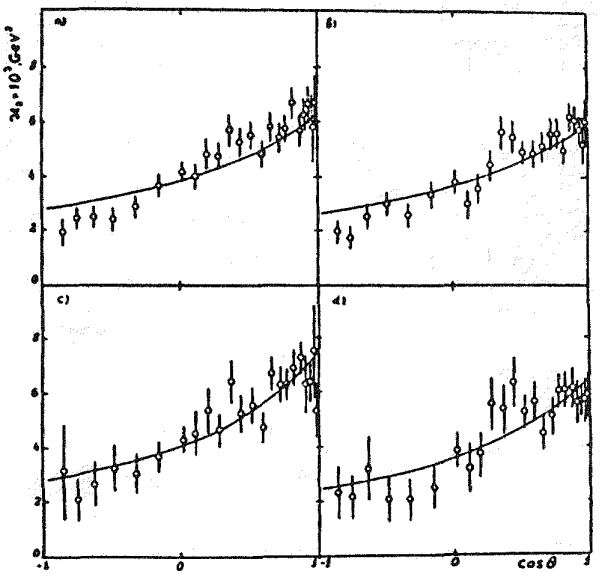

Fig.4

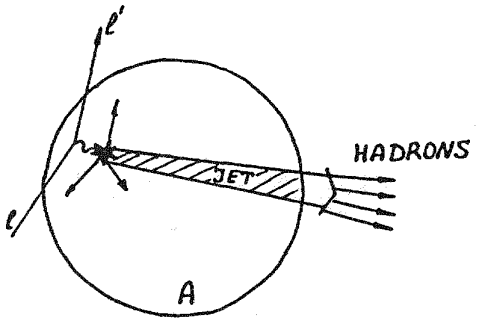

Fig.5

2) How does the quark-gluon jet interact with nuclear matter ?

The first comparision of the inclusive spectra of protons produced in the deep inelastic lepton-nucleus /4/ and hadron-nucleus reactions shows that these spectra are similar. But up to now there are very poor experimental data for reaction

$$l + A \rightarrow l' + b + X\,, \qquad (4)$$

therefore careful measurements of the cumulative particle production in reaction (4) are necessary, especially with measuring Q^2 and ν of the lepton. Such data will permit to answer the following questions:

I) Do the cumulative proton spectra at the deep inelastic lA and hA reactions coinside in the kinematical region forbidden not only for interaction with one nucleon but with nucleon pair also ?

2) Is the ratio of the inclusive cross sections of the cumulative pion production to the proton one at the lA reactions the same as it is at the hA reactions ?

3) What is the value of

$$\rho_{lA} = \frac{E_b\, d\sigma(lA \rightarrow l'bX)}{d^3p_b\, dQ^2 d\nu} \Big/ \frac{d\sigma(lA \rightarrow l'X)}{dQ^2 d\nu} \qquad (5)$$

and what is its A dependence with respect the value of ρ_{hA} and its A dependence ?

4) How does ρ_{lA} depend on ν and Q^2 ?

5) How does coalescence coefficient depend on the emission angle for the deep inelastic lepton-nucleus reactions ?

An experimental answers to these questions may clarify the nature of the local exitation of nuclear matter and, at some extent, the space-time picture of the hadronisation of the quark-gluon jet generated by the lepton-quark scattering.

REFERENCES

I.A.M.Baldin et al.-Yad.Fiz.v.I8,p.79,I973.
2.G.A.Leksin - XVIII Int. Conf. on High Energy Physics,Tbilisi,v.I,p.A6-3,I976.
3.V.B.Gavrilov et al.-ITEP-96,I985.
4.V.I.Efremenko et al.- Phys.Rev.D,v.22, p.258I,I980.
5.K.V.Alankanyan et al.- Yad.Fiz.v.26,p.764, I977.
6.Yu.D.Bayukov et al.- ITEP-I48,I983.
7.Yu.D.Bayukov et al.- Phys.Rev.C,v.20, p.764,I979.
8.Yu.D.Bayukov et al.- Sov.J.Nucl.Phys.v.42, p.II6,I985.
9.L.L.Frankfurt and M.I.Strikman - Phys. Reports,v.76,p.2I5,I98I.
IO.L.A.Kondratyuk and M.Zh.Shmatikov - ITEP-II4,I983.
II.M.V.Kossov and L.M.Voronina -ITEP-I65, I984.
I2.A.M.Baldin - Nucl.Phys.v.A434,p.695,I985.
I3.A.V.Vlasov et al.- Sov.J.Nucl.Phys.V.36, p.536,I982.
I4.V.B.Gavrilov et al. - Z.Phys.A,v.324, p.75,I986.

$(e, e'K^+)$ at small x region

T. Kishimoto

University of Houston Houston Texas 77004

In this short article I would like to show the possibility to investigate the change of nucleon structure in a nucleus by using the exclusive $(e, e'K^+)$ reaction. Studies of the deep inelastic lepton scattering on nuclei show some difference between the structure function of nucleon and that of nucleus[1,2,3]. There is some enhancement for the small x region and depletion at the medium x region (EMC effect). Although there are many successful attempts to explain the effect by incorporating quark degrees of freedom in nuclei, conventional nucleon binding effects in nuclei were also successful to explain the depletion of structure function at the medium x region[4]. The role of small x region seems to be important[5], however, we do not yet have consistent experimental data there.

Although the measured structure function of a nucleon can be understood as a momentum distribution of quarks in nucleon, we need to have models connecting it to the underlying physics. One successful model is the cloudy bag model[6] by which nucleon is described by the coherent sum of baryons and mesons surrounding them. If a nucleon is in a nucleus, there can be a change of nucleon structure in its peripheral region, which consists mostly of mesons i.e. sea quarks. It is quite conceivable that these effects appear in the small x region.

Usually the small x region corresponds to the small Q^2, because energy transfer (ν) is limited in the experiment. The relation is given by

$$x = \frac{Q^2}{2M\nu},$$

where M is proton mass. The small Q^2, for example, $1(GeV/c)^2$ or less, corresponds to the region where we cannot neglect the meson form factor. Therefore to increase Q^2 by using the higher energy beam is one way to study in detail this intriguing small x region. On the other hand study of the change of meson structure of nucleon due to nuclear environment is another way to get close to this problem. Since this kind of study requires relatively low Q^2, it can be done by the relatively low energy CEBAF type

machine. The $(e, e'K^+)$ reaction is quite appropriate to study this kind of meson structure. The advantages of the reaction are three fold.

1) Since there is no strange quark in the nucleus, the K^+ should appear from the sea quark, or in other words, strange mesons coming from the dissociation of nucleon into K^+ and hyperon. In this way we do not see the valence quark contribution, which is unchanged between nucleon and nucleus. Therefore the difference between nucleon and nucleus should be quite clear if it exists.

2) In the inclusive reaction there is some difficulty to resolve the occurrence of deep inelastic scattering from the real photon emission at small x region. At small x region the bremsstrahlung process (real photon emission) cannot be negligible and it becomes complicated for heavier target. Its correction requires the complete knowledge of structure function for all possible bremsstrahlung processes; that is quite difficult. The exclusive reaction can eliminate this real photon emission.

3) Since the K^+ doesn't have much interaction with the nucleon, the final state interaction should be small or calculable[7,8]. We might see the enhancement of K^+ production if propagation of the kaon is enhanced because of, for example, precritical effect of kaon condensation.

There are several experiments done for the $(e, e'K^+)$ reaction on nucleon [9,10,11]. The measured x_F distribution shows fairly good agreement with parton model prediction except for regions that correspond to Λ (1115.6 MeV) and perhaps Λ (1520 MeV) production. Here x_F is given by

$$x_F = P_{parallel}/P_{MAX},$$

where P_{MAX} and $P_{parallel}$ are possible maximum hadron momentum and parallel momentum along the momentum transfer direction. These data can be understood either the configuration of nucleon in terms of hyperons and K^+ or sea quark distribution in nuclei. It is then quite interesting to study in detail the final hyperon excitation, i.e. Λ's and Σ's, by this reaction on a nucleon and make a comparison with models of the nucleon. The reaction on a nucleus could give a change of meson structure of the nucleon in a nuclear environment.

The CEBAF machine can explore the intriguing small x region by looking at rather small Q^2 region where meson form factor plays an important role. The $(e, e'K^+)$ reaction hopefully gives us the information of strange meson distribution in nuclei exclusively.

references
1) J. J. Aubert et al., Phys Lett. 123 B, 275 (1983)
2) A. Bodeck et al., Phys. Rev. Lett. 50, 14331 (1983) and 51, 534 (1983)
3) R. G. Arnold et al., Phys Rev. Lett. 52, 727 (1984)
4) S. V. Akulinichev et al., Phys. Lett. 158B, 485 (1985); S. V. Akulinichev et al., Phys. Rev. Lett. 55, 2239 (1985); B. L. Birbrair et al., Phys. Lett. 166B (1986)
5) E. L. Berger, Interactions between Particle and Nuclear Physics, (Lake Louise, Canada) 165 (1986)
6) S. Theberge and A. Thomas, Nucl. Phys. A393 (1983) 252
7) D. Marlow et al., Phys. Rev. C 25 (1982) 2619
8) AGS proposal EXP 835 (1986)
9) H. Ackerman et al Nucl. Phys. B133 (1978) 397
10) C. J. Bebek et al Phys. Rev. D (1977) 594
11) C. T. Day et al. Phys. Rev. D (1981) 576

Photoproduction of π^+ from ^{14}N

L. Tiator[1], J. Vesper[1*], D. Drechsel[1], N. Ohtsuka[2*] and L.E. Wright[3]

[1] Inst. f. Kernphysik, Universität Mainz, 6500 Mainz
[2] Inst. f. Theor. Physik, Universität Tübingen, 7400 Tübingen
[3] Physics Department, Ohio University, Athens, Ohio 45701

Over the past 3 years the process $^{14}N(\gamma,\pi^+)^{14}C_{gs}$ has become the most completely studied reaction in the field of pion photoproduction. Differential cross sections have been measured at 173 MeV in Mainz[1)] and at 200, 230, 260, 320 and 400 MeV at Bates[2,3)] with most of the data having been analyzed. For a long time pion photoproduction from ^{14}N has been proposed as one of the most interesting reactions in p-shell nuclei. Because of the extremely long lifetime of $^{14}C_{gs}$ a strong suppression of the Gamow-Teller (GT) transition was assumed. In 1977, however, Goulard et al.[4)] speculated that the long lifetime is only due to an almost exact cancellation of the GT single particle transition and meson exchange currents. In a combined analysis of elastic and inelastic electron scattering form factors of ^{14}N, Huffman et al.[5)] found solutions for the nuclear wave function which were consistent with electron scattering and produced a finite GT matrix element. But only in low energy pion photoproduction[1,2)] could it be shown that a finite GT matrix element was neccessary in order to get agreement between theory and experiment. And in a very recent measurement at Mainz at a foreward angle of 25° and photon energy of 173 MeV was the rise of the predicted differential cross section corresponding to a finite GT transition observed[6)]. Fig. 1 shows our calculations in nonlocal DWIA[7)] by using the effective Lagrangian of Blomqvist and Laget[8)] (BL) and distorted pion wave functions from the optical potential of Stricker, McManus and Carr[9)] (SMC). Although there is near perfect agreement between theory and experiment at low energy, a measurement at 320 MeV[3)] revealed a disagreement with the same theory by a factor of 3, which was accounted to partly the lack of unitarization in the BL-operator and also the improper treatment of pion propagation described by SMC potentials.

The aim of this paper is to present a new approach which combines the advantages of the nonlocal DWIA calculation of Tiator and Wright[7)] and the Δ-hole approach of Koch, Moniz and Ohtsuka[10)] and to apply it to the calculation of the differential cross section of the reaction $^{14}N(\gamma,\pi^+)^{14}C_{gs}$. For this purpose we use the full nonlocal Born amplitudes derived from Feynman diagrams, therefore exhibiting a well defined off-shell behaviour. To avoid double counting with the resonance contribution, we project the M_{1+} amplitude out of the isospin 3/2 channel. The resonant part will be evaluated in an extended version of the Δ-hole

approach. In this approach, the ground state of ^{14}N and ^{14}C have open shell structures, such as in the wave function of Cohen-Kurath or Huffmann[5]. The doorway space is spanned by $|\Psi^{(A=13)} \otimes \Delta\rangle$ states which correspond to the $|\Delta \otimes h\rangle$ states in the usual Δ-hole approach. In this way we consider not only the direct photoproduction from initial to final state, $^{14}N(\gamma,\pi^+)^{14}C_{gs}$, but also two-step processes with charge exchange such as $^{14}N(\gamma,\pi^0)^{14}N_{gs}(\pi^0,\pi^+)^{14}C_{gs}$ in a consistent way.

In the following we use the Huffmann H1 wave function and a spreading potential which is adjusted in order to get agreement with elastic pion scattering from ^{14}C in the resonance region, see Fig. 2.

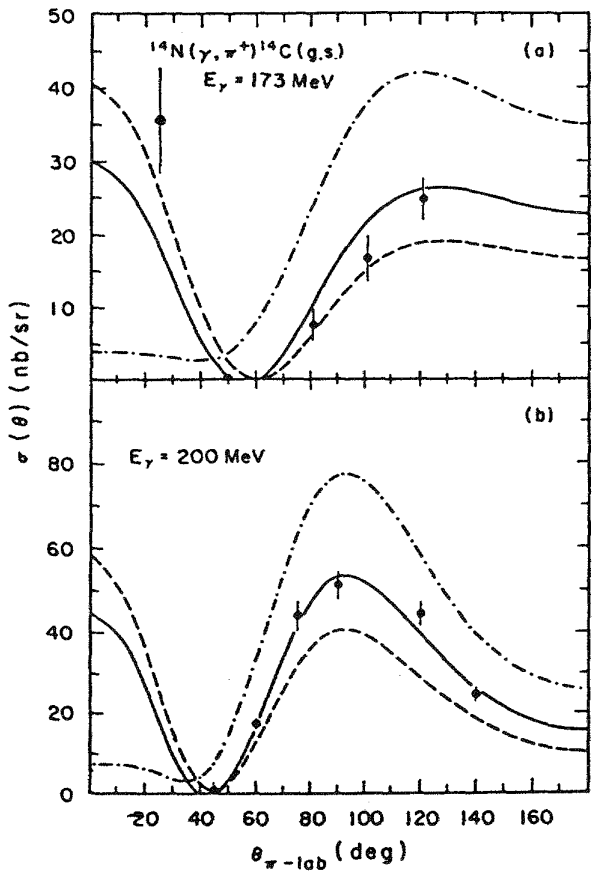

Fig. 1: $^{14}N(\gamma,\pi^+)^{14}C_{gs}$ in nonlocal DWIA at E_γ = 173 MeV (a) and 200 MeV (b). The solid, dashed and dash-dotted lines are obtained with H1, H2 and HF1 wave functions of ref. 5. The Gamow-Teller matrix element for HF1 is zero, but finite for H1 and H2. The data is taken from ref. 1,6 (a) and ref. 2 (b).

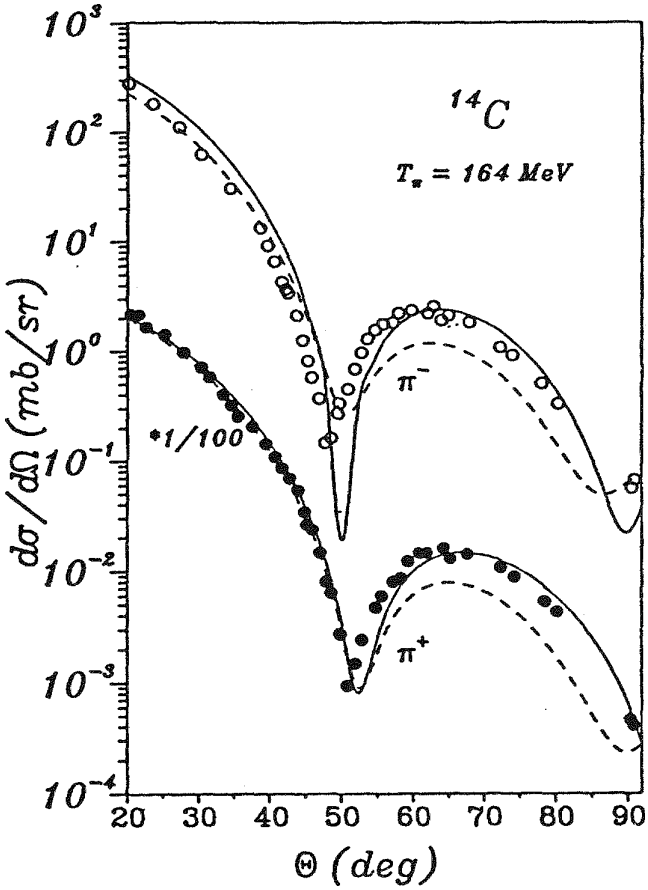

Fig. 2: Pion elastic scattering from ^{14}C at T_π = 164 MeV. The solid line shows our Δ-hole calculation and the dashed line is obtained with an optical potential of ref. 9. The experimental data is taken from ref. 11.

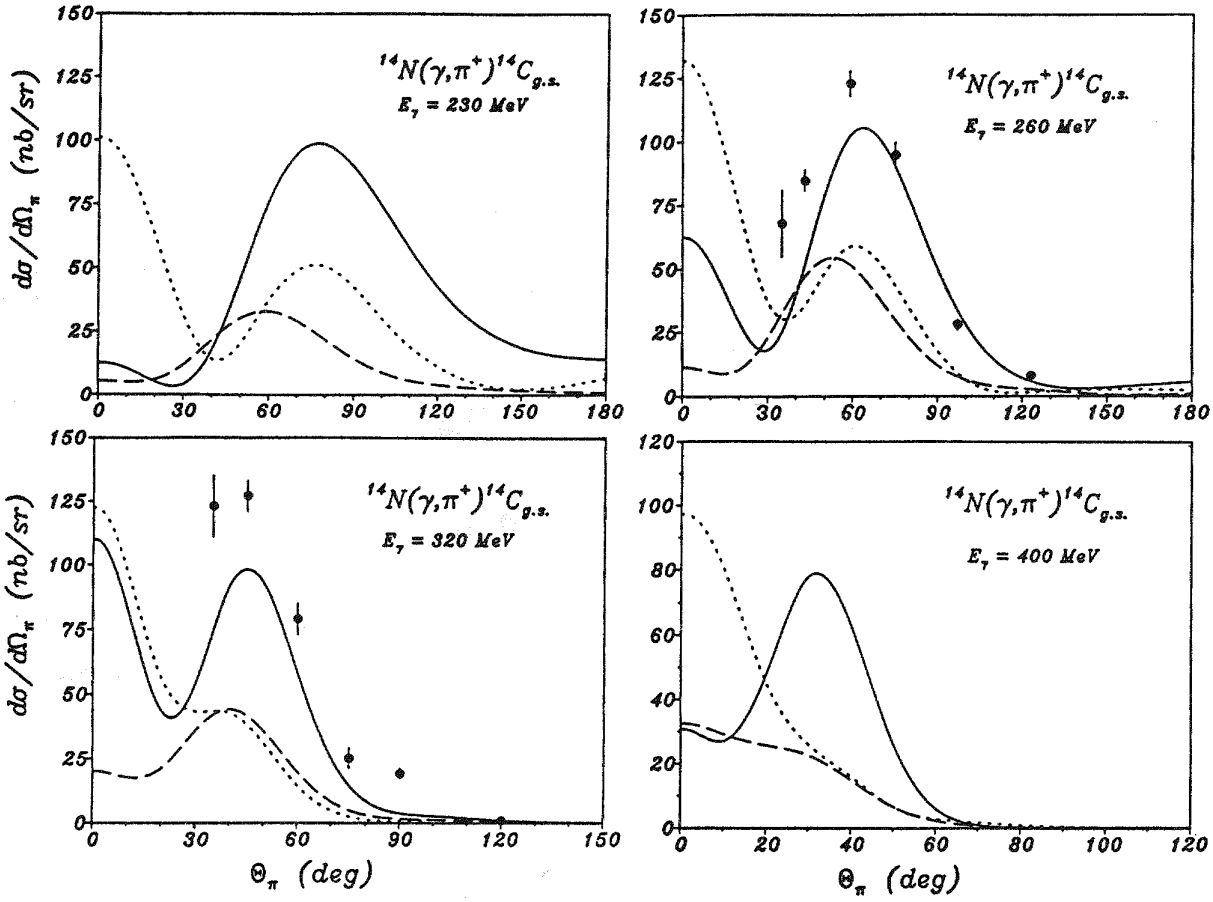

Fig. 3: $^{14}N(\gamma,\pi^+)^{14}C_{gs}$ at different photon energies. The solid line is our Δ-hole calculation and the dotted line shows our standard DWIA calculation. The dashed line shows the resonance contribution in the Δ-hole approach seperately. The experimental data is taken from ref. 18 (260 MeV) and ref. 3 (320 MeV).

In fig. 3 we show our (γ,π) calculations for different photon energies in comparison with the experimental data[11] together with the resonance contribution alone and our standard DWIA calculations. It is important to note, that the Δ-resonance never plays the same dominant role as in γ,π^0 reactions or in pion scattering. In the energy region of the resonance between 260 and 320 MeV, the resonant part alone contributes about 50% while, at smaller energies as well as for higher energies its effect becomes less important. In comparison with other recent calculations we obtain better agreement with the experimental data. In the Δ-hole calculation of Suzuki, Takaki and Koch[12] the resonant contribution at the peak of the 320 MeV data is 15% smaller and the complete calculation is 30% smaller than our results. Wittman and Mukhopadhyay[13] used a nonlocal DWIA approach with a unitarized elementary production operator and Δ-hole pion wave functions distorted by a closed shell nucleus similar to ref. 12.

These results are in very good agreement with the data at 260 MeV but too small by about a factor of 2 at 320 MeV, comparable to ref. 12. In our calculations the data is reasonably well described at both energies: The peak value at 260 MeV is about 15% too small and at 320 MeV it is 25% too small. The reason for the improvement in our calculations is mainly the open shell treatment of not only the initial and final states but also for the intermediate doorway states $|\Psi^{(13)} \otimes \Delta\rangle$ Furthermore our background is evaluated in nonlocal DWIA taking advantage of the well defined off-shell behaviour of Feynman amplitudes.

In conclusion, pion photoproduction from ^{14}N has shown that a systematic experimental survey over the kinematic regime from threshold up to energies above the Δ-resonance is a very powerful tool for finding definite answers to the different aspects of nuclear physics which are investigated by the γ,π probe. Similar efforts would be worthwhile in the case of the mirror nuclei (^{13}C, ^{13}N) and (^{15}N, ^{15}O) for which recent experimental results[14-17] have raised new interesting questions.

* Supported by the Deutsche Forschungsgemeinschaft (SFB 201)

1) K. Röhrich et al, Phys. Lett. **153B** (1985) 203
2) B.H. Cottman et al, Phys. Rev. Lett. 55 (1985) 684
3) P.K. Teng et al, Phys. Lett. **177B** (1986) 25
4) B. Goulard et al, Phys. Rev. **C16** (1977) 1999
5) R.L. Huffman et al, Phys. Rev. **C35** (1987) 1
6) K. Röhrich et al, submitted to Nucl. Phys.
7) L. Tiator and L.E. Wright, Phys. Rev. **C30** (1984) 989
8) K.I. Blomqvist and J.M. Laget, Nucl. Phys. **A280** (1977) 405
9) K. Stricker, H. McManus and J.A. Carr, Phys. Rev. **C19** (1979) 929
10) J.H. Koch, E.J. Moniz and N. Ohtsuka, Ann. of Phys. **154** (1984) 99
11) C.J. Harvey et al, Phys. Rev. **C33** (1986) 1454
12) T. Suzuki, T. Takaki and J.H. Koch, Nucl. Phys. **A460** (1986) 607
13) R. Wittman and N.C. Mukhopadhyay, Phys. Rev. Lett. 57 (1986) 1113
14) P. Stoler et al, Phys. Lett. **143B** (1984) 69
15) S. Kaarsgaarn et al., NIKHEF-K Report (1985)
16) K. Shoda et al, Phys. Lett. **169B** (1986) 17
17) T. Kobayashi et al, contributed paper h-38, p. 676, PANIC 1987
18) P. Stoler and M.D. Seneviratne, private communication

PROGRAM
FOR
THE CEBAF 1987 SUMMER WORKSHOP

JUNE 22 - 26, 1987

Continuous Electron Beam Accelerator Facility
12070 Jefferson Avenue, Newport News, VA 23606

To Be Held At
Christopher Newport College
50 Shoe Lane
Newport News, VA 23606

MONDAY, JUNE 22 *(Sessions through 5:00 p.m. held in Campus Center Theater)*

8:00	Registration begins
9:00 - 9:05	Opening remarks - C. Williamson (MIT)
9:05 - 9:10	Greeting by Richard M. Summerville, Vice President for Academic Affairs, Christopher Newport College
9:10 - 9:30	Welcome and Overview by the Director - H. Grunder (CEBAF)
9:30 - 10:30	CEBAF - A Laboratory for Nuclear Physics - J. Dirk Walecka (CEBAF)

COFFEE

11:00 - 11:30	The Accelerator and its Operation - C. Leemann (CEBAF)
11:30 - 12:00	Engineering, Cost and Schedule - A. Chargin (CEBAF)

LUNCH (at CNC)

2:00 - 2:30	Recommendations of the CEBAF PAC - J. Schiffer (Argonne)
2:30 - 2:45	Discussion - lead by C. Williamson (MIT)

Organization of collaborations

2:45 - 3:15	High Resolution Spectrometers - J. Mougey (CEBAF)

COFFEE

3:15 - 3:45	Large Acceptance Spectrometer (LAS) - B. Mecking (CEBAF)
3:45 - 4:15	The (γ,K) Program - E. Hungerford (Houston)
4:15 - 4:45	Parity Measurements at CEBAF - R. Carlini (LAMPF)

4:45 - 5:00	Organization of Physics Collaboration Meetings - F. Gross (CEBAF)
5:00 - 6:00	Organizational Meetings of the Physics Collaborations *(classrooms - see separate schedule)*
6:00 - 6:15	*Buses to CEBAF*
6:30 - 7:30	Social Hour (at CEBAF)

TUESDAY, JUNE 23 *(Morning sessions held in Campus Center Theater)*

8:30 - 9:20	Coincidence Measurements from Nuclei - W. Bertozzi (MIT)
9:20 - 10:10	Medium Effects in Inelastic Electron Scattering on the Tri-Nucleon System - J. Tjon (Utrecht)
COFFEE	
10:40 - 11:30	Baryon-Baryon Interactions in the Quark Cluster Model - M. Oka (Penn)
11:30 - 12:20	Nuclear Physics with Strange Particles - T. Walcher (Mainz)
LUNCH (at CNC)	
2:00 - 5:00	Physics Collaboration Meetings *(classrooms - see separate schedule)*
5:00 - 6:00	Exploratory Meeting for New Program Collaborations *(Anderson Auditorium - Administration Building - ground floor)*

WEDNESDAY, JUNE 24 *(Morning sessions held in Campus Center Theater)*

8:30 - 9:20	Experimental Studies of Electromagnetic Properties of Few Body Systems - P. Bosted (SLAC/AU)
9:20 - 10:10	Study of Nuclear Correlations and Three-Body Forces with Electrons - J. Laget (Saclay)
COFFEE	
10:40 - 11:30	Hadrons, QCD, and All That - G. Karl (Guelph)
11:30 - 12:20	Relativistic Heavy Ion Collisions - M. Tannenbaum (BNL)
LUNCH (at CNC)	

2:00 - 3:30 Fourth Annual User Group Meeting *(Anderson Auditorium - Administration Building - ground floor)*

3:30 - 5:30 Physics Collaboration meetings *(classrooms - see separate schedule)*

BANQUET

THURSDAY, JUNE 25 *(Sessions through 4:00 p.m. held in Campus Center Theater)*

8:30 - 9:20 Few Nucleon Studies with Polarized p and d Beams at Saturne - Y. Terrien (Saclay)

9:20 - 10:10 Three-Body Forces and Meson Exchange Currents in the Tri-nucleon - J. Friar (LANL)

COFFEE

10:40 - 11:30 Deuteron Form Factors in the Skyrme Approach - E. Nyman (Helsinki)

11:30 - 12:20 Many Body Problems and Electron Scattering - C. Mahaux (Liege)

12:20 - 12:40 The Superconducting Cavities - R. Sundelin (CEBAF)

LUNCH (at CNC)

2:00 - 4:00 Reports of Physics Collaboration Meetings (Plenary Session)

4:00 - 5:30 Program Collaboration Meetings *(Classrooms - see separate schedule)*

5:30 - 6:30 Meeting of New Program Collaborations *(Anderson Auditorium - Administration Building - ground floor and Classrooms)*

FRIDAY, JUNE 26 *(All sessions held in Campus Center Theater)*

Program Collaboration Reports

8:30 - 9:00 High Resolution Spectrometers - C. Papanicolas (Univ. of Ill.)

9:00 - 9:30 Large Acceptance Spectrometer - R.D. McKeown (Caltech)

9:30 - 10:00 The (γ,K) Program - R. E. Chrien (BNL)

10:00 - 10:30 Parity Measurements - R. T. Siegel (W&M)

COFFEE

11:00 - 12:00 Report(s) from Newly Organized Program Collaborations

12:00 - 1:00 Workshop Summary - J. Domingo (SIN)

LUNCH (at CNC)

LIST OF PARTICIPANTS

Gary S. Adams
Physics Dept.
Rensselaer Polytechnic Inst.
Troy, NY 12180

Jurgen Arends
Universitat Bonn
Nussallee 12
D-5300 Bonn #1

Bruce Barrett
Prog. Off. for Nuclear Theory
The National Science Foundation
1800 "G" Street, N.W.
Washington, DC 20550

Omar Benhar
INFN Sezione Sanita
Viale Regina Elena
299 I-00161
Rome, Italy

B.L. Berman
Dept of Physics
Geroge Washington University
Washington, DC 20052

Pierre Bertin
Laboratoire De Phys. Corpusculaire
Universite De Clermont-Ferrand
B.P. 46
63170 Aubiere
France

William Bertozzi
Dept. of Physics
Mass. Inst. of Technology
Bldg 26-441
Cambridge, MA 02139

Fred E. Bertrand
Physics Division
Oak Ridge National Labortory, Bldg. 6000
Martin Marietta Energy System
P.O. Box X
Oak Ridge, TN 37831-6368

Carroll Bingham
Dept. of Physics
University of Tennessee
Knoxville, TN 37996

Paul R. Boberg
Dept of Physics
University of Maryland
College Park, MD 20742

Werner Boeglin
MIT
P.O. Box 846
Middleton, MA 01949

Peter Bosted
SLAC
P.O. Box 4349
Stanford, CA 94305

Warren W. Buck
Dept. of Physics
Hampton University
Hampton, VA 23668

Roger Carlini
Los Alamos Nat. Lab.
MS H847, Group MP-14
Los Alamos, NM 87545

Carl Carlson
Dept. of Physics
College of William & Mary
Williamsburg, VA 23185

Chia-Cheh Chang
Physics Dept.
University of Maryland
College Park, MD 20742

Tom Chapuran
Physics Dept. /E1
Univ. of Pennsylvania
Philadelphia, PA 19104

Robert E. Chrien
Physics Dept.
Brookhaven Nat. Lab.
510 A26-429
Upton, NY 11973

Sang Chun
Dept. of Physics
Hampton University
Hampton, VA 23668

Fritz Coester
Physics Division, Bldg. 203
Argonne National Laboratory
9700 S. Cass Avenue
Argonne, IL 60439-4843

Steve Cotanch
Dept. of Physics
North Carolina State Univ.
Raleigh, NC 27650

Hall Crannell
Dept. of Physics
Catholic University of America
Washington, DC 20064

Francis A. Cucinotta
Mail Stop 160
NASA
Hampton, VA 22365

Donal Day
Dept. of Physics
University of Virginia
Charlottesville, VA 22901

Larry Dennis
Dept. of Physics
Florida State University
Tallahassee, Florida 32306

Veljko Dmitrasinovic
Dept. of Physics
College of William & Mary
Williamsburg, VA 23185

George Dodson
Lab. for Nuclear Science
MIT/BATES 26-429
Cambridge, MA 02139

John Domingo
Swiss Inst. for Nuclear Res.
5432 Villigen
Switzerland

David C. Doughty, Jr.
Christopher Newport College
50 Shoe Lane
Newport News, VA 23606

Edward Dressler
Dept. of Physics
Pennsylvania State Univ.
Abington, PA 19001

John Dubach
Dept. of Phyicss & Astronomy
Univ. of Massachusetts
Amherst, MA 01003

Kim Sh. Egiyan
Yerevan Physical Institute
Markarian Street #2
Yerevan 375036
USSR

R.A. Eisenstein
Nuclear Physics Laboratory
University of Illinois
23 Stadium Drive
Champaign, IL 61820

Kathleen Ensign
Dept. of Physics
College of William & Mary
Williamsburg, VA 23185

S. Fallieros
Physics Dept.
Brown University
Providence, RI 02912

Hamidullah Farhat
Dept. of Physics
Hampton University
Hampton, VA 23663

Manouchehr Farkhondeh
MIT/BATES
P.O. Box 846
Middleton, MA 01949-2846

Mike Finn
Dept. of Physicsy
William & Mary
Williamsburg, VA 23185

Sherman Fivozinsky
U.S. Dept. of Energy
ER-23, GTN
Washington, DC 20545

Gregg Franklin
Physics Dept.
Carnegie-Mellon Univ.Univ. of Minnesota
Pittsburgh, PA 15213Minneapolis, MN 55455

James L. Friar
Los Alamos Nat. Lab.
Theory Division, MS B210
P.O. Box 1663
Los Alamos, NM 87545Durham, NH 03824

Herbert Funsten
Dept. of Physics
College of William & Mary
Williamsburg, VA 23185

Vladimir Gavrilov
Inst. for Theor. & Exp. Physics
B. Chezemushkinskaya UL 25
Moscow 117259
USSR

Gerard P. Gilfoyle
Physics Dept.
University of Richmond
SUNY at Stony Brook
Stony Brook, NY 11794

Kevin Giovanetti
Physics Dept.
Univ. of Virginia
Charlottesville, VA 22901

Vagos Hadjimichael
Dept. of Physics
Fairfield University
Fairfield, CT 06430

Eamon Harper
Dept. of Physics
George Washington Univ.
Washington, DC 20052

Paul Hatchell
Dept. of Physics
University of Wisconsin
Madison, WI

Erik Heide
Dept. of Physcis
Univ. Minnesota
Minnepolis, MN 55455

Jochen Heisenberg
Dept. of Physics
Univ. of New Hampshire

Harry D. Holmgren
SURA
1776 Massachusetts Ave, N.W.
Suite 604
Washington, DC 20036

D. J. Horen
Physics Division, Bldg. 6000
Oak Ridge National Laboratory
P.O. Box X
Oak Ridge, TN 37831-6368

Shian-Shyong Hsiao
Dept. of Physics
N.C. State University, Box 536
Raleigh, NC 27650

Ed Hungerford
Physics Dept.
University of Houston
Houston, TX 77004

Harold E. Jackson, Jr.
Argonne National Lab.
Bldg 203
Argonne, IL 60439

David Jenkins
Physics Dept.
Virginia Tech
Blacksburg, VA 24061

Chueng-Ryong Ji
Physics Dept.
Brooklyn College of CUNY
Brooklyn, NY 11210

Juerg Jourdan
Cal Tech
Kellogg Rad. Lab
Pasadena, CA 91125

John R. Kane
Physics Dept.
William & Mary
Williamsburg, VA 23185

Gabriel Karl
Dept. of Physics
College of Physical Science
University of Guelph
Ontario, Canada N1G2W1

James J. Kelly
Dept. of Physics & Astronomy
Univ. of Maryland
College Park, MD 20742

Ferdous Khan
Dept. of Physics
Old Dominion University
Norfolk, VA 23508

Eberhard Klempt
Dept. of Physics
Universitat Mainz
D-6500 Mainz 1
West Germany

Siegfried Krewald
Kernforschungs Anlage Julich
KFA, 5170 Julich
West Germany

J. Laget
CEN Saclay
DPHN/HE
91191 Gif-Sur-Yvette, Cedex
France

James M. Lambert
Dept. of Physics
Georgetown University
Washington, DC 20052

Donald R. Lehman
Dept. of Physics
George Washington Univ.
Washington, DC 20052

Richard A. Lindgren
Dept. of Physics
University of Virginia
Charlottesville, VA 22901

B. Joseph Lieb
Dept. of Physics
George Mason Univ.
4400 University Drive
Fairfax, VA 22030

John Lightbody
U.S. Dept. of Commerce
National Bureau of Standards
Room B109, Bldg 245
Gaithersburg, MD 20899

Robert Lourie
MIT/LNS 20D-004
77 Massachusetts Avenue
Cambridge, MA 02139

Chris Lyndon
Dept. of Physics
William & Mary
Williamsburg, VA 23185

Ruprecht Machleidt
LANL
Mail Stop H-850
Los Alamos, NM 87545

Richard Madey
Dept. of Physics
Kent State University
Kent, OH 44242

Claude Mahaux
Universite de Liege
Institut de Physique
Sart Tilman
B-4000 Liege 1
Belgium

Mark Manley
Dept. of Physics
Kent State University
Kent, OH 44242

Philippe Martin
Dept. of Physics
Univ. of Petroleum & Minerals
Dhahran 31261
Saudi Arabia

Khin Maung
Dept. of Physics
Old Dominion University
Norfolk, VA 23508

James McCarthy
Physics Dept.
Univ. of Virginia
Charlottesville, VA 22901

Robert McKeown
Div. of Physics & Astronomy
Caltech
Pasadena, CA 91125

Ralph Minehart
BIN 43
SLAC
P.O. Box 4349
Stanford, CA 94305

Rory A. Miskimen
Dept. of Physics
Rm. 417-B
Univ. of Massachusetts
Amherst, MA 01003

Alireza Mokhtari
Physics Dept.
George Washington Univ.
Washington, DC 20052

Philip E. Morris, Jr.
Dept. of Physics
William & Mary
Williamsburg, VA 23185

Gordon S. Mutchler
Physics Dept.
Rice University
P.O. Box 1892
Houston, TX 77251

Reiner Neuhausen
Institut fur Kernphysik
Univ. Mainz
Postfach 3980
D-6500 Mainz
West Germany

John W. Norbury
Physics Dept.
University of Idaho
Moscow, ID 83843

Ebbe Nyman
University of Helsinki
Siltavuorenpenger 2UC
SF-00170
Helsinki-17

M. Oka
Dept. of Physics
Univ. of Pennsylvania
209 S. 33rd St.
Philadelphia, PA 19104

Costas Papanicolas
Dept. of Physics
University of Illinois
1110 W. Green Street
Urbana, IL 61801

C. F. Perdrisat
Physics Dept.
William & Mary
Williamsburg, VA 23185

Gerald A. Peterson
Dept. of Physics & Astronomy
Univ. of Massachusetts
Amherst, MA 01003

Philip Pile
Brookhaven National Lab
Bldg. 510 A
Upton, NY 11973
Italy

Wayne Polyzou
Dept. of Physics & Astronomy
University of Iowa
Iowa City, IA 52240

Volker Ponisch
Niels-Bohr-Institute
Blegdamsvej 17
DK 2100 Copenhagen 0
Denmark

Barry Preedom
Dept. of Physics & Astronomy
Univ. of South Carolina
Columbia, SC 29208

Greg Retzlaff
Saskatchewan Acc Lab
Univ. of Saskatchewan
Saskatoon, Sask.
Canada

Barry G. Ritchie
Dept. of Physics
Arizona State University
Tempe, AZ 85287

Russell L. Robinson
Oak Ridge National Lab
Bldg. 6000
Oak Ridge, TN 37830

Dr. Nathan Rodning
Univ. of Alberta
Nuclear Research Centre
Edmonton, ALTA T6G 2N5
Canada

Giovanni Salme
INFN Sezione Sanita
Viale Regina Elena 299
I-00161 Rome

Francesca Sammarruca
Physics Dept.
VPI
Blacksburg, VA 24061

Betty Orrick Sapp
46 Cresthill Road
Brighton, MA 02135

Wade Sapp
Bates/MIT
Bldg. 26-449
Cambridge, MA 02139

John Schiffer
Physics Division
Argonne National Laboratory
9700 S. Cass Ave.
Argonne, IL 60439

Richard Sealock
Physics Department
Univ. of Virginia
Charlottesville, VA 22903

Kamel K. Seth
Dept. of Physics & Astronomy
Northwestern University
Evanston, IL 60201

Prof. Carl Shakin
Dept. of Physics
Brooklyn College
Brooklyn, NY 11210

Robert Siegel
Dept. of Physics
College of William & Mary
Williamsburg, VA 23185

Paul Souder
201 Physics Building
Syracuse University
Syracuse, NY 13244-1130

Paul Stoler
Dept. of Physics
RPI
Troy, NY 12181

Carey E. Stronach
Dept. of Physics
Virginia State Univ.
Box 358
Petersburg, VA 23803

Peter C. Tandy
Physics Dept.
Kent State Univ.
Kent, OH 44242

M. Tannenbaum
Dept. of Physics
Brookhaven Nat. Lab.
20 Pennsylvania St. Bldg. 510
Upton, NY 11973

Y. Terrien
CEN Saclay DPhN/ME
91191 Gif-Sur-Yvette
Cedex, France

William J. Thompson
Physics Dept.
Univ. of North Carolina
Phillips Hall 039A
Chapel Hill, NC 27514

Stephen T. Thornton
Dept. of Physics
University of Virginia
Charlottesville, VA 22901

Dr. Lothar Tiator
Institut fur Kernphysik
Universitat Mainz
6500 Mainz
West Germany

John Tjon
Institute for Theo. Physics
Utrecht, 3508 TA
The Netherlands

Dr. Toi
P.O. Box 1698
Newport News, VA 23601

Paul Ulmer
College of William & Mary
Williamsburg, VA 23185

Henry S. Valk
School of Physics
Georgia Institute of Technology
Atlanta, GA 30332

J. W. Van Orden
Dept. of Physics
Univ. of Maryland
College Park, MD 20742

Robert L. Varner
Oak Ridge National Laboratory
Bldg. 6000
P.O. Box X
Oak Ridge, TN 37831-6368

Karl F. Von Reden
Univ. of Pittsburgh
100 Allen Hall
Pittsburgh, PA 15260

Thomas Walcher
Institut Fuer Kernphysik
Univ. Mainz
D-6500 Mainz
West Germany

John Watson
Dept. of Physics
Kent State University
Kent, OH 44242

Hans J. Weber
Dept. of Physics
University of Virginia
Charlottesville, VA 22901

Steve Whisnant
Dept. of Physics
Univ. of South Carolina
Columbia, SC 29208

H. Thomas Williams
Dept. of Physics
Washington and Lee Univ.
Lexington, VA 24450

Claude Williamson
Dept. of Physics
MIT
Cambridge, MA 02139

John L. Wood
School of Physics
Georgia Tech
Atlanta, GA 30332

Louis E. Wright
Physics Dept.
Ohio University
Athens, OH 45701

M. Yamazaki
MIT Bates Linear Accelerator
P.O. Box 846
Middleton, MA 01949

Larry Zamick
Physics Dept.
Rutgers University
Piscataway, NJ 08854

Dr. William Ziegler
Dept. of Physics
Univ. of Alberta
Edmonton, Alberta T5M 2M9

Lloyd R. Zumwalt
Nuclear Engineering
North Carolina State Univ.
Raleigh, NC 27650

CEBAF Participants

12070 Jefferson Avenue
Newport News, VA 23606

David Buckle

Volker Burkert

Tony Chargin

Peter Dunn

Franz Gross

Hermann Grunder

Christoph Leemann

John LeRose

Bernhard Mecking

Jean Mougey

Sirish Nanda

Arun Saha

Ron Sundelin

Dirk Walecka

R. Roy Whitney

*U.S. GOVERNMENT PRINTING OFFICE:1987-729-070